

L.-P. Lévy

Magnetism and Superconductivity



Springer

Texts and Monographs in Physics

Series Editors: R. Balian W. Beiglböck H. Grosse E. H. Lieb
N. Reshetikhin H. Spohn W. Thirring

Springer-Verlag Berlin Heidelberg GmbH



<http://www.springer.de/phys/>

Texts and Monographs in Physics

Series Editors: R. Balian W. Beiglböck H. Grosse E. H. Lieb
N. Reshetikhin H. Spohn W. Thirring

From Microphysics to Macrophysics

I + II Methods and Applications
of Statistical Physics By R. Balian

Scattering Theory of Classical and Quantum N -Particle Systems

By J. Dereziński and C. Gérard

Quantum

The Quantum Theory of Particles, Fields,
and Cosmology By E. Elbaz

The Elements of Mechanics

By G. Gallavotti

Supersymmetric Methods in Quantum and Statistical Physics

By G. Junker

CP Violation Without Strangeness

Electric Dipole Moments of Particles,
Atoms, and Molecules
By I. B. Khriplovich and S. K. Lamoreaux

Scattering Theory of Waves and Particles 2nd edition

By R. G. Newton

Generalized Coherent States and Their Applications

By A. Perelomov

The Mechanics and Thermodynamics of Continuous Media

By M. Šilhavý

Large Scale Dynamics of Interacting Particles

By H. Spohn

Renormalization

An Introduction

By M. Salmhofer

Statistical Methods in Quantum

Optics 1. Master Equations and
Fokker–Planck Equations
By H. J. Carmichael

Statistical Mechanics of Lattice Systems

Volume 1: Closed-Form and Exact Solutions
2nd, revised and enlarged edition
By D. A. Lavis and G. M. Bell

Statistical Mechanics of Lattice Systems

Volume 2: Exact, Series
and Renormalization Group Methods
By D. A. Lavis and G. M. Bell

Fields, Symmetries, and Quarks

2nd, revised and enlarged edition By U. Mosel

Conformal Invariance and Critical Phenomena

By M. Henkel

Statistical Mechanics

A Short Treatise

By G. Gallavotti

Quantum Field Theory in Condensed Matter Physics

By N. Nagaosa

Quantum Field Theory in Strongly Correlated Electronic Systems

By N. Nagaosa

Information Theory and Quantum

Physics

Physical Foundations for Under-

standing the Conscious Process

By H.S. Green

Magnetism and Superconductivity

By L.-P. Lévy

Laurent-Patrick Lévy

Magnetism and Superconductivity

Translated by Stephen Lyle
With 129 Figures and 13 Tables



Springer

Professor Laurent-Patrick Lévy
MPI für Festkörperforschung, CNRS
Laboratoire des Champs
Magnétiques Intenses
25, avenue de Martyrs
38042 Grenoble Cedex 9, France

Translator:
Stephen Lyle
8, Impasse du Coteau
69480 Pommiers, France

Editors

Roger Balian

CEA
Service de Physique Théorique de Saclay
91191 Gif-sur-Yvette, France

Nicolai Reshetikhin

Department of Mathematics
University of California
Berkeley, CA 94720-3840, USA

Wolf Beiglböck

Institut für Angewandte Mathematik
Universität Heidelberg, INF 294
69120 Heidelberg, Germany

Herbert Spohn

Zentrum Mathematik
Technische Universität München
80290 München, Germany

Harald Grosse

Institut für Theoretische Physik
Universität Wien
Boltzmanngasse 5
1090 Wien, Austria

Walter Thirring

Institut für Theoretische Physik
Universität Wien
Boltzmanngasse 5
1090 Wien, Austria

Elliott H. Lieb

Jadwin Hall
Princeton University, P.O. Box 708
Princeton, NJ 08544-0708, USA

Title of the original French edition: *Magnétisme et supraconductivité* by L.-P. Lévy, Pierre-André Michel (SESJM) © InterÉditions, Paris 1997

Library of Congress Cataloging-in-Publication Data. Lévy, Laurent-Patrick. [Magnetism and superconductivity/ Laurent-Patrick Lévy; translated by Stephen Lyle. p. cm. – (Texts and monographs in physics, ISSN 0172-5998) Includes bibliographical references and index.
1. Magnetism. 2. Superconductivity. I. Title. II. Series. QC753.2.L495132000
538—dc21 99-056699

ISSN 0172-5998

ISBN 978-3-642-08595-6 ISBN 978-3-662-04271-7 (eBook)

DOI 10.1007/978-3-662-04271-7

This work is subject to copyright. All rights are reserved, whether the whole or part of the material is concerned, specifically the rights of translation, reprinting, reuse of illustrations, recitation, broadcasting, reproduction on microfilm or in any other way, and storage in data banks. Duplication of this publication or parts thereof is permitted only under the provisions of the German Copyright Law of September 9, 1965, in its current version, and permission for use must always be obtained from Springer-Verlag. Violations are liable for prosecution under the German Copyright Law.

© Springer-Verlag Berlin Heidelberg 2000

Originally published by Springer-Verlag Berlin Heidelberg New York in 2000.

Softcover reprint of the hardcover 1st edition 2000

The use of general descriptive names, registered names, trademarks, etc. in this publication does not imply, even in the absence of a specific statement, that such names are exempt from the relevant protective laws and regulations and therefore free for general use.

Typesetting: Data conversion by Satztechnik Katharina Steingraeber, Heidelberg

Cover design: *design & production* GmbH, Heidelberg

Printed on acid-free paper

SPIN: 10678180 55/3144/ba - 5 4 3 2 1 0

Preface

This book was written from lectures given to MSc students following the ‘Matter and Radiation’ course at the University of Grenoble I.

Although magnetism and superconductivity cover a wide area of physics, the course was motivated by a common factor: these phenomena are realisations of thermodynamic states which break certain continuous symmetries. In the case of magnetism, they break rotational invariance. In the case of superconductivity, they break gauge invariance. The aim of the course was to bring out the importance of broken symmetries in condensed matter physics.

The book can be understood with minimal prerequisites and the mathematical techniques used are fairly elementary. However, a basic knowledge of spin and angular momentum is essential, since quantum mechanics lies at the heart of both magnetism and superconductivity. Chapter 2 reviews the main points. The first chapter explains how thermodynamic functions are constructed in the presence of a magnetic field. As the book has two parts, Magnetism (I) and Superconductivity (II), these will be specified between brackets in cross-references to sections and chapters.

I have made a particular effort to present phenomena in magnetism and superconductivity by starting with concrete examples. Some technological applications of superconductivity have also been described.

Limits of size have necessarily imposed some difficult choices. The main omissions concern the magnetism of impurities in metals. Hence, the Kondo effect and heavy fermions have not been touched upon. Among the exact models of magnetism, the solution of the Heisenberg chain using Bethe’s ansatz has not been treated, since excellent monographs already exist. Also omitted are aspects of magnetism related to disorder, such as spin glasses and random field magnets. This is a pity, because these subjects have greatly contributed to conceptual progress in understanding complex organisations of states and will probably be put to use in the coming decade in the context of biological organisation. Finally, many important applications (e.g., neutron scattering, magneto-optics, magnetic recording) have not been treated, for excellent textbooks already exist.

Concerning superconductivity, formal aspects requiring finite temperature Green functions have been omitted. In the end, I was unable to avoid mention of second quantisation in dealing with the BCS theory. More exotic aspects of

superconductivity in quasi-one- and two-dimensional materials have been left out. I would have particularly liked to discuss the possibilities for coexistence between magnetism and superconductivity. Among modern subjects, mesoscopic aspects of superconductivity will be quite accessible on the basis of the present course. A set of examination exercises has been collected together in an appendix. Solutions can be obtained at the Web site *atlas.lpthe.jussieu.fr*.

I would like to thank all those who have contributed to the preparation of this manuscript through their encouragement and advice. In particular, questions from students have been of great help in improving the text.

Laurent-Patrick Lévy

Contents

Part I. Magnetism

1. Magnetic Field and Induction.

Thermodynamics	3
1.1 Magnetostatics	3
1.2 Demagnetising Factors	7
1.3 The Reciprocity Theorem	9
1.4 Magnetic Energy and Work	11
1.5 Thermodynamic Potentials	12
1.6 Magnetocaloric Effects	19
1.7 Einstein–de Haas Effect	20

2. Orbital and Spin Magnetism

Without Interactions	23
2.1 Electrons in a Magnetic Field. The Hamiltonian	23
2.2 Bohm–Aharonov Effect and Permanent Currents	26
2.3 Landau Levels	30
2.4 The Quantum Hall Effect	34
2.5 Orbital Magnetism and Landau Diamagnetism	39
2.6 The Haas–van Alphen Effect	41
2.7 Pauli Paramagnetism of Conduction Electrons	43
2.8 The Zeeman Effect	44
2.9 The Spin–Orbit Interaction	47
2.10 Thermodynamics of Localised Spins	48
2.11 Van Vleck Paramagnetism	50
2.12 The Ionic Anisotropy Field	52
2.13 Crystalline Field	53
2.14 Jahn–Teller Distortion	56
2.15 Disappearance of Orbital Angular Momentum in Transition Ions	58

3. Exchange Interactions

3.1 Direct Exchange Between Spins	61
3.2 Atoms with Two Valence Electrons	62
3.3 The Hund Rules	67

VIII Contents

3.4	The Hydrogen Molecule	68
3.5	Effective Exchange Hamiltonian for a Solid	72
3.6	Hartree–Fock Methods	74
3.7	Superexchange	77
3.8	The Energy of Magnetic States	79
4.	Phase Transitions	83
4.1	Second Order Transitions	83
4.2	Correlation Length, Fluctuations and the Ornstein–Zernike Theory	90
4.3	Critical Exponents and Renormalisation of Fluctuations	93
4.4	Scaling Laws	98
5.	Mean Field	101
5.1	Molecular Field	101
5.2	Susceptibility and Spontaneous Magnetisation	106
5.3	Reaction Field	108
5.4	Antiferromagnetism	110
5.5	Exotic Magnets	113
6.	The Ising Model	117
6.1	One-Dimensional Partition Function	118
6.2	Zero Field Solution	118
6.3	Transfer Matrices	119
6.4	Correlation Functions	121
6.5	Glauber Dynamics	127
6.6	Critical Slowing Down	129
6.7	Lattice Gases	130
7.	The XY Model	133
7.1	The Spin 1/2 XY Chain	135
7.2	The Classical One-Dimensional XY Model	139
7.3	Kosterlitz–Thouless Transition in the Two-Dimensional XY Model	141
8.	Linear Response	147
8.1	Isothermal Response	150
8.2	Adiabatic Response and Fluctuation-Dissipation Theorem ..	152
8.3	Comparing Isothermal and Adiabatic Susceptibilities	159
8.4	Properties of Response Functions	161
8.4.1	Kubo Formulas	161
8.4.2	Kramers–Kronig Relations	162
8.4.3	Time Reversal Symmetries	164
8.4.4	Non-Linear Response	165

8.5	Applications to Resonance Phenomena	166
8.5.1	Bloch Equations	166
8.5.2	Relaxation Between Electron and Nuclear Spins	170
8.5.3	Dipolar Relaxation	171
8.5.4	Exchange Narrowing	172
8.5.5	Ferromagnetic Resonance	173
8.5.6	Ferrimagnetic and Antiferromagnetic Resonance	176
9.	Spin Waves	179
9.1	Spin Hydrodynamics	179
9.2	Elementary Excitations and Magnons	184
9.3	Dipolar Interactions and Magnetostatic Modes	192
9.4	Magnon Thermodynamics	195
9.5	Non-Linear Terms	197
9.6	Spin-Wave Spectroscopy	198
9.7	Parallel Pumping	199
9.8	Other Representations	200
9.9	Hydrodynamic Methods	201
10.	Quantum Spin Chains	205
10.1	One-Dimensional Planar XY Systems	208
10.1.1	Field Theory. The Sine–Gordon Equation	208
10.1.2	XY Phase Correlation Functions. Instantons	214
10.2	Some Theorems	216
10.2.1	The Lieb–Schultz–Mattis Theorem	216
10.2.2	Marshall’s Theorems	217
10.3	Valence Bond States	218
10.3.1	Solid Valence Bond States	221
10.4	The Non-Linear σ Model for Antiferromagnetic Chains	226
11.	Itinerant Magnetism	235
11.1	The Kohn Singularity	239
11.2	The Stoner Model. Magnons in Metals	242
11.3	The Excitonic Insulator. Spin Density Waves	248
11.4	The Hubbard Model	252
11.4.1	Electron Correlations	256
11.4.2	Destruction of Antiferromagnetism by Holes	258
11.4.3	High Temperature Superconductivity	259

Part II. Superconductivity

12. Macroscopic Aspects of Superconductivity	263
12.1 Four Phenomena	263
12.2 Electron–Phonon Interactions	267
12.3 The Two-Fluid Model	270
12.4 The London Equations	271
12.5 London and Pippard Superconductors	272
12.6 Thermodynamics of the Transition	274
12.7 The Intermediate State	276
12.8 Critical Current in a Superconducting Wire	280
12.9 Two Types of Superconductor	283
13. Ginzburg–Landau Theory	285
13.1 Ginzburg–Landau Free Energy	287
13.2 The Ginzburg–Landau Equations	291
13.3 Flux Quantisation	295
13.4 The Little–Parks Effect	299
13.5 Critical Current in a Thin Film	300
13.6 Energy of an Interface Between Normal and Superconducting States	301
13.7 Linearised Ginzburg–Landau Equations	303
13.8 Nucleation of Superconductivity at H_{c2}	303
13.9 Surface Nucleation H_{c3}	305
14. The BCS Theory of Superconductivity	309
14.1 The Electron–Phonon Interaction	309
14.2 The BCS Hamiltonian	311
14.3 Mean Field Approximation and Diagonalisation of the BCS Hamiltonian	314
14.4 BCS Wave Function and Coherent States	319
14.5 Finite Temperatures	322
14.6 Thermodynamic Properties	324
14.7 The Tunnel Effect	324
14.8 Nuclear Relaxation and Ultrasound Absorption	327
14.9 Electromagnetic Screening	331
14.10 Conclusion	336
15. Vortices in Type II Superconductors	337
15.1 Isolated Vortices	337
15.2 Interactions Between Vortices	340
15.3 The Abrikosov Vortex Lattice	342
15.4 Magnetisation Curves	344
15.5 Potential of a Vortex Near a Surface	344

15.6	Dissipation by Vortex Flow	346
15.7	Observing Vortex Motion	349
15.8	Vortex Pinning	350
15.9	Strong Pinning Limit. The Bean Model	351
15.10	Thermal Transport of Flux Lines	352
16.	The Josephson Effect and Quantum Interferometers	355
16.1	Quasi-Particle Tunnelling Current	355
16.2	The Josephson Effect	358
16.3	Microscopic Origins of the Josephson Effect	361
16.4	The Josephson Effect in a Magnetic Field	363
16.5	The AC Josephson Effect	366
16.6	Quantum Interferometers. The AC SQUID	369
16.7	Flux Transformers	373
16.8	Mechanical Analogy for the AC SQUID	373
16.9	The DC SQUID	376
16.10	Electromagnetic Waves	378
17.	Inhomogeneous Superconductivity	381
17.1	The Bogoliubov–de Gennes Equations	381
17.2	Semi-Classical Approximation	384
17.3	Vortex Core States	386
17.4	Interface Between a Superconductor and a Normal Metal. Andreev Reflection	390
17.5	S-N-S Junctions and Andreev States	397
17.6	Electromagnetic Properties of Proximity Structures	399
17.7	Gapless Superconductivity	400
17.8	Collective Modes	402
17.9	Conclusions and Perspectives	404
A.	Representations of Continuous and Point Groups	407
A.1	General Notions	407
A.2	Representations of the Rotation Group	410
A.3	Point Groups	412
A.4	Representations of Point Groups	416
A.5	Application to the Crystalline Field	416
B.	Second Quantisation	421
B.1	State Space for N Free Fermions	421
B.2	Other Representations	422
B.3	Representation of Operators in Second Quantisation	424
B.4	Perturbation Theory	426

C. Exercises	429
C.1 Magnetism	429
C.1.1 Magnetic Textures	429
C.1.2 Long Range Exchange Interaction Between Spin 1/2 Particles and the Mean Field Approximation	430
C.1.3 Spin-Flop Transition for an Antiferromagnet	431
C.1.4 Spin Waves and Quantum Fluctuations in Antiferromagnets	433
C.1.5 Order by Disorder: Ground State Selection Processes in Antiferromagnets Frustrated by Thermal Fluctuations	435
C.2 Superconductivity	438
C.2.1 Superconductors Under Pressure	438
C.2.2 Superconductor Arrays	439
C.2.3 Superconductivity in Inhomogeneous Magnetic Field ..	440
C.2.4 Intermediate State of a Type I Superconductor	441
Bibliography	443
Index	461

Part I

Magnetism

1. Magnetic Field and Induction. Thermodynamics

This book is above all devoted to the microscopic aspects of magnetism. The aim is to study the main magnetic states encountered in nature and their properties. Magnetic solids are generally made up of interacting electrons. These interactions are often complex and it is not always easy to build realistic microscopic models. There are nevertheless many situations in which microscopic models can be justified in a precise way. The procedure then is to determine the ground state and lower energy levels of each magnetic system. In statistical physics, this information can be used to determine thermodynamic properties of the solid. In particular, we can find the equation of state $M(H, T)$ relating magnetisation \mathbf{M} and applied magnetic field \mathbf{H} . Once we know the equation of state, Maxwell's equations deliver all macroscopic properties of the magnetic solid, in particular, the spatial distribution of magnetic field and induction.

This chapter deals with these macroscopic aspects. First we discuss the role of dipolar fields inherent in magnetic solids and approximate methods for solving Maxwell's equations. We then make a complete study of their influence on thermodynamic properties.

1.1 Magnetostatics

Two vector fields are required for a macroscopic description of magnetic phenomena, viz., the magnetic field \mathbf{H} and the magnetic induction \mathbf{B} . The only sources determining the magnetic field \mathbf{H} are macroscopic current sources, i.e., electromagnets. The field \mathbf{H} can then be determined from Ampère's theorem and the boundary conditions that \mathbf{H} must satisfy at the interface between two different magnetic materials. There are also microscopic sources. These are orbital atomic currents and magnetic moments due to spin. We thus define the magnetisation \mathbf{M} as the density of microscopic moments per unit volume. The magnetic induction \mathbf{B} is then the macroscopic mean of the microscopic magnetic field whose sources are macroscopic currents produced by electromagnets and the microscopic density of magnetic moments. Once the mean has been taken, magnetic induction can be expressed as a function of magnetisation and magnetic field:

$$\mathbf{B} = \mathbf{H} + 4\pi\mathbf{M}, \quad (1.1)$$

$$\mathbf{B} = \mu_0(\mathbf{H} + \mathbf{M}), \quad (1.2)$$

depending on the system of units chosen (CGS or MKSA). These will be described shortly. Magnetic field and induction satisfy Maxwell's equations with appropriate boundary conditions. Magnetic induction cannot generally be determined without a supplementary constitutive equation relating magnetisation \mathbf{M} to magnetic field \mathbf{H} . This is because the distribution of atomic moments is not given a priori but depends on the specific physical properties of the system under study. The relation $\mathbf{M}(T, \mathbf{H})$ is the *equation of state* of the magnetic system. With this constitutive equation, (1.2) becomes

$$\mathbf{B} = f(\mathbf{H}, T). \quad (1.3)$$

This equation may become extraordinarily complex for ferromagnetic systems, because the value of \mathbf{B} then depends on all previous values of \mathbf{H} . This is the phenomenon of magnetic hysteresis, caused by the great number of configurations which may be adopted by magnetic domains in a ferromagnetic system. These configurations cannot all be explored by thermodynamic fluctuations and the system is thus left in a metastable state. The aim of the present book is to study the above constitutive equation for the main magnetic solids known. We shall only occasionally have recourse to Maxwell's equations.

Two systems of units are particularly useful. In the Gaussian CGS system, the magnetic field \mathbf{H} is measured in oersteds and coincides in vacuum with the magnetic induction \mathbf{B} , measured in gauss. As the magnetisation \mathbf{M} of a material is also expressed in gauss, the susceptibility $\chi = M/H$ is dimensionless. It is given in e.m.u., that is, electromagnetic units of the Gaussian system. Since magnetisation is an extensive variable, we can define susceptibilities per unit volume $\chi_V = \chi/V$ and per unit mass $\chi_M = \chi/M$. If the material under investigation behaves linearly so that $\mathbf{B} = \mu\mathbf{H}$, the permeability μ is given in terms of susceptibility by

$$\mu = 1 + 4\pi\chi. \quad (1.4)$$

In the CGS system, the speed of light enters explicitly into Maxwell's equations:

$$\nabla \cdot \mathbf{B} = 0, \quad (1.5)$$

$$\nabla \times \mathbf{H} = \frac{4\pi}{c} \mathbf{J} + \frac{1}{c} \frac{\partial \mathbf{D}}{\partial t}. \quad (1.6)$$

The first equation expresses the fact that there are no magnetic monopoles and the second is Ampère's theorem. The second term on the right hand side of (1.6) is the displacement current, which will rarely be considered in this book. The boundary conditions impose continuity of the normal component of \mathbf{B} at the surface, and the jump in tangential component of \mathbf{H} depends on the surface current \mathbf{K} :

$$\mathbf{n} \cdot (\mathbf{B}_2 - \mathbf{B}_1) = 0, \quad (1.7)$$

$$\mathbf{n} \times (\mathbf{H}_2 - \mathbf{H}_1) = \frac{4\pi}{c} \mathbf{K}. \quad (1.8)$$

In the MKSA system, the magnetic field is expressed in ampere-turns per metre since Ampère's theorem brings in current density. 1 ampere-turn/m equals $4\pi \times 10^{-3}$ oersted. It is therefore a small unit of magnetic field. Magnetic induction \mathbf{B} is expressed in tesla or weber/m². In vacuum, it is related to the magnetic field by

$$\mathbf{B} = \mu_0 \mathbf{H}, \quad (1.9)$$

where the vacuum permeability is defined to be $\mu_0 = 4\pi \times 10^{-7}$ henry/m. One tesla equals 10^4 gauss and is therefore a large unit. Magnetisation M is also given in tesla but is related by a factor $10^4/4\pi$ to the magnetisation expressed in gauss in CGS units (see equation (1.2)). Maxwell's equations are simpler in MKSA units:

$$\nabla \cdot \mathbf{B} = 0, \quad (1.10)$$

$$\nabla \times \mathbf{H} = \mathbf{J} + \frac{\partial \mathbf{D}}{\partial t}. \quad (1.11)$$

Boundary conditions on magnetic field and induction are

$$\mathbf{n} \cdot (\mathbf{B}_2 - \mathbf{B}_1) = 0, \quad (1.12)$$

$$\mathbf{n} \times (\mathbf{H}_2 - \mathbf{H}_1) = \mathbf{K}. \quad (1.13)$$

In the MKSA system, we often introduce the magnetic polarisation (not to be confused with current density), defined from magnetisation by

$$\mathbf{J} = \mu_0 \mathbf{M}. \quad (1.14)$$

The susceptibility $\chi = M/H$ is still dimensionless and equals 4π times the e.m.u. susceptibility in the CGS system. Likewise, magnetic polarisability $\bar{\chi} = J/H$ is simply

$$\bar{\chi} = \mu_0 \chi. \quad (1.15)$$

This is given in the same units as μ_0 , namely, henry/m. As in the CGS system, susceptibilities per unit mass and volume can be defined. Permeability μ and relative permeability μ_r are defined from polarisability and susceptibility by

$$\mu = \mu_0 + \bar{\chi} = \mu_0(1 + \chi), \quad (1.16)$$

$$\mu_r = \mu/\mu_0 = 1 + \chi. \quad (1.17)$$

In the MKSA system, introduction of a vacuum permeability is extremely artificial. We shall nevertheless adopt this system in the present book, since it is becoming more and more used as an international standard. Table 1.1 summarises conversions between systems of units [1].

Away from any source of current, the magnetic field obeys $\nabla \times \mathbf{H} = 0$. Hence it is possible to define a magnetic scalar potential ϕ such that

Table 1.1. Magnetic units

Quantity	Symbol	CGS Gaussian	Conversion factor ^a C	MKSA SI
Magnetic induction	B	gauss [G] ^b	10^{-4}	tesla [T], [Wb/m ²]
Magnetic flux	Φ	maxwell [Mx], [G cm ²]	10^{-8}	weber, volt-second
Magnetic potential	U	gilbert [Gb]	$10/4\pi$	ampere [A]
Magnetic field magnetising field	H	oersted [Oe] ^c , [Gb/cm]	$10^3/4\pi$	ampere-turn/m, [A/m]
Magnetisation per unit volume ^d	M	[e.m.u./cm ³] ^e	10^3	[A/m]
Magnetisation per unit volume	$4\pi M$	[G]	$10^3/4\pi$	[A/m]
Magnetic polarisation	J, I	[e.m.u./cm ³]	$4\pi \times 10^{-4}$	[T], [Wb/m ²] ^f
Magnetisation per unit mass	σ, M	[e.m.u./g]	$1, 4\pi \times 10^{-7}$	[A m ² /kg], [Wb m/kg]
Magnetic moment	m, μ	[e.m.u.], [erg/G]	10^{-3}	[A m ²], [Joule/T]
Magnetic dipolar moment	j	[e.m.u.], [erg/G]	$4\pi \times 10^{-10}$	[Wb m]
Susceptibility per unit volume	χ, κ	Dimensionless [e.m.u./cm ³]	4π $(4\pi)^2 \times 10^{-7}$	Dimensionless, [Henry/m]
Susceptibility per unit mass	χ_ρ, κ_ρ	[cm ³ /g], [e.m.u./g]	$4\pi \times 10^{-3}$, $(4\pi)^2 \times 10^{-10}$	[m ³ /kg], [H m ² /kg]
Molar susceptibility	$\chi_{\text{mol}},$ κ_{mol}	[cm ³ /mole]	$4\pi \times 10^{-6},$ $(4\pi)^2 \times 10^{-13}$	[m ³ /mole], [H m ² /mole]
Permeability	μ	Dimensionless	$4\pi \times 10^{-7}$	[H/m], [Wb/A m]
Relative permeability	μ_r	Undefined		Dimensionless
Energy density ^g	W	[erg/cm ³]	10^{-1}	[J/m ³]
Demagnetising factor	N, D	Dimensionless	$1/4\pi$	Dimensionless

^a Multiply the number in CGS units by C to convert to MKSA units.

^b 1 gauss = 10^5 gamma (γ).

^c In basic CGS units, the gauss and oersted are [cm^{-1/2}g^{1/2}s⁻¹].

^d Magnetic moment per unit volume.

^e The e.m.u. (electromagnetic unit), unit of total magnetisation, is not strictly speaking a unit. It corresponds to [G cm³/4 π], or in basic units [cm^{5/2}g^{1/2}s⁻¹/4 π].

^f Recognised MKSA unit, although based on the definition $B = \mu_0 H + J$.

^g $\mathbf{B} \cdot \mathbf{H}$ and $\mu_0 \mathbf{M} \cdot \mathbf{H}$ are expressed in [J/m³] in MKSA units. $\mathbf{M} \cdot \mathbf{H}$ and $\mathbf{B} \cdot \mathbf{H}/4\pi$ are expressed in [erg/cm³] in CGS units.

$$\mathbf{H}(\mathbf{r}) = -\nabla\phi(\mathbf{r}) . \quad (1.18)$$

This magnetic potential is only defined in regions of space where there are no current sources. However, we can always define a vector potential \mathbf{A} for the magnetic induction such that

$$\mathbf{B}(\mathbf{r}) = \nabla \times \mathbf{A}(\mathbf{r}) . \quad (1.19)$$

\mathbf{A} is defined up to addition of a gradient. The vector potential takes on a particular significance in quantum mechanics, as we shall see in the next chapter.

How do we measure magnetic field and induction? If we cut a long, cylindrical cavity with axis along the local magnetic field, the boundary conditions (1.13) imply that the magnetic field inside and outside the cavity are the same. The field measured inside is $\mathbf{H} = \mathbf{B}/\mu_0$. Suppose now that the cavity is in the form of a thin disk normal to the magnetic field. Boundary conditions (1.12) now give the magnetic induction $\mathbf{B} = \mu_0 \mathbf{H}$ inside the cavity equal to that outside. There are other simple cases for which magnetic field and induction inside a material can be determined, without explicitly solving Maxwell's equations, as we shall now show.

1.2 Demagnetising Factors

When the system has ellipsoidal shape,

$$(x/a)^2 + (y/b)^2 + (z/c)^2 = 1 ,$$

we can determine internal and external fields from three numbers N_x , N_y , N_z without having recourse to Maxwell's equations [2]. These are the *demagnetising factors*. A long cylinder can be considered as an ellipsoid by taking $c = \infty$, and a flat disk by taking $a = b = \infty$. We assume that a distant source produces a uniform field $H_0 \hat{\mathbf{z}}$ along $\hat{\mathbf{z}}$ far from the sample. In order to obtain the field inside the ellipsoid, one approach is to use the magnetic potential $\phi(\mathbf{r})$. From the first Maxwell equation,

$$\nabla \cdot \mathbf{B} = \mu_0 \nabla \cdot (\mathbf{H} + \mathbf{M}) = 0 , \quad (1.20)$$

we find that the magnetic potential must obey Poisson's equation

$$\nabla \cdot \mathbf{H} = -\nabla^2 \phi(\mathbf{r}) = \rho_M(\mathbf{r}) , \quad (1.21)$$

where the magnetic charge density $\rho_M(\mathbf{r})$ is given by

$$\rho_M(\mathbf{r}) = -\nabla \cdot \mathbf{M}(\mathbf{r}) . \quad (1.22)$$

Applying Gauss' theorem to a small box of negligible thickness whose two faces are on either side of the interface between ellipsoid and vacuum, we can conclude that there must also be a surface magnetic charge $\sigma_M = \hat{\mathbf{n}} \cdot \mathbf{M}$, where $\hat{\mathbf{n}}$ is the unit vector normal to the surface. Since $\phi(\mathbf{r})$ satisfies Poisson's

equation, we can apply the well known results of electrostatics. This gives the potential inside the ellipsoid as a function of the charge density $\rho_M(\mathbf{r})$ and the surface charge $\sigma_M = \hat{\mathbf{n}} \cdot \mathbf{M}$:

$$\phi(\mathbf{r}) = \mathbf{H}_0 \cdot \mathbf{r} + \int \int \int_V d^3 r' \frac{\rho_M(\mathbf{r}')}{|\mathbf{r} - \mathbf{r}'|} + \int \int_S d^2 r' \frac{\sigma_M(\mathbf{r}')}{|\mathbf{r} - \mathbf{r}'|}. \quad (1.23)$$

An elementary charge at \mathbf{r}' produces a Coulomb potential $1/|\mathbf{r} - \mathbf{r}'|$. We can now show by expansion in terms of harmonics that H and M remain constant throughout the interior of the ellipsoid. Consequently, the ‘magnetic charge’ is zero,

$$\rho_M(\mathbf{r}) = -\nabla \cdot \mathbf{M}(\mathbf{r}) = 0,$$

and the second term in (1.23) disappears. The field inside the ellipsoid is therefore a superposition of the applied field and the field created by the distribution of magnetic charges on the surface. The latter opposes the applied field (see Fig. 1.1). As the magnetisation is uniform, this field is also uniform and proportional to the magnetisation. Hence,

$$H_{\text{int}} = H_0 - N_z M, \quad (1.24)$$

$$B_{\text{int}} = \mu_0 [H_0 + (1 - N_z) M]. \quad (1.25)$$

The coefficient of proportionality N_z is called the demagnetising factor in the z direction because it reduces the field inside the sample. In an analogous way, if the magnetic field is applied along the other principal axes of the ellipsoid ($\hat{\mathbf{x}}$ or $\hat{\mathbf{y}}$), we can define demagnetising factors N_x and N_y . In this coordinate system, for which the principal axes of the ellipsoid are $\hat{\mathbf{x}}$, $\hat{\mathbf{y}}$ and $\hat{\mathbf{z}}$, the only non-zero elements in the demagnetisation tensor \mathbf{N} are its diagonal elements N_x , N_y and N_z . For arbitrary magnetisation \mathbf{M} , the interior field is then

$$\mathbf{H}_{\text{int}} = \mathbf{H}_0 - \mathbf{NM}. \quad (1.26)$$

The sum of the demagnetising factors of an ellipsoid is

$$N_x + N_y + N_z = 1 \quad (1.27)$$

in the MKSA system (and 4π in the CGS system). By symmetry, their values for a sphere are equal: $N_x = N_y = N_z = 1/3$. If we apply a field along the

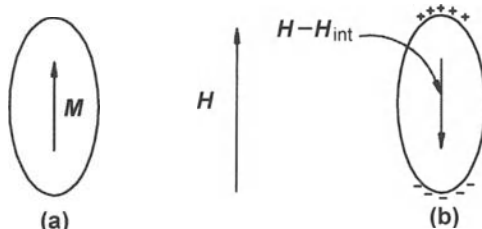


Fig. 1.1. (a) Uniformly magnetised ellipsoid. (b) Magnetic poles at the surface produce a uniform field $H_{\text{int}} - H$ opposing the applied field

Table 1.2. Demagnetising factor for an ellipsoid of revolution

m	N_z	m	N_z	m	N_z	m	N_z
0.0	1	0.2	0.749	1.4	0.249	8.0	0.0286
0.01	0.985	0.25	0.703	1.5	0.232	9.0	0.0239
0.02	0.968	0.3	0.661	1.6	0.219	10.0	0.0199
0.03	0.953	0.4	0.588	1.8	0.194	15.0	0.0103
0.04	0.940	0.5	0.526	2.0	0.173	20.0	0.00676
0.05	0.925	0.6	0.476	2.5	0.135	30.0	0.00342
0.06	0.912	0.7	0.431	3.0	0.109	40.0	0.00207
0.07	0.899	0.8	0.394	3.5	0.0899	50.0	0.00143
0.08	0.886	0.9	0.361	4.0	0.0756	70.0	0.00078
0.09	0.873	1.0	0.330	4.5	0.0645	100.0	0.00042
0.1	0.861	1.1	0.315	5.0	0.0557	200.0	0.00012
0.125	0.829	1.2	0.286	6.0	0.0430	300.0	0.000060
0.167	0.783	1.3	0.266	7.0	0.0350	500.0	0.000023

axis of a long cylinder of revolution, the field inside is equal to that outside, since the tangential component of \mathbf{H} is continuous. We conclude that $N_z \approx O$ and consequently, $N_x = N_y \approx 1/2$, using (1.27). For an applied field normal to a flat disk, it is the normal component of \mathbf{B} which is continuous across the surface. Hence, $N_z \approx 1$ and, using (1.27), $N_x = N_y \approx 0$. For an arbitrary ellipsoid of revolution, tables have been compiled giving demagnetising factors as a function of $m = c/a = c/b$. When $m < 1$, N_z is given as a function of $\cos \psi = m$ by

$$N_z = \frac{1}{\sin^2 \psi} \left(1 - \frac{\psi}{\tan \psi} \right). \quad (1.28)$$

When $m > 1$, we put $1/\cos \psi = m$ and

$$N_z = \frac{1}{\tan^2 \psi} \left[\frac{1}{\sin \psi} \ln \left(\frac{1 + \sin \psi}{\cos \psi} \right) - 1 \right]. \quad (1.29)$$

1.3 The Reciprocity Theorem

One practical problem often encountered in magnetism is to determine the flux induced in a coil by a sample with non-uniform magnetisation per unit volume $\mathbf{M}(\mathbf{r})$ (see Fig. 1.2). The reciprocity theorem relates this flux to the field produced by a current of 1 A in the coil when there is no magnetic sample. The magnetic potential (1.23) produced by the distribution $\mathbf{M}(\mathbf{r})$ can be written more simply by putting $\mathbf{R} = \mathbf{r} - \mathbf{r}'$:

$$\phi(\mathbf{r}) = \int_V d^3 r' \mathbf{M}(\mathbf{r}') \cdot \nabla \frac{1}{|\mathbf{r} - \mathbf{r}'|} = \int_V d^3 r' \mathbf{M}(\mathbf{r}') \cdot \frac{\hat{\mathbf{R}}}{|\mathbf{R}|^2}, \quad (1.30)$$

after integrating by parts. The magnetic field produced by the sample is thus

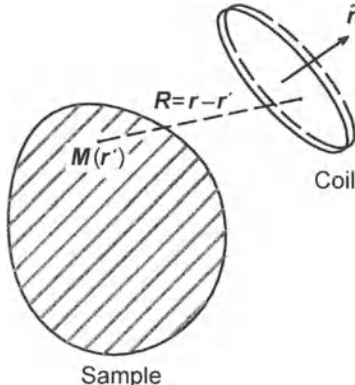


Fig. 1.2. Sample of volume V and magnetisation $\mathbf{M}(\mathbf{r}')$ inducing flux Φ in a detection coil

$$\mathbf{H}(\mathbf{r}) = -\nabla\phi(\mathbf{r}) = \int_V d^3r' \frac{3[\mathbf{M}(\mathbf{r}') \cdot \hat{\mathbf{R}}] \hat{\mathbf{R}} - \mathbf{M}(\mathbf{r}')}{|\mathbf{R}|^3}. \quad (1.31)$$

The magnetic flux through a coil with N turns is therefore

$$\begin{aligned} \Phi &= N\mu_0 \int_S \mathbf{H}(\mathbf{r}) \cdot \hat{\mathbf{n}} d^2r \\ &= N\mu_0 \int_S d^2r \int_V d^3r' \frac{3[\mathbf{M}(\mathbf{r}') \cdot \hat{\mathbf{R}}] (\hat{\mathbf{R}} \cdot \hat{\mathbf{n}}) - \mathbf{M}(\mathbf{r}') \cdot \hat{\mathbf{n}}}{|\mathbf{R}|^3}. \end{aligned} \quad (1.32)$$

Now let $\mathbf{h}(\mathbf{r}')$ be the magnetic field created at point \mathbf{r}' by a current of 1 A in the coil when the sample is removed. From Ampère's theorem, we have

$$\mathbf{v} \cdot \mathbf{h}(\mathbf{r}') = N\mathbf{v} \cdot \oint dl \times \frac{\hat{\mathbf{R}}}{|\mathbf{R}|^2}, \quad (1.33)$$

where \mathbf{v} is an arbitrary vector. Transforming the line integral to a surface integral, we obtain

$$\begin{aligned} \mathbf{v} \cdot \mathbf{h}(\mathbf{r}') &= N \int_S d^2r \hat{\mathbf{n}} \cdot \nabla \times \left[\frac{\hat{\mathbf{R}}}{|\mathbf{R}|^2} \times \mathbf{v} \right] \\ &= -N \int_S d^2r (\mathbf{v} \cdot \nabla) \left[\frac{\hat{\mathbf{R}}}{|\mathbf{R}|^2} \cdot \hat{\mathbf{n}} \right]. \end{aligned} \quad (1.34)$$

Here we have used the vector identity

$$\nabla \times (\mathbf{u} \times \mathbf{v}) = \mathbf{u}(\nabla \cdot \mathbf{v}) - \mathbf{v}(\nabla \cdot \mathbf{u}) + (\mathbf{v} \cdot \nabla)\mathbf{u} - (\mathbf{u} \cdot \nabla)\mathbf{v}. \quad (1.35)$$

Writing $\hat{\mathbf{R}}/|\mathbf{R}|^2$ as the gradient of $1/|\mathbf{R}|$, we find that only the third term is non-zero, since $\nabla^2 1/|\mathbf{R}| \equiv \delta(\mathbf{R})$. Since (1.34) holds for any \mathbf{v} , the field produced by the coil at \mathbf{r}' is

$$\mathbf{h}(\mathbf{r}') = - \int d^2r \nabla \left(\frac{\hat{\mathbf{n}} \cdot \hat{\mathbf{R}}}{|\mathbf{R}|^2} \right) = \int d^2r \frac{3(\hat{\mathbf{n}} \cdot \hat{\mathbf{R}}) \hat{\mathbf{R}} - \hat{\mathbf{n}}}{|\mathbf{R}|^3}. \quad (1.36)$$

Comparing this expression with (1.32), we deduce the reciprocity theorem:

$$\Phi = \mu_0 \int_V d^3 r' \mathbf{M}(r') \cdot \mathbf{h}(r') . \quad (1.37)$$

In other words, if we know the magnetic field $\mathbf{h}(\mathbf{r})$ produced by unit current in a coil when no magnetic sample is present, we can determine the flux produced in the coil by any sample, without having to solve the magnetostatic problem. We need only the magnetisation $\mathbf{M}(\mathbf{r})$. Then we integrate $\mathbf{M}(\mathbf{r}) \cdot \mathbf{h}(\mathbf{r})$ over the region occupied by the sample, as shown in (1.37). The result simplifies detector optimisation and is extremely useful in practice [see Sect. 8.4(I)].

1.4 Magnetic Energy and Work

Consider a solenoid filled with some magnetic material (see Fig. 1.3). If I is the current in the solenoid and n the number of turns per unit length, Ampère's theorem gives the magnetic field at the centre of the solenoid approximately as

$$H = nI . \quad (1.38)$$

Since the divergence of the magnetic induction is zero, we can define the flux of magnetic induction Φ through the tube enclosed by the solenoid by $\Phi = BS$, where S is the cross-sectional area of the solenoid. If the solenoid has length L , it has nL turns and the total flux through all the turns is

$$\Phi = nBLS = nBV , \quad (1.39)$$

where V is the volume of the solenoid. From Faraday's law, a variation in the flux induces an electromotive force in the circuit equal to

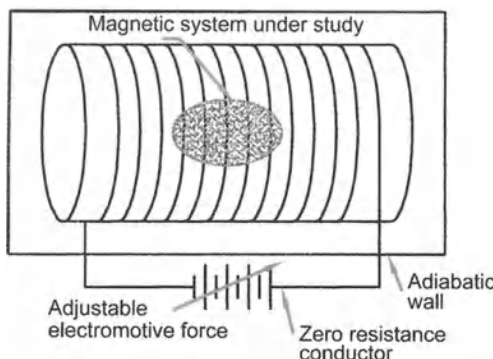


Fig. 1.3. Solenoid of length L and cross-sectional area S containing a magnetic material

$$\mathcal{E} = -\frac{d\Phi}{dt} . \quad (1.40)$$

Consequently, work must be done to maintain the current at its constant value. If dQ is the charge transferred during time dt , the work done is

$$\begin{aligned} dW &= \mathcal{E}dQ = -\frac{d\Phi}{dt}dQ = -Id\Phi \\ &= -\frac{H}{n}nVdB = -VH\mu_0d(H + M) . \end{aligned} \quad (1.41)$$

Then the work done per unit volume of material is

$$dW = -HdB = -\mu_0(HdH + HdM) . \quad (1.42)$$

This work increases the electromagnetic energy by

$$U = \int_0^B HdB = \frac{\mu_0}{2}H^2 + \mu_0 \int_0^M HdM . \quad (1.43)$$

The first term here is the electromagnetic field energy and the second term is the magnetic energy of the magnetised substance. If there is a linear relation between M and H , the energy is quadratic:

$$U = \frac{HB}{2} = \frac{\mu_0 H}{2}(H + M) = (1 + \chi)\frac{\mu_0}{2}H^2 . \quad (1.44)$$

This may seem surprising since the interaction energy of an elementary dipole is

$$U_{\text{int}} = -\boldsymbol{\mu} \cdot \mathbf{B} . \quad (1.45)$$

The reason for this difference is that U represents the change in total energy when a magnetic material is introduced into the field. It therefore includes work done by current sources against electromotive forces. The total magnetic energy is not the same when we work with a constant current source, and hence constant field, and when we work with a constant magnetic induction. In general, field sources are the only ones we are able to control and so it is the constant field energy we must use. Finally, when we calculate the force associated with a change in some coordinate ξ of a magnetic object, we must once again specify that the field H (and hence the current sources) remain constant:

$$F_\xi = - \left(\frac{\partial U}{\partial \xi} \right)_H . \quad (1.46)$$

1.5 Thermodynamic Potentials

The first law of thermodynamics defines the quantity of heat δQ transferred to a system as the change in internal energy minus the work done in magnetising the system. The internal energy of a magnetic solid is therefore

$$dU_S = \delta Q + \mu_0 H dM . \quad (1.47)$$

For a reversible transformation,

$$dU_S = T dS + \mu_0 H dM . \quad (1.48)$$

Entropy and magnetic field can thus be defined as thermodynamic derivatives of the internal energy of a solid:

$$T = \left(\frac{\partial U_S}{\partial S} \right)_M , \quad H = \frac{1}{\mu_0} \left(\frac{\partial U_S}{\partial M} \right)_S . \quad (1.49)$$

As U_S is an exact differential, its partial derivatives satisfy a Maxwell relation:

$$\left(\frac{\partial T}{\partial M} \right)_S = \mu_0 \left(\frac{\partial H}{\partial S} \right)_M . \quad (1.50)$$

The quantity of heat δQ can then be parametrised by

$$\begin{aligned} \delta Q &= \left(\frac{\partial U_S}{\partial T} \right)_M dT + \left[\left(\frac{\partial U_S}{\partial M} \right)_T - \mu_0 H \right] dM \\ &= C_M dT + l dM , \end{aligned} \quad (1.51)$$

where we have defined the specific heat capacity at constant magnetisation

$$C_M = \left(\frac{\partial U_S}{\partial T} \right)_M = \left(\frac{\delta Q}{\delta T} \right)_M = T \left(\frac{\partial S}{\partial T} \right)_M , \quad (1.52)$$

since $\delta Q = T dS$. Likewise, considering entropy S as a thermodynamic function of T and M ,

$$TdS = T \left(\frac{\partial S}{\partial T} \right)_M dT + T \left(\frac{\partial S}{\partial M} \right)_T dM , \quad (1.53)$$

we can re-express the parameter l in (1.51) in terms of the thermodynamic derivative:

$$l = T \left(\frac{\partial S}{\partial M} \right)_T = -T \mu_0 \left(\frac{\partial H}{\partial T} \right)_M . \quad (1.54)$$

Here we have used the Maxwell relation (1.69) associated with the free energy, which will be proven below. These thermodynamic definitions bring out the extensive nature of the magnetic field \mathbf{H} and the intensive nature of magnetisation \mathbf{M} and magnetic induction \mathbf{B} .

The internal energy U_S can generally be determined by methods in statistical physics, from the partition function $U_S = -\partial(\ln Z)/\partial\beta$. Physical quantities can then be calculated from it. However, it is not a true thermodynamic potential measuring the total energy. The electromagnetic field energy has not been included in U_S . We therefore define the total internal energy

$$dU = dU_S + \mu_0 H dH = \delta Q + H dB = T dS + H dB . \quad (1.55)$$

The partial derivatives of U are

$$T = \left(\frac{\partial U}{\partial S} \right)_B, \quad H = \left(\frac{\partial U}{\partial B} \right)_S. \quad (1.56)$$

It is also useful to introduce magnetic enthalpies:

$$\mathcal{H}_S = U_S - \mu_0 H M, \quad (1.57)$$

$$\mathcal{H} = U - H B. \quad (1.58)$$

In differential form

$$d\mathcal{H}_S = T dS - \mu_0 M dH = \delta Q - \mu_0 M dH, \quad (1.59)$$

$$d\mathcal{H} = T dS - B dH. \quad (1.60)$$

The associated Maxwell relation is

$$\left(\frac{\partial T}{\partial H} \right)_S = -\mu_0 \left(\frac{\partial M}{\partial S} \right)_H. \quad (1.61)$$

Equation (1.59) can be used to obtain a new parametrisation of the heat:

$$\begin{aligned} \delta Q &= \left(\frac{\partial \mathcal{H}_S}{\partial T} \right)_H dT + \left[\left(\frac{\partial \mathcal{H}_S}{\partial H} \right)_T + \mu_0 M \right] dH \\ &= C_H dT + h dH, \end{aligned} \quad (1.62)$$

where the specific heat capacity at constant field is

$$C_H = \left(\frac{\partial \mathcal{H}}{\partial T} \right)_H = T \left(\frac{\partial S}{\partial T} \right)_H. \quad (1.63)$$

As for l , the parameter h can be expressed as a thermodynamic derivative. Considering S as a thermodynamic function of T and H ,

$$TdS = T \left(\frac{\partial S}{\partial T} \right)_H dT + T \left(\frac{\partial S}{\partial H} \right)_T dH. \quad (1.64)$$

Using the Maxwell relation (1.78) associated with the Gibbs free energy, we obtain

$$h = T \mu_0 \left(\frac{\partial M}{\partial T} \right)_H. \quad (1.65)$$

The second law of thermodynamics states that thermodynamic equilibrium is reached when entropy is maximal for constant internal energy. It is easy to see that this is equivalent to requiring a minimum of internal energy for constant entropy. (If the internal energy were not minimal, we could extract work and then reinject it in the form of heat, thereby increasing the entropy.) In practice, it is usually the temperature which is kept constant. We must re-express the second law in terms of the minimum of a new thermodynamic function. This will be done explicitly below, by carrying out a Legendre transformation. In the present case, this function is the free energy F (per unit volume),

$$F = U - TS = F_S + \frac{\mu_0}{2} H^2. \quad (1.66)$$

In differential form this is

$$dF = HdB - SdT , \quad (1.67)$$

$$dF_S = \mu_0 H dM - SdT . \quad (1.68)$$

The free energy Maxwell relation is

$$\mu_0 \left(\frac{\partial H}{\partial T} \right)_M = - \left(\frac{\partial S}{\partial M} \right)_T . \quad (1.69)$$

This is very useful for describing magnetocaloric effects. In practice, we first calculate the free energy F_S of a solid from its partition function in statistical physics:

$$F_S = -\frac{1}{\beta} \ln Z . \quad (1.70)$$

We can then construct the total free energy F which is a true thermodynamic potential (reflecting the second law). This can be used to study phase transitions.

Finally, in cases where temperature T and magnetic field H are kept constant, we need yet another thermodynamic potential in order to express the second law as a minimum principle. In these conditions, the Gibbs potential (or Gibbs free energy) G is a minimum. This function is obtained by Legendre transformation [3]. Let b be a particular value of magnetic induction (see Fig. 1.4). At this point, the free energy takes the value $F(b)$. From (1.67), the slope of $F(B)$ at this point is just the magnetic field:

$$H = h(b) = \left(\frac{\partial F}{\partial B} \right)_T (b) . \quad (1.71)$$

The equation of the tangent at b is thus

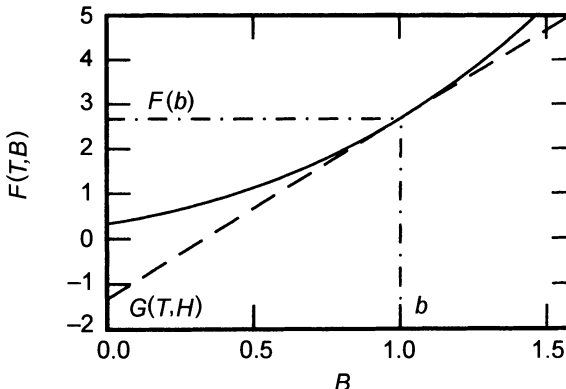


Fig. 1.4. Dependence of free energy on magnetic induction. The slope of the tangent is the magnetic field and the ordinate at the origin is the Gibbs free energy

$$G(H, B) = F(b) + H(B - b) , \quad (1.72)$$

and its ordinate at the origin $B = 0$ is

$$G(H, 0) = F(b) - Hb . \quad (1.73)$$

This depends on H , but also on b which can in turn be expressed in terms of H by means of (1.71): $b = h^{-1}(H)$. Hence we find that

$$G(H) = F(h^{-1}(H)) - Hh^{-1}(H) \quad (1.74)$$

is a function of the slope H and it takes its minimal value at thermodynamic equilibrium. Indeed, if the slope H of the free energy does not change, then a minimal value of G corresponds to a minimal value of F at b . The differential of G is

$$dG = -BdH - SdT . \quad (1.75)$$

If H and T are both fixed, $dG = 0$. Moreover, since $d^2(TS) = d^2(HB) = 0$, we also have $d^2G = d^2U > 0$, in agreement with our construction. If $G(H)$ is known for all values of H , then F can be reconstructed as the envelope of tangents, i.e.,

$$F(B) = G(H) + HB . \quad (1.76)$$

We also define $G_S = G + \mu_0 H^2/2$. Like U_S and F_S , G_S gives an equation of state without being a true thermodynamic potential. The differential relation

$$dG_S = -\mu_0 M dH - SdT \quad (1.77)$$

implies a Maxwell relation:

$$\mu_0 \left(\frac{\partial M}{\partial T} \right)_H = \left(\frac{\partial S}{\partial H} \right)_T . \quad (1.78)$$

The Gibbs free energy is the most useful thermodynamic potential for study of coexisting magnetic phases when the applied field is fixed by current sources. It is also used to study the coexistence of normal and superconducting phases in a magnetic field [intermediate states, see Sect. 12.7(II)].

It often happens that the number of particles in the system is not fixed. This is the case, for example, in an electrical circuit where current sources act as electron reservoirs. It is then useful to specify the mean number of electrons by means of a chemical potential μ . In statistical physics, we work with the grand canonical ensemble. Thermodynamic potentials expressing the second law for constant chemical potential are obtained from the free energies by Legendre transformations:

$$\Omega_F = F - \mu N , \quad \Omega_G = G - \mu N . \quad (1.79)$$

These are the so-called grand canonical potentials. In differential form,

$$d\Omega_F = HdB - SdT - Nd\mu , \quad (1.80)$$

$$d\Omega_G = -BdH - SdT - Nd\mu . \quad (1.81)$$

The value of the chemical potential, specifying the mean number N of particles, is given implicitly by the equation

$$N = - \left(\frac{\partial \Omega_F}{\partial \mu} \right)_{T, B} = - \left(\frac{\partial \Omega_G}{\partial \mu} \right)_{T, H} . \quad (1.82)$$

Finally, there are two thermodynamic relations between C_M and C_H , analogous to the Mayer relation for perfect gases ($C_P - C_V = R$). We use the two parametrisations (1.51) and (1.62) for the heat, obtained from internal energy and enthalpy:

$$\delta Q = C_M dT - T \mu_0 \left(\frac{\partial H}{\partial T} \right)_M dM \quad (1.83)$$

$$= C_H dT + T \mu_0 \left(\frac{\partial M}{\partial T} \right)_H dH . \quad (1.84)$$

We have used relations (1.54) and (1.65), giving l and h in terms of thermodynamic derivatives. Subtracting one equation from the other, we obtain

$$(C_H - C_M) dT = -T \mu_0 \left(\frac{\partial H}{\partial T} \right)_M dM - T \mu_0 \left(\frac{\partial M}{\partial T} \right)_H dH . \quad (1.85)$$

Moreover, there is always an equation of state $M = f(T, H)$. We can therefore express dT in terms of dM and dH as

$$dT = \left(\frac{\partial T}{\partial M} \right)_H dM + \left(\frac{\partial T}{\partial H} \right)_M dH . \quad (1.86)$$

Identifying this with the previous relation, we deduce the thermodynamic identity

$$C_H - C_M = -T \mu_0 \left(\frac{\partial H}{\partial T} \right)_M \left(\frac{\partial M}{\partial T} \right)_H . \quad (1.87)$$

This relation involves a derivative with respect to a constant extensive parameter, which would be difficult to measure. We can remove it by using the standard relation between partial derivatives

$$\left(\frac{\partial H}{\partial T} \right)_M = - \left(\frac{\partial M}{\partial T} \right)_H \left(\frac{\partial H}{\partial M} \right)_T . \quad (1.88)$$

The relation we were seeking becomes

$$C_H - C_M = T \mu_0 \left(\frac{\partial M}{\partial T} \right)_H^2 \left(\frac{\partial H}{\partial M} \right)_T . \quad (1.89)$$

We define the isothermal susceptance κ_T as the derivative of magnetisation with respect to external applied field H , so that

$$\kappa_T = \left(\frac{\partial M}{\partial H} \right)_T . \quad (1.90)$$

This is not the same as the isothermal susceptibility χ_T , which is the derivative of magnetisation with respect to the internal field H_i . Indeed, for a ferromagnetic sample with ellipsoidal shape, we have seen that the internal field is

$$H_i^\alpha = H^\alpha - N_{\alpha\alpha} M^\alpha , \quad (1.91)$$

and consequently

$$\frac{1}{\kappa_T} \Big|_\alpha = \frac{1}{\chi T} \Big|_\alpha + N_{\alpha\alpha} . \quad (1.92)$$

For materials of low susceptibility, susceptance and susceptibility are so close that we will not need to make this distinction. In conclusion, we shall establish a relation between the ratio of specific heat capacities at constant magnetisation and constant field and the ratio of isothermal and adiabatic susceptibilities. We use parametrisations (1.83) and (1.84) for the heat $\delta Q = TdS$. The first of these gives

$$dT = \frac{T}{C_M} dS + \frac{\mu_0 T}{C_M} \left(\frac{\partial H}{\partial T} \right)_M dM . \quad (1.93)$$

Since there is an equation of state relating S , T and M ,

$$dT = \left(\frac{\partial T}{\partial S} \right)_M dS + \left(\frac{\partial T}{\partial M} \right)_S dM . \quad (1.94)$$

The specific heat capacity at constant magnetisation is thus

$$C_M = \mu_0 T \left(\frac{\partial H}{\partial T} \right)_M \left(\frac{\partial M}{\partial T} \right)_S . \quad (1.95)$$

The second parametrisation of δQ leads in the same way to

$$C_H = -\mu_0 T \left(\frac{\partial H}{\partial T} \right)_S \left(\frac{\partial M}{\partial T} \right)_H . \quad (1.96)$$

Dividing one relation by the other, we find the desired identity:

$$\frac{C_H}{C_M} = -\frac{(\partial H/\partial T)_S (\partial T/\partial M)_S}{(\partial H/\partial T)_M (\partial T/\partial M)_H} = \frac{(\partial M/\partial H)_T}{(\partial M/\partial H)_S} = \frac{\kappa_T}{\kappa_S} . \quad (1.97)$$

This can be identified with the ratio of susceptibilities for weakly magnetic materials. We can understand the physical content of this thermodynamic identity, relating specific heats at constant magnetisation and field to isothermal and adiabatic susceptibilities, by studying the linear response of a magnetic system [see Chap. 8(I)].

1.6 Magnetocaloric Effects

The thermodynamics described above enables us to understand magnetocaloric effects occurring in adiabatic processes. In this case,

$$\delta Q = 0 = C_H dT + h dH = C_H dT + T \mu_0 \left(\frac{\partial M}{\partial T} \right)_H dH. \quad (1.98)$$

In most magnetic materials, $(\partial M / \partial T)_H < 0$ and a reduction in magnetic field leads to cooling. As an example, consider a paramagnetic system in a weak field $(\partial M / \partial T)_H = -CH/T^2$, where Curie's constant C is $C_{1/2} = N\mu_0\mu_B^2/k_B$ in the spin 1/2 case. We shall see in Chap. 2 that the constant field specific heat capacity for a spin 1/2 system is $C_H = \mu_0^2 N K_B (\mu_B H / k_B T)^2$. Integrating the above relation, we find that cooling by adiabatic demagnetisation of a magnetic system obeys

$$\ln \left(\frac{T_{\text{fin}}}{T_{\text{ini}}} \right) = - \int_{H_{\text{ini}}}^{H_{\text{fin}}} \mu_0 \left(\frac{\partial M}{\partial T} \right)_H \frac{dH}{C_H(H)}. \quad (1.99)$$

This is known as the magnetocaloric effect. When we consider a spin 1/2 system, it is easy to check that demagnetisation occurs in such a way that H/T remains constant. This is to be expected, since the entropy is constant during a reversible adiabatic transformation, and this can only happen if the partition function is invariant, i.e., if $H/T = \text{const}$. In practice, demagnetisation is stopped before H_{fin} reaches zero since the specific heat of a paramagnetic system tends to zero when $H \rightarrow 0$. The field dependence of the entropy at constant temperature is obtained by integrating the heat $\delta Q = T dS$:

$$S(H, T) - S(0, T) = \mu_0 \int_0^H \left(\frac{\partial M}{\partial T} \right)_H dH. \quad (1.100)$$

If the system is a spin 1/2 paramagnetic solid, its magnetisation is $M = N\mu_B \tanh(\beta\mu_B B)$ [see Sect. 2.10(I)]. Integrating this relation, the entropy of the spins is then

$$S(B, T) = Nk_B [\ln(2 \cosh(\beta\mu_B B)) - \beta\mu_B B \tanh(\beta\mu_B B)]. \quad (1.101)$$

For weak fields, this is approximately $Nk_B \ln 2 - C_{1/2}(H/T)^2/2$, where $C_{1/2}$ is Curie's constant. The entropy is a measure of order in a system, corresponding in this case to the degree of spin alignment. If a large magnetic field polarises the spins, the entropy of the system will be low. When the field is reduced adiabatically, the degree of spin alignment cannot change. For the weaker field, the thermodynamic state corresponds to a system of much lower temperature. We shall see in the next few chapters how interactions between spins and interactions between spins and the crystal lattice can have a significant effect, limiting temperatures attainable through adiabatic demagnetisation. (The argument used for a spin system without interactions can be extended to the case where there is a molecular exchange field h_m .

Now it is the ratio $(H + h_m)/T$ which must stay constant during demagnetisation. Hence the magnetocaloric effect ceases when $H < |h_m|$.) This is why nuclear spins are used to attain the lowest temperatures ($T < 10\mu K$), for they hardly interact at all.

1.7 Einstein–de Haas Effect

Whereas the origin of magnetocaloric effects is energy conservation, magneto-mechanical effects arise from conservation of angular momentum. The total angular momentum of a sample is the sum of electron orbital angular momenta, electron spins, nuclear spins and the angular momentum of the crystal lattice:

$$\mathbf{G} = \langle \mathbf{L} \rangle + \langle \mathbf{S} \rangle + \langle \mathbf{I} \rangle + \mathbf{G}_{\text{latt}} . \quad (1.102)$$

Let us assume that the system has initially zero angular momentum, so that $\langle \mathbf{L} \rangle_0 = \langle \mathbf{S} \rangle_0 = \langle \mathbf{I} \rangle_0 = \mathbf{G}_{\text{latt}} = 0$. The magnetisation induced by an external field \mathbf{H} along $\hat{\mathbf{z}}$ is

$$M = \frac{\mu_B}{\hbar} (g_L \langle L_z \rangle + g_S \langle S_z \rangle) + \mu_N g_I \langle I_z \rangle , \quad (1.103)$$

where μ_B and μ_N are the Bohr and nuclear magnetons and g_L , g_S , g_I are the relevant Landé factors. For free electrons, $g_L \approx 1$ and $g_S \approx 2$. If the system is mechanically isolated, its lattice acquires angular momentum

$$G_{\text{latt}} = -\langle L_z \rangle - \langle S_z \rangle - \langle I_z \rangle , \quad (1.104)$$

which just states that angular momentum is conserved. This is called the Einstein and de Haas effect [4, 5]. It can be used for an experimental determination of the gyromagnetic factor g_S . We define the magneto-mechanical factor to be the ratio of magnetisation to induced angular momentum:

$$g' \mu_B = -\frac{M}{G_{\text{latt}}} = \mu_B \frac{g_L \langle L_z \rangle + g_S \langle S_z \rangle + r g_I \langle I_z \rangle}{\langle L_z \rangle + \langle S_z \rangle + \langle I_z \rangle} , \quad (1.105)$$

where $r = \mu_N/\mu_B$. To simplify, assume that the temperature is sufficiently high to ensure that $k_B T$ is much bigger than the spin-orbit interaction energy, coupling L and S [see Sect. 2.9(I)]. Nuclear polarisation is then negligible. If l and s are the quantum numbers associated with L and S in the ground state of the magnetic ions,

$$\langle L_z \rangle = N \mu_0 \frac{\mu_B l(l+1)}{3k_B T} H , \quad \langle S_z \rangle = N \mu_0 \frac{\mu_B s(s+1)}{3k_B T} H . \quad (1.106)$$

In this high temperature limit, the magneto-mechanical factor is

$$g' = \frac{g_L l(l+1) + g_S s(s+1)}{l(l+1) + s(s+1)} . \quad (1.107)$$

When the temperature is small compared with the spin-orbit interaction, the eigenvalue j of $\mathbf{J} = \mathbf{L} + \mathbf{S}$ in the ground state is a good quantum number determining the magneto-mechanical factor. Indeed, from the definition (1.105), we have [see Sect. 2.8(I)]

$$g' = g_j = \left(\frac{g_L + g_S}{2} + (g_S - g_L) \frac{s(s+1) - l(l+1)}{2j(j+1)} \right). \quad (1.108)$$

Finally, for certain magnetic transition ions, the crystalline field removes all degeneracy in the ground state [see Sect. 2.13(I)]. In such conditions, the mean orbital angular momentum is zero at sufficiently low temperatures [see Sect. 2.15(I)] and the magneto-mechanical factor reduces to the gyromagnetic factor g_S .

In practice, the Einstein-de Haas effect is no longer used to determine gyromagnetic factors, since resonance methods provide a fast and accurate determination [see Chap. 8(I)].

2. Orbital and Spin Magnetism Without Interactions

This chapter is devoted to magnetism in metals and insulators when interactions between electrons can be neglected. In practice, magnetism is due either to the orbital currents of electrons (whether the system be metallic or insulating), or to their spins. The first six sections of this chapter deal with orbital magnetism and the following nine sections with spin magnetism.

2.1 Electrons in a Magnetic Field. The Hamiltonian

In the absence of interaction, all magnetism due to electrons can be described by the Dirac equation [6]. This equation governs the relativistic quantum dynamics of an electron in a static field (electric field $\mathbf{E} = -\nabla\phi$ and magnetic field $\mathbf{B} = \nabla \times \mathbf{A}$). Since electron speeds in a solid are small compared with the speed of light ($v/c \approx 10^{-2}$), we can use the non-relativistic limit of the Dirac Hamiltonian,

$$\mathcal{H} = [\beta mc^2 + V(\mathbf{r})] + c\boldsymbol{\alpha} \cdot (\mathbf{p} - e\mathbf{A}), \quad (2.1)$$

where c is the speed of light and the Dirac matrices

$$\beta = \begin{pmatrix} 1 & 0 \\ 0 & -1 \end{pmatrix}, \quad \boldsymbol{\alpha} = \begin{pmatrix} 0 & \boldsymbol{\sigma} \\ \boldsymbol{\sigma} & 0 \end{pmatrix} \quad (2.2)$$

are expressed in terms of the Pauli matrices $\boldsymbol{\sigma}$ defined in (2.89). The electron charge is denoted $e = -|e|$ and is thus negative. We can distinguish four contributions to the Hamiltonian \mathcal{H} :

$$\mathcal{H} = \mathcal{H}_0 + \mathcal{H}_S + \mathcal{H}_{\text{so}} + V(\mathbf{r}), \quad (2.3)$$

where

$$\mathcal{H}_0 = \frac{1}{2m_*}(\mathbf{p} - e\mathbf{A})^2 = \frac{\boldsymbol{\pi}^2}{2m_*}, \quad (2.4)$$

$$\mathcal{H}_S = -g_S \frac{e}{2m} \mathbf{S} \cdot \mathbf{B}, \quad (2.5)$$

$$\mathcal{H}_{\text{so}} = -\frac{e\hbar}{4mm_*c^2} \boldsymbol{\sigma} \cdot [\mathbf{E} \times (\mathbf{p} - e\mathbf{A})], \quad (2.6)$$

$$V(\mathbf{r}) = e\phi(\mathbf{r}). \quad (2.7)$$

We have neglected non-magnetic relativistic terms like $p^4/2(mc)^2$, and the Darwin retardation term. \mathcal{H}_0 is the Hamiltonian of a free spinless particle in a magnetic field, \mathcal{H}_S is the spin Hamiltonian ($\mathbf{S} = \hbar\boldsymbol{\sigma}/2$), \mathcal{H}_{so} describes the spin-orbit interaction, and $V(\mathbf{r}) = e\phi(\mathbf{r})$ is the electrostatic potential. For conduction electrons in a metal or doped semiconductor, we must introduce the effective mass m_* which takes into account the band structure induced by the periodic lattice potential. In this case, the electrostatic potential $V(\mathbf{r})$ only includes other contributions (impurities, potential differences, etc.). $\boldsymbol{\pi}$ represents the kinetic momentum $m_*\mathbf{v}$ of a Bloch state, whereas $\mathbf{p} \approx \hbar\nabla/\mathrm{i}$ is the momentum operator, conjugate to the position operator \mathbf{r} , i.e., $[r_i, p_j] = i\hbar\delta_{ij}$. In order to recover the Lorentz force on a charged particle in the semi-classical limit, we write the kinetic momentum in the form $\boldsymbol{\pi} = \mathbf{p} - e\mathbf{A}$. Indeed, consider a classical particle of initial momentum \mathbf{p}_0 along the $\hat{\mathbf{x}}$ axis. The particle crosses a region of space of length l in which the induction $\mathbf{B} = B\hat{\mathbf{z}}$ is uniform. The Lorentz force causes the particle to move perpendicularly, in the direction $\mathbf{p}_0 \times \mathbf{B}$. It acquires transverse momentum $\delta\mathbf{p} = -elB\hat{\mathbf{y}}$. As $lB\hat{\mathbf{y}}$ is the change in vector potential $\Delta\mathbf{A}$ across the region, we find that after crossing the region where $B \neq 0$, the particle does indeed have momentum $\mathbf{p}_0 - e\Delta\mathbf{A}$ [7].

The vector potential \mathbf{A} is defined up to addition of a gradient. Gauge invariance is expressed by the fact that the Schrödinger equation

$$\mathcal{H}_0\psi(\mathbf{r}) = \varepsilon\psi(\mathbf{r}) \quad (2.8)$$

remains unchanged when we simultaneously modify both the vector potential \mathbf{A} and the wave function $\psi(\mathbf{r})$ by

$$\mathbf{A}' = \mathbf{A} + \nabla A(\mathbf{r}), \quad (2.9)$$

$$\psi'(\mathbf{r}) = \psi(\mathbf{r}) \exp\left(\frac{\mathrm{i}eA(\mathbf{r})}{\hbar}\right). \quad (2.10)$$

This can be checked by substituting the semi-classical approximation [8, 9] to a stationary state of energy $E = mv_0^2/2 = \boldsymbol{\pi}^2/2m$,

$$\psi'(\mathbf{r}) = a(\mathbf{r}', E) \exp\left(\frac{\mathrm{i}S(\mathbf{r}', \mathbf{r}_0, E)}{\hbar}\right) \psi(\mathbf{r}_0), \quad (2.11)$$

into the Schrödinger equation (2.8). The semi-classical action S , with units [energy \times time], is

$$S(\mathbf{r}', \mathbf{r}_0, E) = \int_{s(\mathbf{r}_0)}^{s(\mathbf{r}')} \mathbf{p}(r) \cdot \mathrm{d}\mathbf{s}, \quad (2.12)$$

where $s(\mathbf{r})$ is the curvilinear coordinate along the classical trajectory, and the classical momentum $\mathbf{p}(r) = m\mathbf{v}_0 + e\mathbf{A}$ is determined from the energy $E = mv_0^2/2$ of the chosen stationary state.

We note as an aside that in most works, the semi-classical approximation is based on the WKB approximation (Wentzel–Kramers–Brillouin) for a 1-

dimensional potential, or for a separable potential in 2 or 3 dimensions. The semi-classical wave function is written as before:

$$\psi(\mathbf{r}', E) \propto \exp(i\beta)/\sqrt{p(\mathbf{r}', E)} , \quad (2.13)$$

where $p(\mathbf{r}', E) = \sqrt{2m_*(E - V(\mathbf{r}'))}$ is the semi-classical kinetic momentum and the phase β can be related to the phase shift occurring at turning points of the trajectory. There is another form of semi-classical approximation which, unfortunately, is rarely discussed (an exception is the book by Gutzwiller). This approximation is valid in any number of dimensions and does not require separability of the particle motion. It is very useful in practice and amounts to calculating the wave function from classical particle trajectories. The value of the wave function at \mathbf{r}' is obtained from its value at \mathbf{r} by the formula

$$\begin{aligned} \psi(\mathbf{r}') = & \frac{2\pi}{(2\pi i\hbar)^{(n+1)/2}} \sum_{\text{cl. path}} \sqrt{(-1)^{n+1} \det(D)} \\ & \times \exp\left(\frac{iS(\mathbf{r}', \mathbf{r}, E)}{\hbar} - i\nu\frac{\pi}{2}\right) \psi(\mathbf{r}) , \end{aligned} \quad (2.14)$$

where the sum is taken over all classical paths running from \mathbf{r} to \mathbf{r}' . As before, S is the semi-classical action

$$S(\mathbf{r}', \mathbf{r}, E) = \sum_{\text{cl. path}} \int_{\mathbf{r}}^{\mathbf{r}'} \mathbf{p}(\mathbf{x}) \cdot d\mathbf{x} . \quad (2.15)$$

The dimension ν measures the number of points conjugate to the origin \mathbf{r} (these being focus points for a bundle of classical trajectories starting at \mathbf{r}). Then

$$D = \frac{1}{|\mathbf{v}||\mathbf{v}'|} \left(-\frac{\partial^2 S}{\partial r \partial r'} \right) \quad (2.16)$$

measures the density of classical trajectories (\mathbf{v} and \mathbf{v}' are classical velocities at initial and final points). This is the so-called van Vleck formula (1928) which can be obtained from Feynman path integrals.

Two gauges are particularly useful:

- The Landau gauge. For uniform magnetic field $\mathbf{B} = B\hat{\mathbf{z}}$,

$$A_y = Bx , \quad A_x = A_z = 0 . \quad (2.17)$$

- The symmetric (Johnson–Lippman) gauge.

$$A_x = -\frac{By}{2} , \quad A_y = \frac{Bx}{2} , \quad A_z = 0 . \quad (2.18)$$

In the symmetric gauge, the Hamiltonian \mathcal{H}_0 is the sum of three terms:

$$\mathcal{H}_0 = \frac{p^2}{2m_*} + \mathcal{H}_L + \mathcal{H}_D , \quad (2.19)$$

where

$$\mathcal{H}_L = -\frac{eB}{2m_*}(xp_y - yp_x) = -\frac{e}{2m}g_L \mathbf{L} \cdot \mathbf{B}, \quad (2.20)$$

$$\mathcal{H}_D = \frac{e^2 B^2}{8m_*}(x^2 + y^2), \quad (2.21)$$

and $g_L = m/m_*$. Here \mathcal{H}_L is the contribution of angular momentum to orbital magnetism, and \mathcal{H}_D is a diamagnetic orbital contribution. Any expectation value of \mathcal{H}_D is positive. As this energy increases quadratically with B , the magnetisation in the ground state $|0\rangle$, $M = -\partial(\langle 0|\mathcal{H}_D|0\rangle)/\partial B$ is negative and in the opposite direction to B . This is the usual definition of diamagnetism. In certain semiconductors, the effective mass m_* can be much lower than the real mass of the electron. For example, $m/m_* = 20$ for gallium arsenide (AsGa) and $m/m_* = 50$ for cadmium telluride (CdTe). \mathcal{H}_0 is then the dominating term in the magnetic Hamiltonian \mathcal{H} .

2.2 Bohm–Aharonov Effect and Permanent Currents

In classical mechanics, gauge invariance expresses the fact that the only observable quantities are values of electromagnetic fields along the particle trajectory. This is no longer true in quantum mechanics, as is illustrated by the Bohm–Aharonov Effect [10]. Consider a ring structure enclosing magnetic flux ϕ (as shown in Fig. 2.1). An electron can pass round the ring from \mathbf{r} to \mathbf{r}' by either of two distinct paths (1) and (2). The amplitude $\psi(\mathbf{r}')$ for finding the electron at \mathbf{r}' is the sum of the semi-classical amplitudes associated with these paths. Each amplitude can be deduced from the semi-classical approximation (2.11):

$$\psi_{1,2}(\mathbf{r}') = \phi_{1,2}(\mathbf{r}') \exp\left(i\frac{e}{\hbar} \int_{\mathbf{r}}^{\mathbf{r}'} \mathbf{A}(\mathbf{s}) \cdot d\mathbf{s}_{1,2}\right), \quad (2.22)$$

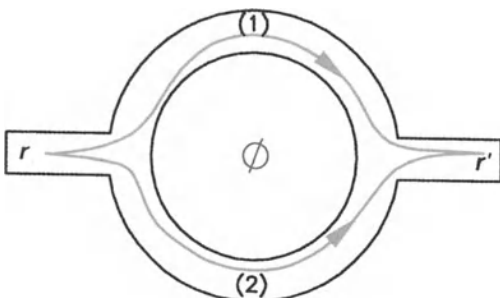


Fig. 2.1. Ring enclosing magnetic flux ϕ . Electrons can pass from \mathbf{r} to \mathbf{r}' along paths on either side of the enclosed flux

$$\phi_{1,2}(\mathbf{r}') = \phi_{1,2}(\mathbf{r}) \exp\left(\frac{i}{\hbar} \int_{\mathbf{r}}^{\mathbf{r}'} \boldsymbol{\pi} \cdot d\mathbf{s}_{1,2}\right), \quad (2.23)$$

where integrals are taken along paths (1) and (2). ϕ_1 and ϕ_2 are the amplitudes corresponding to paths (1) and (2) in the absence of flux. The probability of finding the electron at \mathbf{r}' is therefore

$$\begin{aligned} |\psi(\mathbf{r}')|^2 &= |\psi_1(\mathbf{r}') + \psi_2(\mathbf{r}')|^2 \\ &= |\phi_1|^2 + |\phi_2|^2 + 2\text{Re} \left[\phi_1 \phi_2^* \exp\left(\frac{i}{\hbar} \oint \mathbf{A}(\mathbf{s}) \cdot d\mathbf{s}\right) \right], \end{aligned} \quad (2.24)$$

where we have rewritten the interference term

$$\int_{\mathbf{r}}^{\mathbf{r}'} \mathbf{A}(\mathbf{s}) \cdot d\mathbf{s}_1 - \int_{\mathbf{r}}^{\mathbf{r}'} \mathbf{A}(\mathbf{s}) \cdot d\mathbf{s}_2$$

as the integral of the vector potential along a closed path around the ring. The phase of the interference term depends on the flux enclosed by the ring, since

$$\frac{e}{\hbar} \oint \mathbf{A}(\mathbf{s}) \cdot d\mathbf{s} = \frac{2\pi\phi}{\phi_0},$$

where $\phi_0 = h/|e|$ is the quantum of flux. This phase is gauge invariant. However, it has a non-local character because it involves the magnetic flux within the ring, whereas the electron never enters this region. Interference phenomena are observable if electrons retain a phase memory around the ring. They have been observed in small metallic annular structures of about 1 micron, despite the existence of disorder, which does not affect phase coherence [11, 12].

If we consider a closed insulated ring, the Bohm–Aharonov effect induces a permanent current in it when there is an enclosed flux [15]. Indeed, over a ring structure, the potential $V(s)$ felt by the electron is periodic of period L , where s is the coordinate along the ring, neglecting its width, and L the length of its perimeter. (V may result from defects or impurities, for example.) Consequently, the wave function must be uniform around the ring, so that $\psi(s+L) = \psi(s)$.

Moreover, we can carry out a gauge transformation (2.10). Choosing the gauge function

$$A(s) = - \int_0^s \mathbf{A}(s) \cdot d\mathbf{s},$$

the new vector potential $\mathbf{A}' \equiv 0$ disappears from the Schrödinger equation. The new wave function $\psi'(s)$ must satisfy boundary conditions

$$\psi'(s+L) = \psi(s+L) \exp\left(i \frac{e}{\hbar} \int_0^{s+L} \mathbf{A}(s) \cdot d\mathbf{s}\right)$$

$$\begin{aligned}
&= \psi(s) \exp \left[i \frac{e}{\hbar} \left(\int_0^s + \int_s^{s+L} \right) \mathbf{A}(s) \cdot d\mathbf{s} \right] \\
&= \psi'(s) \exp \left(2i\pi \frac{\phi}{\phi_0} \right), \tag{2.25}
\end{aligned}$$

which are only periodic when the enclosed flux is a multiple of the quantum of flux $\phi/\phi_0 = 0 [\text{mod } n]$. In addition, we can apply Bloch's theorem to the wave function $\psi'(s)$ to give $\psi'(s) = \exp(iks)f(s)$, where $f(s) = f(s+L)$ is a periodic function depending on the potential $V(s)$. Substituting this Bloch wave into the previous equation, we deduce that

$$k_n = \frac{2\pi}{L} \left(n + \frac{\phi}{\phi_0} \right). \tag{2.26}$$

The momentum $p = \hbar k_n$ increases linearly with the flux. Let $E(k_n)$ be the energy levels of the stationary states [when $V = 0$, $E(k_n) = (\hbar k_n)^2 / 2m_*$], represented in Fig. 2.2. Boundary conditions (2.25) require these energy levels to be periodic in k , which is proportional to the flux according to (2.26). This sensitivity of energy to boundary conditions (2.25) is due to a certain rigidity of the wave functions. The speed of the electron in the n th stationary state,

$$v_n = \frac{1}{\hbar} \frac{\partial E_n}{\partial k} = \frac{L\phi_0}{2\pi\hbar} \frac{\partial E_n}{\partial \phi}, \tag{2.27}$$

is periodic in the flux. An electron occupying the n th energy level contributes

$$i_n = \frac{ev_n}{L} = -\frac{\partial E_n}{\partial \phi} \tag{2.28}$$

to a current which is itself periodic. This current, carried by an electron in the n th level, induces a magnetic moment $\mu = i_n S$ which can be observed.

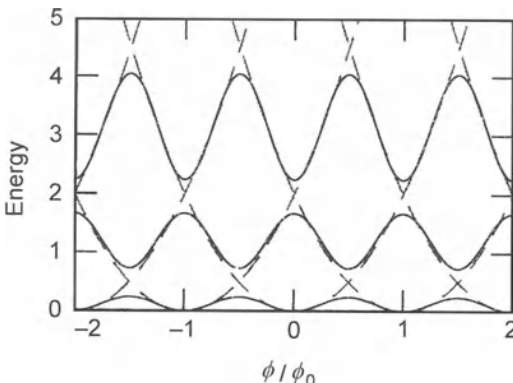


Fig. 2.2. Electronic spectrum in the presence of a spatially periodic potential of period L . This potential opens gaps at wave vectors which are multiples of π/L , corresponding to fluxes which are multiples of $\phi = \phi_0/2$

In practice, the sum of contributions from all the electrons is of the order of the current of an electron at the Fermi level. Although small, the induced magnetic moment from these currents has been observed by several groups [16, 17, 18]. This is an important physical phenomenon because it shows that orbital magnetism originates in gauge invariance, as does the Bohm–Aharonov effect.

Exercise: Aharonov–Casher Effect

There is an effect dual to the Bohm–Aharonov effect for a neutral particle with magnetic moment μ [13]. If a charged particle acquires a phase whilst travelling along a closed path around a tube of flux, we would expect a tube of flux to acquire a phase whenever it follows a closed path around a charged particle.

1. A magnetic moment $\boldsymbol{\mu}$ along the \hat{z} axis moves with velocity \mathbf{v} along the \hat{x} axis. Using the fact that the magnetic field created by the dipole at distance $|\mathbf{r}|$ is

$$\mathbf{B} = \frac{3\hat{r}(\hat{r}\cdot\boldsymbol{\mu}) - \boldsymbol{\mu}}{r^3}, \quad (2.29)$$

find the electric field \mathbf{E} induced in the lab frame. What is the electrostatic energy of a charge q placed at distance r in the (x, y) plane in this electric field?

2. Show that this energy can be rewritten

$$U_{q-\mu} = -\mathbf{v}\cdot(\mathbf{E} \times \boldsymbol{\mu}), \quad (2.30)$$

where \mathbf{E} is the field created by the charge q at distance r .

3. Deduce that the Hamiltonian for the charge interacting with the magnetic moment is

$$\mathcal{H}_{q-\mu} = \frac{(\mathbf{p} - \mathbf{E} \times \boldsymbol{\mu})^2}{2m} - \frac{\mu^2 E^2}{2m}. \quad (2.31)$$

In the absence of the charge, $\nabla \cdot \mathbf{E} = 0$. Define an *electric vector potential* \mathbf{A}_q such that $\mathbf{E} = \nabla \times \mathbf{A}_q$ for the electric field created by a charge q . Show that

$$\mathbf{A}_q = \mathbf{E} \times \hat{z} \quad (2.32)$$

for a line of charge.

4. Using the semi-classical approximation, show that two paths enclosing the charge q are subject to a phase difference $\delta\phi = 2\pi q\mu/h$.
5. Assume that $\mu = h/2e$ for a flux line in a superconductor (a vortex). What is the period of the interference as a function of enclosed charge? This effect has been observed experimentally in arrays of Josephson junctions [14].

2.3 Landau Levels

The Landau levels are the eigenstates of the two-dimensional Hamiltonian $\mathcal{H}_0 - p_z^2/2m_*$, which reduces to

$$\frac{[p_x^2 + (p_y - eA_y)^2]}{2m_*}$$

in the Landau gauge. These states are normalised by assuming that the electrons are contained in a box of volume $V = L_x \times L_y \times L_z$. We shall follow two different approaches here. The first involves directly solving the Schrödinger equation in the Landau gauge. The cyclotron frequency and quantum of flux are defined by

$$\omega_c = \frac{|e|B}{m_*} , \quad \phi_0 = \frac{\hbar}{e} . \quad (2.33)$$

Because of its dependence on effective mass, the cyclotron frequency varies from one material to another. Its value is determined from the definition, so that $\nu_c = \omega_c/2\pi = 27.992g_L B$ GHz, where $g_L = m/m^*$ is the orbital Landé factor and B is given in [T]. The value of the quantum of flux is $\phi_0 = 4.1357 \times 10^{-7}$ G cm² = 4.1357×10^{-15} T m². For superconductors, we will have to introduce the quantum of flux associated with Cooper pairs, viz., $\Phi_0 = \phi_0/2 = 2.0679 \times 10^{-7}$ G cm². In a metal, electrons in the neighbourhood of the Fermi energy have characteristic speed v_F . We can therefore define two characteristic lengths in a magnetic field: the cyclotron radius r_c and the magnetic length l_B :

$$r_c = \frac{\langle v_\perp \rangle}{\omega_c} , \quad l_B = \sqrt{\frac{\phi_0}{2\pi B}} , \quad (2.34)$$

where $\langle v_\perp \rangle = \langle p_\perp/m_* \rangle = \hbar k_\perp/m_*$ is the transverse speed of the electron (with respect to \mathbf{B}), which is of the order of v_F . The magnetic length is $2.5656 \mu\text{m}/(qB)^{1/2}$ if B is given in [G], and $2.5656 \text{ nm}/(qB)^{1/2}$ if B is given in [T] (q is given here in units of $|e|$, i.e., equal to one for an electron). Using the reduced coordinates $X = x/l_B$, $\varepsilon = E/\hbar\omega_c$ and putting $\psi = \exp(i\mathbf{k}_y y)\phi(X)$, Schrödinger's equation in the Landau gauge,

$$-\frac{\hbar^2}{2m_*} \left(\frac{\partial^2 \psi}{\partial X^2} + \left[\frac{\partial}{\partial y} - \frac{ieB}{\hbar} x \right]^2 \psi \right) = E\psi , \quad (2.35)$$

is cast into harmonic oscillator form:

$$\frac{\partial^2 \phi}{\partial X^2} + [2\varepsilon - (X - X_0)^2]\phi = 0 . \quad (2.36)$$

To the parameter $X_0 = k_y l_B$ corresponds the coordinate $x_0 = k_y l_B^2$ on the x axis. For high quantum numbers (semi-classical limit), x_0 represents the coordinate of the centre of a circular orbit. From the definition of quantisation

of a harmonic oscillator in reduced units, $\varepsilon_n = n + 1/2$, we deduce the energy spectrum

$$E_n(k_z) = \left(n + \frac{1}{2} \right) \hbar\omega_c + \frac{(\hbar k_z)^2}{2m_*} . \quad (2.37)$$

It does not depend continuously on k_x and k_y . We have added the kinetic energy of a constant motion parallel to the magnetic field. Wave functions are given in terms of Hermite polynomials H_n by

$$\psi_n(r) = \frac{\exp[i(k_y y + k_z z)]}{\sqrt{L_y L_z}} \exp\left[-\frac{(X - X_0)^2}{2}\right] H_n(X - X_0) . \quad (2.38)$$

There are usually many degenerate states occupying the same Landau level. The only condition on the parameter $x_0 = X_0 l_B$, coordinate of the centre of the cyclotron orbit, is that it must be located somewhere within the sample, i.e., between 0 and L_x . This translates into a condition on the wave vector, viz.,

$$0 \leq k_y \leq \frac{eBL_x}{\hbar} .$$

Let us now determine the degeneracy D of a Landau level, that is, the number of possible states per level. The number of states in the interval dk_y is $dN_y =$

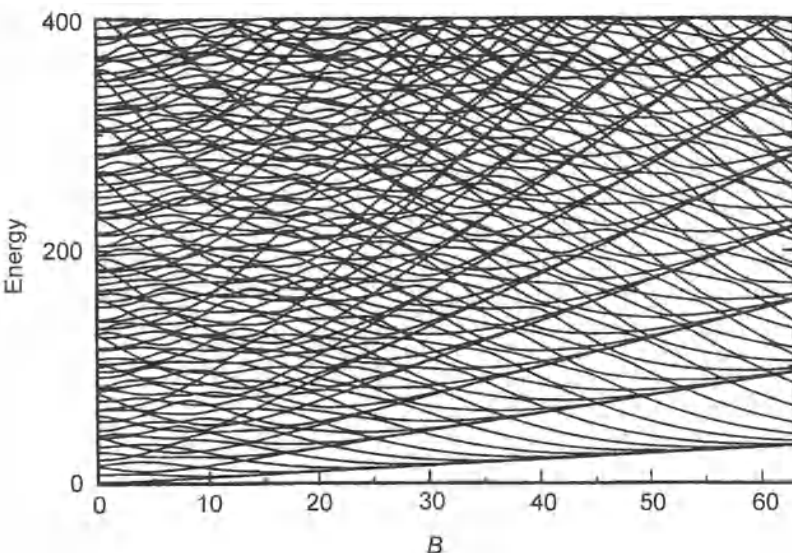


Fig. 2.3. Formation of Landau levels in a square 2-dimensional box [30]. For zero field, energy levels are determined by boundary conditions at the edge of the square. As the magnetic field increases, all energy levels come together around the Landau levels, which are easily identifiable in a strong field. Degeneracy D is then the number of levels in each group forming a Landau level. In this limit, cyclotron orbits are much smaller than the size of the box

$dk_y L_y / 2\pi$. The degeneracy of each Landau level is obtained by summing over all possible values of k_y to give

$$D = L_x L_y \frac{eB}{h} \zeta = \frac{SB}{\phi_0} \zeta , \quad (2.39)$$

where ζ is the spin degeneracy, equal to 2 in a weak field and 1 in a strong field (because of the Zeeman energy). For a 2-dimensional electron gas, the Fermi energy $\varepsilon_F = \hbar^2 k_F^2 / 2m_*$ is determined by the number of particles N and the mean separation Δ between levels. The number of energy levels below ε_F is given by the area of a disk of radius $k_F L / 2\pi$ in phase space, giving $\pi k_F^2 S / (2\pi)^2$, where S is the area $L_x L_y$. Including spin degeneracy, we obtain

$$N = \frac{k_F^2 S}{4\pi} \zeta = \frac{\varepsilon_F}{\Delta} ,$$

where Δ , the mean separation between levels, is energy independent:

$$\Delta = \frac{2\pi\hbar^2}{m_* S \zeta} \quad \text{and} \quad \varepsilon_F = N\Delta . \quad (2.40)$$

The density of states $n_{2D} = 1/\Delta$ is constant in two dimensions. We can calculate the number ν of occupied Landau levels (also called the filling factor):

$$\nu = \frac{N}{D} = \frac{N\phi_0}{\zeta S B} = \frac{N\phi_0}{\zeta \phi} = \frac{N\Delta}{\hbar\omega_c} = \frac{\varepsilon_F}{\hbar\omega_c} . \quad (2.41)$$

We have used $\zeta\phi/\phi_0 = \hbar\omega_c/\Delta$, which follows easily from the definitions. In three dimensions, the highest level filled depends on k_z . It is then convenient to express the degeneracy $D_{3D}(\varepsilon)$ of each level as a function of its energy:

$$\begin{aligned} N &= \int_{-\infty}^{\infty} D_{3D}(\varepsilon) d\varepsilon \\ &= 2 \int_0^{\infty} D_{2D} \frac{L_z dk_z}{2\pi} = 2 \frac{L_z}{2\pi} \int_0^{\infty} D_{2D}(\varepsilon) \frac{dk_z}{d\varepsilon} d\varepsilon . \end{aligned} \quad (2.42)$$

From (2.39) for the 2-dimensional degeneracy, we find

$$D_{3D}(\varepsilon) = \frac{\zeta}{\pi} \frac{B}{\phi_0} \frac{dk_z}{d\varepsilon} . \quad (2.43)$$

There is another way to deal with quantisation into Landau levels. This involves diagonalising the Hamiltonian by means of new operators which can, in the semi-classical limit, be interpreted as the position and momentum of the electron in its orbit. We shall use the symmetric gauge $\mathbf{A} = (\mathbf{B} \times \mathbf{r})/2$ and reduced units $X = x/l_B$, $Y = y/l_B$, $K_x = l_B k_x = l_B p_x / \hbar = d/dX$, $K_y = l_B k_y = l_B p_y / \hbar = d/dY$. Operators Π and \mathbf{R}_0 are then defined by their components

$$\Pi_x = K_x - Y/2 , \quad \Pi_y = K_y + X/2 , \quad (2.44)$$

$$X_0 = X/2 - K_y , \quad Y_0 = Y/2 + K_x . \quad (2.45)$$

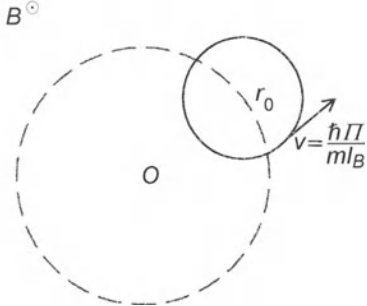


Fig. 2.4. Circular semi-classical orbit centred on r_0 . r_0 takes discrete values and fixes the angular momentum about the origin O . The tangential speed of the electron is related to both the canonical variable Π and the quantised energy values

They satisfy commutation relations

$$[\Pi_y, \Pi_x] = i = [X_0, Y_0]. \quad (2.46)$$

This is easy to check from the definitions and commutation relations $[x, p_x] = [y, p_y] = i\hbar$. The components of $\boldsymbol{\Pi}$ (and \mathbf{R}_0) are therefore conjugate canonical variables. We can also write the Hamiltonian entirely in terms of $|\boldsymbol{\Pi}|$:

$$\mathcal{H}_0 = \frac{\hbar\omega_c}{2} [\Pi_x^2 + \Pi_y^2] = \frac{\hbar\omega_c}{2} \boldsymbol{\Pi}^2, \quad (2.47)$$

which is a constant of the motion. In the semi-classical limit, $\boldsymbol{\Pi}$ is proportional to the electron velocity $\boldsymbol{\Pi} = m_* l_B \mathbf{v}/\hbar$ along its circular trajectory around $\mathbf{r}_0 = l_B \mathbf{R}_0$, the coordinate of the centre of the orbit in the semi-classical limit (see Fig. 2.4). For a uniform field, we can choose a basis in which the operator X_0 (or Y_0) is diagonal (the Landau basis). Alternatively, we can choose a basis diagonalising $R_0^2 = X_0^2 + Y_0^2$ (the Johnson–Lippman basis), which preserves cylindrical symmetry. Quantisation of the energy \mathcal{H}_0 and the possible values of the centre of the semi-classical orbit is achieved by means of the (exact) Einstein–Brillouin–Keller quantisation conditions [8], which generalise the Bohr–Sommerfeld quantisation rules:

$$S_n/\hbar = \oint \Pi_y d\Pi_x = 2\pi(n + 1/2), \quad (2.48)$$

$$S_m/\hbar = \oint X_0 dY_0 = 2\pi(m + 1/2). \quad (2.49)$$

In addition, the integrals

$$\oint \Pi_y d\Pi_x = \pi \Pi_0^2 \quad \text{and} \quad \oint X_0 dY_0 = \pi R_0^2$$

are nothing but areas of disks of radii Π_0 and R_0 , respectively. Hence, the quantisation conditions specify eigenvalues of the energy and the centre r_0 of the semi-classical orbit:

$$\varepsilon_n = \hbar\omega_c(n + 1/2), \quad r_0^2 = (2m + 1)l_B^2. \quad (2.50)$$

We can obtain the energy eigenvalues in an even more elementary way by noticing that the action over a closed orbit is $S_n = \varepsilon T$, where $T = 2\pi/\omega_c$ is the period of the circular orbit.

Eigenstates can be obtained from the ground state via ladder operators

$$a^\dagger = \Pi_y + i\Pi_x, \quad b^\dagger = X_0 + iY_0, \quad (2.51)$$

giving

$$\psi_{n,m}(\mathbf{r}) = (2^{n+m} n! m!)^{-1/2} a^{\dagger n} b^{\dagger m} \psi_0(\mathbf{r}). \quad (2.52)$$

For $m = 0$, wave functions are centred on the origin and have mean spread $\langle n, 0 | r^2 | n, 0 \rangle = (2n + 1)l_B^2$. For $m \neq 0$, wave functions are rings of mean squared distance $\langle n, m | r^2 | n, m \rangle = 2(n + m + 1)l_B^2$ from the origin. Consequently, the magnetic flux enclosed by the (m, n) state is quantised:

$$B\langle n, m | \pi r^2 | n, m \rangle = (n + m + 1)\phi_0, \quad (2.53)$$

in units of the quantum of flux ϕ_0 . Near the critical field H_{c2} , vortices in superconductors are governed by the same equations and enclose exactly one quantum of flux [see Sect. 13.8(II)]. The angular momentum of each semi-classical state, specified by the distance r_0 of the centre of the orbit from the origin together with its energy, is

$$\frac{L_z}{\hbar} = XK_y - YK_x = \frac{1}{2}(\Pi_x^2 + \Pi_y^2 - X_0^2 - Y_0^2) = n - m. \quad (2.54)$$

For the lowest Landau level ($n = 0$), the states with angular momenta $L_z = -m\hbar$, for $0 \leq m \leq m_{\max} \equiv D = \phi/\phi_0$, of which there are of course m_{\max} , all have the same energy as the ground state, i.e., $\hbar\omega_c/2$. Their wave functions can be written in terms of $z = x + iy$ as

$$\psi_{0,m}(z = x + iy) = \frac{z^{*m}}{\sqrt{2\pi l_B^{2m} 2^m m!}} \exp\left(-\frac{|z|^2}{4l_B^2}\right). \quad (2.55)$$

In the same way, it can be shown that the wave functions of the $n = 1$ Landau level are

$$\psi_{1,m}(z = x + iy) = \frac{z^{*m-1}(2|z/l_B|^2 - m)}{\sqrt{2\pi l_B^{2(m-1)} 2^{m+2} (m+1)!}} \exp\left(-\frac{|z|^2}{4l_B^2}\right). \quad (2.56)$$

2.4 The Quantum Hall Effect

When a current \mathbf{J} passes through a conducting band in the presence of magnetic induction \mathbf{B} , a voltage V_H is produced in a direction normal to the current. This is the Hall effect. In other words, the conductivity σ relating current to local electric field

$$\mathbf{J} = \sigma \mathbf{E} \quad (2.57)$$

is a tensor whose off-diagonal terms measure the Hall conductivity. In most metals, the Hall conductivity is proportional to the applied magnetic field. In two dimensions, experiments have shown that Hall conductance is quantised in units of e^2/h , the quantum of conductance [20]. This is the quantum Hall effect. This phenomenon is a spectacular consequence of quantisation into Landau levels. Classically, the equation of motion of an electron in magnetic induction $\mathbf{B} = B\hat{\mathbf{z}}$ is

$$m_* \frac{d\mathbf{v}}{dt} = e(\mathbf{E} + \mathbf{v} \times \mathbf{B}) - \frac{m_* \mathbf{v}}{\tau}, \quad (2.58)$$

where τ is the electron-impurity elastic collision time. In a stationary regime, $d\mathbf{v}/dt = 0$. When the field is large enough ($\omega_c \tau \gg 1$), the last term is negligible and the mean velocity is perpendicular to both \mathbf{E} and \mathbf{B} :

$$v_y = -\frac{E_x}{B}. \quad (2.59)$$

The current density j_y in the $\hat{\mathbf{y}}$ direction is Nev_y/S , where N is the number of electrons. The Hall conductivity is therefore

$$\sigma_{xy} = \frac{j_y}{E_x} = -\frac{Ne}{BS} = -\frac{e}{\phi} N. \quad (2.60)$$

If we assume that the Fermi level is ‘hooked’ onto states spatially localised by impurities and whose energies are located between two Landau levels ν and $\nu+1$, the number of electrons N is the product of the number of occupied levels ν and the degeneracy $D = \zeta\phi/\phi_0$ of each level. The Hall conductivity is then quantised

$$\sigma_{xy} = -\frac{e}{\phi} \nu \zeta \frac{\phi}{\phi_0} = -\nu \frac{\zeta e^2}{h} \quad (2.61)$$

into multiples of e^2/h , the quantum of conductance [19]. From the quantum viewpoint, there are as many electrons (N) as there are available quantum states ($D\nu$). The N -electron quantum state is thus unique and its wave function is a Slater determinant of the $N = D\nu$ independent particles (without interactions). For example, for the lowest Landau level $\nu = 1$, this state is obtained as the determinant of the N states (2.55)

$$\begin{aligned} \psi_{\nu=1}(z_1, \dots, z_N) &= \mathcal{N}_{\nu=1} \begin{vmatrix} 1 & 1 & \dots & 1 \\ z_1 & z_2 & \dots & z_N \\ z_1^2 & z_2^2 & \dots & z_N^2 \\ \vdots & \vdots & & \vdots \\ z_1^{N-1} & z_2^{N-1} & \dots & z_N^{N-1} \end{vmatrix} \exp\left(-\frac{1}{4l_B^2} \sum_1^N |z_i|^2\right) \\ &= \mathcal{N}_{\nu=1} \prod_{i < j} (z_j - z_i) \exp\left(-\frac{1}{4l_B^2} \sum_1^N |z_i|^2\right), \end{aligned} \quad (2.62)$$

which expands as a van der Monde determinant.

This state is explicitly fermionic since the wave function goes to zero whenever two of the z_i and z_j coordinates are equal. It is also incompressible, in the sense that a further electron can only be added into the $\nu + 1$ Landau level. The latter has energy higher by $\hbar\omega_c$. This energy gap represents a discontinuity in the chemical potential $\mu = \partial E / \partial N$. Moreover, the pressure in a 2-dimensional system of area S can be related to the chemical potential by

$$-P \equiv \frac{\partial E}{\partial S} = \frac{\partial E}{\partial N} \frac{\partial N}{\partial S} = \frac{N}{S} \frac{\partial E}{\partial N}, \quad (2.63)$$

since in 2-dimensions $\partial N / \partial S = N/S = \text{const}$. Consequently, the compressibility κ is zero:

$$\frac{1}{\kappa} = -S \frac{\partial P}{\partial S} = S \frac{\partial^2 E}{\partial S^2} = \frac{N^2}{S} \frac{d\mu}{dN} = \infty, \quad (2.64)$$

taking into account the discontinuity in $\mu \equiv \partial E / \partial N$ at integral values of the filling factor ν . In practice, this situation is modified by the existence of localised states between two Landau levels ν and $\nu+1$. The chemical potential rises progressively from one localised state to the next, but the extended state remains incompressible.

As the Fermi level (or equivalently, the chemical potential) is hooked between two Landau levels, there is no extended state (i.e., conducting) at the Fermi level, except at the edge of the sample. The longitudinal conductance σ_{xx} is zero. More precisely, Fig. 2.6 divides up the density of states between extended states centred on Landau levels, which can carry a current, and localised states whose energies lie between Landau levels. The latter do not contribute to charge transfer. For these states, $\sigma_{xx} = 0$ (but $\sigma_{xy} \neq 0$) and diagonal resistivity is

$$\rho_{xx} = \frac{\sigma_{xx}}{\sigma_{xx}^2 + \sigma_{xy}^2} = 0. \quad (2.65)$$

The electron gas is then in a state with no longitudinal resistance, as can clearly be seen in Fig. 2.5. This effect was discovered by von Klitzing, K. and team in 1981 at the Grenoble intense magnetic field laboratory and earned von Klitzing the Nobel prize [20]. The description given here of the whole number quantum Hall effect is rather simplistic. In a disordered system, percolation and discontinuous conduction effects become important [21, 22, 23]. In real systems, edge states are essential [24, 25]. Experiments show (see Fig. 2.5) that, apart from quantisation at whole number multiples of e^2/h , there is also a quantisation for fractional values of the quantum of conductance. These extra Hall plateaus are related to the appearance of collective states induced by Coulomb repulsion between electrons. In these states, the electron gas is also an incompressible fluid. Its excitation levels, separated from the ground state by an energy gap, have fractional charges [26].

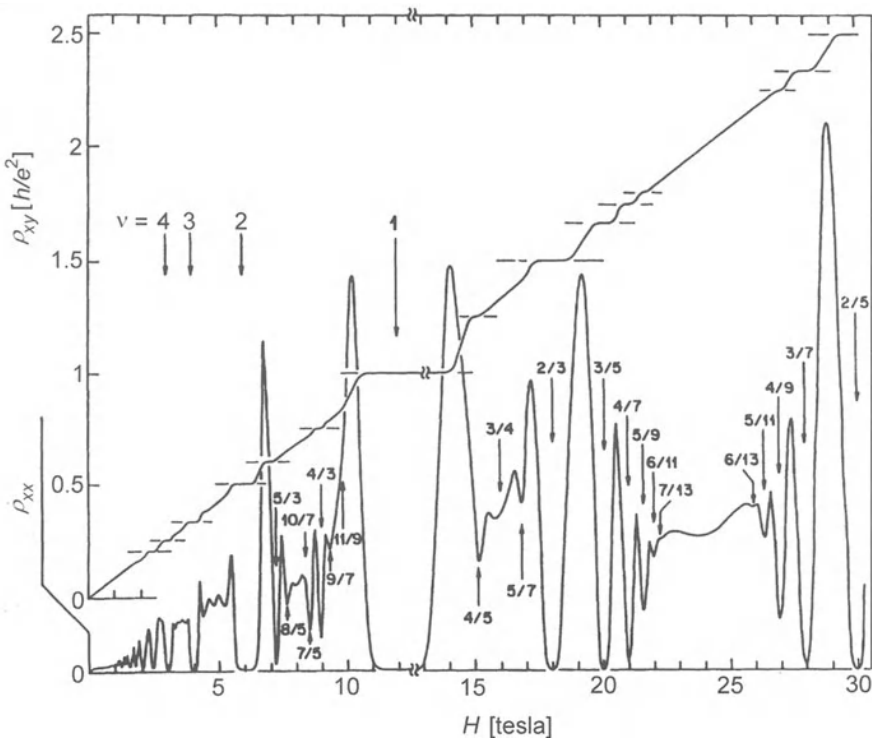


Fig. 2.5. Longitudinal resistivity ρ_{xx} and Hall resistivity of a 2-dimensional electron gas produced at the interface of a very high mobility AsGa-AlAsGa heterojunction. As well as quantisation of the Hall conductance into integral multiples of e^2/h , we observe a quantisation into fractional values of this quantum of conductance. The additional Hall plateaus arise from the appearance of collective states induced by Coulomb interaction between electrons

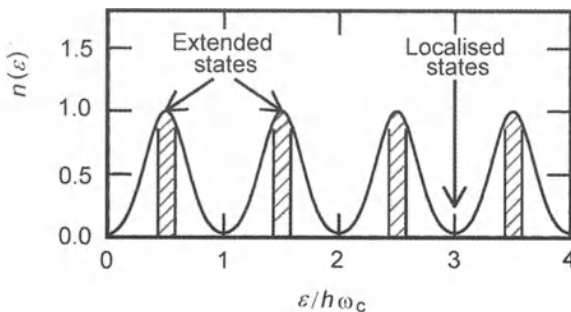


Fig. 2.6. Density of states in a disordered 2-dimensional electron gas in a strong field. Landau levels are widened by the disorder. Only states at the centre of each Landau level are extended and contribute to charge transfer. States located between each Landau level are localised and cannot carry current

**Exercise: Whole Number Quantum Hall Effect
as a Consequence of Gauge Invariance**

There is a simple argument due to Laughlin, R. which leads to quantisation of Hall conductance as a consequence of gauge invariance [27]. This elegant argument only applies when $T = 0$ in small systems. This is because wave functions must be rigid, i.e., they must be sensitive to changes in boundary conditions. We consider a conducting band of width w closed into a cylinder of perimeter L . We apply a radial field $B\hat{r}$ perpendicularly to the band as shown in Fig. 2.7. The field must be big enough to ensure that conduction electrons form Landau levels.

1. What vector potential \mathbf{A} produces a radial field $B\hat{r}$, in a gauge analogous to the Landau gauge? Show that the wave functions of the Landau levels are

$$\psi_{nm}(s) = \exp(iks)\phi_n(z - z_m), \quad (2.66)$$

where z is the coordinate along a generatrix of the cylinder and s the coordinate along the conducting band. Express the possible values of the centre z_m as a function of L , w and the magnetic length l_B . Assume $w \gg l_B$. Does k take continuous or discrete values?

2. Apply magnetic flux ϕ in the cylinder. How does it modify the vector potential \mathbf{A} ? Calculate the shift in z_m induced by the flux ϕ .
3. When $\phi = h/e$, show that a centre z_m shifts by precisely the distance between two consecutive centres. Deduce that a quantum of flux shifts a state in each Landau level from one edge of the band to the other.
4. Assume that flux ϕ increases the voltage across the band by V . By how much is the energy of the system E increased? Using the thermodynamic identity

$$I = -\frac{\partial E}{\partial \phi}, \quad (2.67)$$

analogous to $M = -\partial E / \partial B$, show that the Hall conductance $\sigma_{xy} = I/V$ is quantised.

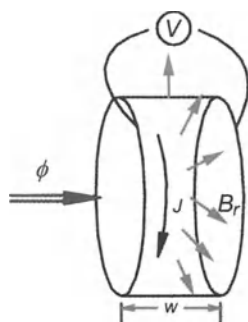


Fig. 2.7. Conducting band closed into the form of a cylinder. A radial magnetic induction B_r is applied. Magnetic flux ϕ is applied in the cylinder

2.5 Orbital Magnetism and Landau Diamagnetism

Quantisation into Landau levels also leads to orbital magnetism, since in classical physics there can be no magnetism (van Leeuwen theorem) [28]. Indeed, classical trajectories are circular. The orbital magnetic moment of each orbit is

$$\boldsymbol{\mu} = \frac{1}{2} \mathbf{r} \times \mathbf{j} = \frac{e}{2} \mathbf{r} \times \mathbf{v} = \frac{mv^2}{2B} \hat{\mathbf{z}} . \quad (2.68)$$

The total magnetic moment is obtained by summing over all orbits. But at any point, there exist two orbits of equal and opposite velocities (see Fig. 2.8). Hence, $\boldsymbol{\mu}_{\text{tot}} = (e/2) \sum_i \mathbf{r}_i \times \mathbf{v}_i = 0$. More precisely, although less intuitively, the free energy F of N uninteracting classical electrons is

$$F = -\frac{N}{\beta} \ln \int d^3r d^3p \exp [-\beta \mathcal{H}_0(\mathbf{r}, \mathbf{p})] , \quad (2.69)$$

where $\mathcal{H}_0 = (\mathbf{p} - e\mathbf{A})^2/2m_* + V(\mathbf{r})$. Making the change of variable $\mathbf{p} \rightarrow \mathbf{p} - e\mathbf{A}$, we find that F is independent of \mathbf{A} and hence of \mathbf{B} . It follows that $\mathbf{m} = -\partial F/\partial B \equiv 0$, and therefore there can be no orbital magnetism in classical physics.

In a quantum description, we must distinguish three different situations:

- (a) $r_c > L$ ($\hbar\omega_c < E_c = \hbar\nu_F/L$), where L is the size of the system;
- (b) $\lambda_F < r_c < L$ ($\varepsilon_F > \hbar\omega_c > E_c$);
- (c) $r_c < \lambda_F$ ($\hbar\omega_c > \varepsilon_F$).

In case (a), the quantum motion is complex and depends on the shape of the system. This is the quantum chaos regime, whose description in terms of

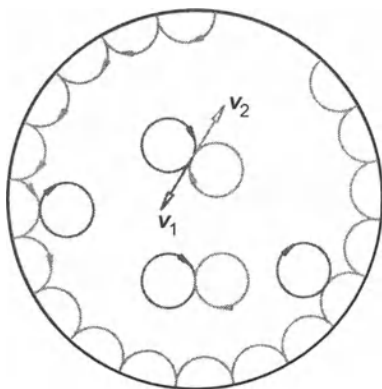


Fig. 2.8. Classical electron trajectories in a magnetic field. At any point \mathbf{r} , there are two trajectories with equal and opposite velocities \mathbf{v}_1 and \mathbf{v}_2 on each trajectory. The contribution of these trajectories to the total orbital moment coming from point \mathbf{r} is therefore zero. Therefore there cannot be orbital magnetism in a classical electron gas

semi-classical orbits is the subject of research at the moment and goes beyond the aims of this book [29, 30]. Landau diamagnetism [31, 32] occurs in case (b) and Haas–van Alphen oscillations [34] in case (c). Landau diamagnetism is easy to calculate when a chemical potential fixes the mean number of particles at some value N . The relevant thermodynamic potential [see Chap. 1(I)] is then $\Omega = F - \mu N$, where F is the free energy of a non-interacting fermion gas. Neglecting the Zeeman spin energy,

$$\Omega = -\frac{1}{\beta} \sum_{i=1}^{\infty} \ln(1 + \exp[\beta(\mu - \varepsilon_i)]) , \quad (2.70)$$

where the sum is taken over all possible states. Energy levels are measured relative to the chemical potential μ (equal to ε_F when $T = 0$). The chemical potential is determined either by an electrode (acting as an electron reservoir), or by the total number of electrons N ,

$$N = -\left(\frac{\partial \Omega}{\partial \mu}\right)_T = \sum_i n(\varepsilon_i) = \sum_i \frac{1}{1 + \exp[-\beta(\mu - \varepsilon_i)]} . \quad (2.71)$$

In 2 dimensions, the degeneracy of each Landau level is $D = \zeta\phi/\phi_0$. We can group together the D states with the same energy to give

$$\Omega = -\frac{1}{\beta} \frac{\zeta\phi}{\phi_0} \sum_{k=0}^{\infty} \ln(1 + \exp \beta[\varepsilon_F - \mu_* B(2k + 1)]) . \quad (2.72)$$

We assume the temperature low enough to replace the chemical potential by ε_F . The orbital moment μ_* is defined by $2\mu_*B = \hbar\omega_c$ ($g_L\mu_B = \mu_*$). As the Landau levels are equally spaced, the sum can be replaced by an integral with the help of Poisson's formula:

$$\sum_{n=0}^p f(n) = \int_{-1/2}^p f(n) dn - \frac{1}{24}[f'(p + 1/2) - f'(-1/2)] . \quad (2.73)$$

Since the function $f(\varepsilon) = \ln[1 + \exp \beta(\varepsilon_F - \varepsilon)]$ we are trying to integrate is zero beyond ε_F , the upper limit can be taken as infinity. The first term does not depend on the magnetic field so we have

$$\begin{aligned} \Omega = & -\frac{\zeta\phi}{2\mu_*B\beta\phi_0} \int_0^{\infty} d\varepsilon \ln[1 + \exp \beta (\varepsilon_F - \varepsilon)] \\ & + \frac{\zeta\phi}{\beta\phi_0} \frac{1}{24}(2\beta\mu_*B) . \end{aligned} \quad (2.74)$$

Now we have $\zeta\phi/\phi_0 = N\mu_*B/\varepsilon_F$, so the first term integrates by parts to give $-N\varepsilon_F/2$. Finally the thermodynamic potential to second order in B becomes

$$\Omega = -\frac{N\varepsilon_F}{2} + \frac{N}{6} \frac{(\mu_*B)^2}{\varepsilon_F} + \dots . \quad (2.75)$$

Hence the Landau susceptibility

$$\chi_L = -\mu_0 \frac{\partial^2 \Omega}{\partial B^2} = -\mu_0 \frac{N\mu_*^2}{3\varepsilon_F} \quad (2.76)$$

is diamagnetic (i.e., negative). In 3 dimensions, the calculation is more difficult. We must first integrate over all states k_z before carrying out the sum over Landau levels.

Exercise

Show that in 3 dimensions the thermodynamic potential is given by

$$\Omega = -\frac{2}{5}N\varepsilon_F + \frac{(\mu_*B)^2 n(\varepsilon_F)}{6}, \quad (2.77)$$

where $n(\varepsilon_F)$ is the density of states at the Fermi level. For a free electron gas, $n(\varepsilon_F) = 3N/2\varepsilon_F$ and the Landau susceptibility is $\chi_L = -\mu_0\mu_*^2 N/2\varepsilon_F$ [40].

2.6 The Haas–van Alphen Effect

In strong fields, few Landau levels are occupied and the discussion above is inadequate. The discrete nature of the Landau levels produces oscillations in the magnetisation which are periodic in $1/B$ [32, 33, 34, 36]. When the number of electrons is fixed, this can be explained in the following way. For a given field B , there are ν occupied Landau levels, each one containing $N/\nu = D = \zeta\phi/\phi_0$ electrons. If there are fewer than $\zeta\phi/\phi_0$ electrons, only the lowest Landau level is populated, the total energy is $E = N\mu_*B$ and the magnetisation is

$$M = -\frac{\partial E}{\partial B} = -N\mu_* . \quad (2.78)$$

In weaker fields such that $2\zeta\phi/\phi_0 > N > \zeta\phi/\phi_0$, electrons partially occupy the second level. Then

$$\begin{aligned} E &= \mu_*B \frac{\zeta\phi}{\phi_0} + 3\mu_*B \left(N - \frac{\zeta\phi}{\phi_0} \right) \\ &= 3\mu_*BN - 2\zeta\mu_*B \frac{\phi}{\phi_0} , \end{aligned} \quad (2.79)$$

$$M = -3\mu_*N + 4\zeta\mu_* \frac{\phi}{\phi_0} , \quad (2.80)$$

which implies that when $\zeta\phi/\phi_0 = N$, the magnetisation jumps from $-N\mu_*$ to $N\mu_*$. Simultaneously, the chemical potential of the system jumps from μ_*B , the ground state energy, to $3\mu_*B$, the energy of the second Landau level. For any electron system, it can be shown that a sudden change in magnetisation with field is associated with a jump in chemical potential with level filling. To do so, we use the Maxwell relation for the grand canonical potential Ω_G defined in (1.81):

$$\mu_0 \left(\frac{\partial M}{\partial \varepsilon_F} \right)_H = \left(\frac{\partial N}{\partial H} \right)_{\varepsilon_F}, \quad (2.81)$$

where the chemical potential has been replaced by the Fermi energy. In 2 dimensions, this gives a relation between the jump in magnetisation ΔM and the jump in chemical potential $\Delta \varepsilon_F$ for a given value of the filling factor $\nu = N/D = N\phi_0/\phi$ (i.e., such that $\partial N/\partial B = N/B$):

$$\frac{\Delta M}{N} = \frac{\Delta \varepsilon_F}{B}. \quad (2.82)$$

This is true whatever the Hamiltonian of the electron system. This relation shows that a sudden change in orbital magnetisation can always be related to the absence of states in a certain region of the spectrum (i.e., to an energy gap).

For fields weaker than $B = N\phi_0/\zeta S$, magnetisation varies linearly with field, from $N\mu_*$ at $B = N\phi_0/\zeta S$ to $-N\mu_*$ at $B = N\phi_0/2\zeta S$. If $3\zeta\phi/\phi_0 > N > 2\zeta\phi/\phi_0$, population of the third Landau level begins. Energy and magnetisation are then

$$\begin{aligned} E &= \mu_* B \frac{\zeta\phi}{\phi_0} + 3\mu_* B \frac{\zeta\phi}{\phi_0} + \left(N - 2 \frac{\zeta\phi}{\phi_0} \right) 5\mu_* B \\ &= 5\mu_* BN - 6\mu_* B \frac{\zeta\phi}{\phi_0}, \end{aligned} \quad (2.83)$$

$$M = -5\mu_* N + 12\mu_* \frac{\zeta\phi}{\phi_0}. \quad (2.84)$$

Hence the magnetisation has a sawtooth variation with filling factor $\nu \propto 1/B$. This dependence is shown in Fig. 2.9. It has recently been observed in a 2-dimensional electron gas of low electron density formed at the interface of a GaAlAs-GaAs heterojunction [37]. Jumps occur at $B = N\phi_0/\zeta\nu S$, where ν is an integer, hence exactly in the middle of a Hall plateau. A glance at Fig. 2.9 will confirm this. If it is the chemical potential $\mu \equiv \varepsilon_F$ which is fixed by an electrode (i.e., an electron reservoir), jumps in magnetisation occur each time a Landau level crosses the chemical potential, that is, when $\hbar\omega_c(\nu+1/2) = \varepsilon_F$. Expressing the Fermi energy ε_F in terms of the number N_0 of electrons in zero field [see (2.40)], these jumps occur when $1/B = \zeta(\nu + 1/2)S/N_0\phi_0$. They are therefore shifted by a half period relative to oscillations for fixed particle number.

When the magnetic field is strong enough to remove spin degeneracy, the period (in $1/B$) of the Haas-van Alphen oscillations is divided by two ($2 \rightarrow \zeta \rightarrow 1$). Jumps in magnetisation now no longer have the same amplitude for odd and even filling factors. This is because the Zeeman energy is not generally the same as the cyclotron energy [38]. Landau levels have width of order \hbar/τ , where τ is the time between each collision with impurities. The Haas-van Alphen effect will therefore be observable when this width is small compared with the spacing $\hbar\omega_c$ between levels. This is Dingle's criterion [39].

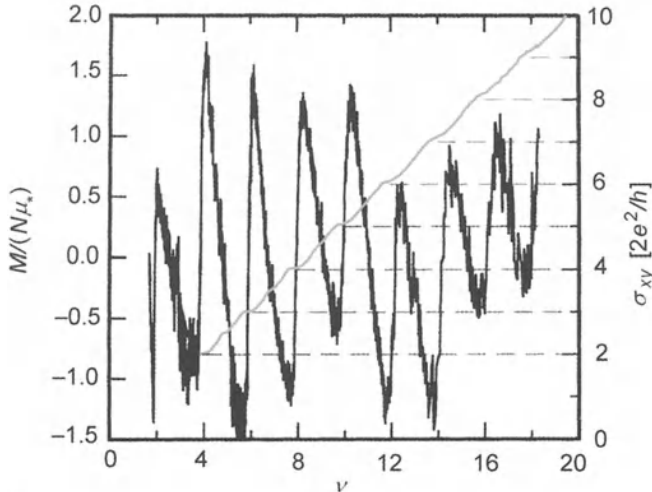


Fig. 2.9. Haas–van Alphen oscillations for a GaAlAs–GaAs heterojunction as a function of filling factor (the number of occupied Landau levels). We can clearly see sudden jumps in magnetisation each time a Landau level is completely filled. These jumps occur exactly at the centre of the Hall plateaus, which are rather narrow here since the heterojunction has very high mobility (there is little disorder to fix the Fermi level between Landau levels)

Likewise, we must have $\mu_* B \gg k_B T$, otherwise many Landau levels will be thermally occupied.

In three dimensions, the Haas–van Alphen effect becomes much more difficult to treat and depends on the shape of the Fermi surface [40]. The dominant contributions to oscillations in magnetisation come from extreme orbits on the Fermi surface. Valuable information can thus be obtained about the shape of the Fermi surface. The Haas–van Alphen effect provides a way of studying the Fermi surface of metals which was widely exploited in the 1950s to 1970s [35].

2.7 Pauli Paramagnetism of Conduction Electrons

Conduction electrons possess spin, a fact we have neglected up to the present. The Fermi seas of \uparrow and \downarrow spins are shifted apart by the Zeeman energy $\pm \mu_B B$. Thermodynamic equilibrium requires the chemical potential, and hence the Fermi energy of the two seas (\uparrow and \downarrow) to be equal. It is the lower end of the bands which is shifted by the Zeeman energy (see Fig. 2.10). The numbers of \uparrow and \downarrow electrons are therefore

$$N_{\pm} = \frac{1}{2} \int_{\pm \mu_B B}^{\infty} d\varepsilon f(\varepsilon) n(\varepsilon) \approx \frac{1}{2} \int_0^{\infty} d\varepsilon f(\varepsilon \mp \mu_B B) n(\varepsilon)$$

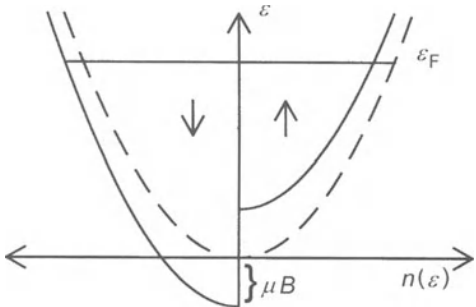


Fig. 2.10. Fermi distribution of \uparrow and \downarrow spins in a magnetic field

$$\approx \frac{N}{2} \mp \frac{\mu_B B}{2} \int_0^\infty d\epsilon \frac{\partial f}{\partial \epsilon}(\epsilon) n(\epsilon) = \frac{N}{2} \pm \frac{n(\epsilon_F)\mu_B B}{2}, \quad (2.85)$$

since the density of states $n(\epsilon_F)$ varies slowly around ϵ_F and

$$\frac{\partial f}{\partial \epsilon} = -\delta(\epsilon - \epsilon_F).$$

As a consequence, the magnetisation is paramagnetic:

$$M = \mu_B N_+ - \mu_B N_- = n(\epsilon_F) \mu_B^2 B = \chi_P H. \quad (2.86)$$

For a free electron gas in three dimensions, $n(\epsilon_F) = 3N/2\epsilon_F$ and the Pauli susceptibility $\chi_P = \partial M / \partial H$ is equal to

$$\chi_P = \mu_0 \mu_B^2 n(\epsilon_F) = \mu_0 \frac{3N\mu_B^2}{2\epsilon_F}. \quad (2.87)$$

If the effective mass is 1, $\mu_* = \mu_B$ and the Pauli susceptibility is three times greater than the Landau susceptibility. In semiconductors of small effective mass, it is always the Landau susceptibility which dominates. In contrast, for transition metals, the d band (and a fortiori for rare earths, the f band) is much narrower and the density of states at the Fermi level much higher than that of a free electron gas. The Pauli susceptibility is then very large. Its wave vector dependence will be studied in Chap. 11 (I). It can give rise to itinerant magnetism in conduction electrons (spin density waves).

2.8 The Zeeman Effect

The contribution of spin $S = \hbar\sigma/2$ to the Hamiltonian \mathcal{H} ($e = -|e| < 0$) is

$$\mathcal{H}_S = -g_S \frac{e}{2m} \mathbf{S} \cdot \mathbf{B}. \quad (2.88)$$

We use the usual representation of the Pauli matrices σ

$$\sigma_x = \begin{pmatrix} 0 & 1 \\ 1 & 0 \end{pmatrix}, \quad \sigma_y = \begin{pmatrix} 0 & -i \\ i & 0 \end{pmatrix}, \quad \sigma_z = \begin{pmatrix} 1 & 0 \\ 0 & -1 \end{pmatrix}. \quad (2.89)$$

The eigenvalues of \mathcal{H}_S are $\pm g_S \mu_B B / 2$ where $\mu_B = |e|\hbar/2m = 0.92741 \times 10^{-24} \text{ J/T} = 0.92741 \times 10^{-20} \text{ erg/Oe}$ is the Bohr magneton. For free electrons, $g_S = 2.0023$, although it varies appreciably in solids (see Sect. 2.11). The gyromagnetic ratio γ is often defined as the ratio of magnetic moment to angular momentum. This ratio $\gamma = g_S e / 2m$ is negative for electron spins, but is usually positive for nuclear spins. In insulating materials, it suffices to retain the orbital term \mathcal{H}_L . The Zeeman Hamiltonian is then

$$\mathcal{H}_z = \mathcal{H}_L + \mathcal{H}_S = -\frac{e}{2m} (g_L \mathbf{L} + g_S \mathbf{S}) \cdot \mathbf{B}. \quad (2.90)$$

The orbital angular momentum \mathbf{L} and the total angular momentum $\mathbf{J} = \mathbf{L} + \mathbf{S}$ are spinors satisfying the usual commutation relations:

$$[J_\alpha, J_\beta] = i\hbar\varepsilon_{\alpha\beta\gamma} J_\gamma, \quad (2.91)$$

$$J_\pm = J_x \pm J_y, \quad (2.92)$$

$$[J_z, J_\pm] = \pm\hbar J_\pm, \quad (2.93)$$

$$[J_+, J_-] = 2\hbar J_z, \quad (2.94)$$

where $\varepsilon_{\alpha\beta\gamma}$ is the completely antisymmetric tensor. The eigenfunctions of \mathbf{L} are often represented by spherical harmonics $Y_{lm}(\theta, \phi)$. Operators L^\pm are ladder operators raising or lowering the value of m by one unit:

$$L^\pm Y_{lm} = \hbar \sqrt{(l \mp m \pm 1)(l \mp m)} Y_{l, m \pm 1}. \quad (2.95)$$

The commutation relations are non-linear. Hence, spin quantum effects often give rise to non-linear effects. In the limit of large j , defined in terms of eigenvalues of J^2 by $J^2|j, m_j\rangle = \hbar^2 j(j+1)|j, m_j\rangle$, we can define normalised operators $\mathcal{J}_\alpha = J_\alpha/\hbar\sqrt{j(j+1)}$ whose components commute approximately

$$[\mathcal{J}_\alpha, \mathcal{J}_\beta] \approx O(1/j). \quad (2.96)$$

This is the semi-classical limit. \mathcal{J} can then be considered as an ordinary unit vector on the surface of a sphere, whose components in the $\hat{\mathbf{z}}$ direction still take on discrete values. Figure 2.11 gives a graphical representation of this vector model. Quantum effects are thus significant for low values of angular momentum ($j = 1/2, 1$).

Since $[\mathcal{H}_z, \mathbf{J}] = 0$, energy eigenstates can be characterised by eigenvalues of J^2 , viz., $\hbar^2 j(j+1)$ and J_z , viz., $\hbar m_j$ where m_j takes values in the range $-j, -j+1, \dots, j-1, j$. When the Zeeman energy is small compared with the spin-orbit interaction coupling \mathbf{L} and \mathbf{S} , it can be obtained by perturbation theory. Expectation values $\langle j, m | \mathcal{H}_z | j, m \rangle$ can then be expressed in terms of the eigenvalues of J_z , by means of the Wigner-Eckart theorem

$$\langle j, m_j | \mathcal{H}_z | j, m_j \rangle = \frac{\langle j || \mathcal{H}_z || j \rangle}{\hbar\sqrt{j(j+1)}} \langle j, m_j | J_z | j, m_j \rangle, \quad (2.97)$$

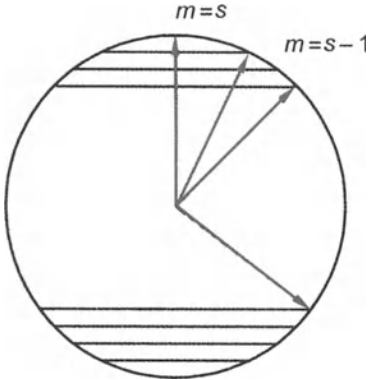


Fig. 2.11. Vector model of spin in the semi-classical limit

where $\langle j||A||j\rangle$ are the reduced matrix elements of the operator $A \equiv \mathcal{H}_z, J_z$. After standard calculations, we find that

$$\varepsilon_{m_j} = g_J \mu_B m_j B , \quad (2.98)$$

where

$$g_J = \left(\frac{g_L + g_S}{2} + (g_S - g_L) \frac{s(s+1) - l(l+1)}{2j(j+1)} \right) . \quad (2.99)$$

This is the anomalous Zeeman effect occurring for solids in which spin-orbit coupling is significant.

Exercise

Prove the above result. Calculate the reduced matrix element, showing that $\hbar\sqrt{j(j+1)}\langle j||\mathcal{H}_z||j\rangle = \langle j, j|\mathcal{H}_z J_z|j, j\rangle$ and expressing $\mathbf{J} \cdot \mathbf{L}$ and $\mathbf{J} \cdot \mathbf{S}$ in terms of J^2, L^2 and S^2 .

When the Zeeman energy is large compared with the spin-orbit interaction coupling \mathbf{L} and \mathbf{S} , it is preferable to use the uncoupled basis $|l, m_l\rangle \otimes |s, m_s\rangle$ in which operators L^2, L_z, S^2 and S_z are diagonal. In this case, the Zeeman energy is

$$\begin{aligned} \varepsilon_{m_l, m_s} &= \langle l, s; m_l, m_s | \mathcal{H}_z | l, s; m_l, m_s \rangle \\ &= (g_L m_l + g_S m_s) \mu_B B . \end{aligned} \quad (2.100)$$

This is the Paschen-Back limit. Orbital and spin contributions are additive and we have the normal Zeeman effect. In practice, this limit is only attained for light atoms (e.g., Li and Be) in intense magnetic fields. This is because the spin-orbit interaction increases as Z^4 and rapidly predominates in heavy atoms.

2.9 The Spin–Orbit Interaction

If we replace \mathbf{B} by $\mathbf{B} + \mathbf{E} \times \mathbf{v}/c^2$ in the Zeeman Hamiltonian, we obtain twice the spin–orbit Hamiltonian (2.6). This suggests that \mathcal{H}_{so} describes a magnetic interaction in the electron frame, induced by the electric field. But this argument is not quite accurate. An electron is accelerated in an electric field and a homogeneous Lorentz transformation is no longer appropriate. The acceleration effect compensates for half the interaction, thereby giving \mathcal{H}_{so} . For a central force potential $V(r) = e\phi(r)$, where $\phi(r)$ is the electrostatic potential of the nucleus and inner electrons, the electric field is $\mathbf{E} = (-\mathbf{r}/er)dV/dr$. We can thus rewrite the spin–orbit Hamiltonian in the form

$$\begin{aligned}\mathcal{H}_{\text{so}} &= -\frac{\hbar}{4mm_*c^2} \left(-\frac{1}{r} \frac{dV}{dr} \right) \boldsymbol{\sigma} \cdot (\mathbf{r} \times \mathbf{p}) \\ &= -\frac{1}{2mm_*c} \left(\frac{1}{r} \frac{dV}{dr} \right) \mathbf{L} \cdot \mathbf{S} = \lambda(r) \mathbf{L} \cdot \mathbf{S}.\end{aligned}\quad (2.101)$$

The matrix elements of the coefficient $\lambda(r)$ depend only on radial electron functions. Since $\mathbf{L} \cdot \mathbf{S} = (J^2 - L^2 - S^2)/2$, the spin–orbit interaction removes the degeneracy in states of different total angular momentum j , i.e.,

$$\langle j | \mathcal{H}_{\text{so}} | j \rangle \propto j(j+1) - l(l+1) - s(s+1).$$

If we neglect screening by inner electron levels, the Coulomb potential produced by a nucleus of charge $Z|e|$ is $V(\mathbf{r}) = -Ze^2/4\pi\epsilon_0 r$ and we have $\lambda(r) = Z\alpha\lambda_c/4\pi m_*r^3$, where $\alpha = e^2/4\pi\epsilon_0\hbar c$ is the fine structure constant and $\lambda_c = \hbar/mc$ the Compton wavelength. The expectation value of the spin–orbit interaction is $\langle \lambda(r) \rangle \propto Z\alpha \langle 1/r^3 \rangle$, which is inversely proportional to the volume occupied by an atomic orbit. This is of the order of a_B^3 , where $a_B = \lambda_c 2\pi Z\alpha$ is the Bohr radius. This is why the spin–orbit interaction increases as $(Z\alpha)^4$ for a localised atomic orbit. Hence the importance of the spin–orbit interaction in heavy atoms.

In metals, the spin–orbit interaction \mathcal{H}_{so} only contributes to the scattering of electrons if there is a lattice defect. Otherwise we can construct Bloch states for which j is a good quantum number, starting from exact eigenfunctions at a site [the Wannier wave function, described in Chap. 3(I)], whose Fourier transforms are the Bloch states of the solid. In the presence of a defect, the spin–orbit interaction contributes to scattering by rotating the electron spin. As it is small compared to the Coulomb interaction scattering the electron, its contribution to the scattering amplitude t can be determined by perturbation theory:

$$\langle \mathbf{k}' | t_{\text{so}} | \mathbf{k} \rangle = \langle \Psi_{\mathbf{k}'\beta} | \mathcal{H}_{\text{so}} | \Psi_{\mathbf{k}\alpha} \rangle = i t_{|\mathbf{k}|}^{\text{so}} (\hat{\mathbf{k}} \cdot \hat{\mathbf{k}}') \hat{\mathbf{k}} \times \hat{\mathbf{k}}' \cdot \boldsymbol{\sigma}_{\alpha\beta}, \quad (2.102)$$

where the $\Psi_{\mathbf{k}\alpha}$ are exact scattering states in the potential due to the impurity and $\boldsymbol{\sigma}$ are the Pauli matrices. The scattering amplitude $t_{|\mathbf{k}|}^{\text{so}}$ is strongly energy dependent. In metals, $Z/k_F a_B$ is large and scattering is always at

low energy. The Born approximation can therefore never be applied. The spin-orbit scattering cross-section σ_{so} is linearly dependent on the amplitude t_{so} :

$$\sigma_{\alpha\beta}(\mathbf{k}, \mathbf{k}') = \left(\frac{m_*}{2\pi\hbar^2} \right)^2 |t_c + it_{\text{so}}\hat{\mathbf{k}} \times \hat{\mathbf{k}}'|^2 \approx \sigma_c + \sigma_{\text{so}}, \quad (2.103)$$

$$\sigma_{\alpha\beta}^{\text{so}} = 2 \left(\frac{m_*}{2\pi\hbar^2} \right)^2 \mathcal{T}m(t_c^* t_{\text{so}}) \hat{\mathbf{k}} \times \hat{\mathbf{k}}' \cdot \boldsymbol{\sigma}_{\alpha\beta}, \quad (2.104)$$

since the Coulomb term dominates. These quantities are difficult to determine theoretically because there are $l_{\max} = Z/k_F a_B$ partial waves. Exhaustive experimental study has shown that the cross-section increases with the charge Z of the impurity as $\sigma_{\text{so}} \propto Z^5$ in the rare metals [43].

2.10 Thermodynamics of Localised Spins

In our discussion of the Zeeman effect, we found that the spin-orbit interaction removed the degeneracy in states of different total angular momentum j . When this interaction is large relative to the temperature, we need only consider the lowest energy j multiplet. The free energy can then be calculated from the eigenvalues of the Zeeman Hamiltonian. Spins at different sites are distinguishable and thermodynamic functions are described by (classical) Boltzmann statistics. The N -spin partition function Z is then the product of N identical partition functions z , one for each spin. Hence,

$$F = -\frac{N}{\beta} \ln \left[\sum_{m=-j}^j \exp(-\beta m g_J \mu_B B) \right]. \quad (2.105)$$

For spin $1/2$, this becomes simply

$$F = -\frac{N}{\beta} \ln[2 \cosh(\beta g_J \mu_B B)]. \quad (2.106)$$

The magnetisation is then $M = -\partial F / \partial B = \chi H$, where χ is the Langevin susceptibility

$$\chi = N \mu_0 \frac{g_J \mu_B j}{B} B_j(\beta g_J j \mu_B B). \quad (2.107)$$

The Brillouin function B_j is defined by

$$B_j(x) = \frac{\sum_{m=-j}^j (m/j) \exp(-mx/j)}{\sum_{m=-j}^j \exp(-mx/j)}. \quad (2.108)$$

It can be written explicitly in terms of common functions:

$$B_j(x) = \frac{2j+1}{2j} \coth \frac{(2j+1)x}{2j} - \frac{1}{2j} \coth \frac{x}{2j}, \quad (2.109)$$

$$B_{1/2}(x) = \tanh x. \quad (2.110)$$

Expanding the Brillouin function to third order in x ,

$$B_j(x) \approx \frac{j+1}{3j}x - \frac{[(j+1)^2 + j^2](j+1)}{90j^3}x^3 + O(x^5), \quad (2.111)$$

it is easy to check that for small values of B ,

$$\chi(T) = N\mu_0 \frac{(g_J\mu_B)^2 j(j+1)}{3k_B T} = \frac{C_j}{T}. \quad (2.112)$$

This is Curie's law and C_j is Curie's constant. The susceptibility of an ensemble of paramagnetic spins diverges when $T \rightarrow 0$. Treating the spins in a purely classical way, the magnetisation is given by

$$m = \frac{\mu}{2} \int_{-1}^1 \exp(-\beta u \mu B) u du = \mu \left(\coth x - \frac{1}{x} \right), \quad (2.113)$$

where $x = \beta \mu B$. The behaviour of magnetisation curves for $j = 1/2$ and $j = 5/2$ according to the classical formula are shown in Fig. 2.12. Magnetisation is saturated more rapidly in the spin $1/2$ case because the relative value of the energy separation between the two levels \uparrow and \downarrow is the greatest. This means that the system is easily blocked in the $|\uparrow\rangle$ state. Classical spin magnetisation saturates very slowly (as $1/H$) because all values of m_z are possible. The $j = 5/2$ case is intermediate.

In the spin $1/2$ case, it is easy to calculate the spin entropy and specific heat:

$$S = -\frac{\partial F}{\partial T} = Nk_B \left[\ln \left(2 \cosh \frac{\beta g_J \mu_B B}{2} \right) - \frac{\beta g_J \mu_B B}{2} \tanh \frac{\beta g_J \mu_B B}{2} \right],$$

$$C = T \frac{\partial S}{\partial T} = \left(\frac{\beta g_J \mu_B B / 2}{\cosh(\beta g_J \mu_B B / 2)} \right)^2 \approx Nk_B \left(\frac{g_J \mu_B B}{2k_B T} \right)^2, \quad (2.114)$$

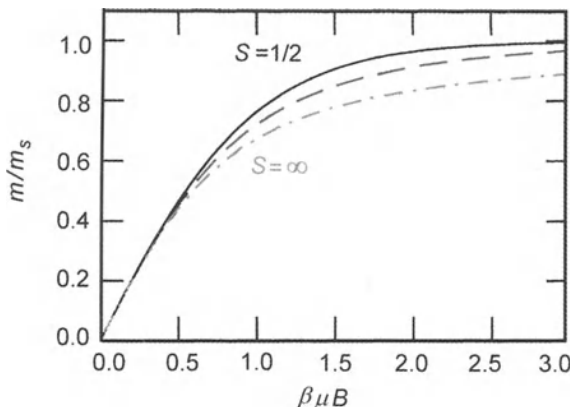


Fig. 2.12. Magnetisation curve for spin $1/2$ (continuous curve), $5/2$ (dashed curve) and classical (broken curve)

where the specific heat approximation is for high temperatures relative to the Zeeman energy. The specific heat is zero when $B = 0$. This is no longer true for interacting spins [see Chap. 5(I)].

Exercise

Show that whatever the value of j , the weak field specific heat is related to the susceptibility by

$$C = \mu_0 \chi \frac{H^2}{T}. \quad (2.115)$$

We can understand the principle of adiabatic demagnetisation from relations (2.114). When a spin system is magnetised at constant field, its entropy decreases and its specific heat increases. Isolating the system and carrying out adiabatic demagnetisation (at constant entropy), the system cools. In practice a small field is always maintained so that the specific heat does not go to zero. This ensures that, in the presence of thermal leakage, the system will not heat up again too quickly.

Exercise

Consider the spin 1 Hamiltonians

$$\mathcal{H} = D(S_z)^2 - \mu H S_z, \quad (2.116)$$

$$\mathcal{H} = E[(S_x)^2 - (S_y)^2] - \mu H S_z. \quad (2.117)$$

Recall that the spin 1 operators can be represented by matrices

$$S_z = \hbar \begin{pmatrix} 1 & 0 & 0 \\ 0 & 0 & 0 \\ 0 & 0 & -1 \end{pmatrix}, \quad S^+ = \hbar \sqrt{2} \begin{pmatrix} 0 & 1 & 0 \\ 0 & 0 & 1 \\ 0 & 0 & 0 \end{pmatrix}, \quad S^- = \hbar \sqrt{2} \begin{pmatrix} 0 & 0 & 0 \\ 1 & 0 & 0 \\ 0 & 1 & 0 \end{pmatrix}. \quad (2.118)$$

1. What are the eigenvalues of these Hamiltonians?
2. What is the free energy of a system of N identical spins with the above Hamiltonians?
3. Deduce the dependence of the susceptibility and the specific heat on temperature.

2.11 Van Vleck Paramagnetism

In certain materials, the orbital angular momentum of the ground state $|0\rangle$ has zero expectation as a consequence of invariance under time reversal (see Sect. 2.15). It might be thought that magnetism would then be purely due to spin in the ground state. In fact, certain excited states have orbital angular

momentum and these contribute to the ground state magnetism in second order perturbation theory. With a view to comparing these contributions, we can use an effective magnetic Hamiltonian acting on spin states in the $|0\rangle$ subspace. To second order,

$$\begin{aligned}\mathcal{H}_{\text{eff}} &= \langle 0 | \mathbf{H}_{\text{so}} + \mathcal{H}_Z | 0 \rangle \\ &= \frac{g_S|e|}{2m} \mathbf{S} \cdot \mathbf{B} - \sum_n \frac{|\langle n | g_L | e | \mathbf{L} \cdot \mathbf{B} / 2m + \lambda \mathbf{L} \cdot \mathbf{S} | 0 \rangle|^2}{E_n - E_0},\end{aligned}\quad (2.119)$$

where the sum is taken over all excited states n of the system. The latter can be classified by means of the irreducible representations of the point symmetry group of the crystal (see Appendix A). The spin Hamiltonian $\mathcal{H}_S \propto \mathbf{S} \cdot \mathbf{B}$ does not contribute in second order perturbation theory (second term); it does not act on orbital wave functions of excited states, orthogonal to the ground state. Expanding out the square of the matrix element in (2.119), we find to second order,

$$\begin{aligned}\mathcal{H}_{\text{eff}} &= \frac{g_S|e|}{2m} \mathbf{S} \cdot \mathbf{B} - \frac{g_L|e|}{2m} \lambda \sum_{i,j} \Lambda_{ij} S_i B_j - \lambda^2 \sum_{i,j} \Lambda_{ij} S_i S_j \\ &\quad - \left(\frac{g_L|e|}{2m} \right)^2 \sum_{i,j} \Lambda_{ij} B_i B_j,\end{aligned}\quad (2.120)$$

where λ is the spin-orbit interaction coefficient (see Sect. 2.9) and

$$\Lambda_{ij} = \sum_n \frac{\langle 0 | L_i | n \rangle \langle n | L_j | 0 \rangle}{E_n - E_0}. \quad (2.121)$$

The tensor Λ has in general three principal axes and three corresponding eigenvalues. Consequently, the Landé factor is also a tensor $g_{ij} = g_S \delta_{ij} - g_L \lambda \Lambda_{ij}$. It diagonalises in the same basis as Λ_{ij} . It is natural, therefore, that the Landé factor should be slightly different from 2.002319 in solids. When the tensor Λ_{ij} has only two eigenvalues Λ_{\perp} and Λ_{\parallel} , the Hamiltonian has eigenvalues

$$E_m^{\parallel} = E_0 + g_{\parallel} \mu_B m B - \left(\frac{g_L|e|}{2m} \right)^2 \Lambda_{\parallel} B^2, \quad (2.122)$$

$$E_m^{\perp} = E_0 + g_{\perp} \mu_B m B - \left(\frac{g_L|e|}{2m} \right)^2 \Lambda_{\perp} B^2. \quad (2.123)$$

Only the second term in each depends on the magnetic quantum number m . The partition function can therefore be factorised into two parts corresponding to the Zeeman and van Vleck contributions. The total susceptibility $\chi = \chi_C + \chi_{VV}$ is made up of two parts: the Langevin susceptibility χ_C [see (2.112)], which obeys a Curie law in $1/T$, and the van Vleck susceptibility χ_{VV} ,

$$\chi_{VV}^{\parallel, \perp} = 2N\mu_B^2 \Lambda_{\parallel, \perp}, \quad (2.124)$$

which is temperature independent. χ_{VV} is anisotropic. It can be significant, either when the ground state is a singlet $S = 0$ (the Curie susceptibility is then zero), or at high temperature, where the Curie term is small. The various regimes are easy to identify by plotting $1/\chi$ as a function of T . The van Vleck susceptibility is important in molecular structures which form preferentially in $S = 0$ states (antiferromagnetism) because of superexchange [see Chap. 3(I)].

2.12 The Ionic Anisotropy Field

The third term in (2.120) represents fine structure or ionic anisotropy. The principal axes of the tensor A have the crystal symmetry. For example, for a cubic crystal, only $A_{xx} = A_{yy} = A_{zz}$ are non-zero. This term then reduces to a constant. However, for a tetragonal crystal, $A_{zz} = A_{\parallel} \neq A_{\perp} = A_{xx} = A_{yy}$. We then define $D = \lambda^2(A_{\parallel} - A_{\perp})$ and, omitting the van Vleck term, the Hamiltonian has a uniaxial ionic anisotropy:

$$\begin{aligned}\mathcal{H} = & g_{\parallel} \mu_B S_z B_z + g_{\perp} \mu_B (B_x S_x + B_y S_y) \\ & + D S_z^2 + \lambda^2 A_{\perp} S(S+1).\end{aligned}\quad (2.125)$$

The last term, which is constant, is generally absorbed into the ground state energy.

Exercise

Determine the spectrum of H for $S = 3/2$ and when \mathbf{B} is oriented along the \hat{z} axis.

When the crystal is orthorhombic or has lower symmetry, the \hat{x} and \hat{y} axes are no longer equivalent. We must introduce a further anisotropy constant $E = \lambda^2(A_{xx} - A_{yy})$. The spin Hamiltonian becomes

$$\begin{aligned}\mathcal{H} = & g_z \mu_B S_z B_z + g_x \mu_B S_x B_x + g_y \mu_B S_y B_y \\ & + D S_z^2 + E(S_y^2 - S_x^2).\end{aligned}\quad (2.126)$$

When the crystal is hexagonal close-packed or triclinic, non-orthonormal bases are needed to diagonalise A .

In crystals with no centre of symmetry, certain exchange interactions (see Chap. 3) introduce a further type of crystalline anisotropy. The exchange energy can be decomposed into symmetric and antisymmetric parts relative to exchange of spins \mathbf{S}_i and \mathbf{S}_j . The antisymmetric part gives rise to the Dzyaloshinskii–Moriya spin anisotropy [44, 45]

$$\mathcal{H}_{DM} = \mathbf{D} \cdot \mathbf{S}_i \times \mathbf{S}_j \quad (2.127)$$

which favours non-collinear spin arrangements.

2.13 Crystalline Field

Up to now we have neglected effects due to the electrostatic field V produced by lattice ions. However, it does have a significant effect on transition ions. These have their magnetic electrons in $3d$ orbitals located on the outer part of the ion, which are therefore highly sensitive to the potential. This is to be contrasted with the rare earth elements where magnetic $4f$ orbitals are buried inside the ion and protected, as it were, by filled $5s^25p^6$ shells. The latter are thus less affected by the electrostatic potential. When we study the crystalline field of the d shells, two distinct situations can arise. Firstly, the crystalline field may be small compared with the Coulomb interaction term between electrons (the Hund term). That term therefore determines the orbital angular momentum and spin in the ground state of the ion. This weak crystalline field limit applies to the $3d$ shell. We can then apply perturbation theory to atomic orbital states. In the opposite situation, more appropriate to the $4d$ and $5d$ shells, the crystalline field is strong and directly determines ionic orbital states. We have relegated this discussion to Appendix A. In the present section, we shall study the weak field limit, taking as example the $3d^1$ configuration (V^{4+} , Ti^{3+}) in which a single d orbital is filled. By electron-hole symmetry, the discussion is the same for the $3d^9$ configuration (Cu^{++}), except that the level structure is reversed since holes have the opposite sign of charge. According to the Hund rules [see Sect. 3.3(I)], the orbital angular momentum is zero ($l = 0$) when the d band is half filled ($3d^5$ configuration). Consequently, the $3d^6$ configuration (Fe^{2+}) is equivalent to the $3d^1$ configuration and the $3d^4$ configuration (Mn^{3+} , Cr^{2+}) is equivalent to the $3d^9$ configuration. The ground state quantum numbers given by the Hund rules [see Chap. 3(I)] are 2D (i.e., $l = 2$, $S = 1/2$). They correspond to the representation $\Gamma_{l=2}$ of the rotation group. The ground state degeneracy $2l + 1 = 5$ (or 10, if spins are included) is reduced by the crystalline field, depending on lattice symmetries. As the crystalline field does not affect spin degeneracy, we need only consider orbital degeneracy. The energy level structure is obtained by decomposing the representation $\Gamma_{l=2}$ of the ground state into irreducible representations of the lattice symmetry group. This rather tedious procedure is described in Appendix A. It is not necessary in the simplest cases. Let us consider the case of a lattice with cubic symmetry. The symmetry group is O_h , the symmetries of the octahedron, containing reflection symmetries σ with respect to the xy , yz and xz planes. We start from the d orbitals,

$$\begin{aligned}\mathcal{Y}_2^{\pm 2} &= \frac{a}{\sqrt{2}}(x \pm i y)^2, & \mathcal{Y}_2^{\pm 1} &= \mp a\sqrt{2}z(x \pm iy), \\ \mathcal{Y}_2^0 &= \frac{a}{\sqrt{3}}(2z^2 - x^2 - y^2),\end{aligned}\tag{2.128}$$

which are not eigenstates of the reflection symmetries, and construct two even orbital states and three odd orbital states by linear combinations. (The

orbitals in (2.128) are proportional to the spherical harmonics $Y_{l=2,m}$, which can be recovered by putting $a = \sqrt{15/\pi}(2r)^{-2}$.) The two even states are:

$$d_{3z^2-r^2} = \mathcal{Y}_2^0, \quad d_{x^2-y^2} = \frac{1}{\sqrt{2}}(\mathcal{Y}_2^2 + \mathcal{Y}_2^{-2}) = a(x^2 - y^2), \quad (2.129)$$

forming a basis for the E representation of the group O . The three odd orbital states are:

$$\begin{aligned} d_{xy} &= \frac{1}{\sqrt{2}}(\mathcal{Y}_2^2 - \mathcal{Y}_2^{-2}) = 2axy, & d_{xz} &= \frac{1}{\sqrt{2}}(\mathcal{Y}_2^{-1} - \mathcal{Y}_2^1) = axz, \\ d_{yz} &= \frac{i}{\sqrt{2}}(\mathcal{Y}_2^1 + i\mathcal{Y}_2^{-1}) = ayz, \end{aligned} \quad (2.130)$$

forming a basis for the F_2 representation. The ground state degeneracy has therefore been reduced to an order 2 degeneracy (E) and an order 3 degeneracy (F_2). To find the energy levels, we treat neighbouring ions as point charges of charge q (this is justified if there is little overlap between neighbouring orbital states). We then expand the potential $V(\mathbf{r}) = (qe/4\pi\epsilon_0) \sum_i 1/|\mathbf{r} - \mathbf{R}_i|$, produced by neighbouring ions, in spherical harmonics:

$$V(r, \theta, \phi) = \sum_{l'} V_{l'} = \sum_{l', m} V_{l', m} r^l Y_l^m(\theta, \phi). \quad (2.131)$$

We now wish to calculate the matrix elements $\langle n; l, m' | V | n; l, m \rangle$ in a basis of atomic D orbitals ($l = 2$). We can thus ignore the l harmonics above 4 (and 6, respectively), since they do not contribute to the overlap of the D (F) orbitals. It is the total orbital angular momentum of the ion which comes in here. If there are two filled d orbitals, the ground state of the ion is F ($l = 3$), according to Hund's rule. (The first Hund rule requires $S = 1$, so that the maximal total orbital angular momentum consistent with the Pauli principle is $l = 3$ [see Chap. 3(I)].) Likewise, we can ignore the odd l and $l = 0$. For a cubic crystal of spacing d , there only remains V_4 for the D states and V_6 for the F states. We can express them in terms of spherical harmonics or Cartesian coordinates:

$$\begin{aligned} V_4(r, \theta, \phi) &= D_4 \left(Y_4^0(\theta, \phi) + \sqrt{\frac{5}{14}}[Y_4^4(\theta, \phi) + Y_4^{-4}(\theta, \phi)] \right) \\ &= C_4[x^4 + y^4 + z^4 - 3r^4/5], \end{aligned} \quad (2.132)$$

$$\begin{aligned} V_6(r, \theta, \phi) &= D_6 \left(Y_6^0(\theta, \phi) + \sqrt{\frac{7}{2}}[Y_6^4(\theta, \phi) + Y_6^{-4}(\theta, \phi)] \right) \\ &= C_6\{x^6 + y^6 + z^6 + (15/4)[x^2(y^4 + z^4) \\ &\quad + y^2(x^4 + z^4) + z^2(x^4 + y^4)] - 15r^6/14\}, \end{aligned} \quad (2.133)$$

where

$$D_4 = \frac{1}{4\pi\epsilon_0 d^5} \frac{7\sqrt{\pi}}{3qe r^4} \quad \text{and} \quad C_4 = \frac{1}{4\pi\epsilon_0 d^5} \frac{35}{4qe}.$$

We must now calculate the matrix elements of V_4 and V_6 . We use the Wigner–Eckart theorem: x^4 is proportional to the matrix element of J_x^4 or L_x^4 . This is straightforward using tables [46]. For example,

$$V_4 = \frac{C_4 \bar{r}^4}{63} \left(\frac{35L_z^4 - a(l)L_z^2 + b(l)}{10} + \frac{L_+^4 + L_-^4}{4} \right), \quad (2.134)$$

where $a(l) = 30l(l+1) - 25$ and $b(l) = 3l(l+1)[l(l+1)-2]$. The ground state is then the triplet, basis of the F_2 representation, with energy

$$E_{F_2} = \varepsilon_0 + \frac{24}{63 \times 5} C_4 \langle r^4 \rangle, \quad (2.135)$$

(the coefficient C_4 is negative for electrons), and the doublet, basis of the E representation, with energy

$$E_E = \varepsilon_0 - \frac{36}{63 \times 5} C_4 \langle r^4 \rangle. \quad (2.136)$$

If the crystal also has a tetragonal symmetry, induced by a Jahn–Teller distortion (see Sect. 2.14), as frequently happens when the crystal contains a transition ion, the ground state degeneracy is then completely removed, as shown in Fig. 2.13. (Note that the symmetry group D_4 only has one-dimensional representations.) In this case the expectation value of the orbital angular momentum is zero (see Sect. 2.15). For crystals containing transition ions (the $3d$, $4d$ and $5d$ series), this mechanism reduces magnetism to spin effects. Some knowledge of representations of the symmetry group considerably reduces the work involved in determining crystalline orbital states. Appendix A provides the practical details needed in this analysis.

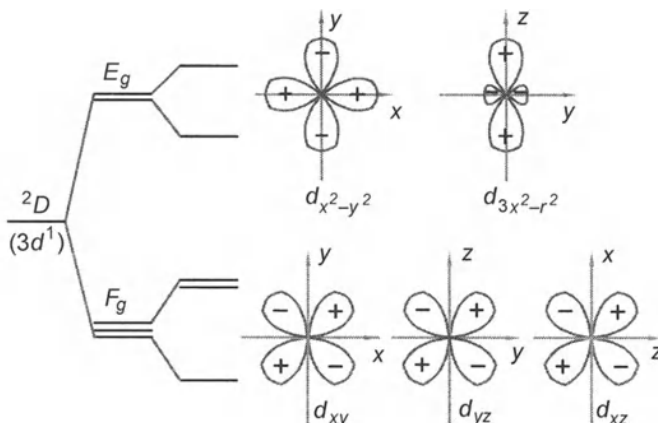


Fig. 2.13. The crystalline field of a cubic crystal reduces the order 5 orbital degeneracy of a 2D state (the $3d^1$ configuration), forming two multiplets of order 2 and 3. Any tetragonal distortion completely removes the orbital degeneracy in these multiplets, so that only spin degeneracy remains

For the rare earths, the total angular momentum j is approximately a good quantum number, the spin-orbit coupling $\propto Z^4$ being much stronger than the crystalline field. It is then better to begin with the coupled basis $|j, m_j\rangle$ when seeking spin-orbital wave functions of the crystal. This requires study of half-integer representations when j takes half integral values.

Exercise

The crystalline field on an ion in an orthorhombic structure can be modelled by a potential of form

$$V_c = aL_x^2 + bL_y^2 + cL_z^2, \quad (2.137)$$

where the constants a , b and c are all different. Show that when the angular momentum of the isolated ion is $l = 1$, V_c removes the orbital degeneracy, leaving only the spin degeneracy $2s + 1$. Show that the expectation value of each component of \mathbf{L} is zero in the ground state.

2.14 Jahn–Teller Distortion

In solids, all orbital degeneracy can be removed at low temperature by a distortion of the crystal lattice known as Jahn–Teller distortion [47, 49, 50]. Indeed, distorting the lattice always leads to a reduction in energy of one of the electron states, thereby lowering the ground state energy. Let us consider an atomic multiplet ($l \neq 0$) in a uniform electric field (the Stark effect). This electric field removes orbital degeneracy for different values of $|m_l|$ by shifting the energies linearly in the field strength (the linear Stark effect) [42]. Another theorem [41] requires the mean energy (centre of gravity) of the states with different $|m|$ values to remain the same. If the system can deform in such a way that non-zero electric field occurs at the ion, the ground state energy is lowered. In a solid, the situation is more complex. Firstly, the crystalline field is not uniform, and secondly, this is a cooperative phenomenon involving all ions in the solid [51].

As an example, let us consider a Cu^{++} ion at an octahedral site in a cube, as in CuCr_2O_4 or K_2CuF_4 crystals. In the crystalline field of the cube (symmetry group O_h), the ground state E is made up of two degenerate orbital states $\langle r|+\rangle = d_{x^2-y^2}$ and $\langle r|-\rangle = d_{3z^2-r^2}$. Since this is a two-level system, we can define Pauli matrices on the subspace spanned by $|+\rangle$ and $|-\rangle$ such that

$$\sigma_z|\pm\rangle = \pm|\pm\rangle, \quad \sigma_x|\pm\rangle = |\mp\rangle. \quad (2.138)$$

In its octahedral site, the Cu^{++} ion forms a bond with the p orbitals of the six neighbouring oxygens (or fluorines) on the \hat{x} , \hat{y} and \hat{z} axes (see Fig. 2.14). These have coordinates (X_i, Y_i, Z_i) . Distortion of the crystal is due to an

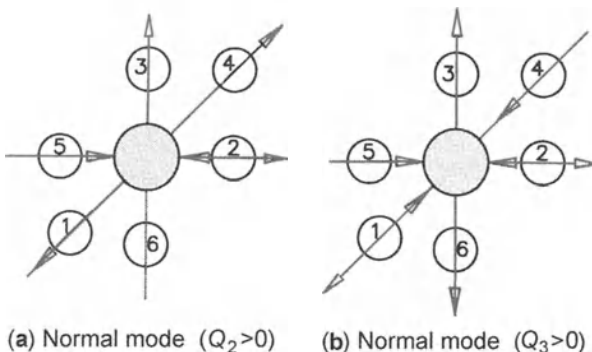


Fig. 2.14. Illustration of the Jahn–Teller theorem in the particular case of orbits $d_{x^2-y^2}$ and $d_{3z^2-r^2}$ (ground state of the $3d^9$ configuration of the Cu^{++} ion in an octahedral environment). (a) Orthorhombic distortion. (b) Tetragonal distortion

anisotropic shift in the various Cu–O or Cu–F bonds, corresponding to longitudinal optical phonons of energy $\hbar\omega_L$ marked on Fig. 2.14. The collective coordinates of these modes are

$$\begin{aligned} Q_2 &= \frac{1}{\sqrt{2}}[X_1 - X_4 + Y_2 - Y_5], \\ Q_3 &= \frac{1}{\sqrt{6}}[2(Z_3 - Z_6) - X_1 + X_4 - Y_2 + Y_5]. \end{aligned} \quad (2.139)$$

The Q_3 mode generates tetragonal distortion along the \hat{z} axis and the Q_2 mode, a symmetric rhombohedral distortion. The potential energy of these elastic distortions is to first harmonic order

$$\mathcal{H}_{\text{ph}} = \frac{\hbar\omega_L}{2}(Q_2^2 + Q_3^2). \quad (2.140)$$

The theory of the crystalline field shows that each of these distortions reduces the ground state degeneracy. The linear coupling between coordinates Q_2 and Q_3 and states $|\pm\rangle$ is then simply

$$\mathcal{H}_c = -g\sqrt{\hbar\omega_L}(\sigma_z Q_3 + \sigma_x Q_2), \quad (2.141)$$

where the Jahn–Teller coupling parameter g has dimensions equal to the square root of an energy and can be calculated from the theory of the crystalline field. Straightforward calculation shows that the eigenvalues and eigenvectors of $\mathcal{H} = \mathcal{H}_c + \mathcal{H}_{\text{ph}}$ in the $|\pm\rangle$ subspace are

$$\varepsilon_{\theta,+} = \frac{\hbar\omega_L Q^2}{2} - g\sqrt{\hbar\omega_L Q^2}, \quad |\theta+\rangle = \cos\frac{\theta}{2}|+\rangle + \sin\frac{\theta}{2}|-\rangle, \quad (2.142)$$

$$\varepsilon_{\theta,-} = \frac{\hbar\omega_L Q^2}{2} + g\sqrt{\hbar\omega_L Q^2}, \quad |\theta-\rangle = -\sin\frac{\theta}{2}|+\rangle + \cos\frac{\theta}{2}|-\rangle, \quad (2.143)$$

where $Q^2 = Q_2^2 + Q_3^2$ and $\tan\theta = Q_2/Q_3$. The zero temperature distortion is determined by minimising the smaller eigenvalue $\varepsilon_{\theta,+}$ with respect to Q to give

$$\varepsilon_{\theta,+} = -\frac{g^2}{2}, \quad Q_{\text{eq}} = \frac{g}{\sqrt{\hbar\omega_L}}. \quad (2.144)$$

The angle θ measuring the relative fractions of distortions Q_3 and Q_2 ,

$$\langle \theta, +|\sigma_z|\theta, +\rangle = \cos \theta, \quad \langle \theta, +|\sigma_x|\theta, +\rangle = \sin \theta, \quad (2.145)$$

remains undetermined. $\theta = 0$ describes tetragonal distortion along the \hat{z} axis, while $\theta = 2\pi/3$ and $\theta = -2\pi/3$ are tetragonal distortions along the \hat{x} and \hat{y} axes, respectively. The value of θ is determined by other contributions, such as the anharmonic vibration terms $\mathcal{H}_{\text{an}} = -\Lambda(Q_3^3 - 3Q_2Q_3^2)$ which favour $\theta = 0$ for $\Lambda > 0$. There are also higher order coupling terms which may contribute to determination of θ . A priori, θ can take different values at different octahedral sites. Two cases are often encountered:

1. All values of θ are the same throughout the crystal. This is a ferromagnetic system of distortions θ_i .
2. When the values θ_0 and $\theta_0 + \pi$ alternate across the crystal, this is an anti-ferromagnetic system. We can then define two sublattices corresponding to the two values of θ , in complete analogy with Néel antiferromagnetism.

Jahn–Teller distortion induces a change in symmetry and thereby generates a second order phase transition [see Chap. 4(I)]. However, anharmonic terms tend to make this transition weakly first order. The harmonic and anharmonic contributions of the phonons are well described by the total free energy F , containing the Jahn–Teller term. In general, the phonon contribution to the free energy is greater in the symmetric phase (cubic) than in the non-symmetric phase (tetragonal). If the Jahn–Teller coupling term g is not large enough, the phonon entropic contributions in the symmetric phase can stabilise it and prevent any Jahn–Teller instability from occurring.

Finally, the spin–orbit interaction is generally incompatible with Jahn–Teller distortion. In fact, the Jahn–Teller coupling distinguishes between two real wave functions. Now the expected value of the spin–orbit Hamiltonian \mathcal{H}_{so} is zero if the orbital functions are real. Jahn–Teller distortion becomes impossible when $\langle \mathcal{H}_{\text{so}} \rangle \gg g^2$. This explains why such distortion does not occur in the rare earths. There are a few counterexamples amongst the heavy transition ions, when the ionic spins have antiferromagnetic organisation, because the orbital states are then no longer equivalent [51].

2.15 Disappearance of Orbital Angular Momentum in Transition Ions

We shall consider here the degeneracy associated with time reversal symmetry T . This often called Kramers degeneracy. To begin with, we neglect spin. It can then be shown that the operator K representing time reversal symmetry (symmetry under $t \rightarrow -t$) is antihermitian,

$$K\psi(\mathbf{r}, t) = \psi^*(\mathbf{r}, t). \quad (2.146)$$

Consider the superposition

$$\begin{aligned} \psi(\mathbf{r}, t) &= \psi_1(\mathbf{r}, t) + \psi_2(\mathbf{r}, t) \\ &= \exp\left(-i\frac{\varepsilon_1 t}{\hbar}\right)\phi_1(\mathbf{r}) + \exp\left(-i\frac{\varepsilon_2 t}{\hbar}\right)\phi_2(\mathbf{r}) \end{aligned} \quad (2.147)$$

of two stationary states ψ_1 and ψ_2 . From the definition of the operator K , the images $\psi'_{1,2}(\mathbf{r}, t) = K\psi_{1,2}(\mathbf{r}, t)$ must satisfy the Schrödinger equation with t replaced by $-t$. Hence the images of $\psi_{1,2}$ are

$$\psi'_{1,2}(\mathbf{r}, t) = K\psi_{1,2}(\mathbf{r}, t) = \exp\left(i\frac{\varepsilon_{1,2} t}{\hbar}\right)K[\phi_{1,2}(\mathbf{r})]. \quad (2.148)$$

As the Schrödinger equation is linear, we must have

$$\begin{aligned} \psi'(\mathbf{r}, t) &= K\psi(\mathbf{r}, t) \\ &= \exp\left(i\frac{\varepsilon_1 t}{\hbar}\right)K[\phi_1(\mathbf{r})] + \exp\left(i\frac{\varepsilon_2 t}{\hbar}\right)K[\phi_2(\mathbf{r})], \end{aligned} \quad (2.149)$$

and this is only possible if the operator K is antihermitian. Applying this property to the matrix elements of the orbital angular momentum \mathbf{L} , we find

$$\langle n|\mathbf{L}|m\rangle = \langle n|K^{-1}K\mathbf{L}K^{-1}K|m\rangle. \quad (2.150)$$

\mathbf{L} is odd with respect to time reversal, so that $K\mathbf{L}K^{-1} = -\mathbf{L}$. Moreover, an antihermitian operator reverses initial and final states: $K|m\rangle = \langle m|^*$ and $\langle n|K^{-1} = |n\rangle^*$. Hence,

$$\langle n|\mathbf{L}|m\rangle = -\langle m|\mathbf{L}|n\rangle^*. \quad (2.151)$$

For the particular case $m = n$, it follows that the expectation value of \mathbf{L} is purely complex. However, this is an observable quantity and measurement in a stationary state must yield a real number. Therefore, $\langle n|\mathbf{L}|n\rangle = 0$. This argument is only valid for non-degenerate states, otherwise $K|n\rangle = \langle n|^* = \langle n'|$. This is the case if the ion contains an odd number of electrons. Materials containing transition ions often exhibit tetragonal distortions which remove all ground state degeneracy. The orbital angular momentum then disappears in the ground state. We deduce that magnetism in materials containing transition ions is mainly due to spin. This result is illustrated by Table 3.1 in Chap. 3(I), comparing the spin moment $2\sqrt{S(S+1)}$ with the moment observed in units of the Bohr magneton. Agreement is good, even if for heavier ions the spin-orbit coupling gives rise to small deviations. Taking spin into account, the time reversal operator is $T = iK\sigma_y$, where K is the complex conjugation operator as above. Time reversal invariance does not remove spin degeneracy. Representing the wave functions of the degenerate doublet ψ^\pm in terms of products of spatial and spin wave functions, $\phi(\mathbf{r})$ and χ , respectively, we have

$$\psi^+(\mathbf{r}) = \phi_1(\mathbf{r})\chi(\uparrow) + \phi_2(\mathbf{r})\chi(\downarrow), \quad (2.152)$$

$$\psi^-(\mathbf{r}) = \phi_2(\mathbf{r})^*\chi(\uparrow) - \phi_1(\mathbf{r})^*\chi(\downarrow). \quad (2.153)$$

Invariance with respect to T requires these two states to be doubly degenerate and to transform by

$$T\psi^+ = \psi^-, \quad (2.154)$$

$$T\psi^- = -\psi^-. \quad (2.155)$$

This doublet of states is called the Kramers doublet [52]. In the presence of a magnetic field, T is no longer a symmetry and there is no Kramers degeneracy.

3. Exchange Interactions

In a solid, interactions between electrons are often significant and extraordinarily complex. Fortunately Pauli's principle restricts the possible wave functions of an electron system. For most insulating solids, the problem of electron interactions can be reduced to a problem of coupled spins. The present chapter discusses this non-trivial equivalence, difficult to justify in practice. The notion of energy exchange is illustrated by several examples from atomic and molecular physics. These will also serve to introduce the tools of second quantisation which are essential for representing states of several electrons.

3.1 Direct Exchange Between Spins

Dipole-dipole interactions between spins, of the order

$$\mu_0 \mu_B^2 / a_0^3 \approx \alpha^2 R_y \approx 1 \text{ K} ,$$

are much too weak to cause ferromagnetism. Electron magnetism comes from the Coulomb interaction between electrons which forces spins into ordered states, because of the Pauli principle. Indeed the latter requires the n -fermion wave function to be completely antisymmetric in the exchange of any two particles (including their spins). Neglecting spin-orbit interactions, the wave function is the product of spatial and spin wave functions. The symmetry of the spatial wave function is determined by the Coulomb interaction which must be minimal in the ground state. Given the global antisymmetry requirement, the spin wave function is then determined too. Exchange interactions therefore result mainly from the chemical bond. In order to understand how a certain ion gives rise to ferromagnetic exchange in an ionic solid, whilst giving antiferromagnetic exchange in a molecular solid, we must begin by examining the chemical bonds.

The main point here is to show that the Hamiltonian for a solid, with its complex electrostatic forces, can be parametrised entirely in terms of the spins of the ions making it up. The parameters in this effective Hamiltonian involve overlaps of exact wave functions of ions in the solid and they are not easy to calculate. Experimental determination is often simpler and more accurate. The effective Hamiltonian is usually taken to be Heisenberg's [53, 54, 55]

$$H_{\text{eff}} = - \sum_{i,j} J_{i,j} \mathbf{S}_i \cdot \mathbf{S}_j , \quad (3.1)$$

where $J_{i,j}$ are the exchange constants and \mathbf{S}_i the total spin of the i th ion in the solid. Although difficult to work with, this Hamiltonian is already vastly simpler than the initial Hamiltonian which described the n electrons of each ion in a solid containing L ions all interacting together via the Coulomb interaction, and included other degrees of freedom too. Before showing how the Hamiltonian can be reduced to this simple form, we begin by studying electrons in an atom, and then in a molecule. In this context the nature of the interactions between electrons is clear.

3.2 Atoms with Two Valence Electrons

Inner electron shells modify the potential felt by valence electrons. Let $U(\mathbf{r})$ be the effective Coulomb potential of the nucleus and inner electron shells given, for example, by the Hartree–Fock approximation (described in Sect. 3.6). Since the spin–orbit coupling remains small compared with Coulomb terms, the wave function of the two valence electrons is a product of spatial and spin wave functions:

$$\Psi(\mathbf{r}_1, \sigma_1; \mathbf{r}_2, \sigma_2) = \psi(\mathbf{r}_1, \mathbf{r}_2) \chi(\sigma_1, \sigma_2) . \quad (3.2)$$

We obtain an approximate form of the Hamiltonian

$$\mathcal{H} = \mathcal{H}_0(\mathbf{r}_1) + \mathcal{H}_0(\mathbf{r}_2) + V(\mathbf{r}_1, \mathbf{r}_2) , \quad (3.3)$$

by treating the Coulomb repulsion

$$V(\mathbf{r}_1, \mathbf{r}_2) = \frac{e^2}{4\pi\epsilon_0 |\mathbf{r}_1 - \mathbf{r}_2|}$$

between the two electrons as a small perturbation. Here, \mathcal{H}_0 is the Hamiltonian of one valence electron,

$$\mathcal{H}_0 = \frac{\mathbf{p}^2}{2m} + U(r) . \quad (3.4)$$

Let $\phi_a(\mathbf{r})$ and $\phi_b(\mathbf{r})$ be its two lowest energy eigenstates, with energies $\varepsilon_a, \varepsilon_b$. The approximation is made by solving the eigenvalue equation $\det(\mathcal{H} - \varepsilon I) = 0$ in a subspace spanned by symmetrised and antisymmetrised combinations of orbital states $\phi_a(\mathbf{r})$ and $\phi_b(\mathbf{r})$. The state space is thereby limited to wave functions

$$\begin{aligned} \psi_S(\mathbf{r}_1, \mathbf{r}_2) &= \frac{1}{\sqrt{2}} [\phi_a(\mathbf{r}_1)\phi_b(\mathbf{r}_2) + \phi_a(\mathbf{r}_2)\phi_b(\mathbf{r}_1)] , \\ \psi_A(\mathbf{r}_1, \mathbf{r}_2) &= \frac{1}{\sqrt{2}} [\phi_a(\mathbf{r}_1)\phi_b(\mathbf{r}_2) - \phi_a(\mathbf{r}_2)\phi_b(\mathbf{r}_1)] . \end{aligned} \quad (3.5)$$

These are eigenstates of the permutation operator P of the two particles, with eigenvalues +1 for the symmetric state ψ_S and -1 for the antisymmetric state ψ_A . With each orbital state we must associate one of the possible spin states,

$$\begin{aligned}\chi_T^+(1, 2) &= \chi_1(\uparrow)\chi_2(\uparrow), & \chi_T^-(1, 2) &= \chi_1(\downarrow)\chi_2(\downarrow), \\ \chi_T^0(1, 2) &= \frac{1}{\sqrt{2}} [\chi_1(\uparrow)\chi_2(\downarrow) + \chi_1(\downarrow)\chi_2(\uparrow)], \\ \chi_S(1, 2) &= \frac{1}{\sqrt{2}} [\chi_1(\uparrow)\chi_2(\downarrow) - \chi_1(\downarrow)\chi_2(\uparrow)],\end{aligned}\quad (3.6)$$

in such a way that the overall wave function (3.2) is antisymmetric, as required by the Pauli principle. These states are eigenstates of S_{tot}^2 , where $\mathbf{S}_{\text{tot}} = \mathbf{S}_1 + \mathbf{S}_2$, with eigenvalues $2\hbar^2$ for the triplet ($S = 1$) and 0 for the singlet ($S = 0$). We wish to establish an isomorphism between the low energy electron states (ψ_S and ψ_A) and the spin states. This isomorphism between the two state spaces can be used to represent the orbital Hamiltonian purely in terms of spin operators. Since \mathcal{H} commutes with the permutation operator P , it is diagonalised in the (S, A) subspace:

$$\mathcal{H} = \begin{pmatrix} \varepsilon_a + \varepsilon_b + u + j & 0 \\ 0 & \varepsilon_a + \varepsilon_b + u - j \end{pmatrix}, \quad (3.7)$$

where u and j are the matrix elements of the Coulomb interaction V between electrons,

$$u = \int d^3r_1 d^3r_2 |\phi_a(\mathbf{r}_1)|^2 V(\mathbf{r}_1, \mathbf{r}_2) |\phi_b(\mathbf{r}_2)|^2, \quad (3.8)$$

$$j = \int d^3r_1 d^3r_2 \phi_a^*(\mathbf{r}_1) \phi_b^*(\mathbf{r}_2) V(\mathbf{r}_1, \mathbf{r}_2) \phi_b(\mathbf{r}_1) \phi_a(\mathbf{r}_2). \quad (3.9)$$

u is called the Hartree or direct term and j the Fock or exchange term. j is the electrostatic energy of the charge distribution $e\phi_a^*(\mathbf{r})\phi_b(\mathbf{r})$ and is a positive quantity. It is therefore the antisymmetric spatial wave function which has the lowest energy. We must associate the (symmetric) spin triplet χ_T with this wave function in order to construct the ground state. The singlet state, associated with the symmetric spatial wave function, lies at energy $2j$ above the ground state energy. Hence Coulomb repulsion favours the state in which spins are parallel. This is the first Hund rule, which will be stated more precisely in the next section. The energy $J = 2j$ is often called the exchange energy for the following reason. When we place the electrons in state $\phi_a(\mathbf{r}_1)\phi_b(\mathbf{r}_2)$, V connects this state with the permuted state $\phi_a(\mathbf{r}_2)\phi_b(\mathbf{r}_1)$ via the matrix element j . Over a small time interval Δt , the amplitude of the permuted state increases as $j\Delta t$. j therefore measures the initial rate of exchange of two numbered electrons in two states.

The spectrum and eigenstates of the spin Hamiltonian

$$\mathcal{H}_{\text{eff}} = E_0 - \frac{j}{2} \boldsymbol{\sigma}_1 \cdot \boldsymbol{\sigma}_2 \quad \text{with} \quad E_0 = \varepsilon_a + \varepsilon_b + u - \frac{j}{2} \quad (3.10)$$

coincide with those of \mathcal{H} itself (here σ_1 and σ_2 are the Pauli matrices for spin 1 and spin 2). Indeed, the exchange term $\sigma_1 \cdot \sigma_2$ can be expressed in terms of the projection operators onto the triplet and singlet states. For spin 1/2, the projection operators are

$$P_T = \frac{1}{4}(3 + \sigma_1 \cdot \sigma_2) , \quad (3.11)$$

$$P_S = \frac{1}{4}(1 - \sigma_1 \cdot \sigma_2) . \quad (3.12)$$

In terms of these the Hamiltonian becomes

$$\mathcal{H}_{\text{eff}} = E_0 - \frac{j}{2}(P_T - 3P_S) , \quad (3.13)$$

which coincides with the restriction of the electron Hamiltonian to the two lowest energy states.

The above analysis can be put into the language of second quantisation (see Appendix B). An antisymmetric wave function for N independent particles can be obtained by successive application of creation operators a_i^\dagger which create a particle in the state i . For example,

$$\begin{aligned} \phi_a(\mathbf{r}) &= \langle \mathbf{r} | a \rangle = \langle \mathbf{r} | a_a^\dagger | 0 \rangle , \\ \psi_A(\mathbf{r}_1, \mathbf{r}_2) &= \frac{1}{\sqrt{2}} [\phi_a(\mathbf{r}_1)\phi_b(\mathbf{r}_2) - \phi_a(\mathbf{r}_2)\phi_b(\mathbf{r}_1)] \\ &= \langle \mathbf{r}_1, \mathbf{r}_2 | a, b \rangle = \langle \mathbf{r}_1, \mathbf{r}_2 | a_a^\dagger a_b^\dagger | 0 \rangle . \end{aligned} \quad (3.14)$$

Since operators a_a^\dagger and a_b^\dagger anticommute, the Pauli principle $|a, b\rangle = -|b, a\rangle$ follows automatically. We then include spin degrees of freedom to obtain the triplet state

$$a_{a\uparrow}^\dagger a_{b\uparrow}^\dagger | 0 \rangle , \quad a_{a\uparrow}^\dagger a_{b\downarrow}^\dagger | 0 \rangle , \quad a_{a\downarrow}^\dagger a_{b\downarrow}^\dagger | 0 \rangle ,$$

and the singlet state

$$a_{a\downarrow}^\dagger a_{b\uparrow}^\dagger | 0 \rangle .$$

From a_i and a_i^\dagger we define field operators $\psi^\dagger(\mathbf{r})$ and $\psi(\mathbf{r})$ by

$$\psi_\sigma^\dagger(\mathbf{r}) = \sum_{i=ab} \phi_i^*(\mathbf{r}) a_{i,\sigma}^\dagger , \quad \psi_\sigma(\mathbf{r}) = \sum_{i=ab} \phi_i(\mathbf{r}) a_{i,\sigma} , \quad (3.15)$$

which create and destroy a particle of spin σ at the point \mathbf{r} . The operator

$$\rho(\mathbf{r}) = \sum_\sigma \psi_\sigma^\dagger(\mathbf{r}) \psi_\sigma(\mathbf{r}) \quad (3.16)$$

measures the electron density at \mathbf{r} . As the Hamiltonian \mathcal{H}_0 only depends on the coordinates of one particle, we can associate an energy density with it by analogy:

$$\varepsilon(\mathbf{r}) = \sum_\sigma \psi_\sigma^\dagger(\mathbf{r}) \mathcal{H}_0(\mathbf{r}) \psi_\sigma(\mathbf{r}) .$$

Integrating over all space, we obtain the representation of \mathcal{H}_0 in terms of number operators $n_{i,\sigma} = a_{i,\sigma}^\dagger a_{i,\sigma}$:

$$\mathcal{H}_0 = \sum_\alpha \varepsilon_\alpha n_\alpha . \quad (3.17)$$

This counts the number of particles in each of the states indexed by α , where $\alpha \equiv a\sigma, b\sigma$. This representation is diagonal in terms of the number operators because the field operators (3.15) were defined on a basis of eigenstates of \mathcal{H}_0 .

The interaction term V between electrons is reexpressed by first writing it in an obviously symmetric form

$$V = \frac{1}{2} \sum_{i \neq j} V(\mathbf{r}_i, \mathbf{r}_j) , \quad (3.18)$$

and then calculating its expectation value. This is done by multiplying by the electron densities at \mathbf{r}_i and \mathbf{r}_j to give

$$V = \frac{1}{2} \int d^3r d^3r' \rho(\mathbf{r}) V(\mathbf{r}, \mathbf{r}') \rho(\mathbf{r}') . \quad (3.19)$$

Using the representation of field operators (3.15) on the basis of states of \mathcal{H}_0 , we obtain the corresponding representation of the interaction potential:

$$V = \frac{1}{2} \sum_{\alpha\beta\gamma\delta} v_{\alpha\beta,\gamma\delta} a_\alpha^\dagger a_\beta^\dagger a_\delta a_\gamma , \quad (3.20)$$

where spin degrees of freedom are implicitly included in indices $\alpha \equiv (i, \sigma)$, $\beta \equiv (j, \sigma')$, and so on. All creation operators have been brought together on the left and destruction operators on the right. A minus sign appears when V is normal ordered in this way, because of anticommutation rules. This is compensated by interchanging a_γ and a_δ . The only non-zero matrix elements

$$v_{\alpha\beta,\gamma\delta} = \int d^3r d^3r' \phi_i^*(\mathbf{r}) \phi_j^*(\mathbf{r}') V(\mathbf{r}, \mathbf{r}') \phi_k(\mathbf{r}) \phi_l(\mathbf{r}') \quad (3.21)$$

are $u = v_{a\sigma b\sigma', a\sigma b\sigma'}$ and $j = v_{a\sigma b\sigma', b\sigma a\sigma'}$. This is because V has no explicit spin dependence. The matrix elements of V can be reexpressed in the space of completely antisymmetric states $|\alpha\beta\rangle = a_\alpha^\dagger a_\beta^\dagger |0\rangle = -|\beta\alpha\rangle$ [see Appendix B, equation (B.35)]:

$$\langle \alpha\beta | V | \gamma\delta \rangle = v_{\alpha\beta,\gamma\delta} - v_{\alpha\beta,\delta\gamma} . \quad (3.22)$$

V does not depend on the spin. Matrix elements between singlet and triplet states are therefore zero so, for example,

$$\langle a\downarrow, b\uparrow | V | a\uparrow, b\downarrow \rangle = 0 .$$

From (3.20) and (3.22) we obtain an equivalent representation of the interaction,

$$V = \frac{1}{4} \sum_{\alpha\beta\gamma\delta} \langle \alpha\beta | V | \gamma\delta \rangle a_\alpha^\dagger a_\beta^\dagger a_\delta a_\gamma , \quad (3.23)$$

which is diagonal in the sense that

$$\langle \alpha\beta | V | \gamma\delta \rangle = V_{\alpha\beta} \delta_{\alpha\gamma} \delta_{\beta\delta} ,$$

when V does not depend explicitly on spin. For example, on triplet states

$$\langle a\uparrow, b\sigma | V | a\uparrow, b\sigma \rangle = u + j ,$$

and on the singlet state,

$$\langle a\downarrow, b\uparrow | V | a\downarrow, b\uparrow \rangle = u - j .$$

Using commutation relations between operators a_α , the interaction can be expressed entirely in terms of the overlap integrals u and j ,

$$V = \frac{1}{2} \sum_{i \neq j, \sigma, \sigma'} \left(u n_{i\sigma} n_{j\sigma'} - j a_{i\sigma}^\dagger a_{i\sigma'} a_{j\sigma'}^\dagger a_{j\sigma} \right) . \quad (3.24)$$

We now eliminate second quantisation operators $a_{i\sigma}$ in favour of spin operators

$$S_i^z = \frac{1}{2} \left(a_{i\uparrow}^\dagger a_{i\uparrow} - a_{i\downarrow}^\dagger a_{i\downarrow} \right) , \quad S_i^+ = a_{i\uparrow}^\dagger a_{i\downarrow} , \quad S_i^- = a_{i\downarrow}^\dagger a_{i\uparrow} , \quad (3.25)$$

to yield once again the total Hamiltonian \mathcal{H}_{eff}

$$\mathcal{H}_{\text{eff}} = \sum_{j \neq i\sigma} \left[\varepsilon_{i\sigma} + \left(u - \frac{j}{2} \right) \frac{\bar{n}_j}{2} \right] n_{i\sigma} - 2j \mathbf{S}_i \cdot \mathbf{S}_j , \quad (3.26)$$

where $\bar{n}_j = n_{j\uparrow} + n_{j\downarrow}$ is the number of electrons per j orbital. (We have used

$$\begin{aligned} & a_{a\uparrow}^\dagger a_{a\uparrow} a_{b\uparrow}^\dagger a_{b\uparrow} + a_{a\downarrow}^\dagger a_{a\downarrow} a_{b\downarrow}^\dagger a_{b\downarrow} \\ &= \frac{1}{2} \left(a_{a\uparrow}^\dagger a_{a\uparrow} + a_{a\downarrow}^\dagger a_{a\downarrow} \right) \left(a_{b\uparrow}^\dagger a_{b\uparrow} + a_{b\downarrow}^\dagger a_{b\downarrow} \right) \\ &+ \frac{1}{2} \left(a_{a\uparrow}^\dagger a_{a\uparrow} - a_{a\downarrow}^\dagger a_{a\downarrow} \right) \left(a_{b\uparrow}^\dagger a_{b\uparrow} - a_{b\downarrow}^\dagger a_{b\downarrow} \right) , \end{aligned} \quad (3.27)$$

an algebraic identity.) In our example we have $i \equiv a$ and $j \equiv b$ so that $\bar{n}_j = 1$. The main interest in these representations (3.20), (3.23) and (3.26) of the Hamiltonian in the language of second quantisation is that they do not depend on the number of particles present. For example, (3.26) is the starting point for the Hartree–Fock approximation, however many interacting electrons there may be. This is the approximation used to demonstrate the Hund rules, which specify spin and angular momentum of the ionic and atomic ground states.

Table 3.1. Configuration of transition ions in the $3d$ shell

Ion	Config.	$^{2S+1}L_j$	$2\sqrt{S(S+1)}$	μ_{exp}	$g_j \sqrt{j(j+1)}$	λ_{so}
Ti $^{3+}$	$3s^2 p^6 d^1$	2D	1.73	1.8	1.55	154
V $^{3+}$	$3s^2 p^6 d^2$	3F	2.83	2.8	1.63	105
Cr $^{3+}$, V $^{2+}$	$3s^2 p^6 d^3$	4F	3.87	3.8	0.77	91
Mn $^{3+}$, Cr $^{2+}$	$3s^2 p^6 d^4$	5D	4.0	4.9	0	88
Fe $^{3+}$, Mn $^{2+}$	$3s^2 p^6 d^5$	6S	5.92	5.9	5.92	0
Fe $^{2+}$	$3s^2 p^6 d^6$	5D	4.9	5.4	6.7	-103
Co $^{2+}$	$3s^2 p^6 d^7$	4F	3.87	4.8	6.63	-178
Ni $^{2+}$	$3s^2 p^6 d^8$	3F	2.83	3.2	5.59	-325
Cu $^{2+}$	$3s^2 p^6 d^9$	2D	1.73	1.9	3.55	-829

Ground states can be found from transition ion configurations using the Hund rules. Values of ionic magnetic moments measured in insulators are given in units of the Bohr magneton. They are always close to the spin value $2\sqrt{S(S+1)}$ in the absence of orbital angular momentum [because Jahn–Teller distortion removes degeneracy, as explained in Sects. 2.14(I) and 2.15(I)]. We also compare μ_{exp} with the value $g_j \sqrt{j(j+1)}$ of the magnetic moment when spin–orbit coupling (*last column*) dominates (no Jahn–Teller distortion). This is never actually the case, even if the magnetic moment is slightly greater than the spin for the heaviest elements (Ni $^{2+}$, Cu $^{2+}$).

The Hund rules only give the ground state configuration. In the discussion of superexchange or van Vleck paramagnetism, excited states enter the process as intermediate (or virtual) states. We must then study excited states in the solid which are very different from those of the ion or atom.

Tables 3.1 and 3.2 specify electronic configurations of transition metals and rare earths, respectively. For unusual ionic configurations, the periodic table at the end of the book can be used.

3.4 The Hydrogen Molecule

In the Heitler–London approximation [57, 58], the mass difference between electrons and nuclei is used to decouple their degrees of freedom and fix the positions of the hydrogen nuclei at \mathbf{R}_a and \mathbf{R}_b . The Hamiltonian describing motion of the two electrons in the field of the two nuclei splits into two hydrogen-like contributions (ions a and b), together with an interaction term including Coulomb repulsion between electrons and attraction towards the other ion (i.e., $1 - b$ and $2 - a$):

$$\mathcal{H} = \mathcal{H}_{1a}(\mathbf{r}_1) + \mathcal{H}_{2b}(\mathbf{r}_2) + V_{\text{int}}(\mathbf{r}_1, \mathbf{r}_2), \quad (3.28)$$

$$\mathcal{H}_{1a} = \frac{p_1^2}{2m} - \frac{e^2}{4\pi\varepsilon_0 r_{1a}}, \quad (3.29)$$

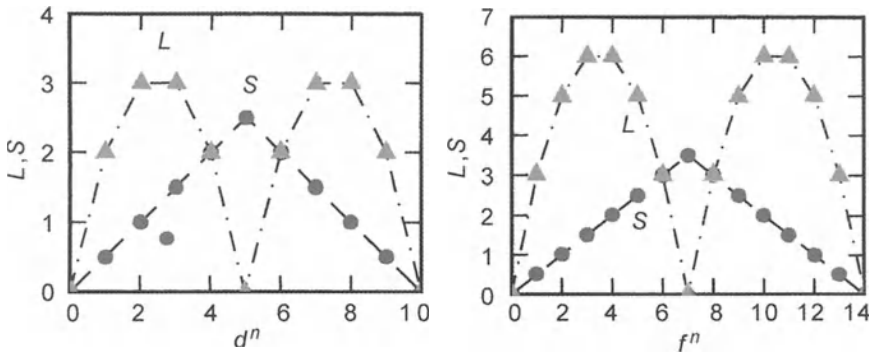


Fig. 3.1. *Left:* Graphical representation of spin and orbital angular momentum of transition ions ($3d$, $4d$ and $5d$ shells). *Right:* The same graph for the rare earths

3.3 The Hund Rules

Magnetic properties of solids depend on total spin and, in certain cases (the rare earths), orbital angular momentum of ions in the material. The Hund rules express the combined effect of Coulomb repulsion (in the Hartree–Fock approximation) and the Pauli principle [56].

Rule 1 Let n denote an atomic shell and l one of the eigenvalues of orbital angular momentum. Electrons occupy the $2(2l+1)$ states of the (n, l) shell in such a way as to maximise the total spin. This rule is not always sufficient to uniquely determine the configuration.

Rule 2 All remaining ambiguity is removed by maximising the total orbital angular momentum L_{tot} .

Consider for example the $3d^2$ configuration (V^{3+} ion). The first rule requires spin $S = 1$. Because of the Pauli principle, one electron is located in an $m_l = 2$ orbital and the other in an $m_l = 1$ orbital, leading to a maximal value of the component $M_L = 2 + 1$ of the total orbital momentum. Adding the two $l = 2$ orbital angular momenta, gives $L = 4, 3, 2, 1$ or 0. But the $L = 4$ orbital state, which includes the component $M_L = 4$, is not consistent with Pauli's principle for total spin $S = 1$. The largest possible value of L is thus $L = 3$, i.e., a ${}^3\text{F}$ ground state of the V^{3+} ion. The $3d^8$ configuration (Ni^{2+}) has two unoccupied orbitals. Considered as positive charges, these holes have a $3d^2$ configuration, giving them the same ground state.

Rule 3 This rule determines whether S and L are parallel or antiparallel. The eigenvalue of total angular momentum $\mathbf{J} = \mathbf{L} + \mathbf{S}$ is $|L - S|$ if the shell is less than half filled, and $L + S$ if it is more than half filled (unoccupied orbitals are considered as holes). This rule comes from the spin-orbit coupling discussed in Sect. 2.9(I), which is also responsible for magnetic anisotropy.

Table 3.2. Rare earth electronic configurations and ground states. Experimental and theoretical values of magnetic moments are given in units of the Bohr magneton. Curie constants of rare earths are also tabulated

Ion	Config.	$^{2S+1}L_J$	$2\sqrt{S(S+1)}$	$\mu = g_j \sqrt{j(j+1)}$	μ_{exp}	C_j
La ³⁺	$4f^0 5s^2 p^6$	0S_0	0	0	0	0
Ce ³⁺	$4f^1 5s^2 p^6$	${}^2F_{5/2}$	6/7	2.54	2.6	0.804
Pr ³⁺	$4f^2 5s^2 p^6$	3H_4	4/5	3.58	3.5	1.60
Nd ³⁺	$4f^3 5s^2 p^6$	${}^4I_{9/2}$	8/11	3.62	3.6	1.64
Pm ³⁺	$4f^4 5s^2 p^6$	6I_4	3/5	2.68	2.7	0.900
Sm ³⁺	$4f^5 5s^2 p^6$	${}^6H_{5/2}$	2/7	0.845	1.5	0.893
Eu ³⁺	$4f^6 5s^2 p^6$	7F_0	0	0	3.4	0
Gd ³⁺	$4f^7 5s^2 p^6$	${}^8S_{7/2}$	2	7.94	8.0	7.88
Tb ³⁺	$4f^8 5s^2 p^6$	7F_6	3/2	9.72	9.5	11.82
Dy ³⁺	$4f^9 5s^2 p^6$	${}^6H_{15/2}$	4/3	10.65	10.5	14.17
Ho ³⁺	$4f^{10} 5s^2 p^6$	5I_8	5/4	10.61	10.4	14.07
Er ³⁺	$4f^{11} 5s^2 p^6$	${}^4I_{15/2}$	6/5	9.58	9.5	11.48
Tm ³⁺	$4f^{12} 5s^2 p^6$	3H_6	7/6	7.56	7.3	7.15
Yb ³⁺	$4f^{13} 5s^2 p^6$	${}^2F_{7/2}$	8/7	4.54	4.5	2.57
Lu ³⁺	$4f^{14} 5s^2 p^6$	0S_0	0	0	0	0

$$V_{\text{int}}(\mathbf{r}_1, \mathbf{r}_2) = \frac{e^2}{4\pi\epsilon_0} \left(\frac{1}{R_{ab}} + \frac{1}{r_{12}} - \frac{1}{r_{2a}} - \frac{1}{r_{1b}} \right), \quad (3.30)$$

where distances r_{1a} , r_{1b} , etc. are defined in Fig. 3.2. Let $\phi_a(\mathbf{r}_1) \equiv \phi(\mathbf{r}_{1a})$ and $\phi_b(\mathbf{r}_2) \equiv \phi(\mathbf{r}_{2b})$ be the ground states of \mathcal{H}_{1a} and \mathcal{H}_{2b} , respectively, with energy ε_0 . In contrast with the situation in the atom, these two orbital states are not orthogonal. This complicates the process of diagonalising the residual Coulomb interaction V_{int} . Symmetrised and antisymmetrised wave functions for the two electrons are

$$\Psi_S(\mathbf{r}_1, \mathbf{r}_2) = [2(1+l^2)]^{-1/2} [\phi_a(\mathbf{r}_1)\phi_b(\mathbf{r}_2) + \phi_a(\mathbf{r}_2)\phi_b(\mathbf{r}_1)], \quad (3.31)$$

$$\Psi_A(\mathbf{r}_1, \mathbf{r}_2) = [2(1-l^2)]^{-1/2} [\phi_a(\mathbf{r}_1)\phi_b(\mathbf{r}_2) - \phi_a(\mathbf{r}_2)\phi_b(\mathbf{r}_1)]. \quad (3.32)$$

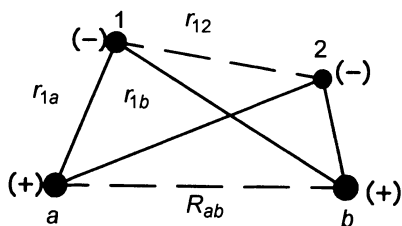


Fig. 3.2. Coordinates of the ions and the two electrons in a hydrogen molecule. Repulsive interactions are represent by dashed lines

These are eigenstates of the permutation operator and hence are not coupled by the perturbation V_{int} , to all orders of the perturbative expansion. These states, having different symmetries, are orthogonal. They have been normalised, taking into account the overlap l of orbitals $\phi_a(\mathbf{r})$ and $\phi_b(\mathbf{r})$. Direct and exchange terms of the interaction $V_{\text{int}}(\mathbf{r}_1, \mathbf{r}_2)$ are defined by

$$l = \int d^3r \phi_a(\mathbf{r})^* \phi_b(\mathbf{r}), \quad (3.33)$$

$$\begin{aligned} u &= \int d^3r_1 d^3r_2 V(\mathbf{r}_1, \mathbf{r}_2) |\phi_a(\mathbf{r}_1)\phi_b(\mathbf{r}_2)|^2 \\ &= \int d^3r_1 d^3r_2 V(\mathbf{r}_1, \mathbf{r}_2) |\phi_a(\mathbf{r}_2)\phi_b(\mathbf{r}_1)|^2, \end{aligned} \quad (3.34)$$

$$j = \int d^3r_1 d^3r_2 V(\mathbf{r}_1, \mathbf{r}_2) \phi_a(\mathbf{r}_1)^* \phi_a(\mathbf{r}_2) \phi_b(\mathbf{r}_2)^* \phi_b(\mathbf{r}_1). \quad (3.35)$$

Spatial wave functions (3.31), (3.32) must be multiplied by spin wave functions of appropriate symmetry, in order to satisfy the Pauli principle. In the subspace spanned by Ψ_S and Ψ_A , the eigenvalue equation

$$\langle \Psi_i | H | \Psi_j \rangle = \mathcal{E} \langle \Psi_i | \Psi_j \rangle \quad (3.36)$$

takes the simple form

$$\begin{pmatrix} 2\varepsilon_0 + (u+j)/(1+l^2) & 0 \\ 0 & 2\varepsilon_0 + (u-j)/(1-l^2) \end{pmatrix} = \mathcal{E} \begin{pmatrix} 1 & 0 \\ 0 & 1 \end{pmatrix}. \quad (3.37)$$

It is not always possible to orthonormalise the basis of products of atomic orbitals. In a cubic lattice, there are 6 neighbours, each having an overlap l with its nearest neighbours. If the condition $6l^2 < 1$ does not hold, there is an orthogonality catastrophe and the ‘atomic’ basis cannot be used.

Still using the correspondence between orbital and spin symmetries, the energy difference between triplet and singlet states of a hydrogen molecule is

$$\Delta E \equiv J = E_S - E_T = -2 \frac{ul^2 - j}{1 - l^4}, \quad (3.38)$$

and the Heisenberg Hamiltonian in spin space is

$$\mathcal{H}_{\text{eff}} = 2\varepsilon_0 + \frac{u - jl^2}{1 - l^4} - \frac{J}{4} - J \mathbf{S}_1 \cdot \mathbf{S}_2 \quad (3.39)$$

$$= E_0 - \frac{J}{2} \left[(\mathbf{S}_1 + \mathbf{S}_2)^2 - \frac{3}{2} \right] = E_0 - \frac{J}{4} \boldsymbol{\sigma}_1 \cdot \boldsymbol{\sigma}_2. \quad (3.40)$$

If we ignore the constant E_0 , eigenvalues of \mathcal{H}_{eff} are $-J/4$ for triplet states and $3J/4$ for the singlet state, which gives the electron spectrum. We have left out \hbar from the spin operators. This Hamiltonian can be transcribed into the language of second quantisation exactly as for an atom with two valence electrons.

When the separation between hydrogen atoms is large enough, l becomes small and the exchange energy

$$J \approx 2(j - ul^2) \quad (3.41)$$

is the difference of two terms. As for an atom, j is an electrostatic energy and always positive. u is also a positive quantity. Hence the exchange energy J is a difference which may be positive (ferromagnetism) or negative (anti-ferromagnetism), depending on the values of u , j and l . Spatially, the ground state is either symmetric or antisymmetric. Calculation shows that, for realistic values of the separation R_{ab} between the two ions, the ground state is spatially symmetric. However, for large values of R_{ab} , it is the antisymmetric state which has lowest energy. This contradicts a theorem about differential operators [59], which requires the ground state wave function to have no nodes. The problem arises because the Heitler–London approximation neglects correlations between electrons by using atomic orbitals. The presence of another atom polarises the atomic orbitals and increases the probability of finding the electron between the two ions. Moreover, when the two electrons exchange, they do not do so along the axis joining the two ions, but rather tend to avoid each other in order to minimise Coulomb repulsion. The exchange energy in the Heitler–London approximation has been calculated as a function of R_{ab} by Sugiura [60]:

$$J = Ry \left[-\frac{56}{45} + \frac{4}{15} \left(\gamma + \ln \frac{R}{a} \right) \right] \left(\frac{R}{a} \right)^3 \exp \left(-\frac{2R}{a} \right), \quad (3.42)$$

where γ is Euler's constant and Ry the Rydberg energy, equal to 27.2 eV. For large distances, J becomes positive because of the divergent logarithmic term. Therefore, the Heitler–London approximation gives neither the sign nor the value of the exchange energy correctly at large distances. This puts considerable limits on its usefulness, since it cannot be used as a starting point for perturbative calculation.

Finally, an atom cannot be considered as the limit of a hydrogen molecule when $R_{ab} \rightarrow 0$ since the two orbitals then become identical and when $l \rightarrow 1$, the basis Ψ_S , Ψ_A is no longer defined. This basis can then no longer be used as a basis for orbital functions. We must extend the basis to include the first excited state of the atom (see Sect. 3.2).

Exercise: Antiferromagnetic Exchange Between Three Spins

Consider three spins $1/2$, antiferromagnetically coupled ($J < 0$) in a magnetic field \mathbf{H} along the \hat{z} axis. The Hamiltonian is

$$\mathcal{H} = |J|(\mathbf{S}_1 \cdot \mathbf{S}_2 + \mathbf{S}_2 \cdot \mathbf{S}_3 + \mathbf{S}_3 \cdot \mathbf{S}_1) - \gamma \mathbf{B} \cdot (\mathbf{S}_1 + \mathbf{S}_2 + \mathbf{S}_3). \quad (3.43)$$

1. Which operators commute with \mathcal{H} ? Deduce good quantum numbers for the system.
2. What is the spectrum of the Hamiltonian? Determine the degeneracy of each state and plot the Zeeman diagram.
3. Construct projection operators onto each subspace and interpret the ground state degeneracy physically.

3.5 Effective Exchange Hamiltonian for a Solid

The above results can be generalised to solids when the overlap between atomic orbitals is small [62]. Eigenstates of free atoms are close enough to orbital states of the solid to justify using their quantum numbers. Rotation invariance in the spin space of each atom remains a good symmetry.

A bijective correspondence between orbital and spin states is obtained by introducing a mixed representation of states

$$\Psi_\chi(\mathbf{r}_1, \dots, \mathbf{r}_N; \sigma_1, \dots, \sigma_N) = \mathcal{A}\Phi(\mathbf{r}_1, \dots, \mathbf{r}_N)\chi(\sigma_1, \dots, \sigma_N), \quad (3.44)$$

where the wave function of the solid $\Phi(\mathbf{r}_1, \dots, \mathbf{r}_N)$ is a product over site number of the *exact* wave functions in the potential of the solid. (The number of electrons N is generally greater than the number of sites L , since each ion has several valence orbitals.) These wave functions constitute an orthonormal basis. Each wave function is antisymmetrised at each site so that the Pauli principle is satisfied for the individual atoms. $\chi(\sigma_1, \dots, \sigma_N)$ is an arbitrary spin wave function of all the electrons and \mathcal{A} is the global antisymmetrisation operator, over all sites in the solid, viz.,

$$\mathcal{A} = \frac{1}{N!} \sum_P \delta_P P_{ij} P_\sigma^{ij}. \quad (3.45)$$

The sum here is over all possible permutations of electrons. δ_P is the sign of the permutation and P_{ij} permutes the i and j coordinates,

$$P_{ij} \langle \dots, \mathbf{r}_i, \dots, \mathbf{r}_j, \dots | \Phi \rangle = \langle \dots, \mathbf{r}_j, \dots, \mathbf{r}_i, \dots | \Phi \rangle. \quad (3.46)$$

Likewise, P_σ^{ij} permutes the i and j spins,

$$P_\sigma^{ij} \langle \dots, \sigma_i, \dots, \sigma_j, \dots | \chi \rangle = \langle \dots, \sigma_j, \dots, \sigma_i, \dots | \chi \rangle. \quad (3.47)$$

If all spins are spin 1/2, this permutation operator can be expressed in terms of the Pauli matrices for the i and j spins,

$$P_\sigma^{ij} = \frac{1}{2}(1 + \boldsymbol{\sigma}_i \cdot \boldsymbol{\sigma}_j). \quad (3.48)$$

Exercise

Check that $P_\sigma^2 = 1$ and $P_\sigma |\uparrow\downarrow\rangle = |\downarrow\uparrow\rangle$.

In this representation, the matrix elements of the Hamiltonian are linear combinations of spin matrix elements. Since permutations commute with the Hamiltonian and have a group structure, the matrix element

$$\langle \Psi_\chi | \mathcal{H} | \Psi'_\chi \rangle = \frac{1}{N!^2} \langle \Phi | \otimes \langle \chi | \sum_{P'} \delta_{P'} P' P'_\sigma \mathcal{H} \sum_P \delta_P P P_\sigma | \Phi \rangle \otimes | \chi \rangle \quad (3.49)$$

decomposes into a sum of products of space and spin matrix elements:

$$\langle \Psi_\chi | \mathcal{H} | \Psi'_\chi \rangle = \sum_P \delta_P V_P \langle \chi | P_\sigma | \chi' \rangle \quad \text{where} \quad V_P = \langle \Phi | \mathcal{H} | P_{ij} \Phi \rangle . \quad (3.50)$$

The eigenvalue equation

$$\det (\langle \Psi_1 | \mathcal{H} | \Psi_2 \rangle - E \langle \Psi_1 | \Psi_2 \rangle) = 0 \quad (3.51)$$

determining the energy spectrum of the solid is thus equivalent to the secular equation in spin space, viz.,

$$\det \left[\sum_P \delta_P (V_P - \mathcal{E}) P^\sigma \right] = 0 , \quad (3.52)$$

as far as physical states are concerned. In order to obtain the Heisenberg effective Hamiltonian, we use the representation (3.48) of the spin permutation operator in terms of Pauli matrices. The k, k' matrix element of the secular equation in spin space is then

$$(\langle \Phi_k | \mathcal{H} | \Phi_k \rangle - \mathcal{E}) \delta_{k, k'} - \sum_{i>j} n_i n_j \langle \Phi_k | (\mathcal{H} - \mathcal{E}) P_{ij} \frac{1}{2} (1 + \boldsymbol{\sigma}_i^\alpha \cdot \boldsymbol{\sigma}_j^\beta) | \Phi_{k'} \rangle . \quad (3.53)$$

Indices α and β pick out electrons at sites i and j , while factors n_i and n_j count the number of permutations of electrons between sites i and j . For ions with more than one electron in the outer shell, we use the Wigner–Eckart theorem [see Sect. 2.8(I)] to eliminate the electron spin operator $\boldsymbol{\sigma}_i^\alpha \cdot \boldsymbol{\sigma}_j^\beta$ in favour of total spin operators \mathbf{S}_i and \mathbf{S}_j at sites i and j . We find

$$\boldsymbol{\sigma}_i^\alpha \cdot \boldsymbol{\sigma}_j^\beta \propto \frac{4}{n_i n_j} \mathbf{S}_i \cdot \mathbf{S}_j . \quad (3.54)$$

When the orbital wave functions are not degenerate, the spin dependent part of the secular equation simplifies to

$$-2 \sum_{i>j} \langle \chi_k | \mathbf{S}_i \cdot \mathbf{S}_j | \chi_{k'} \rangle \int d^3 r_1 \dots d^3 r_n \Phi_k (\mathcal{H} - \mathcal{E}) P_{ij} \Phi_{k'} . \quad (3.55)$$

We can use this to represent the secular equation approximately by an effective Hamiltonian

$$\mathcal{H}_{\text{eff}} = \mathcal{E}_\Phi + \Delta \mathcal{E}_\Phi - 2 \sum_{i>j} J_{ij} \mathbf{S}_i \cdot \mathbf{S}_j . \quad (3.56)$$

As for the hydrogen molecule, coefficients J_{ij} are orbital overlap integrals,

$$J_{ij} \propto \sum_{\alpha\beta} \int d^3 r_1 \dots d^3 r_n \langle \Phi_k | (\mathcal{H} - \mathcal{E}_\Phi) | \Phi_{k'} \rangle . \quad (3.57)$$

It is interesting to consider some deviations from the Heisenberg Hamiltonian. Very often the crystalline field destroys rotational invariance at each site. We must then introduce exchange constants J_x^{ij} , J_y^{ij} and J_z^{ij} for each crystalline axis. The Heisenberg Hamiltonian becomes anisotropic:

$$\mathcal{H}_{\text{eff}} = - \sum_{i>j} (J_x^{ij} S_i^x S_j^x + J_y^{ij} S_i^y S_j^y + J_z^{ij} S_i^z S_j^z) . \quad (3.58)$$

Among higher order corrections to the bilinear Heisenberg Hamiltonian, the biquadratic terms

$$\mathcal{H}_{\text{bi}} = - \sum_{i>j} K_{ij} (\mathbf{S}_i \cdot \mathbf{S}_j)^2 \quad (3.59)$$

often arise but rarely exceed 5% of the direct exchange. In metals, other types of exchange occur, which we shall analyse in Chap. 11(I).

3.6 Hartree–Fock Methods

Neglecting interactions between electrons, an orthogonal basis of states can be defined for a solid. Denote by $U(\mathbf{r})$ the periodic potential due to ions in the crystal, including the effects of nuclei and inner electron shells. The Schrödinger equation for electrons in the outer shell d_α is

$$\mathcal{H}_0 \phi_{d_\alpha}(\mathbf{k}, \mathbf{r}) = \left(-\frac{\hbar^2 \nabla^2}{2m} + U(\mathbf{r}) \right) \phi_{d_\alpha}(\mathbf{k}, \mathbf{r}) = \varepsilon_{d_\alpha}(\mathbf{k}) \phi_{d_\alpha}(\mathbf{k}, \mathbf{r}) . \quad (3.60)$$

States $\phi_{d_\alpha}(\mathbf{k}, \mathbf{r})$ form energy bands $\varepsilon_{d_\alpha}(\mathbf{k})$ indexed by orbitals d_α of the localised ions giving rise to them. In this context, the wave functions ϕ_{d_α} , called d_α ligands [61, 63], are Bloch waves

$$\phi_{d_\alpha}(\mathbf{k}, \mathbf{r}) = \exp(i\mathbf{k} \cdot \mathbf{r}) f_{d_\alpha}(\mathbf{k}, \mathbf{r}) , \quad (3.61)$$

where the f_{d_α} are periodic functions over the lattice. These states form an orthonormal basis of 1-electron states:

$$\int d^3r \phi_{d_\alpha}^*(\mathbf{k}', \mathbf{r}) \phi_{d_\beta}(\mathbf{k}, \mathbf{r}) = \delta_{\alpha\beta} \delta(\mathbf{k} - \mathbf{k}') . \quad (3.62)$$

In this chapter, we are interested in quasi-insulating systems with low dispersion $\varepsilon_{d_\alpha}(\mathbf{k}) \approx \varepsilon_{d_\alpha}^0$. In this limit, the Wannier basis is more appropriate. This is defined as the Fourier transform of the Bloch basis,

$$\begin{aligned} \phi_{d_\alpha}(\mathbf{r} - \mathbf{R}_i) &= \frac{1}{\sqrt{V}} \sum_{\mathbf{k}} \exp[i\mathbf{k} \cdot (\mathbf{r} - \mathbf{R}_i)] f_{d_\alpha}(\mathbf{k}, \mathbf{r}) , \\ \varepsilon_{d_\alpha}^{ij} &= \sum_{\mathbf{k}} \exp(-i\mathbf{k} \cdot \boldsymbol{\tau}_{ij}) \varepsilon_{d_\alpha}(\mathbf{k}) = \varepsilon_{d_\alpha}^0 + t_{d_\alpha}(\boldsymbol{\tau}_{ij}) , \end{aligned} \quad (3.63)$$

where $\boldsymbol{\tau}_{ij} = \mathbf{R}_j - \mathbf{R}_i$. These wave functions, localised around \mathbf{R}_i , are close to the atomic orbitals $\psi_{d_\alpha}(\mathbf{r} - \mathbf{R}_i)$. The energy $\varepsilon_{d_\alpha}^{ij}$ of a Wannier state depends on a hopping integral $t_{d_\alpha}^{ij}$ which measures the kinetic energy of delocalisation from site \mathbf{R}_i to site \mathbf{R}_j and determines the width of the d_α band. In an insulator this is a small quantity compared with the separation between valence and conduction bands. This basis is useful because it remains orthonormal,

$$\int d^3r \phi_{d_\alpha}^*(\mathbf{r} - \mathbf{R}_i) \phi_{d_\beta}(\mathbf{r} - \mathbf{R}_j) = \delta_{\alpha\beta} \delta_{ij} , \quad (3.64)$$

whilst incorporating the complex structure of the solid. In this basis, an N -electron state can be specified using second quantisation operators $a_{\alpha i \sigma}^\dagger$, where α specifies the type of d orbital, i the site and σ the spin:

$$|\phi_N\rangle = \prod_1^N a_{\alpha i \sigma}^\dagger |0\rangle . \quad (3.65)$$

In an insulator, the degenerate α orbitals must be completely filled. In this basis, the Hamiltonian \mathcal{H}_0 becomes, in terms of second quantisation operators $a_{\alpha i \sigma}^\dagger$,

$$\mathcal{H}_0 = \sum_{\alpha i \sigma} \left(\varepsilon_{d_\alpha}^0 a_{\alpha i \sigma}^\dagger a_{\alpha i \sigma} + \sum_j \tau_{d_\alpha}^{ij} a_{\alpha j \sigma}^\dagger a_{\alpha i \sigma} \right) . \quad (3.66)$$

The effect of the off-diagonal hopping terms $\tau_{d_\alpha}^{ij}$ in the Wannier basis will be studied in the next section. The N -electron ground state cannot be of the form (3.65), for two reasons. Firstly, interactions between electrons have not yet been taken into account and secondly, these are not eigenstates of $\mathbf{S}_{\text{tot}} = \sum_{i=1}^N \mathbf{S}_i$, which commutes with the total Hamiltonian. To include the interaction

$$V = \frac{1}{2} \sum_{i \neq j} V(\mathbf{r}_i, \mathbf{r}_j) \quad (3.67)$$

between electrons, we transcribe this potential into the language of second quantisation. We follow the same procedure used in Sect. 3.2, except that here there are many orbital states. This raises no additional problems and we find the total Hamiltonian

$$\begin{aligned} \mathcal{H} = & \sum_{\alpha i \sigma} \left[\varepsilon_{d_\alpha}^0 + \sum_{(\beta j) \neq (\alpha i)} \bar{n}_{\beta j} \left(u_{\alpha \beta}^{ij} - \frac{j_{\alpha \beta}^{ij}}{2} \right) \right] n_{\alpha i \sigma} \\ & - \sum_{(\beta j) \neq (\alpha i)} 2j_{\alpha \beta}^{ij} \mathbf{S}_{\alpha i} \cdot \mathbf{S}_{\beta j} , \end{aligned} \quad (3.68)$$

where $\bar{n}_{\beta j} = n_{\beta j \uparrow} + n_{\beta j \downarrow}$ is the total occupation number of state βj and the overlap integrals u and j are generalisations of (3.8), (3.9), viz.,

$$\begin{aligned} u_{\alpha \beta}^{ij} &= \int d^3r d^3r' |\phi_{d_\alpha}(\mathbf{r} - \mathbf{R}_i)|^2 V(\mathbf{r}, \mathbf{r}') |\phi_{d_\beta}(\mathbf{r}' - \mathbf{R}_j)|^2 , \\ j_{\alpha \beta}^{ij} &= \int d^3r d^3r' \phi_{d_\alpha}^*(\mathbf{r} - \mathbf{R}_i) \phi_{d_\beta}^*(\mathbf{r}' - \mathbf{R}_j) \\ &\quad \times V(\mathbf{r}, \mathbf{r}') \phi_{d_\beta}(\mathbf{r} - \mathbf{R}_i) \phi_{d_\alpha}(\mathbf{r} - \mathbf{R}_j) . \end{aligned} \quad (3.69)$$

Just as in the previous section, we do indeed find a Heisenberg Hamiltonian. It is not diagonal since each particle interacts with all other particles. The

Hartree–Fock approximation consists in defining the new (spin dependent) eigenstates $\psi_{d_\alpha\sigma}(\mathbf{r} - \mathbf{R}_i)$. These states ψ_{d_α} are defined as solutions of the Schrödinger equation in a potential equal to the sum of $U(\mathbf{r})$ and the mean potential \bar{V} induced by all the other particles, represented by the second and third terms of (3.70). This equation

$$\begin{aligned} 0 &= (\mathcal{H}_0 - \varepsilon_{\alpha i \sigma}^{\text{HF}}) \psi_{d_\alpha}^\sigma(\mathbf{r} - \mathbf{R}_i) \\ &+ \sum_{\beta j \sigma'} \left[\int d^3 r' V(\mathbf{r}, \mathbf{r}') |\psi_{d_\beta}^{\sigma'}(\mathbf{r}' - \mathbf{R}_j)|^2 \right] \psi_{d_\alpha}^\sigma(\mathbf{r} - \mathbf{R}_i) \\ &- \sum_{\beta j} \psi_{d_\beta}^\sigma(\mathbf{r} - \mathbf{R}_j) \int d^3 r' \psi_{d_\beta}^{\sigma*}(\mathbf{r}' - \mathbf{R}_j) V(\mathbf{r}, \mathbf{r}') \psi_{d_\alpha}^\sigma(\mathbf{r}' - \mathbf{R}_i) \end{aligned} \quad (3.70)$$

must be solved in a self-consistent way since the ψ_{d_α} determine the mean potential \bar{V} . Note that the last term (associated with exchange) only connects states having parallel spins. It therefore favours ferromagnetism for repulsive interactions. This is the Hund rule again. This integro-differential equation can be solved iteratively. At each stage, we evaluate the potential \bar{V} produced by the other particles using wave functions obtained in the previous iteration [64]. In practice, such a procedure is efficient and gives excellent results for small systems. We define operators $b_{\alpha i \sigma}^\dagger$ creating a particle in the state $\psi_{d_\alpha}^\sigma(\mathbf{r} - \mathbf{R}_i)$. As states ψ incorporate the mean effects of the other particles, the operator b^\dagger is said to create a quasi-particle of energy ε^{HF} . In this quasi-particle basis, we define an antisymmetrised N -electron state by

$$|\psi_N\rangle = \prod_1^N b_{\alpha i \sigma}^\dagger |0\rangle . \quad (3.71)$$

In this basis, the Hamiltonian has diagonal form in the Hartree–Fock approximation:

$$\mathcal{H}_{\text{HF}} = \sum_{\alpha i \sigma} \varepsilon_{\alpha i \sigma}^{\text{HF}} b_{\alpha i \sigma}^\dagger b_{\alpha i \sigma} . \quad (3.72)$$

In practice, we do not have to solve the integro-differential equation (3.70) in order to obtain quasi-particle energies. This is because Hartree–Fock states ψ have the property

$$\langle \phi_N | \mathcal{H} | \psi_N \rangle = \langle \phi_N | \mathcal{H} | \phi_N \rangle . \quad (3.73)$$

We can just apply contraction rules (see Appendix B) to the biquadratic operators appearing in \mathcal{H} . For example,

$$n_{\alpha i \sigma} n_{\beta j \sigma'} \rightarrow \langle |n_{\alpha i \sigma}| \rangle n_{\beta j \sigma'} + n_{\alpha i \sigma} \langle |n_{\beta j \sigma'}| \rangle - \langle |n_{\alpha i \sigma}| \rangle \langle |n_{\beta j \sigma'}| \rangle , \quad (3.74)$$

$$\boldsymbol{\sigma}_{\alpha i} \cdot \boldsymbol{\sigma}_{\beta j} \rightarrow \langle |\boldsymbol{\sigma}_{\alpha i}| \rangle \cdot \boldsymbol{\sigma}_{\beta j} + \boldsymbol{\sigma}_{\alpha i} \cdot \langle |\boldsymbol{\sigma}_{\beta j}| \rangle - \langle |\boldsymbol{\sigma}_{\alpha i}| \rangle \cdot \langle |\boldsymbol{\sigma}_{\beta j}| \rangle . \quad (3.75)$$

(There is some ambiguity in these contraction rules. They implicitly assume that particle number is fixed in physical states of the system. If particle number is not fixed, as happens in superconductors, we must also include contractions $\langle |a^\dagger a^\dagger| \rangle_{\text{cc}}$ and $a^\dagger a^\dagger \langle |c c| \rangle$.) Mean values are taken either as expectations

in the N -particle ground state relative to \mathcal{H}_0 , or as a thermodynamic mean over the N -particle states of \mathcal{H}_0 , defined by

$$\langle |A| \rangle = \text{Tr} [\exp(-\beta \mathcal{H}_0) A] .$$

In the latter case, the Hartree–Fock approximation is called the *mean field approximation*, the basics of which will be studied in Chap. 5(I). In any case, the energy of a quasi-particle is

$$\varepsilon_{\alpha i \pm}^{\text{HF}} = \varepsilon_{\alpha i} + \sum_{(\beta j) \neq (\alpha i)} \left(u_{\alpha \beta}^{ij} - \frac{j_{\alpha \beta}^{ij}}{2} \right) \frac{\rho_{\beta j}}{2} \mp \sum_{(\beta j) \neq (\alpha i)} 2 j_{\alpha \beta}^{ij} s_{\beta}^j , \quad (3.76)$$

where $\rho = \langle |n| \rangle$ and $s = \langle |S| \rangle$ are the mean electron density and polarisation, respectively. The second term in this equation can be interpreted as a molecular potential U_m acting on the quasi-particle $\psi_{\alpha i \sigma}$, induced by all other quasi-particles. Likewise, the last term is a molecular magnetic field h_m acting on the quasi-particle spin. This microscopic field is the origin of magnetism [see Chap. 5(I)]. These ideas of quasi-particle and molecular field also form the basis for the Landau theory of Fermi fluids [65]. As $\varepsilon_{\sigma}^{\text{HF}}$ depends on spin σ , the Hartree–Fock Hamiltonian is explicitly spin dependent, despite the fact that the N -particle microscopic Hamiltonian is not. This is Pauli's principle again. In practice, we rarely need to consider all interaction terms $u_{\alpha \beta}^{ij}, j_{\alpha \beta}^{ij}$. The most important term is $u_{\alpha \alpha}^{ii}$. It plays a critical role in the magnetism of metals and also in the magnetism of molecular crystals, which are dominated by superexchange (see next section). The direct exchange term between nearest neighbours $j_{\alpha \beta}^{i i+1}$ is general an order of magnitude smaller and governs magnetism in insulators. Interactions between second neighbours are rarely relevant, except in molecular solids via superexchange.

3.7 Superexchange

The metal fluoride compounds MnF_2 , FeF_2 and CoF_2 , which are all anti-ferromagnetic at low temperature, serve to illustrate the problems raised in determining electron wave functions. Overlap between Mn^{++} orbitals ($3d^5$, $S = 5/2$, $L = 0$) is negligible because the F^- ion is interposed between the Mn^{++} ions. Superexchange, put forward by Kramers [66], attributes antiferromagnetism between manganese ions to indirect transmission of magnetism by F^- anions. One of the p electrons of the F^- ion is transferred to the manganese ion $\text{Mn}^{++} \rightarrow \text{Mn}^+$, producing an excited configuration $3d^6$ ($S = 2$, $L = 2$). The F ion then only has one electron, which it can exchange with one of the d orbitals of the other Mn^{++} ion (see Fig. 3.3). Using this excited state in a second order perturbative calculation, we obtain an effective exchange between Mn^{++} ions, called superexchange. More precisely, the ground state wave function of the manganese ion is a mixture of atomic orbitals

$$\Psi_{\text{ground}} = \Phi_{\text{Mn}^{++}} \Phi_{\text{F}^-} + \varepsilon \Phi_{\text{Mn}^+} \Phi_{\text{F}} . \quad (3.77)$$

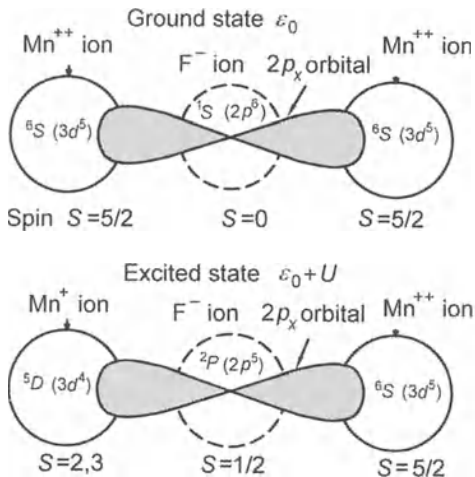


Fig. 3.3. Ionic and excited configurations of metal fluoride or metal oxide compounds, giving rise to antiferromagnetic superexchange

The mixture of the excited configuration is responsible for magnetic properties. This kind of exchange can only generally arise if wave functions (p_x here) of the F^- anion are not orthogonal to wave functions of the Mn^{++} cation (d_{xy} , d_{xz} or d_{yz} , hereafter denoted d_α). This type of exchange is very common in ionic crystals. Oxides and fluorides are almost all antiferromagnetic.

An approximate treatment of superexchange can be built upon the Wannier basis (Sect. 3.6) [63]. Here we allow an electron to hop from one orbital to another to form an excited state of the solid. Indeed, up to now, atoms have been treated as being sufficiently well separated to ensure that the only relevant physical process is two-electron exchange imposed by the Pauli principle. By allowing individual electrons to hop from one site to another, we assume that they can form bands in the solid, as mentioned in the last section. The electrons form a (magnetic) insulator only if the band is completely filled, the other fillings giving rise to a metallic magnetic state [see Chap. 11(I)].

Let us suppose that we know the one-electron wave functions $\phi_{d_\alpha}(\mathbf{k}, \mathbf{r})$ in the periodic potential of the solid [see (3.61)], indexed by the atomic orbital d_α . These wave functions are Bloch states and form d_α bands associated with d_α ligands. The hopping amplitudes $t_{d_\alpha}^{ij}$ (3.63) giving the dispersion of the bands are small here and the hopping Hamiltonian in (3.66)

$$\mathcal{H}_{\text{hop}} = \sum_{\alpha i \neq j \sigma} t_{d_\alpha}^{ij} a_{\alpha i \sigma}^\dagger a_{\alpha j \sigma} \quad (3.78)$$

can be treated as a perturbation. In superexchange, direct exchange integrals j are negligible and only the Hubbard interaction term $u_{\alpha \alpha}^{ii} \equiv u_\alpha^i$ is significant. Hence,

$$\mathcal{H} = \sum_{\alpha i \sigma \sigma'} (\varepsilon_{d_\alpha}^0 + u_\alpha n_{\alpha i \sigma'}) n_{\alpha i \sigma}. \quad (3.79)$$

As the hopping Hamiltonian only couples electrons in the same d_α ligand, there is no point in specifying the ligand in the perturbation treatment of \mathcal{H}_{hop} . To first order, $\langle \phi_N | \mathcal{H}_{\text{hop}} | \phi_N \rangle = 0$. To second order,

$$\delta E_N = - \sum_{\phi^*} \frac{|\langle \phi^* | \mathcal{H}_{\text{hop}} | \phi_N \rangle|^2}{u} \approx - \langle \phi_N | \frac{\mathcal{H}_{\text{hop}}^2}{u} | \phi_N \rangle. \quad (3.80)$$

To carry out the sum over intermediate states, we have assumed that transfers of several electrons do not contribute so that we can use the completeness relation $\sum |\phi^* \rangle \langle \phi^*| = 1$. Superexchange can then be represented by an effective Hamiltonian

$$\mathcal{H}_{\text{eff}} = - \frac{\mathcal{H}_{\text{hop}}^2}{u} \equiv - \sum_{i \neq j \sigma \sigma'} \frac{|t_{ij}^2|}{u} a_{i\sigma}^\dagger a_{j\sigma} a_{j\sigma'}^\dagger a_{i\sigma'}. \quad (3.81)$$

But the combination of operators $a_{i\sigma}^\dagger a_{i\sigma'} a_{j\sigma'}^\dagger a_{j\sigma}$ is exactly the combination appearing in the exchange term (3.24). This term decomposes into an electron density contribution $n_{i\sigma} n_{j\sigma'}$ and a spin exchange term. Explicitly,

$$\mathcal{H}_{\text{eff}} = - \sum_{i \neq j \sigma \sigma'} \frac{|t_{ij}^2|}{2u} n_{i\sigma} n_{j\sigma'} + \sum_{i \neq j} \frac{2|t_{ij}^2|}{u} \mathbf{S}_i \cdot \mathbf{S}_j, \quad (3.82)$$

where we have used the definition (3.25) of spin operators in terms of second quantisation operators. There is thus an antiferromagnetic exchange induced by the kinetic hopping term. The sign of the exchange clearly comes from the following fact: when the spins are antiparallel, the electron can hop from one site to another whilst satisfying Pauli's principle. Since spin wave functions are orthogonal, spatial orbitals can increase their overlap in order to lower their *kinetic* energy. The origin of superexchange is not the Coulomb interaction between electrons but rather the kinetic term inherent in fermions; when orbitals overlap, the delocalisation kinetic energy is reduced, thereby favouring antiferromagnetic configurations.

Before attempting an approximate solution of the effective Hamiltonians, it will be interesting to compare energies of the simpler magnetic states.

3.8 The Energy of Magnetic States

In the Wannier basis, a general N -electron state is

$$|\phi_N\rangle = \prod_1^N a_{i\sigma}^\dagger |0\rangle. \quad (3.83)$$

and its wave function can be expressed as a Slater determinant:

$$\langle \dots \mathbf{r}_j \sigma_j \dots | \phi_N \rangle = \frac{1}{\sqrt{N!}} \begin{vmatrix} \phi_1(\mathbf{r}_1) \sigma_1 & \phi_2(\mathbf{r}_1) \sigma_1 & \dots & \phi_n(\mathbf{r}_1) \sigma_1 \\ \phi_1(\mathbf{r}_2) \sigma_2 & \phi_2(\mathbf{r}_2) \sigma_2 & \dots & \phi_n(\mathbf{r}_2) \sigma_2 \\ \vdots & \vdots & \vdots & \vdots \\ \phi_1(\mathbf{r}_n) \sigma_n & \phi_2(\mathbf{r}_n) \sigma_n & \dots & \phi_n(\mathbf{r}_n) \sigma_n \end{vmatrix}, \quad (3.84)$$

where the ϕ_i are Wannier orbitals. The formalism of second quantisation avoids heavy manipulations with Slater determinants. Unfortunately these states are not eigenstates of S_{tot} which commutes with \mathcal{H} . To take advantage of these good quantum numbers, and expand an antisymmetric state (3.83) in terms of eigenstates of S_{tot} , we construct projection operators onto one of the spin states, generally $S_{\text{tot}} = 0$ (antiferromagnetic system) or $S_{\text{tot}} = NS$ (ferromagnetic system). The projection onto the ferromagnetic state is constructed by noticing that

$$\begin{aligned} P_S^\perp &= \frac{1}{N} [NS(NS+1) - S_{\text{tot}}^2] \\ &= \frac{1}{N} \left[NS(NS+1) - NS(S+1) - 2 \sum_{i>j} \mathbf{S}_i \cdot \mathbf{S}_j \right], \end{aligned} \quad (3.85)$$

$$P_{1/2}^\perp = \frac{N-1}{4} - \frac{1}{2N} \sum_{i>j} \boldsymbol{\sigma}_i \cdot \boldsymbol{\sigma}_j \quad (3.86)$$

projects onto the subspace orthogonal to the ferromagnetic state [of maximal spin, viz., $S_{\text{tot}} = \sqrt{NS(NS+1)}$]. In general, we can thereby construct projection operators onto subspaces orthogonal to any given value of total spin. Multiplying together $S-1$ projection operators perpendicular to all spin spaces other than the one we are seeking, we can construct a projector onto the chosen spin value.

In the ferromagnetic state, all spins are parallel and symmetric under permutation. The ferromagnetic state is therefore

$$|F_N\rangle = \prod_1^N a_i^\dagger |0\rangle \otimes |\uparrow \dots \uparrow\rangle. \quad (3.87)$$

The expectation value of the Hartree–Fock Hamiltonian in this state is

$$E_F = \sum_{i \neq j}^N \varepsilon_{ij} + \sum_{i \neq j} (u_{ij} - j_{ij}), \quad (3.88)$$

where $\varepsilon_{ij} = \varepsilon_i \delta_{ij}$ for an insulator and the Hartree terms u_{ij} and Fock terms j_{ij} are defined in (3.69). For translation invariant systems, it is useful to express the ground state energy as a sum over the conjugate space. In order to do so, we define Fourier transforms

$$\varepsilon(\mathbf{k}) = \sum_{\tau_{ij}} \exp(i\mathbf{k} \cdot \boldsymbol{\tau}_{ij}) \varepsilon_{ij}, \quad (3.89)$$

$$V(\mathbf{k}, \mathbf{k}') = \sum_{\tau_{im}, \tau_{jl}} \exp(i\mathbf{k} \cdot \tau_{im} - i\mathbf{k}' \cdot \tau_{jl}) V_{ij, lm}, \quad (3.90)$$

$$V_{ij, lm} = \int d^3r d^3r' \phi_i^*(\mathbf{r}) \phi_j^*(\mathbf{r}') V(\mathbf{r}, \mathbf{r}') \phi_l(\mathbf{r}) \phi_m(\mathbf{r}'), \quad (3.91)$$

where $\tau_{ij} = \mathbf{R}_j - \mathbf{R}_i$. The energy of the ferromagnetic state is then

$$E_F = \sum_{\mathbf{k}} [\varepsilon(\mathbf{k}) + V(\mathbf{k}, \mathbf{k}) - V(\mathbf{k}, -\mathbf{k})]. \quad (3.92)$$

$V(\mathbf{k}, \mathbf{k})$ coincides with the direct or Hartree term and $V(\mathbf{k}, -\mathbf{k})$ with the exchange or Fock term. When V depends only on $\mathbf{r} - \mathbf{r}'$ (this never happens for electrons in a periodic lattice potential!), $V(\mathbf{k}, \mathbf{k}')$ is a function of the difference $\mathbf{k} - \mathbf{k}'$. The direct term $V(0)$ is then the mean potential created by all the other electrons (the mean field), whilst the exchange interaction $V(2\mathbf{k})$ depends on the centre of mass momentum of the two particles.

Let us consider briefly the antiferromagnetic state. Apart from the singlet state $S = 0$, whose wave function is completely antisymmetric, there is another state which plays an important role, namely the Néel state. In this state, spins at neighbouring sites are oriented oppositely, i.e.,

$$\psi_{\text{N\'eel}} = |\psi_{\text{sp}}\rangle \otimes |\uparrow, \downarrow, \uparrow, \downarrow, \dots\rangle, \quad (3.93)$$

where the spatial state $|\psi_{\text{sp}}\rangle$ is not specified since neighbouring spin states are orthogonal. It must be chosen so as to minimise the Coulomb energy. Although $|\psi_{\text{N\'eel}}\rangle$ is not an eigenstate of S_{tot} , we can arrange for its energy to be close to the singlet energy by judicious choice of $|\psi_{\text{sp}}\rangle$. When the spatial state is a product of Wannier states $|\psi_{\text{sp}}^{\text{prod}}\rangle$, the orthogonality of neighbouring spin states makes the energy calculation particularly simple in the Néel state:

$$E_{\text{N\'eel}}^{\text{prod}} = \sum_{i \neq j} (\varepsilon_{ij} + V_{ij, ij}). \quad (3.94)$$

In the conjugate space,

$$E_{\text{N\'eel}}^{\text{prod}} = \sum_{i \neq j} [\varepsilon(\mathbf{k}) + V(0)]; \quad (3.95)$$

We can now see that the Néel state in this approximation has much higher energy than the singlet energy. The reason for this is our choice of spatial wave function as a product of Wannier states at each site. Although such a choice is justified in the context of the Hartree–Fock approximation, this approximation neglects any spatial correlation between electrons at neighbouring sites. By choosing a variational spatial wave function (e.g., a linear combination of product states), a much lower Néel state energy can be obtained [see also Sect. 11.4.2(I)]. For thermodynamic reasons, it is the Néel state which is generally the most stable in three dimensions. (When antiferromagnetic correlations develop over a correlation length ξ , the transition from state $|\uparrow, \downarrow, \uparrow, \dots\rangle$ to state $|\downarrow, \uparrow, \downarrow, \dots\rangle$, which would allow formation

of the linear combination corresponding to the singlet state, is only possible via a tunnelling matrix element between these two states. In three dimensions, detailed study shows that these matrix elements do not grow as fast as $\sqrt{F(\xi)} \propto \xi^{3/2}$, where $F(\xi)$ is the free energy of a correlated region. Quantum effects then become less relevant as the transition is approached. Such arguments cannot be made in one or two dimensions, where there is no long range magnetic organisation.) The singlet state $S = 0$ is stabilised by very large quantum effects in one dimension and significant quantum effects in two dimensions, as we shall see in Chaps. 7(I) and 10(I).

4. Phase Transitions

4.1 Second Order Transitions

How does a system change from a paramagnetic state at high temperature to a ferromagnetic state at $T = 0$? Landau was the first to emphasise the importance of symmetries in phase transitions [67, 68]. In its paramagnetic phase a system is isotropic and invariant under rotation. In contrast, the ferromagnetic state has a spontaneous magnetisation which fixes some special orientation in space. This direction breaks rotational invariance. Hence, paramagnetic and ferromagnetic states do not possess the same symmetry. Landau pointed out that a symmetry cannot change gradually: either it exists or it does not exist. A (second order) phase transition must separate states with different symmetries.

When a symmetry is broken, there is generally an order parameter characterising the non-symmetric state. According to Landau, any parameter whose mean value is zero in the symmetric state and non-zero in the non-symmetric state can be taken as an order parameter. For example, magnetisation $\langle \mathbf{M} \rangle$ is an order parameter for a ferromagnetic system, and alternating magnetisation $\langle \mathbf{N}^\dagger \rangle$ is an order parameter for an antiferromagnetic system. The amplitude $\langle \phi \rangle$ of the macroscopic ground state wave function is an order parameter for a boson gas or a superconductor. (There are also many second order transitions in crystalline phases. In a binary alloy such as brass (CuZn), which has face-centred cubic structure, the order parameter is the proportion of atoms at a given crystallographic site, i.e., $[p(\text{Cu}) - p(\text{Zn})]/[p(\text{Cu}) + p(\text{Zn})]$.) This idea nevertheless has a precise meaning: the order parameter is an extra variable required to specify the macroscopic state of a system. For a paramagnetic system in zero field ($H = 0$), $M = 0$ by invariance with respect to time and the state is uniquely specified by variables V and T (or P and T). In non-superconducting metals, gauge invariance ensures that $\langle \phi \rangle = 0$, as we shall see in Chap. 13(II). It is important to understand that an order parameter can have a well defined phase, in addition to an amplitude. This phase governs macroscopic properties of superconductors and superfluids. At the very least, an order parameter can take on two signs (as in the Ising model), but in general it must specify one or more angles. By symmetry, the free energy does not depend on these phase variables since the various directions can be connected by the original symmetry.

Once the symmetry is broken, a new variable is needed to completely specify the state of the system. It is then straightforward to show that the free energy

$$F_Z = -k_B T \ln Z(T, V, M \equiv M_{\min})$$

in the ordered phase is a different function to the one describing the disordered phase, even if the new variable M is eliminated using the minimum condition

$$\frac{\partial F_Z}{\partial M}(T, V, M_{\min}) = \mu_0 H \equiv 0.$$

Assume we can calculate $Z(T, V, M)$ directly, and hence obtain

$$F_Z = -k_B T \ln Z(T, V, M). \quad (4.1)$$

Here F_Z does not coincide with the free energy at thermodynamic equilibrium as we defined it in Chap. 1. The partition function $Z(T; V, M)$ and $F_Z(T, V, M)$ do not necessarily describe states of thermodynamic equilibrium as long as the value of M has not been specified. In fact, M must be considered here as a variable independent of H . At thermodynamic equilibrium, the free energy $F(V, T)$ we usually observe is obtained by minimising $F_Z(T, V, M)$ with respect to M . Hence the condition

$$\frac{\partial F_Z}{\partial M}(M_{\min}) = \mu_0 H = 0, \quad (4.2)$$

in the absence of magnetic field. Above T_c , this condition is trivially satisfied, by rotation invariance. Below T_c , (4.2) is no longer a trivial requirement. If the solution M_{\min} of (4.2) is substituted into (4.1), we thereby obtain a new function $F_S(V, T) = F_Z(V, T, M_{\min})$. It does not coincide with the function $F(V, T)$ describing the free energy above T_c . The free energy is not analytic at T_c and there is a phase transition. It is the second derivatives of F (susceptibility and specific heat) which are singular at T_c , whilst the first derivatives (magnetisation and entropy) are continuous. In particular, there is no latent heat at a second order phase transition.

At a first order phase transition, the singularity in the free energy is quite different. When $T > T_c$, the Gibbs free energy $G = F + PV$ is an analytic function of volume in the form of an asymmetric double potential well such that one minimum at V_1 is less than the other at V_2 (see Fig. 4.1). Lowering the temperature, this asymmetry becomes less marked. At T_c the two wells are finally symmetric, $G(T_c, V_1) = G(T_c, V_2)$, and such that $(\partial G / \partial V)_{T=T_c} = 0$. Hence,

$$-P = \left(\frac{\partial F}{\partial V_1} \right)_{T_c} = \left(\frac{\partial F}{\partial V_2} \right)_{T_c}. \quad (4.3)$$

Below T_c , $G(T, V_1) > G(T, V_2)$. The system jumps discontinuously from V_1 to V_2 . This implies a discontinuity in the derivatives of the Gibbs free energy $G(P, T) = F + PV$, expressed in terms of intensive variables P and T .

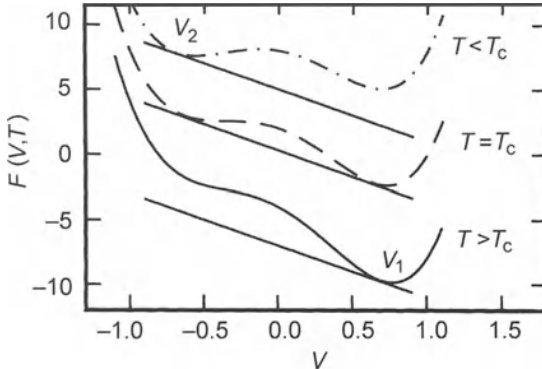


Fig. 4.1. First order transition. Thermodynamic equilibrium is the minimum point at which the slope takes the given value $-P$. At the critical temperature this slope occurs simultaneously at both minima V_1 and V_2 . The state jumps discontinuously from V_1 ($T > T_c$) to V_2 ($T < T_c$)

These ideas of symmetry and order parameter may not be obvious in some systems [69]. Certain magnetic glasses (spin glasses) have a ‘hidden’ microscopic order parameter which does not correspond to a macroscopic variable in the usual sense of the term since it describes the rigidity of the system. Here is the difficulty with the order parameter idea: we can never be sure that some hidden order will not appear, such as alternating magnetisation N^\dagger in antiferromagnetism or phase $\langle \phi \rangle$ in superconductivity. These were hidden variables for many years. This difficulty with the order parameter idea is well illustrated in 2-dimensional systems. According to the Mermin–Wagner theorem [70] [see Chap. 7(I)], no long range order can break a continuous symmetry in two dimensions. Nevertheless, Kosterlitz and Thouless have shown in their study of the 2-dimensional XY model that an order parameter might be of purely topological character [71] [see Chap. 7(I)]. In such 2-dimensional systems, the main fluctuations are vortices. Individually, these alter the topology of the phase field of the magnet or superconductor; but pairing together topological defects of opposite (topological) charge, the topological integrity of the phase field is restored. Below a topological transition, all vortices are paired. Above the transition, their pairing energy falls to zero, releasing a gas of free vortices which destroys the topological integrity of the system.

Even in Landau theory, a symmetry may change discontinuously, as in a first order transition. Close to transition, certain response functions diverge (susceptibility) in such a way that magnetisation fluctuations can be very large locally. If there are significant magneto-elastic couplings in the material considered, fluctuations in magnetisation can induce distortion of the crystal lattice. There is then a first order phase transition which occurs just before we reach the critical temperature associated with change of symmetry.

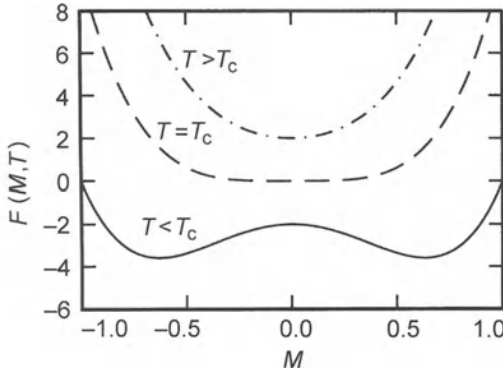


Fig. 4.2. Dependence of $F_Z(M, T)$ on M at different temperatures. When T crosses T_c , the curvature $a(T)$ of F at $M = 0$ changes sign

When a ferromagnetic system has small magnetisation \mathbf{M} , the free energy F_Z can be expanded in powers of its order parameter \mathbf{M} ,

$$F_Z - F_0 = a(T)M^2 + \frac{b(T)}{2}M^4 + \frac{c(T)}{3}M^6 - \mu_0 \mathbf{M} \cdot \mathbf{H}, \quad (4.4)$$

where the last term describes energy of spins in an external field \mathbf{H} . Let us begin by assuming that $H = 0$. Coefficients $b(T)$, $c(T)$ are positive and slowly varying near T_c . The other coefficient $a(T)$, however, changes sign and is zero at T_c . It is therefore appropriate to limit the expansion to the close neighbourhood of T_c , viz., $a(T) = \alpha\tau$, where $\tau = (T - T_c)/T_c$ is the reduced temperature. For $T > T_c$, the minimum of F_Z is obviously at $M = 0$ and $F_S = F_Z(M = 0) = F_0$, as expected from rotation invariance. However, when $T < T_c$, the first term is negative and the minimum of F_Z is no longer at $M = 0$. We can check this by taking the partial derivative with respect to M^2 ,

$$\frac{\partial F_Z}{\partial M^2} = 0 = \alpha \frac{T - T_c}{T_c} + bM^2 + cM^4 + \dots . \quad (4.5)$$

Keeping the first two terms, we obtain

$$M^2 = \frac{\alpha}{b} \frac{T_c - T}{T_c} . \quad (4.6)$$

Substituting this value of magnetisation into expansion (4.5) of the free energy F_Z , we find that for $T < T_c$,

$$F_S(T) = F_0 - \frac{\alpha^2}{2b} \left(\frac{T - T_c}{T_c} \right)^2 . \quad (4.7)$$

F_S is not the same analytic function above ($F_S = F_0$) and below T_c . If we apply a weak magnetic field H above T_c , we must include magnetic energy $-\mu_0 \mathbf{M} \cdot \mathbf{H}$ in the free energy (4.5). Minimising with respect to M , we find

$$M = \frac{\mu_0 H T_c}{2\alpha|T - T_c|}, \quad \chi = \frac{\mu_0 T_c}{2\alpha|T - T_c|}. \quad (4.8)$$

The susceptibility diverges at T_c . At the critical temperature, the magnetisation obtained by minimising F_Z behaves non-analytically in H :

$$M = \left(\frac{\mu_0 H}{2b} \right)^{1/3}. \quad (4.9)$$

At T_c , the susceptibility $\chi = M/H$ is not constant and diverges even in a weak field. $\chi(H, T)$ is not an analytic function at the critical point ($T = T_c, H = 0$). This is true however we approach the critical point (either by varying the field at constant temperature T_c , or by changing the temperature in zero field). Similarly we may check that the specific heat $C = -T\partial^2 F_Z / \partial T^2$ is zero for $T > T_c$ and equal to

$$C_M(H = 0) = \frac{\alpha^2 T}{b T_c^2} \quad (4.10)$$

below T_c . The specific heat is discontinuous at T_c with a jump of $\Delta C = \alpha^2/b T_c$. Any singularity in the susceptibility or specific heat indicates a second order phase transition, since these are second derivatives of the free energy.

If the magneto-elastic coupling is significant, the free energy must include those elastic contributions from the lattice which are coupled to magnetisation. (Magneto-elastic coupling can be induced by lattice vibrations which modulate magnetic exchange, the latter having exponential dependence on interatomic distance. It is thus highly sensitive to pressure changes. We can even induce tetragonal distortion by applying sufficient pressure to increase the magneto-elastic coupling.) The simplest form of elastic and magneto-elastic terms is [see Sect. 2.14(I)]

$$F_{\text{dist}} = dQ M^2 + \frac{e}{2} Q^2, \quad (4.11)$$

where Q is an elastic deformation of the crystal (e.g., the difference between lattice spacings along two axes of the lattice) and e the elastic modulus. (Distortions of a cubic lattice correspond to modes Q_2 and Q_3 in Fig. 2.14(I). They couple with M_y and M_z , respectively. Although it would be more correct to include this anisotropy in the magneto-elastic coupling, this would not be very helpful.) Minimising F_{dist} with respect to Q , we find that $Q_{\text{eq}} = -dM^2/e$, i.e.,

$$F_{\text{dist}} = -\frac{d^2 M^4}{2e}. \quad (4.12)$$

If this term exceeds $b(T)M^4/2$, the coefficient of M^4 changes sign. When $b' = b - d^2/2e$ becomes negative, the function F_Z has three minima. The phase transition then becomes weakly first order [72]. This is shown in Fig. 4.4 where $F_Z(M)$ is plotted as a function of temperature in the presence of an applied field H . At T_c , magnetisation appears in a discontinuous way as we

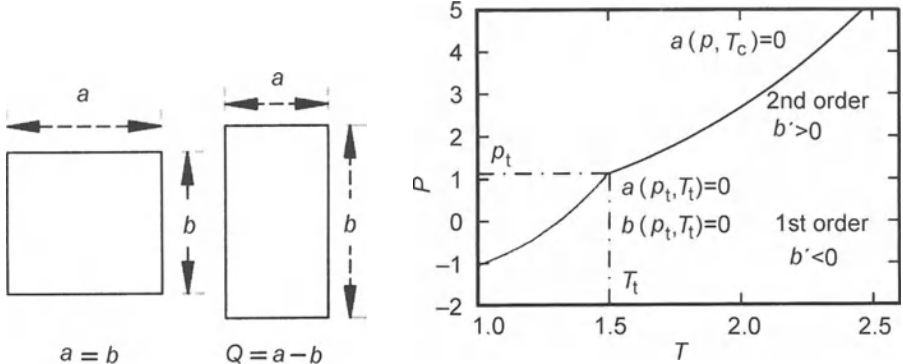


Fig. 4.3. Left: example of cubic \rightarrow tetragonal distortion. Right: P , T -phase diagram where the tricritical point t is reached when magneto-elastic coupling induces a sign change in b'

move from the central minimum ($M_1 \approx 1$) to the minimum M_2 . Varying a physical parameter such as pressure, the coefficient b' may go to zero at a certain temperature T_t . At this temperature, transition is determined by the balance between coefficients a and c . The point (T_t, P_t) on the phase diagram then corresponds to a tricritical point. This point separates regions where the transition is first order from those where behaviour is second order. Near a tricritical point, the order parameter which minimises free energy is

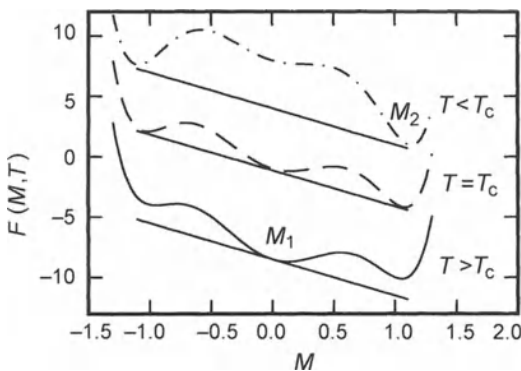


Fig. 4.4. First order magnetic phase transition. Even in the presence of an applied field H , imposing slope $-\mu_0 H$ at an equilibrium state, the free energy F_Z has three minima as a function of M when $b' < 0$. At T_c , the system moves discontinuously from one minimum $M_1 \approx 0$ to another M_2 . Metastability effects, such as supercooling, are also possible, as in any first order transition. These curves should be contrasted with the first order transition in Fig. 4.1 and the second order transition in Fig. 4.2

$$\frac{\partial F_Z}{\partial M^2} = 0 = a + cM^4, \quad M = \left(\frac{\alpha(T - T_c)}{cT_c} \right)^{1/4} \quad (4.13)$$

and the critical exponent β equals $1/4$ rather than $1/2$, as obtained previously. For certain systems there may be competition between two order parameters, one associated with antiferromagnetic order N and the other with a secondary ferromagnetic order M which couples to N in the presence of an applied field. The above methods can be generalised by expanding the free energy in powers of M and N , then minimising with respect to both parameters. In this case the novelty lies in coupling terms between the two order parameters. These introduce a tricritical point separating paramagnetic, ferromagnetic and antiferromagnetic phases. A well known example is FeCl_2 [74].

In some cases, symmetries forbid second order transition. In a magnet, invariance with respect to time excludes the possibility of a third order invariant M^3 in the free energy. This is not always so. If no symmetry forbids a third order invariant, then the transition must be first order for a simple reason, viz., the condition $\partial F_Z / \partial M$ and $M = 0$ no longer defines a minimum. The conclusion is the same: the second order transition will occur if energy considerations do not intervene to induce a discontinuous first order jump in the non-symmetric state. In general, the non-symmetric state is the low temperature state, except for helium 3, because the paramagnetic entropy of the solid (Curie law obeying Boltzmann statistics) is greater than the paramagnetic entropy of the liquid (Pauli susceptibility governed by Fermi statistics). A magnetic field produces magnetisation in the paramagnetic phase and breaks rotation symmetry. The phase transition is smoothed by the field, since the change of symmetry is no longer abrupt.

In a finite system, the free energy

$$F_Z = -k_B T \ln [\text{Tr} \exp(-\beta(\mathcal{H} - \mu N))]$$

is always an analytic, and even an entire function of magnetisation [see Chap. 6(I)]. The singularity in F_Z appears when we take the thermodynamic limit $N \rightarrow \infty$. This is because the probability of a thermodynamic fluctuation being sufficient to push the system from the $+M$ state to the $-M$ state becomes extraordinarily small when the system becomes large, i.e., it is of order $\exp(-\sqrt{N}) \approx \exp(-10^{12})$. The system becomes spontaneously non-ergodic, exploring only a tiny fraction of phase space. The above remarks show how carefully we must treat numerical simulations carried out for small systems, which are still ergodic. The presence of a phase transition may be completely hidden by effects of the small size of the system.

4.2 Correlation Length, Fluctuations and the Ornstein–Zernike Theory

We have been considering homogeneous and uniform systems. In these conditions, magnetic order appears suddenly at T_c . Neutron scattering experiments (or light scattering for transparent magnetic systems) show that systems are not homogeneous above T_c and fluctuate violently. This type of behaviour is well known close to the critical point of a liquid; here density fluctuations are so great that they scatter light, causing critical opalescence. Neutron scattering experiments also show that order exists over short distances, i.e., spins are correlated over a distance ξ called the correlation length. At distances shorter than ξ , spins are ordered. This quantity diverges when $T \rightarrow T_c$. Over larger distance scales, the system is a heterogeneous assembly of domains of size ξ . Near T_c , symmetric and non-symmetric phases have similar energies and thermodynamic fluctuations can easily induce a locally non-zero value of the order parameter. Let δF be the variation in free energy associated with a fluctuation in the order parameter. The probability of this fluctuation is

$$P(\delta F) = \exp\left(-\frac{\delta F}{k_B T}\right). \quad (4.14)$$

In order to generalise the expansion of the free energy as a function of the order parameter, we assume that $M(\mathbf{r})$ varies with \mathbf{r} over distances of order ξ . Then we can describe its spatial fluctuations [73]. Changes in direction of $M(\mathbf{r})$ increase the free energy because the order parameter has a certain stiffness allowing it to come back to equilibrium. To first order the simplest stiffness term respecting rotation invariance of the spins is proportional to $(\nabla M)^2$ [see Chap. 9(I)]. The free energy describing this non-homogeneous order parameter is given by integrating the free energy density

$$F_Z - F_0 = \int d^3r \left(\frac{\Gamma}{2} (\nabla M)^2 + aM^2 + \frac{b}{2} M^4 - \mu_0 \mathbf{M} \cdot \mathbf{H} \right), \quad (4.15)$$

over the volume V of the system. F_Z is then a functional of $M(\mathbf{r})$. These hydrodynamic fluctuations $\delta \mathbf{M} = M(\mathbf{r}) - \mathbf{M}_0$ of the order parameter about its mean value \mathbf{M}_0 are very close to the spin wave modes described in Chap. 9(I). They are transverse to \mathbf{M}_0 , i.e., $\delta \mathbf{M} \cdot \mathbf{M}_0 = 0$. We decompose fluctuations δM into a Fourier sum

$$\delta M = \frac{1}{\sqrt{V}} \sum_{\mathbf{k}} \tilde{m}_{\mathbf{k}} \exp(i\mathbf{k} \cdot \mathbf{r}) \quad (4.16)$$

of components $\tilde{m}_{\mathbf{k}}$ transverse to \mathbf{M}_0 . The free energy fluctuation (4.15) now appears as a sum of *independent* contributions associated with each component $\tilde{m}_{\mathbf{k}}$ ($\ll M_0$) of the magnetisation fluctuations:

$$F_Z - \bar{F} = \sum_{\mathbf{k}^*} (\Gamma k^2 + 2a + 6bM_0^2) |m_{\mathbf{k}}|^2, \quad (4.17)$$

where the star indicates that the sum over \mathbf{k} is taken over a half sphere of directions, because components $\tilde{m}_{\mathbf{k}}$ and $\tilde{m}_{-\mathbf{k}}$ have been grouped together. \bar{F} is the contribution to free energy of the mean value M_0 of the order parameter. The probability (4.14) of a free energy fluctuation is therefore the product of contributions from each component $\tilde{m}_{\mathbf{k}}$, since these are independent. The mean amplitude of each component $\tilde{m}_{\mathbf{k}}$ is calculated by Gaussian quadrature. We integrate over fluctuations transverse to M_0 . The volume element is thus $d^2m_{\mathbf{k}} = 2\pi m_{\mathbf{k}} dm_{\mathbf{k}}$ and the Gaussian integrals are

$$\int_0^\infty x^{2n+1} \exp(-\alpha x^2) dx = n!/(2\alpha)^{n+1}. \quad (4.18)$$

This gives

$$\langle |m_{\mathbf{k}}|^2 \rangle = \frac{\langle |m_{\mathbf{k}}|^2 \exp(-\beta F) \rangle}{\langle \exp(-\beta F) \rangle} = \frac{1}{\Gamma k^2 + 2a + 6bM_0^2}. \quad (4.19)$$

Above T_c , when there is zero field, $M_0 \rightarrow 0$, we see that small wave vectors have large fluctuation amplitudes, limited only by the *correlation length*

$$\xi = 2\pi \sqrt{\frac{\Gamma T_c}{2\alpha(T - T_c)}}, \quad (4.20)$$

which diverges near T_c . Physically, long wavelength fluctuations involve infinitesimal energy because the restoring force Γk^2 tends to zero when $k \rightarrow 0$. The contribution of fluctuations to the free energy can be calculated likewise, giving

$$\begin{aligned} \delta F &= -\frac{1}{\beta} \ln \prod_{\mathbf{k}^*} \int d^2m_{\mathbf{k}} \exp[-\beta(\Gamma k^2 + 2a + 6bM_0^2)|m_{\mathbf{k}}|^2] \\ &= -\sum_{\mathbf{k}^*} \frac{1}{\beta} \ln \int_0^\infty 2\pi m_{\mathbf{k}} dm_{\mathbf{k}} \exp[-\beta(\Gamma k^2 + 2a + 6bM_0^2)|m_{\mathbf{k}}|^2]}, \end{aligned} \quad (4.21)$$

where the sum is taken over all amplitudes $m_{\mathbf{k}}$ of possible fluctuations. Carrying out the integration,

$$\delta F = -k_B T \sum_{\mathbf{k}^*} \ln \left(\frac{\pi k_B T}{\Gamma k^2 + 2a + 6bM_0^2} \right). \quad (4.22)$$

The contribution of fluctuations to susceptibility is given by the thermodynamic definition of the field $\partial F / \partial M_0 \equiv \mu_0 H = \mu_0 M_0 / \chi$. Hence,

$$\frac{1}{2\chi} = \frac{1}{\mu_0} \frac{\partial F}{\partial M_0^2} = \frac{a}{\mu_0} + \frac{1}{\mu_0} \sum_{\mathbf{k}} \frac{6b k_B T}{\Gamma k^2 + 2a}. \quad (4.23)$$

(Large values of k give a divergent contribution. The origin of this divergence lies in the classical treatment of spin waves. Taking into account their boson statistics,

$$\frac{k_B T}{\Gamma k^2 + 2a} \rightarrow \frac{1}{\exp[\beta(\Gamma k^2 + 2a)] - 1}, \quad (4.24)$$

and the contribution of these fluctuations converges naturally.) These fluctuations also contribute to specific heat. From its definition

$$C_{\text{fl}} = -\frac{T}{V} \frac{\partial^2 \delta F}{\partial T^2}$$

in terms of the free energy (4.22), we obtain, keeping only the most divergent term ($a = \alpha\tau$),

$$\begin{aligned} C_{\text{fl}} &\approx \frac{4\alpha^2}{V} \sum_{\mathbf{k}^*} (\Gamma k^2 + 2a + 6bM_0^2)^{-2} \\ &= 2\alpha^2 \int \frac{d^3k}{(2\pi)^3} (\Gamma k^2 + 2a + 6bM_0^2)^{-2} \\ &= \frac{\alpha k_B}{4\pi\Gamma^{3/2}} \frac{1}{\sqrt{2a + 6bM_0^2}}, \end{aligned} \quad (4.25)$$

after integrating over all wave vectors. We have replaced the sum over \mathbf{k} by an integral, normalising volumes,

$$\sum_{\mathbf{k}} \rightarrow V \int \frac{d^3k}{(2\pi)^3}. \quad (4.26)$$

This description of fluctuations serves to establish the limits of applicability of Landau theory. The above discussion explicitly assumes that the amplitude of long wavelength fluctuations remains small. To see whether this condition is fulfilled, we compare the contribution of fluctuations C_{fl} given by (4.25) with the discontinuity in specific heat ΔC at transition given by (4.10). This contribution must be small compared with ΔC [75]. Finally, the expansion (4.15) of F_Z as a function of a local order parameter is restricted to the neighbourhood of T_c ($\tau \ll 1$). Combining these two conditions, we obtain

$$\frac{b^2(k_B T_c)^2}{2\alpha\Gamma^3} \ll \frac{|T - T_c|}{T_c} \ll 1. \quad (4.27)$$

The limits of validity of Landau theory are therefore controlled by the values of Γ , α and b . In superconductors, the lower limit is so small that Landau theory is almost always valid. Concerning superfluidity of helium-4, the theory is never applicable, whereas superfluidity of helium-3 can almost always be described by Landau theory. For magnetic transitions, the lower limit lies between 0.1 and 0.3 so that Landau theory has limited applicability and deviations from it soon become significant. We shall now analyse the effect of fluctuations on a phase transition, when they begin to predominate.

4.3 Critical Exponents and Renormalisation of Fluctuations

Landau theory does not provide a satisfactory description of critical behaviour for many magnets close to transition [76, 77, 78, 79]. We use reduced variables

$$\tau = \frac{|T - T_c|}{T_c}, \quad h = \frac{\mu H}{k_B T_c}, \quad (4.28)$$

which parametrise ‘distance’ from the critical point ($T = T_c, H = 0$). Experiments show that magnetisation, susceptibility, specific heat and correlation length have power law behaviour close to T_c :

$$M(T) \propto \tau^\beta, \quad M(h) \propto h^{1/\delta}, \quad (4.29)$$

$$\chi(T) \propto \tau^{-\gamma}, \quad C(T) \propto \tau^{-\alpha}, \quad (4.30)$$

$$\xi(T) \propto \tau^{-\nu}. \quad (4.31)$$

Exponents $\alpha, \beta, \gamma, \delta$ and ν are the critical exponents and take irrational values, whereas in Landau theory they have values $\alpha = 0, \beta = 1/2, \gamma = 1, \delta = 3$ and $\nu = 1/2$.

Landau theory assumes analyticity above T_c once all spatial fluctuations of magnetisation have been averaged ($M_0 = \overline{M(\mathbf{r})}$). Analyticity is lost only when we take the thermodynamic average of mean magnetisation,

$$\langle M_0 \rangle = \int \exp[-\beta F(M_0, T)] M_0 d^3 M_0.$$

When we carry out the above average with Boltzmann weighting factor $\exp[-\beta F(M_0, T)]$, we find that equilibrium magnetisation corresponds to a minimum of F . From this condition, we can deduce the non-analytic forms (4.8) for specific heat and (4.7) for susceptibility. Landau theory is motivated by hydrodynamic considerations. Landau assumed that only fluctuations on an atomic scale are relevant, and that, once these are averaged out, magnetisation is a continuous function of space which only varies under the influence of an external force. $M(\mathbf{r})$ can then be obtained from a classic equation. This is how the Ginzburg–Landau theory [Chap. 13(II)] describes the order parameter of a superconductor. In a universe of dimension greater than or equal to 4, the Landau viewpoint is correct. Unfortunately, below 4 dimensions, fluctuations on all length scales up to the correlation length are significant and Landau theory is no longer valid. The free energy is a functional of $M(\mathbf{r})$ which is no longer analytic on any length scale.

The role of long wavelength fluctuations is easy to treat near $d = 4$, because they remain small. We therefore only consider fluctuations whose wavelength is large relative to atomic dimensions. (There exist other truncations which result in renormalisation of fluctuations up to the atomic length scale [81]. Here we follow the continuous approach of K. Wilson and M. Fisher [82].)

Once we have averaged over atomic fluctuations, magnetisation is a continuous functional of $M(\mathbf{r})$, as in Landau theory. But long wavelength fluctuations are still present in $M(\mathbf{r})$ and we must determine what form they can take. If L is a length greater than atomic dimensions, suppose that fluctuations of wavelength $\lambda < 2\pi L$ have been averaged out. $M(\mathbf{r})$ then only contains Fourier components of wavelength greater than $2\pi L$. We thus write

$$M(\mathbf{r}) = \int_{\mathbf{k}} \exp(i\mathbf{k} \cdot \mathbf{r}) m_{\mathbf{k}}, \quad (4.32)$$

where the integral

$$\int_{\mathbf{k}} \text{ means } \int \frac{d^d k}{(2\pi)^d},$$

d is the dimension of space, and we integrate $|k|$ up to $1/L$. Averaging over long wavelength fluctuations reduces to integrating over the $m_{\mathbf{k}}$, just as in Ornstein–Zernike theory [73]. However, in this case we do not limit ourselves to a harmonic theory in which each fluctuation is independent of the others. We take into account coupling between fluctuations of different wavelengths. As in Ornstein–Zernike theory, fluctuations are weighted by a Boltzmann factor $\exp(-\mathcal{F})$, where we introduce dimensionless free energies $\mathcal{F} = \beta F$ and Hamiltonians $\mathcal{H} = \beta H$. The size of fluctuations implies that coefficients a and b in the functional (4.15) also depend on scale L . We therefore introduce a (dimensionless) free energy depending on scale L , below which fluctuations have been averaged out:

$$\mathcal{F}_L = \int d^d r \left[\Gamma(\nabla M)^2(\mathbf{r}) + a_L M^2(\mathbf{r}) + \frac{b_L}{2} M^4(\mathbf{r}) \right], \quad (4.33)$$

where we have put $\beta\Gamma/2 \rightarrow \Gamma$, $\beta a \rightarrow a_L$, and $\beta b \rightarrow b_L$. Later we will justify the fact that Γ has negligible L dependence in the absence of a field. Non-analyticity of \mathcal{F}_L is a consequence of the L dependence of a and b , which only persists up to the correlation length ξ . Beyond this, fluctuations are negligible. We can then use Landau theory, once parameters a_L , b_L have been renormalised by short distance fluctuations. In other words, we can substitute a_{ξ} , b_{ξ} into (4.6) to obtain the spontaneous magnetisation. As the correlation length is non-analytic at T_c , the ξ dependence of a_{ξ} , b_{ξ} leads to subtle behaviour at the critical point.

To begin with, we seek to average fluctuations in the interval from L to $L + \delta L$, weighting with the Boltzmann factor $\exp(-\mathcal{F}_L)$. The result is a free energy $\mathcal{F}_{L+\delta L}$ for a magnetisation function denoted $M_{\mathcal{H}}(\mathbf{r})$, for wavelengths greater than $L + \delta L$. The Fourier components of $M_{\mathcal{H}}$ are the same $m_{\mathbf{k}}$ except that components between $1/L$ and $1/(L + \delta L)$ have disappeared. How many degrees of freedom $m_{\mathbf{k}}$ have thereby been eliminated? The volume of phase space eliminated is of the order of $V\delta L/L^{d+1}$. Rather than choosing the $m_{\mathbf{k}}$ as integration variables, it is convenient to use linear combinations of them corresponding to localised wave packets. Let $\psi_n(\mathbf{r})$ be an orthonormal basis

of $V\delta L/L^{d+1}$ functions, whose wave vectors lie between $1/L$ and $1/(L + \delta L)$ and occupy a volume of order $\delta V = L^{d+1}/\delta L$. In this basis, the magnetisation fluctuation becomes

$$M(\mathbf{r}) = M_{\mathcal{H}}(\mathbf{r}) + \sum_n m_n \psi_n(\mathbf{r}) . \quad (4.34)$$

We can integrate the m_n separately since the ψ_n are orthogonal. To simplify, consider a single integration $M(\mathbf{r}) = M_{\mathcal{H}}(\mathbf{r}) + m\psi(\mathbf{r})$ and assume $M_{\mathcal{H}}$ varies only slightly over the volume δV occupied by ψ . Then

$$\exp(-F_{L+\delta L}[M_{\mathcal{H}}]) = \int_{-\infty}^{\infty} dm \exp(-F_L[M_{\mathcal{H}} + m\psi]) \quad (4.35)$$

can be calculated by expanding $F_L[M_{\mathcal{H}} + m\psi]$. Since

$$\int d^d r [\nabla \psi(\mathbf{r})]^2 \approx 1/L^2 ,$$

we find that

$$\begin{aligned} \exp(-F_{L+\delta L}[M_{\mathcal{H}}]) &= \exp(-F_L[M_{\mathcal{H}}]) \\ &\times \int_{-\infty}^{\infty} dm \exp \left[\left(\frac{\Gamma}{L^2} + a_L \right) m^2 + 3b_L M_{\mathcal{H}}^2 m^2 \right] . \end{aligned} \quad (4.36)$$

Calculating this Gaussian integral with the standard result

$$\int_{-\infty}^{\infty} dx \exp(-\alpha x^2) = \sqrt{\pi/\alpha} ,$$

and taking the logarithm, we obtain

$$F_{L+\delta L}[M_{\mathcal{H}}] \approx F_L[M_{\mathcal{H}}] + \frac{1}{2} \ln \left(\frac{\Gamma}{L^2} + a_L + 3b_L M_{\mathcal{H}}^2 \right) . \quad (4.37)$$

This expression only takes into account fluctuations over the volume occupied by $\psi(\mathbf{r})$. It must be extended to the whole of V by integrating over all m_n .

When L is comparable with the correlation length, Γ/L^2 and a_L have the same order of magnitude [see (4.19) and (4.20)]. Therefore, at lengths intermediate between atomic distances and the correlation length ξ , a_L is small compared with Γ/L^2 . Using the approximation $\ln(1+x) \approx x - x^2/2$, the logarithm in (4.37) can be expanded in powers of $M_{\mathcal{H}}$ to give

$$\ln \left(\frac{\Gamma}{L^2} + a_L + 3b_L M_{\mathcal{H}}^2 \right) \approx \ln \frac{\Gamma}{L^2} + 3b_L \frac{L^2}{\Gamma} M_{\mathcal{H}}^2 \quad (4.38)$$

$$- \frac{9}{2} b_L^2 \frac{L^4}{\Gamma^2} M_{\mathcal{H}}^4 - 3a_L b_L \frac{L^4}{\Gamma^2} M_{\mathcal{H}}^2 . \quad (4.39)$$

We still have to integrate over all m_n . Noting that each ψ_n contributes in proportion to the volume it occupies in phase space, the difference in free energy (4.37) at length scales L and $L + \delta L$ is

$$\begin{aligned} F_{L+\delta L}[M_{\mathcal{H}}] - F_L[M_{\mathcal{H}}] &\approx \text{const.} \\ &+ \frac{V\delta L}{2L^{d+1}} \left(3b_L \frac{L^2}{\Gamma} M_{\mathcal{H}}^2 - \frac{9}{2} b_L^2 \frac{L^4}{\Gamma^2} M_{\mathcal{H}}^4 - 3a_L b_L \frac{L^4}{\Gamma^2} M_{\mathcal{H}}^2 \right). \end{aligned} \quad (4.40)$$

However, the difference in free energy between length scales L and $L + \delta L$ is [see (4.33)]

$$\begin{aligned} F_{L+\delta L} - F_L &\approx \text{const.} \\ &+ \frac{V}{L^{d+1}} \left[(a_{L+\delta L} - a_L) M_{\mathcal{H}}^2 + \frac{b_{L+\delta L} - b_L}{2} M_{\mathcal{H}}^4 \right]. \end{aligned} \quad (4.41)$$

If we now identify the coefficients of $M_{\mathcal{H}}^2$ and $M_{\mathcal{H}}^4$ in the last two equations, we obtain renormalisation equations relating values of coefficients a_L and b_L at two neighbouring length scales:

$$a_{L+\delta L} - a_L = \frac{3}{2} b_L \left(\frac{L^{1-d}}{\Gamma} - a_L \frac{L^{3-d}}{\Gamma^2} \right) \delta L, \quad (4.42)$$

$$b_{L+\delta L} - b_L = -\frac{9}{2} b_L \frac{L^{3-d}}{\Gamma^2} \delta L. \quad (4.43)$$

These are often written in differential form:

$$L \frac{da_L}{dL} = \frac{3}{2} b_L \left(\frac{L^{2-d}}{\Gamma} - a_L \frac{L^{4-d}}{\Gamma^2} \right), \quad (4.44)$$

$$L \frac{db_L}{dL} = -\frac{9}{2} b_L \frac{L^{4-d}}{\Gamma^2}. \quad (4.45)$$

These renormalisation equations can be applied up to the correlation length. Beyond, a_L and b_L change only slightly due to saturation of the logarithm and dominance of a_L over Γ/L^2 . When $d > 4$, a_L and b_L tend to constant values at large scales, as in Landau theory. When $d < 4$, b_L and a_L behave at large scales as

$$b_L \approx \frac{2(4-d)}{9} \Gamma^2 L^{d-4}, \quad (4.46)$$

$$a_L \approx u L^{(d-4)/3} - \frac{4-d}{2+d} \Gamma L^{-2}, \quad (4.47)$$

where u can be related to the microscopic value of a and is proportional to $T - T_c$. At large distances, the energy of a fluctuation ΓL^{-2} (elastic restoring energy) tends to zero and hence

$$a_L \propto L^{(d-4)/3} (T - T_c). \quad (4.48)$$

Exercise

Check the asymptotic behaviour of a_L and b_L as given in (4.46) and (4.47) for the case $d < 4$. What is their behaviour when $d > 4$? What can you deduce?

As before, the correlation length is reached when elastic energy $\Gamma(\nabla M)^2$ and condensation energy $a_L M^2$ are close to one another, i.e., $\Gamma/\xi^2 \approx a_\xi$. This implies

$$\xi \propto \sqrt{\frac{\Gamma}{a_\xi}} = \sqrt{\frac{\Gamma}{T - T_c}} \xi^{(4-d)/6}. \quad (4.49)$$

Putting $\varepsilon = 4 - d$, the critical exponent ν associated with the correlation length is then

$$\nu = \frac{1}{2} \frac{1}{1 - \varepsilon/6}. \quad (4.50)$$

This equals 0.6 in three dimensions and 3/4 in two dimensions. In an analogous way, since the spontaneous magnetisation is proportional to $\sqrt{a_\xi/b_\xi}$, the critical exponent β is

$$\beta = \frac{1}{2} - \frac{\varepsilon}{3} \frac{1}{1 - \varepsilon/6}. \quad (4.51)$$

The critical exponents are obtained here as expansions in powers of $4 - d$ and are non-trivial. They result from coupling of fluctuations on different scales. Some terms in the renormalisation equations tend to 0 at large scales. They become smaller as we approach the critical point and are not relevant to critical behaviour. The critical temperature T_c is a fixed point $da_L/dL = 0$ and $db_L/dL = 0$ of the renormalisation equations. The system is scale invariant, having the same structure at all lengths, and the free energy no longer depends on L . The behaviour of the free energy becomes independent of microscopic details of the system. This explains why critical behaviour is the same for so many different systems. Critical phenomena are thus universal. It can in fact be shown that critical exponents depend only upon the dimension and the number of components of the order parameter. The ideas behind scaling relations are based on the following observation: any thermodynamic quantity can be described using a scaling function and this imposes universal relations between critical exponents.

Finally, the renormalisation equations have other trivial fixed points. They correspond to limits $T \rightarrow \infty$ and $T \rightarrow 0$, where the system is either completely disordered or completely ordered. These fixed points are stable, whereas T_c is an unstable fixed point, in the sense that iteration of the renormalisation equations moves the system away from the critical point.

Renormalisation has had a considerable impact on contemporary physics. Apart from its application to critical phenomena, de Gennes has used it to formulate the modern theory of polymers [83]. Wilson's solution to Kondo's problem is another remarkable success for contemporary physics [84]. Finally, application of scaling ideas to the metal-insulator transition has laid the foundations for the theory of disordered systems [85].

4.4 Scaling Laws

Since fluctuations renormalise physical parameters up to the correlation length, any macroscopic physical quantity can be expressed as a function of correlation length which measures the distance to the critical point. Widom has used this to introduce a scaling law hypothesis: any deviation from the critical point corresponding to identical correlation lengths has the same effects if we measure it on scales where the correlation lengths correspond [86]. Mathematically, this hypothesis [86, 87, 88] requires the free energy F to be a homogeneous function of reduced variables $\tau = |T - T_c|/T_c$ and $h = \mu H/k_B T_c$, i.e.,

$$F(\lambda^u \tau, \lambda^v h) = \lambda F(\tau, h). \quad (4.52)$$

Differentiating with respect to h , magnetisation also obeys a homogeneity condition:

$$\begin{aligned} m &= -\lambda \frac{\partial F(\tau, h)}{\partial h} = -\lambda^v \frac{\partial F(\lambda^u \tau, \lambda^v h)}{\partial \lambda^v h} \\ &\Leftrightarrow \lambda M(\tau, h) = \lambda^v M(\lambda^u \tau, \lambda^v h). \end{aligned} \quad (4.53)$$

In the special case when $h = 0$, this becomes

$$M(\tau, 0) = \lambda^{v-1} M(\lambda^u \tau, 0). \quad (4.54)$$

This equation is true for any value of λ . Choosing $\lambda = \tau^{-1/u}$,

$$M(\tau, 0) = \tau^{(1-v)/u} m_0, \quad (4.55)$$

where $m_0 = M(1, 0)$ is often called the critical amplitude. Identifying this expression with the definition of the critical exponent β , we find

$$\beta = \frac{1-v}{u}. \quad (4.56)$$

Using the same procedure when $\tau = 0$,

$$M(0, h) = \lambda^{v-1} M(0, \lambda^v h), \quad (4.57)$$

and putting $\lambda = h^{-1/v}$, we obtain

$$M(0, h) = h^{1/v-1} m_1. \quad (4.58)$$

We can now eliminate scaling exponents u and v in terms of measurable critical exponents β and δ :

$$\delta = \frac{v}{1-v}, \quad u = \frac{1}{\beta} \frac{1}{\delta+1}, \quad v = \frac{\delta}{\delta+1}. \quad (4.59)$$

The scaling law for susceptibility is obtained in the same way, taking the second derivative of free energy with respect to h . It is easy to check that

$$\lambda^{2v} \chi(\lambda^u \tau, \lambda^v h) = \lambda \chi(\tau, h). \quad (4.60)$$

Choosing $\lambda = \tau^{-1/u}$ at $h = 0$,

$$\chi(\tau, 0) = \tau^{-(2v-1)/u} \chi_0 . \quad (4.61)$$

We can thereby identify the critical exponent γ to be

$$\gamma = \frac{2v - 1}{u} . \quad (4.62)$$

Expressions for scaling exponents u and v in terms of critical exponents lead to the Widom relation between β , γ and δ , viz.,

$$\gamma = \beta(\delta - 1) . \quad (4.63)$$

If we differentiate free energy with respect to temperature, we obtain in a similar way the scaling law for specific heat,

$$\lambda^{2u} C(\lambda^u \tau, \lambda^v h) = \lambda C(\tau, h) . \quad (4.64)$$

Putting $h = 0$ and $\lambda = \tau^{-1/u}$, we obtain the exponent α of the specific heat in terms of u : $\alpha = 2 - 1/u$. Identifying exponents leads to the Griffiths relation [89] between α , β and γ :

$$\alpha + 2\beta + \gamma = 2 . \quad (4.65)$$

Finally, when we analyse the behaviour of correlation functions with scale λ , we can obtain a hyperscaling relation which depends on the dimension d of space. This relation is

$$dv = 2 - \alpha = 2\beta + \gamma . \quad (4.66)$$

Exercise

Check that scaling relations (4.63), (4.65) and (4.66) are satisfied for the critical exponents in 4-dimensional Landau theory.

The last relation is not quite so general as the Widom and Griffiths relations since it is not valid for transitions whose fixed point is at zero temperature. (A magnet in a random magnetic field has a fixed point at $T = 0$ and hence has no hyperscaling relation.)

The most important physical consequence of the scale invariance hypothesis is existence of a scaling function. Suppose we have measured the magnetisation as a function of τ and h near the critical point. All experimental data can be fitted onto a single curve defined by

$$M(\tau, h) = \tau^\beta M \left(1, \frac{h}{\tau^{\beta\delta}} \right) . \quad (4.67)$$

The exponent $\phi = \beta\delta$ is the *crossover exponent*. The curve M/τ^β as a function of the single parameter $h/\tau^{\beta\delta}$ is illustrated in Fig 4.5 for CrBr_3 , a ferromagnetic magnet [90, 91]. This curve, the scaling function, describes the state equation of the magnet in the neighbourhood of the critical point. Scaling laws are observed experimentally in magnets for reduced temperatures τ in

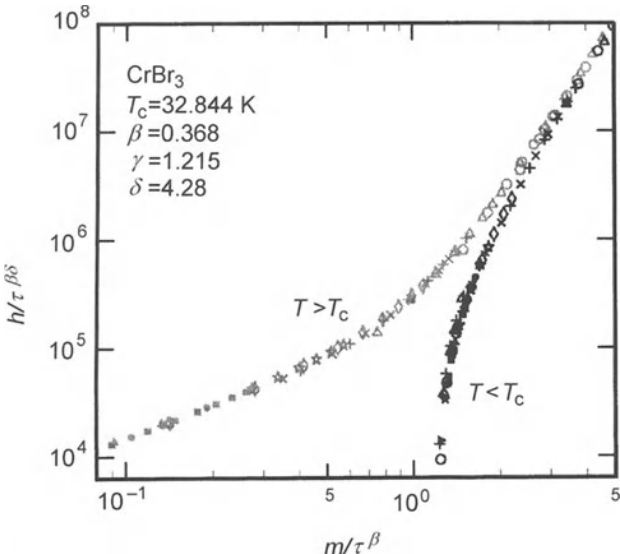


Fig. 4.5. Example of a scaling law obtained by Faraday rotation of the ferromagnetic magnet CrBr_3 [90, 91]. The whole set of data collected at all reduced temperatures and fields lies on the same curve, whilst the reduced temperature varies between 10^{-4} and 0.2. Curves above and below T_c have the same asymptotic slope, showing that critical exponents are the same on either side of transition

the range 10^{-1} – 10^{-4} , because lack of homogeneity in samples causes local variations in critical temperature. The most beautiful scaling laws have been observed at the superfluid transition of helium for values of τ in the range 10^{-1} – 10^{-5} [92].

Finally, there is also a dynamic scaling law [93] relating characteristic relaxation time of a system near a critical point to its correlation length. This scaling law will be discussed in Sect. 6.6(I) in the context of the Ising model.

5. Mean Field

Landau theory gives the magnetic states of matter near their critical temperature. However, it neglects the effects of fluctuations. This hypothesis seems justified for temperatures much smaller than the critical temperature. If we neglect Gaussian fluctuations in the order parameter, it is in fact possible to construct a microscopic theory of magnetism generalising Landau theory to all temperatures. This is mean or molecular field theory. Despite certain limitations, the method can describe qualitatively almost all types of magnetic order occurring in three-dimensional magnets. In addition, many refinements have been made to this theory, extending it to effects of reaction fields and Gaussian fluctuations. It has thus become an essential tool in condensed matter physics.

5.1 Molecular Field

The molecular field approximation amounts to linearising the Heisenberg Hamiltonian

$$\mathcal{H} = -J \sum_{i \neq j}^N \mathbf{S}_i \cdot \mathbf{S}_j - \gamma \mu_0 \sum_{i=1}^N \mathbf{S}_i \cdot \mathbf{H} \quad (5.1)$$

around the thermodynamic mean $\langle \mathbf{S}_i \rangle$ of the i th spin. This in turn is equivalent to neglecting quadratic fluctuations in $\mathbf{S}_i - \langle \mathbf{S}_i \rangle$. Substituting

$$\mathbf{S}_i = \langle \mathbf{S}_i \rangle + (\mathbf{S}_i - \langle \mathbf{S}_i \rangle) \quad (5.2)$$

into (5.1), we obtain the *mean field Hamiltonian*

$$\mathcal{H}_{\text{mf}} = -\gamma \mu_0 \sum_{i=1}^N \mathbf{S}_i \cdot (\mathbf{h}_i + \mathbf{H}) + J \sum_{i \neq j}^N \langle \mathbf{S}_i \rangle \cdot \langle \mathbf{S}_j \rangle, \quad (5.3)$$

where \mathbf{h}_i is the mean of the local field at site i , viz.,

$$\gamma \mu_0 \mathbf{h}_i = 2J \sum_{j \text{ s.t. } j \neq i} \langle \mathbf{S}_j \rangle. \quad (5.4)$$

This local field is precisely the molecular field \mathbf{h}_m^i defined by the Hartree-Fock approximation in (3.76). It therefore has a precise microscopic meaning

which is more general than we might expect from the spin Hamiltonian (5.1) and (5.3). If the i th spin has a great many neighbours, it seems plausible to neglect variations in molecular field from one site to another (a reasonable approximation in three dimensions and an exact one in four or more dimensions). In such conditions, we replace the molecular field \mathbf{h}_i by its mean \mathbf{h}_m over the sample. (This further averaging is only necessary in the presence of disorder or non-homogeneity.) For exchange $J_{ij} \equiv J$ between nearest neighbours,

$$|h_m| = \frac{2zJ\hbar S}{g\mu_0\mu_B} \sigma \approx \frac{zJ\hbar S}{\mu_0\mu_B} \sigma = \alpha M , \quad (5.5)$$

where $\sigma = M/Ng\mu_B S$ is the normalised order parameter of the magnet and z the number of neighbouring spins (magnetic coordination). Whereas the molecular field is proportional to the number of neighbours, local field fluctuations increase as the square root \sqrt{z} . For long range interactions, $z \rightarrow \infty$ and fluctuations become negligible. The mean field approximation is then exact. This result is rigorously demonstrated in Exercise C.1.2 (Appendix C). The molecular field is also proportional to magnetisation, the only vector defining the macroscopic order parameter of the magnet. The parameter α relating h_m to magnetisation becomes, in terms of microscopic constants,

$$\alpha = \frac{2zJ\hbar}{\mu_0(g\mu_B)^2 N} . \quad (5.6)$$

It increases with magnetic coordination z . The mean field equation determines the magnetisation produced by induction $B = \mu_0(h_m + H) = \mu_0(\alpha M + H)$ in a self-consistent way. To simplify this analysis, we shall consider the spin 1/2 case [94, 95]. The magnetisation of the system is determined by Langevin's equation

$$\begin{aligned} M &= N\mu \tanh[\beta\mu_0\mu(H + h_m)] \\ &= N\mu \tanh[\beta\mu_0\mu(H + \alpha M)] , \end{aligned} \quad (5.7)$$

where $\mu = g\mu_B/2$. The parameter α given by (5.6) is generally determined experimentally. Let us begin by assuming that the external field is zero $H = 0$. Figure 5.1 shows a graphical solution of the problem, as the intersection of $y = M/N\mu$ and $y = \tanh(\alpha\beta\mu_0\mu M)$. At high temperatures, the only possible solution is $M = 0$ and the partition function is the same as that for N free spins, $Z = 2^N$. Below the critical temperature

$$T_c = \frac{\alpha N \mu_0 \mu^2}{k_B} = \frac{zJ\hbar}{2k_B} , \quad (5.8)$$

the equation has three possible solutions when the magnetic field is zero: the trivial solution $M = 0$, which is in fact unstable ($\partial^2 F / \partial M^2 \leq 0$, see Sect. 5.2), and

$$M = \pm \mu N \sigma . \quad (5.9)$$

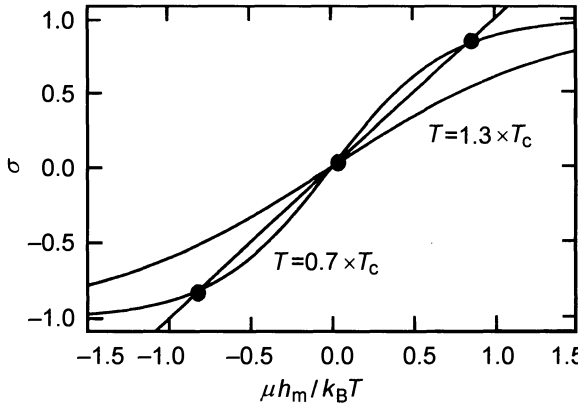


Fig. 5.1. Graphical determination of spontaneous magnetisation above and below T_c . Below T_c , solution $M = 0$ is excluded because the condition for thermodynamic stability $\partial H/\partial M = \mu_0^{-1} \partial^2 F/\partial M^2 > 0$ is not satisfied

Here the normalised order parameter σ is a solution of the Weiss equation

$$\sigma = \tanh \left[\frac{T_c}{T} (\sigma + h) \right], \quad (5.10)$$

where the reduced field is defined by $h = \mu H/k_B T_c$. σ is normalised so that $\sigma \rightarrow 1$ when $T \rightarrow 0$. The magnetisation M is then the saturation magnetisation $N\mu$. In zero field, we can rewrite the mean field equation in the equivalent form

$$\begin{aligned} \frac{T}{T_c} &= \frac{2\sigma}{\ln(1+\sigma) - \ln(1-\sigma)} \\ &= \frac{2\sigma}{2(\sigma + \sigma^3/3 + \sigma^5/5 + \dots)}. \end{aligned} \quad (5.11)$$

Near T_c where σ is small, the order parameter has the same temperature dependence as in Landau theory, i.e., $\sigma = \sqrt{3}(T_c/T - 1)$. (To the next order we find

$$\sigma^2 = \frac{5}{6} \left[\sqrt{1 - \frac{18}{5} \left(1 - \frac{T_c}{T} \right)} - 1 \right]. \quad (5.12)$$

It is straightforward to check that the magnetisation below T_c is reduced: $\sigma^2 \approx 3\tau - 27\tau^2/20$.) It is no accident that the temperature dependence should be the same. The mean field approximation neglects fluctuations in just the same way as Landau theory. Expanding the mean field equation (5.10) for $T > T_c$, we find that susceptibility obeys the Curie–Weiss law

$$\chi = \frac{C}{T - T_c}, \quad (5.13)$$

in which $C = \mu_0 N \mu^2 / k_B$ is the Curie constant. As in Landau theory, susceptibility is singular at T_c . If we assume that, for $T < T_c$, eigenstates of the magnet can be represented as products of eigenstates for each spin 1/2 in a molecular field h_m , the partition function associated with these non-trivial solutions is

$$\begin{aligned} Z &= (2 \cosh \beta \mu h_m)^N = (2 \cosh \sigma T_c / T)^N \\ &= (2 \cosh \tanh^{-1} \sigma)^N = (2 / \sqrt{1 - \sigma^2})^N. \end{aligned} \quad (5.14)$$

The mean field approximation is therefore equivalent to a factorisation of the partition function into N identical factors. In this approximation there are two types of error. Firstly, we implicitly assume that the molecular field \mathbf{h}_i acting at site i does not depend on the orientation of spin \mathbf{S}_i . Now, depending on its orientation, the spin \mathbf{S}_i can polarise its neighbours since the induced field $\mathbf{h}_k = J_{ki} \mathbf{S}^i$ varies. In their turn, all neighbouring spins \mathbf{S}_k react back on spin \mathbf{S}_i through the exchange term. This induces a reaction field \mathbf{h}_i^r of the i th spin on itself given by

$$\mathbf{h}_i^r = \sum_k J_{ik} J_{ki} \chi_k^{-1} \langle \mathbf{S}^i \rangle.$$

In Sect. 5.3, we will show how to include effects of this reaction field in the mean field approximation. A second error arises from the existence of collective modes of low energy spins. These excitations are spin waves similar to phonons in a crystal. They play a crucial role at low temperatures where reversal of individual spins in the exchange field h_i can no longer occur, so that spin waves are the only remaining elementary excitations.

When we calculate the free energy F of a magnet in the mean field approximation, we must add the electromagnetic field energy to the free energy of the spin configuration [see Chap. 1(I)]. The energy contained in the electromagnetic field is

$$\int_0^M h_m(m) dm = N^2 \mu^2 \alpha \int_0^\sigma s ds = N^2 \mu^2 \alpha \frac{\sigma^2}{2} = N k_B T_c \frac{\sigma^2}{2}. \quad (5.15)$$

The free energy and internal energy $U = \partial(\beta F) / \partial \beta = F - T \partial F / \partial T$ of the magnet are then

$$F = -N k_B T \ln 2 + \frac{N k_B T}{2} \ln(1 - \sigma^2) + N k_B T_c \frac{\sigma^2}{2}, \quad (5.16)$$

$$U = -N k_B T_c \frac{\sigma^2}{2}. \quad (5.17)$$

From the internal energy, it is easy to evaluate the specific heat per spin:

$$C_\sigma = \frac{1}{N} \frac{\partial U}{\partial T} = -k_B T_c \sigma \frac{\partial \sigma}{\partial T} = \frac{k_B T_c^2 (1 - \sigma^2) \sigma^2}{T [T - T_c (1 - \sigma^2)]}. \quad (5.18)$$

This gives $c_\sigma = 3k_B/2$ at transition.

Exercise

Prove explicitly relation (5.18) for the specific heat per spin.

When $T \ll T_c$, (5.11) gives a magnetisation exponentially close to saturation, i.e., $\sigma = 1 - \exp(2T_c/T)$. The specific heat is exponentially small at low temperatures, $c_\sigma = 4k_B(T_c/T)^2 \exp(-2T_c/T)$, since the only excitations retained here are individual spin flips in the exchange field (which is of the order of $k_B T_c/\mu$). We shall see that at low temperatures the specific heat is dominated by very long ‘hydrodynamic’ excitations (or spin waves) which have much lower energies. Mean field theory can of course be extended to any spin value. The mean field equation is expressed in terms of the Brillouin function [96], already encountered in Chap. 2(I),

$$M = N\mu B_S(\beta\mu\alpha M), \quad (5.19)$$

where $\mu = \mu_B g_S S$ as before. Saturation magnetisation is $M(T=0) = N\mu$ since $B(\infty) = 1$. The argument of the Brillouin function is

$$y = N\mu^2\beta\alpha[M/M(0)] = bM/M(0) = b\sigma,$$

where σ is the normalised order parameter. Expanding the Brillouin function,

$$B_S(y) = \frac{S+1}{3S} \left(y - \frac{2S^2 + 2S + 1}{30S^2} y^3 + \dots \right), \quad (5.20)$$

we obtain the dependence of critical temperature and order parameter $\sigma = M(T)/M(0)$ near T_c on spin value S :

$$T_c = \frac{N\mu^2\alpha(S+1)}{3k_B S}, \quad (5.21)$$

$$\sigma^2 = \frac{10}{3} \frac{(S+1)^2}{2S^2 + 2S + 1} |\tau|, \quad (5.22)$$

where $\tau = (T - T_c)/T_c$. In terms of the order parameter, the internal energy is given directly by

$$U = -\frac{3}{2} N k_B T_c \frac{S}{S+1} \sigma^2. \quad (5.23)$$

The discontinuity in specific heat at T_c increases with spin S :

$$\Delta c_\sigma = 5k_B \frac{S(S+1)}{S^2 + (S+1)^2}, \quad (5.24)$$

equalling $5k_B/2$ in the classical limit $S \rightarrow \infty$. At low temperatures, the specific heat still decreases exponentially, but more slowly:

$$c_\sigma(T \ll T_c) \approx \frac{9k_B}{(S+1)^2} \left(\frac{T_c}{T} \right)^2 \exp \left(\frac{3}{S+1} \frac{T_c}{T} \right). \quad (5.25)$$

Once again there are further hydrodynamic contributions to specific heat which are much greater at low temperatures.

Exercise

Check relations (5.21–5.24) explicitly.

5.2 Susceptibility and Spontaneous Magnetisation

Figure 5.2 shows a graphical solution of (5.10) for the order parameter $\sigma(H) = M(H)/M_0$, by translation of the function $\tanh(T_c\sigma/T)$ of $T_c h/T = \mu H/k_B T$. When $T < T_c$, the order parameter can have three possible determinations in a certain range of values of the field. It can be shown quite generally [by means of the fluctuation-dissipation theorem discussed in Chap. 8(I)] that the susceptibility of a spin system can never be negative. (Diamagnetism is basically an orbital property.) Any region where $\partial\sigma/\partial H < 0$ is therefore unstable. Let h_1 be the value of the field at the point where

$$\frac{\partial\sigma}{\partial h}(h_1) = 0,$$

as indicated in Fig. 5.3. As the magnetic field decreases from $+\infty$ down to some value $h \leq -h_1$, the order parameter jumps discontinuously at $-h_1$ because the system becomes thermodynamically unstable. Similarly when h increases from $-\infty$ to $+h_1$. This is magnetic hysteresis. As an illustration, the dependence of the reduced field $h = \mu H/k_B T_c$ on $-\sigma$ has been plotted at constant temperature. These curves are analogous to isotherms of a van der Waals gas, which also exhibit a thermodynamically unstable region. Regions where $\sigma > 0$ for $h < 0$ and vice versa describe states very similar to superheated liquids and supercooled vapours. For a magnet, nucleation of a phase with opposite magnetisation is difficult. This is why hysteresis

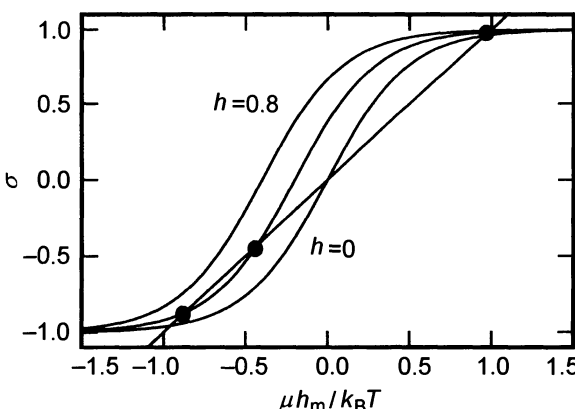


Fig. 5.2. Graphical solution of the Weiss equation in the presence of a magnetic field. Only those solutions corresponding to positive susceptibility are thermodynamically stable

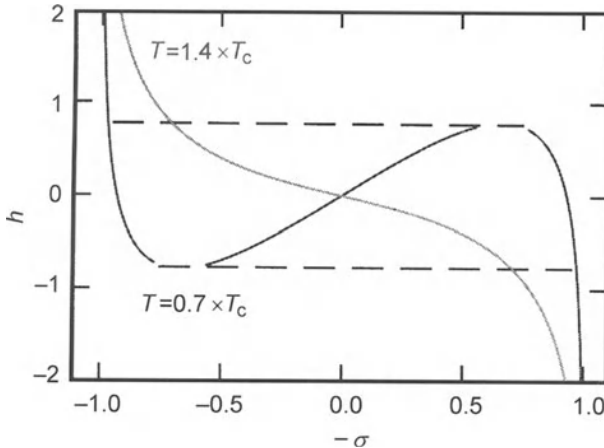


Fig. 5.3. Dependence of h on $-\sigma$ below T_c (full curve) and above (dotted curve). Below T_c the system jumps irreversibly from one orientation of magnetisation to the other along the horizontal dashed lines

effects are so important in magnets. To give a correct description of magnetic hysteresis, we must understand that a state of uniform magnetisation rarely corresponds to a minimum of magnetostatic energy. Indeed, it is possible to lower the sum of *exchange energy* and *dipolar energy* by forming domains whose size and shape depend on:

- exchange energy J , which determines the energy required to form an interface between two domains;
- magnetic moment μ , which determines the dipolar energy scale;
- the shape of the sample, which influences the details;
- disorder (impurities), which lowers the energy of walls between domains and contributes to pinning them.

Above T_c , the linear susceptibility is obtained by expanding the mean field equation to first order in M :

$$M = N\mu B_S[\beta\mu(H + \alpha M)] \approx N\mu^2\beta \frac{S+1}{3S}(H + \alpha M). \quad (5.26)$$

This gives the Curie–Weiss susceptibility

$$\chi = \frac{C_S}{T - T_c}, \quad (5.27)$$

where the Curie constant is

$$C_S = N \frac{(g_S\mu_B)^2 S(S+1)}{3k_B}. \quad (5.28)$$

Ferromagnetism can be detected at high temperatures. Plotting $1/\chi$ as a function of temperature (Curie–Weiss graph), we obtain a straight line which

intersects the temperature axis at T_c . Consequently, when this intersection is clearly positive, the system tends towards ferromagnetism. If the intersection is negative, it tends towards antiferromagnetism, which we shall describe in Sect. 5.4. In weak fields, we can define a susceptibility below T_c through $M(T, H)/M_0 \approx \sigma(T) + \chi(T)H$. By similar analysis to that carried out for susceptibility, we find

$$\chi(T) = \frac{1 - \sigma^2}{T - T_c(1 - \sigma^2)}, \quad (5.29)$$

which diverges as $1/(T_c - T)$ when $T \rightarrow T_c^-$, with the same critical exponent ($\gamma = 1$) as above T_c . This symmetry is observed for all second order phase transitions and is a consequence of scaling laws.

Exercise

Demonstrate (5.29) explicitly.

Exercise: Demagnetisation of a Ferromagnetic System

Consider a spin 1/2 system with ferromagnetic exchange J in an external magnetic field h .

1. What is the free energy above and below the Curie temperature?
2. What is the entropy of the system as a function of temperature and magnetic field?
3. Deduce that a ferromagnetic system cannot be cooled below its Curie temperature by adiabatic demagnetisation.

5.3 Reaction Field

We shall simplify our study of the reaction field by considering a magnet made up of Ising spins which can only take on the two values ± 1 . Let S^0 denote a particular spin. The exchange field $h_0 = \sum_j J_{j0}S^j$ acting on spin S^0 is not independent of its orientation. In fact, S^0 contributes a quantity

$$h_j(S^0) = J_{j0}S^0, \quad (5.30)$$

to the exchange field of its neighbours. The thermodynamic mean of this quantity is

$$\langle h_j(S^0) \rangle = J_{j0}\langle S^0 \rangle = J_{j0}m^0.$$

Denoting the local susceptibility of spin S^j by χ_j , the thermodynamic mean $m^j = \langle S^j \rangle$ of the magnetisation at site j is shifted by an amount

$$\delta m^j = J_{j0}\chi_j m^0 \quad (5.31)$$

by the effects of the field $h_j(S^0)$. This polarisation of neighbouring spins by spin S^0 therefore induces a reaction field

$$\langle h_0^r \rangle = \sum_j J_{0j} \delta m^j = \sum_j J_{0j} J_{j0} \chi_j m^0 \quad (5.32)$$

on the spin S^0 . Although the exchange field h_0 is not independent of S^0 , the cavity field $h_c = h_0 - h_r$ is, since the reaction of neighbouring spins on S^0 has been subtracted. As h_c is a random variable whose mean is independent of S^0 , the thermodynamic mean of spin S^0 can be determined by replacing the cavity field by its mean value. We then obtain the Onsager equations

$$m_0 = \mu \tanh \beta \mu \langle h_0^c \rangle , \quad (5.33)$$

$$\langle h_0^c \rangle = \langle h_0 \rangle - \langle h_0^r \rangle = \sum_j (J_{0j} m^j - J_{0j}^2 \chi_j m^0) . \quad (5.34)$$

Their solution defines the mean field approximation [97]. To a first approximation, the local susceptibility is

$$\chi_j = \left(\frac{\partial m_j}{\partial h_j} \right)_T = \frac{\beta \mu^2}{\cosh^2 \beta \mu h_j} = \beta(\mu^2 - m_j^2) , \quad (5.35)$$

where \cosh^{-2} has been rewritten as $1 - \tanh^2$ and we have used the mean field equation. For any magnetic system, the mean squared local magnetisation taken over sites neighbouring S_0 is specified by the parameter $q \approx z^{-1} \sum_j m_j^2$ such that

$$\sum_j J_{0j}^2 m_j^2 = \langle J^2 \rangle z \mu^2 q , \quad (5.36)$$

where z is the magnetic coordination of the site. The Onsager equations then take the very general form

$$m_0 = \mu \tanh \beta \mu \langle h_c \rangle , \quad (5.37)$$

$$\langle h_c \rangle = \langle h_0 \rangle - \langle J^2 \rangle z \mu (1 - q) m_0 . \quad (5.38)$$

In disordered magnets such as spin glasses, the exchange term J_{ij} is a random variable whose typical value is $\langle J_{ij}^2 \rangle = \langle J^2 \rangle$. Onsager's equations can be applied to these systems, in which the reaction field is large [98, 99]. Although such disordered magnets do not exhibit spontaneous magnetisation, the mean value of q is nevertheless an order parameter, called the Edwards-Anderson order parameter. It is just the mean squared local magnetisation [100, 101]. The Onsager reaction field method provides a recursive construction of the partition function, as is illustrated by the following demonstration of Onsager's equations. Adding a spin S^0 to an equilibrium ensemble of N spins, the exchange field on this spin, and its variance, are given by

$$\langle h \rangle_N = \sum_{k=1}^N J_{0k} m_k , \quad (5.39)$$

$$\begin{aligned}
\langle(h - \langle h \rangle_N)^2\rangle &= \sum_{k,l=1}^N J_{0k} J_{0l} \langle(S_k - m_k)(S_l - m_l)\rangle \\
&\approx \sum_k J_{0k}^2 \langle(S_k - m_k)^2\rangle \\
&\approx \langle J^2 \rangle z \mu^2 (1 - q) ,
\end{aligned} \tag{5.40}$$

where the $m_k = \langle S^k \rangle_N$ are the expectation values of S^k without the new spin S^0 . As the m_k are independent of m_0 , local fields h have Gaussian distribution with variance $\bar{h}_N = \langle J^2 \rangle z \mu^2 (1 - q)$. For each configuration of N spins there correspond two configurations of $N + 1$ spins (including S^0), and their energies are $E_N = \mp \beta \mu h$. The probability of having an $(N + 1)$ -spin system with given local field h at spin S^0 together with a given value of this spin is therefore

$$\mathcal{P}(h, S_0) = K \exp\left(-\frac{(h - \langle h \rangle_N)^2}{\bar{h}_N} + \beta \mu h S_0\right). \tag{5.41}$$

K is a factor normalising the distribution to unity. As anticipated, this distribution is no longer Gaussian and is correlated with the value of S_0 . It is then easy to calculate the mean magnetisation and the mean field from this probability distribution:

$$\begin{aligned}
m_0 &= \langle S_0 \rangle_{N+1} = \sum_{S_0} \int dh \mathcal{P}(h, S_0) S_0 \\
&= \mu \tanh \beta \mu \langle h \rangle_N ,
\end{aligned} \tag{5.42}$$

$$\langle h \rangle_{N+1} = \langle h \rangle_N + \beta \mu^2 (1 - q) \tanh \beta \mu \langle h \rangle_N . \tag{5.43}$$

These are the same as Onsager's equations, obtained previously by a different method. The partition function Z_{N+1} of the $N + 1$ spins is constructed recursively from the function Z_N . It no longer separates into a product of N identical terms. The Onsager procedure nevertheless gives the thermodynamic functions and free energy of the system.

5.4 Antiferromagnetism

In an antiferromagnetic system, spins are arranged alternately \uparrow, \downarrow across the lattice. (Such an arrangement assumes that there is no frustration of exchange over the lattice formed by the spins.) Néel was the first to generalise the idea of molecular field by separating the lattice formed by the spins into two interpenetrating sublattices (a) and (b), depending on spin direction \uparrow or \downarrow [102]. In such a situation, sublattice (a) exerts molecular field h_a on sublattice (b), whilst sublattice (b) exerts molecular field h_b on sublattice (a). For spin 1/2, the constitutive equations of the mean field approximation have form

$$\sigma_a = \tanh\left(\beta\mu H - \frac{T_N}{T}\sigma_b\right) = \tanh\left(\frac{T_N}{T}(h - \sigma_b)\right), \quad (5.44)$$

$$\sigma_b = \tanh\left(\beta\mu H - \frac{T_N}{T}\sigma_a\right) = \tanh\left(\frac{T_N}{T}(h - \sigma_a)\right), \quad (5.45)$$

where we have defined the (Néel) critical temperature as before by $T_N = N\mu^2\alpha/k_B$ and also the reduced field $h = \alpha\mu NH$, in units of the order parameters σ_a and σ_b for each sublattice (a) and (b). In the absence of a magnetic field, these two parameters are clearly opposed to one another: $\sigma_a = -\sigma_b = \sigma$. The mean field equations are exactly the same as those we solved earlier for ferromagnetic systems. T_N is then the critical temperature of the system. In the presence of a magnetic field, two macroscopic variables describe the system: magnetisation $M = N\mu(\sigma_a + \sigma_b)/2$ and the alternating order parameter $\sigma = (\sigma_a - \sigma_b)/2$. Above transition, the susceptibility is obtained by adding the two equations (5.44, 5.45) and linearising. This gives

$$M = \frac{C_{1/2}}{T + T_N} H. \quad (5.46)$$

The susceptibility does not diverge at transition. Only one magnetic wave, with wave vector $2\pi/a$ where a is the lattice spacing, couples to the alternating susceptibility $\chi^\dagger = \partial\sigma/\partial(h_a - h_b)$, and the latter diverges at transition. Such a wave is produced by a polarised neutron beam in which one component of the neutron wave vector is a multiple of $2\pi/a$. Hence the great utility of neutron scattering in the study of antiferromagnetism. Below transition, there are two susceptibilities depending on whether the magnetic field is applied along the axis of magnetisation of the sublattices (longitudinal susceptibility) or perpendicular to it (transverse susceptibility). Let us begin with longitudinal susceptibility. For weak fields, the magnetisation of the sublattices is $\sigma_a = \sigma + \chi_{\parallel}^a h$ and $\sigma_b = -\sigma + \chi_{\parallel}^b h$. Expanding (5.44) and (5.45) to first order in h , we obtain

$$\begin{aligned} \sigma_a &= \frac{T_N(1 - \chi_{\parallel}^b)h/T + \tanh(T_N\sigma/T)}{1 + (T_N/T)(1 - \chi_{\parallel}^b)h\tanh(T_N\sigma/T)} \\ &= \frac{T_N(1 - \chi_{\parallel}^b)h/T + \sigma}{1 + (T_N/T)(1 - \chi_{\parallel}^b)h\sigma}, \end{aligned} \quad (5.47)$$

$$\begin{aligned} \sigma_b &= \frac{T_N(1 - \chi_{\parallel}^a)h/T - \tanh(T_N\sigma/T)}{1 - (T_N/T)(1 - \chi_{\parallel}^a)h\tanh(T_N\sigma/T)} \\ &= \frac{T_N(1 - \chi_{\parallel}^a)h/T - \sigma}{1 - (T_N/T)(1 - \chi_{\parallel}^a)h\sigma}. \end{aligned} \quad (5.48)$$

Subtracting one equation from the other, we find immediately that $\chi_{\parallel}^a = \chi_{\parallel}^b = \chi_{\parallel}$. Adding them together,

$$2H\chi_{\parallel} = \frac{\sigma + (1 - \chi_{\parallel})HT_N/T}{1 + (1 - \chi_{\parallel})H\sigma T_N/T} - \frac{\sigma - (1 - \chi_{\parallel})HT_N/T}{1 - (1 - \chi_{\parallel})H\sigma T_N/T}$$

$$\approx 2(1 - \chi_{\parallel})(1 - \sigma^2)HT_N/T. \quad (5.49)$$

At low fields, longitudinal susceptibility is therefore given by

$$\chi_{\parallel} = \frac{C(1 - \sigma^2)}{T + T_N(1 - \sigma^2)}. \quad (5.50)$$

This susceptibility tends to zero as $T \rightarrow 0$ and is maximal at the transition T_N , where it equals $C/2T_N$. As the Néel temperature is of the same order as the exchange constant J/k_B , the susceptibility of an antiferromagnet is inversely proportional to the exchange. Regarding transverse susceptibility, we note that the resultant field $\mathbf{h}_r^{a,b} = \mathbf{h}_m^{a,b} + \mathbf{H}_{\perp}$ on each sublattice makes an angle $|\theta| \approx H_{\perp}/(H_{\perp}^2 + h_m^2)^{1/2}$, as shown in Fig. 5.4a. The magnetisation of each sublattice is collinear with the resultant local field so the transverse magnetisation is $M/M_0 = 2\sigma|\theta| = 2\sigma H_{\perp}/(H_{\perp}^2 + h_m^2)^{1/2}$. The transverse susceptibility $\chi_{\perp} = 2\sigma/h_m = \mu M_0/k_B T_N$ is therefore constant and equal to $C/2T_N$ as shown in Fig. 5.4b. Above T_N , the susceptibility is of course isotropic since there is no longer any alternating magnetisation.

A uniaxial anisotropy energy $D \sum_i (S_i^z)^2$ stabilises the orientation of the order parameter in an antiferromagnet (along the \hat{z} axis when D is negative). When we apply a magnetic field in this direction, the order parameter remains collinear with the field (and the anisotropy axis) up to a critical field H_{sf} , the spin-flop field, at which the order parameter suddenly swings into the plane perpendicular to the field (i.e., the (\hat{x}, \hat{y}) plane) [119]. The physical reason for this is simple. With this orientation, the system obtains a Zeeman energy greater than the energy in a collinear orientation. When the field is strong enough, the difference of Zeeman energy between the two orientations exceeds the anisotropy energy and the order parameter flips over suddenly

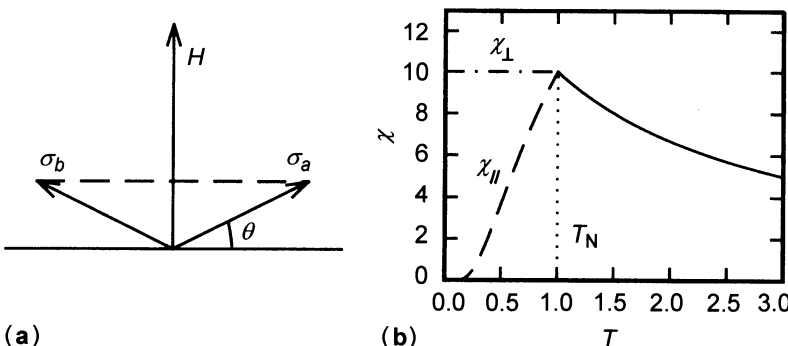


Fig. 5.4. (a) Orientation of order parameters σ_a and σ_b relative to the applied field $H_{\perp} = H\hat{y}$ and to the order parameter $\sigma = \sigma\hat{z}$ in zero field. (b) Temperature dependence of longitudinal and transverse susceptibility

into the perpendicular plane. This is of course a first order transition, since the order parameter is non-zero at transition. A detailed study of the spin-flop transition can be found in Exercise C.1.3 of Appendix C.

Exercise

Check that below T_N the magnetic field dependence of the Gibbs free energy is

$$G_S(H) \approx G_S(0) - \frac{\mu_0}{2} \left(\chi_{\parallel} H_{\parallel}^2 + \chi_{\perp} H_{\perp}^2 \right). \quad (5.51)$$

Deduce the orientation of the order parameter relative to the applied field in the most stable thermodynamic state.

5.5 Exotic Magnets

Spin Density Waves

If the wave vector associated with the alternating magnetisation is not commensurate with lattice spacing, we speak of a spin density wave. Usually, the spin density wave vector can vary below transition, but locks in with lattice periodicity at lower temperatures, via a first order phase transition. We then speak of the commensurate-incommensurate phase transition. Quasi-1-dimensional organic conductors are particularly prone to this type of instability because their Fermi surfaces have rather strong meshing properties in one direction. Spin density wave states are described in Chap. 11(I) in the context of itinerant magnetism.

Ferrimagnetism

If a magnet has both a spontaneous and an alternating magnetisation, we speak of ferrimagnetism. Such systems have two order parameters M and N which are generally coupled. The associated ferromagnetic and antiferromagnetic transitions do not always occur together. In most cases, ferrimagnetism results from two different ions forming two sublattices of different magnetisation. Ferrimagnetic magnets have quite interesting hydrodynamic modes. Their resonance modes are discussed in Chap. 8(I) as an example of a linear response.

Helimagnets

Here spins rotate through some angle θ as we move through each atomic layer along the \hat{c} axis of an anisotropic lattice (e.g., tetragonal or hexagonal). This angle is not necessarily a submultiple of 2π . (An angle $\theta = \pi$ corresponds

to an antiferromagnet with two sublattices, and $\theta = \pi/2$ corresponds to one with four sublattices, etc.) The spins thus form a spiral which may or may not be commensurate with the lattice. The best known example of this type of order is Holmium, whose spiral locks in with lattice periodicity at low temperatures [120]. The complexity of this order parameter gives rise to very rich hydrodynamic modes which will be studied in Chap. 9(I).

Frustrated Antiferromagnets

Two types of frustration are observed in antiferromagnets. Firstly, an antiferromagnetic interaction between second neighbours may oppose antiferromagnetic order between nearest neighbours. The system cannot satisfy all constraints with just two sublattices. Usually it will resolve its frustration by forming an ensemble of sublattices with complex geometry [104, 105, 106, 107]. But other interesting possibilities also exist. The system may form a fluid phase in which spins remain strongly correlated [108]. (An example of this exotic state seems to have been created in a 2-dimensional Kagomé lattice. The lattice is made up of an ensemble of stars of David touching at their points. Triangles in the lattice have only one common apex, and this generates a high level of degeneracy.) These spin liquids have highly quantum properties and are being actively studied at the present time [see Chap. 11(I)] [109, 110, 111, 112, 113].

A second form of frustration in antiferromagnets comes from the lattice. The 2-dimensional triangular lattice [114, 115, 116, 117], the 3-dimensional face-centred cubic lattice and also certain tetragonal structures, are not compatible with antiferromagnetism because the product of exchange interactions over a closed loop in the lattice is negative. In this situation, the exchange bonds cannot all be satisfied. This leads to a high level of degeneracy in the ground state which also comprises a large number of sublattices. In this case, the interesting processes are ones which remove degeneracies [118]. Examples are (a) thermal fluctuations, (b) quantum fluctuations [120], and (c) disorder [121]. These competing selection processes can give rise to particularly rich phase diagrams [122, 123]. This is another rather poorly understood area of magnetism.

Disordered Magnets

Two other types of frustrated magnets involve disorder. Spin glasses are magnets in which interactions between spins are sometimes ferromagnetic, sometimes antiferromagnetic. Although it may seem paradoxical, these systems exhibit a second order phase transition in a frozen phase in which spins maintain fixed directions relative to one another [100, 124, 125]. These systems exhibit some properties characteristic of glasses, such as slow relaxation and hysteresis. In addition, the organisation of their states reveals a complexity similar to that of neuronal networks in the human brain [99].

Another disordered magnet can be produced in certain materials. These are random field magnets, in which the external magnetic field applied to each spin fluctuates randomly from one spin to another. This system has a rather special phase transition in which thermal fluctuations play no role (i.e., they are irrelevant) [126, 127]. The transition is governed by the field fluctuations, giving rise to new phase transition behaviour.

There are many other ordered and disordered magnetic systems and they are active subjects of research around the world. The aim is often technological: magnetism, and more recently magneto-optics, provide a means for storing huge quantities of data. With regard to magneto-optic recording by laser which is being developed (and sold) at the present time, technological and commercial stakes are high, given the storage demands required in databases on information highways.

6. The Ising Model

There are very few models of interacting spins which are exactly solvable by the methods of statistical physics. Among these, the Ising model is exactly solvable in one dimension [128]. In this case, fluctuations are so large that the phase transition is pushed right down to absolute zero temperature. In two dimensions, the model is still exactly solvable in zero field, a result due to Onsager (1944) [129, 130]. Phase transition now occurs at a finite critical temperature. Depending on the magnetic coordination z of the lattice, the critical temperature $k_B T_c$ is $1.51866 \times J$ for the honeycomb lattice ($z = 3$), $2.26918 \times J$ for the square lattice ($z = 4$), and $3.64096 \times J$ for the triangular lattice ($z = 6$). Not only does the critical temperature differ from that given by mean field theory, but critical exponents ($\alpha = 0$, $\beta = 1/8$, $\gamma = 7/4$, $\delta = 15$ and $\nu = 1$) do not coincide with those in Landau theory. Onsager's solution gives a concrete example of the significance of fluctuations. These strongly renormalise critical behaviour. Hence the importance of the 2-dimensional Ising model as a test for modern theories of phase transition.

As a first step towards the Ising Hamiltonian, consider a magnet in which spins S exhibit a large uniaxial ionic anisotropy. This is described by the Hamiltonian

$$\mathcal{H} = -J \sum_{i \neq j} \mathbf{S}_i \cdot \mathbf{S}_j + \sum_i [D(S_z^i)^2 - \gamma \mu_0 \mathbf{H} \cdot \mathbf{S}_i] . \quad (6.1)$$

If the ionic anisotropy term D is large negative, spins are always blocked in one of the states $+S$ or $-S$. Thermodynamic properties can then be studied by keeping only the \hat{z} spin component:

$$\mathcal{H} = -J \sum_{i \neq j} \sigma_i \sigma_j - h \sum_i \sigma_i , \quad (6.2)$$

where $\sigma_i = \pm 1$ and the magnetic field h is expressed here in energy units. Despite the simple appearance of this Hamiltonian, the model has not yet been solved in three dimensions. It plays an important role in statistical physics. Among other things, it has been used to study separation of fluid phases or binary alloys, through the lattice gas model (C.N. Yang) [131, 132], which will be discussed in Sect. 6.7. In addition, P.G. de Gennes has shown that the Ising model can also be applied to complex systems like polymers

[133]. In the present chapter, we shall study this key model, to which many monographs have already been devoted [134, 135, 136, 137].

6.1 One-Dimensional Partition Function

In one dimension, the Hamiltonian of the N spins can be written as

$$\mathcal{H} = -J \sum_{i=1}^{N-1} \sigma_i \sigma_{i+1} - \sum_i h_i \sigma_i . \quad (6.3)$$

To simplify evaluation of thermodynamic functions, we assume spins are arranged on a ring and identify spin $N + 1$ with spin 1. In the thermodynamic limit $N \rightarrow \infty$, these cyclic boundary conditions have no effect on results. The partition function is then

$$\begin{aligned} Z_N &= \text{Tr} [\exp(-\beta \mathcal{H})] \\ &= \sum_{\dots \sigma_i=\pm 1 \dots} \exp \left(\nu \sum_{i=1}^{N-1} \sigma_i \sigma_{i+1} + B_i \sigma_i \right) , \end{aligned} \quad (6.4)$$

where $\nu = \beta J$ and $B_i = \beta h_i$.

6.2 Zero Field Solution

As thermodynamic properties are independent of boundary conditions, we calculate the partition function for an open chain, i.e., a chain in which spins 1 and N can independently take values ± 1 . In the partition function, we can thus evaluate the trace over states of spin σ_N ,

$$\begin{aligned} Z_N &= \left[\sum_{\dots \sigma_{N-1}=\pm 1} \exp \left(\nu \sum_{i=1}^{N-2} \sigma_i \sigma_{i+1} \right) \right] \left[\sum_{\sigma_N=\pm 1} \exp(\nu \sigma_{N-1} \sigma_N) \right] \\ &= Z_{N-1} \times 2 \cosh \nu , \end{aligned} \quad (6.5)$$

since we have

$$\begin{aligned} \sum_{\sigma_N=\pm 1} \exp(\nu \sigma_{N-1} \sigma_N) &= \exp(\nu \sigma_{N-1}) + \exp(-\nu \sigma_{N-1}) \\ &= 2 \cosh \nu , \end{aligned} \quad (6.6)$$

whatever the value of σ_{N-1} . Using this recurrence relation, and directly evaluating the partition function for a 2-spin chain,

$$Z_2 = \sum_{\sigma_1, \sigma_2=\pm 1} \exp(\nu \sigma_1 \sigma_2) = 4 \cosh \nu , \quad (6.7)$$

we obtain the partition function

$$Z_N = 2(2 \cosh \nu)^{N-1} \quad (6.8)$$

for N coupled Ising spins. It is straightforward to calculate free energy, entropy and specific heat per spin from the partition function:

$$f = -\frac{1}{\beta} \ln(2 \cosh \nu) , \quad (6.9)$$

$$s = -\frac{\partial f}{\partial T} = k_B [\ln(2 \cosh \nu) - \nu \tanh \nu] , \quad (6.10)$$

$$c = T \frac{\partial s}{\partial T} = k_B \nu^2 \frac{1}{\cosh^2 \nu} . \quad (6.11)$$

Notice that for any positive value of ν , f is an analytic function, and hence there is no phase transition above absolute zero temperature. The entropy at high temperature ($\nu \rightarrow 0$) is the same as for free spins, i.e., $k_B \ln 2$. The specific heat is non-zero even for zero field, a typical feature of interacting spins. However, when $T \rightarrow 0$ or $T \rightarrow \infty$, the specific heat tends to zero. When we study correlation functions in Sect. 6.4, we shall see that the system becomes ordered at zero temperature. To handle the Ising model in the presence of a field, or in dimensions greater than one, we must use other techniques.

6.3 Transfer Matrices

With our periodic boundary conditions $N+1 \equiv 1$, we can rewrite the partition function as

$$Z_N = \sum_{\sigma} \prod_{i=1}^N \mathcal{L}(\sigma_i, \sigma_{i+1}) , \quad (6.12)$$

where

$$\mathcal{L}(\sigma, \sigma') = \exp \left[\nu \sigma \sigma' + \frac{B}{2} (\sigma + \sigma') \right] . \quad (6.13)$$

The sum over possible configurations takes the form of a matrix product. Summing over $\sigma_2 = \pm 1, \dots, \sigma_N = \pm 1$, we have

$$Z_N = \sum_{\sigma_i=\pm 1} \mathcal{L}^N(\sigma_1, \sigma_1) , \quad (6.14)$$

where $\mathcal{L}^N(\sigma, \sigma')$ is the σ, σ' matrix element of the N th power of the matrix \mathcal{L} ,

$$\mathcal{L} = \begin{pmatrix} \mathcal{L}(+1, +1) & \mathcal{L}(+1, -1) \\ \mathcal{L}(-1, +1) & \mathcal{L}(-1, -1) \end{pmatrix} = \begin{pmatrix} \exp(\nu + B) & \exp(-\nu) \\ \exp(-\nu) & \exp(\nu - B) \end{pmatrix} . \quad (6.15)$$

Since Z_N is the trace of \mathcal{L}^N , it can be expressed in terms of the eigenvalues of \mathcal{L} as

$$Z_N = \lambda_1^N + \lambda_2^N . \quad (6.16)$$

The eigenvalue equation for \mathcal{L} is

$$\det(\mathcal{L} - \lambda I) = \lambda^2 - 2\lambda \exp \nu \cosh B + 2 \sinh 2\nu = 0 . \quad (6.17)$$

The two eigenvalues are therefore

$$\lambda_{1,2} = \cosh B \exp \nu \pm [\exp(2\nu) \sinh^2 B + \exp(-2\nu)]^{1/2} . \quad (6.18)$$

Since the ratio λ_2/λ_1 is much less than 1 for all values of ν , we find

$$\begin{aligned} -\beta f &= \lim_{N \rightarrow \infty} \frac{\ln Z_N}{N} = \lim_{N \rightarrow \infty} \frac{1}{N} \ln [\lambda_1^N (1 + (\lambda_2/\lambda_1)^N)] = \ln \lambda_1 \\ &= \ln \left\{ \exp \nu \cosh B + [\exp(2\nu) \sinh^2 B + \exp(-2\nu)]^{1/2} \right\} . \end{aligned} \quad (6.19)$$

In zero field $B = 0$, we retrieve $\ln(2 \cosh \nu)$ as expected. This method can be generalised to an Ising chain in which exchange constants J_n between neighbouring sites n and $n + 1$ fluctuate, so that they must be described by a probability distribution $P(J_n)$. To each exchange constant J_n there corresponds a transfer matrix \mathcal{L}_n . In zero field $B = 0$, all transfer matrices \mathcal{L}_n commute. They can therefore be simultaneously diagonalised. The partition function can then be determined for an arbitrary distribution $P(J_n)$:

$$Z_N = \prod_n 2 \cosh \beta J_n , \quad (6.20)$$

$$f = -\frac{1}{\beta N} \sum_n \ln(2 \cosh \beta J_n) = -\frac{1}{\beta} \langle \ln(2 \cosh \beta J) \rangle . \quad (6.21)$$

The disordered Ising chain can thus be completely solved. For antiferromagnetic interactions, short range order is represented by a spin density wave with temperature dependent wave vector [138, 139].

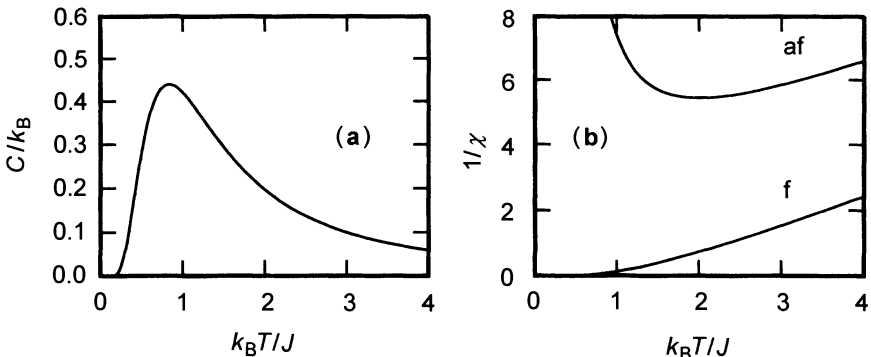


Fig. 6.1. (a) Specific heat in the 1-dimensional Ising model. The specific heat is maximal when $k_B T$ is of the same order as J . (b) Reciprocal susceptibility as a function of temperature for ferromagnetic and antiferromagnetic exchange, f and af , respectively. In practice, divergence of susceptibility in the ferromagnetic chain is only observable for infinitesimal fields

When there is no disorder, the magnetisation is evaluated from the partition function $Z(\nu, B)$,

$$m = -\frac{\partial(\beta f)}{\partial B} = \frac{\sinh B}{[\sinh^2 B + \exp(-4\nu)]^{1/2}}. \quad (6.22)$$

In zero field, the magnetisation is zero at all finite temperatures and the system remains ‘paramagnetic’. For ferromagnetic exchange in weak fields, the susceptibility diverges at low temperatures according to

$$\chi = \frac{\exp(2J/k_B T)}{k_B T}. \quad (6.23)$$

However, as soon as the magnetic field is of order $k_B T \exp(-4J/k_B T)$, saturation is reached (ferromagnetic case) and susceptibility falls back to zero. Critical behaviour therefore occurs at $T = 0$. This becomes explicit when we work out correlation functions.

6.4 Correlation Functions

For the Ising chain, the correlation function between spins k and l is defined by

$$\begin{aligned} \langle \sigma_k \sigma_l \rangle &= \frac{1}{Z_N} \sum_{\sigma} \sigma_k \sigma_l \exp(-\beta \mathcal{H}) \\ &= \frac{1}{Z_N} \sum_{\sigma} \sigma_k \sigma_l \exp \left(\nu \sum_{i=1}^N \sigma_i \sigma_{i+1} + B \sigma_i \right) \\ &= \frac{1}{Z_N} \sum_{\sigma} \mathcal{L}(\sigma_1, \sigma_2) \dots \mathcal{L}(\sigma_{k-1}, \sigma_k) \sigma_k \mathcal{L}(\sigma_k, \sigma_{k+1}) \dots \\ &\quad \mathcal{L}(\sigma_{l-1}, \sigma_l) \sigma_l \mathcal{L}(\sigma_l, \sigma_{l+1}) \dots \mathcal{L}(\sigma_N, \sigma_1). \end{aligned} \quad (6.24)$$

As before, we can sum over all configurations except $\sigma_k = \pm 1$ and $\sigma_l = \pm 1$. The correlation function is then given by

$$Z_N \langle \sigma_k \sigma_l \rangle = \sum_{\sigma_k, \sigma_l = \pm 1} \sigma_k \mathcal{L}^{N-l+k}(\sigma_k, \sigma_l) \sigma_l \mathcal{L}^{l-k}(\sigma_l, \sigma_k), \quad (6.25)$$

where $\mathcal{L}^{N-l+k}(\sigma_k, \sigma_l)$ is the σ_k, σ_l element of the 2×2 matrix \mathcal{L}^{N-l+k} . The matrix \mathcal{L}^s can be written in terms of eigenvalues and eigenvectors of the matrix \mathcal{L} . For example, in zero field, these are given by

$$\lambda_1 = 2 \cosh \nu, \quad \lambda_2 = 2 \sinh \nu, \quad (6.26)$$

$$\Phi_1 = \frac{1}{\sqrt{2}} \begin{pmatrix} 1 \\ 1 \end{pmatrix}, \quad \Phi_2 = \frac{1}{\sqrt{2}} \begin{pmatrix} 1 \\ -1 \end{pmatrix}. \quad (6.27)$$

The matrix \mathcal{L}^s is then given by

$$\mathcal{L}^s(\sigma, \sigma') = \sum_{j=1}^2 \lambda_j^s \Phi_j(\sigma) \Phi_j(\sigma') . \quad (6.28)$$

Using the expression $Z_N = \lambda_1^N + \lambda_2^N$ for the partition function, we evaluate the correlation function from identities (6.25) and (6.28) :

$$Z_N \langle \sigma_k \sigma_l \rangle = \sum_{\sigma_k, \sigma_l} \sum_{i,j=1}^2 \lambda_i^{N-l+k} \Phi_i(\sigma_k) \Phi_i(\sigma_l) \lambda_j^{l-k} \sigma_l \Phi_j(\sigma_l) \Phi_j(\sigma_k) . \quad (6.29)$$

Hence,

$$\langle \sigma_k \sigma_l \rangle = \left[1 + \left(\frac{\lambda_2}{\lambda_1} \right)^N \right] \sum_{i,j=1}^2 \left(\frac{\lambda_i}{\lambda_1} \right)^{N-l+k} \left(\frac{\lambda_j}{\lambda_1} \right)^{l-k} (\Phi_i | \sigma \Phi_j)^2 , \quad (6.30)$$

where we have used the scalar product notation

$$(\Phi_i | \sigma \Phi_j) = \sum_{\sigma=\pm 1} \Phi_i(\sigma) \sigma \Phi_j(\sigma) . \quad (6.31)$$

Whatever the temperature, the ratio λ_2/λ_1 of the eigenvalues of \mathcal{L} is always less than 1. Depending on the value of i (1 or 2), we have

$$\lim_{N \rightarrow \infty} (\lambda_i / \lambda_1)^{N-l+k} \rightarrow 1 \text{ or } 0 \quad (6.32)$$

in the thermodynamic limit. Hence in this limit, the correlation function is always given by

$$\langle \sigma_k \sigma_l \rangle = \sum_{j=1}^2 (\lambda_j / \lambda_l)^{l-k} (\Phi_1 | \sigma \Phi_j)^2 . \quad (6.33)$$

This expression is easy to evaluate in zero field since the scalar product $(\Phi_1 | \sigma \Phi_j) = 0$ or 1, for $j = 1$ or 2, respectively. From the correlation function, we define a correlation length ξ by

$$\langle \sigma_k \sigma_l \rangle = (\tanh \nu)^{|l-k|} \equiv \exp(-|l-k|/\xi) , \quad (6.34)$$

which diverges at low temperatures according to

$$\xi = \frac{1}{\ln(\tanh \nu)} \approx \frac{1}{2} \exp(2\beta J) . \quad (6.35)$$

Apart from minor changes of notation, the above discussion carries over almost word for word to two dimensions [129, 130, 140]. For example, the correlation function for two spins in the same row and in the k th and l th column is given by (6.33), where the λ_j and Φ_j are now eigenvalues and eigenvectors of the column transfer matrix (2^M in number, where M is the number of spins per column), and N is the number of rows. In zero field, the dominant eigenvector is completely symmetric. The $j = 1$ term in (6.33) is then identically zero. At temperatures below the critical point, the larger eigenvalue λ_1 becomes asymptotically degenerate and hence

$$\lim_{M \rightarrow \infty} \lambda_2/\lambda_1 \rightarrow 1 \quad (T < T_c) , \quad (6.36)$$

so that (6.33) implies

$$\lim_{|l-k| \rightarrow \infty} \lim_{M \rightarrow \infty} \langle \sigma_k \sigma_l \rangle = (\Phi_1 | \sigma \Phi_2)^2 > 0 . \quad (6.37)$$

This in turn implies the existence of long range order. Generally, it can be shown that long range order exists if and only if the larger eigenvalue is asymptotically degenerate [141].

Exercise. Magnetostriiction

Consider a ferromagnetic Ising chain in field h [142]. The n th atom, of mass M , is located at $x_n + na$ relative to its equilibrium position na , where n is a whole number. Lattice vibrations are described by a harmonic oscillator (phonon) Hamiltonian,

$$\mathcal{H}_{\text{ph}} = \sum_n \left[\frac{p_n^2}{2M} + \frac{1}{2} M \omega_0^2 (x_{n+1} - x_n)^2 \right] . \quad (6.38)$$

Lattice vibrations modulate magnetic exchange, which depends on relative positions of atoms n and $n + 1$. To second order,

$$J(x_{n+1} - x_n) = J(0) \left[1 + \eta_1 \frac{x_{n+1} - x_n}{a} + \eta_2 \frac{(x_{n+1} - x_n)^2}{a^2} + \dots \right] . \quad (6.39)$$

1. Deduce the magnetic Hamiltonian $\mathcal{H}_{0,1,2}$ to orders 0, 1, 2 in terms of $(x_{n+1} - x_n)^{0,1,2}$.
2. Assume that the spin configuration $\{\sigma\} \equiv \sigma_1, \dots, \sigma_n, \dots$ is given. Show that the first order correction to the Ising Hamiltonian can be eliminated by a translation $x'_n = x_n + \Delta x_n$, where Δx_n depends on the spin configuration $\{\sigma\}$.
3. Deduce the expression

$$\mathcal{H} = \mathcal{H}_{\text{ph}} + \mathcal{H}_0 + \frac{1}{2} N \frac{J^2(0) \eta_1^2}{M \omega_0^2 a^2} + \mathcal{H}_2 , \quad (6.40)$$

for the total Hamiltonian and conclude that magneto-elastic coupling contracts the chain. If the initial length of the chain is $L = na + \langle x_N - x_0 \rangle$, the final length is

$$L' = L - \frac{\eta_1}{M \omega_0^2 a} U(T) , \quad (6.41)$$

where $U(T)$ is the zero field internal energy in the Ising model.

4. Deduce that the expansion coefficient is related to the magnetic specific heat per unit length c_M , by the thermodynamic identity

$$\alpha = \frac{1}{L} \left(\frac{\partial L}{\partial T} \right) = - \frac{\eta_1}{M \omega_0^2 a} c_M(T) . \quad (6.42)$$

This result is known as magnetostriiction.

5. To first order, the effect of \mathcal{H}_2 is to renormalise J and the speed of sound $c = \omega_0 a$. By making a mean field type approximation,

$$\begin{aligned}\mathcal{H}_2 = & -\frac{J(0)\eta_2}{a^2} \sum_n [\langle x_{n+1} - x_n \rangle^2 \sigma_n \sigma_{n+1} \\ & + (x_{n+1} - x_n)^2 \langle \sigma_n \sigma_{n+1} \rangle - \langle x_{n+1} - x_n \rangle^2 \langle \sigma_n \sigma_{n+1} \rangle] ,\end{aligned}\quad (6.43)$$

determine the new exchange constant and renormalised speed of sound.

Exercise. The Lee and Yang Zeros

Lee and Yang have shown that the partition function Z_N for an Ising model in a space of arbitrary dimensions can be considered as a complex function of $\zeta = \exp(-2B) = \exp(-2\beta h)$. In the 1-dimensional Ising model, it can be shown that $Z_N(\zeta)$ is a polynomial of degree N whose zeros $\zeta_j = \exp(i\theta_j)$ all lie on the unit circle in the complex plane. Once the zeros are known, we can determine their distribution $g(\nu, \theta)$. This depends on temperature through $\nu = \beta J$. The function g determines all analyticity properties of the free energy and the phase diagram of the system. Magnetisation, susceptibility and specific heat can thus be calculated from the distribution $g(\nu, \theta)$ of zeros of the partition function. All results obtained with this 1-dimensional model remain valid in higher dimensions, except that now the distribution $g(\nu, \theta)$ of zeros must be determined numerically.

1. Show that the zeros of Z_N can be written

$$\zeta_j = a_j + i\sqrt{1 - a_j^2}, \quad (6.44)$$

$$a_j = -\exp(-4\nu) + [1 - \exp(-4\nu)] \cos\left(\frac{(2j+1)\pi}{N}\right), \quad (6.45)$$

where $2j+1$ lies in the interval $[-N, N]$.

2. Show that in the interval $[0, 2 \arcsin \exp(-2\nu)]$ the distribution of zeros of Z_N , $g(\nu, \theta)$, is zero, but that in the interval $[2 \arcsin \exp(-2\nu), \pi]$ the function $g(\nu, \theta)$ takes the form

$$g(\nu, \theta) = \frac{1}{2\pi} \frac{\sin(\theta/2)}{[\sin^2(\theta/2) - \exp(-4\nu)]^{1/2}}. \quad (6.46)$$

The function $g(\nu, \theta)$ is normalised to unity in the interval $[-\pi, \pi]$.

3. Let $-J$ be the ground state energy per spin. Show that the free energy per spin can be expressed in terms of $g(\nu, \theta)$ by the relation

$$f = -J - h + \frac{1}{\beta} \int_0^\pi \ln(\zeta^2 - 2\zeta \cos \theta + 1) d\theta. \quad (6.47)$$

4. Deduce that the magnetisation $m(\zeta)$ has a cut on the unit circle but is an analytic function inside and outside the circle.

$$\begin{aligned} m &= 1 - 4\zeta \int_0^\pi d\theta g(\nu, \theta) \frac{\zeta - \cos \theta}{\zeta^2 - 2\zeta \cos \theta + 1} \\ &= 1 - 2\zeta \int_{-\pi}^\pi d\theta g(\nu, \theta) \frac{g(\nu, \theta)}{\zeta - \exp(i\theta)}. \end{aligned} \quad (6.48)$$

5. Using the explicit form (6.46) for the distribution of zeros, show that the magnetisation is given in terms of ζ by

$$m(\nu, \zeta) = \left[\frac{\zeta^2 - 2\zeta + 1}{\zeta^2 - 2\zeta[1 - 2\exp(-2\nu)] + 1} \right]^{1/2} \quad (6.49)$$

and calculate the susceptibility.

Solution

Since the partition function is given by $Z_N = \lambda_1^N + \lambda_2^N$, its zeros ζ_j correspond to the N complex roots of -1 , namely,

$$\left(\frac{\lambda_2}{\lambda_1} \right)^N = -1, \quad \frac{\lambda_2}{\lambda_1} = \exp \left[i \frac{(2j+1)\pi}{N} \right] \equiv \exp(i\phi_j). \quad (6.50)$$

Moreover, the eigenvalues of the transfer matrix (6.18) are given in terms of $\nu = \beta J$ and $B = \beta h$ by

$$\lambda_{1,2} = \exp \nu \cosh B \left[1 \pm \left\{ 1 + [\exp(-4\nu) - 1]/\cosh^2 B \right\}^{1/2} \right] \quad (6.51)$$

$$= \exp \nu \cosh B \left[1 \pm \sqrt{1-b} \right], \quad (6.52)$$

where b is defined in terms of $\zeta = \exp(-2B)$ by

$$b = \frac{4u\zeta}{(1+\zeta)^2}, \quad (6.53)$$

and $u = 1 - \exp(-4\nu)$. We first determine b_j as a function of $\exp(i\phi_j)$ and then ζ_j as a function of b_j . Since

$$\frac{\lambda_2}{\lambda_1} = \exp(i\phi_j) = \frac{1 - \sqrt{1-b_j}}{1 + \sqrt{1-b_j}} \quad \text{or} \quad b_j = \frac{1}{\cos^2 \phi_j/2}, \quad (6.54)$$

we find from (6.53) that ζ_j is a solution of the quadratic equation

$$1 + \zeta^2 + 2\zeta(1 - 2u \cos^2 \phi_j/2) = 0. \quad (6.55)$$

Its solutions can be written in the following form:

$$\zeta^j = \zeta_r^j \pm i\sqrt{1 - \zeta_r^2}, \quad (6.56)$$

$$\begin{aligned} \zeta_r^j &= 2u \cos^2 \phi_j/2 - 1 = u - 1 + u \cos \phi_j \\ &= -\exp(-4\nu) + [1 - \exp(-4\nu)] \cos \phi_j. \end{aligned} \quad (6.57)$$

In order to obtain the distribution of angles θ over the unit circle, we differentiate the real part of a zero:

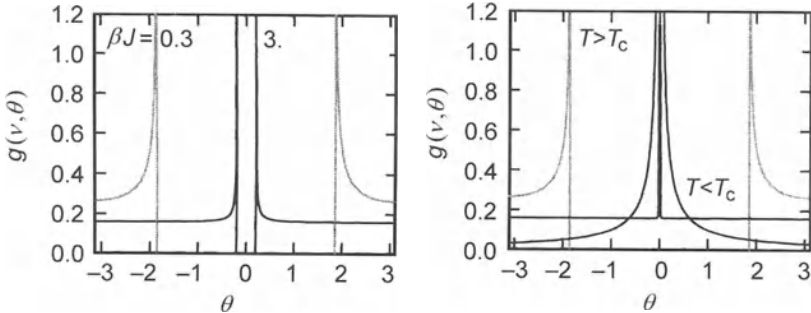


Fig. 6.2. *Left:* The Lee and Yang distribution of zeros in the 1-dimensional Ising model. *Right:* The same distribution in two dimensions

$$\cos \theta = -\varepsilon + (1 - \varepsilon) \cos \phi , \quad (6.58)$$

$$\sin \theta d\theta = (1 - \varepsilon) \sin \phi d\phi , \quad (6.59)$$

where $\varepsilon = \exp(-4\nu)$. Using the first relation, we can rewrite $(1 - \varepsilon) \sin \phi$ in terms of $\cos \theta$, viz.,

$$\begin{aligned} (1 - \varepsilon) \sin \phi &= [(1 - \varepsilon)^2 - (\cos \theta + \varepsilon)^2]^{1/2} \\ &= 2 \cos(\theta/2) [1 - \varepsilon - \cos^2(\theta/2)]^{1/2} \\ &= 2 \cos(\theta/2) [\sin^2(\theta/2) - \varepsilon]^{1/2} . \end{aligned} \quad (6.60)$$

By expressing $\sin \theta$ in terms of the half-angle, and noting that the distribution of angles ϕ is uniform and equal to $1/2\pi$, we obtain the distribution of zeros (6.46). Since $\cos \theta$ can only vary between -1 and $1 - 2\varepsilon$, there is no value of θ between 0 and $\arccos(1 - 2\varepsilon) = 2\arcsin[\exp(-2\nu)]$. Note that when $T \rightarrow 0$, $\varepsilon \rightarrow 0$, the distribution g is non-zero everywhere except at $\theta = 0$. Since the partition function is a degree N polynomial with zeros ζ_j , we can write

$$Z_N = Z_0 \prod_{j=1}^N (\zeta - \zeta_j) . \quad (6.61)$$

For large values of ζ , $Z_N \approx \lambda_1^N \approx \exp(\nu + B)\zeta^N$, which specifies the constant $Z_0 = \exp N(\nu + B)$. We deduce that the free energy per spin is

$$f = -\frac{1}{N\beta} \ln Z_N = -J - h + k_B T \sum_j \ln[\zeta - \exp(i\theta_j)] . \quad (6.62)$$

This does indeed agree with (6.47) in the thermodynamic limit. The magnetisation (6.48) is obtained by simply differentiating: $m = -\partial f / \partial h = 2\beta\zeta \partial f / \partial \zeta$.

6.5 Glauber Dynamics

Up to now, we have only considered equilibrium properties. The relaxation of an interacting Ising spin system cannot be obtained from its Hamiltonian because it eliminates intrinsic spin dynamics (precession in the local field). Relaxation phenomena can nevertheless be described by means of a phenomenological equation which specifies the transition rate Γ from one spin configuration $\sigma \equiv \sigma_1, \dots, \sigma_N$ to another $\sigma' \equiv \sigma'_1, \dots, \sigma'_N$. This master equation takes the form

$$\frac{d}{dt} P(\sigma, t) = \Gamma(\sigma|\sigma') P(\sigma', t), \quad (6.63)$$

where each σ represents an N -spin configuration. In general, we assume that transition from one configuration to another involves changing a single spin (Glauber dynamics) [143, 144, 145]. In this case, the transition rate is

$$\Gamma(\sigma|\sigma') = \sum_i \sigma_i \sigma'_i \delta^i(\sigma|\sigma') w_i(\sigma'), \quad (6.64)$$

where the function δ^i is zero if configurations σ, σ' differ by any spin other than i . The transition probability w_i of spin i is imposed by the principle of detailed balance,

$$w_i = \frac{1}{\tau} [1 - \sigma_i \tanh(\beta h_i)], \quad (6.65)$$

where the local field h_i at site i is

$$h_i = h + J(\sigma_{i-1} + \sigma_{i+1}). \quad (6.66)$$

Indeed, the principle of detailed balance requires occupation of states \uparrow and \downarrow of spin i to be stationary at equilibrium, i.e.,

$$\Gamma_i(\uparrow|\downarrow) n_i(\uparrow) = \Gamma_i(\downarrow|\uparrow) n_i(\downarrow). \quad (6.67)$$

This condition specifies the transition probability w_i for a Boltzmann distribution $n_i(\sigma) = \exp(-\beta \sigma_i h_i)$. Expectation values of local magnetisation and thermodynamic field are then

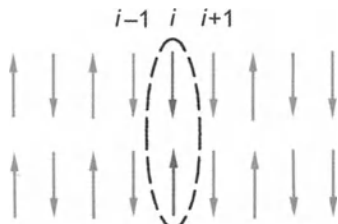


Fig. 6.3. Example of two configurations differing only by reversal of a single spin, spin i . Glauber dynamics only connects configurations of this type

$$\langle \sigma_i \rangle = \sum_{\sigma} \sigma_i P(\sigma|t) , \quad (6.68)$$

$$\langle \tanh(\beta h_i) \rangle = \sum_{\sigma} \tanh(\beta h_i) P(\sigma|t) , \quad (6.69)$$

and relaxation of local magnetisation is described by

$$\tau \frac{d}{dt} \langle \sigma_i \rangle = -\langle \sigma_i \rangle + \langle \tanh(\beta h_i) \rangle . \quad (6.70)$$

At equilibrium ($d/dt \rightarrow 0$), this equation resembles the mean field equation except that here the local field h_i , rather than its mean value $\langle h_i \rangle$, determines local magnetisation. In one dimension, h_i fluctuates enormously from one site to another and the mean field approximation is very poor. The dynamical equation can nevertheless be solved to all orders in its expansion in powers of $h(t)$ [146]. We shall only treat the first order (linear response):

$$\tanh(\beta h_i) = x_i + y_i(\sigma_{i-1} + \sigma_{i+1}) + z_j \sigma_{i-1} \sigma_{i+1} , \quad (6.71)$$

where coefficients x_i , y_i and z_i are given to first order in the applied field h , or the corresponding reduced parameter $B = \beta h$, by

$$x = (1 - \gamma^2/2)B , \quad (6.72)$$

$$y = \gamma/2 , \quad (6.73)$$

$$z = -\gamma^2 B/2 , \quad (6.74)$$

and $\gamma = \tanh(2\beta J)$. We can then reduce the dynamical equation to

$$\tau \frac{d}{dt} \langle \sigma_i \rangle = -[(1 - 2y)\langle \sigma_i \rangle - x - z\langle \sigma_{i-1} \sigma_{i+1} \rangle] . \quad (6.75)$$

As we are only considering the linear response, the correlation function $\langle \sigma_{i-1} \sigma_{i+1} \rangle$ can be replaced by its equilibrium value $a^2 \equiv \tanh^2 \nu$. In such conditions, the magnetic response is causal,

$$M(t) = \int_{-\infty}^{\infty} \chi(t' - t) h(t') dt' , \quad (6.76)$$

and the dynamical susceptibility is

$$\chi(t) = \frac{\beta N}{\tau \cosh 2\beta J} \theta(t) \exp \left[-(1 - \gamma) \frac{t}{\tau} \right] . \quad (6.77)$$

The relaxation time of the magnetisation is no longer the microscopic time τ , but rather

$$\tau' = \frac{\tau}{1 - \gamma} = \exp(2\nu) \cosh(2\nu) \tau \approx 2\xi^2 \tau , \quad (6.78)$$

which diverges as ξ^2 at low temperatures, where ξ is the correlation length defined in (6.34). This slowing down near the critical temperature (here, $T = 0$) is typical behaviour in the neighbourhood of a phase transition. It suggests that there may be dynamical scaling laws, as we shall now investigate [147].

6.6 Critical Slowing Down

We interpret the characteristic time τ' as the maximal relaxation time of an arbitrary configuration in volume ξ^d , where d is the dimension of the space (in the previous example, $d = 1$). Quite generally, we can make a dynamical scaling law hypothesis in which the maximal relaxation time for volume ξ^d at the critical point grows as

$$\tau' \propto \xi^z. \quad (6.79)$$

z is the dynamical critical exponent. In the 1-dimensional Ising model, we found $z = 2$. Using arguments very similar to those developed in Chap. 4(I), we can obtain a dynamical scaling function. Explicitly, a dynamical scaling law expresses the fact that, if we increase the frequency at which we study a system by some scaling factor λ , we obtain the same effect as if we had reduced the relaxation time by a factor $1/\lambda$. Now reducing the correlation length by a factor of $1/\lambda^{1/z}$ has just this effect, dividing the relaxation time by a factor λ . Therefore, in order to accelerate relaxation of the system by the scaling factor, it suffices to move away from the critical point by a factor $1/\lambda^{1/z\nu}$. We thus express the fact that the free energy and its derivatives are homogeneous functions of $\tau = (T - T_c)/T_c$ and ω . For example, this homogeneity condition requires the susceptibility to take the form

$$\chi(\tau, \omega) = \lambda \chi(\lambda^x \tau, \lambda^y \omega). \quad (6.80)$$

At zero frequency, we should retrieve the static scaling law. In particular, choosing $\lambda = \tau^{-1/x}$,

$$\chi(\tau, 0) = \frac{\chi(1, 0)}{\tau^{1/x}} \equiv \frac{\chi(1, 0)}{\tau^\gamma}, \quad (6.81)$$

and hence $1/x = \gamma$. The frequency dependence of the susceptibility should be $\omega\tau' \propto \omega\tau^{-z\nu}$, implying $y = z\nu/\gamma$. Choosing a scaling factor $\lambda = \tau^{-\gamma}$ in scaling law (6.80), we obtain the scaling function

$$\chi(\tau, \omega) = \tau^{-\gamma} \chi(1, \omega\tau^{-z\nu}). \quad (6.82)$$

If we choose $\lambda = \omega^{-\gamma/z\nu}$, this scaling function can be written equivalently

$$\chi(\tau, \omega) = \omega^{-\gamma/z\nu} \chi(\tau\omega^{-1/z\nu}, 1). \quad (6.83)$$

Analyticity properties of the complex susceptibility $\chi = \chi' + i\chi''$ give the asymptotic form of the susceptibility at low frequencies ($\omega\tau' \ll 1$)

$$\chi'(\omega) = \frac{\chi_0}{\tau^\gamma}, \quad (6.84)$$

$$\chi''(\omega) = \frac{\chi_0 \omega}{\tau^{\gamma+z\nu}}, \quad . \quad (6.85)$$

whilst at high frequencies,

$$\chi'(\omega) \propto \left(\frac{1}{\omega^{1/z\nu}\tau} \right)^\gamma \cos\left(\frac{\pi\gamma}{z\nu}\right), \quad (6.86)$$

$$\chi''(\omega) \propto \left(\frac{1}{\omega^{1/z\nu}\tau} \right)^\gamma \sin\left(\frac{\pi\gamma}{z\nu}\right). \quad (6.87)$$

It is not difficult to obtain dynamical scaling functions associated with other thermodynamic functions, and their behaviour in a magnetic field.

6.7 Lattice Gases

Consider a lattice with V sites and N particles [131]. A single particle can occupy each node in the lattice. Only particles occupying neighbouring sites can interact, with energy $-A$. Thus,

$$\begin{aligned} J_{ij} &= -A, & i, j \text{ neighbours,} \\ &= 0 & \text{otherwise.} \end{aligned} \quad (6.88)$$

We introduce binary parameters t_i at each site such that

$$\begin{aligned} t_i &= +1, & \text{if } i \text{ is occupied,} \\ &= 0, & \text{if } i \text{ is not occupied.} \end{aligned} \quad (6.89)$$

The interaction energy in a specific configuration is

$$\mathcal{H} = \sum_{ij*} t_i t_j, \quad (6.90)$$

$$\mathcal{H} = \sum_{i=1}^V t_i t_{i+1} \quad (\text{1D}), \quad (6.91)$$

where $ij*$ under the sum indicates that it should be taken over nearest neighbours. There is also a condition on the number of particles,

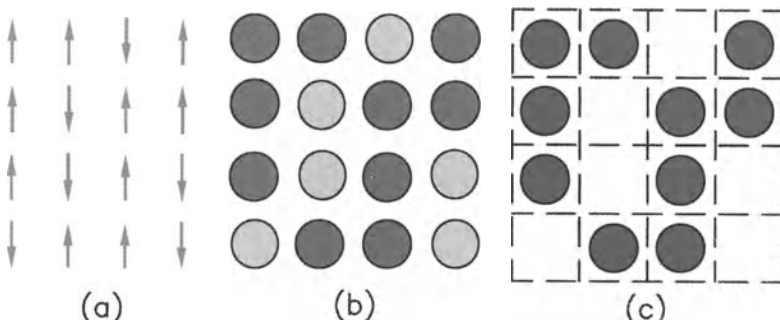


Fig. 6.4. In the Ising model, a configuration can be represented as: (a) an arrangement of spins, (b) an arrangement of atoms in a binary alloy, (c) a configuration of atoms on a lattice having V sites partially filled by N particles

$$N = \sum_{i=1}^V t_i . \quad (6.92)$$

The canonical partition function is

$$Z(N, V, T) = \sum_{\sum_1^V t_i = N} \exp(-\beta \mathcal{H}) . \quad (6.93)$$

As usual, we eliminate the constraint on the number of particles by fixing its mean value with a chemical potential. In this grand canonical ensemble,

$$Z_G(\mu, V, T) = \sum_t \exp \beta \left(A \sum_{ij*} t_i t_j - \mu \sum_{i=1}^V t_i \right) , \quad (6.94)$$

where the sum is taken over all configurations. This is equivalent to the partition function of an ensemble of V spins on a lattice, viz.,

$$Z(\mathcal{H}, V, T) = \sum_{\sigma} \exp \beta \left(J \sum_{ij*} \sigma_i \sigma_j + h \sum_{i=1}^V \sigma_i \right) . \quad (6.95)$$

We can identify (6.94) and (6.95) if variables σ_i and t_i are related by

$$\sigma_i = 1 - 2t_i \quad (6.96)$$

and corresponding parameters J and h are defined by

$$J = A/4 , \quad (6.97)$$

$$2h = \mu - zA/2 , \quad (6.98)$$

where z is the coordination of a site on the lattice. We can then relate the thermodynamic functions of the gas to those of the corresponding magnet. For example, the gas pressure is

$$p = \frac{1}{\beta V} \ln Z_G(\mu, V, T) = -f - zJ/2 - h , \quad (6.99)$$

where f is free energy per spin. Density ρ is naturally related to magnetisation M by

$$\rho = (1 - M)/2 . \quad (6.100)$$

Likewise, isothermal compressibility K_T and constant volume specific heat C_V are related to susceptibility and specific heat at constant magnetisation, respectively:

$$4\rho^2 K_T = \chi_T , \quad (6.101)$$

$$\rho C_V = C_M . \quad (6.102)$$

We can conclude that, in a binary alloy composed of two types of atom A and B, we can naturally introduce a binary variable which equals 1 if a site is occupied by an A atom and -1 if it is occupied by a B atom. We come back to the Ising model.

7. The XY Model

When we studied phase transitions, we emphasised the importance of fluctuations in low-dimensional systems. Indeed, restoring forces which tend to bring the system back towards equilibrium decrease quadratically with distance ($\Gamma M_0^2/L^2$). Many long wavelength fluctuations are excited because they involve only an infinitesimal energy. In a low-dimensional system, they make dominant contributions to thermodynamic quantities and long range order cannot develop. Considering only Gaussian fluctuations [Ornstein–Zernike theory, see Sect. 4.2(I)], a phase transition is indicated by a zero in the inverse magnetic susceptibility

$$\frac{\mu_0}{2\chi} = a(T) + \sum_{\mathbf{k}} \frac{6bk_B T}{\Gamma k^2 + 2a(T)} . \quad (7.1)$$

In mean field theory, the first term $a(T) = \alpha(T - T_c)/T_c$ is zero at T_c . The second term gives the contribution of linear fluctuations to the susceptibility. If this contribution is much greater than $|a(T)|$ at all temperatures, the system has no phase transition since the susceptibility loses its singularity. It is straightforward to estimate the contribution from fluctuations of wavelength greater than L in one and two dimensions:

$$\left. \frac{\mu_0}{2\chi} \right|_{\text{fl}} = \frac{6bk_B T}{4\pi^2} \frac{L\xi}{\Gamma} \arctan \frac{\xi}{L} , \quad d = 1 , \quad (7.2)$$

$$\left. \frac{\mu_0}{2\chi} \right|_{\text{fl}} = \frac{6bk_B T}{4\pi^2} \frac{L^2}{\Gamma} \ln \left(1 + \frac{\xi^2}{L^2} \right) , \quad d = 2 . \quad (7.3)$$

These quantities diverge when $\xi \rightarrow \infty$. Consequently, these fluctuations always dominate the magnetic condensation energy and destroy long range order in dimensions less than or equal to two. For systems with continuous symmetry, there is a rigorous theorem due to Mermin and Wagner [148] which shows that no long range magnetic order can exist in dimensions less than or equal to two. More precisely, only an external field H can induce magnetisation, and it is bounded by inequalities [149, 150]

$$|M(T)| \leq C \frac{(\mu H)^{1/3}}{(k_B T)^{2/3}} , \quad d = 1 , \quad (7.4)$$

$$|M(T)| \leq \frac{C'}{[k_B T \ln(\mu H)]^{1/2}} , \quad d = 2 . \quad (7.5)$$

In this chapter, we shall examine the XY model defined by Hamiltonian

$$\mathcal{H} = -J \sum_{i,j} (S_i^+ S_j^- + S_i^- S_j^+) - \mu \mu_0 \mathbf{H} \cdot \sum_i \mathbf{S}_i , \quad (7.6)$$

which can be considered as the limit as $J_z \rightarrow 0$ of an anisotropic Heisenberg Hamiltonian. (Note that, in the present chapter, the exchange constant differs by a factor of two from its definition elsewhere in the book.) Alternatively, the XY Hamiltonian can also describe integer spin magnetic systems with strong planar ionic anisotropy, in which spins are blocked in their $m_z = 0$ states. In the semi-classical limit, spins can be represented by their angles in the XY plane. Rotations in the XY plane form a continuous symmetry group and this excludes magnetic order in one or two dimensions. However, the absence of long range order does not mean that there is no phase transition of some other type. Below a critical temperature T_{KT} , correlation functions in two dimensions no longer decrease exponentially as they would in a paramagnetic system, but rather as a power law

$$C(\mathbf{r}) = \langle \mathbf{S}(0) \cdot \mathbf{S}(\mathbf{r}) \rangle \propto \frac{1}{r^{\eta(T)}} , \quad (7.7)$$

where the critical exponent $\eta(T)$ depends continuously on temperature,

$$0 < \eta(T) = \frac{k_B T}{4\pi J} < 1/4 . \quad (7.8)$$

Moreover, the static susceptibility $\chi(T)$ can be related to spin-spin correlation functions by

$$\chi(T) = 2\pi\mu_0\mu_B^2 \int_{r_0}^{\infty} C(\mathbf{r}) r \, dr \rightarrow \infty . \quad (7.9)$$

The susceptibility is therefore infinite at all temperatures below T_{KT} . The low temperature phase is thus ‘critical’ and in zero field the interval $[0, T_{\text{KT}}]$ is a critical line on the phase diagram. The rather odd behaviour is related to the fact that there is topological order which, in the low temperature phase, forbids topological defects in the field of spin vectors. In this phase, these topological defects or *vortices* are paired together, the members of each pair having opposite topological charges. This influences the vector field in their neighbourhood, without destroying its topological integrity over large distances.

Before tackling the 2-dimensional XY model, it is instructive to examine a rigorous treatment [151, 152] of the 1-dimensional model in two limits:

- the extreme quantum limit ($S = 1/2$) in which spins form an almost ordered spin fluid, but without manifesting any long range order;
- the classical limit $S = \infty$.

7.1 The Spin 1/2 XY Chain

Consider a magnetic field in the \hat{z} direction. In one dimension, the XY Hamiltonian can be diagonalised using a non-linear representation of spin operators in terms of fermionic operators. This is the Jordan–Wigner transformation [153]. Operator S_i^+ is represented in terms of the density $a_j^\dagger a_j$ of fermions on the left of site i , viz.,

$$S_i^+ = a_i^\dagger \exp \left(i\pi \sum_{j < i} a_j^\dagger a_j \right) , \quad (7.10)$$

$$S_i^z = a_i^\dagger a_i - 1/2 . \quad (7.11)$$

When a_i are fermions,

$$\{a_i, a_j^\dagger\} = \delta_{ij} , \quad \{a_i, a_j\} = 0 , \quad (7.12)$$

spin operators have the right commutation relations. For example,

$$[S_i^+, S_i^-] = a_i^\dagger a_i - a_i a_i^\dagger = a_i^\dagger a_i - 1 + a_i^\dagger a_i 2S_z . \quad (7.13)$$

For nearest neighbours, we find that

$$\begin{aligned} S_i^+ S_{i+1}^- &= a_i^\dagger \exp \left(i\pi a_i^\dagger a_i \right) a_{i+1} \\ &= a_i^\dagger (1 - a_i^\dagger a_i + \dots) a_{i+1} = a_i^\dagger a_{i+1} , \end{aligned} \quad (7.14)$$

since $a_i^\dagger a_i^\dagger = 0$ (two fermions cannot occupy the same site). The Hamiltonian is then a quadratic form in the a_i ,

$$\mathcal{H} = -J \sum_i (a_i^\dagger a_{i+1} + a_i a_{i+1}^\dagger) - B \sum_i \left(a_i^\dagger a_i - \frac{1}{2} \right) , \quad (7.15)$$

where $B = \mu_0 \mu_B H$ is proportional to the Zeeman energy. By a Fourier transform, operators a_i can be redefined in terms of quanta $|k\rangle = a_k^\dagger |0\rangle$, and free waves are described by

$$a_k = \frac{1}{\sqrt{N}} \sum_i \exp(-ikR_i) a_i , \quad (7.16)$$

$$N\delta(R_i - R_j) = \sum_k \exp[ik(R_i - R_j)] , \quad (7.17)$$

$$\{a_k, a_{k'}^\dagger\} = \delta(k - k') . \quad (7.18)$$

The Hamiltonian then takes a diagonal form,

$$\mathcal{H} = \sum_k \varepsilon_k a_k^\dagger a_k + BN/2 , \quad (7.19)$$

describing a free fermion gas. Fermion wave vectors are $k = 2\pi i / Na$, where a is the lattice spacing, and their dispersion relation ε_k is

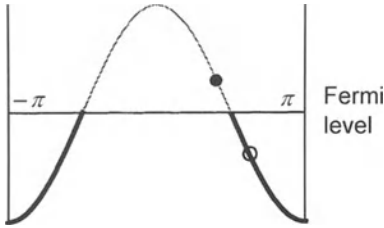


Fig. 7.1. Energy of states in an antiferromagnetic XY chain as a function of ka . The quasi-particle and quasi-hole excited in an elementary excitation are also represented

$$\varepsilon_k = -[2J \cos(ka) + B]. \quad (7.20)$$

The second term in (7.19) gives the chemical potential of the fermion gas as $B/2$, i.e., half the spin flip energy in the applied field. At zero temperature and for zero field ($B = 0$), all negative energy states are filled and the Fermi level is $\mu \equiv \varepsilon_F = 0$. For antiferromagnetic exchange, the zero field ground state is such that all states whose wave vectors ka lie in $[-\pi, -\pi/2]$ and $[\pi/2, \pi]$ are filled, whilst all states whose wave vectors lie in $[-\pi/2, \pi/2]$ are empty. For large N , the ground state energy is $-2NJ/\pi$. A hole in the Fermi sea, called a *spinon*, corresponds to an excitation with angular momentum $\hbar/2$. For this reason, these excitations cannot be observed directly in experiments [154]. The elementary excitations generated by a spin flip are particle-hole pairs, each carrying angular momentum \hbar . Such modes of wave vector k are very close to spin waves in ordered magnets [see Chap. 9(I)]. In the present case they are composite structures and their energy is the sum of the energy of a quasi-particle (spinon) of wave vector q_1 and that of a quasi-hole of wave vector $q_2 = k - q_1$. Since the Fermi surface consists of two points $\pm\pi/2a$, their dispersion relation, defined by

$$E_k = \varepsilon_{q_1} + \varepsilon_{q_2}, \quad k = q_1 + q_2, \quad (7.21)$$

is doubly degenerate. For each wave vector k , there is a continuum of magnons corresponding to spinons whose wave vectors belong to the segment $A - A'$ (see Fig. 7.2 left). The lower limit of the continuum is at $q_1 = \pi/2$, $q_2 = k - \pi/2$ (points A or A') and the upper limit at $q_1 = q_2 = k/2$ (point B):

$$E_{\min}(k) = 2|J|[\cos \pi/2 + \cos(k - \pi/2)] = 2|J| \sin k, \quad (7.22)$$

$$E_{\max}(k) = 2|J|[\cos(k - \pi)/2 + \cos(k - \pi)/2] = 2|J| \sin k/2. \quad (7.23)$$

The simplest way to determine thermodynamic quantities is to start from the free energy of the free spinon gas,

$$F = -\frac{Na}{\pi\beta} \int_{-\pi/a}^{\pi/a} dk \ln[1 + \exp(-\beta\varepsilon_k)]. \quad (7.24)$$

This gives a constant susceptibility at low temperatures,

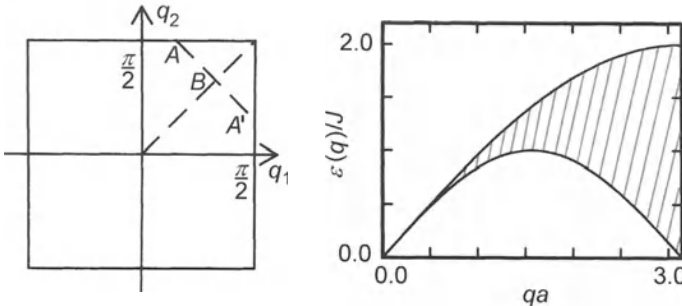


Fig. 7.2. *Left:* Wave vectors q_1 , q_2 forming a composite magnon of wave vector k . The lower limit of the spectrum is at A (A') and the upper limit at B . *Right:* Continuum forming the magnon spectrum

$$\chi = 2N\mu_0 \frac{\mu_B^2}{2|J|}, \quad (7.25)$$

characteristic of antiferromagnetic interactions. As for any Fermi fluid, the specific heat is linear at low temperatures, with a maximum when $k_B T$ is of the order of $2|J|$. At $T = 0$, correlation functions are, of course, those of a free fermion gas:

$$\begin{aligned} \langle S_j^+ S_i^- \rangle &= \langle a_j^\dagger \exp \left(-i\pi \sum_{k=j}^{i-1} a_k^\dagger a_k \right) a_i \rangle \\ &= (-1)^{|i-j|} \frac{1}{\pi} \int_{-\pi/2}^{\pi/2} \exp[ik(R_j - R_i)] dk \\ &\propto \frac{(-1)^{|i-j|} a}{|R_j - R_i|}. \end{aligned} \quad (7.26)$$

They decrease as a power law with exponent $\eta = 1$. Despite its 1-dimensional structure, the system therefore remains ‘almost ordered’, with very slowly decreasing correlation functions. This property is in fact specific to chains of half-integer spins; chains of integer spins form a disordered singlet state at zero temperature [see Chap. 10(I)].

An exchange interaction along \hat{z} ,

$$\mathcal{H}_z = 2\Delta \sum_i S_i^z S_{i+1}^z = 2\Delta \sum_i (n_i - 1/2)(n_{i+1} - 1), \quad (7.27)$$

does not fundamentally change the ground state, which remains a fermion gas occupying the same states, provided $\Delta \leq J$. The fermions nevertheless interact strongly and this greatly complicates the theory. When $\Delta > J$, the system has a gap of the order of $\Delta - J$ in its excitation spectrum and the ground state coincides with that of the corresponding Ising model, i.e., ferromagnetic for $\Delta > 0$, and antiferromagnetic for $\Delta < 0$. The model is

exactly solvable by Bethe's ansatz for any value of Δ [155, 156, 157, 158, 159]. Because of interactions, introducing a hole into the Fermi sea modifies all other fermion wave vectors. This strongly renormalises the hole energy. As an example, in the isotropic Heisenberg chain, the energy of a hole with wave vector q is

$$\varepsilon(q) = \pi|J|\cos q , \quad (7.28)$$

rather than $2|J|\cos q$. Interactions also modify the ground state energy:

$$E_g = 2|J|N \left(\frac{1}{4} - \ln 2 \right) = -2|J|N \times 0.443 . \quad (7.29)$$

This is to be compared with the energy of the Néel state, $E_N = -2|J|N \times 1/4$. As we might expect, quantum fluctuations lower the ground state energy, rather as thermal fluctuations lower the free energy in a classical system. Magnons are composite particle-hole objects made of two spinons, as before. Their spectrum is exactly the same as that of the XY chain (see Fig. 7.2), after the renormalisation of the exchange constant $J \rightarrow \pi J/2$ mentioned previously. Figure 7.3 shows explicitly how a reversed spin of angular momentum \hbar spontaneously decomposes into two spinons of angular momentum $\hbar/2$ [160]. This is referred to as spinon deconfinement. There is still a qualitative difference between the isotropic Heisenberg chain and the XY chain. Spinons can form bound states, confined over a length determined by the wave vector. These are called *strings*. Such excitations do not alter S_z and only contribute to the energy via the holes they create. However, their contributions to entropy are fundamental to an analysis of thermodynamic properties [161]. At long wavelengths, the (J, Δ) Heisenberg model can be described as a Luttinger liquid [162]. This rather formal approach leads to a precise description of correlation functions. Many monographs devoted to the Heisenberg and XY models give a complete description [151, 165, 166]. Let us just mention that, by choosing decreasing exchange interactions $\sin^2 \pi n/N \approx 1/r^2$, the Heisenberg model can once again be described as a free fermion gas [163, 164], with ground state

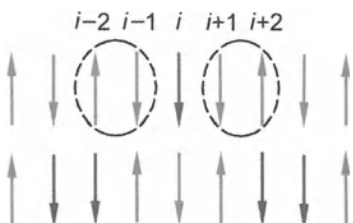


Fig. 7.3. Starting from the antiferromagnetic ground state of the isotropic chain, the spin i is flipped. By exchange of spins $i - 2, i - 1$, and spins $i + 1, i + 2$, two defects in the antiferromagnetic structure propagate towards the left and right. These defects restore translation invariance, broken by antiferromagnetic order

$$|\psi\rangle = P_G |\phi\rangle, \quad P_G = \prod_{i=1}^N (1 - n_i^\uparrow n_i^\downarrow), \quad |\phi\rangle = \prod_{|k|<\pi/a} a_{k\uparrow}^\dagger a_{k\downarrow}^\dagger |0\rangle. \quad (7.30)$$

The (Gutzwiller) projection operator P_G ensures that there is only one spin state at each site, whilst all magnon states (from $-\pi/a$ to π/a rather than just within $[-\pi/2a, \pi/2a]$) are occupied.

In conclusion, all spin 1/2 chains form a fermion gas whose ground state has the same ‘almost ordered’ structure as the XY model, provided that $\Delta \leq J$.

7.2 The Classical One-Dimensional XY Model

In the classical limit, spins are represented by their angles in the XY plane. In terms of these angles, the classical XY Hamiltonian becomes

$$\mathcal{H} = -2J \sum_i \cos(\theta_i - \theta_{i+1}) = \sum_i \mathcal{H}_{i,i+1}. \quad (7.31)$$

This also models a chain of Josephson junctions [see Chap. 16(II)], in which angles θ_i are phases of each superconducting island. All terms $\mathcal{H}_{i,i+1}$ commute in this model and we can write the partition function

$$Z = \int \prod_\alpha \frac{d\theta_\alpha}{p_i} \exp(-\beta \mathcal{H}) \quad (7.32)$$

as an ordered sequence of integrations:

$$Z = \dots \frac{1}{\pi} \int_{-\pi}^{\pi} \exp(-\beta \mathcal{H}_{i,i+1}) \frac{1}{\pi} \int_{-\pi}^{\pi} \exp(-\beta \mathcal{H}_{i+1,i+2}) \dots. \quad (7.33)$$

The functions $\exp(-\beta \mathcal{H}_{i,i+1})$ can be expanded in terms of a Fourier basis

$$\exp[2\beta J \cos(\theta_i - \theta_{i+1})] = I_0(2\beta J) + \sum_{n \neq 0} I_n(2\beta J) \exp[in(\theta_i - \theta_{i+1})], \quad (7.34)$$

where I_n are modified Bessel functions. This suggests a matrix representation of the partition function using a transfer matrix,

$$\exp[\beta J \cos(\theta_i - \theta_{i+1})] = \psi_i^\dagger z_i \psi_{i+1}. \quad (7.35)$$

ψ_i is a column vector with components $\psi = (\exp[i\theta_1] \dots \exp[in\theta_i])$ and z_i is a diagonal matrix with entries $z_{n,m} = z_n \delta_{nm} = 2I_n(2\beta J)$. Integration over angles reduces the expression in (7.33) to a product of transfer matrices z_i , and the partition function is its trace:

$$Z = \text{Tr}(z^N) = \sum_n z_n^N \rightarrow z_0^N. \quad (7.36)$$

In the thermodynamic limit, this is dominated by the largest eigenvalue $z_0 = 2I_0(2\beta J)$. The free energy then becomes simply

$$F = -Nk_B T \ln[2I_0(2\beta J)] . \quad (7.37)$$

Its internal energy,

$$U = -2NJ \langle \cos(\theta_i - \theta_{i+1}) \rangle = -2NJ \frac{I_1(2\beta J)}{I_0(2\beta J)} , \quad (7.38)$$

tends to $2NJ$, the classical energy of the ferromagnetic or antiferromagnetic state. Its specific heat,

$$C = Nk_B \left(\frac{2J}{k_B T} \right)^2 \left(\frac{1}{2} + \frac{I_2}{2I_0} - \frac{I_1^2}{I_0^2} \right) , \quad (7.39)$$

tends to a constant value $Nk_B/2$ at low temperatures. In this limit, the kinetic energy is just that of a perfect gas having one particle per spin, in agreement with the principle of equipartition of energy. A simple calculation shows that the correlation length $\xi = 4J/k_B T$ diverges when $T \rightarrow 0$. The system therefore has a phase transition at $T = 0$, like the 1-dimensional Ising model.

Exercise

Show that the correlation function for the classical XY chain is

$$\langle \cos(\theta_i - \theta_j) \rangle = \frac{\sum_{i=1}^{\infty} I_n(2\beta J)^{|i-j|}}{\sum_{i=0}^{\infty} I_n(2\beta J)^{|i-j|}} , \quad (7.40)$$

and deduce the correlation length at low temperatures.

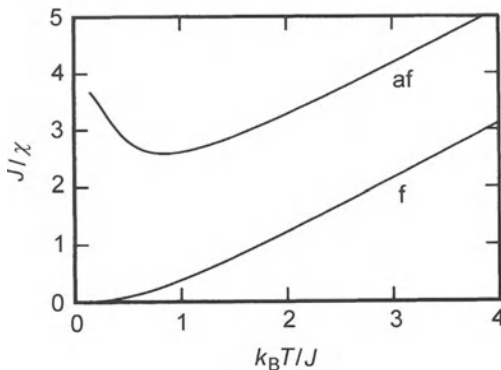


Fig. 7.4. Susceptibility in the classical 1-dimensional XY model, for ferromagnetic and antiferromagnetic interactions. General behaviour resembles that in the 1-dimensional Ising model (see Fig. 6.1). For antiferromagnetic interactions, susceptibility tends to a constant value at low temperatures

If a magnetic field is applied in the XY plane, its Zeeman interaction with the spins is

$$\mathcal{H}_{i,i+1} = -\frac{B}{2}(\cos \theta_i + \cos \theta_{i+1}) . \quad (7.41)$$

For small values of the field $B = \mu_0 \mu_B H$, its contribution to the free energy can be calculated to second order by perturbation methods. We can then evaluate the susceptibility in the classical XY model:

$$\chi = \frac{\mathcal{C} I_0 + I_1}{T I_0 - I_1} = \frac{\mathcal{C}}{T} \frac{1 + U/2NJ}{1 - U/2NJ} , \quad (7.42)$$

where \mathcal{C} is Curie's constant and U the internal energy. Note that I_1 changes sign when J changes sign, whereas I_0 remains unchanged. We can thus conclude that $X = T\chi/\mathcal{C}$ satisfies the symmetry relation

$$X(\beta J) X(-\beta J) = 1 . \quad (7.43)$$

The Ising model and the isotropic Heisenberg model in one dimension satisfy the same symmetry relations in the classical limit. This symmetry is destroyed by quantum fluctuations, which are much more significant in antiferromagnetic systems [see Chap. 10(I)].

7.3 Kosterlitz–Thouless Transition in the Two-Dimensional XY Model

Since it is impossible to stabilise long range order in two dimensions, it is natural to study fluctuations at low temperatures [167, 168, 169, 170]. Consider the order parameter of an XY magnet,

$$M(\mathbf{r}) = |m(\mathbf{r})| \exp[i\theta(\mathbf{r})] , \quad (7.44)$$

whose amplitude and phase may fluctuate. As there is short range order at sufficiently low temperatures, the Landau free energy always has a local minimum with well defined amplitude $|m(\mathbf{r})| = \sqrt{|a|}/b$. However, the phase is not specified by this local minimum and can fluctuate in an arbitrary way. Amongst all possible phase fluctuations, topological defects correspond to phase fields such that the integral around a closed path takes a value

$$\oint \phi(\mathbf{r}) = 2\pi Q , \quad (7.45)$$

where the *topological charge* Q of the defect can only take integer values. Some examples of topological defects in an XY magnet are shown in Fig. 7.5. In addition, we must include spin waves, fluctuations associated with continuous deformations of the order parameter $\phi(\mathbf{r})$. These also contribute to the free energy, as they do in ordered magnets at finite temperatures. Because defects have well defined topological charges, we can always factorise the contribution

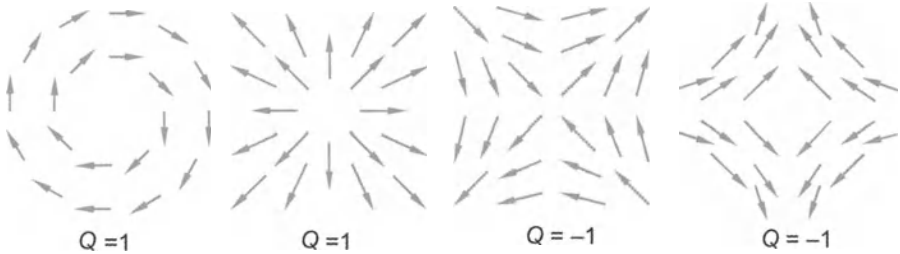


Fig. 7.5. Configuration of spin vortices on a square lattice. Configurations on the *left* have charge $Q = +1$, whereas textures on the *right* have charge $Q = -1$. All the configurations can be generated from the first by successively rotating spins through $\pi/2$

of these vortices to the partition function. This means that we can study their contribution to the free energy separately. The decomposition

$$\phi(\mathbf{r}) = \psi(\mathbf{r}) + \bar{\phi}(\mathbf{r}) \quad (7.46)$$

is defined by local minimisation of a free energy fluctuation

$$\begin{aligned} \delta F &= J \int d^2 r [(\nabla \psi)^2 + 2(1 - \cos \delta \bar{\phi})] \\ &\approx J \int d^2 r [(\nabla \psi)^2 + (\nabla \bar{\phi})^2], \end{aligned} \quad (7.47)$$

where we have linearised fluctuations associated with the vortex, since we seek to understand low temperature behaviour. The spin wave contribution increases continuously with temperature, whilst topological defects induce a phase transition. Let us estimate the contribution to the elastic energy of a vortex. The gradient of the phase ϕ is constant on a circle of radius r centred on the core of the vortex. In fact,

$$\nabla \bar{\phi}(\mathbf{r}) = \frac{2\pi Q}{2\pi r}. \quad (7.48)$$

Its elastic energy

$$\begin{aligned} u_v &= \int_a^R J(\nabla \phi)^2 2\pi r dr \\ &= 2\pi J \int_a^R \left(\frac{Q}{r}\right)^2 r dr = 2\pi J Q^2 \ln\left(\frac{R}{a}\right) \end{aligned} \quad (7.49)$$

is bounded by the size R of the system and the atomic spacing a . We can compare this energy with its entropy s_v . The number w of possible configurations of the vortex is determined by the number of ways we can position it. Since there are R^2/a^2 available sites,

$$s_v = k_B \ln w = 2k_B \ln(R/a). \quad (7.50)$$

At low temperatures, the free energy of an isolated vortex,

$$f_v = u_v - T s_v = 2(\pi J - k_B T) \ln(R/a), \quad (7.51)$$

is dominated by the elastic energy. Isolated vortices can only appear above a critical temperature

$$k_B T_{KT} \approx \pi J, \quad (7.52)$$

when $f_v < 0$. In practice, this temperature is lower because there are vortex pairs at low temperatures and their interactions favour the appearance of free vortices. The transition temperature is thereby renormalised according to

$$\frac{\pi J}{k_B T_{KT}} - 1 = 2\pi \exp\left(-\pi^2 \frac{J}{k_B T_{KT}}\right). \quad (7.53)$$

If there are no vortices, spin waves destroy long range order. However, correlations between spins decrease very slowly as power laws which we shall now determine. If there are no topological defects, the spin correlation function can be expanded in powers of $\theta(0) - \theta(\mathbf{r})$ to give

$$\begin{aligned} \langle \mathbf{S}(0) \cdot \mathbf{S}(\mathbf{r}) \rangle &= \langle \cos[\theta(0) - \theta(\mathbf{r})] \rangle \\ &= 1 + \sum_{n=1}^{\infty} \frac{(-1)^n}{(2n)!} \langle [\theta(0) - \theta(\mathbf{r})]^{2n} \rangle. \end{aligned} \quad (7.54)$$

In the case of Gaussian fluctuations, all moments of $\theta(0) - \theta(\mathbf{r})$ can be expressed in terms of the variance, i.e.,

$$\langle [\theta(0) - \theta(\mathbf{r})]^{2n} \rangle = (2n - 1)!! \langle [\theta(0) - \theta(\mathbf{r})]^2 \rangle^n. \quad (7.55)$$

Since $(2n - 1)!!/(2n)! = 1/n!2^n$, the correlation function can be written in terms of the second moment alone:

$$\langle \mathbf{S}(0) \cdot \mathbf{S}(\mathbf{r}) \rangle \approx \exp\left[-\frac{1}{2} \langle [\theta(0) - \theta(\mathbf{r})]^2 \rangle\right]. \quad (7.56)$$

At equilibrium, phase fluctuations are translation invariant, i.e., $\theta(0) - \theta(\mathbf{r}) \equiv \theta(\mathbf{R}) - \theta(\mathbf{R} + \mathbf{r})$. They can therefore be parametrised in Fourier transform space by

$$\theta(\mathbf{R}) - \theta(\mathbf{R} + \mathbf{r}) = \int \frac{d^2 q}{4\pi^2} [\exp i\mathbf{q} \cdot \mathbf{R} - \exp i\mathbf{q} \cdot (\mathbf{R} + \mathbf{r})] \theta(q). \quad (7.57)$$

Quadratic fluctuations are parametrised by the same Fourier amplitude $|\theta(q)|^2$,

$$\frac{1}{2} [\theta(0) - \theta(\mathbf{r})]^2 = \int \frac{d^2 q}{4\pi^2} (1 - \cos \mathbf{q} \cdot \mathbf{r}) |\theta(q)|^2, \quad (7.58)$$

whose thermodynamic average reduces to a Gaussian integral [see Sect. 4.2(I)]

$$\langle |\theta(q)|^2 \rangle = \int_{-\infty}^{\infty} d\theta \theta^2 \sqrt{\frac{\beta J q^2}{\pi}} \exp(-\beta J q^2 \theta^2) = \frac{kT}{2Jq^2}. \quad (7.59)$$

It only remains to calculate the angular average over all possible q directions of

$$\int_0^{2\pi} d\theta [1 - \cos(qr \cos \theta)] = 2\pi[1 - J_0(qr)] , \quad (7.60)$$

where J_0 is the Bessel function of order 0. Phase fluctuations are obtained by integrating over all wave vectors q ,

$$\begin{aligned} \langle [\theta(0) - \theta(\mathbf{r})]^2 \rangle &= \frac{k_B T}{2\pi J} \int_0^{\pi/a} \frac{1 - J_0(qr)}{q} dq \\ &\approx \frac{k_B T}{2\pi J} \ln(\pi r/a) , \end{aligned} \quad (7.61)$$

because for large values of r , we can ignore (after change of variable) the Bessel function contribution. Hence the spin-spin correlation function decreases as a power law

$$\langle \mathbf{S}(0) \cdot \mathbf{S}(\mathbf{r}) \rangle = \left(\frac{\pi a}{r} \right)^{\eta(T)} , \quad (7.62)$$

where the critical exponent $\eta(T) = kT/4\pi J$ is a continuous function of temperature, attaining its maximal value of $1/4$ at the transition temperature T_{KT} .

In order to understand the low temperature phase, we must take into account interactions between vortices. We begin by determining the phase field $\bar{\phi}(\mathbf{r})$ associated with a vortex distribution of charge

$$\rho(\mathbf{r}) = \sum_i Q_i \delta(\mathbf{r} - \mathbf{r}_i) . \quad (7.63)$$

Since the field of a vortex is a Coulomb field, $\bar{\phi}(\mathbf{r})$ must satisfy Poisson's equation

$$\nabla^2 \bar{\phi}(\mathbf{r}) = 2\pi \rho(\mathbf{r}) . \quad (7.64)$$

The Green function for the two-dimensional Coulomb potential is

$$g(\mathbf{r} - \mathbf{r}') = \frac{1}{2\pi} \ln \left(\frac{|\mathbf{r} - \mathbf{r}'|}{a} \right) ,$$

where g is defined by the requirement

$$\nabla_{\mathbf{u}}^2 g(\mathbf{u} - \mathbf{u}') = \delta(\mathbf{u} - \mathbf{u}') . \quad (7.65)$$

The general solution of (7.64) is obtained by superposing the contribution from each charge to give

$$\phi(\mathbf{r}) = 2\pi \int d^2 r g(\mathbf{r} - \mathbf{r}') \rho(\mathbf{r}') . \quad (7.66)$$

Integrating by parts the energy of the vortex field,

$$\begin{aligned} U_v &= J \int d^2r [\nabla \bar{\phi}(\mathbf{r})]^2 \\ &= J \int dl \bar{\phi}(\mathbf{r}) \nabla \bar{\phi}(\mathbf{r}) \cdot \mathbf{n} - 2\pi J \int d^2r \bar{\phi}(\mathbf{r}) \rho(\mathbf{r}), \end{aligned} \quad (7.67)$$

we obtain the total energy due to phase fluctuations,

$$U = J \int d^2r (\nabla \psi)^2 - 4\pi^2 J \int \int d^2r d^2r' \rho(\mathbf{r}) g(\mathbf{r} - \mathbf{r}') \rho(\mathbf{r}') + \mu, \quad (7.68)$$

where the chemical potential μ is determined by the surface term. It is defined by requiring global neutrality $\sum_i Q_i = 0$. This expresses the fact that vortices can only appear in pairs. Consequently, the contribution from topological defects is equivalent to an effective Hamiltonian of positive and negative charges in Coulomb interaction, viz.,

$$\mathcal{H}_{\text{eff}}^v = -2\pi J \sum_{i \neq j} Q_i Q_j \ln |\mathbf{r}_i - \mathbf{r}_j|/a + \mu, \quad (7.69)$$

where the chemical potential μ determines the average vortex density. The energy of a pair $+Q, -Q$, which is of the order of

$$u_{vv} = 2\pi J Q^2 \ln \left(\frac{\rho + a}{a} \right), \quad (7.70)$$

is much smaller than the energy of either vortex. This is because the average distance ρ between vortices $+Q$ and $-Q$ is

$$\langle \rho^2 \rangle = \frac{\int_a^\infty dr r^3 \exp[4\pi\beta Q^2 J \ln(r/a)]}{\int_a^\infty dr r \exp[4\pi\beta Q^2 J \ln(r/a)]} = a^2 \frac{2\pi\beta Q^2 J - 1}{2\pi\beta Q^2 J - 2}, \quad (7.71)$$

and this is close to the atomic spacing a . At low temperatures, a gas of $+Q, -Q$ pairs is energetically favoured, thus rendering the system electrically neutral. The phase field ϕ is then dipolar, i.e., inversely proportional to the distance d between pairs (in two dimensions). The residual interaction between pairs reduces to polarisation effects. These can be described by a dielectric constant $\epsilon(\mathbf{r})$, which is strongly dependent on average vortex density. Pair energies are renormalised phenomenologically by this dielectric constant,

$$U_{vv} = 2\pi J Q^2 \frac{\ln(|\mathbf{r}|/a)}{\epsilon(\mathbf{r})}, \quad (7.72)$$

at all temperatures. This brings out the fact that the divergence of susceptibility χ below T_{KT} indicates critical behaviour at all temperatures between 0 and T_{KT} . By renormalisation methods [see Chap. 4(I)], we can then determine the effective coupling between pairs as a function of temperature. Behaviour is highly singular in the neighbourhood of T_{KT} because the susceptibility has an essential divergence for $T \geq T_{KT}$,

$$\chi(T) \propto \exp \left(\frac{2.625}{\sqrt{\tau}} \right), \quad (7.73)$$

where $\tau = (T - T_{KT})/T_{KT}$. At transition, specific heat variations are too small to be detected. However, the spin stiffness constant Γ , which tends to J when $T \rightarrow 0$ (and tends to the superfluid density in superconductors and superfluids) makes a universal jump at transition, given by

$$\Gamma(T_{KT}) = \frac{2}{\pi} k_B T_{KT}. \quad (7.74)$$

A superfluid helium 4 film adsorbed onto a surface is also described by the XY model, where angle θ is the phase of the local order parameter. In this analogy, the spin stiffness constant Γ can be identified with helium atom density ρ_s in the superfluid state. This quantity can be precisely measured using a mechanical oscillator whose period depends on the inertial mass of the helium film, given by the normal component of the density $\rho_n = \rho - \rho_s$. The variation ΔP of oscillator period with temperature is proportional to the inertial mass variation and hence to ρ_s . This dependence is plotted in Fig. 7.6, for helium films of different thicknesses. The jump $\Delta P \propto \rho_s \equiv \Gamma$ is proportional to transition temperature T_{KT} , as expected from (7.74). This experimental confirmation using adsorbed helium 4 films [171, 172, 173] is one of the most significant successes of the theory proposed by Kosterlitz and Thouless. It has since been applied in contexts as varied as superconducting films [174], Josephson junction arrays [175], two-dimensional magnetism, 1-dimensional conductors, magnetism in $1+1$ (time) dimensions [176], and the crystal roughening transition and crystal growth [177].

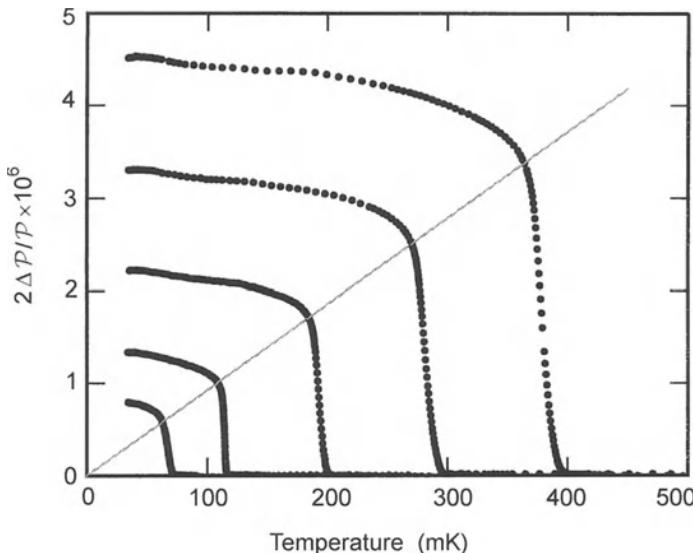


Fig. 7.6. Superfluid density of a helium film as a function of transition temperature. All curves end on a straight line whose slope is universal

8. Linear Response

In a sufficiently weak magnetic field (i.e., such that the Zeeman energy is small compared with k_B), an ensemble of paramagnetic spins does not manifest much alignment. Many spins are in reversed states with energies well above the ground state energy. What processes lead to this thermal disorder? We can cite dipolar interaction as an example: a Bohr magneton creates a magnetic field of order 1 T at a distance of 3 Å (the field of a nuclear magneton at this distance is a thousand times weaker). In such conditions, quantum states of spins coupled by dipolar interactions cannot be those of isolated spins. Nevertheless, at high temperatures, spatial correlations between spins become negligible. This is because dipolar fields are then fluctuating rapidly and can be considered as random ‘forces’ (equivalent to Langevin forces [178, 179]). Such effects bring the system towards thermodynamic equilibrium. Fluctuations then have only a slight effect *on average* with regard to thermodynamic quantities. Fluctuations in dipolar fields can nevertheless induce transitions between the various states accessible at neighbouring sites. In this way, they decrease temporal correlations between spins. It is the correlation functions and response functions which are sensitive to fluctuations.

Let us characterise temporal correlations between two quantities. We shall consider the μ and ν components of the total spin $S^\mu = \sum_r s^\mu(r)$, where $s(r)$ is the spin of the ion at point r . We first define the time evolution of this operator,

$$S^\mu(t) = \exp\left(i\frac{\mathcal{H}_0}{\hbar}t\right) S^\mu(0) \exp\left(-i\frac{\mathcal{H}_0}{\hbar}t\right). \quad (8.1)$$

This is the evolution of S^μ from 0 to t when it is isolated from the thermostat, \mathcal{H}_0 being the Hamiltonian when there are no external forces. The temporal correlation function between S^μ and S^ν is defined by

$$\begin{aligned} C^{\mu\nu}(\tau = t' - t) &= \langle S^\mu(t') S^\nu(t) \rangle \\ &= \frac{1}{Z_0} \text{Tr} [\exp(-\beta\mathcal{H}_0) S^\mu(t') S^\nu(t)] , \end{aligned} \quad (8.2)$$

where $Z_0 = \text{Tr}[\exp(-\beta\mathcal{H}_0)]$ and Tr indicates the trace of the operator in square brackets. These correlation functions, defined for a system in thermodynamic equilibrium, depend only on the time interval $\tau = t' - t$.

Two observations allow us to show that the correlation functions are stationary: the evolution operator $\exp(-i\mathcal{H}_0 t/\hbar)$ commutes with the density matrix, and the trace of a product of operators is invariant under cyclic permutation, i.e.,

$$\text{Tr}[AB \exp(-\beta\mathcal{H}_0)] = \text{Tr}[\exp(-\beta\mathcal{H}_0)AB].$$

In the classical limit, all quantities commute and correlation functions $C^{\mu\nu}(\tau)$ and $C^{\mu\nu}(-\tau)$ would be indistinguishable. It is therefore natural to introduce symmetrised correlation functions

$$C_S^{\mu\nu}(\tau) = \frac{1}{2}\langle S^\mu(t')S^\nu(t) + S^\nu(t)S^\mu(t') \rangle = \frac{1}{2}\langle \{S^\mu(t'), S^\nu(t)\} \rangle. \quad (8.3)$$

When we are interested in quantities having average values at equilibrium, the connected correlation functions are more useful. These are the correlation functions of the associated fluctuations,

$$\begin{aligned} \mathcal{S}^{\mu\nu}(\tau) &= \langle [S^\mu(\tau) - \langle S^\mu \rangle][S^\nu(0) - \langle S^\nu \rangle] \rangle \\ &= \langle S^\mu(\tau)S^\nu \rangle - \langle S^\mu \rangle \langle S^\nu \rangle. \end{aligned} \quad (8.4)$$

The usual definition given here must be modified when correlation functions do not decouple at infinite times, i.e., when

$$\lim_{\tau \rightarrow \pm\infty} \langle S^\mu(\tau)S^\nu \rangle \neq \langle S^\mu \rangle \langle S^\nu \rangle.$$

A better definition is then (see Sect. 8.3)

$$\mathcal{S}^{\mu\nu}(\tau) = \langle S^\mu(\tau)S^\nu(0) \rangle - \langle S^\mu(\infty)S^\nu \rangle. \quad (8.5)$$

These correlation functions can, of course, be generalised to any physical quantity (e.g., density, current, energy). Finally, by analogy, we define spatio-temporal correlations $\langle C^{\mu\nu}(\mathbf{R} \equiv \mathbf{r}' - \mathbf{r}, \tau) \rangle$ by

$$C^{\mu\nu}(\mathbf{R}, \tau) = \frac{1}{V} \sum_{\mathbf{r}} \langle S^\mu(\mathbf{r} + \mathbf{R}, \tau)S^\nu(\mathbf{r}, 0) \rangle, \quad (8.6)$$

$$\mathcal{S}^{\mu\nu}(\mathbf{R}, \tau) = \frac{1}{V} \sum_{\mathbf{r}} \langle [S^\mu(\mathbf{r} + \mathbf{R}, \tau) - \langle S^\mu \rangle][S^\nu(\mathbf{r}, 0) - \langle S^\nu \rangle] \rangle, \quad (8.7)$$

The Fourier transform of $\mathcal{S}^{\mu\nu}(\mathbf{R}, t)$,

$$\mathcal{S}^{\mu\nu}(\mathbf{q}, \omega) = \frac{1}{\sqrt{V}} \sum_{\mathbf{R}} \int_{-\infty}^{\infty} dt \exp[-i(\mathbf{q} \cdot \mathbf{R} - \omega t)] \mathcal{S}^{\mu\nu}(\mathbf{R}, t), \quad (8.8)$$

is called the *structure factor*. This quantity can be measured by neutron scattering experiments. It characterises elementary excitations of a magnetic system, to be studied in the next chapter. The physics of neutron scattering can be found in several textbooks [180, 181, 182].

Fluctuations also play an important role when we study response (for example, of total spin $\langle S^\mu(t) \rangle$) to a time dependent magnetic field $H^\nu(t)$ (for example, a harmonically varying field $H^\nu(t) = H_0^\nu \cos \omega t$). The Zeeman perturbation is expressed in reduced form

$$\mathcal{H}_Z(t) = - \sum_{\nu} S^{\nu} h_{\nu}(t), \quad (8.9)$$

where $h_{\nu} = \mu_0 \gamma H_{\nu}$ and γ is the gyromagnetic factor. For a small perturbation, the response will be a *linear* function of field components $h_{\nu}(t)$, viz.,

$$\langle S^{\mu}(t) \rangle = \sum_{\nu} \int_{-\infty}^t dt' \chi^{\mu\nu}(t-t') h_{\nu}(t'). \quad (8.10)$$

In this context, susceptibilities $\chi^{\mu\nu}(\tau)$ are called response functions. These functions are causal, in the sense that

$$\chi^{\mu\nu}(\tau) = 0 \quad \text{for } \tau < 0, \quad (8.11)$$

since there can be no response before the perturbation. Physically, the response function $\chi^{\mu\nu}(\tau)$ represents the response of the system to an impulsive excitation $h_{\nu}(t) = \delta(t)$.

There are two distinct limits when we study the linear response of a system. The processes relaxing magnetisation towards equilibrium (such as the dipolar field) may be very rapid compared with oscillations of the magnetic field; the magnetisation is then able to follow the applied field almost instantaneously. In this case, the system responds at constant temperature and this is called an *isothermal response*. On the other hand, the frequency may be very high compared with the system's relaxation rate; the magnetisation cannot keep in step with the applied field. We then have an *adiabatic response*, since it is just the response of spins which are isolated from the outside world. In practice, we always find ourselves in an intermediate situation. We can imagine that Fourier components of fluctuations at the frequency of the applied field will be particularly effective in delaying magnetisation response relative to field h_{ν} . In such conditions, the magnetic field does non-zero magnetic work $\oint H^{\nu}(t) dM_{\nu}(t)$ on the system because any phase delay in the magnetisation amounts to a dissipation of energy (see Sect. 8.3). Spin fluctuations therefore govern magnetic energy dissipation in a time dependent field. This fundamental relation between the linear response to a small excitation and the fluctuations of a system at equilibrium was originally discovered in the context of electrical conductivity [185, 186, 187]. It is known as the fluctuation-dissipation theorem and we shall study it in the present chapter. It is a correspondence of great practical importance. The response to an applied force gives invaluable information about fluctuations of a system at equilibrium. For example, we can deduce temporal correlations of spins which are difficult to measure directly. Conversely, symmetries of the microscopic Hamiltonian (e.g., with respect to time reversal) impose rigorous symmetries upon correlations between various quantities. The fluctuation-dissipation theorem expresses relationships between response functions and correlation functions which can be used to establish Onsager's reciprocity relations between the various response functions of the system (see Sect. 8.4) [183, 184].

The physical origin of the fluctuation-dissipation theorem can be viewed as a relation between emission of electromagnetic fluctuations induced by fluctuations in a spin system and absorption of electromagnetic energy required to maintain thermodynamic equilibrium. This viewpoint will be developed in Sect. 8.2. The system must also obey the principle of detailed balance,

$$n_i \nu(i \rightarrow j) = n_j \nu(j \rightarrow i). \quad (8.12)$$

This expresses the fact that the number of spins in transition from quantum state $|i\rangle$ to state $|j\rangle$ is equal to the number of spins going the other way. In this expression, $\nu(i \rightarrow j)$ is the transition rate and n_i the occupation number of state $|i\rangle$. This principle is one of the foundations of statistical physics, so the fluctuation-dissipation theorem has very wide validity. Deviations have only been observed for systems outside equilibrium (aging of metastable states [188]).

8.1 Isothermal Response

A response can be treated as isothermal when the excitation frequency is less than all relaxation frequencies of the system. Strictly speaking, this limit is only reached for the quasi-static limit discussed in the next section. In practice, the frequency range for which a response can be considered as isothermal depends on both the system and the relevant physical quantity [189, 190, 191]. Indeed, conservation laws imply that certain quantities will relax very slowly towards equilibrium through intermediate ‘hydrodynamic’ modes whose frequencies tend to zero at long wavelengths (see the next chapter). As an example, let us consider a Zeeman perturbation. We assume that the time dependence of the total Hamiltonian,

$$\mathcal{H} = \mathcal{H}_0 + \mathcal{H}_Z = \mathcal{H}_0 - \sum_{\nu} S^{\nu} h_{\nu}, \quad (8.13)$$

entering through h_{ν} , is quasi-static. The isothermal response $\langle S^{\mu} \rangle$ can then be defined as

$$\delta \langle S^{\mu} \rangle = \frac{\text{Tr} [S^{\mu} \exp(-\beta \mathcal{H})]}{\text{Tr} [\exp(-\beta \mathcal{H})]} - \frac{\text{Tr} [S^{\mu} \exp(-\beta \mathcal{H}_0)]}{\text{Tr} [\exp(-\beta \mathcal{H}_0)]}. \quad (8.14)$$

The linear response is just the first term in the expansion of $\delta \langle S^{\mu} \rangle$ in powers of h_{ν} . However, this expansion involves a difficulty: operators S^{ν} (and hence also \mathcal{H}_Z) do not commute with \mathcal{H}_0 . We must therefore transpose methods used for time dependent perturbations to the density matrix $\exp[-\beta(\mathcal{H}_0 + \mathcal{H}_Z)]$. We can make use of the formal analogy with the time evolution operator $\exp[-it(\mathcal{H}_0 + \mathcal{H}_Z)/\hbar]$. Define an operator [192]

$$V(\beta) \equiv V(it/\hbar) = U_{\mathcal{H}}(\tau) U_{\mathcal{H}_0}^{-1}(\tau) = \exp[-\beta \mathcal{H}] \exp[\beta \mathcal{H}_0]. \quad (8.15)$$

The derivative of V with respect to β is equivalent to the derivative with respect to an imaginary time parameter $\tau = -i\hbar\beta$ of the corresponding evolution operators, bearing in mind that

$$[\mathcal{H}, \exp(-\lambda\mathcal{H})] = [\mathcal{H}_0, \exp(-\lambda\mathcal{H}_0)] = 0. \quad (8.16)$$

Hence,

$$\begin{aligned} \frac{dV(\beta)}{d\beta} &= \exp[-\beta\mathcal{H}]\mathcal{H}_0 \exp[\beta\mathcal{H}_0] - \exp[-\beta\mathcal{H}]\mathcal{H} \exp[\beta\mathcal{H}_0] \\ &= -\exp[-\beta\mathcal{H}]\mathcal{H}_Z \exp[\beta\mathcal{H}_0] \\ &= V(\beta) \exp[-\beta\mathcal{H}_0] \left\{ \sum_{\nu} S^{\nu} h_{\nu} \right\} \exp[\beta\mathcal{H}_0] \\ &= \sum_{\nu} h_{\nu} V(\beta) S^{\nu}(i\hbar\beta), \end{aligned} \quad (8.17)$$

where we have generalised definition (8.1) to imaginary times. This differential equation is equivalent to the integral equation

$$V(\beta) = 1 + \sum_{\nu} h_{\nu} \int_0^{\beta} V(\lambda) S^{\nu}(i\hbar\lambda) d\lambda, \quad (8.18)$$

as is easily checked by differentiating. As for time dependent perturbations, this integral equation can be solved iteratively. The first order solution is obtained by replacing V in the integral of (8.18) by its value for $h_{\nu} = 0$, viz., $V = 1$. We find

$$V(\beta) \approx 1 + \sum_{\nu} h_{\nu} \int_0^{\beta} S^{\nu}(i\hbar\lambda) d\lambda, \quad (8.19)$$

$$\begin{aligned} \exp(-\beta\mathcal{H}) &= V(\beta) \exp(-\beta\mathcal{H}_0) \\ &\approx \exp(-\beta\mathcal{H}_0) + \\ &\quad \sum_{\nu} h_{\nu} \int_0^{\beta} d\lambda \exp(-\lambda\mathcal{H}_0) S^{\nu} \exp[(\lambda - \beta)\mathcal{H}_0]. \end{aligned} \quad (8.20)$$

We can now substitute (8.20) in the definition (8.14) of the isothermal response, keeping only terms linear in h_{ν} . This leads to

$$\begin{aligned} \delta\langle S^{\mu} \rangle &= \sum_{\nu} h_{\nu} \left\{ \frac{\text{Tr} \left[S^{\mu} \int_0^{\beta} d\lambda \exp(-\lambda\mathcal{H}_0) S^{\nu} \exp(\lambda - \beta)\mathcal{H}_0 \right]}{\text{Tr} [\exp(-\beta\mathcal{H}_0)]} \right. \\ &\quad \left. - \frac{\text{Tr} [S^{\mu} \exp(-\beta\mathcal{H}_0)]}{\text{Tr} [\exp(-\beta\mathcal{H}_0)]} \frac{\text{Tr} \left[\int_0^{\beta} d\lambda \exp(-\lambda\mathcal{H}_0) S^{\nu} \exp(\lambda - \beta)\mathcal{H}_0 \right]}{\text{Tr} [\exp(-\beta\mathcal{H}_0)]} \right\} \\ &= \sum_{\nu} h_{\nu} \int_0^{\beta} d\lambda [\langle S^{\mu}(-i\hbar\lambda) S^{\nu} \rangle - \langle S^{\mu}(-i\hbar\lambda) \rangle \langle S^{\nu} \rangle], \end{aligned} \quad (8.21)$$

where we have used invariance of the trace under cyclic permutation. Response functions are just the coefficients of the h_ν . They have been written in terms of connected correlation functions [\mathcal{S} given in (8.4)] with imaginary arguments $-i\hbar\lambda$. These can be obtained by analytic continuation of the temporal correlation functions. Explicitly, isothermal susceptibilities are defined by

$$\begin{aligned}\chi_T^{\mu\nu} &= \int_0^\beta d\lambda [\langle S^\mu(-i\hbar\lambda)S^\nu \rangle - \langle S^\mu(-i\hbar\lambda) \rangle \langle S^\nu \rangle] \\ &= \int_0^\beta d\lambda \{[\langle S^\mu(-i\hbar\lambda) - \langle S^\mu(-i\hbar\lambda) \rangle](S^\nu - \langle S^\nu \rangle)\} \\ &= \int_0^\beta d\lambda \mathcal{S}^{\mu\nu}(-i\hbar\lambda).\end{aligned}\tag{8.22}$$

These are the static response functions. Connected correlation functions at imaginary times can be found directly by taking their derivative with respect to temperature.

We shall now examine the other limit mentioned earlier, in which the system does not have time to exchange heat with the thermostat during the oscillation period of the magnetic field.

8.2 Adiabatic Response and the Fluctuation-Dissipation Theorem

In order to study the adiabatic response, we shall assume that the system is in thermodynamic equilibrium with a thermostat at $t = -\infty$, then isolated and the perturbation switched on adiabatically. The isolated system behaves like a Hamiltonian system. We can study the time development of initial states (eigenstates of \mathcal{H}_0) under the perturbation $\mathcal{H}_Z(t)$, using time dependent perturbation theory [193, 194, 195]. Let $|i\rangle$ be eigenstates of \mathcal{H}_0 of energy ε_i^0 , and $|\psi_i(t)\rangle$ their time development under the effect of the perturbation. The expectation value of a quantity such as total spin S^μ is defined by

$$\langle S^\mu(t) \rangle = \frac{1}{Z_0} \sum_i \exp(-\beta\varepsilon_i^0) \langle \psi_i(t) | S^\mu | \psi_i(t) \rangle,\tag{8.23}$$

$$\begin{aligned}\delta\langle S^\mu(t) \rangle &= \langle S^\mu(t) \rangle - \frac{1}{Z_0} \sum_i \exp(-\beta\varepsilon_i^0) \langle i | S^\mu | i \rangle \\ &= \langle S^\mu(t) \rangle - \langle S^\mu(-\infty) \rangle,\end{aligned}\tag{8.24}$$

where $\exp(-\beta\varepsilon_i^0)/Z_0$ is the initial population of state $|i\rangle$ at $t = -\infty$. The fact that the perturbation is switched on adiabatically allows us to follow the time development of each state i without altering its population [196]. The time dependence of states $|\psi_i(t)\rangle$ is found in the interaction basis

$$|i\rangle_{\text{int}} = \exp(i\mathcal{H}_0 t/\hbar)|i\rangle , \quad (8.25)$$

$$|\psi_i(t)\rangle_{\text{int}} = \exp(i\mathcal{H}_0 t/\hbar)|\psi_i(t)\rangle , \quad (8.26)$$

defined in such a way that the state $|i\rangle_{\text{int}}$ is stationary when there is no interaction (i.e., $d|i\rangle_{\text{int}}/dt = 0$). In this basis, first order perturbation theory relates $|\psi_i(t)\rangle_{\text{int}}$ to $|i\rangle_{\text{int}}$:

$$|\psi_i(t)\rangle_{\text{int}} = \left[1 - \frac{i}{\hbar} \int_{-\infty}^t dt' \mathcal{H}_Z^{\text{int}}(t') \right] |i\rangle_{\text{int}} , \quad (8.27)$$

where $\mathcal{H}_Z^{\text{int}}$ is the Zeeman perturbation in the interaction basis, given by

$$\mathcal{H}_Z^{\text{int}}(t) = \exp\left(i\frac{\mathcal{H}_0}{\hbar}t\right) \mathcal{H}_Z(t) \exp\left(-i\frac{\mathcal{H}_0}{\hbar}t\right) . \quad (8.28)$$

We obtain the linear response $\delta\langle S^\mu(t)\rangle$ by substituting (8.27) into the definition (8.24):

$$\delta\langle S^\mu(t)\rangle = -\frac{1}{Z_0} \frac{i}{\hbar} \int_{-\infty}^t dt' \text{Tr} \{ \exp(-\beta\mathcal{H}_0) [S_\mu(t), \mathcal{H}_Z^{\text{int}}(t')] \} . \quad (8.29)$$

The evolution operator $\exp(-i\mathcal{H}_0 t'/\hbar)$ and density matrix $\exp(-\beta\mathcal{H}_0)$ commute. We can therefore express the response in the basis of stationary states $|i\rangle$ as the expectation value of a commutator:

$$\delta\langle S^\mu(t)\rangle = \frac{i}{\hbar} \int_{-\infty}^t dt' \langle [\mathcal{H}_Z(t'), S^\mu(t-t')] \rangle , \quad (8.30)$$

where we have once again used the invariance of the trace under cyclic permutations of operators. Using definition (8.9) of the Zeeman perturbation, we obtain the definition of adiabatic susceptibility $\tilde{\chi}^{\mu\nu}$,

$$\delta\langle S^\mu(t)\rangle = \sum_\nu \int_{-\infty}^\infty dt' \tilde{\chi}^{\mu\nu}(t-t') h_\nu(t') , \quad (8.31)$$

$$\begin{aligned} \tilde{\chi}^{\mu\nu}(t) &= \frac{i}{\hbar} \langle [S^\mu(t), S^\nu] \rangle \quad \text{for } t > 0 , \\ &= 0 \quad \text{for } t < 0 . \end{aligned} \quad (8.32)$$

Thermodynamic averages are always weighted by the initial density matrix $\exp(-\beta\mathcal{H}_0)$ at $t = -\infty$. This is another demonstration that the linear response is causal. Let us decompose the perturbation $h_\nu(t)$ into Fourier components,

$$h_\nu(t) = \frac{1}{2\pi} \int_{-\infty}^\infty h_\nu(\omega) \exp(-i\omega + \eta)t , \quad (8.33)$$

where η is an infinitesimal quantity which represents the perturbation being switched on adiabatically. We can then define the Fourier transform of the susceptibility from (8.32),

$$\begin{aligned}\delta\langle S^\mu(t)\rangle &= \frac{1}{2\pi} \sum_\nu \int_{-\infty}^{\infty} d\omega h_\nu(\omega) \exp(-i\omega + \eta)t \\ &\quad \times \int_{-\infty}^t dt' \tilde{\chi}^{\mu\nu}(t-t') \exp(-i\omega + \eta)(t'-t),\end{aligned}\quad (8.34)$$

$$\begin{aligned}\tilde{\chi}^{\mu\nu}(\omega + i\eta) &= \int_0^{\infty} d\tau \tilde{\chi}^{\mu\nu}(\tau) \exp(i\omega - \eta)\tau \\ &= \frac{i}{\hbar} \int_0^{\infty} d\tau \langle [S^\mu(\tau), S^\nu] \rangle \exp(i\omega - \eta)\tau.\end{aligned}\quad (8.35)$$

Since the spin operators are Hermitian, it is easy to check that

$$\tilde{\chi}_{\mu\nu}(\omega)^* = \tilde{\chi}_{\mu\nu}(-\omega), \quad (8.36)$$

in other words, the real part $\tilde{\chi}'(\omega)$ of $\tilde{\chi}(\omega)$ is an even function of ω , whilst the imaginary part $\tilde{\chi}''(\omega)$ is an odd function, $\tilde{\chi}(\omega) = \tilde{\chi}'(\omega) + i\tilde{\chi}''(\omega)$. In order to obtain the usual forms of the fluctuation-dissipation theorem, we will make a distinction between response functions associated with physical quantities which are odd with respect to time reversal [denoted $R(t)$], and those associated with even quantities. In the former category, we find the components $S^\mu(t)$ of total spin which we have been considering up until now. In the second category, an example is density $n(t)$. The Fourier transform of the commutator $[R(t), S^\nu]$ between response $R(t)$ and excitation S^ν is given in terms of response functions:

$$\begin{aligned}&\frac{i}{\hbar} \int_{-\infty}^{\infty} dt \langle [R(t), S^\nu] \rangle \exp(i\omega t) \\ &= \frac{i}{\hbar} \int_0^{\infty} dt \{ \langle [R(t), S^\nu] \rangle \exp(i\omega - \eta)t + \langle [R(-t), S^\nu] \rangle \exp(-i\omega - \eta)t \} \\ &= \tilde{\chi}(\omega + i\eta) - \tilde{\chi}(-\omega + i\eta) = 2i\tilde{\chi}''(\omega) \quad \text{when } R(t) = -R(-t), \\ &= \tilde{\chi}(\omega + i\eta) + \tilde{\chi}(-\omega + i\eta) = 2\tilde{\chi}'(\omega) \quad \text{when } R(t) = R(-t).\end{aligned}\quad (8.37)$$

Finally, we establish the thermodynamic identity

$$\begin{aligned}&\int_{-\infty}^{\infty} dt \langle S^\nu S^\mu(t) \rangle \exp(i\omega t) \\ &= \int_{-\infty}^{\infty} \frac{dt}{Z_0} \text{Tr} \left[e^{-\beta \mathcal{H}_0} S^\nu \exp \left(i \frac{\mathcal{H}_0}{\hbar} t \right) S^\mu \exp \left(-i \frac{\mathcal{H}_0}{\hbar} t \right) \right] e^{i\omega t} \\ &= \int_{-\infty}^{\infty} \frac{dt}{Z_0} \text{Tr} \left[e^{-\beta \mathcal{H}_0} e^{i\mathcal{H}_0(t-i\hbar\beta)/\hbar} S^\mu e^{-i\mathcal{H}_0(t-i\hbar\beta)/\hbar} S^\nu \right] e^{i\omega t} \\ &= \exp(-\beta\hbar\omega) \int_{-\infty}^{\infty} dt \langle S^\mu(t) S^\nu \rangle e^{i\omega t}.\end{aligned}\quad (8.38)$$

The fluctuation-dissipation theorem is obtained by substituting (8.38) into (8.37). For odd $R(t)$,

$$\tilde{\chi}''(\omega) = \frac{1}{2\hbar}[1 - \exp(-\beta\hbar\omega)]C(\omega); \quad (8.39)$$

for even $R(t)$,

$$\tilde{\chi}'(\omega) = \frac{i}{2\hbar}[1 - \exp(-\beta\hbar\omega)]C(\omega). \quad (8.40)$$

The fluctuation-dissipation theorem is usually expressed in terms of symmetrised correlation functions (8.3), which have a well defined classical limit:

$$\tilde{\chi}''(\omega) = \frac{1}{\hbar} \tanh\left(\frac{\beta\hbar\omega}{2}\right) C_S(\omega) \quad \text{when } R(t) = -R(-t), \quad (8.41)$$

$$\tilde{\chi}'(\omega) = \frac{i}{\hbar} \tanh\left(\frac{\beta\hbar\omega}{2}\right) C_S(\omega) \quad \text{when } R(t) = R(-t). \quad (8.42)$$

At high temperatures $\beta\hbar\omega \ll 1$, Planck's constant drops out:

$$\tilde{\chi}''(\omega) = \frac{\omega}{2k_B T} C_S(\omega) \quad \text{when } R(t) = -R(-t), \quad (8.43)$$

$$\tilde{\chi}'(\omega) = \frac{i\omega}{2k_B T} C_S(\omega) \quad \text{when } R(t) = R(-t). \quad (8.44)$$

This is the classical limit of the fluctuation-dissipation theorem.

In this form, the theorem can be interpreted as a relation between the electromagnetic power emitted by magnetic fluctuations in a sample and the power the sample absorbs from an oscillating magnetic field.

Physical Interpretation of the Fluctuation-Dissipation Theorem

We are interested in the electromagnetic field emitted by an ensemble of fluctuating magnetic moments. When electromagnetic wavelengths are long compared with characteristic dimensions of sample and detector, the field distribution is determined by the magnetostatic problem. We consider the magnetic flux induced by the magnetic field of the sample in a small coil [see Fig. 1.2(I) and Sect. 1.3(I)]. The reciprocity theorem gives this flux in terms of local magnetisation $\mathbf{M}(\mathbf{r}, t) = \gamma\mathbf{S}(\mathbf{r}, t)$ and field $\mathbf{h}(\mathbf{r})$ created by the coil when a current of one ampere flows through it, viz.,

$$\Phi(t) = \gamma \int_V d^3r \mathbf{S}(\mathbf{r}, t) \cdot \mathbf{h}(\mathbf{r}). \quad (8.45)$$

Electromagnetic noise induced in the coil can be described by the flux-flux correlation function. Equation (8.43) then relates noise to spin-spin correlation functions:

$$\langle \Phi(t')\Phi(t) \rangle = \gamma^2 \int_V d^3r' \int_V d^3r \langle \mathbf{S}^\mu(\mathbf{r}', t') \mathbf{S}^\nu(\mathbf{r}, t) \rangle h_\mu(\mathbf{r}') h_\nu(\mathbf{r}). \quad (8.46)$$

Let us examine how this expression simplifies in some particular situations. When magnetic fluctuations are isotropic,

$$\langle \mathbf{S}^\mu(\mathbf{r}', t') \mathbf{S}^\nu(\mathbf{r}, t) \rangle = \frac{\delta_{\mu\nu}}{3} \langle \mathbf{S}(\mathbf{R}, \tau) \cdot \mathbf{S}(0, 0) \rangle = \delta_{\mu\nu} C(\mathbf{R}, \tau), \quad (8.47)$$

where $\mathbf{R} = \mathbf{r}' - \mathbf{r}$ and $\tau = t' - t$. The electromagnetic noise is then determined by the spatio-temporal correlation function $C(\mathbf{R}, \tau)$,

$$\langle \Phi(\tau) \Phi(0) \rangle = \gamma^2 \int_V d^3 r' \int_V d^3 r C(\mathbf{R}, \tau) \mathbf{h}(\mathbf{r}) \cdot \mathbf{h}(\mathbf{r}'). \quad (8.48)$$

Two limits are possible, depending on whether the correlation functions vary over large distances relative to the coil size (as happens in a ferromagnetic domain) or small distances (typical of a paramagnet). In the first case, $C(\mathbf{R}, \tau)$ no longer depends on R and

$$\langle \Phi(\tau) \Phi(0) \rangle = \gamma^2 C(\tau) \left| \int_V d^3 r \mathbf{h}(\mathbf{r}) \right|^2. \quad (8.49)$$

In the other case, $C(\mathbf{R}, \tau) = N \delta(R) \langle \mathbf{S}(\tau) \cdot \mathbf{S}(0) \rangle$, where N is the number of spins in the sample. Electromagnetic fluctuations then reduce to temporal spin-spin fluctuations,

$$\langle \Phi(\tau) \Phi(0) \rangle = \gamma^2 C(\tau) N \int_V d^3 r |\mathbf{h}(\mathbf{r})|^2. \quad (8.50)$$

In both cases, electromagnetic noise is proportional to spin-spin correlation functions $C(\tau)$. The spectrum of electromagnetic power emitted is proportional to $|\Phi^2(\omega)|$, the Fourier transform of $\langle \Phi(\tau) \Phi(0) \rangle$. Hence, the spectral distribution of noise is described by the correlation function $C(\omega)$. Although it is difficult to detect, magnetic noise has been observed experimentally using quantum detectors [SQUIDs, described in Chap. 16(II)] [197, 198], which are highly sensitive to magnetic flux, in a superconducting detection coil.

Let us now assume that an oscillating current of amplitude I and frequency ω passes through the same coil. The magnetic field produced is $I \mathbf{h}(\mathbf{r}) \cos \omega t$. The adiabatic susceptibility, assumed isotropic and spatially uniform, determines the magnetic response

$$\begin{aligned} \delta \langle \mathbf{S}(\mathbf{r}, t) \rangle &= \mu_0 \gamma I \mathbf{h}(\mathbf{r}) \operatorname{Re} [\tilde{\chi}(\omega) \exp(-i\omega t)] \\ &= \mu_0 \gamma I \mathbf{h}(\mathbf{r}) [\tilde{\chi}'(\omega) \cos \omega t + \tilde{\chi}''(\omega) \sin \omega t], \end{aligned} \quad (8.51)$$

where Re denotes the real part. The work done by the magnetic field on the system in one cycle of period $T = 2\pi/\omega$ is [see Chap. 1(I)]

$$\begin{aligned} W &= \int_0^{2\pi/\omega} dt \int_V d^3 r \mathbf{H}(\mathbf{r}, t) \cdot d\mathbf{M}(\mathbf{r}, t) \\ &= - \int_0^{2\pi/\omega} dt \int_V d^3 r \mathbf{M}(\mathbf{r}, t) \cdot d\mathbf{H}(\mathbf{r}, t) \\ &= -\mu_0 \gamma^2 I^2 \int_V d^3 r |\mathbf{h}(\mathbf{r})|^2 \int_0^T d(\cos \omega t) [\tilde{\chi}'(\omega) \cos \omega t + \tilde{\chi}''(\omega) \sin \omega t] \\ &= \pi \mu_0 \gamma^2 I^2 \tilde{\chi}''(\omega) N \int_V d^3 r |\mathbf{h}(\mathbf{r})|^2, \end{aligned} \quad (8.52)$$

after integrating the magnetisation by parts. The power dissipated is thus work divided by the period $2\pi/\omega$, i.e.,

$$\mathcal{P} = \mu_0 \gamma^2 I^2 \frac{\omega}{2} \tilde{\chi}''(\omega) N \int_V d^3r |\mathbf{h}(\mathbf{r})|^2 . \quad (8.53)$$

According to the fluctuation-dissipation theorem (8.43), we can replace $\tilde{\chi}''(\omega)$ in this expression by $\omega C(\omega)/k_B T$. We then identify $\gamma^2 C(\omega) \int_V d^3r |\mathbf{h}(\mathbf{r})|^2$ with the electromagnetic noise $|\Phi(\omega)|^2$ induced by the sample in thermodynamic equilibrium [see (8.50)]. We can thus define the dissipative resistance of the sample in terms of electromagnetic noise induced in the coil,

$$\mathcal{R} = \frac{\mathcal{P}}{I^2} = \frac{1}{4k_B T} \omega^2 |\Phi(\omega)|^2 . \quad (8.54)$$

Since the electromotive force induced by fluctuations in flux $\Phi(t)$ is $\mathcal{E} = -d\Phi/dt = i\omega\Phi$, the last equation can also be written

$$\mathcal{R} = \frac{\mathcal{E}^2(\omega)}{4k_B T} . \quad (8.55)$$

In other words, the electromotive force induced per spectral unit is $\mathcal{E} = \sqrt{4k_B T \mathcal{R}}$. It was in this form that Johnson and Nyquist originally discovered the fluctuation-dissipation theorem for electrical circuits. This equivalence between electrical and magnetic forms of the theorem shows that magnetic dissipation can be represented by an additional resistance in the circuit. Resonant absorption can therefore be detected through reduction in the quality factor of a resonant LC circuit whose inductance produces the magnetic field. This is the principle used for detection of nuclear magnetic and electron-spin resonances. In this context, magnetic energy $\mu_0 \int_V d^3r |\mathbf{h}(\mathbf{r})|^2 / 2$ in the sample is parametrised by inductance L of the coil and the filling factor η which measures the fraction of electromagnetic energy contained in the sample

$$\frac{\mu_0}{2} \int_V d^3r |\mathbf{h}(\mathbf{r})|^2 = \eta \frac{1}{2} L (I = 1)^2 , \quad (8.56)$$

since the field \mathbf{h} is the field produced by a current of 1 ampere.

In a 2-level system (e.g., a spin 1/2 ensemble in a magnetic field), it is not difficult to obtain, using the above discussion, the Einstein relations between spontaneous and stimulated emission, together with Planck's radiation law. From the Bloch equations [see Sect. 8.5.1 and equation (8.113)], we can determine the transverse susceptibility of the spins χ_{xx} , where $\hat{\mathbf{x}}$ is the coil axis,

$$\begin{aligned} \tilde{\chi}'_{xx} + i\tilde{\chi}''_{xx} &= \frac{\langle S_z \rangle}{2} \left[\frac{1}{(\omega - \Omega_L) + i/T_2} + \frac{1}{(\omega + \Omega_L) + i/T_2} \right] \\ &= \frac{\langle S_z \rangle}{2} \left[\frac{(\Omega_L - \omega)T_2^2}{1 + (\omega - \Omega_L)^2 T_2^2} + i \frac{T_2}{1 + (\omega - \Omega_L)^2 T_2^2} \right] \\ &\quad + (\Omega_L \leftrightarrow -\Omega_L) , \end{aligned} \quad (8.57)$$

where $\langle S_z \rangle = (\hbar/2) \tanh(\beta\hbar\Omega_L/2)$ is the average spin value at equilibrium. Combining this with the fluctuation-dissipation theorem, we deduce that the spin-spin correlation function is

$$C_{xx}(\omega) \approx \frac{\hbar^2}{4} \frac{T_2}{1 + (\omega - \Omega_L)^2 T_2^2}, \quad (8.58)$$

since $C_{xx}(\omega) \neq 0$ only if $\omega \approx \Omega_L$. The part of the electromagnetic power radiated by spins which is absorbed by the resistance $\mathcal{R}_{\text{coil}}$ of the coil is

$$\begin{aligned} \mathcal{P}_{\text{exch}}(\omega) &= \frac{\mathcal{E}^2}{\mathcal{R}_{\text{coil}}} = \frac{\omega^2 |\Phi(\omega)|^2}{\mathcal{R}_{\text{coil}}} \\ &\approx \eta \frac{L\Omega_L^2}{\mathcal{R}_{\text{coil}}} \frac{N\gamma^2\hbar^2}{4} \frac{T_2}{1 + (\omega - \Omega_L)^2 T_2^2}, \end{aligned} \quad (8.59)$$

where we have used the definition (8.56) of the filling factor to parametrise the induced flux (8.48). Integrating over all frequencies, we obtain the total absorbed power,

$$\mathcal{P}_{\text{exch}} = \frac{1}{\pi} \int_0^\infty \mathcal{P}_{\text{exch}}(\omega) d\omega = \eta \frac{L\Omega_L^2}{\mathcal{R}_{\text{coil}}} \frac{N\gamma^2\hbar^2}{4}. \quad (8.60)$$

(Note that we need only integrate over positive frequencies, since $\chi''(\omega)$ is symmetric, and this amounts to multiplying the Fourier integral by a factor of 2.) The power absorbed by the coil is temperature independent. There can be no energy transfer between sample and coil unless the latter is at a temperature T_{coil} which differs from the sample temperature T . Indeed, its resistance generates current noise, given by the Nyquist formula

$$|I(\omega)|^2 = \frac{2\hbar\omega}{\mathcal{R}_{\text{coil}}} \coth\left(\frac{\hbar\omega}{2k_B T_{\text{coil}}}\right). \quad (8.61)$$

The power absorbed by the sample is determined by (8.53), susceptibility (8.58), and filling factor (8.56),

$$\mathcal{P}_{\text{coil}}(\omega) = \frac{\eta L}{\mathcal{R}_{\text{coil}}} \frac{\gamma^2\hbar\Omega_L^2}{2} \coth\left(\frac{\hbar\Omega_L}{2k_B T_{\text{coil}}}\right) \frac{N\langle S_z \rangle T_2}{1 + (\omega - \Omega_L)^2 T_2^2}, \quad (8.62)$$

since χ'' has a resonance at $\omega \approx \Omega_L$. Moreover, the magnetisation

$$N\langle S_z \rangle = \frac{\hbar}{2}(N_\uparrow - N_\downarrow) \quad (8.63)$$

is proportional to the population difference between the two levels. After integrating over all frequencies, the power radiated by the coil which is absorbed in the sample is

$$\mathcal{P}_{\text{coil}} = \frac{\eta L}{\mathcal{R}_{\text{coil}}} \frac{\gamma^2\hbar\Omega_L^2}{4} \coth\left(\frac{\hbar\Omega_L}{2k_B T_{\text{coil}}}\right) (N_\uparrow - N_\downarrow). \quad (8.64)$$

We can now parametrise the energy flux between sample and coil by the coefficient of spontaneous emission $A = \eta\hbar\gamma^2 L\Omega_L/\mathcal{R}_{\text{coil}} = \eta\hbar\gamma^2 Q$, where Q is the quality factor of the coil:

$$\begin{aligned}\mathcal{P}_{\text{exch}} - \mathcal{P}_{\text{coil}} &= \frac{A\hbar\Omega_L}{2} \left[N - (N_\uparrow - N_\downarrow) \coth \left(\frac{\hbar\Omega_L}{2k_B T_{\text{coil}}} \right) \right] \\ &= A\hbar\Omega_L \left[N_\downarrow - \frac{N_\uparrow - N_\downarrow}{\exp(\hbar\Omega_L/k_B T_{\text{coil}}) - 1} \right].\end{aligned}\quad (8.65)$$

We recognise here Einstein's equations describing energy exchange between the electromagnetic field and the 2-level system. We see that energy transfer is zero when $T = T_{\text{coil}}$. We also find the Planck radiation law, since the resonant electromagnetic mode of the coil has occupation

$$\langle n \rangle = [\exp(\hbar\Omega_L/k_B T_{\text{coil}}) - 1]^{-1}$$

at equilibrium. Conversely, we can view Planck's law as a consequence of the relation between Einstein coefficients A (representing spontaneous emission) and B (associated with stimulated emission). This relation is nothing other than the fluctuation-dissipation theorem in another guise. We have therefore shown that the physical origin of the theorem lies in the principle of detailed balance (8.12), which allowed us to relate the Einstein coefficients A and B .

When electromagnetic wavelengths are short compared with all characteristic lengths, the Planck radiation law can also be demonstrated from the fluctuation-dissipation theorem (a partial treatment of this problem is given in Sommerfeld's book [199]).

8.3 Difference Between Isothermal and Adiabatic Susceptibilities

It might be thought that adiabatic susceptibility tends to isothermal susceptibility as the frequency tends to 0. The following example shows that this is not true. Let us assume that S_z is a conserved quantity, so that $[\mathcal{H}_0, S_z] = 0$. From the definition (8.32), we deduce that

$$[\mathcal{H}_0, S_z] = 0 \Rightarrow \tilde{\chi}(\omega) \equiv 0. \quad (8.66)$$

But the isothermal susceptibility (the Curie susceptibility, for paramagnetic spins) is not zero. If the system is in equilibrium with a thermostat, this should not perturb the system's response in any significant way. However, the return to equilibrium remains fundamentally different in each case. Correlation functions must necessarily tend to zero at infinite times ($\lim_{t \rightarrow \infty} \langle \delta S^\mu(t) \delta S^\nu(0) \rangle \rightarrow 0$), if the system is in thermodynamic equilibrium with the thermostat. This is not necessarily the case if the system is isolated, because energy is conserved. Indeed, even if S_z is not a constant of motion, its fluctuations are generally coupled to the energy (through the Zeeman term); and since the energy cannot evolve in an isolated system, correlation functions do not tend to zero, as illustrated in Fig. 8.1. Let us relate this difference between isothermal and adiabatic susceptibilities to the infinite time limits of the correlation functions, defined by

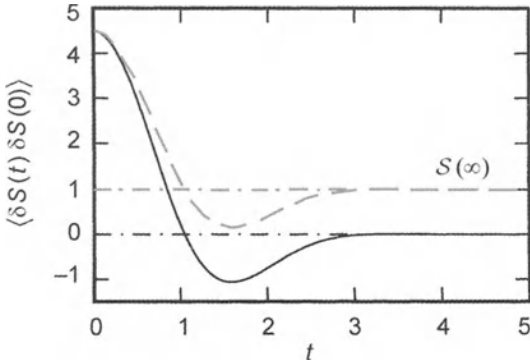


Fig. 8.1. Time dependence of correlation functions. *Continuous curve*: system in contact with thermostat. *Dashed curve*: isolated system. The difference between isothermal and adiabatic susceptibilities is given by $\mathcal{S}(\infty)$

$$\lim_{\tau \rightarrow \pm\infty} \mathcal{S}^{\mu\nu}(\tau) = \langle \delta S^\mu(\tau) \delta S^\nu(0) \rangle = \mathcal{S}^{\mu\nu}. \quad (8.67)$$

If S^μ is not a conserved quantity, correlation functions often decouple,

$$\lim_{\tau \rightarrow \pm\infty} \langle S^\mu(\tau) S^\nu(0) \rangle = \langle S^\mu \rangle \langle S^\nu \rangle, \quad (8.68)$$

which implies that $\mathcal{S}^{\mu\nu} = 0$. This can never happen for conserved quantities. For example, $C_{zz}(t) \equiv (\hbar/2)^2$ for an ensemble of independent spin 1/2 entities. On the other hand, $\langle S_z \rangle = (\hbar/2) \tanh(\beta\mu H)$ and consequently, $C_{zz} \neq \langle S_z \rangle^2$.

The isothermal response (8.22) is an integral over imaginary times of the correlation function $\mathcal{S}(\tau)$. By analytic continuation, the integral becomes in Fourier space,

$$\begin{aligned} \chi_T^{\mu\nu} &= \int_0^\beta d\lambda S^{\mu\nu}(-i\hbar\lambda) \\ &= \int_0^\beta d\lambda \frac{1}{2\pi} \int_{-\infty}^\infty d\omega S^{\mu\nu}(\omega) \exp(-\lambda\hbar\omega) \\ &= \frac{1}{2\pi} \int_{-\infty}^\infty d\omega S^{\mu\nu}(\omega) \frac{1 - \exp(-\beta\hbar\omega)}{\hbar\omega}. \end{aligned} \quad (8.69)$$

The correlation functions at zero frequency cannot be obtained by dividing (8.39) by $[1 - \exp(-\beta\hbar\omega)]$, because $\mathcal{S}(\omega)$ has a singularity as $\omega \rightarrow 0$. Correlation functions

$$\tilde{\mathcal{S}}^{\mu\nu}(\tau) = \mathcal{S}^{\mu\nu}(\tau) - \mathcal{S}^{\mu\nu} \quad (8.70)$$

have a regular Fourier transform when $\omega \rightarrow 0$, since they tend to 0 when $\tau \rightarrow \pm\infty$. We deduce that

$$\mathcal{S}^{\mu\nu}(\omega) = 2\pi \mathcal{S}^{\mu\nu} \delta(\omega) + \tilde{\mathcal{S}}^{\mu\nu}(\omega). \quad (8.71)$$

Since $\tilde{\mathcal{S}}(\omega)$ is a regular function, the fluctuation-dissipation theorem (8.39) implies

$$\tilde{\mathcal{S}}^{\mu\nu}(\omega) = 2\hbar\mathcal{P} \left[\frac{\tilde{\chi}_{\mu\nu}''(\omega)}{1 - \exp(-\beta\hbar\omega)} \right], \quad (8.72)$$

where \mathcal{P} is the principal part of the function. Substituting (8.71) and (8.72) into (8.58), we obtain a relation between isothermal and adiabatic susceptibilities, viz.,

$$\chi_T^{\mu\nu} = \beta\mathcal{S}^{\mu\nu} + \frac{1}{\pi}\mathcal{P} \int_{-\infty}^{\infty} d\omega \frac{\tilde{\chi}_{\mu\nu}''(\omega)}{\omega}. \quad (8.73)$$

The Kramers–Kronig relations (8.84) then imply

$$\chi_T^{\mu\nu} = \beta\mathcal{S}^{\mu\nu} + \tilde{\chi}'_{\mu\nu}(0) - \tilde{\chi}'_{\mu\nu}(\infty). \quad (8.74)$$

This explicitly relates isothermal and adiabatic susceptibilities [200]. For an ensemble of paramagnetic spins, the first term

$$\beta\mathcal{S}^{\mu\nu} = \beta \left(\frac{\hbar}{2} \right)^2 [1 - \tanh^2(\beta\mu H)] = \beta \left(\frac{\hbar}{2} \right)^2 \frac{1}{\cosh^2(\beta\mu H)} \quad (8.75)$$

does indeed give the Curie susceptibility. It is therefore essential!

8.4 Properties of Response Functions

8.4.1 Kubo Formulas

The Kubo formulas give formal representations of response functions which often prove useful. We can eliminate the commutator in definitions (8.32) using the identity

$$\int_0^\beta d\lambda \frac{d}{d\lambda} \exp(\lambda\mathcal{H}_0) S^\nu \exp(-\lambda\mathcal{H}_0) = \exp(\beta\mathcal{H}_0) S^\nu \exp(-\beta\mathcal{H}_0) - S^\nu.$$

We find that

$$\begin{aligned} \tilde{\chi}^{\mu\nu} &= \frac{i}{Z_0\hbar} \text{Tr} [\exp(-\beta\mathcal{H}_0) S^\mu(t) S^\nu - \exp(-\beta\mathcal{H}_0) S^\nu S^\mu(t)] \\ &= \frac{i}{Z_0\hbar} \int_0^\beta d\lambda \text{Tr} \left[\exp(-\beta\mathcal{H}_0) \frac{d}{d\lambda} \exp(\lambda\mathcal{H}_0) S^\nu \exp(-\lambda\mathcal{H}_0) S^\mu(t) \right]. \end{aligned} \quad (8.76)$$

This can be condensed into the simple formula

$$\begin{aligned} \tilde{\chi}^{\mu\nu}(\omega) &= \int_0^\infty dt \int_0^\beta d\lambda \langle \dot{S}^\nu(-i\hbar\lambda) S^\mu(t) \rangle \exp(i\omega - \eta)t \\ &= - \int_0^\infty dt \int_0^\beta d\lambda \langle \dot{S}^\mu(t - i\hbar\lambda) S^\nu \rangle \exp(i\omega - \eta)t, \end{aligned} \quad (8.77)$$

due to Kubo. In the above formulas, the derivative is defined formally by

$$\dot{S}^\mu(-i\hbar\lambda) = -i\hbar \frac{d}{d\lambda} S^\mu(-i\hbar\lambda).$$

The change of sign associated with permutation of S^μ and S^ν reflects the presence of the commutator in (8.32). The Fourier transform can be calculated explicitly by introducing a complete set of states between the two spin operators:

$$\tilde{\chi}^{\mu\nu}(\omega) = \sum_{i,j} [p(\varepsilon_j) - p(\varepsilon_i)] \frac{\langle i|S^\nu|j\rangle \langle j|S^\mu|i\rangle}{(\varepsilon_j - \varepsilon_i - \hbar\omega) + i\eta}, \quad (8.78)$$

where $p(\varepsilon) = \exp(-\beta\varepsilon)/Z_0$ is the occupation probability of the state under consideration. This is the magnetic analogue of the Kubo formula for electrical conductivity.

Conductivity is the current response to the potential exciting electrical charge. The derivative in (8.77) then allows us to transform charge-current correlations into current-current correlations. This is what leads to the differences between (8.78) and the usual Kubo formula.

Decomposing the denominators of (8.78) into principal parts, we obtain the absorption

$$\tilde{\chi}_{\mu\nu}''(\omega) = \pi \sum_{i,j} [p(\varepsilon_i) - p(\varepsilon_j)] \langle i|S^\nu|j\rangle \langle j|S^\mu|i\rangle \delta(\varepsilon_j - \varepsilon_i - \hbar\omega), \quad (8.79)$$

which can also be obtained more directly using the Fermi golden rule. We shall describe an application of Kubo's formula to the study of electron-spin resonances in Sect. 8.5.

8.4.2 Kramers–Kronig Relations

Because response functions are causal, we can define the Fourier transform (8.32) as an integral over positive times. We can then analytically continue the response functions (8.32) in the upper complex plane $\text{Im}(\omega) > 0$, since the exponential factor in the Fourier transform guarantees convergence of the integral. The response functions nevertheless have non-zero limits as $\omega \rightarrow \infty$. With regard to magnetic susceptibility, it is the real part $\tilde{\chi}'(\omega)$ which tends to a non-zero value $\tilde{\chi}'(\infty)$. The imaginary part tends to zero; beyond all relaxation frequencies of the system, there can be no more absorption. Before applying the Kramers–Kronig relations to a system, we must carefully study its analyticity properties and in particular its asymptotic behaviour. Response functions must decrease faster than $1/|\omega|$ when $\omega \rightarrow \pm\infty$. To simplify, we shall only consider magnetic systems for which $\chi(z = \omega + i\eta) - \chi'(\infty)$ tends to zero when $\omega \rightarrow \pm\infty$. This function also has poles in the complex plane, corresponding to physical resonances (the collective modes). Since such resonances are damped, poles of $\chi(z)$ must lie in the lower complex plane.

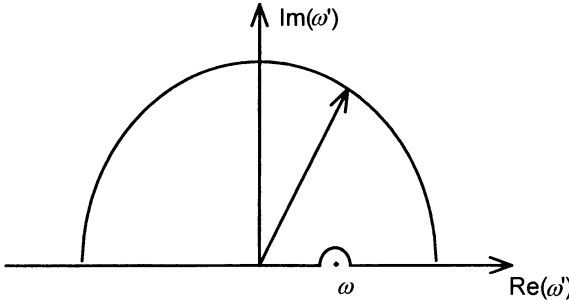


Fig. 8.2. Integration contour C in the upper complex plane. The integral over the semi-circle tends to zero ($\eta > 0$), when the radius tends to infinity

Consequently, Cauchy's theorem applied to the contour C shown in Fig. 8.2 must give zero,

$$\oint_C dz \frac{\tilde{\chi}(z) - \tilde{\chi}'(\infty)}{z - \omega} = 0 , \quad (8.80)$$

since we avoid the pole $z = \omega$. The integration reduces to one along the real axis since the response function is exponentially small along the semi-circle of radius $R \rightarrow \infty$. Using the decomposition into principal parts of

$$\frac{1}{\omega' - \omega + i\eta} = \mathcal{P} \frac{1}{\omega' - \omega} - i\pi\delta(\omega' - \omega) , \quad (8.81)$$

and separating real and imaginary parts of the integral, we obtain

$$\tilde{\chi}'(\omega) - \tilde{\chi}'(\infty) = \frac{1}{\pi} \mathcal{P} \int_{-\infty}^{\infty} \frac{\tilde{\chi}''(\omega')}{\omega' - \omega} d\omega' , \quad (8.82)$$

$$\tilde{\chi}''(\omega) = -\frac{1}{\pi} \mathcal{P} \int_{-\infty}^{\infty} \frac{\tilde{\chi}'(\omega') - \tilde{\chi}'(\infty)}{\omega' - \omega} d\omega' . \quad (8.83)$$

These are known as the Kramer–Kronig relations and they are useful for two reasons. Firstly, we can determine the dispersive part of the susceptibility $\tilde{\chi}'(\omega)$ from absorption measurements [governed by $\tilde{\chi}''(\omega)$], over a sufficiently wide frequency range (or vice versa). Secondly, if $\tilde{\chi}'(\omega)$ and $\tilde{\chi}''(\omega)$ can only be measured over a limited frequency range, we can find out whether there is significant absorption at experimentally inaccessible frequencies. Indeed, transformation (8.82) of $\tilde{\chi}''(\omega)$ over part of the spectrum would not correctly reproduce measurements of $\tilde{\chi}'(\omega)$ if part of the ‘spectral weighting’ were ignored. When $\omega \rightarrow \infty$, (8.82) gives the sum rule

$$\tilde{\chi}'(0) - \tilde{\chi}'(\infty) = \int_{-\infty}^{\infty} \frac{\tilde{\chi}''(\omega')}{\omega'} d\omega' , \quad (8.84)$$

which we have already used in (8.74) to relate isothermal and adiabatic susceptibility. In 2-level systems, $\chi''(\omega)$ only differs from zero in the neighbourhood of $\omega \approx \omega_0$. In this case,

$$\tilde{\chi}'(0) - \tilde{\chi}'(\infty) = \frac{2}{\omega_0} \int_0^\infty \tilde{\chi}''(\omega') d\omega' . \quad (8.85)$$

Static susceptibility is proportional to the area under the absorption curve, a result which is widely used in Nuclear Magnetic Resonance (NMR). In practice, the Kramers–Kronig relations are modified so as to eliminate the divergence of the integral at $\omega = \omega'$. The definition of the principal part requires

$$\mathcal{P} \int_{-\infty}^\infty \frac{d\omega'}{\omega' - \omega} = 0 . \quad (8.86)$$

This identity can be multiplied by $\tilde{\chi}''(\omega)$ and subtracted from (8.82). Making use of frequency symmetry relations (8.36), we obtain

$$\tilde{\chi}'(\omega) - \tilde{\chi}'(\infty) = \frac{2}{\pi} \int_0^\infty \frac{\omega' \tilde{\chi}''(\omega') - \omega \tilde{\chi}''(\omega)}{\omega'^2 - \omega^2} d\omega' , \quad (8.87)$$

$$\tilde{\chi}''(\omega) = \frac{2}{\pi} \int_0^\infty \frac{\omega \tilde{\chi}'(\omega') - \omega' \tilde{\chi}'(\omega)}{\omega'^2 - \omega^2} d\omega' . \quad (8.88)$$

In this form, the Kramers–Kronig relations no longer have singularities at $\omega \approx \omega'$ and are ideal for numerical simulations. In addition, $\tilde{\chi}'(\infty)$ no longer enters into determination of $\tilde{\chi}''(\omega)$. Finally, we note that the Kramers–Kronig relations cannot be applied to electrical conductivity, which does not converge rapidly enough as $\omega \rightarrow \pm\infty$. We can, however, relate it to the dielectric constant using the last Maxwell equation,

$$\tilde{\varepsilon}''(\omega) = \frac{\sigma'(\omega) - \sigma'(0)}{\omega} , \quad \tilde{\varepsilon}'(\omega) = \frac{\sigma''(\omega)}{\omega} , \quad (8.89)$$

and then apply the Kramers–Kronig relations; the dielectric constant has the same analyticity properties as the susceptibility.

8.4.3 Time Reversal Symmetries

Excitations other than Zeeman perturbations can be represented in the form

$$V = -Eh(t) , \quad (8.90)$$

where E is the operator representing the physical quantity which couples to ‘force’ h . Time reversal symmetry amounts to exchanging initial and final states and reversing the magnetic field ($H \rightarrow -H$). Hence,

$$\langle i|E|j\rangle = \langle i|E^\dagger|j\rangle = \langle j|E|i\rangle^* = \eta_E \langle j|E|i\rangle , \quad (8.91)$$

where η_E represents the symmetry of operator E with respect to time reversal. Momentum, current, angular momentum and spin are all odd operators. Density and energy are even operators. From these relations, introducing a complete set of states, we obtain the symmetries of the correlation functions with respect to time reversal:

$$\begin{aligned} C_{RE}(\tau, H) &= \langle R(\tau)E \rangle_H = \eta_R \eta_E \langle ER(-\tau) \rangle_{-H} \\ &= \eta_R \eta_E \langle E(\tau)R \rangle_{-H} = C_{ER}(\tau, -H). \end{aligned} \quad (8.92)$$

Definitions (8.32) and (8.35), giving response functions in terms of correlation functions, thus lead to the Onsager reciprocity relations

$$\tilde{\chi}_{RE}(\omega) = \eta_E \eta_R \tilde{\chi}_{ER}(\omega). \quad (8.93)$$

Usually, we consider response functions such that $\eta_E = \eta_R$, in which case the susceptibility tensor is symmetric. Antisymmetric response functions (e.g., magnetisation density) are such that $\eta_E = -\eta_R$. The above relation then implies that they go to zero in the static limit. The Onsager reciprocity relations have many applications, notably concerning thermoelectric and thermomagnetic effects [201], and multiterminal transport measurements [202, 203].

8.4.4 Non-Linear Response

The perturbation expansion (8.27) of states $|\psi_{\text{int}}(t)\rangle$ expressed in the interaction basis can be continued to higher orders. We can thereby formulate a theory of non-linear response. Higher order response functions can be defined [204],

$$\begin{aligned} \langle S^\mu(t) \rangle &= \langle S^\mu \rangle_0 + \\ &\sum_{n=1} \frac{1}{n!} \int \chi^{\mu\nu_1\dots\nu_n}(t, t_1, \dots, t_n) h_{\nu_1}(t_1) \dots h_{\nu_n}(t_n) dt_1 \dots dt_n, \end{aligned} \quad (8.94)$$

where non-linear susceptibilities depend only on time intervals $\tau = t - t_1$, $\tau_{n-1} = t_{n-1} - t_n$,

$$\chi(\tau, \tau_1, \dots, \tau_{n-1}) = \left(\frac{i}{n} \right)^n \theta(\tau) \theta(\tau_1) \dots \theta(\tau_{n-1}) \quad (8.95)$$

$$\langle [\dots [S^\mu(\tau + \dots + \tau_{n-1}), S^{\nu_1}(\tau_1 + \dots + \tau_{n-1})], \dots, S^{\nu_n}] \rangle$$

and are causal functions of all applied fields $h_{\nu_1}, \dots, h_{\nu_n}$. It is straightforward to generalise the time reversal symmetries of the response functions. However, the fluctuation-dissipation theorem can only be generalised at the second order. The reason for this is as follows: knowing the response functions for $\tau, \tau_1, \dots, \tau_{n-1}$ all positive, we cannot reconstitute the correlation functions in regions where some times are positive and some are negative. To second order, the procedure can still be applied because of time reversal symmetries. In this case, the generalisation of relation (8.42) for symmetrised correlation functions is [205, 206]

$$\begin{aligned} C_S^{\mu\nu_1\nu_2} &= 2\text{Re} \{ E(\omega, \omega_1) \chi^{\mu\nu_1\nu_2}(\omega, \omega_1) \\ &\quad + E(-\omega_1, \omega - \omega_1) \chi(-\omega_1, \omega - \omega_1) \\ &\quad + E(\omega_1 - \omega, -\omega) \chi^{\mu\nu_1\nu_2}(\omega_1 - \omega, -\omega) \} , \end{aligned} \quad (8.96)$$

where the spectral function $E(\omega, \omega_1)$ is defined by

$$E(\omega, \omega_1) = -\hbar^2 \left[\frac{1 + e^{\beta\hbar\omega} + (e^{\beta\hbar(\omega-\omega_1)} + e^{\beta\hbar\omega_1})/2}{3(1 - e^{\beta\hbar(\omega-\omega_1)})(1 - e^{\beta\hbar\omega_1})} \right]. \quad (8.97)$$

The relation between adiabatic and isothermal susceptibilities involves further difficulties, analysed in the references cited here.

8.5 Applications to Resonance Phenomena

8.5.1 Bloch Equations

Many works have been devoted to nuclear magnetic resonance [207, 208, 209, 210] and electron-spin resonance [211, 212]. We shall therefore restrict discussion to the main points. Two experimental methods are used in resonance spectroscopy: continuous methods to which the linear response theory can be applied as it stands, and pulsed methods which require certain generalisations. In the latter case, an intense pulse of radiofrequency magnetic field flips spins over rather abruptly, and this cannot be described as an adiabatic perturbation. After such a rotation, spins nevertheless remain in thermodynamic equilibrium amongst themselves, since this state is obtained by a uniform rotation of an equilibrium state. In the laboratory frame, the expected value of the total spin precesses rapidly around the applied magnetic field. However, we can place ourselves in a frame precessing with the Larmor frequency about the applied magnetic field. The expected value of the spin then evolves much more slowly and we often find that, in this frame, spins remain in thermodynamic equilibrium locally. We can then introduce the idea of spin temperature. The system returns towards the state of global thermodynamic equilibrium as a result of interactions such as the dipolar interaction and anisotropic exchange interactions, which do not conserve total spin. These interactions are denoted \mathcal{H}_I . The state of global equilibrium is described by the density matrix

$$\rho_0 = \frac{1}{Z_0} \exp(-\beta\mathcal{K}_0) \quad \text{where} \quad \mathcal{K}_0 = \mathcal{H}_0 + \mathcal{H}_I + \mathcal{H}_Z. \quad (8.98)$$

\mathcal{H}_0 is the lattice Hamiltonian, $\mathcal{H}_Z = -\mathbf{S} \cdot \mathbf{h}_0$ is the Zeeman Hamiltonian in a uniform field $\mathbf{h}_0 = h_0 \hat{\mathbf{z}}$ (expressed in reduced units), and \mathbf{S} the total spin. A local spin equilibrium can be described by generalising this density matrix to

$$\rho(t) = \frac{1}{Z(t)} \exp[-\beta_L(t)\mathcal{H}_0 - \beta(t)\mathcal{H}_I + \beta_Z(t)\mathbf{S}(t) \cdot \mathbf{h}(t)], \quad (8.99)$$

parametrised by three temperatures $\beta_L(t) = 1/k_B T_L$, $\beta_Z(t) = 1/k_B T_Z$ and $\beta(t) = 1/k_B T$, which have slowly varying time dependence. $\mathbf{h}(t)$ is a fictitious thermodynamic field such that $\langle \mathbf{S} \rangle(t) = -\partial \ln(Z)/\partial \mathbf{h}(t)$ is the expected value

of the spin observed at time t . In other words, deviations of the fictitious field from \mathbf{h}_0 are related to deviations in the expected value of the spin at equilibrium by the *isothermal* susceptibility tensor,

$$\mathbf{h}(t) - \mathbf{h}_0 = (\chi_T)^{-1} \delta \langle \mathbf{S}(t) \rangle . \quad (8.100)$$

If $\langle \mathbf{S} \rangle(t)$ evolves slowly compared with the time required to establish local equilibrium, there is always a density matrix (8.99) in which parameters β_Z and β relax slowly towards the lattice temperature β_L , and \mathbf{h} relaxes towards \mathbf{h}_0 . The distinction between temperatures β_I , β_Z and β is only significant when specific heats associated with the various contributions to \mathcal{K}_0 (i.e., \mathcal{H}_0 , \mathcal{H}_Z and \mathcal{H}_I) are very different, and provided that energy exchange processes between the various reservoirs are slow. For nuclear spins, energy scales $\langle \mathcal{H}_0 \rangle \gg \langle \mathcal{H}_Z \rangle \gg \langle \mathcal{H}_I \rangle$ are well separated and we can indeed speak of distinct thermodynamic reservoirs. In the case of electron spins, \mathcal{H}_Z and \mathcal{H}_I are often comparable and there is no need to distinguish between β and β_Z , except possibly in very intense fields. To simplify the discussion, we shall assume that $\beta = \beta_Z = \beta_L$, but that $\mathbf{h} \neq \mathbf{h}_0$, so that we can treat situations in which the local equilibrium differs from global equilibrium. The Larmor precession of $\langle \mathbf{S} \rangle$ is obtained by keeping only the Zeeman Hamiltonian in the equation of motion of the density matrix,

$$i\hbar \frac{d\rho}{dt} = -[\rho(t), \mathcal{H}] = [\rho(t), \mathbf{S}] \cdot \mathbf{h}_0 . \quad (8.101)$$

Multiplying by S^μ and taking the trace, we deduce equations of motion for the expected value $\langle \mathbf{S} \rangle = \text{Tr}[\rho(t)\mathbf{S}]$,

$$\begin{aligned} \frac{d\langle S^\mu(t) \rangle}{dt} &= -\frac{i}{\hbar} \sum_\nu \text{Tr} \{ S^\mu [\rho(t), S^\nu] h_0^\nu \} \\ &= \frac{i}{\hbar} \sum_\nu h_0^\nu \text{Tr} \{ \rho(t) [S^\mu, S^\nu] \} \\ &= \langle \mathbf{S} \rangle \times \mathbf{h}_0|_\mu . \end{aligned} \quad (8.102)$$

The longitudinal component $\langle S^z \rangle$ is constant and transverse components of spin $S^\pm = S^x \pm iS^y$ carry out uniform circular motion,

$$\frac{d\langle S^\pm(t) \rangle}{dt} = \mp i\Omega_L \langle S^\pm(t) \rangle , \quad (8.103)$$

at the Larmor frequency $\Omega_L \equiv |\mathbf{h}_0|$. This motion is a uniform precession about \mathbf{h}_0 . Viewing from a frame rotating at the Larmor frequency amounts to changing to the interaction basis defined in (8.25). Indeed, the operator generating a rotation through $\theta = \Omega_L t$ about $\hat{\mathbf{z}}$ (see Appendix A)

$$\Gamma(\Omega_L t, \hat{\mathbf{z}}) = \exp \left(-i \frac{S_z}{\hbar} \Omega_L t \right) \quad (8.104)$$

is just the evolution operator of the Zeeman Hamiltonian in a field $-\mathbf{h}_0$. In this basis, the equation of motion of the density matrix is

$$-i\hbar \frac{d\rho_t}{dt} = -[\rho_t(t), \mathcal{H}_t] = -[\rho_t(t), \mathcal{H} + \mathbf{S} \cdot \mathbf{h}_0]. \quad (8.105)$$

When we keep only the Zeeman Hamiltonian, $\mathcal{H} = \mathcal{H}_Z$, the density matrix and all expectation values are stationary in this frame. Relaxation therefore comes from \mathcal{H}_I , which does not conserve total spin. The equations of motion reduce to

$$\frac{d\langle S^\mu(t) \rangle_t}{dt} = \frac{i}{\hbar} \text{Tr} \{ [\rho_t(t), \mathcal{H}_I] S^\mu \} = \frac{i}{\hbar} \text{Tr} \{ \rho_t(t) [\mathcal{H}_I, S^\mu] \}. \quad (8.106)$$

We assume that the density matrix is in local equilibrium [see (8.99)] in the rotating frame. This assumption will be justified later. By analogy with (3.22), we express deviations of the density matrix $\rho(t)$ from global equilibrium $\rho_0 = \exp(-\beta\mathcal{K}_0)/Z$,

$$\begin{aligned} \rho(t) - \rho_0 &= \frac{1}{Z} \mathbf{h}(t) \cdot \int_0^\beta d\lambda \exp(-\lambda\mathcal{K}_0) \mathbf{S}(t) \exp(\lambda\mathcal{K}_0) \\ &\approx \beta \mathbf{h}(t) \cdot \mathbf{S}(t) \quad \text{when } \beta h \ll 1. \end{aligned} \quad (8.107)$$

We also expand $\mathbf{S}(t)$ to first order in perturbation theory:

$$\mathbf{S}(t) = \mathbf{S} + \frac{i}{\hbar} \int_0^t d\tau [\mathcal{H}_I(\tau), \mathbf{S}(\tau)]. \quad (8.108)$$

Substituting (8.108) into (8.107) and (8.106), we obtain equations of motion in the rotating frame to second order in \mathcal{H}_I ,

$$\frac{d\langle S^\mu(t) \rangle_t}{dt} = \sum_\nu [G_0^{\mu\nu} + G_1^{\mu\nu}(t)] (\chi^{-1})_{\nu\eta} \langle S^\eta(t) \rangle_t, \quad (8.109)$$

where G_0 and G_1 are, in the high temperature limit,

$$G_0^{\mu\nu} = \frac{i\beta}{\hbar Z_0} \text{Tr} \{ S^\nu [\mathcal{H}_I, S^\mu] \} = \frac{i\beta}{\hbar Z_0} \text{Tr} \{ \mathcal{H}_I [S^\mu, S^\nu] \}, \quad (8.110)$$

$$G_1^{\mu\nu}(t) = -\frac{\beta}{\hbar^2} \int_0^t d\tau \langle [\mathcal{H}_I(\tau), S^\nu(\tau)] [S^\mu, \mathcal{H}_I] \rangle. \quad (8.111)$$

G_0 is almost always zero, if the system is invariant under rotation (this excludes polarised systems). With regard to G_1 , its integrand decreases in a time τ_c which is very short compared with other characteristic times, because spin is not conserved by the Hamiltonian \mathcal{H}_I . This means that *local* equilibrium is attained very quickly. For times $t > \tau_c$, G_1 is time independent and the density matrix $\rho(t)$ corresponds to a local equilibrium of the system in the rotating frame, thereby justifying the assumption made earlier. It may happen that spins are strongly coupled to long wavelength hydrodynamic modes which relax slowly towards equilibrium. The time dependence of $G(t)$ is then relevant and affects spin dynamics. This is the case for ferromagnets, in which there are long range dipolar interactions, giving rise to ‘magnetostatic’ modes. These will be studied in the next chapter. In such a situation, the hypotheses required to deduce Bloch’s equations cannot be justified. When

the susceptibility is isotropic, or when deviations of $\langle \mathbf{S} \rangle$ at equilibrium are small, the equations of motion (8.109) become, in the laboratory frame,

$$\frac{d\langle S^z(t) \rangle}{dt} = -\frac{1}{T_1} [\langle S^z(t) \rangle - \langle S_{\text{eq}}^z \rangle] , \quad (8.112)$$

$$\frac{d\langle S^\pm(t) \rangle}{dt} = \mp i(\Omega_L + \delta\Omega) \langle S^\pm(t) \rangle - \frac{1}{T_2} \langle S^\pm(t) \rangle . \quad (8.113)$$

These are Bloch's equations. The parameter $\delta\Omega_L$ shifts the resonance line and is called the *Knight shift* in nuclear magnetic resonance. The parameter T_1 measures the relaxation time of longitudinal magnetisation towards equilibrium and T_2 the same for transverse magnetisation. T_2 is usually much shorter than T_1 , since energy conserving processes can contribute to T_2 but not to T_1 . The above analysis leads to explicit determination of these parameters in terms of \mathcal{H}_I :

$$\begin{aligned} \delta\Omega &= \frac{\beta}{\hbar\chi} \langle S^- [S^+, \mathcal{H}_I] \rangle \\ &\quad + \frac{\beta}{\hbar^2\chi} \text{Im} \left\{ \int_0^\infty d\tau \langle [\mathcal{H}_I(\tau), S^-(\tau)] [S^+, \mathcal{H}_I] \rangle \exp(i\Omega_L\tau) \right\} , \end{aligned} \quad (8.114)$$

$$\frac{1}{T_1} = \frac{\beta}{\hbar^2\chi} \int_0^\infty d\tau \langle [\mathcal{H}_I(\tau), S^z(\tau)] [S^z, \mathcal{H}_I] \rangle , \quad (8.115)$$

$$\frac{1}{T_2} = \frac{\beta}{\hbar^2\chi} \text{Re} \left\{ \int_0^\infty d\tau \langle [\mathcal{H}_I(\tau), S^-(\tau)] [S^+, \mathcal{H}_I] \rangle \exp(i\Omega_L\tau) \right\} . \quad (8.116)$$

It is not difficult to generalise these formulas when βh_0 is of order 1, starting from (8.107) [213]. Likewise when the susceptibility tensor is anisotropic, the Bloch equations can be generalised and become non-linear.

Exercise

Determine these non-linear equations, assuming that the susceptibility tensor χ is diagonal in the laboratory frame and that its components are $\chi_{zz} \equiv \chi_\parallel$ and $\chi_{xx} = \chi_{yy} = \chi_\perp$.

We assumed that parameters \mathbf{h}_0 and \mathbf{S}_0 were spatially uniform. When $\langle S^\mu(\mathbf{r}, t) \rangle$ depends on \mathbf{r} , we must take into account the existence of spin currents \mathbf{J}^μ which tend to bring the system back towards a spatially uniform state. The Bloch equations are modified, replacing $d\langle S^\mu \rangle/dt$ by $\partial\langle S^\mu \rangle/\partial t + \nabla \cdot \mathbf{J}^\mu$. For each physical system, constitutive equations exist, relating spin currents to magnetisation gradients, temperature gradients and gradients of other 'hydrodynamic' variables. In the simplest systems, $\mathbf{J}_\mu = -D\nabla S_\mu$, introducing a dissipative diffusion term into the Bloch equations. When the system has broken symmetries, this analysis is no longer valid, as we shall see in the next chapter.

8.5.2 Relaxation Between Electron and Nuclear Spins

As an example, let us determine the relaxation times T_1 and T_2 for nuclear spins coupled to electron spins via a contact hyperfine interaction at each site in the lattice. This interaction

$$\mathcal{H}_I = A \sum_i \mathbf{S}_i \cdot \mathbf{I}_i \quad (8.117)$$

does not conserve all components of the total nuclear spin $\mathbf{I} = \sum_i \mathbf{I}_i$. We shall also assume that transverse fluctuations of electron spins can be described by the correlation function

$$C_{+-}(t) = \langle S^-(t)S^+ \rangle = \langle S_\perp^2 \rangle \exp(-t/\tau), \quad (8.118)$$

where τ is the *electronic* correlation time. Using commutators

$$[\mathcal{H}_I, I_z] = \frac{A\hbar}{2}(I^-S^+ - I^+S^-), \quad (8.119)$$

$$[\mathcal{H}_I, I^\pm] = \pm A\hbar(I^\pm S_z - I_z S^\pm), \quad (8.120)$$

and relations (8.115), (8.116), we can calculate relaxation times T_1 and T_2 explicitly. We introduce a complete set of states between the two commutators appearing in definitions (8.115) and (8.116). For T_1 we find

$$\begin{aligned} \frac{1}{T_1} &= \frac{A^2\beta}{2\chi} \sum_{\alpha\beta} \int_0^\infty d\tau \left\{ \exp(-i\Omega_L\tau) \langle S^+(\tau)S^- \rangle \langle \alpha|I^-|\beta \rangle \langle \beta|I^+|\alpha \rangle \right. \\ &\quad \left. + \exp(i\Omega_L\tau) \langle S^-(\tau)S^+ \rangle \langle \alpha|I^+|\beta \rangle \langle \beta|I^-|\alpha \rangle \right\} \\ &= \frac{A^2\beta\langle S_\perp^2 \rangle}{2\chi} \frac{2I(I+1)(2I+1)}{3} \left(\frac{1}{i\Omega_L + \tau^{-1}} + \frac{1}{-i\Omega_L + \tau^{-1}} \right) \\ &= A^2\langle S_\perp^2 \rangle (2I+1) \frac{\tau}{1 + (\Omega_L\tau)^2}, \end{aligned} \quad (8.121)$$

where we have used $\chi = \beta I(I+1)/3$ for the Curie susceptibility and $\langle I^-I^+ \rangle = 2I(I+1)(2I+1)/3$. Calculations for T_2 and $\delta\Omega_L$ are almost identical, yielding

$$\delta\Omega_L = A(2I+1) \left[\langle S_z \rangle + A\langle S_\perp^2 \rangle \tau \frac{\Omega_L\tau}{1 + (\Omega_L\tau)^2} \right], \quad (8.122)$$

$$\frac{1}{T_2} = A^2(2I+1)\tau \left[\langle S_\parallel^2 \rangle + \langle S_\perp^2 \rangle \frac{1}{1 + (\Omega_L\tau)^2} \right]. \quad (8.123)$$

The electron relaxation time τ varies with temperature and controls the temperature dependence of relaxation rates and the Knight shift. Relaxation is fastest when τ is comparable with the nuclear precession period $2\pi/\Omega_L$. In other words, it is the Fourier components of fluctuations at the Larmor frequency which relax nuclear spins, as shown in Fig. 8.3.

Exercise

Check expressions (8.122) and (8.123) for $1/T_2$ and the Knight shift.

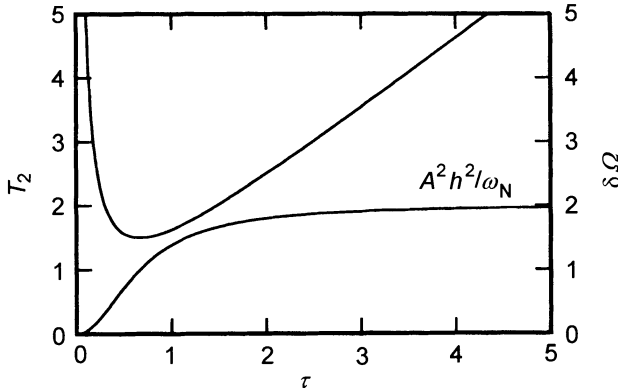


Fig. 8.3. Dependence of $1/T_2$ and Knight shift $\delta\Omega$ on electron relaxation time τ

8.5.3 Dipolar Relaxation

Dipolar interactions do not conserve total spin and are very effective in relaxing electron spins. Let us evaluate the associated relaxation times in the simplest cases. As before, we express the dipolar Hamiltonian (with gyro-magnetic factors normalised to unity) in terms of S^\pm and S^z ,

$$\mathcal{H}_I = \sum_{i \neq j} \left(\frac{1 - 3 \cos^2 \theta_{ij}}{R_{ij}^3} \right) \left[\frac{1}{2} (S_i^+ S_j^- + S_i^- S_j^+) + S_i^z S_j^z \right], \quad (8.124)$$

where $R_{ij} = |\mathbf{R}_{ij}| = |\mathbf{r}_j - \mathbf{r}_i|$ is the distance between spins i and j , and θ_{ij} is the angle between \mathbf{R}_{ij} and the $\hat{\mathbf{z}}$ axis. We then calculate commutators,

$$[S_k^z, \mathcal{H}_I] = \hbar \sum_{i \neq j} \left(\frac{1 - 3 \cos^2 \theta_{ij}}{R_{ij}^3} \right) (S_i^+ S_j^- - S_i^- S_j^+) \delta_{ik}, \quad (8.125)$$

$$[S_k^\pm, \mathcal{H}_I] = \pm 2\hbar \sum_{i \neq j} \left(\frac{1 - 3 \cos^2 \theta_{ij}}{R_{ij}^3} \right) (S_i^z S_j^\pm - S_i^\pm S_j^z) \delta_{ik}. \quad (8.126)$$

These are substituted into definitions (8.115) and (8.116) and a complete set of states introduced between the two commutators in order to carry out the time integral $\int_0^\infty \langle \alpha | [\mathcal{H}_I, S^{z, \pm}(\tau)] | \beta \rangle$. The integral leads to energy denominators of type $1/[i(\varepsilon_\beta - \varepsilon_\alpha) + \hbar/\tau_{sl}]$. Spin levels have width \hbar/τ_{sl} . The relaxation time τ_{sl} may be interpreted as the spin-lattice relaxation time, after which spins remain permanently in thermodynamic equilibrium. τ_{sl} must be brought explicitly into the calculation of $1/T_1$, because the energy difference $\varepsilon_\beta - \varepsilon_\alpha$ is in this case identically zero; the longitudinal relaxation comes in through an energy conserving spin-flip process. Calculation of $1/T_1$ becomes more or less identical to the calculation in the previous section:

$$\begin{aligned}\frac{1}{T_1} &= \frac{2\beta}{\chi} \sum_i \left(\frac{1 - 3\cos^2\theta_{ij}}{R_{ij}^3} \right)^2 \langle S_i^+ S_i^- \rangle \langle S_j^- S_j^+ \rangle \tau_{\text{sl}} \\ &= \frac{8S(S+1)(2S+1)^2}{3} \frac{\tau_{\text{sl}}}{\hbar^2} \mu^4 \sum_i \left(\frac{1 - 3\cos^2\theta_{ij}}{R_{ij}^3} \right)^2,\end{aligned}\quad (8.127)$$

where we have reintroduced the magnetic moment of the spins S , fixing the dipolar energy scale. The angular average of $(1 - \cos^2\theta)^2$ gives $4/5$ and the sum of $1/R_{ij}^6$ over a cubic lattice of spacing a is

$$\sum_i \frac{1}{R_{ij}^6} = \frac{25}{3} \frac{1}{a^6}. \quad (8.128)$$

In this simple case, the longitudinal relaxation rate is

$$\frac{1}{T_1} = S(S+1)(2S+1)^2 \frac{200\mu^4}{9a^6} \frac{\tau_{\text{sl}}}{\hbar^2}. \quad (8.129)$$

We can directly determine the spin-lattice relaxation time. However, there are other terms in the total Hamiltonian which may considerably modify the behaviour of the system, as we shall now show.

Exercise

Determine the relaxation time $1/T_2$ and the Knight shift for a dipolar interaction.

8.5.4 Exchange Narrowing

Exchange interactions have a significant effect on relaxation processes. Reversal of two neighbouring spins by the dipolar interaction involves an exchange energy. When this energy is large, such processes are effectively forbidden. Alternatively, we may consider that states out of equilibrium induced by the dipolar interaction precess very rapidly around the exchange field, thereby greatly reducing the spectral components of dipolar fluctuations at the Larmor frequency. The time dependence of matrix elements

$$\langle \alpha | [\mathcal{H}_I(\tau), S(\tau)] | \beta \rangle \propto \exp(-i\Omega_{\beta\alpha} - 1/\tau_{\text{sl}})\tau \quad (8.130)$$

in the dipolar relaxation is considerably modified here because frequencies $\Omega_{\alpha\beta} = (\varepsilon_\beta - \varepsilon_\alpha)/\hbar$ are randomly modulated in time by exchange fields. We must therefore average the time dependence of

$$\langle \alpha | [\mathcal{H}_I(\tau), S(\tau)] | \beta \rangle \propto \exp[-i\phi(\tau)] \equiv \exp \left[-i \int_0^\tau dt \Omega_{\beta\alpha}(t) \right] \quad (8.131)$$

over all possible exchange frequencies. We assume that the distribution of phases $\phi(t)$ is a Gaussian centred on $\Omega_{\beta\alpha}\tau$, of width $\Omega_{\text{ex}}\tau$. We can then evaluate the expectation value of the random phase $\phi(\tau)$,

$$\begin{aligned}\langle \exp[-i\phi(\tau)] \rangle &= \exp(-i\Omega_{\beta\alpha}\tau) \exp\left(-\frac{1}{2}\langle \phi(t) - \Omega_{\beta\alpha}t \rangle^2\right) \\ &= \exp(-i\Omega_{\beta\alpha}\tau) \exp\left(-\frac{1}{2}\Omega_{\text{ex}}^2\tau^2\right).\end{aligned}\quad (8.132)$$

When the exchange frequency is large compared with the Larmor frequency, the time integral determining relaxation times T_1 and T_2 becomes

$$\int_0^\infty d\tau \exp\left[-\frac{1}{2}\Omega_{\text{ex}}^2\tau^2\right] = \frac{\sqrt{2\pi}}{2\Omega_{\text{ex}}}.\quad (8.133)$$

In other words, relaxation times T_1 and T_2 become much longer, since the width $\approx 1/\tau_{\text{sl}}$ of the spin levels is replaced by the exchange frequency Ω_{ex} .

There may be a distribution of Larmor frequencies of width $\Delta\Omega_L$ throughout the sample. This can happen in an inhomogeneous magnetic field, for example. The width of the absorption line associated with transverse magnetisation $\langle S^+ \rangle$ is then determined by

$$\frac{1}{T_2^*} = \frac{1}{T_2} + \Delta\Omega_L.\quad (8.134)$$

We speak of inhomogeneous broadening. The shape of the absorption line depends on the exact distribution of Larmor frequencies. However, if the exchange between spins, characterised by Ω_{ex} , exceeds the inhomogeneous broadening, the absorption line becomes Lorentzian again, as we can check from (8.132).

Exercise

Make this argument explicit. How should the argument be modified to take into account the diffusion of spins in a sample placed in an inhomogeneous magnetic field?

There are many relaxation processes in ferromagnets apart from the dipolar process. They involve crystalline morphology, chemical structure, which plays an important role in spin-lattice relaxation, and the exact nature of collective modes [see Chap. 9(I)]. Several monographs have been written about these aspects [215, 216, 217].

8.5.5 Ferromagnetic Resonance

Exchange interactions are usually isotropic in ferromagnetic systems. The exchange field, which is then proportional to magnetisation, does not contribute to the Bloch equations. This is because the magnetisation cannot precess about itself. In order to take anisotropic terms into account, and such terms always appear through demagnetising fields, we give a phenomenological description of the dependence of its free energy on the order parameter,

$$\Delta F_s = -\frac{1}{2} \kappa_\mu^{-1} M_\mu^2 + \mathbf{M} \cdot \mathbf{H} + F_A , \quad (8.135)$$

where the anisotropy energy F_A depends on the system. As an example, let us consider a uniaxial anisotropy $F_A = DM_z^2$ or $F_A = DM_x^2$. Even if the exchange and susceptibility χ are isotropic, the susceptance $\kappa \equiv (\kappa)_\mu$ defined in (1.90) is not, because the demagnetising field reduces the applied field within the sample by an amount which depends upon its direction. The internal magnetic field is in this case

$$H_\mu^i = \left(\frac{\partial F}{\partial M_\mu} \right) = \frac{1}{\kappa} \Big|_\mu M_\mu + H_\mu + H_\mu^A \approx H_\mu - N_\mu M_\mu + H_\mu^A , \quad (8.136)$$

where the anisotropy field $\mathbf{H}^A = \partial F_A / \partial \mathbf{M}$ equals $2DM_z \hat{\mathbf{z}}$ or $2DM_x \hat{\mathbf{x}}$, depending on the anisotropy axis. Let us assume that, at equilibrium, the magnetisation $M_0 \hat{\mathbf{z}}$ is collinear with the magnetic field chosen along $\hat{\mathbf{z}}$. We are interested in *linear* precession modes of the magnetisation. We expand $\mathbf{M}(t)$ about $M_0 \hat{\mathbf{z}}$,

$$\mathbf{M}(t) = M_0 \hat{\mathbf{z}} + \mathbf{m}(t) . \quad (8.137)$$

The Bloch equations for an anisotropy along $\hat{\mathbf{z}}$,

$$\frac{d}{dt} \begin{vmatrix} m_x \\ m_y \\ m_z \end{vmatrix} = \gamma \begin{vmatrix} m_x \\ m_y \\ M_0 \end{vmatrix} \times \begin{vmatrix} -N_x m_x \\ -N_y m_y \\ H - N_z M_0 + 2DM_0 \end{vmatrix} , \quad (8.138)$$

can be linearised:

$$\frac{dm^+}{dt} = -i\gamma \{ [H + (2D + N_\perp - N_z)M_0]m^+ + N_\Delta M_0 m^- \} , \quad (8.139)$$

$$\frac{dm^-}{dt} = i\gamma \{ [H + (2D + N_\perp - N_z)M_0]m^- + N_\Delta M_0 m^+ \} , \quad (8.140)$$

where $N_\perp = (N_x + N_y)/2$ and $N_\Delta = (N_x - N_y)/2$. Harmonic solutions $m^\pm = m_0^\pm \exp(-i\omega t)$ can be obtained from the roots of the determinant of this linear system, viz.,

$$\omega_0^2 = \gamma^2 \{ [H + (2D + N_\perp - N_z)M_0]^2 + (N_\Delta M_0)^2 \} . \quad (8.141)$$

Even when there is no anisotropy, the resonant frequency depends on the orientation of the sample relative to the magnetic field. For example, if the plate is oriented perpendicularly to the field, $N_z = 1$, $N_\perp = 0 = N_\Delta$ and

$$\omega_0 = |\gamma|(H - M_0) , \quad (8.142)$$

whilst a plate positioned parallel to the field has demagnetising factors $N_\perp = 1/2 = N_\Delta$ and $N_z = 0$, and therefore has resonant frequency

$$\omega_0^2 = \gamma^2 H(H + M_0) . \quad (8.143)$$

When the anisotropy axis is perpendicular to the field, the transverse magnetisation satisfies similar equations of motion:

$$\frac{dm^x}{dt} = \gamma[H + (N_y - N_z)M_0]m^y, \quad (8.144)$$

$$\frac{dm^y}{dt} = -\gamma[H + (2D + N_x - N_z)M_0]m^x, \quad (8.145)$$

but the resonant modes

$$\omega_0^2 = \gamma^2[H + (N_y - N_z)M_0][H + (2D + N_x - N_z)M_0] \quad (8.146)$$

are very different. In fact, if the anisotropy field $H_A = 2DM_0$ is large compared with the applied field, the resonant frequency increases as the square root of the field,

$$\omega_0 \approx |\gamma| \sqrt{H(H + H_A)} \approx |\gamma| \sqrt{HH_A}. \quad (8.147)$$

This dependence is due to an elliptical motion of the transverse magnetisation, because deviations m_x also involve the transverse anisotropy energy. This flattens the precession along the $\hat{\mathbf{y}}$ axis, as shown in Fig. 8.4.

Exercise: Transverse Susceptibility

1. Explicitly determine solutions $m_x(t)$ and $m_y(t)$ in the presence of an alternating field $h_x \pm ih_y = h_0 \exp(\mp i\omega t)$.
2. Check that the anisotropy field causes spins to precess elliptically.
3. Deduce the transverse susceptibility tensor.

We also note that during precession, component m_z is no longer constant, but oscillates at twice the Larmor frequency (see Fig. 8.4). This effect is used in parallel pumping methods, discussed in the next chapter.

We have not yet taken into account relaxation processes bringing the magnetisation back towards equilibrium. In ferromagnetic systems, longitudinal

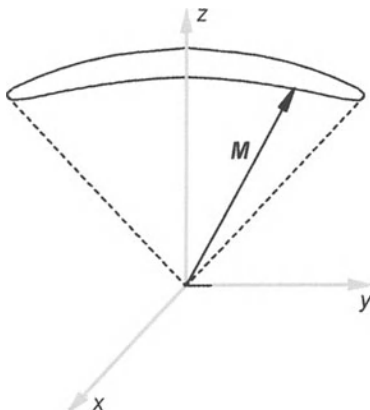


Fig. 8.4. Precession of the magnetisation of a ferromagnet in the presence of a plane uniaxial anisotropy along the $\hat{\mathbf{x}}$ axis, which forces spins into the (y, z) plane

and transverse relaxation times, T_1 and T_2 , respectively, are often equal [218]. Magnetisation relaxation processes are therefore often included in a different way, using the Landau and Lifshitz term [219],

$$-\frac{\lambda}{M^2} \mathbf{M} \times \mathbf{M} \times \mathbf{H}_i . \quad (8.148)$$

In the low amplitude limit this gives relaxation times

$$T_1 = T_2 = \frac{M_0}{\lambda H} . \quad (8.149)$$

Another form sometimes used is the Gilbert term [220],

$$-\frac{\alpha}{M} \mathbf{M} \times \frac{d\mathbf{M}}{dt} . \quad (8.150)$$

In this case, relaxation times T_1 and T_2 are frequency dependent:

$$T_1 = T_2 = \frac{1}{\alpha\omega} . \quad (8.151)$$

When we consider non-linear dynamics, the various forms for the dissipative terms are no longer equivalent.

8.5.6 Ferrimagnetic and Antiferromagnetic Resonance

Ferrimagnetic systems [mentioned in Sect. 5.5(I)] comprise two distinct sublattices associated with different ions. The two sublattices do not fully compensate one another and the system has a spontaneous magnetisation. When we study the dynamics of such systems, we must treat the magnetisation of the two sublattices as independent variables, coupled together by exchange interactions. In order to write the Bloch equations associated with each sublattice, we determine internal fields by variation of the free energy with the magnetisations \mathbf{M}_a and \mathbf{M}_b of each sublattice a and b ,

$$\Delta F_s = -\alpha \mathbf{M}_a \cdot \mathbf{M}_b + D_a (M_z^a)^2 + D_b (M_z^b)^2 + (\mathbf{M}_a + \mathbf{M}_b) \cdot \mathbf{H} , \quad (8.152)$$

where the first term comes from the molecular field coupling the two sublattices. We have neglected demagnetising factors. Internal fields acting on the sublattices a and b are

$$\mathbf{H}_a = \frac{\partial F}{\partial \mathbf{M}_a} = -\alpha \mathbf{M}_b + 2D_a M_z^a \hat{\mathbf{z}} + \mathbf{H} , \quad (8.153)$$

$$\mathbf{H}_b = \frac{\partial F}{\partial \mathbf{M}_b} = -\alpha \mathbf{M}_a + 2D_b M_z^b \hat{\mathbf{z}} + \mathbf{H} . \quad (8.154)$$

Introducing deviations of the magnetisation from equilibrium values, $\mathbf{M}_a = M_a^0 \hat{\mathbf{z}} + \mathbf{m}_a(t)$ and $\mathbf{M}_b = M_b^0 \hat{\mathbf{z}} + \mathbf{m}_b(t)$, it is easy to write down the linearised Bloch equations for each sublattice:

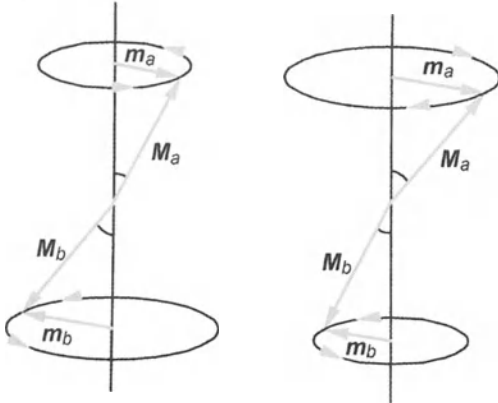


Fig. 8.5. *Left:* Ferromagnetic precession mode. Magnetisations of the two sublattices precess in the same direction about the magnetic field. *Right:* Antiferromagnetic precession mode. The two sublattices precess in opposite directions about the magnetic field. The difference in precession frequencies is the exchange frequency

$$\frac{dm_a^\pm}{dt} = \pm i\gamma_a [(H + 2D_a M_a^0 + \alpha M_b^0)m_a^\pm + \alpha M_a^0 m_b^\pm] , \quad (8.155)$$

$$\frac{dm_b^\pm}{dt} = \pm i\gamma_b [(H + 2D_b M_b^0 - \alpha M_a^0)m_b^\pm - \alpha M_b^0 m_a^\pm] . \quad (8.156)$$

These are coupled two-by-two. There are therefore two distinct normal modes. The normal frequencies can be determined directly from the characteristic equation of this linear system. However, the nature of these modes can be brought out more clearly if we assume that gyromagnetic factors $\gamma_a \approx \gamma_b$ and anisotropy energies $D_a \approx D_b$ are the same. We can then define two order parameters $M = M_a^0 + M_b^0$ (magnetisation), $N = M_a^0 - M_b^0$ (alternating magnetisation), and also the corresponding dynamical variables $\mathbf{m} = \mathbf{m}_a + \mathbf{m}_b$, $\mathbf{n} = \mathbf{m}_a - \mathbf{m}_b$, to obtain the coupled equations of the two order parameters,

$$\frac{dm^\pm}{dt} = \pm i\gamma [(H + DM)m^\pm + (DN - \alpha M/2)n^\pm] , \quad (8.157)$$

$$\frac{dn^\pm}{dt} = \pm i\gamma [(H + DM - \alpha N)n^\pm + (DN + \alpha M/2)m^\pm] . \quad (8.158)$$

If we neglect coupling terms, resonant frequencies in the frame rotating at the Larmor frequency $\gamma(H + DM)$ are 0 and $-\gamma\alpha N$. The first mode is the ferromagnetic precession mode, since the magnetisations of the two sublattices precess at the same speed. In the second mode, the two sublattices precess in opposite directions and their relative precession frequency is the exchange frequency. This is an antiferromagnetic mode, illustrated in Fig. 8.5. Terms coupling the dynamics of the two order parameters come from two sources: partly from the anisotropy and partly from the imperfect compensation be-

tween the two sublattices. When coupling is weak, we can obtain resonant frequencies from perturbation theory:

$$\Omega_L \approx \gamma \left[(H + HM) + \frac{(\alpha M/2)^2 - (BN)^2}{\alpha N} \right], \quad (8.159)$$

$$\Omega_L \approx \gamma \left[(H + HM - \alpha N) - \frac{(\alpha M/2)^2 - (BN)^2}{\alpha N} \right]. \quad (8.160)$$

Precession frequencies of the two modes are therefore pushed apart (level repulsion). In antiferromagnetic systems, the order parameter at equilibrium \mathbf{N} is collinear with the anisotropy axis (of Ising type) if the magnetic energy is dominated by anisotropy. Otherwise, the order parameter \mathbf{N} moves round perpendicular to the magnetic field above the spin-flop transition [see Chap. 5(I) and Exercise C.1.3, Appendix C]. Of course, modes are of a quite different nature above this transition.

Exercise

Study the precession modes of an antiferromagnet above the spin-flop transition.

9. Spin Waves

9.1 Spin Hydrodynamics

The existence of hydrodynamic modes is usually a consequence of conservation laws. Deviations from equilibrium associated with the conserved variables cannot relax locally. They must be transported over greater distances. This process is all the slower as wavelengths corresponding to deviations are long. In a fluid, there are three conservation laws: conservation of mass, momentum (a vector) and energy. All these laws can be expressed in the same way:

$$\frac{\partial \rho(\mathbf{r}, t)}{\partial t} + \frac{\nabla \cdot \mathbf{g}(\mathbf{r}, t)}{m} = 0 , \quad (9.1)$$

$$\frac{\partial g_i(\mathbf{r}, t)}{\partial t} + \nabla_j \tau_{ij}(\mathbf{r}, t) = 0 , \quad (9.2)$$

$$\frac{\partial \varepsilon(\mathbf{r}, t)}{\partial t} + \nabla \cdot \mathbf{j}_\varepsilon(\mathbf{r}, t) = 0 , \quad (9.3)$$

where ρ , $\mathbf{g} = m\rho\mathbf{v}$ and ε are respectively the particle density, momentum density and energy density (which has units of pressure). τ_{ij} and \mathbf{j}_ε are the momentum and energy flux, respectively. The three equations are not sufficient to describe the hydrodynamics of a fluid, since the fluxes have not yet been specified. Given that all other degrees of freedom have microscopic relaxation times and reach a local equilibrium, we can relate these fluxes to variations in local thermodynamic variables [221]. Such constitutive equations relate momentum and energy fluxes to pressure, and velocity and temperature gradients. They depend on microscopic properties of the fluid through transport coefficients such as viscosities and thermal conductivity. Constitutive equations generally couple the dynamics of the momentum and energy. For example, fluid viscosity contributes to energy dissipation and temperature gradients also generate a flow of matter.

As an example, the constitutive equations for a liquid are

$$\langle \tau_{ij} \rangle = P\delta_{ij} - \eta \left(\nabla_i v_j + \nabla_j v_i - \frac{2}{3} \nabla \cdot \mathbf{v} \delta_{ij} \right) - \zeta \nabla \cdot \mathbf{v} \delta_{ij} , \quad (9.4)$$

$$\langle \mathbf{j}_\varepsilon \rangle = (\varepsilon + P)\mathbf{v} + \kappa \nabla T , \quad (9.5)$$

where P and T are the pressure and temperature of the fluid. η and ζ are the first (shear) and second coefficients of viscosity, and κ the thermal conductivity. Pressure and temperature gradients are related to density and energy gradients by the thermodynamic identities

$$\nabla X = \left(\frac{\partial X}{\partial n} \right)_\varepsilon \nabla n + \left(\frac{\partial X}{\partial \varepsilon} \right)_n \nabla \varepsilon , \quad (9.6)$$

where $X \equiv p, T$.

These dynamical equations nevertheless possess natural modes or hydrodynamic modes, corresponding to sound propagation $\omega = \pm ck$ and heat diffusion $\omega = -iD_Q k^2$, respectively [222]. As we shall see later, such modes are only well defined for long wavelengths, i.e., small k .

In paramagnetic systems, apart from the energy, the only conserved magnetic variable is the spin density $\tilde{\sigma}$ (or equivalently, the magnetisation),

$$\frac{\partial \tilde{\sigma}(\mathbf{r}, t)}{\partial t} + \nabla \cdot \tilde{\mathbf{j}}_\sigma(\mathbf{r}, t) = 0 . \quad (9.7)$$

We make a distinction here between vectors describing spin operator expectation values $\tilde{\sigma}, \tilde{h}$, which carry a tilde, and their gradients $\nabla \sigma_x, \nabla \sigma_y, \nabla \sigma_z$ with respect to coordinates \mathbf{r} , written in bold. The spin current $\tilde{\mathbf{j}}$ thus has nine components, indexed by α, j , proportional to $\partial \sigma_\alpha / \partial r_j$. The conservation law (9.7) is a consequence of rotational invariance of the microscopic Hamiltonian, which implies $[\mathbf{S}_{\text{tot}}, \mathcal{H}] = 0$. This hydrodynamic equation assumes that local thermodynamic equilibrium has been reached by the magnetisation and hence that the hydrodynamic evolution is sufficiently slow. When there is an *external* magnetic field, the magnetisation generally precesses too quickly and $[\mathbf{S}_{\text{tot}}, \mathcal{H}] \neq 0$. In the frame precessing at the Larmor frequency about the magnetic field, the magnetisation is stationary and in thermodynamic equilibrium. The hydrodynamic equation (9.7) must therefore be interpreted in this frame. In the laboratory frame, the spin dynamics includes an extra term associated with this uniform precession [223],

$$\frac{\partial \tilde{\sigma}(\mathbf{r}, t)}{\partial t} - \gamma \tilde{\sigma}(\mathbf{r}, t) \times \tilde{h} + \nabla \cdot \tilde{\mathbf{j}}_\sigma(\mathbf{r}, t) = 0 , \quad (9.8)$$

where γ is the gyromagnetic factor of the spins S . In a paramagnetic system, constitutive relations generally couple magnetisation and energy fluxes, j_σ and j_ε , respectively,

$$\mathbf{j}_{\sigma_z} = - \left(D_\sigma \nabla \sigma_z + L_{21} \frac{\nabla T}{T} \right) , \quad (9.9)$$

$$\mathbf{j}_Q = \mathbf{j}_\varepsilon - \frac{\varepsilon + P}{\rho} \mathbf{v} = -(\kappa \nabla T + T L_{12} \nabla \sigma_z) , \quad (9.10)$$

because spin reversal during a collision can only occur if its Zeeman energy is converted into kinetic energy (conservation of energy). The spin diffusion coefficient D_σ is generally a tensor, but reduces to a constant in isotropic systems. Coupling coefficients L_{12} and L_{21} are small, so hydrodynamic modes

associated with diffusion of spins and heat $Q = \varepsilon(\mathbf{r}, t) - (\varepsilon + P)\rho(\mathbf{r}, t)/\rho$ decouple:

$$\frac{\partial \tilde{\sigma}}{\partial t} - \gamma \tilde{\sigma} \times \tilde{h} - D_\sigma \nabla^2 \tilde{\sigma} = 0 , \quad (9.11)$$

$$\frac{\partial Q}{\partial t} - D_Q \nabla^2 Q = 0 . \quad (9.12)$$

There are thus three hydrodynamic modes:

- transverse diffusion of spins, $\omega \mp \gamma|h| = -iD_\sigma^\perp k^2$;
- longitudinal diffusion of spins, $\omega = -iD_\sigma^\parallel k^2$;
- heat diffusion, $\omega = -iD_Q k^2$.

Exercise

Establish these dispersion relations and show that the heat diffusion coefficient is given by $D_Q = \kappa/\rho C_p$, where κ is thermal conductivity and C_p is specific heat per unit volume.

When the system has a second order transition which breaks a continuous symmetry (rotational symmetry for magnets), hydrodynamic modes are profoundly modified. Indeed, one or more new hydrodynamic modes appear below T_c , associated with fluctuations transverse to the order parameter and of long wavelength λ (Goldstone theorem [224]). These fluctuations are slow, and hence hydrodynamic, because restoring forces bringing the order parameter back towards equilibrium tend to zero as $\lambda \rightarrow \infty$. Since the fluctuations are transverse to the order parameter, they tend to restore the symmetry which it breaks. In a magnet, the associated hydrodynamic modes are spin waves. In a superfluid, fluctuations in the phase of the order parameter generate a supercurrent, transporting matter or energy without dissipation. In a superconductor, the phase fluctuations generate charge fluctuations which oscillate at the plasma frequency because the Coulomb interaction is long range; there are no hydrodynamic modes, except in the neighbourhood of the critical temperature [see Chap. 17(II)]. Fluctuation modes transverse to the order parameter are called Goldstone modes, because of the Goldstone theorem mentioned above, which associates one or more hydrodynamic modes to a continuous symmetry broken by the order parameter. Ising systems have no continuous symmetry and hence there are no Goldstone modes.

We can develop these ideas in the context of a ferromagnet. When there is no anisotropy, the free energy does not depend on the direction of the spontaneous magnetisation density $\propto \tilde{\sigma}$. As this direction is arbitrary, we can rotate it by means of an infinitesimal magnetic field without expending any energy. Since a global rotation of the spins requires no energy, we only need a very small energy to change the direction of the magnetisation over a very long wavelength $\lambda = 2\pi/k$. Let us impose boundary conditions such

that spins on either side of the sample are at an angle θ to each other. If we assume that, from one site to the next, spins (considered here as classical) are rotated in the x direction through an angle $\delta\theta = \theta a/L_x$, where a is the atomic spacing and L_x the sample length, this configuration has energy

$$E_\theta = -J\hbar^2 s^2 \sum_i \cos(\delta\theta_i) = -N J \hbar^2 s^2 \left[1 - \frac{(\delta\theta)^2}{2} \right] \quad (9.13)$$

$$= -N J \hbar^2 s^2 + \frac{N J \hbar^2 a^2}{2} \left(\frac{S\theta}{L_x} \right)^2 = E_0 + V \frac{\Gamma(\nabla\tilde{\sigma})^2}{2}. \quad (9.14)$$

$E_0 = -N J s^2$ is the ground state energy, V the volume of the system, σ the spin density and $\Gamma \approx J\hbar^2 z a^2 / 3v$ the spin stiffness constant ($v = V/N$ is the atomic volume and z the coordination of the 3-dimensional lattice). To first order, this energy change $\delta E = E_\theta - E_0$ must be proportional to $|\nabla\sigma|^2$, the only derivative of the spin density which is invariant under a rotation in spin space. This spin torsion energy is equivalent to the Zeeman energy in an effective field $\gamma\tilde{h}_{\text{eff}}(\mathbf{r}) = -\Gamma\nabla^2\tilde{\sigma}(\mathbf{r})$. Introducing a magnetic potential $h_\alpha = -\nabla \cdot \phi_\alpha$, we can integrate the second term in the free energy,

$$\delta F = \int d^3r \left[\frac{\Gamma}{2} (\nabla\tilde{\sigma})^2 - \gamma\tilde{\sigma}(\mathbf{r}) \cdot \tilde{h}(\mathbf{r}) \right], \quad (9.15)$$

by parts and thereby complete the quadratic form $(\nabla\tilde{\sigma} + \gamma\tilde{\phi}/\Gamma)^2$. It follows that the free energy

$$\delta F = \int d^3r \left[\frac{\Gamma}{2} \left(\nabla\tilde{\sigma} + \gamma \frac{\tilde{\phi}}{\Gamma} \right)^2 - \frac{\gamma^2}{2\Gamma} |\tilde{\phi}|^2 \right] \quad (9.16)$$

is a minimum when

$$\phi_{\min} = -\frac{\Gamma}{\gamma} \nabla\tilde{\sigma} \Rightarrow \tilde{h}_{\text{eff}} = \frac{\Gamma}{\gamma} \nabla^2\tilde{\sigma}. \quad (9.17)$$

We obtain the dynamical equation of the spin density by replacing

$$H = \int d^3r \frac{\Gamma}{2} (\nabla\tilde{\sigma})^2 \quad \text{by} \quad \gamma \int d^3r \tilde{\sigma} \cdot \tilde{h}_{\text{eff}}.$$

This is equivalent to precession of the spins in the effective field \tilde{h}_{eff} :

$$\frac{\partial\tilde{\sigma}}{\partial t} = \gamma\tilde{\sigma} \times \tilde{h}_{\text{eff}} = \Gamma\tilde{\sigma} \times \nabla^2\tilde{\sigma}. \quad (9.18)$$

We can also establish the spin density hydrodynamics from its classical equation of motion, in the form of a Poisson bracket

$$\frac{\partial\tilde{\sigma}}{\partial t} = [\tilde{\sigma}, H]_{\text{pb}}, \quad (9.19)$$

and using the angular momentum algebra of $\tilde{\sigma}$ [225],

$$[\sigma_x(\mathbf{r}), \sigma_y(\mathbf{r}')]_{\text{pb}} = \sigma_z(\mathbf{r}) \delta(\mathbf{r} - \mathbf{r}'). \quad (9.20)$$

(As for spin, the other relations are obtained by cyclic permutations.) We thus come back to (9.18), starting from

$$H = \int d^3r \frac{\Gamma}{2} (\nabla \tilde{\sigma})^2 .$$

Indeed,

$$\begin{aligned} [\sigma_\alpha(\mathbf{r}), (\nabla' \sigma(\mathbf{r}'))^2]_{\text{pb}} &= 2 \sum_\beta \nabla' \sigma_\beta(\mathbf{r}') \cdot \nabla' [\sigma_\alpha(\mathbf{r}), \sigma_\beta(\mathbf{r}')]_{\text{pb}} \\ &= 2 \sum_\beta \nabla' \sigma_\beta(\mathbf{r}') \cdot \nabla' \varepsilon_{\alpha\beta\gamma} \sigma_\gamma(\mathbf{r}) \delta(\mathbf{r} - \mathbf{r}') . \end{aligned} \quad (9.21)$$

We then integrate $\nabla' \delta(\mathbf{r} - \mathbf{r}')$ by parts to obtain

$$[\sigma_\alpha(\mathbf{r}), H]_{\text{pb}} = -2 \frac{\Gamma}{2} \sum_\beta \varepsilon_{\alpha\beta\gamma} (\nabla^2 \sigma_\beta) \sigma_\gamma . \quad (9.22)$$

We obtain the dispersion relation of the normal modes by describing fluctuations in the spin density transverse to $\sigma_0 \hat{\mathbf{z}}$ as a *spin wave*,

$$\begin{aligned} \tilde{\sigma} &= \sigma_0 \hat{\mathbf{z}} + \tilde{\sigma}_\perp \\ &= \sigma_0 \hat{\mathbf{z}} + \delta\sigma [\cos(\mathbf{k} \cdot \mathbf{r} - \omega t) \hat{\mathbf{x}} + \sin(\mathbf{k} \cdot \mathbf{r} - \omega t) \hat{\mathbf{y}}] , \end{aligned} \quad (9.23)$$

and linearising the equation of motion (9.18) around $\sigma_0 \hat{\mathbf{z}}$ to obtain

$$\omega = \Gamma \sigma_0 k^2 , \quad (9.24)$$

where σ_0 is the equilibrium spin density. As in paramagnetic systems, we have a quadratic dispersion relation. In this case, however, modes are reactive and propagating, rather than diffusive, as they are in paramagnetic systems. The modes are reactive because there is a restoring force, bringing the system back towards equilibrium. Figure 9.1 gives a visual representation of spin waves. A spatial modulation of spin precession propagates either parallel or perpendicular to the magnetic field.

It might be thought that an antiferromagnet would have similar hydrodynamic modes to a ferromagnet. This is not the case. Unlike ferromagnets, they have an order parameter $\tilde{\mathbf{n}}(\mathbf{r}, t)$, the alternating magnetisation, which does

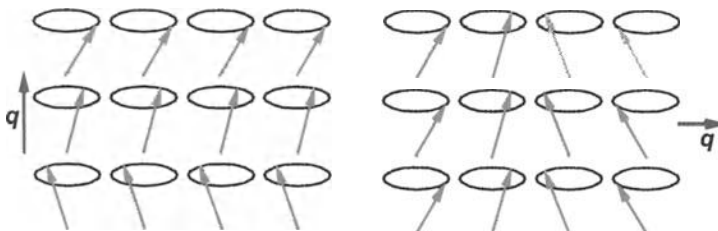


Fig. 9.1. Representation of spin waves propagating along the magnetic field (*left*), and perpendicular to the magnetic field (*right*)

not satisfy a conservation law above the transition. This is to be contrasted with (9.7) for ferromagnetic systems, where $\tilde{\sigma}$ happens to be a conserved quantity. In Sect. 9.9 we shall describe hydrodynamic modes in systems with a more complex order parameter, such as antiferromagnets with several sub-lattices, and helimagnets, making use only of symmetry considerations and thermodynamics.

The only restrictions on the above analysis are:

- deviations are long wavelength and small amplitude;
- dynamics are slow.

There is no restriction on the spin value. At short wavelengths, spin waves become more or less well defined reactive modes, depending on the available dissipation and diffusion mechanisms. It is nevertheless possible to give a precise quantum definition in the large spin limit, using approximate representations of spin operators.

Exercise: Spin Waves in a Magnetic Field

1. Check that in a uniform field the Bloch equation for a ferromagnet is

$$\frac{\partial \tilde{\sigma}}{\partial t} = \gamma \tilde{\sigma} \times \tilde{h}_{\text{eff}}, \quad h_{\text{eff}} = h\hat{z} + \frac{\Gamma}{\gamma} \nabla^2 \sigma. \quad (9.25)$$

2. Linearising this equation around the ground state $\tilde{\sigma} = \sigma_0 \hat{z} + \delta \tilde{\sigma}$, obtain the dynamics of the transverse spin density $\delta \sigma^+ = \delta \sigma_x + i \delta \sigma_y$. Deduce the spin-wave dispersion relation.
3. In an inhomogeneous magnetic field, establish an analogy with the Schrödinger equation for a particle of mass m in a potential $U(\mathbf{r})$. What is the mass m and the potential $U(\mathbf{r})$?
4. Assume that the ferromagnet is a long cylinder of length L with axis along the \hat{x} axis and cross-section sufficiently small to justify neglecting magnetisation gradients in the \hat{y} and \hat{z} directions. The magnetisation satisfies boundary conditions such that the spin current $\tilde{j} \propto \nabla \tilde{\sigma}$ is zero at the ends $x = \pm L/2$. We assume that the magnetic field is inhomogeneous $\tilde{h} = h(r)\hat{z} = (h_0 + Gx)\hat{z}$. Write down the semi-classical action of the particle of mass m in potential $U(\mathbf{r})$. Using the Bohr–Sommerfeld quantisation rules, deduce the stationary states. Show that these stationary states correspond to spatially localised spin waves at the end of the sample [226].

9.2 Elementary Excitations and Magnons

Up to now we have been considering spins either as classical variables (vectors or binary variables in the case of the Ising model), or as generators of the rotation group in spin space. Eigenstates of these operators often have rather

special properties, which vary greatly with the value of the spin. For example, a rotation through 4π in real space is required to reproduce the eigenstates of half-integer spins, whereas a rotation through 2π is sufficient for integer spins. When a magnetic system becomes ordered, spins select a particular direction in space and thermal fluctuations do not allow the system to explore all possible spin directions. In such conditions, we may say in semi-classical terms (considering spins as vectors) that spins deviate only by very small angles from their equilibrium positions. In this limit, spin operators can be represented by bosons (see Sect. 2.2). This considerably simplifies the study of elementary excitations above the ground state. Of course, if the ground state is disordered, as happens in one dimension [see Chap. 7, 10(I)], we cannot neglect large amplitude rotations. We must then take into account the quantum complexity of spinors.

We can give a concrete illustration of the quantum modes by choosing the magnetic Hamiltonian

$$\mathcal{H} = - \sum_{i \neq j} J_{ij} \hbar^2 \tilde{S}_i \cdot \tilde{S}_j + D \hbar^2 (S_{z,x}^i)^2 + \mu H S_i^z , \quad (9.26)$$

whose exchange may be ferromagnetic $J > 0$ or antiferromagnetic $J < 0$. S is expressed here in units of \hbar and $\mu = g_S \mu_B$ is the magnetic moment. Apart from its physical significance, the ionic anisotropy term D is interesting because different methods must be used to diagonalise it, depending on whether it is oriented parallel DS_z^2 or perpendicular DS_x^2 to the magnetic field. We will not take dipolar interactions into account, although they are important in all ferromagnetic systems. They can be treated in every way like the ionic anisotropy term, despite the added complexity.

Holstein–Primakoff Transformation

The transformation of the spin Hamiltonian in terms of harmonic oscillators [227] is based upon the relations [see Chap. 2(I)]

$$S_i^+ |m\rangle = \sqrt{(s-m)(s+m+1)} |m+1\rangle , \quad (9.27)$$

$$S_i^- |m\rangle = \sqrt{(s-m+1)(s+m)} |m-1\rangle , \quad (9.28)$$

satisfied by eigenstates of spin operators of spin s at the i th site. The ground state of a ferromagnet is characterised by the eigenvalues of S_i^z being maximal $m = \pm s$ at all sites. In order to linearise the deviation of S_i^z around $-s$, we introduce the deviation operator $\hat{n}_i = s + S_z$ which has quantum numbers $n = s + m$. Eigenstates $|n\rangle$ of \hat{n}_i correspond to eigenstates $|m\rangle$ of S_z , where $n = s + m$. We can therefore rewrite the last equation in terms of \hat{n} ,

$$S_i^+ |n\rangle = \sqrt{2s} \sqrt{n+1} \sqrt{1-n/2s} |n+1\rangle , \quad (9.29)$$

$$S_i^- |n\rangle = \sqrt{2s} \sqrt{1-(n-1)/2s} \sqrt{n} |n-1\rangle . \quad (9.30)$$

This suggests introducing harmonic oscillator operators [230],

$$a^\dagger |n\rangle = \sqrt{n+1} |n+1\rangle , \quad (9.31)$$

$$a |n\rangle = \sqrt{n} |n-1\rangle , \quad (9.32)$$

in terms of which spin operators become

$$S_i^+ = \sqrt{2s} a_i^\dagger f_i(s) , \quad (9.33)$$

$$S_i^- = \sqrt{2s} f_i(s) a_i , \quad (9.34)$$

$$S_i^z = -s + a_i^\dagger a_i , \quad (9.35)$$

where $f_i(s) = \sqrt{1 - a_i^\dagger a_i / 2s}$. This transformation preserves commutation relations if operators a and a^\dagger are bosons, i.e.,

$$[S_i^z, S_j^\pm] = \pm S_i^\pm \delta_{ij} , \quad [S_i^+, S_j^-] = 2S_i^z \delta_{ij} \Leftrightarrow [a_i, a_j^\dagger] = \delta_{ij} . \quad (9.36)$$

Exercise

Check the equivalence of these commutation relations.

The number of excited bosons is the eigenvalue of the number operator $\hat{n}_i = s + S_i^z = a_i^\dagger a_i$. If the n_i were independent, their average numbers $\langle n_i \rangle$ at thermodynamic equilibrium would be given by Bose–Einstein statistics. The transformation from S to a^\dagger and a , due to Holstein and Primakoff, is non-linear. It is only useful if we can expand the square root to first order (or if necessary, to second order). After transformation to the Fourier space, we can then express the Hamiltonian as a sum of *independent* harmonic oscillators, which we interpret as elementary excitations of the system. This transformation implicitly assumes a large value for s . Whilst commutation relations are preserved by the non-linear transformation, they become approximate as soon as we expand the square root. The Holstein–Primakoff transformation is therefore a semi-classical approximation (in $1/s$), for small oscillation amplitudes of S_\perp . The Holstein–Primakoff transformation has a simple geometrical interpretation in the classical limit. The quantity $1 - x$, where $n = xs$, is the projection of the unit vector parallel to the spin on the \hat{z} axis. Let θ be the angle of stereographic projection of the unit sphere onto the plane tangent to the south pole. The geometry drawn in Fig. 9.2 shows that $\sin^2 \theta = x/2$ and hence that $\sqrt{n} = |a| = \sqrt{2s} \sin \theta$, which we interpret as the oscillation amplitude of spin i , is proportional to the angle of stereographic projection. The stereographic projection of the unit vector parallel to the spin is given in terms of a by $2|a|/\sqrt{2s - |a|^2}$.

Using the procedure of Sect. 3.8(I), we diagonalise the exchange interaction by transforming to the Fourier transform space:

$$a_i = \frac{1}{\sqrt{N}} \sum_{\mathbf{k}} \exp(i\mathbf{k} \cdot \mathbf{R}_i) a_{\mathbf{k}} , \quad a_{\mathbf{k}} = \frac{1}{\sqrt{N}} \sum_i \exp(-i\mathbf{k} \cdot \mathbf{R}_i) a_i , \quad (9.37)$$

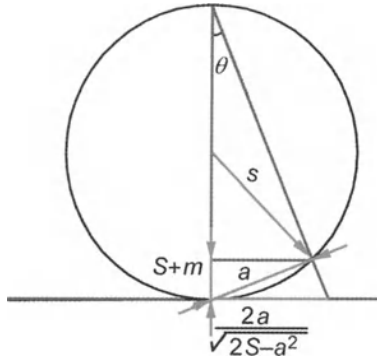


Fig. 9.2. Stereographic projection of a vector on the sphere of radius s onto the tangent plane at the south pole. The Holstein–Primakoff amplitude a is the arc subtended between the end of S and the south pole

$$N\delta(\mathbf{R}_i - \mathbf{R}'_i) = \sum_{\mathbf{k}} \exp i\mathbf{k} \cdot (\mathbf{R}_i - \mathbf{R}'_i),$$

$$[a_{\mathbf{k}}, a_{\mathbf{k}'}^\dagger] = \delta(\mathbf{k} - \mathbf{k}'). \quad (9.38)$$

Relations between a_i^\dagger and $a_{\mathbf{k}}^\dagger$ are obtained by complex conjugation. $a_{\mathbf{k}}$ and $a_{\mathbf{k}}^\dagger$ are annihilation and creation operators for the magnon of wave vector \mathbf{k} . They were obtained from spin operators S_i^+ and S_i^- by carrying out a change of variables. In this case, the formalism of second quantisation appears as a change of representation and introduces no new physical content. Spin operators can be expanded to third order in the new a operators as follows:

$$S_i^+ = \sqrt{\frac{2s}{N}} \sum_{\mathbf{k}} \exp(-i\mathbf{k} \cdot \mathbf{R}_i) a_{\mathbf{k}}^\dagger \quad (9.39)$$

$$- \frac{1}{N\sqrt{8Ns}} \sum_{\mathbf{kk}'\mathbf{k}''} \exp[-i(\mathbf{k} + \mathbf{k}' - \mathbf{k}'') \cdot \mathbf{R}_i] a_{\mathbf{k}}^\dagger a_{\mathbf{k}'}^\dagger a_{\mathbf{k}''} + \dots,$$

$$S_i^- = \sqrt{\frac{2s}{N}} \sum_{\mathbf{k}} \exp(i\mathbf{k} \cdot \mathbf{R}_i) a_{\mathbf{k}} \quad (9.40)$$

$$- \frac{1}{N\sqrt{8Ns}} \sum_{\mathbf{kk}'\mathbf{k}''} \exp[-i(\mathbf{k} - \mathbf{k}' - \mathbf{k}'') \cdot \mathbf{R}_i] a_{\mathbf{k}}^\dagger a_{\mathbf{k}'} a_{\mathbf{k}''} + \dots,$$

$$S_i^z = -s + \frac{1}{N} \sum_{\mathbf{kk}'} \exp[-i(\mathbf{k} - \mathbf{k}') \cdot \mathbf{R}_i] a_{\mathbf{k}}^\dagger a_{\mathbf{k}'} . \quad (9.41)$$

The Hamiltonian can now be diagonalised. The Zeeman energy, when expressed in terms of the magnon operators,

$$\mathcal{H}_Z = \mu H \sum_i S_i^z$$

$$\begin{aligned}
&= -\mu H \sum_i \left[s - \frac{1}{N} \sum_{\mathbf{k}\mathbf{k}'} \exp[-i(\mathbf{k} - \mathbf{k}') \cdot \mathbf{R}_i] a_{\mathbf{k}}^\dagger a_{\mathbf{k}'} \right] \\
&= -\mu H N s + \mu H \sum_{\mathbf{k}} a_{\mathbf{k}}^\dagger a_{\mathbf{k}} ,
\end{aligned} \tag{9.42}$$

is indeed a sum of elementary harmonic excitations. For ferromagnetic exchange interactions between nearest neighbours, we sum exchange contributions over relative positions δ of neighbouring ions, viz.,

$$\begin{aligned}
\mathcal{H}_{\text{ex}} &= -J\hbar^2 \sum_{i, \delta} \tilde{S}_i \cdot \tilde{S}_{i+\delta} \\
&= -J\hbar^2 \sum_{i, \delta} \left[\frac{1}{2} (S_i^+ S_{i+\delta}^- + S_i^- S_{i+\delta}^+) + S_i^z S_{i+\delta}^z \right] \\
&= -\frac{J\hbar^2 s}{N} \sum_{i, \delta} \sum_{\mathbf{k}\mathbf{k}'} \left[\exp(i\mathbf{k} \cdot \mathbf{R}_i) \exp[-i\mathbf{k}' \cdot (\mathbf{R}_i + \delta)] a_{\mathbf{k}} a_{\mathbf{k}'}^\dagger \right. \\
&\quad \left. + \exp(-i\mathbf{k} \cdot \mathbf{R}_i) \exp[i\mathbf{k}' \cdot (\mathbf{R}_i + \delta)] a_{\mathbf{k}}^\dagger a_{\mathbf{k}'} \right] \\
&\quad + \left[s - \frac{1}{N} \sum_{\mathbf{k}\mathbf{k}'} \exp[-i(\mathbf{k} - \mathbf{k}') \cdot \mathbf{R}_i] a_{\mathbf{k}}^\dagger a_{\mathbf{k}'} \right] \\
&\quad \times \left[s - \frac{1}{N} \sum_{\mathbf{k}\mathbf{k}'} \exp[-i(\mathbf{k} - \mathbf{k}') \cdot (\mathbf{R}_i + \delta)] a_{\mathbf{k}}^\dagger a_{\mathbf{k}'} \right] .
\end{aligned} \tag{9.43}$$

Neglecting fourth order terms and letting z denote the coordination of each site (the number of neighbours), we obtain

$$\begin{aligned}
\mathcal{H}_{\text{ex}} &= -J\hbar^2 s \sum_{\mathbf{k}\delta} \left[\exp(-i\mathbf{k} \cdot \boldsymbol{\delta}) a_{\mathbf{k}} a_{\mathbf{k}}^\dagger + \exp(i\mathbf{k} \cdot \boldsymbol{\delta}) a_{\mathbf{k}}^\dagger a_{\mathbf{k}} \right] \\
&\quad - Nz J\hbar^2 s^2 + 2z J\hbar^2 s \sum_{\mathbf{k}} a_{\mathbf{k}}^\dagger a_{\mathbf{k}} .
\end{aligned} \tag{9.44}$$

We define the sum over the crystal lattice

$$\eta_{\mathbf{k}} = \frac{1}{z} \sum_{\delta} \exp i\mathbf{k} \cdot \boldsymbol{\delta} , \tag{9.45}$$

which takes on a simple form for a cubic lattice with nearest neighbour exchange, viz.,

$$\eta_{\mathbf{k}} = \frac{1}{3} (\cos k_x a + \cos k_y a + \cos k_z a) , \tag{9.46}$$

where a is the lattice constant. As the average of $\eta_{\mathbf{k}}$ over the whole lattice is zero,

$$\sum_{\mathbf{k}} \eta_{\mathbf{k}} = 0 , \tag{9.47}$$

the exchange Hamiltonian also takes on a harmonic form

$$\mathcal{H}_{\text{ex}} = -NzJ\hbar^2 s^2 + 2zJ\hbar^2 s \sum_{\mathbf{k}} (1 - \eta_{\mathbf{k}}) a_{\mathbf{k}}^\dagger a_{\mathbf{k}} . \quad (9.48)$$

Anharmonic terms have been neglected. These appear to first and third order in the Holstein–Primakoff approximation, through $S_i^z S_j^z$ and $S_i^+ S_j^-$, respectively. Separation between harmonic and anharmonic terms is only well defined if creation and annihilation operators are ordered according to some specified convention (see Appendix B). The *normal ordering* convention consists in arranging for all creation operators to be on the left and all annihilation operators on the right. For example, the term $a_{\mathbf{k}}^\dagger a_{\mathbf{k}'} a_{\mathbf{q}}^\dagger a_{\mathbf{q}'}$ must be rewritten

$$a_{\mathbf{k}}^\dagger a_{\mathbf{k}'} a_{\mathbf{q}}^\dagger a_{\mathbf{q}'} = a_{\mathbf{k}}^\dagger a_{\mathbf{q}}^\dagger a_{\mathbf{k}'} a_{\mathbf{q}'} + \delta(\mathbf{q} - \mathbf{k}') a_{\mathbf{k}}^\dagger a_{\mathbf{q}'} . \quad (9.49)$$

In the exchange Hamiltonian, harmonic terms generated by the second term of (9.49) do not contribute to the final Hamiltonian (9.48) because of the sum rule (9.47). The effect of remaining anharmonic terms is analysed in Sect. 9.6. The ionic anisotropy term is interesting because different methods must be used to diagonalise it, depending on its orientation relative to the magnetic field. When anisotropy conserves axial symmetry about the $\hat{\mathbf{z}}$ axis,

$$\begin{aligned} \mathcal{H}_a &= D\hbar^2 \sum_i (S_i^z)^2 \\ &= D\hbar^2 \sum_i \left[s - \frac{1}{N} \sum_{\mathbf{kk}'} \exp[-i(\mathbf{k} - \mathbf{k}') \cdot \mathbf{R}_i] a_{\mathbf{k}}^\dagger a_{\mathbf{k}'} \right]^2 \\ &= ND\hbar^2 s^2 - (2s + 1)D\hbar^2 \sum_{\mathbf{k}} a_{\mathbf{k}}^\dagger a_{\mathbf{k}} , \end{aligned} \quad (9.50)$$

where terms of order four have been neglected, as previously. For this axial symmetry, the total Hamiltonian $\mathcal{H} = \mathcal{H}_Z + \mathcal{H}_{\text{ex}} + \mathcal{H}_a$ is well represented by a set of harmonic oscillators of frequency $\omega_{\mathbf{k}}$,

$$\mathcal{H} = E_0 + \sum_{\mathbf{k}} \hbar \omega_{\mathbf{k}} a_{\mathbf{k}}^\dagger a_{\mathbf{k}} , \quad (9.51)$$

$$E_0 = -\mu H N s + D\hbar^2 N s^2 - NzJ\hbar^2 s^2 , \quad (9.52)$$

$$\omega_{\mathbf{k}} = \gamma H + D\hbar(2s + 1) + 2zJ\hbar s(1 - \eta_{\mathbf{k}}) . \quad (9.53)$$

The physical interpretation is then clear: low energy excitations above the ground state E_0 are spin waves of wave vector \mathbf{k} . They behave like elementary excitations (magnons) which are independent of one another. Each carries one unit \hbar of angular momentum. Operators $a_{\mathbf{k}}^\dagger$ and $a_{\mathbf{k}}$ increase and decrease their numbers by one unit. Such a description is only consistent if magnon lifetimes are long compared with their period $2\pi/\omega_{\mathbf{k}}$. The anharmonic terms we neglected in (9.51) play the role of diffusing magnons amongst each other. These processes determine their lifetime. It can be

shown that, at long wavelengths, the magnon lifetime τ_k is very long. In fact, $\hbar/\tau_k \approx \Gamma(ka)^4$, where $\Gamma = zJ\hbar^2a^2s/3$ is the spin stiffness constant [see (9.51)], in the Holstein–Primakoff approximation. In this long wavelength limit, magnons are just the hydrodynamic modes discussed in the last section. (In practice, Γ is renormalised by non-linear terms to give the stiffness constant Γ occurring in the hydrodynamic approach.) As the dispersion relation $\omega_k = \gamma H + D\hbar(2s+1) + \Gamma k^2$ is quadratic, we always have $\omega_k \tau_k \gg 1$, i.e., magnons are well defined modes. At short wavelengths, the magnon lifetimes induced by anharmonic terms become much shorter and the magnons are no longer well defined.

For an axial anisotropy, the magnon dispersion relation (9.53) exhibits an anisotropy gap $\Delta = D\hbar^2(2s+1)$, even in zero field. In fact, when $D > 0$, the anisotropy energy must be supplied in order to reduce $|S_z|$ by one unit.

A transverse anisotropy in the \hat{x} direction breaks rotational invariance about the \hat{z} axis. The ionic anisotropy term is then no longer diagonal. In fact,

$$\begin{aligned} S_i^x &= \frac{1}{2}(S_i^+ + S_i^-) \\ &= \sqrt{\frac{s}{2N}} \sum_{\mathbf{k}} \left[\exp(i\mathbf{k} \cdot \mathbf{R}_i) a_{\mathbf{k}} + \exp(-i\mathbf{k} \cdot \mathbf{R}_i) a_{\mathbf{k}}^\dagger \right]. \end{aligned} \quad (9.54)$$

The ionic anisotropy couples magnons whose wave vectors are \mathbf{k} and $-\mathbf{k}$, since

$$\mathcal{H}_a = \frac{D\hbar^2 s}{2N} \sum_i \left\{ \sum_{\mathbf{k}} \left[\exp(i\mathbf{k} \cdot \mathbf{R}_i) a_{\mathbf{k}} + \exp(-i\mathbf{k} \cdot \mathbf{R}_i) a_{\mathbf{k}}^\dagger \right] \right\}^2 \quad (9.55)$$

$$= \frac{ND\hbar^2 s}{2} + D\hbar^2 s \sum_{\mathbf{k}} a_{\mathbf{k}}^\dagger a_{\mathbf{k}} + \frac{D\hbar^2 s}{2} \sum_{\mathbf{k}} (a_{\mathbf{k}} a_{-\mathbf{k}} + a_{\mathbf{k}}^\dagger a_{-\mathbf{k}}^\dagger). \quad (9.56)$$

The total Hamiltonian is no longer diagonal in the Holstein–Primakoff magnon basis. It now takes the form

$$\mathcal{H} = E_0 + \sum_{\mathbf{k}} \left(\xi_{\mathbf{k}} a_{\mathbf{k}}^\dagger a_{\mathbf{k}} + \frac{\Delta_{\mathbf{k}}}{2} a_{\mathbf{k}} a_{-\mathbf{k}} + \frac{\Delta_{\mathbf{k}}^*}{2} a_{\mathbf{k}}^\dagger a_{-\mathbf{k}}^\dagger \right), \quad (9.57)$$

where E_0 , $\xi_{\mathbf{k}}$ and $\Delta_{\mathbf{k}}$ are given by

$$E_0 = -N\mu s H + \frac{ND\hbar^2 s}{2} - NzJ\hbar^2 s^2, \quad (9.58)$$

$$\xi_{\mathbf{k}} = \mu H + D\hbar^2 s + 2zJ\hbar^2 s(1 - \eta_{\mathbf{k}}), \quad (9.59)$$

$$\Delta_{\mathbf{k}} = D\hbar^2 s. \quad (9.60)$$

The $\Delta_{\mathbf{k}}$ are independent of \mathbf{k} here, because the ionic anisotropy is a point interaction, like the electron-phonon interaction which gives rise to superconductivity. When we introduce a long range interaction like the dipolar interaction, the Hamiltonian (9.57) has the same form, but the \mathbf{k} dependence

of energies $\xi_{\mathbf{k}}$ and $\Delta_{\mathbf{k}}$ is different [228]. This Hamiltonian can be diagonalised by a rotation in the magnon subspace $(\mathbf{k}, -\mathbf{k})$ [229, 231]. Indeed, the Hamiltonian (9.57) becomes in matrix form

$$\mathcal{H} = E_0 + \frac{1}{2} \sum_{\mathbf{k}} \left(X_{\mathbf{k}}^\dagger H_{\mathbf{k}} X_{\mathbf{k}} - \xi_{\mathbf{k}} \right), \quad (9.61)$$

where $H_{\mathbf{k}}$ is a 2×2 matrix and $X_{\mathbf{k}}$ a vector operator:

$$H_{\mathbf{k}} = \begin{pmatrix} \xi_{\mathbf{k}} & \Delta_{\mathbf{k}}^* \\ \Delta_{\mathbf{k}} & \xi_{\mathbf{k}} \end{pmatrix}, \quad X_{\mathbf{k}} = \begin{pmatrix} a_{\mathbf{k}} \\ a_{-\mathbf{k}}^\dagger \end{pmatrix}. \quad (9.62)$$

$H_{\mathbf{k}}$ cannot be diagonalised by a unitary transformation. We must preserve the commutation relations satisfied by operators $a_{\mathbf{k}}$, in order to describe harmonic oscillations. We therefore use a Bogoliubov transformation S such that $\sigma_z S \sigma_z S^\dagger = 1$. We have

$$[X_{\mathbf{k}}, X_{\mathbf{k}}^\dagger] = X_{\mathbf{k}} X_{\mathbf{k}}^{*\top} - (X_{\mathbf{k}}^* X_{\mathbf{k}}^\top)^\top = \begin{pmatrix} 1 & 0 \\ 0 & -1 \end{pmatrix} \equiv \sigma_z. \quad (9.63)$$

Denote by $c_{\mathbf{k}}$ the operators which diagonalise \mathcal{H} in (9.61), and define a vector operator, analogous to $X_{\mathbf{k}}$:

$$Y_{\mathbf{k}} = \begin{pmatrix} c_{\mathbf{k}} \\ c_{-\mathbf{k}}^\dagger \end{pmatrix}. \quad (9.64)$$

Let $S_{\mathbf{k}}$ be the Bogoliubov transformation such that $X_{\mathbf{k}} = S_{\mathbf{k}} Y_{\mathbf{k}}$,

$$a_{\mathbf{k}} = u_{\mathbf{k}} c_{\mathbf{k}} + v_{\mathbf{k}}^* c_{-\mathbf{k}}^\dagger, \quad (9.65)$$

$$a_{-\mathbf{k}}^\dagger = u_{-\mathbf{k}}^* c_{-\mathbf{k}}^\dagger + v_{-\mathbf{k}} c_{\mathbf{k}}. \quad (9.66)$$

In order to preserve the commutation relation (9.63), which amounts to $[c_{\mathbf{k}}, c_{\mathbf{k}}^\dagger] = 1$ or $[Y_{\mathbf{k}}, Y_{\mathbf{k}}^\dagger] = \sigma_z$, we find that S must satisfy

$$S \sigma_z S^\dagger = \sigma_z. \quad (9.67)$$

This in turn implies the condition

$$|u_{\mathbf{k}}|^2 - |v_{\mathbf{k}}|^2 = 1 \quad (9.68)$$

between $u_{\mathbf{k}}$ and $v_{\mathbf{k}}$, which can be interpreted as a hyperbolic rotation ($u_{\mathbf{k}} = \cosh \theta_{\mathbf{k}}$, $v_{\mathbf{k}} = \sinh \theta_{\mathbf{k}}$). Finally, to get the Hamiltonian into diagonal form, we must have $Y_{\mathbf{k}}^\dagger E_{\mathbf{k}} Y_{\mathbf{k}} = X_{\mathbf{k}}^\dagger H_{\mathbf{k}} X_{\mathbf{k}}$. In view of (9.67), this is equivalent to

$$H_{\mathbf{k}} S_{\mathbf{k}} = \sigma_z S_{\mathbf{k}} \sigma_z E_{\mathbf{k}}. \quad (9.69)$$

$E_{\mathbf{k}}$ is the ‘eigenvalue’ of $H_{\mathbf{k}}$. In terms of components $u_{\mathbf{k}}$ and $v_{\mathbf{k}}$, this homogeneous linear system of equations

$$\xi_{\mathbf{k}} u_{\mathbf{k}} + \Delta_{\mathbf{k}}^* v_{-\mathbf{k}} = E_{\mathbf{k}} u_{\mathbf{k}}, \quad (9.70)$$

$$\Delta_{\mathbf{k}} u_{\mathbf{k}} + \xi_{-\mathbf{k}} v_{-\mathbf{k}} = -E_{\mathbf{k}} v_{-\mathbf{k}}, \quad (9.71)$$

has a non-trivial solution only if the determinant is zero. This gives the dispersion relation for the magnons:

$$\begin{aligned} E_{\mathbf{k}} &= \sqrt{\xi_{\mathbf{k}}^2 - |\Delta_{\mathbf{k}}|^2} \\ &= \sqrt{(\mu H + \Gamma k^2)(\mu H + \Gamma k^2 + 2D\hbar^2 s)} . \end{aligned} \quad (9.72)$$

In the limit $k \rightarrow 0$, the resonant frequency $\gamma\sqrt{H(H + H_a)}$ increases with the anisotropy field $H_a = 2D\hbar^2 s/\mu$, and we can use this fact to determine its value. Magnons have no anisotropy gap in zero field ($\omega \rightarrow 0$), unlike the case for axial anisotropy. If $\phi_{\mathbf{k}}$ is the phase of $\Delta_{\mathbf{k}} = |\Delta_{\mathbf{k}}| \exp(i\phi_{\mathbf{k}})$, the matrix $S_{\mathbf{k}}$ becomes

$$S_{\mathbf{k}} = \begin{bmatrix} \sqrt{\frac{\xi_{\mathbf{k}} + E_{\mathbf{k}}}{2E_{\mathbf{k}}}} & -\sqrt{\frac{\xi_{\mathbf{k}} - E_{\mathbf{k}}}{2E_{\mathbf{k}}}} \exp(-i\phi_{\mathbf{k}}) \\ -\sqrt{\frac{\xi_{\mathbf{k}} - E_{\mathbf{k}}}{2E_{\mathbf{k}}}} \exp(i\phi_{\mathbf{k}}) & \sqrt{\frac{\xi_{\mathbf{k}} + E_{\mathbf{k}}}{2E_{\mathbf{k}}}} \end{bmatrix} . \quad (9.73)$$

The Hamiltonian (9.57) is a sum of independent harmonic oscillators,

$$\mathcal{H} = E'_0 + \sum_{\mathbf{k}} E_{\mathbf{k}} c_{\mathbf{k}}^\dagger c_{\mathbf{k}} , \quad (9.74)$$

where $E'_0 = E_0 + (1/2) \sum_{\mathbf{k}} (E_{\mathbf{k}} - \xi_{\mathbf{k}})$. The corresponding normal modes are linear combinations of magnons propagating in opposite directions. We can form an intuitive idea of these modes by considering the limit $k = 0$, and drawing the precession of a unit vector parallel to the spins (classical limit). We find that this vector follows an elliptical path whose eccentricity depends on the ratio $D\hbar^2 s/\mu H$ between ionic anisotropy and external field (see Fig. 8.4).

In the BCS theory of superconductivity, the Bogoliubov transformation is used to diagonalise the attractive interaction between two electrons propagating in opposite directions. The only difference is that the matrix S is then unitary, since electrons are fermions.

9.3 Dipolar Interactions and Magnetostatic Modes

In the last section, we only considered short range interactions, i.e., exchange and ionic anisotropy. In this case, spin-wave frequencies tend, in the limit $k \rightarrow 0$, to the precession frequency of the uniform magnetisation, given by the Bloch equation

$$\frac{\partial \tilde{\sigma}(\mathbf{r}, t)}{\partial t} = \frac{\partial \langle \tilde{S} \rangle}{\partial t} = -\frac{i}{\hbar} \left\langle [\tilde{S}, \mathcal{H}] \right\rangle \approx \gamma \tilde{\sigma}(\mathbf{r}, t) \times \tilde{H}(\tilde{r}, t) . \quad (9.75)$$

The dipolar interaction, behaving as $1/r^3$, does not decrease sufficiently quickly to make the total dipolar energy independent of sample shape, since

$\int_V d^3r/r^3$ is of order 1. When the mode wavelength $\lambda = 2\pi/k$ becomes comparable with the size of the sample, we must take into account boundary conditions on the electromagnetic field at the surface of the sample (the component of $\tilde{b}(\mathbf{r}, \omega)$ normal to the surface and the tangential component of $\tilde{h}(\mathbf{r}, \omega)$ must both be continuous). These induce magnetic surface charges $\tilde{m}(\mathbf{r}, \omega)$ oscillating at the same frequency ω . This electromagnetic field then reacts upon spins, whose precession modes become more complex. The dynamical equation of the spins, i.e., the Bloch equation, must be solved simultaneously with Maxwell's equations for the electromagnetic field. The resulting normal modes are known as *magnetostatic modes* (or Walker modes [232, 233]) and are the true normal modes of the system at long wavelengths.

As an example, we shall study the magnetostatic modes of a vertical cylinder whose diameter a is small compared with its length. We express the magnetisation in terms of its transverse fluctuations $\tilde{m}(\mathbf{r}) \exp(-i\omega t)$ and its equilibrium value $M_0 \hat{\mathbf{z}}$, and likewise for fluctuations $\tilde{h}(\mathbf{r}, t)$ in the magnetic field around H_0 ,

$$\tilde{M}(\mathbf{r}, t) = \tilde{M}_0 + \tilde{m}(\mathbf{r}) \exp(-i\omega t), \quad (9.76)$$

$$\tilde{H}(\mathbf{r}, t) = \tilde{H}_0 + \tilde{h}(\mathbf{r}) \exp(-i\omega t). \quad (9.77)$$

We seek stationary solutions satisfying the linearised Bloch equation (9.75),

$$i\frac{\omega}{\gamma} m_x(\mathbf{r}) = m_y(\mathbf{r}) H_0 - M_0 h_y(\mathbf{r}), \quad (9.78)$$

$$i\frac{\omega}{\gamma} m_y(\mathbf{r}) = -m_x(\mathbf{r}) H_0 + M_0 h_x(\mathbf{r}). \quad (9.79)$$

We define two circular polarisations \pm of the field and magnetisation by

$$m^\pm = m_x \pm im_y, \quad h^\pm = h_x \pm ih_y. \quad (9.80)$$

The corresponding dynamic susceptibilities, given by $m^\pm = \chi^\pm h^\pm$, and hence

$$\chi^\pm = \frac{\gamma M_0}{\omega \pm \gamma H_0}, \quad (9.81)$$

are diagonal [see (9.78) and (9.79)]. Near the resonance $\omega \approx \gamma H_0$, χ^+ becomes negligible compared with χ^- . Moreover, the magnetic field \mathbf{h} and induction \mathbf{b} must satisfy Maxwell's equations

$$\begin{aligned} \frac{1}{\mu_0} \nabla \cdot \mathbf{b} &= \nabla \cdot (\mathbf{h} + \mathbf{m}) \\ &= \frac{\partial h_z}{\partial z} + [1 + \kappa(\omega)] \left[\frac{\partial h_x}{\partial x} + \frac{\partial h_y}{\partial y} \right] = 0, \\ \nabla \times \mathbf{h} &= 0, \end{aligned} \quad (9.82)$$

where $\kappa(\omega) \approx \chi^-/2$. In order to determine normal modes, we introduce the magnetic scalar potential

$$\mathbf{h} = -\nabla\phi, \quad (9.83)$$

thereby reducing (9.82) to a scalar equation,

$$-\frac{\partial^2 \phi}{\partial z^2} = [1 + \kappa(\omega)] \nabla_{\perp}^2 \phi, \quad (9.84)$$

where

$$\nabla_{\perp}^2 = \frac{\partial^2}{\partial x^2} + \frac{\partial^2}{\partial y^2} = \frac{\partial^2}{\partial \rho^2} + \frac{1}{\rho} \frac{\partial}{\partial \rho} + \frac{1}{\rho^2} \frac{\partial^2}{\partial \theta^2}, \quad (9.85)$$

and ρ, θ, z are cylindrical coordinates for \mathbf{r} . The two circular polarisations are given in terms of their components in cylindrical coordinates by

$$h^{\pm} = (h_{\rho} \pm i h_{\theta}) \exp(\pm i\theta), \quad m^{\pm} = (m_{\rho} \pm i m_{\theta}) \exp(\pm i\theta). \quad (9.86)$$

We begin by looking for modes propagating along the cylinder axis, such that the magnetisation $m^-(\rho, \theta, z)$ and the field $h^-(\rho, \theta, z)$ are independent of θ . The magnetic potential ϕ must then take the form

$$\phi = \exp(i(kz + \theta)) f(\rho), \quad (9.87)$$

in such a way that

$$m^- = \kappa(\omega) h^- = -\kappa(\omega) \left(\frac{\partial f}{\partial \rho} + \frac{f}{\rho} \right) \exp(ikz). \quad (9.88)$$

Continuity of the tangential component (h_{θ}, h_z) of \tilde{h} at the surface of the cylinder requires continuity of both ϕ and b_{ρ} , and also continuity of $\partial\phi/\partial\rho + \kappa(\partial\phi/\partial\rho + \phi/\rho)$ with $\kappa = 0$ outside the cylinder. When $1 + \kappa > 0$, equivalent to $\omega > \gamma(H + M_0/2)$, solutions f of radial equation (9.84) are modified Bessel functions and are physically unacceptable because $f \rightarrow \infty$ when $\rho \rightarrow 0, \infty$. Hence, there can only be propagating modes when $1 + \kappa < 0$. Near the Larmor frequency, $\kappa \rightarrow -\infty$, the boundary condition at $\rho = 0$ becomes simply $df/d\rho + f/\rho = 0$. The solutions of (9.84) satisfying this boundary condition are then

$$\phi = \exp(i(kz + \theta)) J_1(\lambda_n \rho), \quad h^- = -\exp(ikz) J_0(\lambda_n \rho), \quad (9.89)$$

where the λ_n are determined by the condition $J_1(\lambda_n a) = 0$. Bearing in mind that ϕ is a solution of the Helmholtz equation,

$$\nabla_{\perp}^2 J_1(\lambda_n \rho) \exp(i\theta) = -J_1(\lambda_n \rho) \exp(i\theta)/\lambda_n^2,$$

frequencies of magnetostatic modes are determined by the condition $\kappa(\omega_n) = -k^2/\lambda_n^2$ [see (9.84)]. This implies

$$\omega_n = \gamma \left(H_0 + \frac{M_0}{2} \frac{\lambda_n^2}{k^2} \right). \quad (9.90)$$

This $1/k^2$ behaviour of magnetostatic modes can be contrasted with the Γk^2 dispersion of spin waves. We see why magnetostatic modes are only significant for long wavelengths. They are also very sensitive to slowly varying ‘potentials’ over the sample, produced by a magnetic field gradient, for example.

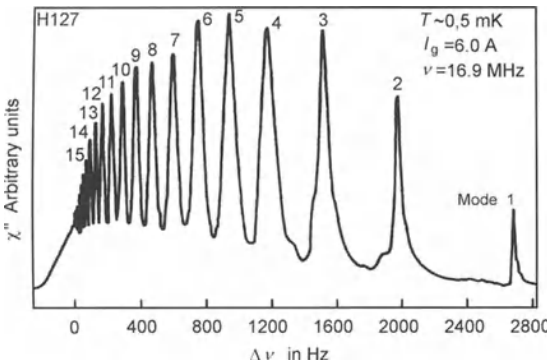


Fig. 9.3. Spectrum of magnetostatic modes in a cylindrical crystal of solid helium 3, in the presence of a small field gradient which localises modes spatially. From Osheroff and Cross [234]

Figure 9.3 illustrates the spectrum of magnetostatic modes in the presence of such a gradient [234]. For larger values of k , boundary conditions on \mathbf{h} and \mathbf{b} no longer influence spin dynamics. In this case, the Bloch equation alone controls collective spin modes. It is then sufficient to carry out the procedure described in the last section to diagonalise the dipolar Hamiltonian by a Bogoliubov transformation. We obtain the spin-wave dispersion relation which now depends on the direction of propagation of the spin wave relative to the magnetic field.

9.4 Magnon Thermodynamics

At low enough temperatures, few magnons are thermally excited and their non-linear interactions can be neglected. Magnons are then pure harmonic oscillator modes satisfying Bose–Einstein statistics. At temperature T , $\langle n_{\mathbf{k}} \rangle$ magnons of wave vector \mathbf{k} and frequency $\omega_{\mathbf{k}}$ are excited, where

$$\langle n_{\mathbf{k}} \rangle = \langle a_{\mathbf{k}}^\dagger a_{\mathbf{k}} \rangle = \frac{1}{\exp(\hbar\omega_{\mathbf{k}}/k_B T) - 1} . \quad (9.91)$$

These hydrodynamic modes can affect the thermodynamic properties of ferromagnets. The magnetisation per unit volume is reduced:

$$\begin{aligned} M(T) &= \frac{g\mu_B}{V} \sum_i \langle S_i^z \rangle = \frac{g\mu_B}{V} \sum_i (-S + \langle n_i \rangle) \\ &= M(0) + \frac{g\mu_B}{V} \sum_{\mathbf{k}} \langle n_{\mathbf{k}} \rangle . \end{aligned} \quad (9.92)$$

The $n_{\mathbf{k}}$ are introduced by Fourier transforming the a_i . If ionic anisotropy and magnetic field are negligible, the energy of magnons in a cubic crystal is, in the long wavelength limit (9.53),

$$\hbar\omega_{\mathbf{k}} = \frac{J\hbar^2 z s a^2}{d} k^2 = \Gamma k^2 , \quad (9.93)$$

where $d = 1, 2, 3, \dots$ is the space dimension. In these conditions, the drop in magnetisation is given by the total density of excited magnons,

$$M(0) - M(T) = \frac{g\mu_B}{V} \frac{\Omega V}{(2\pi)^d} \int_0^\infty \frac{k^{d-1} dk}{\exp(\Gamma k^2/k_B T) - 1} , \quad (9.94)$$

where $\Omega = 2\pi, 4\pi, \dots$ is the total solid angle in d dimensions. After change of variable, this suppression of magnetisation by hydrodynamic fluctuations reduces to

$$M(0) - M(T) = \frac{g\mu_B \Omega}{2(2\pi)^d} \int_0^\infty \left(\frac{k_B T}{\Gamma} \right)^{d/2} I_d , \quad (9.95)$$

where

$$I_d = \int_0^\infty \frac{x^{d/2-1} dx}{\exp x - 1} . \quad (9.96)$$

In one and two dimensions, the integral I_d diverges for small values of x , going as $1/x$ in one dimension and $\ln x$ in two dimensions. The divergent contribution comes from magnons of long wavelength and small energies $\hbar\omega_{\mathbf{k}}$. In physical terms, spins are not sufficiently rigid at long wavelengths to maintain any long range order in one and two dimensions. In one dimension, it can be checked that even at $T = 0$, the system is not ordered. This is due to long wavelength quantum fluctuations which are sufficient to destroy ferromagnetism. (In two dimensions, correlation functions decrease according to a power law at $T = 0$ [see Chap. 7(I)], indicating a quasi-order over large distances.) We will examine low energy excitations in highly quantum systems in Chap. 10(I).

In three dimensions, $I_3 = \sqrt{\pi}/2 \zeta(3/2)$, where the zeta function takes the value $\zeta(3/2) \approx 2.37$ and

$$M(T) - M(0) \approx \zeta(3/2) g\mu_B \left(\frac{k_B T}{4\pi\Gamma} \right)^{3/2} . \quad (9.97)$$

This is Bloch's $T^{3/2}$ law [235]. In mean field theory, the only thermodynamic excitations retained are individual spin reversals in their molecular field h_m . They contribute an exponential behaviour to $M(T) - M(0)$ at low temperatures. In this limit, hydrodynamic fluctuations make a much more significant contribution to the thermodynamics than excitations associated with reversal of a single spin. Quite generally, the partition function of a boson gas is obtained by summing over all states:

$$Z = 1 + e^{-x} + e^{-2x} + \dots + e^{-nx} + \dots = \frac{1}{1 - e^{-x}} , \quad (9.98)$$

and the free energy is therefore

$$F = \frac{1}{\beta} \sum_{\mathbf{k}} \ln [1 - \exp(-\hbar\omega_{\mathbf{k}}/k_B T)] . \quad (9.99)$$

The internal energy $U = \partial(\beta F)/\partial\beta$ and specific heat $C = \partial U/\partial T$ are then given by

$$U = \sum_{\mathbf{k}} \hbar\omega_{\mathbf{k}} n_{\mathbf{k}}, \quad C = k_B \sum_{\mathbf{k}} \frac{x^2}{4 \sinh^2 x}, \quad (9.100)$$

where $x = \hbar\omega_{\mathbf{k}}/k_B T$. At low temperatures, the specific heat also varies as $T^{3/2}$,

$$C_H = \frac{15k_B}{4} \zeta(5/2) \left(\frac{k_B T}{4\pi\Gamma} \right)^{3/2}, \quad (9.101)$$

where $\zeta(5/2) \approx 1.34$. If we wish to determine the specific heat at higher temperatures, we must take into account all non-linear terms in the expansion of s in terms of a and a^\dagger . In practice, beyond the domain of validity of the spin-wave approximation, the mean field approximation discussed in Chap. 5(I) is the only reasonable alternative, except in one dimension [see Chap. 10(I)].

9.5 Non-Linear Terms

In Sect. 9.2, the spin Hamiltonian (9.26) was reduced by neglecting, among other things, the 4-magnon interaction terms

$$a_{\mathbf{k}}^\dagger a_{\mathbf{q}}^\dagger a_{\mathbf{k}} a_{\mathbf{q}} \delta(\mathbf{k} + \mathbf{q} - \mathbf{k}' - \mathbf{q}').$$

These can be interpreted as a scattering of two magnons initially in states \mathbf{k} and \mathbf{q} into two magnons in states \mathbf{k}' and \mathbf{q}' . Because of these interaction terms, magnons are not exactly normal modes of the system, even at zero temperature [236].

More precisely, the dominant order 4 contributions are those of the exchange Hamiltonian. An approximate treatment can be made by keeping only biquadratic terms among the quartic terms. We neglect terms which cannot be factorised into terms of type $a_{\mathbf{k}}^\dagger a_{\mathbf{k}}$. This is the *random phase approximation*, based on the idea that magnons of different wave vector are not coherent. It is not always a very satisfactory hypothesis. In the presence of transverse anisotropy, there is coherent coupling between the \mathbf{k} and $-\mathbf{k}$ states, and non-linear terms can in certain cases give rise to magnon bound states. The random phase approximation nevertheless allows us to estimate the frequency shift induced by the other magnons. In this approximation,

$$\mathcal{H}_{\text{ex}}^{(4)} = -\frac{Jz}{N} \sum_{\mathbf{k}\mathbf{q}} (1 + \eta_{\mathbf{k}-\mathbf{q}} - \eta_{\mathbf{k}} - \eta_{\mathbf{q}}) a_{\mathbf{k}}^\dagger a_{\mathbf{k}} a_{\mathbf{q}}^\dagger a_{\mathbf{q}} . \quad (9.102)$$

This biquadratic Hamiltonian can be reduced to an effective harmonic Hamiltonian by averaging over thermal populations of $a_{\mathbf{k}}^\dagger a_{\mathbf{k}}$ and $a_{\mathbf{q}}^\dagger a_{\mathbf{q}}$. The effective

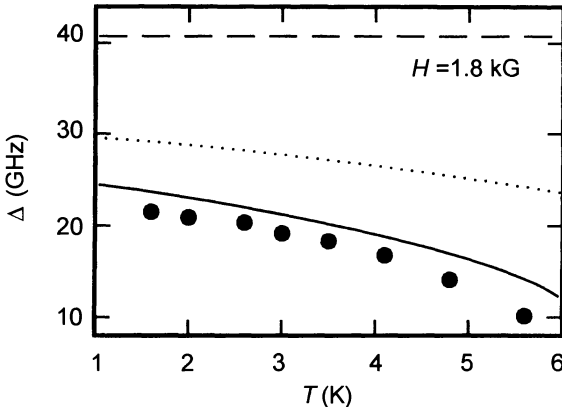


Fig. 9.4. Magnetisation of CsNiF_3 , a quasi-1-dimensional ferromagnet, as a function of temperature. The *dotted curve* takes into account fourth order terms in the exchange Hamiltonian, weighted by the magnon thermal population. The *continuous curve* also includes non-linear excitations (solitons), described in Chap. 10(I)

Hamiltonian is obtained by expanding the $\eta_{\mathbf{k}}$ to fourth order and averaging over angles:

$$H_{\text{eff}} = \sum_{\mathbf{k}} \hbar \omega_{\mathbf{k}}(T) a_{\mathbf{k}}^\dagger a_{\mathbf{k}} , \quad (9.103)$$

$$\frac{\omega_{\mathbf{k}}(T)}{\omega_{\mathbf{k}}} = \mathcal{R} = 1 - \frac{1}{zN} \sum_{\mathbf{q}} \frac{\omega_{\mathbf{q}}}{J\hbar s^2} \langle n_{\mathbf{q}} \rangle . \quad (9.104)$$

The factor \mathcal{R} can be interpreted as a renormalisation of the spin stiffness constant $\Gamma \rightarrow \mathcal{R}\Gamma$. The stiffness constant is reduced at high temperatures. Thermodynamic properties are altered and there are deviations from Bloch's law (see Fig. 9.4) [237]. The frequency shift of the collective modes with temperature is easily observed, either by electron resonance, or by scattering neutrons on thermally excited magnons.

9.6 Spin-Wave Spectroscopy

How can spin waves be excited at $T = 0$? If we apply a spatially inhomogeneous electromagnetic field $\tilde{h}(\mathbf{r}, t) = \tilde{h}_0 \cos(\mathbf{q} \cdot \mathbf{r} - \omega t)$, where \tilde{h}_0 is perpendicular to the equilibrium magnetisation, the Zeeman Hamiltonian for the interaction between this field and the spins is

$$\mathcal{H}_{\text{Z}} = \frac{g_S}{2} \mu_B [S^+(\mathbf{q}) h^-(\mathbf{q}) + S^-(\mathbf{q}) h^+(\mathbf{q})] , \quad (9.105)$$

where $S^+(\mathbf{q}) = \sqrt{2s} a_{\mathbf{q}}^\dagger$ and $h^\pm(\mathbf{q}) = h_0 \exp(\mp i\omega t)/2$. There is a couple $\tilde{M}_0 \times \tilde{h}$ on the magnetisation and a component of magnetisation appears transverse

to M_0 , spatially modulated by the wave vector \mathbf{q} . This magnetisation $\tilde{m}(\mathbf{q})$ oscillates at the frequency of the inhomogeneous magnetic field \tilde{h} . When this frequency coincides with the frequency $\omega_{\mathbf{q}}$ of the spin wave with the same wave vector, resonance occurs. We can therefore carry out spectroscopy of spin waves by resonance. The response $m(\mathbf{q})$ can be quantified by finding the transverse susceptibility

$$\chi_{+-}(\mathbf{q}, \omega) \approx 2\chi_{xx}(\mathbf{q}, \omega) = 2\chi_{yy}(\mathbf{q}, \omega).$$

The equation of motion of $\langle a_{\mathbf{q}}^\dagger \exp(i\omega t) \rangle$ is

$$\begin{aligned} i\hbar \times (i\omega) \langle a_{\mathbf{q}}^\dagger \rangle &= \langle [a_{\mathbf{q}}^\dagger, \mathcal{H} + \mathcal{H}_Z] \rangle \\ &= -\hbar\omega_{\mathbf{q}} \langle a_{\mathbf{q}}^\dagger \rangle - \frac{gs\mu_B h_0}{2} \sqrt{2s}, \end{aligned} \quad (9.106)$$

where \mathcal{H} is the spin-wave Hamiltonian (9.51). We deduce the transverse susceptibilities, such that $\langle S^+ \rangle = \chi_{+-} h^-$,

$$\begin{aligned} \chi_{+-}(\mathbf{q}, \omega) &= \frac{g_s s \gamma}{(\omega - \omega_{\mathbf{q}}) + i\gamma_{\mathbf{q}}/2}, \\ \chi_{-+}(\mathbf{q}, \omega) &= -\frac{g_s s \gamma}{(\omega + \omega_{\mathbf{q}}) + i\gamma_{\mathbf{q}}/2}. \end{aligned} \quad (9.107)$$

Spin-wave modes are given by the poles of the transverse susceptibility. The magnon lifetime $\tau_{\mathbf{q}} = 1/\gamma_{\mathbf{q}} \propto 1/\Gamma q^4$ has been put into (9.107) phenomenologically. This relation expresses the elementary nature of spin waves: the system responds exclusively at frequency $\omega_{\mathbf{q}}$ when excited by a wave vector \mathbf{q} . Finally, we observe that the susceptibility is related to correlation functions at equilibrium by the fluctuation-dissipation theorem [see Chap. 8(I)]. The susceptibility (9.107) therefore also determines transverse correlation functions,

$$\begin{aligned} \langle S^+(\mathbf{q}, \omega) S^-(-\mathbf{q}) \rangle &= \hbar N \coth(\beta\hbar\omega/2) \chi''_{+-}(\mathbf{q}, \omega) \\ &= g_s s \mu_B N \coth(\beta\hbar\omega/2) \frac{\gamma_{\mathbf{q}}/2}{(\omega - \omega_{\mathbf{q}})^2 + \gamma_{\mathbf{q}}^2/4}. \end{aligned} \quad (9.108)$$

From these, we can in turn extract spatio-temporal correlation functions by Fourier transform. Consequently, measurements of dynamic susceptibilities contain invaluable information: they determine all spatio-temporal correlation functions at equilibrium.

9.7 Parallel Pumping

Spin waves of arbitrary wave vector can be generated through parametric excitation by a magnetic field oscillating in the direction parallel to the equilibrium magnetisation. This excitation method is non-linear. Indeed, the Zeeman Hamiltonian associated with a spatially uniform field oscillating in the z direction is

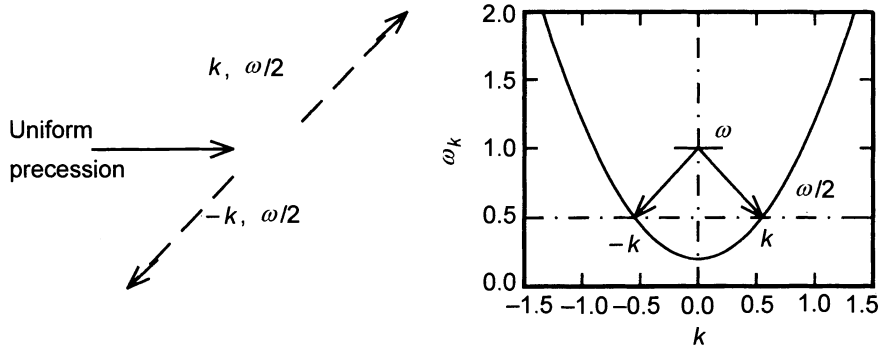


Fig. 9.5. Parametric pumping of magnon pairs by a spatially uniform oscillating field

$$\mathcal{H}_{\parallel} = -g_S \mu_B h_z \cos \omega t \sum_{\mathbf{k}} a_{\mathbf{k}}^\dagger a_{\mathbf{k}} . \quad (9.109)$$

But when there is transverse anisotropy or dipolar interactions, the $a_{\mathbf{k}}$ are no longer normal modes of the system. We can nevertheless find the new normal modes by diagonalisation in the $c_{\mathbf{k}}$ basis. Expressing the $a_{\mathbf{k}}$ in terms of the $c_{\mathbf{k}}$, the Hamiltonian describing parametric excitation parallel to the magnetisation is

$$\begin{aligned} \mathcal{H}_{\parallel} = & -g_S \mu_B h_z \cos \omega t \\ & \times \sum_{\mathbf{k}} \left(|u_{\mathbf{k}}|^2 c_{\mathbf{k}}^\dagger c_{\mathbf{k}} + |v_{\mathbf{k}}|^2 c_{-\mathbf{k}} c_{-\mathbf{k}}^\dagger + u_{\mathbf{k}} v_{\mathbf{k}} c_{-\mathbf{k}} c_{\mathbf{k}} + u_{\mathbf{k}}^* v_{\mathbf{k}}^* c_{\mathbf{k}}^\dagger c_{-\mathbf{k}} \right) . \end{aligned} \quad (9.110)$$

The last term describes the creation of two magnons propagating in opposite directions, as shown in Fig. 9.5. This is parallel pumping of transverse magnons by a longitudinal field. We can visualise the coupling by considering the precession of the magnetisation which, in the presence of transverse anisotropy, is elliptical rather than circular. The component m_z of the magnetisation is no longer constant in time, but oscillates at twice the transverse precession frequency. A longitudinal magnetic field couples to this longitudinal magnetisation and, if the excitation frequency equals twice the precession frequency, resonance occurs. All magnons whose frequencies $\omega_{\mathbf{k}}$ satisfy

$$\omega_{\mathbf{k}} = \frac{\omega}{2} \quad (9.111)$$

can thereby be excited.

9.8 Other Representations

The magnons considered above correspond to modes linearised around the ferromagnetic ground state. In 1- and 2-dimensional systems, there is no

long range order, and we cannot define linearised modes around a disordered state. J. Villain has shown that we can nevertheless define spin-wave modes, provided their wavelength remains shorter than the correlation length [238]. The method was conceived for systems with planar anisotropy, causing spins to line up in a plane. Spin operators are represented in terms of S_z and an angle operator Φ ,

$$S_i^+ = \exp(i\phi_i) \sqrt{S(S+1) - S_i^z(S_i^z + 1)}, \quad (9.112)$$

with commutation relations

$$[\Phi_i, S_j^z] = i\hbar\delta_{ij}. \quad (9.113)$$

In the semi-classical limit, S^+ and S_z are components of \mathbf{S} in the (x, y) plane and along \hat{z} . Note that Φ and S_z are conjugate canonical variables, like position x and momentum p_x in quantum mechanics. They therefore satisfy an uncertainty relation $\delta\Phi \times \delta S_z \approx 1$. For this reason we cannot maintain S entirely within the (x, y) plane without delocalising the angular variable and this explains why the exchange interaction is not always sufficient to localise spin variables in low-dimensional systems. We can nevertheless define local excitations analogous to spin waves by expanding the square root in (9.112) in the semi-classical limit (large S). The main difference with Holstein–Primakoff magnons is that Φ and S_z are the quantised variables, rather than deviations from the ground state.

Another useful representation is provided by the Schwinger bosons [239]. Boson operators a and b are defined in terms of spin operators by

$$S^z = a^\dagger a - b^\dagger b, \quad S^+ = a^\dagger b, \quad S^- = ab^\dagger, \quad (9.114)$$

where boson occupation numbers $n_a = a^\dagger a$ and $n_b = b^\dagger b$ must satisfy

$$n_a + n_b = 2s. \quad (9.115)$$

The condition (9.115) clearly contains all spinor physics. The spin-wave approximation consists in neglecting this constraint. An intermediate approximation is obtained by introducing a potential into the Hamiltonian via a Lagrange multiplier, in such a way that the energy minimum occurs when the constraint (9.115) is satisfied. The norm of the spin is then only equal to s on average, which amounts to saying that spins are ‘soft’ [240].

9.9 Hydrodynamic Methods

The Holstein–Primakoff transformation can be generalised to simple antiferromagnets and ferrimagnets (see Exercise C.1.4, Appendix C). In the case of more complex magnets, such as antiferromagnets with non-collinear sublattices or helimagnets, the complexity of the order parameter makes it difficult to quantise deviations of spins from the ground state. We must then resort

to a hydrodynamic description (see Sect. 9.1) which, although phenomenological, is very general, being based upon conservation laws and symmetries of the system [241].

This approach makes use of the following properties. A deviation from equilibrium involving most of the degrees of freedom of a system made up of a very large number of particles relaxes towards local equilibrium in a microscopic relaxation time τ_c . However, certain hydrodynamic macroscopic variables relax much more slowly. This may be due to conservation laws, consequences of symmetries of the microscopic Hamiltonian, or it may be due to long range order. The thermodynamic state of a system breaking a continuous symmetry must be characterised by a new hydrodynamic variable. Intuitively, conserved variables relax slowly because conservation laws forbid local relaxation. They must be ‘transported’ over distances comparable with the characteristic wavelength of the deviation from equilibrium. We would therefore expect the relaxation time to be longer if the characteristic wavelengths are themselves longer. We have also seen that variations in the long wavelengths transverse to the direction breaking the symmetry (the *easy* direction of the magnet) relax slowly because restoring forces become infinitesimal when the wavelength tends to infinity.

Hydrodynamics provides a description of the dynamics of conserved variables of long wavelengths and low frequency ω , when all other degrees of freedom reach local equilibrium in a time $\tau \ll \omega^{-1}$. Hydrodynamic equations assume in addition that:

- deviations from equilibrium can be expanded in powers of spatial gradients;
- forces tending to restore equilibrium are linear in the deviations.

Hydrodynamic Modes of Complex Magnets

Energy and spin density are conserved variables, even in the absence of broken symmetry. They are always hydrodynamic variables. When there is a broken symmetry, other hydrodynamic variables may appear, depending on the nature of the order parameter. This is not so in ferromagnets because the order parameter, the spin density, is already a conserved variable. However, in antiferromagnets, the order parameter is alternating spin density $\tilde{n}(\mathbf{r}, t)$. Fluctuations transverse to this parameter are then new hydrodynamic variables. In general, two angles θ_1 and θ_2 are needed to specify the orientation of $\tilde{n}(\mathbf{r})$ relative to its equilibrium position. For a non-collinear order parameter (e.g., helimagnet, antiferromagnet with non-collinear sublattices), three angles $\theta_1, \theta_2, \theta_3 \equiv \tilde{\theta}$ are required to specify an arbitrary rotation of the order parameter.

In order to determine the local thermodynamic equilibrium of variables $\tilde{\sigma}$ and $\tilde{\theta}$, we use an effective magnetic field which gives the local spin density via the susceptibility,

$$\gamma\sigma_\alpha = \chi^{\alpha\beta} h_\beta , \quad \text{or} \quad h^\alpha = [\chi^{-1}]_{\alpha\beta} \gamma\sigma^\beta . \quad (9.116)$$

We assume χ is diagonal in the chosen basis. With regard to thermodynamic fields $\tilde{\phi}$ conjugate to the angles $\tilde{\theta}$ which specify the local orientation of the order parameter, we identify two cases. If there is no magnetic anisotropy, uniform rotation of the order parameter involves no energy transfer and thermodynamic fields ϕ are conjugate to gradients of angles $\tilde{\theta}$ [242],

$$\phi_\alpha = \Gamma^\alpha \nabla \theta_\alpha . \quad (9.117)$$

We have also assumed that the stiffness tensor Γ is diagonal. In such conditions, we can integrate the differential of the local internal energy,

$$d\varepsilon = \delta Q + \delta W = T ds + \sum_\alpha \gamma h_\alpha d\sigma_\alpha + \phi_\alpha \cdot d(\nabla \theta_\alpha) , \quad (9.118)$$

giving the change in free energy ΔF at constant temperature

$$\Delta F = d\varepsilon - T ds = \frac{1}{2} \int d^3r \left[\frac{(\gamma \sigma_\alpha)^2}{\chi_\alpha} + \Gamma^\alpha |\nabla \theta_\alpha|^2 \right] . \quad (9.119)$$

If there is in addition an anisotropy energy associated with uniform rotation of the order parameter, we must add to (9.119) the relevant free energy of anisotropy $F_a(\theta)$ for the system under consideration [243]. Likewise for the Zeeman energy $-\gamma \tilde{\sigma} \cdot \tilde{H}$ in a magnetic field. The dynamical equations satisfied by $\tilde{\sigma}$ and $\tilde{\theta}$ can be obtained either from the Schrödinger equation, or more simply by writing the classical equation of motion of $\tilde{\sigma}$ and $\tilde{\theta}$ in terms of Poisson brackets [see (9.19) and (9.20)],

$$\frac{\partial \tilde{\sigma}}{\partial t} = [\tilde{\sigma}, \Delta F]_{\text{pb}} , \quad \frac{\partial \tilde{\theta}}{\partial t} = [\tilde{\theta}, \Delta F]_{\text{pb}} , \quad (9.120)$$

and using the angular momentum algebra of the classical variables $\tilde{\sigma}$ and $L_\alpha \equiv \partial/\partial \theta_\alpha$,

$$[\sigma_\alpha(\mathbf{r}), \sigma_\beta(\mathbf{r}')]_{\text{pb}} = \varepsilon_{\alpha\beta\gamma} \sigma_\gamma(\mathbf{r}) \delta(\mathbf{r} - \mathbf{r}') , \quad (9.121)$$

$$\left[\sigma_\alpha(\mathbf{r}), \frac{\partial}{\partial \theta_\beta(\mathbf{r}')} \right]_{\text{pb}} = \frac{\partial}{\partial \theta_\alpha(\mathbf{r}')} \delta_{\alpha\beta} \delta(\mathbf{r} - \mathbf{r}') . \quad (9.122)$$

$\tilde{\sigma}$ and \tilde{L} are indeed the generators of the group of rotations in 3-dimensional space, in perfect analogy with the situation in quantum mechanics. The dynamical equations are now

$$\frac{\partial \tilde{\sigma}}{\partial t} = \gamma \left[\tilde{\sigma} \times (\tilde{h}_\sigma + \tilde{H}) \right] + \nabla \cdot (\Gamma \nabla \theta) + \frac{\partial F_a}{\partial \tilde{\theta}} , \quad (9.123)$$

$$\frac{\partial \tilde{\theta}}{\partial t} = \frac{\partial F}{\partial \tilde{\sigma}} , \quad (9.124)$$

where $h_\sigma^\alpha = \chi_\alpha^{-1} \gamma \sigma^\alpha$. These equations can be linearised and after Fourier transform we obtain

$$\frac{\partial \delta\tilde{\sigma}}{\partial t} = \gamma \left(\tilde{\sigma} \times \delta\tilde{h}_\sigma - \tilde{H} \times \delta\tilde{\sigma} \right) + (\Lambda + \Gamma k^2) \delta\tilde{\theta}, \quad (9.125)$$

$$\frac{\partial \delta\tilde{\theta}}{\partial t} = \frac{\gamma^2}{\chi} \delta\tilde{\sigma}. \quad (9.126)$$

The matrix Λ depends on the anisotropy in the system and may not be symmetric. As an example, we consider a helimagnet [see Sect. 5.5(I)] in zero field and with negligible ionic anisotropy. Susceptibility and spin stiffness tensors reflect the anisotropy of the structure. In a helimagnet we have $\chi_1 = \chi_2 \neq \chi_3$, and the Γ_α^i are equal for $i, \alpha = 1, 2$. The above equations give three hydrodynamic modes corresponding to the three different polarisations of spin waves. Dispersion relations are linear in k ,

$$\omega_\alpha = c_\alpha k, \quad (9.127)$$

where

$$c_\alpha = \frac{\gamma}{\sqrt{\chi_\alpha}} \left(\sum_i \frac{\Gamma_\alpha^i k_i^2}{k^2} \right)^{1/2}. \quad (9.128)$$

Speeds c_α of spin waves are anisotropic. These linear dispersion relations should be contrasted with the quadratic behaviour in ferromagnets. Indeed, the order parameter of a ferromagnet, magnetisation, is a conserved quantity, and this is no longer the case here. Magnetisation and fluctuations transverse to the order parameter are distinct hydrodynamic variables here, with coupled dynamics which leads to this linear dispersion. The dispersion relation (9.128) can be applied to antiferromagnets, in which the susceptibility and spin stiffness constant are isotropic. Indeed, we determined the susceptibility of an antiferromagnet of spins s in Chap. 5(I) [see (5.50)]: $\chi = C_s/2T_N$, where $C_s \approx (\gamma\hbar^2)s(s+1)/3k_B$ is the Curie constant per spin, $T_N = 2J\hbar^2zs(s+1)/3k_B$ and z is the lattice coordination. Moreover, the spin stiffness constant is $\Gamma = J\hbar^2s^2a^2/2$. In terms of microscopic parameters, the spin-wave dispersion relation (9.128) becomes

$$\omega_{\mathbf{k}} = J\hbar s \sqrt{2z} |\mathbf{k}| a. \quad (9.129)$$

The same result is obtained in Exercise C.1.4, Appendix C, using the Holstein–Primakoff transformation. If there is a magnetic field or anisotropy, certain modes have a finite frequency at $k = 0$. Indeed, any uniform rotation of an order parameter or the magnetisation requires some energy, and this energy induces a gap in the excitation spectrum.

In conclusion, the existence of long wavelength hydrodynamic modes does not depend on s being large. In fact we have only used symmetry considerations and conservation laws. However, if a spin 1/2 system has no broken symmetries, as happens in one dimension, elementary excitations of a spin 1/2 chain are no longer spin waves; they are spinons, more closely related to reversals of individual spins than to spatial modulations of a hydrodynamic variable [see Chap. 7(I) and Chap. 10(I)].

10. Quantum Spin Chains

In low-dimensional systems, fluctuations have such large effects that there is generally no long range order. It is then crucial to distinguish between quantum and thermal fluctuations.

Thermal fluctuations populate low-energy states. As temperatures increase, the energy and momentum of excitations are renormalised by their interactions with other excited states [244]. Temperature thus strengthens interactions between excited states without fundamentally changing their nature.

In contrast, quantum fluctuations change the very nature of all states in a system, right down to the ground state. They have a simple origin: we cannot simultaneously specify all components of a quantum spin. The effect tends to restore rotational invariance of the ground state, even when the classical energy of the magnet favours an ordered state. This competition between order (via energy) and disorder (via quantum fluctuations) is a delicate matter in one dimension and new quantum states may result. For example, the spin 1/2 antiferromagnetic XY chain studied in Chap. 7(I) does not adopt a Néel state but rather forms a spin liquid equivalent to a Fermi liquid. Many other states are possible. As an example, consider a magnetic chain with uniaxial anisotropy $D(S^z)^2$, whose generic Hamiltonian

$$\frac{\mathcal{H}_0}{J} = \sum_i \left[-\frac{1}{2}(S_i^+ S_{i+1}^- + S_i^- S_{i+1}^+) - \Delta S_i^z S_{i+1}^z + D(S_i^z)^2 \right] \quad (10.1)$$

describes both ferromagnetic ($\Delta > 0$) and antiferromagnetic interactions ($\Delta < 0$). In the latter case, reversing x and y components of even spins ($i = 2p$, $S_{2p}^x \rightarrow -S_{2p}^x$, $S_{2p}^y \rightarrow -S_{2p}^y$) without altering odd ones, leaves spin commutation relations unchanged, and (10.1) becomes the Hamiltonian of a genuine antiferromagnet. For integer spins ($S = 1, 2$, etc.), the possible phases at $T = 0$ can be represented as a function of D and Δ on the diagram in Fig. 10.1 [247]. Apart from the ferromagnetic and antiferromagnetic Néel phases, we also find an XY phase in which correlation functions decrease more slowly than for the spin 1/2 XY chain encountered in Chap. 7(I). But the most interesting feature is the two singlet phases $S = 0$. There is a liquid phase (Haldane) [245, 246] and a gaseous phase [248]. These are phases of an entirely quantum nature as can be seen immediately by comparing with

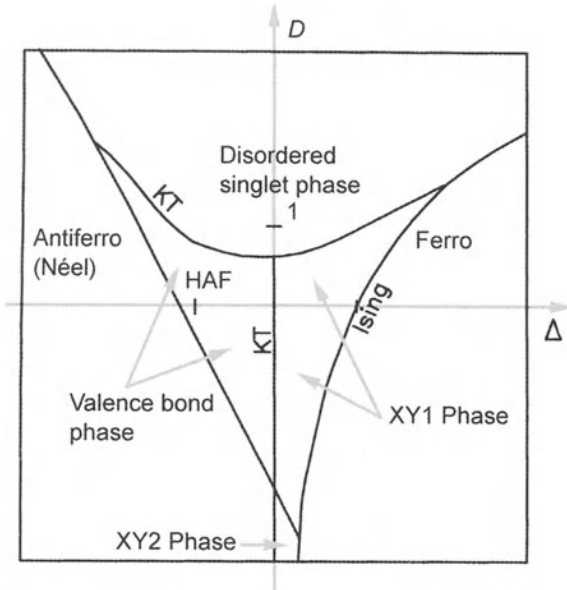


Fig. 10.1. $T = 0$ phase diagram for integer spin chains as a function of uniaxial anisotropy D and exchange anisotropy Δ . There are six different phases: two ordered phases (ferro and Néel), two XY phases and two singlet phases (liquid and gaseous). This diagram should be compared and contrasted with the diagram for half-integer spin chains (see Fig. 10.2)

the same diagram for half-integer spin chains (cf. Fig. 10.2); these phases are now replaced by the XY phase in this part of the diagram. Moreover, spin 1/2 antiferromagnetic chains often display instabilities (spin-Peierls transition [50]) near dimerised phases in which neighbouring spins pair together to form singlet states, breaking translation invariance. Such a diversity in ground states is all the more significant in that transitions between phases are not controlled by temperature. Thermodynamic stability between phases is often formulated in terms of competition between the various energy contributions from the Hamiltonian and entropic contributions governed by temperature. Even at zero temperature, an analogous description is possible for quantum phases. In each system, we can define a coupling constant g which gauges the size of quantum fluctuations. For example, the coupling constant for an antiferromagnet is $g^2 = z/S$, where z is the number of neighbours (usually 2 or 4) and S the spin. The parameter g measures quantum delocalisation of the spins and, for quantum systems, can be considered as analogous to temperature. These quantum fluctuations increase with g . They can lower the system energy, just as entropy reduces the free energy of a classical system. They lead to the liquid and gaseous singlet phases and stabilise dimerised phases. In all these states, correlations between spins are very short range.

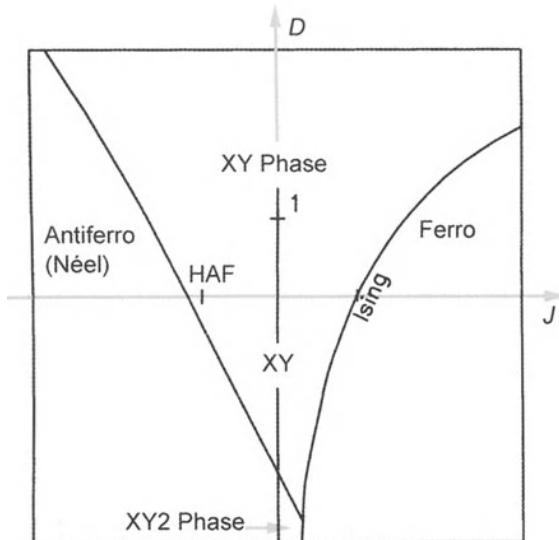


Fig. 10.2. Phase diagram for half-integer spin chains. There are four different phases: two ordered phases (ferro and Néel) and two XY phases. Singlet phases, if they exist, can only appear for very large values of D . Positions of lines separating the various phases are only approximate here

Compared with ferromagnetic and antiferromagnetic phases, they can be considered to be disordered by quantum fluctuations, rather as a paramagnetic phase is disordered by temperature. When energy contributions are of the same order as fluctuations, we obtain XY phases. In these phases, correlations between spins decrease by a power law; these are almost-ordered phases. Finally, interactions can stabilise ordered phases (ferromagnetic or Néel) at zero temperature. As for all phase transitions, symmetry properties are very important. Rotation invariance is partially broken in the XY phase and completely broken in the ferromagnetic phase. In the Néel phase, translation invariance is also broken. Dimerised phases only break translation invariance. Singlet phases break neither rotation nor translation invariance but involve non-local correlation functions which we shall discuss further [176]. Transition between two phases may correspond either to a crossing over of two energy levels (first order transition), or to the breaking of some continuous symmetry (second order transition).

Topological invariants play a special role in describing spin chains. Fluctuations mean that the order parameter associated with spins can rotate through integer multiples of 2π . For XY and ferromagnetic systems, quantum fluctuations cannot undo knots in the order parameter; the number of turns it goes through between $x = -\infty$ and $x = \infty$ is therefore an invariant, known as the topological charge Q . Every topological defect corresponds to a well defined non-linear excitation of the Hamiltonian, the soliton. This is

an excitation which is localised in space and propagates without dispersion [252]. State space can then be divided into sectors according to the value of Q , the number of solitons. In antiferromagnetic systems, topological charge is not conserved because quantum fluctuations allow the system to move from one sector to another by the tunnel effect (thereby leading to spontaneous generation of solitons at singular space-time events known as instantons). But rotation through $2\pi Q$ introduces a phase factor $\exp(2\pi iSQ)$ in the spin wave function. This has no effect for whole number spins, when $\exp(2\pi iSQ) = 1$, and the tunnel effect can induce transitions with $\Delta Q = 1$ between sectors. Such spontaneous soliton generation destroys long range antiferromagnetic order. But for half-integer spins, the phase factor only equals 1 when $Q = 2$. The tunnel effect can no longer connect even and odd sectors in state space. More physically, the phase factor $\exp(2\pi iSQ) = \pm 1$ leads to a momentum difference of $\hbar\pi/a$ between even and odd sectors, and this cannot be absorbed. Generation of soliton pairs is much more difficult. Ordered phases (XY and Néel) are therefore stabilised unless there are sufficiently large antiferromagnetic interactions between second neighbours.

Even if the ground state is ordered, temperature excites linear and non-linear modes which destroy long range order. In the presence of low-energy non-linear modes, magnetic correlations are soon destroyed. This is because, unlike harmonic excitations which bring the system back towards equilibrium, solitons can break the order parameter into disjoint segments. All physical parameters are then strongly renormalised by fluctuations and this causes unusual temperature behaviour.

Given the importance of topological excitations, we shall study planar (XY) ferromagnets in which their effects are typical.

10.1 One-Dimensional Planar XY Systems

10.1.1 Field Theory. The Sine–Gordon Equation

Solitons are basically classical objects. They are often encountered in non-linear systems with one space and one time dimension [251]. They are sometimes used as propagation modes in optical fibres because they lend themselves particularly well to digital coding. Consider a 1-dimensional magnet with large planar anisotropy $D > 0$, described by Hamiltonian

$$\mathcal{H} = -J \sum_i [\mathbf{S}_i \cdot \mathbf{S}_{i+1} + D(S_i^z)^2 - \mu H S_i^x] , \quad (10.2)$$

in a magnetic field H perpendicular to the chain axis. The Villain representation is particularly well suited to planar systems [see Sect. 9.8(I)] [238]. The component S_i^z and the angle ϕ_i made by the projection of \mathbf{S}_i in the (x, y) plane are conjugate canonical variables. In the classical limit they satisfy the Poisson bracket algebra

$$[\phi(x), S_z(x')]_{\text{pb}} = \delta(x - x') \implies [\exp(i\phi(x)), S_z(x')]_{\text{pb}} = i \exp(i\phi(x)) \delta(x - x') ,$$

and generate equations of motion

$$\begin{aligned} \frac{\partial \phi(x)}{\partial t} &= [\mathcal{H}, \phi(x)]_{\text{pb}} = -2DS_z(x) , \\ \frac{\partial S_z(x)}{\partial t} &= [\mathcal{H}, S_z(x)]_{\text{pb}} = -J\hat{S}^2a^2 \frac{\partial^2 \phi}{\partial x^2} + \mu H \hat{S} \sin \phi , \end{aligned} \quad (10.3)$$

where a is the lattice constant and $\hat{S} = \sqrt{S(S+1)}$. Classical dynamics of the phase field are then described by the sine–Gordon equation [254]

$$\frac{\partial^2 \phi(x, t)}{\partial t^2} = 2Dja^2\hat{S}^2 \left[\frac{\partial^2 \phi(x, t)}{\partial x^2} - \frac{\mu H}{Ja^2\hat{S}} \sin \phi(x, t) \right] . \quad (10.4)$$

In a large enough magnetic field, the phase field makes small oscillations about $\phi = 0$ ($\sin \phi \approx \phi$). These are spin waves of wave vector q and frequency

$$\omega = J\hat{S}^2ag^2\sqrt{q^2 + m^2} , \quad (10.5)$$

where

$$g = \left(\frac{2D}{J\hat{S}^2} \right)^{1/4} \quad \text{and} \quad m = \sqrt{\frac{\mu H}{Ja^2\hat{S}}} \quad (10.6)$$

play the same roles as the coupling constant and particle mass in the Klein–Gordon relativistic scalar field theory. Neither S_x nor S_z commute with the Hamiltonian and they are therefore not conserved quantities. However, in a quantum theory, the action of conjugate canonical variables (such as S_z and Φ) over a period is quantised in units of Planck's constant:

$$\oint S_z d\Phi = nh . \quad (10.7)$$

This quantises the amplitude of the spin waves. Equivalently, it quantises their momentum (in units of $\hbar q$) and energy (in units of $\hbar\omega$).

Identifying $c = J\hat{S}^2ag^2 = \sqrt{2DJ\hat{S}^2a^2}$ with the speed of light, (10.4) can be checked for invariance under a Lorentz transformation

$$t = \gamma \left(t' - \frac{x'}{v} \right) , \quad (10.8)$$

$$x = \gamma(x' - vt') , \quad (10.9)$$

where $\gamma^{-2} = 1 - (v/c)^2$. It is then possible to generate progressive solutions of the sine–Gordon equation from static solutions by means of a relativistic Lorentz transformation. These solutions have a first integral

$$\frac{1}{2} \left(\frac{\partial \phi}{\partial x} \right)^2 = m_0^2 - m^2 \cos \phi , \quad (10.10)$$

where m_0 is an integration constant. Localised solutions must satisfy $\phi \rightarrow \pm 1$ when $x \rightarrow \pm\infty$, and this implies $m_0 = m$. By quadrature, we thus obtain a static soliton

$$\tan \frac{\phi}{4} = \exp [\pm m(x - x_0)] . \quad (10.11)$$

This is indeed a topological defect, with charge

$$Q \equiv \frac{1}{2\pi} \int_{-\infty}^{\infty} \frac{\partial \phi}{\partial x} dx = \pm 1 , \quad (10.12)$$

since ϕ represented in Fig. 10.3 varies through $\pm 2\pi$ over a characteristic distance of $1/m$. Solitons behave like free particles. Their interactions are limited to phase shifts without inducing any scattering. More generally, solutions to (10.10) are elliptic functions (cn) [255]

$$\sin \frac{\phi}{2} = \text{cn} \left[\frac{\sqrt{m_0^2 + m^2}}{2} (x - x_0), k \right] - \text{const.} \quad (10.13)$$

Here, the parameter $k^2 = 2m^2/(m_0^2 + m^2)$ governs both spatial periodicity and the non-linear nature of the solution. As $k \rightarrow 1$, the spatial periodicity of the elliptic function cn tends to infinity and we obtain a soliton once again ($\text{cn} \rightarrow 1/\cosh$). As well as static solutions (relative to their centre of mass), there is another family of solutions known as *breathers*. These have internal degrees of freedom. When localised, they oscillate relative to the centre of mass, as described by

$$\tan \left[\frac{\phi(x, t)}{4} \right] = \frac{qc}{\omega} \frac{\sin \omega t}{\cosh qx} , \quad (10.14)$$

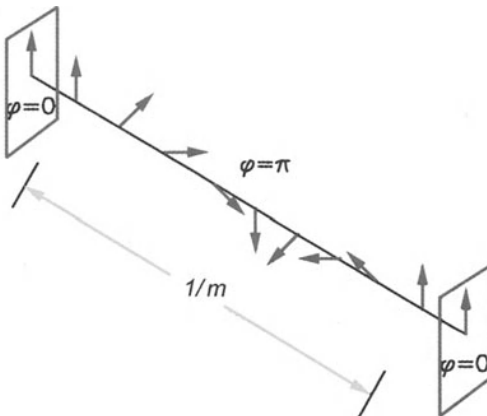


Fig. 10.3. Classical picture of the soliton of a planar magnet. Angle ϕ rotates through 2π as x changes from $-\infty$ to ∞

where internal frequency ω and spatial extent q^{-1} are related by the dispersion relation

$$m^2 = q^2 + \left(\frac{\omega}{c}\right)^2. \quad (10.15)$$

Breathers can be considered as soliton-antisoliton bound states [$1/\cosh qx \rightarrow 2\exp(\mp qx)$ as $x \rightarrow \pm\infty$]. They have zero topological charge. They can also be generalised to periodic structures [255]. Once we have identified the elementary excitations, we can obtain a general solution by a principle of non-linear superposition,

$$\tan\left(\frac{\phi_3 - \phi_0}{2}\right) = \pm \frac{\lambda_1 + \lambda_2}{\lambda_1 - \lambda_2} \tan\left(\frac{\phi_1 - \phi_2}{2}\right), \quad (10.16)$$

where the ϕ_i are solutions of the sine-Gordon equation and the λ_i are particular constants. Existence of this superposition principle is related to the fact that the sine-Gordon equation is completely integrable using inverse methods described in many text books [251, 252].

Conjugate canonical variables can be identified from (10.3) and (10.4):

$$\Phi = \phi/g, \quad \Pi = gS_z. \quad (10.17)$$

Equations of motion can then be generated from Hamilton's equations using the Hamiltonian

$$\mathcal{H} = Ja\hat{S}^2g^2 \int dx \frac{1}{2} \left[\left(\frac{\partial \Phi}{\partial x} \right)^2 + \Pi^2 \right] - \frac{m^2}{g^2} (\cos g\Phi - 1). \quad (10.18)$$

We thereby determine the momentum carried by the phase field,

$$P = - \int \frac{dx}{a} \Pi \left(\frac{\partial \Phi}{\partial x} \right), \quad (10.19)$$

which, like the energy, is a conserved quantity.

It is instructive to determine the angular momentum, momentum and energy of the elementary excitations. Components of angular momentum carried by a soliton of speed v are

$$S - S_x = S \int \frac{dx}{a} (1 - \cos \phi) = \frac{4S}{\gamma ma}, \quad (10.20)$$

$$\begin{aligned} S_z &= -\frac{1}{2D} \frac{\partial \phi [\gamma(x-vt)]}{\partial t} \\ &= \frac{2v}{2Da} \int_{-\infty}^{\infty} \frac{du}{\cosh u} = \frac{2\pi v}{2Da}, \end{aligned} \quad (10.21)$$

where $\gamma^{-2} = 1 - (v/c)^2$. These quantities are conserved because the soliton is a static object in the centre of mass frame. Its momentum and energy are found analogously:

$$P = \frac{4m\gamma v}{2Da} \int_{-\infty}^{\infty} \frac{du}{\cosh^2 u} = \frac{8m\gamma v}{2Da}, \quad (10.22)$$

$$E = 8m\gamma Ja\hat{S}^2. \quad (10.23)$$

This corresponds to a classical relativistic particle of mass $8m$ propagating at speed v . Note that the momentum $P = 4m\gamma S_z/\pi$ of the soliton is proportional to its angular momentum S_z which, in quantum theory, is quantised in units of \hbar . However, the quantum definition of the momentum of a spin chain requires more careful analysis [256]. The wave function of the chain can be represented as a product of N spin states,

$$|\psi\rangle = \prod_{i=1}^N |\hat{\Omega}_i\rangle, \quad (10.24)$$

where the $|\hat{\Omega}_i\rangle$ form a basis of semi-classical states of the i th spin [257]. The operator translating through one lattice spacing $T_a = \exp(iaP)$ generates the momentum operator P . Its matrix elements are

$$\langle\psi|T_a|\psi\rangle = \prod_{i=1}^N \langle\hat{\Omega}_i|\hat{\Omega}_{i+1}\rangle. \quad (10.25)$$

For a static soliton, state $|\hat{\Omega}_{i+1}\rangle$ can be obtained from $|\hat{\Omega}_i\rangle$ by rotation through an angle $\phi_{i+1} - \phi_i$ about \hat{z} . The rotation operator

$$\exp\left[i\frac{S_z}{\hbar}(\phi_{i+1} - \phi_i)\right]$$

can then be used to calculate the matrix element:

$$\begin{aligned} \langle\psi|T_a|\psi\rangle &= \prod_{i=1}^N \exp\left(im_z a \frac{\partial\phi_i}{\partial x}\right) \\ &= \exp\left(im_z \int \frac{\partial\phi}{\partial x} dx\right) = \exp(2\pi im_z Q), \end{aligned} \quad (10.26)$$

where m_z is the value of the S_z quantum number. For half-integer spins, this adiabatic phase is not a multiple of 2π , and it generates an additional momentum

$$P_0 = 2\frac{\pi}{a}Qm_z \equiv 2\frac{\pi}{a}SQ. \quad (10.27)$$

This has a purely quantum origin, stemming from the 4π periodicity of half-integer spins. The total momentum of a soliton is therefore quantised in units of angular momentum

$$P_{\text{tot}} = P_0 + P = m_z \left(2\frac{\pi}{a}Q + \frac{4\hbar m}{\pi}\right). \quad (10.28)$$

Quantum fluctuations also affect the soliton energy in two different ways. On the one hand, spin waves have a zero point energy so that $\langle \cos g\Phi \rangle \approx$

$\exp(-g^2\langle\Phi^2\rangle/4)$. This renormalisation of the potential is equivalent to a mass renormalisation [261]

$$m \longrightarrow \hat{m} = m \times \exp\left(-\frac{1}{4}g^2\langle\Phi^2\rangle\right) \approx m \times \left(\frac{\mu H}{128J\hat{S}}\right)^{g^2/16\pi}. \quad (10.29)$$

In addition to this, zero point fluctuations are not the same around the soliton as they are in the ground state. In other words, there is a difference in zero point energy between sectors $Q = 1$ and $Q = 0$ and this constitutes a further quantum correction to the soliton energy. To first order, this correction

$$E_q = 8\hat{m}\left(1 - \frac{\hbar g^2}{8\pi}\right)Ja\hat{S}^2 \quad (10.30)$$

amounts to renormalising the coupling constant by

$$g^2 \longrightarrow \hat{g}^2 = g^2/(1 - \hbar g^2/8\pi).$$

We can extend this analysis to breathers. In the centre of mass frame, momentum is zero. Classically, values of the energy

$$E = 16q\gamma Ja\hat{S}^2 \quad (10.31)$$

range from 0 to twice the energy of one soliton [cf. (10.23)]. This is to be expected since a breather is a composite structure made up of two interacting solitons. However, it is rather surprising to find that a breather can have an infinitesimal energy. This is in fact no longer the case in quantum mechanics, which imposes a quantisation of internal oscillation frequencies. In classical mechanics, the energy of a particle in periodic motion is the derivative of the total action $\mathcal{S} = \int_0^T L dt$ with respect to the period $T = 2\pi/\omega$, whence

$$E(T) = 16Ja\hat{S}\sqrt{m^2 - \left(\frac{2\pi}{Tc}\right)^2} = \frac{d\mathcal{S}}{dT}. \quad (10.32)$$

The total action is obtained by quadrature:

$$\mathcal{S} = 32\pi \frac{Ja\hat{S}^2}{c} \left[\arccos\left(\frac{\omega}{mc}\right) - \sqrt{\left(\frac{mc}{\omega}\right)^2 - 1} \right]. \quad (10.33)$$

We can now apply the Bohr–Sommerfeld quantisation rule to the reduced action

$$S = \oint \Pi d\Phi = \mathcal{S} + ET = 32\pi \frac{Ja\hat{S}^2}{c} \arccos\left(\frac{\omega}{mc}\right) = 2\pi n\hbar, \quad (10.34)$$

in order to obtain the quantisation of oscillation frequencies and energy:

$$\frac{\omega_n}{mc} = \cos\left(\frac{n\hbar g^2}{16}\right) \Rightarrow E_n = 16Ja\hat{S}^2\gamma \sin\left(\frac{n\hbar g^2}{16}\right). \quad (10.35)$$

This rather simplistic analysis does not take zero point fluctuations into account and these would renormalise the coupling constant $g^2 \longrightarrow \hat{g}^2$

[258, 259, 260]. For small coupling constants ($\hbar g^2 \ll 1$), we obtain the energy $\varepsilon_k = \hbar mc\gamma$ of magnons whose phase speeds $v = ck/m$ coincide with the breather speed in the laboratory frame. When g is small, the $n = 1$ breather coincides with a magnon. This suggests interpreting breathers as bound states of n magnons. In an ordered magnet, interaction between magnons is negligible. This means that bound states cannot form and gives magnons there bosonic characteristics: the energy of n magnons is n times the energy of one magnon. Here, the n magnons making up the breather interact all the more as the number of magnons in the state increases, and this gradually reduces their binding energy $E_{n+1} - E_n$. In fact, n cannot exceed a value $n_{\max} = 8\pi/\hbar g^2$, beyond which the breather spontaneously dissociates into a soliton-antisoliton pair. In particular, when $n_{\max} < 1$, the only stable excitations of a sine-Gordon system are the solitons.

10.1.2 XY Phase Correlation Functions. Instantons

When the magnetic field tends to zero, the action of the phase field between 0 and t reduces to

$$\begin{aligned} S(0, t) &= \int_0^t dt \mathcal{L} = Ja\hat{S}^2 \int_0^t dt \int dx \frac{1}{2} \left[\frac{1}{c^2} \left(\frac{\partial \phi}{\partial t} \right)^2 - \left(\frac{\partial \phi}{\partial x} \right)^2 \right] \\ &= i \frac{Ja\hat{S}^2}{2c} \int_0^{\tau=ict} d\tau \int_{-\infty}^{\infty} dx \left[\left(\frac{\partial \phi}{\partial x} \right)^2 + \left(\frac{\partial \phi}{\partial \tau} \right)^2 \right], \end{aligned} \quad (10.36)$$

where we have made the change of variable $\tau = ict$ in order formally to restore the Euclidean metric. This representation of the action in terms of an imaginary time allows us to express the evolution operator

$$\begin{aligned} U(t) &= \exp \left(i \frac{S(0, t)}{\hbar} \right) \\ &= \exp \left\{ - \frac{Ja\hat{S}^2}{2\hbar c} \int_0^{\tau=ict} d\tau \int_{-\infty}^{\infty} dx \left[\left(\frac{\partial \phi}{\partial x} \right)^2 + \left(\frac{\partial \phi}{\partial \tau} \right)^2 \right] \right\} \end{aligned} \quad (10.37)$$

as the density matrix of the classical XY model in the complex plane. The parameter $\beta^{-1} = 2\hbar c/a = 2J\hat{S}^2\hbar g^2$ plays the role of the temperature ($k_B T$) in the classical model. Spatio-temporal correlations

$$\langle \mathbf{S}(x, t) \cdot \mathbf{S}(0) \rangle = Z^{-1} \text{Tr} \{ \exp [-S(\beta)] \mathbf{S}(x, t) \cdot \mathbf{S}(0) \} \quad (10.38)$$

are then obtained from the correlation function in the classical XY model by straightforward analytic continuation of its partition function Z . The same goes for any other expectation value. Weak couplings $\hbar g^2 \ll 1$ correspond to the limit $T \rightarrow 0$, where the classical correlation function has been calculated in Sect. 7.2. We deduce by analytic continuation that

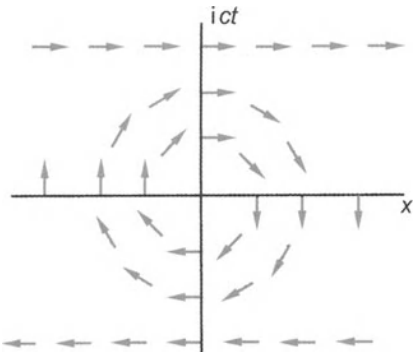


Fig. 10.4. Pictorial representation of an instanton as a vortex in space-time

$$\begin{aligned}\langle \mathbf{S}(x, t) \cdot \mathbf{S}(0, 0) \rangle &= \langle \cos[\phi(x, t) - \phi_0] \rangle \\ &= \left(\frac{\pi a}{x^2 + (ict)^2} \right)^{\eta/2} = \left(\frac{\pi a}{x^2 - (ct)^2} \right)^{\eta/2},\end{aligned}$$

where the exponent η becomes in this case

$$\eta = \frac{k_B T}{4\pi J} \longrightarrow \frac{\hbar g^2}{2\pi}. \quad (10.39)$$

More generally, we can find the dynamics of a quantum theory in one space and one time dimension by examining the thermodynamics of the corresponding 2-dimensional classical model. The physics of quantum phases is closely related to topological excitations, as in the case of the XY phase. In the $(x, \tau = ict)$ plane, the equivalent of a vortex is the instanton. As shown in Fig. 10.4, this structure allows the system to pass from a $\phi = -\pi$ state at times $t \ll 0$ to a $\phi = 0$ state when $t \gg 0$. The corresponding action $\mathcal{S}(-t, t)$ is proportional to the energy of the vortex in the classical XY model. Now, in semi-classical physics, the probability of tunnelling from one configuration to another is related to $\exp[-\mathcal{S}(-t, t)]$ where $t \rightarrow \infty$. An instanton is therefore an elementary process relating different states by tunnelling [264]. The tunnelling process is only significant if the instanton action $\mathcal{S}(-t, t)$ remains finite or, equivalently, the classical vortex energy is finite. Although the vortex energy in the XY model increases logarithmically with distance, the presence of other vortices (instantons) cuts off this weak divergence at infinite times and the corresponding action remains finite. As in classical theory, instanton-anti-instanton pairs of equal and opposite topological charge have smaller action and contribute even when coupling constants (which here play the role of temperature) are weak. As in the classical XY model, instanton-anti-instanton bound states do not destroy the ordered phase, provided that the coupling constant remains below a critical coupling constant g_{KT} ; above this value, instanton-anti-instanton pairs dissociate. In classical theory, dissociation of vortex pairs occurs at the Kosterlitz-Thouless transition. The

temperature T_{KT} of this transition is defined in (7.52). In an analogous way, the critical coupling constant

$$\frac{k_{\text{B}}T_{\text{KT}}}{J} \approx Q^2\pi \iff 2\hbar g_{\text{KT}}^2 \approx Q^2\pi \quad (10.40)$$

depends on the instanton topological charge. For integer spin chains, instantons with topological charge $Q = 1$ can dissociate and the critical coupling constant corresponds to a D/J value of

$$\frac{D}{J} = \frac{\pi^2}{8} S(S+1) . \quad (10.41)$$

This expression underestimates the ratio D/J which actually takes the value 0.8 for spin 1. This is to be expected since the critical coupling constant (\simeq temperature) of the Kosterlitz–Thouless transition is always reduced by the presence of a finite density of instantons [see (7.53)]. For half-integer chains, momentum conservation inhibits dissociation of $Q = \pm 1$ defects. The transition is governed by dissociation of $Q = \pm 2$ defects and the critical coupling constant is then much higher [see (10.40)].

It is interesting to consider the disordered phase when $g > g_{\text{KT}}$. Instantons connect all directions of the order parameter and restore rotation invariance. But the only quantum state invariant under rotation is the singlet $|S=0\rangle$. We can thus identify this state with the gaseous singlet phase in the phase diagram of Fig. 10.1. We therefore reach the paradoxical conclusion that a ferromagnetic system with sufficiently large planar anisotropy can form a singlet state, like an antiferromagnet. This clearly illustrates the extent to which quantum fluctuations may transform the classical states upon which we base our physical intuition!

In conclusion, let us mention that in a transverse magnetic field the sine–Gordon phase is not destroyed by quantum fluctuations. Indeed, the instanton action becomes infinite in the sine–Gordon model. As a result, the probability of connecting the various sectors $\phi = 2n\pi$ of the ground state by tunnelling becomes negligible and the broken symmetry is thereby maintained.

The methods described in this section can be transposed to many other 1-dimensional models of magnetism, provided the corresponding classical solutions are known. All integrable classical models can be obtained systematically by inverse methods [251, 252, 265]. As an example, we could mention the isotropic ferromagnetic chains [266] for which all non-linear solutions are known [263, 267]. Further equally relevant models have been studied in some depth [265, 268, 269].

10.2 Some Theorems

10.2.1 The Lieb–Schultz–Mattis Theorem

For a half-integer spin chain whose Hamiltonian is invariant under translation and rotation of spins ($D = 0$), there is a rigorous theorem due to Lieb, Schultz

and Mattis which specifies the ground state [270, 271]. Either there is no energy gap between ground state and first excited state, or the ground state is degenerate and spontaneously breaks translation invariance, i.e., forms a dimerised structure. In order to show that there is no gap, we need only construct a state $|\psi_1\rangle$ orthogonal to the ground state $|\psi_0\rangle$ such that

$$\Delta E = \langle\psi_1|\mathcal{H} - E_0|\psi_1\rangle = \mathcal{O}(1/2N) , \quad (10.42)$$

where $2N + 1$ is the number of spins in a chain with periodic boundary conditions ($\mathbf{S}_{2N+1} \equiv \mathbf{S}_1$). Consider the state

$$|\psi_1\rangle = U|\psi_0\rangle , \quad U = \exp \left[\frac{i\pi}{l} \sum_{j=-l}^l (j+l) S_j^z \right] , \quad (10.43)$$

where l is a whole number of order N . U has the effect of twisting consecutive spins through roughly π/l . This torsion being infinitesimal, the additional energy is small. For example,

$$U^\dagger S_i^+ S_{i+1}^- U = \exp(i\pi/l) S_i^+ S_{i+1}^- \quad (10.44)$$

and the additional energy ΔE for the Heisenberg Hamiltonian is

$$\begin{aligned} \Delta E &= \frac{J}{2} \left\{ \left[\exp \left(-\frac{i\pi}{l} \right) - 1 \right] \langle\psi_0|S_i^+ S_{i+1}^-|\psi_0\rangle \right. \\ &\quad \left. + \left[\exp \left(\frac{i\pi}{l} \right) - 1 \right] \langle\psi_0|S_i^- S_{i+1}^+|\psi_0\rangle \right\} \\ &\propto 2N [\cos(\pi/l) - 1] = \mathcal{O}(1/2N) . \end{aligned} \quad (10.45)$$

It only remains to show that $|\psi_1\rangle$ is orthogonal to $|\psi_0\rangle$. This brings in the half-integral nature of the spins explicitly. Carrying out a parity reversal $i \rightarrow -i$ followed by a rotation by π about y , $S_i^z \rightarrow -S_{-i}^z$, the operator U transforms by

$$U \longrightarrow U \exp(-2\pi i S_{\text{tot}}^z) \equiv -U , \quad (10.46)$$

precisely because spins are half integral. If $|\psi_0\rangle$ has even parity, then $|\psi_1\rangle$ must be odd. Hence, $|\psi_1\rangle$ is orthogonal to $|\psi_0\rangle$. The only other alternative is that $|\psi_0\rangle$ spontaneously breaks parity. The ground state then forms a dimerised state which is naturally degenerate since its image under parity has the same energy.

10.2.2 Marshall's Theorems

These specify the ground state for antiferromagnetic systems in which spins can be separated into two sublattices A and B [272, 273]. In this case, a state is specified by the value S of the total spin of the sublattice and its component M along z :

$$|\psi(S, M)\rangle = |\psi(S, M)\rangle_A \otimes |\psi(S, -M)\rangle_B . \quad (10.47)$$

Marshall's first theorem requires the lowest energy state amongst states of given M value to take the form

$$|\psi_0(M)\rangle = \sum_S (-1)^{S+M} a(S, M) |S, M\rangle , \quad (10.48)$$

where all amplitudes $a(S, M)$ are positive. As a corollary, it can be shown that the ground state of an antiferromagnet is a non-degenerate singlet

$$S_{\text{tot}} |\psi_0\rangle = 0 . \quad (10.49)$$

By making a judicious choice for the phases in a family of variational states, taking Marshall's theorem into account, excellent approximations can be obtained [275]. Among the possible families of variational states, valence bond states play a key role in describing antiferromagnetic spin chains.

10.3 Valence Bond States

When quantum fluctuations dominate, the ground state is often a singlet. It is therefore useful to give a complete description of these singlet states, taking spin 1/2 chains as an example. There are many ways of combining $2N$ spin 1/2 states to form a singlet state. An exhaustive description of the subspace of singlet states can be obtained from the valence bond algebra. The idea is to evaluate all possible states that can be formed from an arbitrary pair of spins i, j . Thus for spin 1/2, we can form either a singlet or a triplet. We introduce a condensed notation to describe these states:

$$[i, j] \equiv \frac{1}{\sqrt{2}} (| \downarrow_i \uparrow_j \rangle - | \uparrow_i \downarrow_j \rangle) , \quad (10.50)$$

$$\{i, j\}_1 \equiv | \uparrow_i \uparrow_j \rangle , \quad \{i, j\}_0 \equiv \frac{1}{\sqrt{2}} (| \uparrow_i \downarrow_j \rangle + | \downarrow_i \uparrow_j \rangle) , \quad \{i, j\}_{-1} \equiv | \downarrow_i \downarrow_j \rangle .$$

It is straightforward to check that the singlet state obtained by adding two triplet states $\{i, j\}$ and $\{k, l\}$ can be written as a linear combination of singlet valence bonds, i.e.,

$$[\{i, j\} \{k, l\}] = [i, k] [j, l] + [i, l] [j, k] . \quad (10.51)$$

Exercise

Establish this result, using the fact that the spin 0 state formed by addition of two spin 1 states with components $-1, 0, 1$ takes the form

$$|0\rangle = \frac{1}{\sqrt{3}} (|1, -1\rangle - |0, 0\rangle + |-1, 1\rangle) .$$

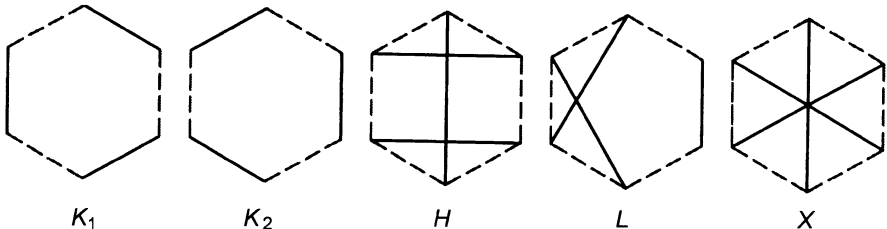


Fig. 10.5. Five possible products of valence bonds for the benzene structure. Only the first two, the Kekulé states, are physical

This construction of singlet states by contraction of two higher spins ($S = q/2$) generalises to the case where these spins are themselves obtained by addition of q spin 1/2 states. We can show that any singlet wave function can be written as a linear combination of products of valence bond states [275, 278]:

$$|S\rangle = \sum_{i_\alpha, j_\eta} a(i_1 j_1, \dots i_\alpha j_\alpha, \dots i_n j_n) [i_1 j_1] \dots [i_\alpha j_\alpha] \dots [i_n j_n]. \quad (10.52)$$

For example, benzene contains 6 spin 1/2 states and there are therefore $C_{N=6}^{N/2=3} = 12$ possible products of valence bonds. The main configurations are shown in Fig. 10.5. The first two products $|K_1\rangle$ and $|K_2\rangle$ are the Kekulé states [276]. They break translation invariance and consequently enter the ground state in the form of a linear combination

$$\begin{aligned} |S\rangle_{\text{benzene}} &= \frac{1}{\sqrt{2}}(|K_1\rangle + |K_2\rangle) \\ &= \frac{1}{\sqrt{2}}([12][34][56] + [23][45][61]), \end{aligned} \quad (10.53)$$

in such a way as to restore translation invariance. There is indeed a spin chain which has just this state as its ground state (see the following section). Such terminology is ideally suited to systems built up of dimers, in which the product of the $[i_\alpha j_\alpha]$ (where α indexes each dimer) dominates other contributions to the wave function. Hence the wave function for a chain with alternating antiferromagnetic couplings, with Hamiltonian

$$\mathcal{H}_1 = \sum_{i=1}^N [J_1(1+\delta)\mathbf{S}_{2i-1} \cdot \mathbf{S}_{2i} + J_1(1-\delta)\mathbf{S}_{2i} \cdot \mathbf{S}_{2i+1}], \quad (10.54)$$

is close to the Kekulé state

$$|K_1\rangle = [12][34] \dots [2N, 1], \quad (10.55)$$

when $\delta \rightarrow 1$. As δ decreases, the wave function contains valence bonds of longer and longer range. In the extreme case of the Heisenberg chain ($S = 1/2$, $\delta = 0$), the range of valence bonds making up the ground state becomes

infinite. This is understandable, since its ground state is almost ordered. Generally speaking, the more closely a magnetic state resembles a state with long range order, the greater the range of the valence bonds describing it. This is illustrated in the next exercise.

It is not difficult to calculate matrix elements of spin operators $\mathbf{S}_i \cdot \mathbf{S}_j$ between any valence bond states, making use of the identities:

$$\mathbf{S}_i \cdot \mathbf{S}_j[i, j] = -\frac{3}{4}[i, j], \quad (10.56)$$

$$\mathbf{S}_j \cdot \mathbf{S}_k[i, j][k, l] = \frac{1}{4}[i, j][k, l] - \frac{1}{2}[j, k][l, i], \quad (10.57)$$

$$\mathbf{S}_j \cdot \mathbf{S}_k[i, j]\{k, l\} = \frac{1}{4}[i, j]\{k, l\} + \frac{1}{2}[j, k]\{i, l\}, \quad (10.58)$$

$$\mathbf{S}_i \cdot \mathbf{S}_j\{i, j, k, \dots\} = \frac{1}{4}\{i, j, k, \dots\}. \quad (10.59)$$

These are often expressed in the form of graphical rules [277].

Exercise: The Néel Wave Function as a Valence Bond State

A Néel state composed of $2N$ spin $1/2$ states is divided into two sublattices A and B each containing N spins. Total spins of the two sublattices are maximal, that is, equal to $N/2$. The Néel state $|N/2, N/2\rangle_A \otimes |N/2, -N/2\rangle_B$ is not a singlet state but can easily be made rotation invariant by application of Marshall's theorem,

$$|N\rangle = \frac{1}{\sqrt{N+1}} \sum_{m=-N/2}^{N/2} (-1)^m |N/2, m\rangle_A \otimes |N/2, -m\rangle_B, \quad (10.60)$$

which is a singlet.

1. Show that the state $|N/2, m\rangle_A \otimes |N/2, -m\rangle_B$ contains $C_N^{m+N/2}$ distinct spin configurations (see Appendix A).
2. Consider a general spin configuration with the property that the component of S_z in each sublattice equals $\pm m$, i.e.,

	Sublattice A	Sublattice B
Spin \uparrow	$N/2 + m$	$N/2 - m$
Spin \downarrow	$N/2 - m$	$N/2 + m$

We seek a correspondence between these spin configurations and valence bond configurations in which one element of the bond is a spin in sublattice A and the other a spin in sublattice B . Show that these spin configurations occur in $(N/2+m)!(N/2-m)!$ bond configurations. Deduce that their amplitude is proportional to

$$(-1)^{N/2-m} \left(\frac{N}{2} + m\right)! \left(\frac{N}{2} - m\right)! = (-1)^{N/2} N! \frac{(-1)^m}{C_N^{N/2+m}}. \quad (10.61)$$

3. Observing that there are $N!$ possible bonds between the two sublattices, and identifying the last factor in (10.61) with the amplitude in the Néel state of a configuration with given sublattice magnetisation $S_z = m$, deduce that

$$|N\rangle = \sum_{i_\alpha \in A, j_\alpha \in B} [i_1 j_1] \dots [i_\alpha j_\alpha] \dots [i_N j_N]. \quad (10.62)$$

In the Néel state, all bond configurations have the same weight, whatever their length.

Exercise: Energy and Magnetisation in the Néel State

1. From (10.56) and (10.57), check that the energy of the Néel state (10.62) equals $-J/4$ per bond.
2. Show that expectation

$$\frac{1}{2N} \sum \langle (2S_i^z)^2 \rangle = 1/3.$$

Justify this result in terms of the Hamiltonian isotropy.

10.3.1 Solid Valence Bond States

Majumdar–Ghosh State

Consider a family of spin 1/2 ladders with the structure illustrated in Fig. 10.6. They have Hamiltonian $\mathcal{H} = \mathcal{H}_1 + \mathcal{H}_2$, where \mathcal{H}_1 is defined by (10.54) and

$$\mathcal{H}_2 = J_2 \sum_{i=1}^{2N} \mathbf{S}_{i-1} \cdot \mathbf{S}_{i+1}. \quad (10.63)$$

A certain degree of magnetic frustration exists in this system because not all antiferromagnetic bonds can be satisfied. Ground states for these ladders are known for certain values of parameters J_1 , J_2 , δ . When $\delta = 0$ and $J_2 = 0$, or equally when $J_1 = 0$, the system reduces to Heisenberg chains with the same type of ground state as the XY chain [see Chap. 7(I)] and with correlations which decrease slowly as $1/|i - j|$.

When $\delta = 0$ and $J_2 = J_1/2$, the ground state, which has energy $-3J_1/8$ per spin, is generated by the Kekule states $|K_1\rangle$ and $|K_2\rangle$ shown in Fig. 10.6 [278, 279]. These states have ordered valence bonds and are therefore solid valence bond states. Of course, quantum fluctuations lower their energy below the energy of the Néel state ($-J/4$). Let $\mathcal{J}_i = \mathbf{S}_{i-1} + \mathbf{S}_i + \mathbf{S}_{i+1}$ be the total spin of three consecutive spins $i - 1$, i and $i + 1$. The operator

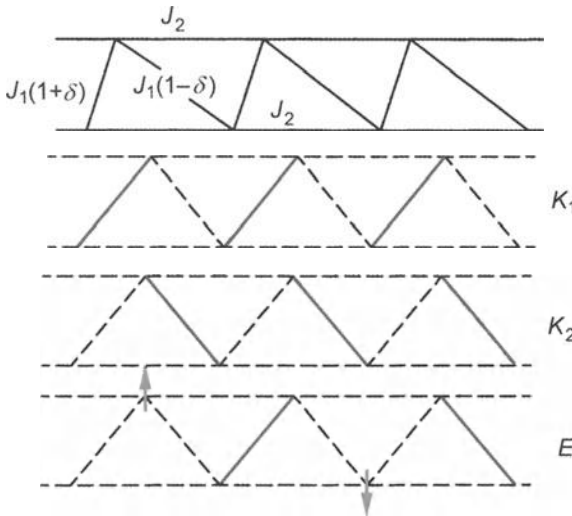


Fig. 10.6. (a) Spin ladder with magnetic frustration. (b) When $\delta = 0$ and $J_2 = J_1/2$, the ground state can be generated from Kekulé states $|K_1\rangle$ and $|K_2\rangle$. (c) Excited state made up from two free spins separating a $|K_1\rangle$ and a $|K_2\rangle$ state

$$\begin{aligned} \mathcal{P}_{3/2}(i-1, i, i+1) &= \mathcal{J}_i^2 - \frac{3}{4} \\ &= 2(\mathbf{S}_{i-1} \cdot \mathbf{S}_i + \mathbf{S}_i \cdot \mathbf{S}_{i+1} + \mathbf{S}_{i-1} \cdot \mathbf{S}_{i+1}) + \frac{3}{2} \end{aligned} \quad (10.64)$$

projects the value of the total spin \mathcal{J}_i onto the $3/2$ subspace, because $\mathcal{P}_{3/2}$ annihilates all states such that $\mathcal{J}_i = 1/2$. The Majumdar–Ghosh Hamiltonian can be written as a sum of projection operators $\mathcal{P}_{3/2}$:

$$\mathcal{H} = \frac{J_1}{4} \left[\sum_{i=1}^{2N} \left(\mathcal{J}_i^2 - \frac{3}{4} \right) - 3N \right]. \quad (10.65)$$

In the Kekulé state, \mathcal{J}_i^z takes values $\pm 1/2$. As this state is rotation invariant, we can deduce that all the \mathcal{J}_i assume their smallest value, viz., $1/2$. Consequently, Kekulé states have the lowest energy. Among the linear combinations of $|K_1\rangle$ and $|K_2\rangle$, $|\psi\rangle = (|K_1\rangle + |K_2\rangle)/2$ is the only eigenstate with zero momentum; it is therefore the ground state. In this state, valence bonds have minimal length and hence correlations between spins are very short range, not exceeding one lattice spacing. The valence bonds are ordered but spins are disordered, as in a liquid state, and we speak of a *spin liquid*.

We can also define an order parameter ψ by

$$2\langle S_i^+ S_{i+1}^- - S_{i-1}^+ S_i^- \rangle = (-1)^i |\psi|. \quad (10.66)$$

This describes states with solid valence bonds since it equals 1 in the Kekulé state and 0 in either the antiferromagnetic state or the paramagnetic state.

[Another possible definition of the order parameter would be $2\langle \mathbf{S}_i \cdot \mathbf{S}_{i+1} \rangle + 1/2 = (-1)^i |\psi|$.] It is known today that the Kekule state is still the ground state on the line $\delta = 1 - 2J_2/J_1$, which constitutes a disorder line on the (J_1, J_2, δ) phase diagram [279, 280].

Excited states, shown on Fig. 10.6, are made up of two free spins behaving like two defects, which separate a $|K_1\rangle$ state from a $|K_2\rangle$ state. These excitations form a continuum above a band whose dispersion relation $\varepsilon(q) = J_1(5/4 - |\cos q|)$ has two minima, one at $q = 0$ and the other at $q = \pi$ [279]. Consequently, these excitations are separated from the ground state by an energy gap $\Delta = J_1/4$, half the exchange interaction $J_2 = J_1/2$. The excitation spectrum and correlation functions found here should be contrasted with the isotropic Heisenberg model, which has long range spin correlations and continuous excitation spectrum ranging from 0 to $2J$. The two models therefore belong to different universality classes. It would seem that the Majumdar–Ghosh model belongs to the same universality class [250] as Haldane’s liquid phase [245], describing integer spin antiferromagnetic chains.

It is known today that we must have a finite interaction between second neighbours $J_2 \approx 0.298J_1$ [280, 281], in order to induce an energy gap in the Heisenberg model excitation spectrum and hence to place it in the new universality class. The relationship between this transition and the properties of the non-linear sigma model with a topological term will be explored at the end of the present chapter.

AKLT State

Valence bond states can be used for spins greater than $1/2$. The idea is to consider a spin S state as a composite structure built up from $2S$ spins $\sigma = 1/2$, and then to construct valence bond states from elementary components, i.e., the spins σ [283]. This approach is useful for the spin 1 case, giving a concrete picture of the Haldane liquid phase. Consider the Hamiltonian

$$\mathcal{H}/J = \sum_{i=1}^N \mathbf{S}_i \cdot \mathbf{S}_{i+1} - \beta (\mathbf{S}_i \cdot \mathbf{S}_{i+1})^2 \quad (10.67)$$

for a spin $S = 1$ chain. β is a biquadratic term which is not particularly relevant to real physical systems. However, numerical simulations [282] have shown that, as long as the parameter $|\beta|$ is lower than $1/2$, the ground state of (10.67) remains of the same type, whatever the value of $|\beta| < 1/2$. We thereby obtain a concrete picture of the ground state in an isotropic antiferromagnetic chain by studying the Hamiltonian proposed by AKLT [283], in which $\beta = -1/3$. Two adjacent spins \mathbf{S}_i and \mathbf{S}_{i+1} ($S = 1$) in the chain combine to give a total spin $\mathcal{J}_i = \mathbf{S}_i + \mathbf{S}_{i+1}$, which can take values 0, 1 and 2. Operators

$$\mathcal{P}_\perp^0(i, i+1) = \frac{1}{4}(\mathbf{S}_i + \mathbf{S}_{i+1})^2 = 1 + \frac{1}{2}\mathbf{S}_i \cdot \mathbf{S}_{i+1}, \quad (10.68)$$

$$\mathcal{P}_\perp^1(i, i+1) = \frac{1}{6}[(\mathbf{S}_i + \mathbf{S}_{i+1})^2 - 2] = \frac{1}{3}(1 + \mathbf{S}_i \cdot \mathbf{S}_{i+1}) \quad (10.69)$$

project an arbitrary state onto subspaces orthogonal to $\mathcal{J} = 0$ and $\mathcal{J} = 1$, respectively. Hence their product

$$\mathcal{P}_2(i, i+1) = \mathcal{P}_\perp^0 \mathcal{P}_\perp^1 = \frac{1}{3} + \frac{1}{2} \mathbf{S}_i \cdot \mathbf{S}_{i+1} + \frac{1}{6} (\mathbf{S}_i \cdot \mathbf{S}_{i+1})^2 \quad (10.70)$$

projects onto the subspace $\mathcal{J} = 2$.

Exercise

Show that

$$\mathcal{P}_0(i, i+1) = -\frac{1}{3} + \frac{1}{3} (\mathbf{S}_i \cdot \mathbf{S}_{i+1})^2, \quad (10.71)$$

$$\mathcal{P}_1(i, i+1) = 1 - \frac{1}{2} \mathbf{S}_i \cdot \mathbf{S}_{i+1} + \frac{1}{2} (\mathbf{S}_i \cdot \mathbf{S}_{i+1})^2 \quad (10.72)$$

are projectors onto subspaces $\mathcal{J} = 0$ and $\mathcal{J} = 1$ and check the completeness relation $\mathcal{P}_0 + \mathcal{P}_1 + \mathcal{P}_2 = 1$.

As for the Majumdar–Ghosh Hamiltonian, the AKLT Hamiltonian can be expressed as a sum of projection operators onto the $\mathcal{J} = 2$ subspaces of each bond:

$$\frac{\mathcal{H}_{\text{AKLT}}}{J} = 2 \sum_{i=1}^N \mathcal{P}_2(i, i+1) - \frac{2N}{3}. \quad (10.73)$$

Its ground state is represented graphically in Fig. 10.7 [284]. It is a valence bond state in which each component $\sigma = 1/2$ of the spin $S = 1$ at site i is contracted in a (singlet) valence bond with one of the $\sigma = 1/2$ spins at a neighbouring site. That is,

$$|S\rangle_{\text{AKLT}} = [12] [23] \dots [i-1, i] [i, i+1] \dots [N, 1]. \quad (10.74)$$

This state cannot have a projection onto the $\mathcal{J} = 2$ subspaces of each bond $i, i+1$, since two of the spin 1/2 components form a singlet. It is therefore an eigenstate and its energy $E_0 = -2NJ/3$ is smaller than the expectation value of $\mathcal{H}_{\text{AKLT}}$ in the Néel state ($-NJ/3$). Since \mathcal{J} assumes the smallest possible value at each bond, we have found the ground state. As for the Majumdar–Ghosh state, spin-spin correlation functions [285] decrease exponentially over a length $a/\ln 3$ which is of the order of the lattice constant. This state with its

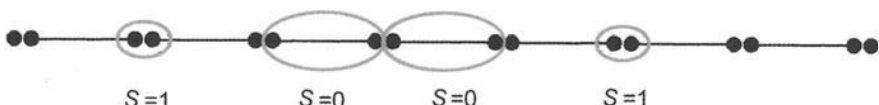


Fig. 10.7. Solid valence bond AKLT state. Each spin 1 is decomposed into two spin 1/2 components combined into valence bonds with neighbouring spins. At each end of the chain is an unmatched spin 1/2 which can be observed experimentally

ordered valence bonds has spin correlations which are typical of a liquid state (and there is a formal analogy between the AKLT state and the Laughlin state describing the fractional quantum Hall effect) [285, 290]. The first excited state is a triplet separated from the ground state by an energy gap $\Delta = 0.35J$ [285]. This is slightly less than the gap for the isotropic chain ($\Delta = 0.41J$) [286, 287, 289].

Physical Interpretation of the Haldane Liquid State

The AKLT state (10.74) can be expanded in a linear combination of products of $2N$ spin 1/2 states:

$$\begin{aligned} |S\rangle_{\text{AKLT}} &= \frac{1}{2^{N/2}} \sum_{\text{bonds}} (-1)^P [(\uparrow_1 \downarrow_2)(\downarrow_2 \uparrow_3)(\uparrow_3 \downarrow_4)(\uparrow_4 \downarrow_5)(\downarrow_5 \uparrow_6)\dots] \\ &= \frac{1}{2^{N/2}} \sum_{\text{config}} (-1)^P [\uparrow_1, -1_2, 1_3, 0_4, -1_5, \dots], \end{aligned} \quad (10.75)$$

where σ_i^z components have been added at each site to specify the S_i^z component of the i th spin ($S = 1$). Since the σ_i^z components of each valence bond are opposite, the S_i^z can never take the same values, either +1 or -1, at two successive sites. This describes an antiferromagnetic order without positional order. In other words, a spin with $S_z^i = +1$ can have any number of neighbours with component $S_z^j = 0$, but must eventually encounter a spin such that $S_z^k = -1$, i.e.,

$$S_i^z = +1, \quad S_k^z = -1, \quad \text{and} \quad S_j^z = 0 \quad \text{if} \quad i < j < k. \quad (10.76)$$

The fewer spins there are with $S_j^z = 0$, the closer the state approximates an antiferromagnetic state. A revealing way of representing the same state [250] is as follows: to a state $S_i^z = +1$ we associate a fictive particle at site i with spin $\sigma_z = +1/2$; likewise, to a state $S_i^z = -1$ we associate a fictive particle with spin $\sigma_z = -1/2$, and all spin states with $S_z^j = 0$ remain unoccupied. This representation describes a fluid with antiferromagnetic order. The total absence of positional order means we must introduce a non-local order parameter

$$\psi_1 = - \left\langle \exp \left(i\pi \sum_{i=1}^n S_i^z \right) S_n^z \right\rangle, \quad (10.77)$$

suitable for describing this Haldane liquid phase. Figure 10.8 shows a configuration of spins $\sigma_i^z = \pm 1/2$ in the state (10.75), the configuration of spins S_i^z , and that of the corresponding fluid of fictive particles ($\sigma = \pm 1/2$), as well as local values of the order parameter. The more spins $S_i^z = 0$ there are, the smaller the order parameter becomes and the more dilute the fluid. A chemical potential can be associated with the fluid of fictive particles. This potential increases as the density diminishes. In the Hamiltonian (10.1), the

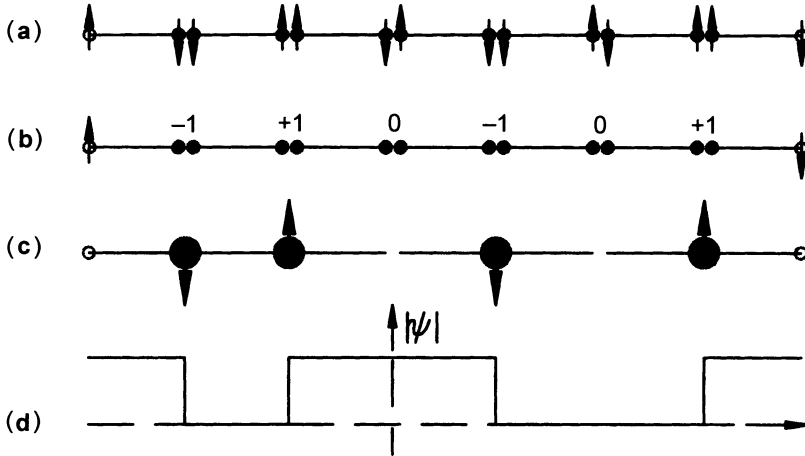


Fig. 10.8. (a) Spin 1/2 configuration specifying the valence bond state. (b) Corresponding spin 1 configuration. (c) State of the fluid of fictive particles $\sigma = \pm 1/2$. (d) Local values of the order parameter

planar anisotropy term $D > 0$ (which favours the $S_z^i = 0$ state) plays the role of chemical potential for the Haldane liquid. When the chemical potential is large enough, we go from a liquid to a gaseous phase whose order parameter becomes

$$\psi_g = - \left\langle \exp \left(i\pi \sum_{i=1}^n S_i^z \right) \right\rangle . \quad (10.78)$$

In this phase, there remains only a dilute gas of particles occurring in pairs $\sigma_z = \pm 1/2$.

Valence bond states have been used to construct two concrete examples of a singlet ground state. As it has not been possible to carry out an exact study of excited states, no clear difference between integer and half-integer spins has come out. The non-linear σ models make this difference more explicit [245, 246].

10.4 The Non-Linear σ Model for Antiferromagnetic Chains

It is interesting to study topological defects associated with antiferromagnetic chains in order to understand their role in quantum magnetism. As for the XY chain, we use semi-classical methods appropriate to large spin values S . In this limit, we expect local antiferromagnetic order. At long wavelengths, the local direction of the alternating magnetisation \mathbf{n} is a collective coordinate with slow dynamics. In an antiferromagnet, local magnetisation \mathbf{l} is also a

conserved quantity which should therefore be included in any hydrodynamic description. This approach will be illustrated here for the ladder structure shown in Fig. 10.6 [291, 292]. The Hamiltonian is $\mathcal{H} = \mathcal{H}_1 + \mathcal{H}_2$ where \mathcal{H}_1 and \mathcal{H}_2 were defined in (10.54) and (10.63). We carry out a hydrodynamic expansion in $1/S$ about the antiferromagnetic state. This assumes that S is large and also that frustration in the model is not large enough to change the classical ground state. Let

$$2\hbar S \mathbf{n}_{2i} = \mathbf{S}_{2i} - \mathbf{S}_{2i-1}, \quad (10.79)$$

$$2\hbar a \mathbf{l}_{2i} = \mathbf{S}_{2i-1} + \mathbf{S}_{2i}, \quad (10.80)$$

where $2a$ is the lattice constant. We can check that these variables obey commutation relations:

$$\begin{aligned} \left[l_{2i}^\alpha, l_{2j}^\beta \right] &= i\varepsilon^{\alpha\beta\gamma} l_{2i}^\gamma \frac{\delta_{ij}}{2a} \rightarrow [l^\alpha(x), l^\beta(x')] = i\varepsilon^{\alpha\beta\gamma} \delta(x - x'), \\ \left[n_{2i}^\alpha, l_{2j}^\beta \right] &= i\varepsilon^{\alpha\beta\gamma} n_{2i}^\gamma \frac{\delta_{ij}}{2a} \rightarrow [n^\alpha(x), l^\beta(x')] = i\varepsilon^{\alpha\beta\gamma} \delta(x - x'), \\ \left[n_{2i}^\alpha, n_{2j}^\beta \right] &= i\varepsilon^{\alpha\beta\gamma} l_{2i}^\gamma \frac{a^2}{S^2} \frac{\delta_{ij}}{2a} \rightarrow [n^\alpha(x), n^\beta(x')] \approx 0, \end{aligned} \quad (10.81)$$

taking the continuous limit $\delta_{ij}/2a \rightarrow \delta(x - x')$ and neglected contributions of order $1/S^2$. Moreover, vectors \mathbf{n} and \mathbf{l} must remain orthogonal,

$$\mathbf{n}(x) \cdot \mathbf{l}(x) \equiv 0 \quad \text{and} \quad \mathbf{n}^2 = 1 + \frac{1}{S} - \frac{a^2}{S^2} \mathbf{l}^2. \quad (10.82)$$

The vector \mathbf{l} appears as the generator of local rotations in the group $O(3)$, whilst \mathbf{n} transforms as a vector. In fact, \mathbf{l} is the angular momentum of a material particle placed at the end of the vector \mathbf{n} , and is therefore generated by its dynamics. Indeed the equations of motion of spin \mathbf{S}_{2i} are

$$\begin{aligned} -\frac{\partial \mathbf{S}_{2i}}{\partial t} &= J_1(1 + \delta) \mathbf{S}_{2i} \times \mathbf{S}_{2i-1} + J_1(1 - \delta) \mathbf{S}_{2i} \times \mathbf{S}_{2i+1} \\ &\quad + J_2 \mathbf{S}_{2i} \times (\mathbf{S}_{2i-2} + \mathbf{S}_{2i+2}), \end{aligned} \quad (10.83)$$

and these determine, to first order in $|\mathbf{l}| \ll 1$, the equations of motion of \mathbf{n} :

$$-\mathbf{S} \frac{\partial \mathbf{n}}{\partial t} = 4J_1 a S \mathbf{n} \times \mathbf{l}. \quad (10.84)$$

\mathbf{l} can then be expressed in terms of \mathbf{n} ,

$$\mathbf{l} \approx \frac{1}{4J_1 a} \mathbf{n} \times \frac{\partial \mathbf{n}}{\partial t}. \quad (10.85)$$

Note that, in the presence of a magnetic field, we can just move to the rotating frame

$$\frac{\partial \mathbf{n}}{\partial t} \rightarrow \frac{\partial \mathbf{n}}{\partial t} - \gamma \mathbf{n} \times \mathbf{H}. \quad (10.86)$$

In order to specify the dynamics of \mathbf{l} , we must expand the interaction energy between spins in terms of the gradients of $\mathbf{n}(x)$ and $\mathbf{l}(x)$. Keeping only first and second order terms,

$$\mathbf{S}_{2i-1} \cdot \mathbf{S}_{2i} \approx -S(S+1) + 2a^2 \mathbf{l}^2(x), \quad (10.87)$$

$$\begin{aligned} \mathbf{S}_{2i} \cdot \mathbf{S}_{2i+1} &= [\mathbf{S}\mathbf{n}(x-a) + a\mathbf{l}(x-a)] \cdot [-\mathbf{S}\mathbf{n}(x+a) + a\mathbf{l}(x+a)], \\ &\approx -S(S+1) + 2a\mathbf{l}^2(x) + 2a^2 S^2 \left(\frac{\partial \mathbf{n}}{\partial x} \right)^2 \\ &\quad - 2a^2 S \left(\mathbf{l} \cdot \frac{\partial \mathbf{n}}{\partial x} + \frac{\partial \mathbf{n}}{\partial x} \cdot \mathbf{l} \right), \end{aligned} \quad (10.88)$$

$$\begin{aligned} \mathbf{S}_{2i-1} \cdot \mathbf{S}_{2i+1} &= [\mathbf{S}\mathbf{n}(x-a) + a\mathbf{l}(x-a)] \cdot [\mathbf{S}\mathbf{n}(x+a) + a\mathbf{l}(x+a)], \\ &\approx S(S+1) - 2a^2 S^2 \left(\frac{\partial \mathbf{n}}{\partial x} \right)^2. \end{aligned} \quad (10.89)$$

The second derivative of \mathbf{n} satisfies the identity

$$\mathbf{n} \cdot \frac{\partial^2 \mathbf{n}}{\partial x^2} + \frac{\partial^2 \mathbf{n}}{\partial x^2} \cdot \mathbf{n} = -2 \left(\frac{\partial \mathbf{n}}{\partial x} \right)^2, \quad (10.90)$$

obtained by twice differentiating $\mathbf{n}^2 = \text{constant}$. Likewise, the scalar product

$$\mathbf{n} \cdot \frac{\partial \mathbf{l}}{\partial x} = -\mathbf{l} \cdot \frac{\partial \mathbf{n}}{\partial x} \quad (10.91)$$

is the derivative of $\mathbf{n} \cdot \mathbf{l} = 0$.

By taking the continuous limit in this way, we obtain an effective Hamiltonian for the low-energy degrees of freedom described by vector fields \mathbf{l} and \mathbf{n} ,

$$\begin{aligned} \mathcal{H}_{\text{eff}} &= a \int dx \left[J_1 \mathbf{l}^2 - 2J_1 S(1-\delta) \left(\mathbf{l} \cdot \frac{\partial \mathbf{n}}{\partial x} + \frac{\partial \mathbf{n}}{\partial x} \cdot \mathbf{l} \right) \right. \\ &\quad \left. + 2(J_1(1-\delta) - 2J_2) S^2 \left(\frac{\partial \mathbf{n}}{\partial x} \right)^2 \right]. \end{aligned} \quad (10.92)$$

We can now recognise the Hamiltonian of the non-linear σ model [291, 293, 294],

$$\mathcal{H} = \frac{4J_1 a}{g^2} \int_{-\infty}^{\infty} dx \left[g^2 \left(1 - \frac{\Theta}{4\pi} \frac{\partial \mathbf{n}}{\partial x} \right)^2 + \frac{1}{g^2} \left(\frac{\partial \mathbf{n}}{\partial x} \right)^2 \right], \quad (10.93)$$

in which the coupling constant

$$g^2 = \frac{2}{S \sqrt{1 - \delta^2 - 4J_2/J_1}} \quad (10.94)$$

increases with frustration J_2 and tends to infinity when $J_2/J_1 = (1 - \delta^2)/4$. Before examining the role of the topological angle

$$\Theta = 2\pi(1-\delta)S, \quad (10.95)$$

we study the dynamics of this model when there is no topological term, i.e., when $\Theta = 0$. The first step is to identify conjugate canonical variables. As in the XY model, coordinates of vector \mathbf{n} are specified by its component n_z

and the angle ϕ made by its projection in the (x, y) plane. Let Π_z and Π_ϕ denote the variables canonically conjugate to n_z and ϕ , that is, satisfying

$$[\phi(x), \Pi_\phi(x')] = i\delta(x - x') , \quad [n_z(x), \Pi_z(x')] = i\delta(x - x') , \quad (10.96)$$

$$\begin{aligned} [\phi(x), n_z(x')] &= [\Pi_\phi(x), \Pi_z(x')] \\ &= [\phi(x), \Pi_z(x')] = [n_z(x), \Pi_\phi(x')] = 0 . \end{aligned}$$

Commutation relations (10.81) show immediately that we can identify Π_ϕ with l_z . Likewise, from the equation of motion (10.83), we can relate Π_z to l^+ :

$$\Pi_z = \frac{i}{2(1 - n_z^2)} (n^- l^+ - n^+ l^-) . \quad (10.97)$$

We can now put the Hamiltonian into canonical form,

$$\begin{aligned} \mathcal{H} = \frac{4J_1 a}{g^2} \int_{-\infty}^{\infty} dx &\left[g^2 \left(\Pi_z (1 - n_z^2) \Pi_z + \frac{\Pi_\phi^2}{1 - n_z^2} \right) \right. \\ &\left. + \frac{1}{g^2} \left(\frac{\partial \mathbf{n}}{\partial x} \right)^2 \right] . \end{aligned} \quad (10.98)$$

Hamilton's equations,

$$\begin{aligned} i \frac{\partial \phi}{\partial t} &= [\phi, H] , \quad i \frac{\partial n_z}{\partial t} = [n_z, H] , \\ i \frac{\partial \Pi_\phi}{\partial t} &= [\Pi_\phi, H] , \quad i \frac{\partial \Pi_z}{\partial t} = [\Pi_z, H] , \end{aligned} \quad (10.99)$$

completely specify the dynamics of the system. We thus obtain the Lagrangian

$$\begin{aligned} \mathcal{L} &= \int dx \left[\frac{\partial n_z}{\partial t} \Pi_z + \frac{\partial \phi}{\partial t} \Pi_\phi \right] - \mathcal{H} \\ &= \frac{1}{g^2} \int_{-\infty}^{\infty} dx \left[\frac{1}{c} \left(\frac{\partial \mathbf{n}}{\partial t} \right)^2 - c \left(\frac{\partial \mathbf{n}}{\partial x} \right)^2 \right] , \end{aligned} \quad (10.100)$$

where $c = 4J_1 a / g^2$. The Lorentz invariance of the non-linear σ model is rendered quite explicit here. As in the XY model, the speed c of the spin waves plays the role of the speed of light. The equations of motion can also be obtained from the Euler–Lagrange equations for the field \mathbf{n} ,

$$\frac{\partial}{\partial t} \left(\frac{\delta \mathcal{L}}{\delta \partial_t \mathbf{n}} \right) + \frac{\partial}{\partial x} \left(\frac{\delta \mathcal{L}}{\delta \partial_x \mathbf{n}} \right) = \frac{\delta \mathcal{L}}{\delta \mathbf{n}} , \quad (10.101)$$

provided we incorporate the constraint $\mathbf{n}^2 \approx 1$ into the Lagrangian density \mathcal{L} by introducing a Lagrange multiplier,

$$L \longrightarrow L + \lambda(\mathbf{n}^2 - 1) .$$

This can be eliminated from the equations of motion

$$\frac{1}{c^2} \frac{\partial^2 \mathbf{n}}{\partial t^2} - \frac{\partial^2 \mathbf{n}}{\partial x^2} + \lambda \mathbf{n} = 0 , \quad (10.102)$$

by taking scalar and vector products:

$$0 = \mathbf{n} \cdot \left(\frac{1}{c^2} \frac{\partial^2 \mathbf{n}}{\partial t^2} - \frac{\partial^2 \mathbf{n}}{\partial x^2} \right) + \left[\frac{1}{c^2} \left(\frac{\partial \mathbf{n}}{\partial t} \right)^2 - \left(\frac{\partial \mathbf{n}}{\partial x} \right)^2 \right] , \quad (10.103)$$

$$0 = \frac{g^2}{c} \frac{\partial l}{\partial t} - \mathbf{n} \times \frac{\partial^2 \mathbf{n}}{\partial x^2} . \quad (10.104)$$

The classical solutions in this model are known and quantum properties can be studied by the instanton method [264]. The instanton action is finite. Note first that the topological term Θ occurring in the initial Hamiltonian (10.93) can be generated in the non-linear σ model (10.98) by carrying out a canonical transformation [296] [i.e., one which preserves commutation relations (10.99)],

$$\tilde{\phi} = \phi , \quad \tilde{n}_z = n_z , \quad (10.105)$$

$$\tilde{\Pi}_\phi = \Pi_\phi + \frac{\Theta}{4\pi} \frac{\partial n_z}{\partial x} , \quad \tilde{\Pi}_z = \Pi_z - \frac{\Theta}{4\pi} \frac{\partial \phi}{\partial x} .$$

The Hamiltonian is invariant under this canonical transformation,

$$\begin{aligned} \mathcal{H} = \tilde{\mathcal{H}} &= c \int dx \left[g^2 \left(\tilde{\Pi}_z + \frac{\Theta}{4\pi} \frac{\partial \phi}{\partial x} \right) (1 - n_z^2) \left(\tilde{\Pi}_z + \frac{\Theta}{4\pi} \frac{\partial \phi}{\partial x} \right) \right. \\ &\quad \left. + \frac{1}{1 - n_z^2} \left(\Pi_\phi - \frac{\Theta}{4\pi} \frac{\partial n_z}{\partial x} \right) + \frac{1}{g^2} \left(\frac{\partial n_z}{\partial x} \right)^2 \right] , \end{aligned} \quad (10.106)$$

which also preserves the equations of motion. In this form, we recognise the Hamiltonian (10.93) of the non-linear σ model with topological term Θ . This term has an effect on the phase of wave functions via the action $\tilde{\mathcal{S}} = \int \tilde{\mathcal{L}} dt$, exactly as the vector potential affects the electron phase (Bohm–Aharonov effect), without modifying the equations of motion. Indeed, the Lagrangian becomes

$$\begin{aligned} \tilde{\mathcal{L}} &= \int dx \left[\frac{\partial n_z}{\partial t} \tilde{\Pi}_z + \frac{\partial \phi}{\partial t} \tilde{\Pi}_\phi - \tilde{H} \right] \\ &= \mathcal{L} + \frac{\Theta}{4\pi} \int dx \mathbf{n} \cdot \frac{\partial \mathbf{n}}{\partial t} \times \frac{\partial \mathbf{n}}{\partial x} , \end{aligned} \quad (10.107)$$

shifting the action by

$$\tilde{\mathcal{S}} - \mathcal{S} = \frac{\Theta}{4\pi} \int \int dt dx \mathbf{n} \cdot \frac{\partial \mathbf{n}}{\partial t} \times \frac{\partial \mathbf{n}}{\partial x} \equiv \Theta \mathcal{Q} . \quad (10.108)$$

Imposing periodic boundary conditions on the field $\mathbf{n}(x, t)$,

$$\mathbf{n}(-\infty, t) = \mathbf{n}(\infty, t) \quad \text{and} \quad \mathbf{n}(x, -\infty) = \mathbf{n}(x, \infty) ,$$

a point x, t of space-time can be considered as the stereographic projection of a point \mathbf{z} on the surface of a sphere (see Fig. 9.2). Hence, the mapping which associates vector $\mathbf{n}(x, t) \equiv \mathbf{n}(\mathbf{z})$ with $\mathbf{z} \equiv x, t$ is a bijection from the sphere (\mathbf{z}) onto a sphere (\mathbf{n}), and integral Q represents the number of turns made by \mathbf{n} as \mathbf{z} covers the sphere. Note in this respect that the surface element of the sphere is

$$dS = \sin \theta d\theta \frac{\partial n_\theta}{\partial \theta} \frac{\partial n_\phi}{\partial \phi} = \mathbf{n} \cdot \frac{\partial \mathbf{n}}{\partial t} \times \frac{\partial \mathbf{n}}{\partial x}. \quad (10.109)$$

Q is therefore a whole number and a topological invariant. We can thus deduce that the physics is periodic in Θ with 2π periodicity. If there is no dimerisation ($\Theta = 2\pi S$), spin chains must therefore be equivalent to the non-linear σ model with $\Theta = 0$ when S is integer valued, and with $\Theta = \pi$ when S is half-integer valued. Although the topological angle Θ comes into the global action for the whole chain, it originates in the periodicity of the spin states, a local feature. In order to bring this out, it will be useful to discretise the model once again by putting [294]

$$a \frac{\partial \mathbf{n}}{\partial x} = \mathbf{n}(j) - \mathbf{n}(j+1), \quad (10.110)$$

and then eliminating the minus sign by defining a vector field $\tilde{\mathbf{n}}$ such that $\tilde{\mathbf{n}}(j) = \mathbf{n}(j)$ and $\tilde{\mathbf{n}}(j+1) = -\mathbf{n}(j+1)$. In this version, the Hamiltonian of the non-linear σ model becomes

$$\mathcal{H} = \frac{4J_1}{g^2} \sum_j \left[g^2 l'^2(j) + \frac{1}{g^2} \tilde{\mathbf{n}}(j) \cdot \tilde{\mathbf{n}}(j+1) \right], \quad (10.111)$$

where the angular momentum \mathbf{l}' differs from \mathbf{l} by the vector potential \mathbf{A} of a monopole [257] placed at the centre of the sphere traced out by the end of the vector \mathbf{n} ,

$$\mathbf{l}'(j) = \mathbf{l}(j) + \frac{\Theta}{2\pi} \mathbf{A}(j). \quad (10.112)$$

(In one of the possible gauges,

$$A_\phi = -\cot \theta, \quad (10.113)$$

where θ is the angle between \mathbf{n} and $\hat{\mathbf{z}}$.)

We can now examine properties of this system in the strong coupling limit $g^2 \gg 1$. The total energy is dominated by the kinetic energy $l'^2(j)$. The possible values of l'^2 and l'_z can be obtained either by solving the Schrödinger equation directly when a magnetic monopole is present, or by using semi-classical quantisation methods in the presence of an adiabatic phase [297],

$$l'^2(j) = \left(l + \frac{\Theta}{2\pi} \right) \left(l + 1 + \frac{\Theta}{2\pi} \right), \quad (10.114)$$

$$l'_z(j) = m + \frac{\Theta}{2\pi}. \quad (10.115)$$

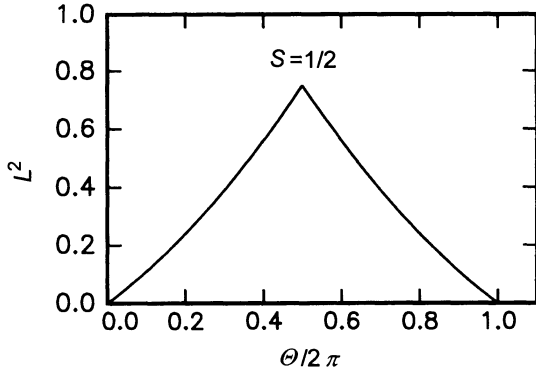


Fig. 10.9. Kinetic energy as a function of topological angle Θ . The ground state is non-degenerate unless $\Theta = \pi$, in which case angular momentum is quantised in half-integer values

The ground state has non-zero angular momentum except when $\Theta = 0$. Figure 10.9 shows that l'^2 attains its maximum value of $3/4$ when $\Theta = \pi$. At this point, l' is quantised in half-integer values and there is degeneracy at each site since $l'_z(j)$ can take values $\pm 1/2$. When $\Theta < \pi$, the ground state is unique,

$$l'^2 = \frac{\Theta}{2\pi} \left(1 + \frac{\Theta}{2\pi} \right) , \quad (10.116)$$

$$l'_z = \frac{\Theta}{2\pi} . \quad (10.117)$$

The same is true for $\Theta > \pi$, where

$$l'_z = -1 + \Theta/2\pi , \quad l'^2 = (\Theta/2\pi - 2)(\Theta/2\pi - 1) .$$

This is a rather unusual chiral state since, as for a ferromagnetic state, it breaks time reversal invariance. The first excited state $l = 1$ is separated from the ground state by a gap of the order of J_1 , except when $\Theta = \pi$, in which case degeneracy can only be removed by the effects of the (very small) antiferromagnetic interaction $\tilde{\mathbf{n}}(j) \cdot \tilde{\mathbf{n}}(j+1)$. In other words, the kinetic term l'^2 acts as a projector onto the subspace of states with $\sigma_z = \pm 1/2$. On this subspace, the matrix elements of $\tilde{\mathbf{n}}(j) \cdot \tilde{\mathbf{n}}(j+1)$ are proportional to the matrix elements of $\sigma(j) \cdot \sigma(j+1)$ (Wigner–Eckart theorem). This allows us to identify this model with the isotropic Heisenberg chain, which has no gaps in its excitation spectrum. For weaker couplings $g^2 \leq 1$, it is not known whether the model has this structure.

Hence half-integer spin chains (with $\delta = 0$) have a very special almost ordered structure because angular momentum cannot remove $\sigma = \pm 1/2$ degeneracy. All other systems have a gap in their excitation spectra, generated either by spin dimerisation ($\delta \neq 0$), or by quantum fluctuations which restore rotation invariance when spins are integer valued.

Many aspects of spin chains remain to be explored. For example, only qualitative studies have yet been made of phase transitions between the various quantum states in Figs. 10.1 and 10.2 [250].

11. Itinerant Magnetism

The metallic state is characterised by the high kinetic energy of conduction electrons, imposed by the Pauli principle. In metallic systems, spontaneous magnetisation necessarily generates a difference between the total kinetic energy of \uparrow spins and \downarrow spins, because chemical potentials of the two Fermi seas (\uparrow and \downarrow) remain the same. Figure 11.3 shows the \uparrow and \downarrow Fermi seas of an electron gas, which has polarisation $\sigma = (N_\uparrow - N_\downarrow)/N$. The sum of kinetic energies of spin \uparrow (+) and spin \downarrow (-) electrons

$$\mathcal{E}_k(\pm) = \int_{\mp IN\sigma/V}^{\varepsilon_F} \varepsilon n(\varepsilon) d\varepsilon , \quad (11.1)$$

is always greater than the kinetic energy in the unpolarised state. [$n(\varepsilon_F)$ is the density of states at the Fermi level.] In terms of electron polarisation σ , the increase in kinetic energy is of order

$$\Delta\mathcal{E}_k = \frac{(N_\uparrow - N_\downarrow)^2}{2n(\varepsilon_F)} = \frac{N^2\sigma^2}{2n(\varepsilon_F)} , \quad (11.2)$$

implying a value of $2N\varepsilon_F\sigma^2/3$ for a free electron gas. This is a considerable increase for a metal whose Fermi energy and electron density are already rather high. The shift between \uparrow and \downarrow Fermi seas becomes energetically possible only if electron polarisation lowers the Coulomb energy even more. As for an atom, the Coulomb interaction between two electrons with parallel spins is weaker because antisymmetry of spatial wave functions tends to keep them further apart. Let $r_s a_B$ denote the mean distance between electrons, where a_B is the Bohr radius and r_s a dimensionless parameter. The Coulomb energy, of the order of $e^2/4\pi\varepsilon_0 r_s a_B$, decreases as $1/r_s$ when electron density ($\propto 1/r_s^3$) is decreased. In contrast, the r_s dependence of the kinetic energy is $\varepsilon_F \propto 1/r_s^2$ [$\varepsilon_F \propto k_F^2 \propto 1/(r_s a_B)^2$]. Ferromagnetic instability becomes more probable when interactions dominate, that is, at very low electron densities. Unfortunately, it is clear today [298, 299] that a free electron gas cannot have ferromagnetic instability. Two phenomena tend to stabilise the Fermi sea. Firstly, in its unpolarised state, electron positions are correlated in such a way as to minimise Coulomb interactions. For this reason, the interaction energy is only slightly lower in the ferromagnetic state than in the unpolarised state. Secondly, at very low densities, the ferromagnetic state must compete with a state in which electrons crystallise into a regular triangular

lattice, the Wigner crystal [300]. In very weakly doped semiconductors II–VI ($\text{Hg}_x\text{Cd}_{1-x}\text{Te}$), experiments show that electrons condense into an electronic solid [301], thereby confirming Wigner's arguments. The ferromagnetism of transition metals belonging to the $3d$ series [e.g., Fe ($3d^64s^2$), Co ($3d^74s^2$), Ni ($3d^84s^2$)] can only be explained by appealing to the rather special band structure of $3d$ states in metallic contexts [302, 303].

Table 11.1. Magnetisation, magnetic moment per atom, Curie temperature and Curie constant for ferromagnetic metals

Material	$M(T = 0)$ [emu/mole]	μ/μ_B	T_c [K]	C [emu/mole K]
Fe	1752	2.22	1093	1.26
Co	1449	1.72	1428	1.22
Ni	510	0.53	650	0.31

In these metals, a certain number of d_α orbitals are filled. It might therefore be thought that their magnetism comes from sufficiently localised d_α orbitals [304, 305]. Metallic features could then be imputed to delocalised s orbitals playing no ferromagnetic role. This simplified view is quite appropriate for the rare earths since the $4f$ orbitals are highly localised within the ions.

In the rare earths, $4f$ valence orbitals are protected inside the ion by the $5s$ and $5p$ orbitals. These $5s$ and $5p$ orbitals constitute the metallic bands. In many materials, there is sufficiently little hybridisation between $4f$ states and metallic bands to ensure that the latter retain their localised character. Although the magnetism of rare earths can to a large extent be formulated in terms of localised spins, electronic degrees of freedom remain significant since they allow an exchange interaction to be transmitted between localised spins.

However, such a view is far from accurate for transition ions. The d_α orbitals form bands of width greater than one electron-volt and their magnetism cannot be explained in terms of localised states. Moreover, neutron and X-ray scattering experiments [306, 307] have shown that the magnetic moment of each electron in the $3d_\alpha$ bands is close to the Bohr magneton, although there is strong global compensation between bands (in nickel, magnetic polarisation reduces to $\approx 0.53\mu_B$ per atom). Even if the $3d_\alpha$ electrons are in Bloch states, there is always a finite probability of two electrons being at the same site. Coulomb repulsion between two electrons thus remains effective even if the Fermi surface significantly alters its characteristics. In fact, there is competition between this Hund term and quantum delocalisation which gives rise to the electron kinetic energy. Whether or not there is magnetic instability depends exclusively on the number of electrons contributing to energy exchange. Since exchange is above all a scattering process requiring access to unoccupied states, only electrons close to the Fermi level can contribute to magnetic exchange in a metal. We can estimate the conditions in

which a magnetic instability may occur. Let I denote the reduction in potential energy caused by reversing a spin. If the electron gas has polarisation σ , the total gain in potential energy will be of order

$$\begin{aligned}\Delta E_{\text{int}} &= -I \left[N_{\uparrow}^2 + N_{\downarrow}^2 - 2 \left(\frac{N}{2} \right)^2 \right] \\ &= -\frac{N^2 I}{4} [(1 + \sigma)^2 + (1 - \sigma)^2 - 2] = -\frac{N^2 I}{2} \sigma^2.\end{aligned}\quad (11.3)$$

An instability is only possible when the sum $\Delta E_k + \Delta E_{\text{int}}$ is negative, which gives Stoner's criterion (cf. Sect. 11.2),

$$In(\varepsilon_F) > 1, \quad (11.4)$$

where I is determined by the Coulomb exchange interaction and $n(\varepsilon_F)$ is the density of states at the Fermi level. This criterion involves microscopic aspects of exchange, through the term I , and the number of participating electrons, through the term $n(\varepsilon_F)$. It is fairly universal, depending little on the model under consideration. In particular, the Hubbard model (see Sect. 11.4), which is more appropriate for description of narrow bands, leads to the same criterion. The three ferromagnetic metals in the $3d$ series, iron, nickel and cobalt, all satisfy Stoner's condition. In general, the wider the d bands, the smaller the density of states at the Fermi level. This is why metals in the $4d$ and $5d$ transition series, with bands two or three times wider than those in the $3d$ series, are not magnetic [308]. (Certain metals in the $4d$ series, such as palladium, are nevertheless very close to magnetic instability. This is revealed by the formation of giant magnetic moments when dilute quantities of impurity are introduced into these metals.) We can also understand why copper is not magnetic. Its $3d$ bands are completely filled and its Fermi level lies in the (very wide) $4s$ level (see Fig. 11.1). In contrast, the Fermi level of nickel falls in the $3d$ band which is only partially filled, to the advantage of the $4s$ band. Nickel is ferromagnetic and considered to be the best example of an itinerant magnet. The great success of the Stoner model stems from its simplicity [309]. It describes the main ferromagnetic features of metals and alloys in the $3d$ series, without appealing to either the structure of the $3d$ bands or hybridisation effects.

However, there is one aspect of the problem which is not taken into account by the Stoner criterion, namely the shape and structure of the Fermi surface. In certain metals of the $3d$ series and also in highly anisotropic organic conductors, some regions of the Fermi surface have nesting properties: one part of the Fermi surface occupied by the d_α can be fitted into an unfilled part of another band d_β , by translating through a wave vector \mathbf{Q}_0 (cf. Fig. 11.5). In this case, there are many states \mathbf{k} near the Fermi surface of each band such that

$$\varepsilon_{d_\alpha}(\mathbf{k}) = \varepsilon_{d_\beta}(\mathbf{k} + \mathbf{Q}_0). \quad (11.5)$$

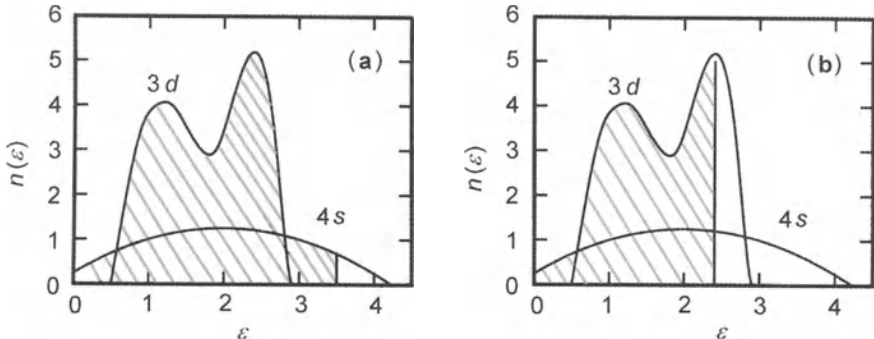


Fig. 11.1. (a) Density of states in the $3d$ and $4s$ bands of copper. The Fermi level lies in the $4s$ band which is rather wide and in which the density of states is consequently rather low. (b) The same graph for nickel. The Fermi level lies at a maximum of the density of states in the much narrower $3d$ band. The Stoner criterion is therefore satisfied

A small perturbation coupling these degenerate states can then generate a magnetic instability. Such quasi-degeneracies have the effect of amplifying susceptibility $\chi(\mathbf{q})$ near the nesting vector $\mathbf{q} \approx \mathbf{Q}_0$ (see Sect. 11.1). [$\chi(\mathbf{q})$ measures the response $\mathbf{m}(\mathbf{q})$ to an exchange magnetic field $\mathbf{h}(\mathbf{q}) = h_0 \cos(\mathbf{q} \cdot \mathbf{r})$ of spatial period $2\pi/|\mathbf{q}|$.] Now the exchange interaction couples just the occupied states $|\alpha, \mathbf{k}, \uparrow\rangle$ of the d_α band with unoccupied states (holes) $|\beta, \mathbf{k} + \mathbf{Q}_0, \downarrow\rangle$ of the d_β band. Since these states are quasi-degenerate, a magnetic instability of wave vector $\mathbf{Q} \approx \mathbf{Q}_0$ may appear before the Stoner criterion $In(\varepsilon_F) > 1$ can be satisfied. The electron gas then forms a spin density wave. In this state the magnetisation density $\sigma(\mathbf{r}) = \sigma_0 \cos(\mathbf{Q} \cdot \mathbf{r})$ is modulated with period $2\pi/|Q|$.

The order parameter of a spin density wave may be more complex. It is a superposition of helicoidal structures in which spins \mathbf{S}_i rotate around a wave vector \mathbf{Q} , making an angle θ_Q with that vector ($(\mathbf{S}_i \cdot \mathbf{Q}) = \cos \theta_Q$). In practice, the most stable spin density waves formed in itinerant systems are linearly polarised states, i.e., superpositions of two spirals in opposite directions.

The wave vector $\mathbf{Q} \approx \mathbf{Q}_0$ is not necessarily commensurable with the period of the reciprocal lattice $G = 2\pi/a$. We then speak of an incommensurable spin density wave. This kind of instability becomes all the more probable as the nested section of the Fermi surface increases. The Fermi surface for an electron gas exhibits very pronounced nesting properties in one dimension, and weaker ones in two and three dimensions. This explains why many highly anisotropic organic conductors (quasi-one- or two-dimensional) form cascades of spin density waves at low temperatures [310]. Spin density wave states also exist in other materials, amongst which chromium is the best known example. Chromium possesses two bands with significant nesting properties, viz., a band of occupied states (electrons) with a band of unoccupied states (holes).

This nesting structure, proposed by Lomer [311], has led to identification of the microscopic mechanism which triggers the formation of a spin density wave. Many examples are known amongst metals, alloys and organic conductors: chromium, manganese, γ -iron; alloys of Cr and Mn, Cr and Ni, Mn and Fe; but also vanadium sulfates and selenides such as V_3S_4 , V_3Se_4 , V_5S_8 , V_5Se_8 , and $CrBr_2$ together with a whole series of 1-dimensional organic materials in the Bechgaard salt family. The microscopic basis for these magnetic states is the Overhauser mechanism [312]. Electron-hole pairs with parallel spins, each belonging to one of the two nested bands, are bound together by exchange. These neutral bound states are often called excitons by analogy with semiconductors. In the nested sections of the Fermi surface, a gap appears in the one-particle excitation spectrum. Electrons in these regions of the Fermi surface can no longer contribute to electrical conduction, which requires free electrons or holes. The state describing this type of spin density wave is often called an excitonic insulator, because electron-hole pairs cannot be broken apart once the spin density wave has been established. This state closely resembles the BCS state of a superconductor, except that in that case Cooper pairs of charge $2e$ are formed from two electrons with antiparallel spins (Cooper channel), whereas here the excitonic insulator (electron-hole channel) is formed by a neutral electron-hole pair.

Although somewhat simplistic, this theory explains many experimental details on the phase diagram of chromium and its alloys, even if the elementary excitation spectrum observed by neutron scattering remains largely unexplained by present spin wave theories.

Before going on to study the Stoner model and the excitonic insulator, it will be useful to understand how the susceptibility $\chi(\mathbf{q})$ depends on the wave vector of an electron gas without interactions.

11.1 The Kohn Singularity

Let us consider the magnetic response of an electron gas to an exchange induction $\mathbf{b}(\mathbf{q}) = b \cos(\mathbf{q} \cdot \mathbf{r})$ of wave vector \mathbf{q} . We use perturbation theory to estimate the energy change induced by Zeeman interaction of the spins with \mathbf{b} , viz.,

$$\mathcal{H}_z = g_S |\gamma| \sum_{\alpha i} \mathbf{S}_{\alpha i} \cdot \mathbf{b} \cos(\mathbf{q} \cdot \mathbf{r}), \quad (11.6)$$

where $\gamma = e/2m$ is the gyromagnetic factor. Here $\mathbf{S}_{\alpha i}$ is the spin of an electron in a Wannier d_α orbital centred on site i . In the limit $q \rightarrow 0$, uniform susceptibility is obtained by choosing the quantisation axis along z , and $\mathbf{b} = b \hat{\mathbf{x}}$ along x , so as to ensure that \mathcal{H}_z has no diagonal elements in the limit $\mathbf{q} \rightarrow 0$. Hence,

$$\mathcal{H}_z = \frac{g_S |\gamma| b}{2} \sum_{\alpha i} (S_{\alpha i}^+ + S_{\alpha i}^-) [\exp(i\mathbf{q} \cdot \mathbf{r}) + \exp(-i\mathbf{q} \cdot \mathbf{r})]. \quad (11.7)$$

Substituting expression (3.25) for spin operators in terms of second quantisation operators, then taking their Fourier transform

$$a_{\alpha i} = \frac{1}{\sqrt{V}} \sum_{\mathbf{k}} \exp(i\mathbf{k} \cdot \mathbf{R}_i) a_{\alpha \mathbf{k}}, \quad (11.8)$$

the Zeeman Hamiltonian becomes [see Sect. 3.8(I)]

$$\begin{aligned} \mathcal{H}_z = \frac{g_S \mu_B b}{4} \sum_{\alpha \beta \mathbf{k}} & \left[D_{\mathbf{k}, \mathbf{k}-\mathbf{q}}^{\alpha \beta} \left(a_{\beta \mathbf{k}-\mathbf{q} \uparrow}^\dagger a_{\alpha \mathbf{k} \downarrow} + a_{\beta \mathbf{k}-\mathbf{q} \downarrow}^\dagger a_{\alpha \mathbf{k} \uparrow} \right) \right. \\ & \left. + D_{\mathbf{k}, \mathbf{k}+\mathbf{q}}^{\alpha \beta} \left(a_{\beta \mathbf{k}+\mathbf{q} \uparrow}^\dagger a_{\alpha \mathbf{k} \downarrow} + a_{\beta \mathbf{k}+\mathbf{q} \downarrow}^\dagger a_{\alpha \mathbf{k} \uparrow} \right) \right], \end{aligned} \quad (11.9)$$

where D is the matrix element of $\exp(i\mathbf{q} \cdot \mathbf{r})$ between two Bloch states,

$$D_{\mathbf{k}, \mathbf{k}+\mathbf{q}}^{\alpha \beta} = \langle \beta, \mathbf{k} + \mathbf{q} | \exp(i\mathbf{q} \cdot \mathbf{r}) | \alpha, \mathbf{k} \rangle. \quad (11.10)$$

For a free electron gas, $D \equiv \delta_{\alpha \beta}$. In general, this Hamiltonian has no diagonal matrix elements. Second order perturbation theory gives the energy correction

$$\begin{aligned} \mathcal{E}_z = \left(\frac{g_S \mu_B h}{4} \right)^2 \sum_{\alpha \beta \mathbf{k} \sigma} & \left[\frac{|D_{\mathbf{k}, \mathbf{k}-\mathbf{q}}^{\alpha \beta}|^2 |\langle a_{\beta, \mathbf{k}-\mathbf{q}, -\sigma}^\dagger a_{\alpha \mathbf{k} \sigma} \rangle|^2}{\varepsilon_{\alpha \mathbf{k}} - \varepsilon_{\beta \mathbf{k}-\mathbf{q}}} \right. \\ & \left. + \frac{|D_{\mathbf{k}, \mathbf{k}+\mathbf{q}}^{\alpha \beta}|^2 |\langle a_{\beta, \mathbf{k}+\mathbf{q}, -\sigma}^\dagger a_{\alpha \mathbf{k} \sigma} \rangle|^2}{\varepsilon_{\alpha \mathbf{k}} - \varepsilon_{\beta \mathbf{k}+\mathbf{q}}} \right]. \end{aligned} \quad (11.11)$$

Contributions to this sum come from states in which \mathbf{k} is inside the Fermi surface and $\mathbf{k} + \mathbf{q}$ outside. The thermodynamic mean of $|\langle a_{\mathbf{k}+\mathbf{q}}^\dagger a_{\mathbf{k}} \rangle|^2$ therefore reduces to the product of occupation numbers of the occupied states in the α band and the holes in the β band, i.e., $f_{\mathbf{k}}^\alpha (1 - f_{\mathbf{k}+\mathbf{q}}^\beta)$, where f is the Fermi function $f(\varepsilon) = [\exp \beta(\varepsilon - \varepsilon_F) + 1]^{-1}$. The energy correction

$$\begin{aligned} \mathcal{E}_z = -\frac{g_S^2 \mu_B^2 b^2}{8} \sum_{\alpha \beta \mathbf{k}} & \left[|D_{\mathbf{k}, \mathbf{k}-\mathbf{q}}^{\alpha \beta}|^2 \frac{f_{\mathbf{k}}^\alpha (1 - f_{\mathbf{k}-\mathbf{q}}^\beta)}{\varepsilon_{\mathbf{k}-\mathbf{q}}^\beta - \varepsilon_{\mathbf{k}}^\alpha} \right. \\ & \left. + |D_{\mathbf{k}, \mathbf{k}+\mathbf{q}}^{\alpha \beta}|^2 \frac{f_{\mathbf{k}}^\alpha (1 - f_{\mathbf{k}+\mathbf{q}}^\beta)}{\varepsilon_{\mathbf{k}+\mathbf{q}}^\beta - \varepsilon_{\mathbf{k}}^\alpha} \right] \end{aligned} \quad (11.12)$$

is simplified by making the change of variable $\mathbf{k} \rightarrow \mathbf{k} + \mathbf{q}$ in the first term. Identifying the result with $-\chi(\mathbf{q})b^2/2\mu_0$, we deduce the susceptibility

$$\chi(\mathbf{q}) = \mu_0 \frac{g_S^2 \mu_B^2}{2} \sum_{\alpha \beta \mathbf{k}} |D_{\mathbf{k}, \mathbf{k}+\mathbf{q}}^{\alpha \beta}|^2 \frac{f_{\mathbf{k}}^\alpha - f_{\mathbf{k}+\mathbf{q}}^\beta}{\varepsilon_{\mathbf{k}-\mathbf{q}}^\beta - \varepsilon_{\mathbf{k}}^\alpha}. \quad (11.13)$$

In order to proceed further with this calculation, we would need to know the structure of the Bloch states and bands. We can nevertheless observe that energy denominators cancel at the nesting wave vector \mathbf{Q}_0 of the α band (occupied) on the β band (empty). This gives rise to a singularity (the

Kohn singularity [313]) in the susceptibility at the nesting vector \mathbf{Q}_0 . We pursue the study of this singularity by calculating the susceptibility of a free electron gas in one, two and three dimensions. For a one-dimensional electron gas at zero temperature, we convert the above sum into an integral:

$$\begin{aligned}\chi(q) &= \mu_0 g_S^2 \mu_B^2 \frac{2mN}{\hbar^2 V} \int_{-k_F}^{k_F} \frac{dk}{2\pi} \frac{1}{(k+q)^2 - k^2} \\ &= \mu_0 \frac{g_S^2 \mu_B^2 N}{\varepsilon_F V} \frac{k_F}{q} \ln \left| \frac{2k_F + q}{2k_F - q} \right|. \end{aligned}\quad (11.14)$$

The Lindhard susceptibility diverges logarithmically as $q \rightarrow 2k_F$. This divergence arises from electrons located at $k = k_F - \delta k$, whose energy $\varepsilon - \varepsilon_F = -v_F \hbar \delta k / m$ relative to the Fermi level is degenerate with respect to that of holes at $k = -k_F - \delta k$. Indeed, the energy of a hole relative to the Fermi level is minus the energy of the corresponding electron, viz., $\varepsilon_F - \varepsilon = -v_F \hbar \delta k / m$, and it has opposite spin. The point $-k_F$ is therefore nested onto the point $+k_F$ of the Fermi surface. This greatly increases the probability of instability for the spin density wave in one dimension. (Since electric polarisability has the same singularity at $q \approx 2k_F$, there is competition between spin and charge density waves and superconductivity.) In three dimensions, the above integral is carried out in two stages:

$$\begin{aligned}\chi(|\mathbf{q}|) &= \mu_0 g_S^2 \mu_B^2 \frac{2m}{\hbar^2} \int_0^{k_F} \frac{k^2 dk}{4\pi^2} \int_0^\pi \frac{\sin \theta d\theta}{q^2 + 2kq \cos \theta} \\ &= \mu_0 g_S^2 \mu_B^2 \frac{2m}{\hbar^2} \int_0^{k_F} \frac{k dk}{8\pi^2 q} \ln \frac{2k+q}{2k-q} \\ &= \mu_0 \frac{3g_S^2 \mu_B^2 N}{8\varepsilon_F V} W\left(\frac{2k_F}{q}\right), \end{aligned}\quad (11.15)$$

where $W(u)$ is given by

$$W(u) = \frac{1}{2} + \frac{1}{4u} (u^2 - 1) \ln \left| \frac{1+u}{1-u} \right|, \quad (11.16)$$

so that $W \rightarrow 1$ as u (or q) tends to zero. [We have used the integral

$$\int u du \ln(1 \pm u) = \frac{1}{2}(u^2 - 1) \ln(1 \pm u) - \frac{1}{2} \left(\frac{u^2}{2} \mp u \right) \quad (11.17)$$

and the relation between the number of electrons N , the volume V and k_F , viz., $N/V = k_F^3/3\pi^2$.] This function is monotonic decreasing from $q = 0$ to $q = \infty$ with a singularity in its derivative at $q = 2k_F$. Since it has no maximum, the free electron gas in three dimensions has no spin density wave instability. Of course, true solids do not have spherical Fermi surfaces and may have nesting properties leading to a maximum for $\chi(q)$. In two dimensions, we find an intermediate situation with

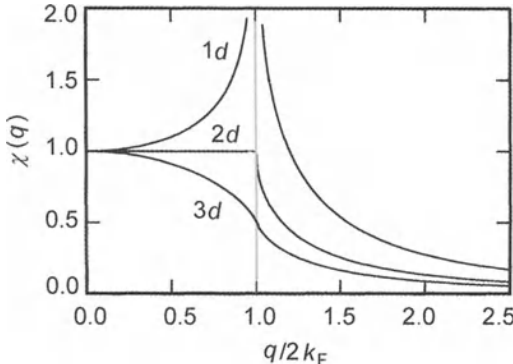


Fig. 11.2. Susceptibility of a free electron gas as a function of wave vector \mathbf{q} in one, two and three dimensions. The divergence of $\chi(\mathbf{q})$ as $q \rightarrow 2k_F$ only occurs in one dimension

$$\begin{aligned}\chi(q) &= \chi(0) \left[1 - \sqrt{1 - 4k_F^2/q^2} \right] \quad \text{for } q > 2k_F , \\ \chi(q) &\approx \chi(0) \quad \text{for } q < 2k_F .\end{aligned}\tag{11.18}$$

This evolution of $\chi(q)$ with dimension is illustrated in Fig. 11.2.

Before going on to study how excitonic insulators can form when $\chi(\mathbf{q})$ has a maximum for some value $\mathbf{q} = \mathbf{Q}_0$ (the nesting vector of the Fermi surface), it will be useful to examine the way in which a ferromagnetic instability can develop at $q = 0$ when $\chi(\mathbf{q})$ is monotonic decreasing.

11.2 The Stoner Model. Magnons in Metals

The Stoner model provides a tangible idea of magnetism in metals without appealing to band structure. It applies to itinerant electrons whose kinetic energy is considerably greater than the interaction energy between electrons.

The metallic state profoundly modifies the Coulomb interaction between electrons. The whole electron gas responds collectively to the Coulomb potential produced by each charge. This leads to a rapid decrease in the potential beyond some characteristic distance, the Thomas–Fermi length, of order the distance between electrons. This is the phenomenon of *screening*. The Coulomb potential $U(r) = -e^2/4\pi\epsilon_0 r$ between two electrons, with Fourier transform $U(\mathbf{q}) = -e^2/\epsilon_0 |\mathbf{q}|^2$, is screened by the other charges and hence decreases exponentially with distance,

$$U_{\text{scr}}(\mathbf{r}) = -\frac{e^2}{4\pi\epsilon_0} \frac{\exp(-q_{\text{TF}}r)}{r} , \quad U_{\text{scr}}(\mathbf{q}) = \frac{e^2}{\epsilon_0} \frac{1}{q^2 + q_{\text{TF}}^2} .\tag{11.19}$$

The Thomas–Fermi length is $\lambda_{\text{TF}} = 2\pi/q_{\text{TF}}$, where $q_{\text{TF}}^2 \approx e^2 n(\epsilon_F)/\epsilon_0$. In transition metals, it is less than the distance between electrons. The very

short range of this residual potential means that we can replace $U_{\text{scr}}(\mathbf{q})$ by a constant $e^2/\varepsilon_0 q_{\text{TF}}^2$. The Coulomb interaction then reduces to a contact term $U(\mathbf{r}) = I\delta(\mathbf{r})$. In second quantisation, this potential takes the form

$$U = I \int d^3r \rho_\uparrow(\mathbf{r}) \rho_\downarrow(\mathbf{r}), \quad (11.20)$$

where the spins of the density operators $\rho(\mathbf{r}) = \psi^\dagger(\mathbf{r})\psi(\mathbf{r})$ are opposite because the Pauli principle forbids electrons with parallel spins at the same point. In the language of second quantisation, U is expressed in the basis of Bloch states, taking Fourier transforms of field operators,

$$\psi(\mathbf{r}) = \frac{1}{\sqrt{V}} \exp(i\mathbf{k} \cdot \mathbf{r}) a_{\mathbf{k}\sigma}. \quad (11.21)$$

We thus obtain the Stoner representation of the Hamiltonian:

$$\mathcal{H} = \sum_{\mathbf{k}\sigma} \varepsilon_{\mathbf{k}} a_{\mathbf{k}\sigma}^\dagger a_{\mathbf{k}\sigma} + \frac{I}{V} \sum_{\mathbf{k}\mathbf{k}'\mathbf{q}\sigma} a_{\mathbf{k}-\mathbf{q},\sigma}^\dagger a_{\mathbf{k}'+\mathbf{q},-\sigma}^\dagger a_{\mathbf{k}',-\sigma} a_{\mathbf{k},\sigma}. \quad (11.22)$$

In the same way, the Zeeman Hamiltonian

$$\mathcal{H}_z = \frac{g_S \mu_B}{2} \sum_i \int \psi^\dagger(r) \boldsymbol{\sigma} \psi(r) \cdot \mathbf{b}(\mathbf{r})$$

has representation

$$\mathcal{H}_z = g_S \mu_B \sum_{\mathbf{q}} \left[\frac{S^+(\mathbf{q}) b^-(\mathbf{q}) + S^-(\mathbf{q}) b^+(\mathbf{q})}{2} + S^z(\mathbf{q}) b^z(\mathbf{q}) \right], \quad (11.23)$$

where $\mathbf{b}(\mathbf{q})$ are the Fourier components of the magnetic induction and spin operators have form

$$\begin{aligned} S^+(\mathbf{q}) &= \sum_{\mathbf{k}} a_{\mathbf{k}-\mathbf{q}\uparrow}^\dagger a_{\mathbf{k}\downarrow}, & S^-(\mathbf{q}) &= \sum_{\mathbf{k}} a_{\mathbf{k}-\mathbf{q}\downarrow}^\dagger a_{\mathbf{k}\uparrow}, \\ S^z(\mathbf{q}) &= \frac{1}{2} \sum_{\mathbf{k}} (a_{\mathbf{k}-\mathbf{q}\uparrow}^\dagger a_{\mathbf{k}\uparrow} - a_{\mathbf{k}-\mathbf{q}\downarrow}^\dagger a_{\mathbf{k}\downarrow}). \end{aligned} \quad (11.24)$$

$\mathcal{H} + \mathcal{H}_z$ cannot be diagonalised exactly. In order to identify the elementary excitations, we require equations of motion of an excitation $\mathbf{k} \downarrow \Rightarrow \mathbf{k} - \mathbf{q} \uparrow$:

$$\begin{aligned} i\hbar \frac{d}{dt} \langle a_{\mathbf{k}-\mathbf{q}\uparrow}^\dagger a_{\mathbf{k}\downarrow} \rangle &= \left\langle \left[a_{\mathbf{k}-\mathbf{q}\uparrow}^\dagger a_{\mathbf{k}\downarrow}, \mathcal{H} + \mathcal{H}_z \right] \right\rangle \\ &= (\varepsilon_{\mathbf{k}} - \varepsilon_{\mathbf{k}-\mathbf{q}}) \langle a_{\mathbf{k}-\mathbf{q}\uparrow}^\dagger a_{\mathbf{k}\downarrow} \rangle \\ &+ \frac{I}{V} \sum_{\mathbf{p}, \mathbf{r}} \left[\left\langle a_{\mathbf{p}-\mathbf{r}\downarrow}^\dagger a_{\mathbf{k}-\mathbf{q}+\mathbf{r}\uparrow}^\dagger a_{\mathbf{p}\downarrow} a_{\mathbf{k}\downarrow} - a_{\mathbf{k}-\mathbf{q}-\mathbf{r}\uparrow}^\dagger a_{\mathbf{p}+\mathbf{r}\downarrow}^\dagger a_{\mathbf{p}\downarrow} a_{\mathbf{k}\downarrow} \right\rangle \right] \\ &+ \frac{g_S \mu_B b \exp(i\omega t)}{4} \left[\left\langle a_{\mathbf{k}-\mathbf{q}\uparrow}^\dagger a_{\mathbf{k}+\mathbf{q}\uparrow} - a_{\mathbf{k}-2\mathbf{q}\downarrow}^\dagger a_{\mathbf{k}\downarrow} \right\rangle + n_{\mathbf{k}-\mathbf{q}\uparrow} - n_{\mathbf{k}\downarrow} \right], \end{aligned} \quad (11.25)$$

where a transverse magnetic field $\mathbf{b}(\mathbf{r}) = b \cos(\mathbf{q} \cdot \mathbf{r}) \exp(i\omega t) \hat{x}$ has been included. Only coherent contributions from \mathbf{k} and $\mathbf{k} - \mathbf{q}$ states can have macroscopic consequences. Incoherent contributions can only cause magnetisation or density fluctuations. This random phase approximation is equivalent to the mean field approximation, where only mean values of the fields are considered. Hence, we need only retain quadratic contractions of quartic operators in (11.25) (see Appendix B), and we have

$$\begin{aligned} & \left[\varepsilon_{\mathbf{k}} - \varepsilon_{\mathbf{k}-\mathbf{q}} + \frac{2I}{V} \sum_{\mathbf{p}} (n_{\mathbf{p}\uparrow} - n_{\mathbf{p}\downarrow}) - \hbar\omega \right] \langle a_{\mathbf{k}-\mathbf{q}\uparrow}^\dagger a_{\mathbf{k}\downarrow} \rangle \\ &= \frac{2I}{V} (n_{\mathbf{k}\uparrow} - n_{\mathbf{k}\downarrow}) \sum_{\mathbf{p}} \langle a_{\mathbf{p}-\mathbf{q}\uparrow}^\dagger a_{\mathbf{p}\downarrow} \rangle - \frac{gs\mu_B b}{4} (n_{\mathbf{k}\uparrow} - n_{\mathbf{k}\downarrow}). \end{aligned} \quad (11.26)$$

As in the Hartree–Fock approximation, we define quasi-particles whose energy is modified by the mean potential of all the other particles, i.e.,

$$\varepsilon_{\mathbf{k}\pm}^{\text{HF}} = \varepsilon_{\mathbf{k}} + \frac{2I}{V} \sum_{\mathbf{p}} n_{\mathbf{p}\pm} = \varepsilon_{\mathbf{k}} + nI(1 \mp \sigma), \quad (11.27)$$

where $n = N/V$ and $\sigma = (N_\uparrow - N_\downarrow)/N$ are electron density and polarisation, respectively. The energy shift due to interactions depends only upon particle spin. Hence \uparrow and \downarrow spins shift uniformly as shown in Fig. 11.3. This quasi-particle spectrum describes two independent bands of \uparrow and \downarrow spins, and thermodynamic potentials are sums of those for the two Fermi seas. The specific heat $C = \gamma T$ is therefore linear at low temperatures, with Sommerfeld constant

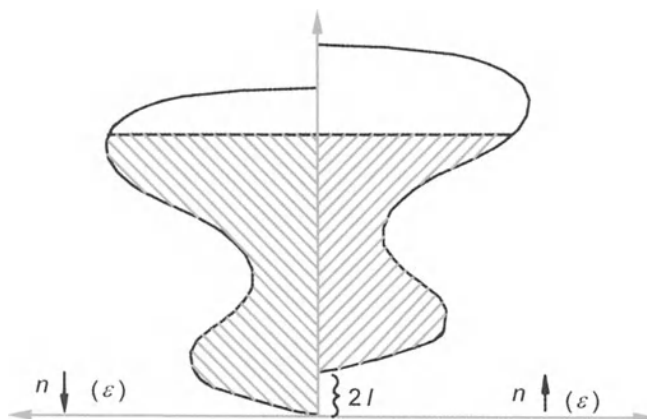


Fig. 11.3. The Stoner model. Electronic bands are uniformly shifted energetically by the molecular field, in a way which depends on their spin. Zero temperature polarisation depends on I , ε_F and the band shape

$$\gamma = \frac{\pi^2 k_B^2}{6} [n(\varepsilon_F + NI\sigma/V) + n(\varepsilon_F - NI\sigma/V)] \quad (11.28)$$

equal to the sum of contributions from each band.

We can find the magnetisation $\langle S^+(\mathbf{q}) \rangle$ by summing over all contributions from excitations $\langle a_{\mathbf{k}-\mathbf{q}\uparrow}^\dagger a_{\mathbf{k}\downarrow} \rangle$. Equation (11.26) can then be solved explicitly to obtain the dynamic susceptibility of the system:

$$\chi(\mathbf{q}, \omega) = \mu_0 \frac{g_S^2 \mu_B^2}{V} \frac{\Gamma(\mathbf{q}, \omega)}{1 - 2I\Gamma(\mathbf{q}, \omega)/V}, \quad (11.29)$$

where the structure factor Γ is given by

$$\Gamma(\mathbf{q}, \omega) = \sum_{\mathbf{q}} \frac{f_{\mathbf{k}-\mathbf{q}\uparrow} - f_{\mathbf{k}\downarrow}}{\hbar\omega + \varepsilon_{\mathbf{k}}^{\text{HF}} - \varepsilon_{\mathbf{k}-\mathbf{q}}^{\text{HF}}}. \quad (11.30)$$

In the zero field paramagnetic phase, Γ is proportional to the susceptibility $\chi_0(\mathbf{q}, \omega)$ of the free electron gas [$\varepsilon_{\mathbf{k}\sigma}^{\text{HF}} = \varepsilon_{\mathbf{k}}$, see (11.13)]. The static susceptibility $\chi(\mathbf{q}, \omega \rightarrow 0)$ [see (11.29) and (11.30)] is increased by the Stoner factor

$$S = \frac{1}{1 - 4I\chi_0(\mathbf{q})/\mu_0 g_S^2 \mu_B^2} \quad (11.31)$$

relative to that for the free electron gas. When $S \rightarrow 0$, the Fermi surface has an instability and the system becomes magnetic. When $\chi_0(\mathbf{q})$ has its maximum at $\mathbf{q} = 0$, this magnetic instability coincides with the Stoner criterion [see (11.4)]. Indeed, expressing the Pauli susceptibility (2.87) $\chi_0(0) = \mu_0 g_S^2 \mu_B^2 n(\varepsilon_F)/4$ in terms of the density of states, we come back to Stoner's criterion:

$$I = \frac{4I\chi(0)}{\mu_0 g_S^2 \mu_B^2} = In(\varepsilon_F). \quad (11.32)$$

At temperatures $T < T_c$ below the magnetic instability, $n_{\mathbf{k}\uparrow} \neq n_{\mathbf{k}\downarrow}$. The molecular field shifts quasi-particle energies apart by $\varepsilon_{\mathbf{k}\uparrow} - \varepsilon_{\mathbf{k}\downarrow} = 2IN\sigma/V$. The magnetic polarisation σ is then determined by the integral equation

$$N\sigma = \int_{-IN\sigma/V}^{-\varepsilon_F} n(\varepsilon_{\mathbf{k}}) d^3k - \int_{IN\sigma/V}^{\varepsilon_F} n(\varepsilon_{\mathbf{k}}) d^3k. \quad (11.33)$$

Even at zero temperature, the magnetic polarisation σ rarely exceeds 10% in ferromagnetic metals and alloys. The increase in electron kinetic energy is then of the order of 1% of the total energy. If we inject a current into a normal metal via a junction between a ferromagnetic metal and a normal metal, this injected current is polarised. It quickly relaxes the equilibrium in the normal metal over the inelastic collision length. This polarised current has nevertheless been observed experimentally [314].

Even for cases where the Stoner criterion is not fulfilled, susceptibility enhancement by the Stoner factor gives rise to giant magnetic moments when an impurity such as iron is diluted in a metal close to magnetic instability (e.g., palladium [308]). Indeed, the local field of the impurity polarises the

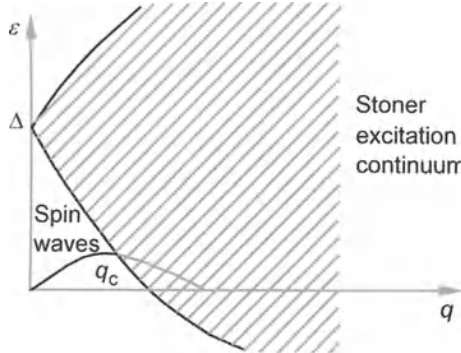


Fig. 11.4. Stoner excitation continuum and spin wave modes of a ferromagnet. Beyond wave vector \mathbf{q}_c , spin waves decay into Stoner excitations

electron gas locally and the Stoner factor then amplifies its response, creating a bubble of polarised electrons in the vicinity of the impurity.

At finite frequencies $\omega \neq 0$, the structure factor

$$\Gamma(\mathbf{q}, \omega - i\eta) = \Gamma'(\mathbf{q}, \omega) + i\Gamma''(\mathbf{q}, \omega)$$

has an imaginary part associated with poles $\hbar\omega = \varepsilon_{\mathbf{k}\uparrow}^{\text{HF}} - \varepsilon_{\mathbf{k}-\mathbf{q}\downarrow}^{\text{HF}}$. These poles correspond to Stoner excitations. The Zeeman energy shift of an electron in exchange field I when its spin reverses is absorbed by a change in kinetic energy:

$$\hbar\omega = 2\mu_B H + nI\sigma + \frac{\hbar^2 q^2}{2m_*} + \frac{\hbar^2 \mathbf{q} \cdot \mathbf{k}}{m_*}. \quad (11.34)$$

When $\mathbf{q} \rightarrow 0$, these excitations have a gap $\Delta = 2\mu_B H + nI\sigma$ and form a continuum between $\Delta - \hbar^2 q k_F / m_*$ and $\Delta + \hbar^2 q k_F / m_*$, as shown in Fig. 11.4. In contrast, if the electron spin is not reversed, then there is no gap in the electronic excitation spectrum. There is therefore no particular modification in states close to the Fermi surface. Only the volume of the Fermi sea occupied by \downarrow spins decreases in favour of the volume occupied by \uparrow spins.

At long wavelengths, $\Gamma''(\mathbf{q}, \omega)$ is small since there are few Stoner excitations. The imaginary susceptibility [see (11.29)],

$$\chi''(\mathbf{q}, \omega) = \frac{g_S^2 \mu_B^2}{4} \frac{\Gamma''(\mathbf{q}, \omega)}{[1 - 2I\Gamma'(\mathbf{q}, \omega)/V]^2 + 4I^2 \Gamma''(\mathbf{q}, \omega)^2/V^2}, \quad (11.35)$$

also has an absorption peak when

$$\frac{2I}{V} \Gamma(\mathbf{q}, \omega_{\text{sw}}) = 1. \quad (11.36)$$

These resonances correspond to the spin wave modes of the magnet. To obtain the dispersion relation at long wavelengths, we expand $\Gamma'(\mathbf{q}, \omega)$ in powers of q and ω . After a straightforward calculation [315], we find

$$\hbar\omega_{\mathbf{q}} - 2\mu_B H = \frac{1}{N_\uparrow - N_\downarrow} \sum_{\mathbf{k}} \left[\frac{1}{2} (n_{\mathbf{k}\uparrow} + n_{\mathbf{k}\downarrow}) (\mathbf{q} \cdot \nabla_{\mathbf{k}})^2 \varepsilon_{\mathbf{k}} - \frac{1}{I\sigma} (n_{\mathbf{k}\uparrow} - n_{\mathbf{k}\downarrow}) (\mathbf{q} \cdot \nabla_{\mathbf{k}} \varepsilon_{\mathbf{k}})^2 \right]. \quad (11.37)$$

We obtain the same quadratic dependence on \mathbf{q} as we did for localised spin systems in Chap. 9(I). The first term corresponds to additional kinetic energy acquired by electrons to make up for the change in direction of the macroscopic polarisation. This term is always positive and goes to zero for a filled band. The second term corresponds to the reduction of kinetic energy when the spin deviates from the plane in which the macroscopic polarisation varies. As the wave vector increases, the Stoner excitation contribution also increases and Γ'' grows accordingly. The spin wave modes are thereby enlarged. Finally, beyond q_c , these modes decay into the continuum, as shown in Fig. 11.4.

Spin wave modes can be observed elsewhere than in the ferromagnetic phase. A magnetic field suffices to polarise the electron gas and induce an exchange field, proportional to the mean spin density, about which individual spins precess. Even though the mean spin density cannot precess about itself, spin currents can precess about the exchange field. This gives transverse spin scattering modes a reactive character [65]. Corresponding hydrodynamic modes are then called paramagnons [315, 317, 318, 319]. Not only have these been observed above transition in ferromagnets, but they have also been seen in normal metals and Fermi liquids [320, 321, 322]. Whatever the type of system, they can be explained by invoking a molecular exchange field induced by spin polarisation [323].

Stoner modes can make a significant contribution to the specific heat at low temperatures. In weak ferromagnets (e.g., ZrZn₂, $T_c = 25$ K, which has magnetic moment $0.12\mu_B$ per atom, or Sc₃In, $T_c = 6$ K, $\mu = 0.045\mu_B$), a T^2 law is observed for the decrease in magnetisation, rather than the $T^{3/2}$ behaviour of the Bloch law.

Two types of refinement exist for the Stoner model. Firstly, a more realistic treatment can be made of the exchange interaction, which is not really a contact interaction, but depends on electron density in the solid as $U(r) \propto [\rho(r)]^{1/3}$. Indeed, when spins are parallel, electrons are further apart due to the Pauli principle, leaving a deficiency in electron density of parallel spins in their vicinity. The radius of this exchange hole is of order $4\pi r^3 \rho(r)/3 = 1$, and this determines the characteristic distance $r \propto \rho^{1/3}$ over which the exchange potential varies. Secondly, we can include the various bands and their hybridisations to obtain a realistic description of ferromagnetic metals.

The weakness of the Stoner model arises from the mean field approximation. Fluctuations are particularly relevant near T_c and in weak ferromagnets. More realistic descriptions of the fluctuations have been made despite the complexity of the subject [324].

Finally, when $\chi_0(\mathbf{q})$ reaches its maximum at $\mathbf{q} = \mathbf{Q}_0$, magnetic instability develops at the wave vector $\mathbf{q} = \mathbf{Q}_0$ as the Stoner factor $S \rightarrow \infty$ (11.30), rather than at $\mathbf{q} = 0$. The system then forms a spin density wave (SDW). The Stoner model can reveal this magnetic instability, but cannot describe the condensed phase. Indeed, owing to the random phase approximation, the exchange field is zero on average. We must therefore study the microscopic structure of the magnetic order parameter in more detail [325].

One description of SDWs, close to the Stoner model, consists in postulating that the spin \uparrow and \downarrow Fermi seas shift apart in the reciprocal space of a vector \mathbf{Q}_0 . Such a description is not compatible with the band structure of real metals.

11.3 The Excitonic Insulator. Spin Density Waves

A spin density wave appears in a metal when nesting of the Fermi surface allows electrons in one band to form bound states with holes in another nested band (see Fig. 11.5) [326, 327].

Only the coupling terms between these states are relevant. A realistic way of simplifying the problem is to replace the section of the Fermi surface occupied by electrons with a sphere of radius k_F^a and the section occupied by holes with a sphere of radius k_F^b . The latter is close to, but not necessarily equal to k_F^a , in order to model imperfect nesting. Let $k_F = (k_F^a + k_F^b)/2$ and $\delta = v_F \hbar (k_F^b - k_F^a)/2m$. The displacement between the centres of the two spheres is \mathbf{Q}_0 [328]. Let a^\dagger and b^\dagger be operators creating electrons in the two nested sections (a) and (b) of the Fermi surface. The Hamiltonian has form

$$\mathcal{H} = \sum_{\mathbf{k}\sigma} (\varepsilon_{\mathbf{k}}^a n_{\mathbf{k}\sigma}^a + \varepsilon_{\mathbf{k}}^b n_{\mathbf{k}\sigma}^b) + \frac{I}{V} \sum_{\mathbf{k}\mathbf{k}'\mathbf{q}\sigma} a_{\mathbf{k}-\mathbf{q}\sigma}^\dagger a_{\mathbf{k}\sigma} b_{\mathbf{k}'+\mathbf{q}-\sigma}^\dagger b_{\mathbf{k}'-\sigma} , \quad (11.38)$$

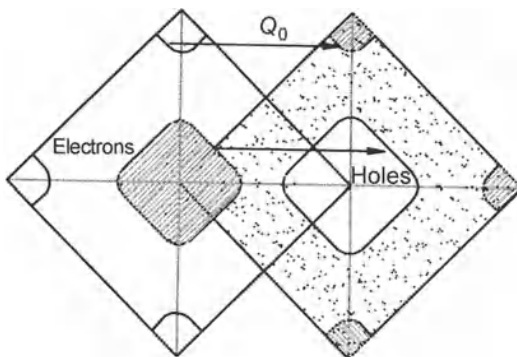


Fig. 11.5. Structure of the a and b bands in chromium, projected onto the plane $(1, 0, 0)$. There is nesting of occupied states in the a band with unoccupied states in the b band. The nesting vector $\mathbf{Q}_0 = 0.96\mathbf{G}$ is close to the vector $\mathbf{G} = 2\pi/a$ of the reciprocal lattice

where intraband exchange terms have been neglected, together with all other inert sections of the Fermi surface. The system becomes an excitonic insulator when a macroscopic number of excitons (electron-hole pairs) condenses out. In second quantisation this means that there is some wave vector \mathbf{Q} (not necessarily the same as \mathbf{Q}_0) such that

$$\langle a_{\mathbf{k}\sigma}^\dagger b_{\mathbf{k}'-\sigma} \rangle = e_{\mathbf{k}\sigma}^* \delta(\mathbf{k}' - \mathbf{k} - \mathbf{Q}) \quad (11.39)$$

is non-zero for any \mathbf{k} . Since destruction of a b electron with spin $-\sigma$ is equivalent to creation of a hole with spin σ , the operator $a_\sigma^\dagger b_{-\sigma}$ creates an electron-hole pair whose total spin is $S = 1$ in the ground state (i.e., it is a triplet). The numbers e^* resemble the eigenvalues of an exciton number operator, except that they are complex. They all have the same phase in the condensed state. The order parameter of the excitonic insulator,

$$\Delta = \frac{I}{V} \sum_{\mathbf{k}} e_{\mathbf{k}\sigma}, \quad (11.40)$$

then takes on a macroscopic value. Associating expectation values of electron-hole pairs $\langle a_{\mathbf{k}\sigma}^\dagger b_{\mathbf{k}+\mathbf{Q}, -\sigma} \rangle$ with amplitudes of Cooper pairs $\langle a_{\mathbf{k}\sigma}^\dagger a_{-\mathbf{k}, -\sigma}^\dagger \rangle$ in the theory of superconductors [see Chap. 14(II)], there is a perfect analogy between the excitonic insulator and the superconducting state. We can therefore follow the prescription of the BCS theory [see Sect. 14.3(II)]. We define a mean Hamiltonian (the BCS Hamiltonian) in which we retain only terms of first order in the deviation from equilibrium $[\delta(a^\dagger b) = a_{\mathbf{k}\sigma}^\dagger b_{\mathbf{k}+\mathbf{Q}, -\sigma} - e_{\mathbf{k}\sigma}^*]$. We thereby obtain the effective Hamiltonian $\mathcal{H}_{ei} \approx \mathcal{H} - \mu N_{op}$, given by

$$\begin{aligned} \mathcal{H}_{ei} &= \sum_{\mathbf{k}\sigma} \left[\varepsilon_{\mathbf{k}}^a a_{\mathbf{k}\sigma}^\dagger a_{\mathbf{k}\sigma} + \varepsilon_{\mathbf{k}}^b b_{\mathbf{k}\sigma}^\dagger b_{\mathbf{k}\sigma} \right] \\ &\quad - \sum_{\mathbf{k}\sigma} \left[\Delta a_{\mathbf{k}\sigma}^\dagger b_{\mathbf{k}+\mathbf{Q}, -\sigma} + \Delta^* b_{\mathbf{k}+\mathbf{Q}, \sigma}^\dagger a_{\mathbf{k}, -\sigma} \right] + \sum_{\mathbf{k}\sigma} e_{\mathbf{k}\sigma}^* \Delta \\ &= E_I + \sum_{\mathbf{k}\sigma} X_{\mathbf{k}\sigma}^\dagger H_{\mathbf{k}} X_{\mathbf{k}\sigma}, \end{aligned} \quad (11.41)$$

where energies are measured relative to the chemical potential (of order ε_F), i.e., $\varepsilon_{\mathbf{k}} \Rightarrow \varepsilon_{\mathbf{k}} - \mu$, the term $E_I = \sum_{\mathbf{k}} e_{\mathbf{k}}^* \Delta$ is the mean interaction energy, and

$$X_{\mathbf{k}\sigma}^\dagger = \begin{pmatrix} a_{\mathbf{k}\sigma} \\ b_{\mathbf{k}+\mathbf{Q}, -\sigma} \end{pmatrix}, \quad H_{\mathbf{k}} = \begin{pmatrix} \varepsilon_{\mathbf{k}}^a & \Delta \\ \Delta^* & \varepsilon_{\mathbf{k}+\mathbf{Q}}^b \end{pmatrix}, \quad (11.42)$$

where

$$\varepsilon_{\mathbf{k}}^a \approx \xi_{\mathbf{k}} + \delta, \quad \varepsilon_{\mathbf{k}+\mathbf{Q}}^b \approx -\xi_{\mathbf{k}} + \delta + C. \quad (11.43)$$

In these formulas, $\xi_{\mathbf{k}} = v_F \hbar (k - k_F)/m$ and $C = v_F \hbar |\mathbf{Q} - \mathbf{Q}_0|/m$ measures the departure from commensurability of the spin density wave and the nesting vector \mathbf{Q}_0 . As in the BCS theory, this effective Hamiltonian can be diagonalised by a Bogoliubov transformation, which is unitary for fermions [see

Chap. 14(II)] and preserves their commutation relations. Operators c and d representing excitonic quasi-particles are defined by

$$X_{\mathbf{k}\sigma} = S_{\mathbf{k}} Y_{\mathbf{k}\sigma} = \begin{pmatrix} a_{\mathbf{k}\sigma} \\ b_{\mathbf{k}+\mathbf{Q}, -\sigma} \end{pmatrix} = \begin{pmatrix} u_{\mathbf{k}} & v_{\mathbf{k}}^* \\ -v_{\mathbf{k}} & u_{\mathbf{k}}^* \end{pmatrix} \begin{pmatrix} c_{\mathbf{k}, \sigma} \\ d_{\mathbf{k}, -\sigma}^\dagger \end{pmatrix}. \quad (11.44)$$

Eigenvalues of $H_{\mathbf{k}}$ give energies of c and d quasi-particles:

$$E_{\mathbf{k}}^c = \delta + C/2 + E_{\mathbf{k}}, \quad E_{\mathbf{k}}^d = \delta + C/2 - E_{\mathbf{k}}, \quad (11.45)$$

$$E_{\mathbf{k}} = \sqrt{\xi_{\mathbf{k}}^2 + |\Delta|^2 - C\xi_{\mathbf{k}} + C^2/4}. \quad (11.46)$$

There is thus a gap of 2Δ in the energy spectrum. In terms of the $c_{\mathbf{k}}$ and $d_{\mathbf{k}}$ quasi-particles, the Hamiltonian becomes diagonal:

$$\mathcal{H}_{\text{ei}} = E_{\text{ei}} + \sum_{k < k_F} E_{\mathbf{k}}^c c_{\mathbf{k}\sigma}^\dagger c_{\mathbf{k}\sigma} + \sum_{k > k_F} E_{\mathbf{k}}^d d_{\mathbf{k}\sigma}^\dagger d_{\mathbf{k}\sigma}, \quad (11.47)$$

where the ground state energy of the excitonic insulator is

$$E_{\text{ei}} = \sum_{\mathbf{k}} (-\varepsilon_{\mathbf{k}}^b + E_{\mathbf{k}}^d) + E_I. \quad (11.48)$$

Introducing the common density of states for a and b electrons,

$$\begin{aligned} n(\xi, \eta) &= \sum_{\mathbf{k}} \delta \left[\xi - \frac{1}{2} (\varepsilon_{\mathbf{k}+\mathbf{Q}}^b - \varepsilon_{\mathbf{k}}^a) \right] \delta \left[\eta - \frac{1}{2} (\varepsilon_{\mathbf{k}+\mathbf{Q}}^b + \varepsilon_{\mathbf{k}}^a) \right] \\ &= \frac{n_0}{C} [\theta(\eta - \delta + C) - \theta(\eta - \delta - C)], \end{aligned} \quad (11.49)$$

where θ is the Heaviside step function, we can determine the condensation energy

$$E_{\text{ei}} - E_I = \int d\xi d\eta n(\xi, \eta) [E^d(\xi) - \varepsilon_b(\xi)]$$

of the excitonic insulator. More generally, we can find the difference in free energy ΔG from the paramagnetic state. The energy gap and departure from commensurability C are found by minimising E_{ei} with respect to C and Δ . The result leads to the phase diagram in Fig. 11.6. For nesting deviations δ which are small compared with Δ , the wave vector $\mathbf{Q} = \mathbf{Q}_0$ of the spin density wave remains equal to the nesting vector ($C = 0$). In this case, coefficients $u_{\mathbf{k}}$ and $v_{\mathbf{k}}$ of the Bogoliubov transformation have the same form as they do in the BCS theory [see Sect. 14.3(II)], viz.,

$$\begin{aligned} |u_{\mathbf{k}}|^2 &= \frac{1}{2} \left(1 + \frac{\xi_{\mathbf{k}}}{|E_{\mathbf{k}}|} \right), \quad |v_{\mathbf{k}}|^2 = \frac{1}{2} \left(1 - \frac{\xi_{\mathbf{k}}}{|E_{\mathbf{k}}|} \right), \\ 2u_{\mathbf{k}}^* v_{\mathbf{k}} &= -\frac{\Delta}{E_{\mathbf{k}}}. \end{aligned} \quad (11.50)$$

We can now determine condensation amplitudes

$$\begin{aligned} e_{\mathbf{k}, \sigma} &= \left\langle a_{\mathbf{k}\sigma}^\dagger b_{\mathbf{k}+\mathbf{Q}, -\sigma} \right\rangle = \left\langle \left(u_{\mathbf{k}} c_{\mathbf{k}}^\dagger + v_{\mathbf{k}} d_{\mathbf{k}} \right) \left(-v_{\mathbf{k}} c_{\mathbf{k}} + u_{\mathbf{k}}^* d_{\mathbf{k}}^\dagger \right) \right\rangle \\ &= u_{\mathbf{k}}^* v_{\mathbf{k}} (1 - n_{\mathbf{k}}^c - n_{\mathbf{k}}^d). \end{aligned} \quad (11.51)$$

When $C \rightarrow 0$, $n(\xi, \eta) \rightarrow n_0 \delta(\eta)$, the sum of (11.51) over all electronic states gives a gap

$$\begin{aligned} \Delta &= n_0 I \int d\xi_{\mathbf{k}} \frac{\Delta}{2E_{\mathbf{k}}} [1 - f(E_{\mathbf{k}} + \delta) - f(E_{\mathbf{k}} - \delta)] \\ &= \Delta n_0 \int_0^{\varepsilon_m} \frac{d\xi_{\mathbf{k}}}{2E_{\mathbf{k}}} \left[\tanh \frac{\beta}{2}(E_{\mathbf{k}} + \delta) + \tanh \frac{\beta}{2}(E_{\mathbf{k}} - \delta) \right], \end{aligned} \quad (11.52)$$

which is identical to the BCS equation when $\delta = 0$. ε_m is a cutoff energy for the Coulomb interaction, typically of the order of the Fermi energy. For perfect nesting ($\delta = 0$), there is a gap whatever the value of I , since

$$\Delta = \varepsilon_m \exp [-1/n_0 I].$$

When $\delta \neq 0$, a minimum value of interaction I is required before a spin density wave can form. The transition temperature is plotted as a function of δ in Fig. 11.6. This model also predicts another spin density wave phase whose wave vector is incommensurable with \mathbf{Q}_0 and \mathbf{G} (the vector of the reciprocal lattice closest to \mathbf{Q}_0). It can be observed in chromium, where $\mathbf{Q} \neq \mathbf{G}$ varies continuously with temperature. The spin density wave in chromium is illustrated in Fig. 11.7. Its amplitude is modulated with period about 26 times the atomic lattice spacing, which coincides with the incommensurability $2\pi/|\mathbf{Q} - \mathbf{G}|$. Diluting a small quantity of manganese or nickel into the chromium, the spin density wave becomes commensurable with the lattice. This behaviour is easily explained in terms of the Rice model, introducing

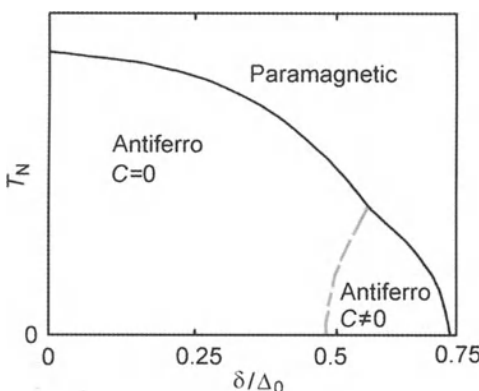


Fig. 11.6. Excitonic insulator phase diagram in the Rice model. There are three phases: the paramagnetic phase; the $C = 0$ phase, stable under small nesting deviations; and an incommensurable $C \neq 0$ phase, stable under intermediate nesting deviations

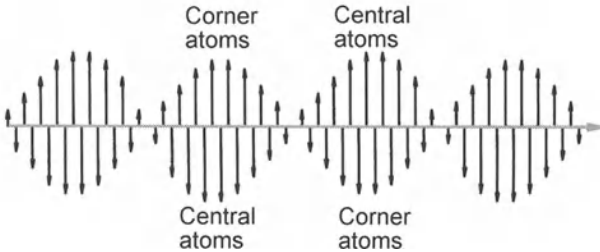


Fig. 11.7. Graphical representation of the spin density wave in chromium. The amplitude modulation coincides with the incommensurability of the wave vector \mathbf{Q} with $G = 2\pi/a$

scattering by the impurities. The phase diagram of chromium can then be reproduced completely, as well as that for its alloys, starting from an excitonic insulator model [329].

In real physical systems, the gap in the excitation spectrum only partially opens on the Fermi surface. Conductivity anomalies are thus only slight at transition and the system is certainly not insulating, as it would be if all electron-hole pairs had condensed. Nevertheless, accurate measurements have shown that in the Bechgaard salts about 30% of electrons no longer contribute to transport. This is explained well by the existence of a gap over an appreciable section of the Fermi surface.

Many aspects of spin density waves remain to be investigated. Some systems, such as the γ -Fe, would appear to exhibit no nesting properties. Others, such as MnZn and FeRh, reveal coexisting ferromagnetism and spin density waves [330]. Finally, collective modes observed by neutron scattering on chromium and its alloys have still to receive a satisfactory explanation [331].

11.4 The Hubbard Model

This model is both the best studied and the least understood in magnetism. It was developed to describe narrow band metals for which the Coulomb repulsion term between two electrons at one of the L lattice sites dominates all other terms, including kinetic energy [332]. The model has a simple Hamiltonian:

$$\mathcal{H} = -t \sum_{\langle ij \rangle \sigma} a_{i\sigma}^\dagger a_{j\sigma} + U \sum_i n_{i\uparrow} n_{i\downarrow}, \quad (11.53)$$

where $n_{i\sigma} = a_{i\sigma}^\dagger a_{i\sigma}$ is the occupation number of the Wannier state $\phi(\mathbf{R}_i, \mathbf{r})$ of spin σ centred on site i . This model is quite realistic if this is the only band to be partially filled. We define the filling n of the band as the number of electrons per site. $n = \langle n_{i\uparrow} \rangle + \langle n_{i\downarrow} \rangle$ varies between 0 and 2, but since there is a particle-hole symmetry, we need only study the model when n varies between 0 and 1. For low filling, the Hubbard model reduces to the Stoner model

(under the substitution $2I \leftrightarrow U$), when we use the Bloch basis $\phi(\mathbf{k}, \mathbf{r})$ in place of the Wannier basis [see Sect. 3.6(I)]. The term t describes the hopping integral between nearest neighbours i and j , denoted $\langle ij \rangle$, and measures the band width. An exact solution only exists in one dimension [333]. Many approximation methods, generally untested, have been put forward to obtain information about the ground state in higher dimensions. Several monographs [334, 335, 336] and many articles have been devoted to the subject. The main difficulty lies in the fact that the Hartree–Fock approximation, which linearises the interaction term U about the expected filling $\langle n_i \rangle$ [$n_{i\sigma} = \langle n_{i\sigma} \rangle + (n_{i\sigma} - \langle n_{i\sigma} \rangle)$], viz.,

$$\mathcal{H} = -t \sum_{\langle ij \rangle \sigma} a_{i\sigma}^\dagger a_{j\sigma} + U \sum_i (\langle n_{i\uparrow} \rangle n_{i\downarrow} + n_{i\uparrow} \langle n_{i\downarrow} \rangle - \langle n_{i\uparrow} \rangle \langle n_{i\downarrow} \rangle) , \quad (11.54)$$

is only justified in infinite dimensions [337, 338]. For smaller fillings, the Hartree–Fock approximation predicts a ferromagnetic instability when the Stoner criterion is satisfied, i.e., when $Un(\varepsilon_F)/2 > 1$. Electron polarisation is then defined by

$$\sigma = \frac{\langle n_{i\uparrow} \rangle - \langle n_{i\downarrow} \rangle}{n} ,$$

and in terms of operators $a_{\mathbf{k}\sigma}$ (Fourier images of operators $a_{i\sigma}$), the Hamiltonian is diagonal, coinciding with the Stoner Hamiltonian in the Hartree–Fock approximation,

$$\mathcal{H} = \sum_{\mathbf{k}\sigma} \varepsilon_{\mathbf{k}\sigma}^{\text{HF}} a_{\mathbf{k}\sigma}^\dagger a_{\mathbf{k}\sigma} , \quad (11.55)$$

$$\varepsilon_{\mathbf{k}\pm}^{\text{HF}} = -tz\eta_{\mathbf{k}} + \frac{Un}{2}(1 \mp \sigma) , \quad (11.56)$$

where

$$\eta_{\mathbf{k}} = \frac{1}{z} \sum_{\delta_{\langle ij \rangle}} \exp(i\mathbf{k} \cdot \delta_{\langle ij \rangle}) .$$

The ground state

$$|\Psi\rangle = \prod_{i=1}^{N_\uparrow} a_{i\uparrow}^\dagger \prod_{i=1}^{N_\downarrow} a_{i\downarrow}^\dagger |0\rangle \quad (11.57)$$

is composed of two Fermi spheres of two independent quasi-particles. In the ferromagnetic ground state, we have $N_\uparrow \neq N_\downarrow$. In the Hartree–Fock approximation, there is no difference between the Stoner model and the Hubbard model for small fillings. The Hubbard model nevertheless provides a simpler way of studying correlations between electrons, whose effects are ignored in the Hartree–Fock approximation. These effects reduce the gain in potential energy in the ferromagnetic state. This in turn amounts to renormalising the parameter U (of order 10 eV) to a much smaller value \mathcal{T} , of order t , the

band width (between 100 meV and 1 eV) (see Sect. 11.4.2). The Stoner criterion must therefore be used with renormalised parameters $Tn(\varepsilon_F)/2 > 1$. Even when renormalised, the Hartree–Fock approximation is wrong in one dimension; this is shown by the exact solution of Lieb and Wu. No well-tested approximation has yet been produced to describe the two-dimensional Hubbard model. Among tractable models, Gutzwiller's variational wave functions [339] give an estimate of ground state energy, despite the fact that correlations described by these wave functions are not always realistic.

If there is one electron per site ($n = 1$), the Hubbard model possesses an antiferromagnetic ground state in the mean field approximation. In the special case where $t = 0$, there are two degenerate spin states at L sites, or 2^L degenerate states. No energy is required to reverse a spin, whereas adding a charge requires energy U . Consequently, at least at this point of the phase diagram, there is a separation between spin and charge excitations. When $n = 1$ and t is small, there are two bands separated by an energy of about U (see Fig. 11.8). The lower band of width $\approx t$ is completely filled. It is therefore an insulator ($U \gg k_B T$) in which charges are localised by Coulomb repulsion. This is the Mott insulator. (In disordered systems, charges can be localised by destructive interference during scattering from impurities. This is the Anderson insulator where disorder dominates and interactions between electrons are secondary.) There must therefore be a metal-insulator transition depending on n . Today we have several possible scenarios for this transition [340, 341], although they remain poorly understood. It is thought that part of the physics of high temperature superconductors composed of CuO₂ planes can be described by a 2-dimensional Hubbard model near $n = 1$. This has stimulated considerable interest over the past few years.

When $n = 1$, the antiferromagnetism of the Hubbard model is well understood. For small values of t , perturbation theory can be applied to the

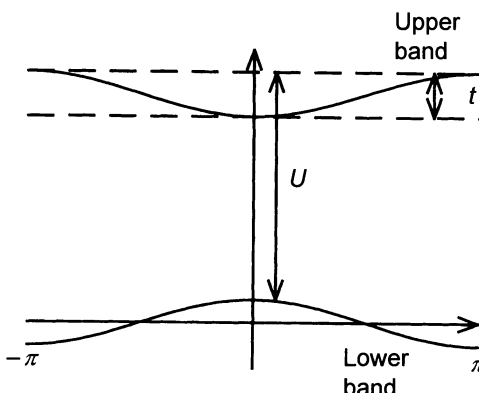


Fig. 11.8. The two bands of the Hubbard model when the Hund term U is much greater than the band width t . If the lower band is not completely filled, we can use an effective Hamiltonian $t - J$ which describes interactions in the lower band

hopping Hamiltonian, exactly as in superexchange studies [see Sect. 3.7(I)]. In the lower Hubbard band (LHB), the hopping term can be replaced by an effective Hamiltonian [see (3.82)],

$$\mathcal{H}_{\text{LHB}} = -t \sum_{\langle ij \rangle \sigma} P_0 a_{i\sigma}^\dagger a_{j\sigma} P_0 + J \sum_{\langle ij \rangle} \left(\mathbf{S}_i \cdot \mathbf{S}_j - \frac{n_i n_j}{4} \right) , \quad (11.58)$$

where the exchange integral $J = 2|t|^2/U$ is always antiferromagnetic (positive). The first term is the projection (by means of operator P_0) of the hopping Hamiltonian onto the lower Hubbard band, only relevant when $n \neq 1$. This is the $t - J$ model, which describes the strong coupling limit ($U \gg t$) of the Hubbard model. When the spin density waves are antiferromagnetic, orthogonality of states is ensured, allowing spatial wave functions to spread out and thereby lower their kinetic energy. In other words, the delocalisation energy imposed by the Pauli principle is minimal in an antiferromagnetic configuration. When the coupling is not strong enough, we may appeal to the mean field approach, used in describing the excitonic insulator and which also leads to an antiferromagnetic ground state.

When $n \leq 1$, the Hilbert space is greatly extended since we have $N - L \equiv (n - 1)L$ holes to share out over L sites, each having two states, i.e.,

$$\frac{L!}{(N/2)!^2(N - L)!} \gg 2^L$$

possible states. When a hole moves within an antiferromagnetic Néel state, unsatisfied magnetic bonds are generated along its path, as shown in Fig. 11.9. Charge degrees of freedom are therefore coupled to spins. Only quantum fluctuations can then repair locally the Néel walls produced by holes. The coupling is thus very effective in destroying antiferromagnetic order. The various magnetic states which can be induced by hole motion are discussed in Sect. 11.4.2. But before tackling this problem, it will be useful to understand the physical origins of correlations between particles, which are not included in the mean field.

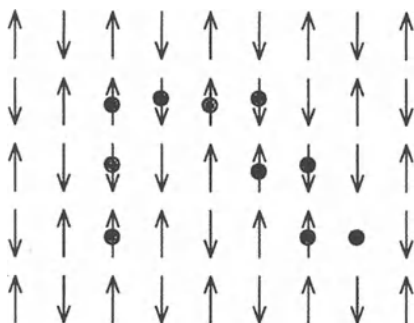


Fig. 11.9. Example of a hole trajectory generating a defect line (Néel wall) in the magnetic lattice

11.4.1 Electron Correlations

Small spatial correlations between particles in an antiferromagnetic state can considerably reduce the Coulomb interaction between electrons, at the expense of a very small increase in kinetic energy [342]. This may seem paradoxical. How is it that small spatial correlations can control such large energy changes? In the low filling limit, a particle at site i produces potential $U(\mathbf{r} - \mathbf{R}_i)$ for the other particles. It will be useful in a first approximation to ignore the crystal lattice, so that we can concentrate on correlations between two particles i and j . The product of their unperturbed wave functions is a plane wave of form

$$\langle \mathbf{r}_i, \mathbf{r}_j | \mathbf{k}, \mathbf{q} \rangle = \exp i(\mathbf{k} \cdot \mathbf{r}_i + \mathbf{q} \cdot \mathbf{r}_j),$$

and their interaction $U(\mathbf{r}_i - \mathbf{r}_j)$ only depends on their separation. The centre of mass wave function can therefore be separated from the relative coordinate,

$$\begin{aligned} \langle \mathbf{r}_i, \mathbf{r}_j | \mathbf{k}, \mathbf{q} \rangle &= \exp \frac{i}{2} (\mathbf{r}_i + \mathbf{r}_j)(\mathbf{k} + \mathbf{q}) \exp \frac{i}{2} (\mathbf{r}_i - \mathbf{r}_j)(\mathbf{k} - \mathbf{q}) \\ &= \langle \mathbf{R} | \mathbf{P} \rangle \langle \mathbf{r} | \mathbf{p} \rangle, \end{aligned}$$

where $\mathbf{P} = \mathbf{k} + \mathbf{q}$ and $\mathbf{p} = (\mathbf{k} - \mathbf{q})/2$. The presence of a hard core potential considerably modifies the wave function $\langle \mathbf{r} | \mathbf{p} \rangle \rightarrow \langle \mathbf{r} | \psi_{\mathbf{p}} \rangle$. It acquires a node at the origin ($\mathbf{r} = 0$) so as to avoid the singularity of the potential. The perturbative approximation $\langle \mathbf{p} | U | \mathbf{p} \rangle$ to the interaction energy $\Sigma_{\mathbf{p}} = E_{\mathbf{p}} - \varepsilon_{\mathbf{p}}$ is then wildly inaccurate. We must solve the Schrödinger equation

$$E_{\mathbf{p}} |\psi_{\mathbf{p}}\rangle = [\varepsilon_{\mathbf{p}} + U(\mathbf{R})] |\psi_{\mathbf{p}}\rangle, \quad (11.59)$$

with boundary conditions $\langle \mathbf{r} | \psi_{\mathbf{p}} \rangle \rightarrow \langle \mathbf{r} | \mathbf{p} \rangle$ as $\mathbf{p} \cdot \mathbf{r} \rightarrow -\infty$ appropriate to a scattering problem. The solution can be expressed in the form [343]

$$|\psi_{\mathbf{p}}\rangle = |\mathbf{p}\rangle + \sum_{\mathbf{q}} \frac{\langle \mathbf{q} | t | \mathbf{p} \rangle}{\varepsilon_{\mathbf{p}} - \varepsilon_{\mathbf{q}} + i\eta} |\mathbf{q}\rangle, \quad (11.60)$$

where scattering matrix elements $\langle \mathbf{q} | t | \mathbf{p} \rangle$ satisfy the integral equation (the factor of 2 comes from the reduced mass $\mu = m/2$)

$$\langle \mathbf{q} | t | \mathbf{p} \rangle = \langle \mathbf{q} | U | \mathbf{p} \rangle + \sum_{\mathbf{k}} \langle \mathbf{q} | U | \mathbf{k} \rangle \frac{1}{2(\varepsilon_{\mathbf{p}} - \varepsilon_{\mathbf{k}}) + i\eta} \langle \mathbf{k} | t | \mathbf{p} \rangle. \quad (11.61)$$

The overlap between the two electron wave functions is greatly reduced: their states are correlated. In order to completely specify the correlations and determine the energy of the states, we must include spin degrees of freedom and the Pauli principle. For a spin triplet state $S = 1$, the spatial wave function is antisymmetric (-) and for a singlet state $S = 0$ it is symmetric (+). Exchanging coordinates is equivalent to substituting $\mathbf{p} \rightarrow -\mathbf{p}$, so the scattering amplitude in these states is

$$\langle \mathbf{q} | t^{\pm} | \mathbf{p} \rangle = \frac{\langle \mathbf{q} | t | \mathbf{p} \rangle \pm \langle -\mathbf{q} | t | \mathbf{p} \rangle}{2}.$$

The corresponding energies are

$$E_{\mathbf{p}}^{\pm} = \varepsilon_{\mathbf{p}} + \frac{1}{2} \text{Re} (\langle \mathbf{p}|t|\mathbf{p}\rangle \pm \langle \mathbf{p}|t|-\mathbf{p}\rangle) . \quad (11.62)$$

The energy difference between singlet and triplet states is just $\text{Re}\langle \mathbf{p}|t|-\mathbf{p}\rangle$, which is of the order of the band width t when the Coulomb repulsion U is large.

Because of the lattice and the other particles, the interaction between two electrons is no longer translation invariant. The scattering theory must be slightly generalised [323, 344]. The scattering matrix \mathcal{T} in the medium comprising the lattice + other particles is defined by an integral equation which can be written either in the Wannier basis $\langle \mathbf{r}|i\rangle = \phi(\mathbf{r} - \mathbf{R}_i)$, or in the Bloch basis $\langle \mathbf{r}|\mathbf{k}\rangle = \exp(i\mathbf{k} \cdot \mathbf{r})f_{\mathbf{k}}(\mathbf{r})$ (where f is periodic):

$$\begin{aligned} \langle i, j | \mathcal{T}^0 | k, l \rangle &= U \delta(\mathbf{R}_i - \mathbf{R}_k) \delta(\mathbf{R}_j - \mathbf{R}_l) \\ &\quad + \sum_{m, n} \langle i, j | \mathcal{T}^0 | m, n \rangle \langle m, n | G | k, l \rangle U \delta(\mathbf{R}_k - \mathbf{R}_l) , \end{aligned} \quad (11.63)$$

$$\begin{aligned} \langle \mathbf{k}_1, \mathbf{k}_2 | \mathcal{T}^0 | \mathbf{q}_1, \mathbf{q}_2 \rangle &= U \delta(\mathbf{k}_1, \mathbf{k}_2; \mathbf{q}_1, \mathbf{q}_2) \\ &\quad + \sum_{\mathbf{p}_1, \mathbf{p}_2} \langle \mathbf{k}_1, \mathbf{k}_2 | \mathcal{T}^0 | \mathbf{p}_1, \mathbf{p}_2 \rangle \langle \mathbf{p}_1, \mathbf{p}_2 | G | \mathbf{q}_1, \mathbf{q}_2 \rangle U \delta(\mathbf{q}_1 + \mathbf{q}_2) . \end{aligned} \quad (11.64)$$

This generalises (11.61). The function $\delta(\mathbf{k}_1, \mathbf{k}_2; \mathbf{q}_1, \mathbf{q}_2) = 1$ when $\mathbf{k}_1 + \mathbf{k}_2 = \mathbf{q}_1 + \mathbf{q}_2 + \mathbf{K}$, where \mathbf{K} belongs to the reciprocal lattice. The Green function G for two independent particles on the periodic lattice has a particularly simple expression in the Bloch basis:

$$\langle \mathbf{p}_1, \mathbf{p}_2 | G | \mathbf{q}_1, \mathbf{q}_2 \rangle = \frac{1}{L} \frac{\delta(\mathbf{p}_1, \mathbf{p}_2; \mathbf{q}_1, \mathbf{q}_2)}{\varepsilon_{\mathbf{q}_1} + \varepsilon_{\mathbf{q}_2} - \varepsilon_{\mathbf{p}_1} - \varepsilon_{\mathbf{p}_2}} , \quad (11.65)$$

where L is the number of sites. The self-energy of a quasi-particle is obtained by adding the contributions of all pairs containing that quasi-particle. Substituting \mathcal{T} for t in (11.62) and summing over all pairs, we obtain the energy of the quasi-particle \mathbf{p} of spin \pm as

$$\begin{aligned} E_{\mathbf{p}\pm} &= \sum_{\langle \mathbf{q} \rangle} \text{Re} \left[\left(\langle \mathbf{p}, \mathbf{q} | \mathcal{T} | \mathbf{p}, \mathbf{q} \rangle - \frac{1}{2} \langle \mathbf{p}, \mathbf{q} | \mathcal{T} | \mathbf{q}, \mathbf{p} \rangle \right) n(\mathbf{q}) \right. \\ &\quad \left. \mp \frac{1}{2} \langle \mathbf{p}, \mathbf{q} | \mathcal{T} | \mathbf{q}, \mathbf{p} \rangle \sigma(\mathbf{q}) \right] , \end{aligned} \quad (11.66)$$

where the sum over q , $\langle \mathbf{q} \rangle$ is restricted to occupied states and $\sigma(\mathbf{q})$ is the electron polarisation at wave vector \mathbf{q} .

As the density increases, the wave functions of each particle must acquire more and more nodes in order to escape the cost of Coulomb repulsion at sites occupied by the other particles. We thus obtain a strongly correlated fermion system. Although we have seen how to include two-particle correlations using non-perturbative scattering theory, there is no method for determining, even

qualitatively, the features of N -body correlations. Several scenarios have been proposed to describe the transition from a metallic state of independent quasi-particles (Fermi liquid) to a correlated metallic state [345], and then to a Mott insulator. However, this crucial problem remains completely open.

11.4.2 Destruction of Antiferromagnetism by Holes

In two dimensions, the correlation functions of the antiferromagnetic state decrease slowly [algebraically, see Chap. 7(I)] with distance. A merely infinitesimal exchange between adjacent planes is enough to stabilise long range order. The antiferromagnetic state is drastically altered by displacement of a hole, because such motion occurs via spin transfer from the occupied site to the location of the hole. The magnetic defect line (see Fig. 11.9) left by the hole limits its displacement because the magnetic energy $\mathcal{E}_m = 2J\mathcal{L}$ of a Néel wall of length \mathcal{L} cannot exceed its kinetic energy t . At long wavelengths, Néel walls appear like a dipole moment induced by hole motion. In a mean field description, the main effect of a low hole concentration is to modify the ground state. The latter is no longer an antiferromagnet with two sublattices, but rather a *spiral phase* [346]. Figure 11.10 shows the orientation of spins in sublattice B neighbouring spin S_i^A in sublattice A . In directions \hat{x} and \hat{y} , spins rotate relative to S_i^A in such a way that the chirality $C = S_i^A \cdot (S_{i+\hat{x}}^B \times S_{i+\hat{y}}^B)$ is non-zero. The order parameter $C \propto t(1-x)/J$ increases linearly with hole concentration $1-x$. Some experimental evidence exists in one of the copper oxides La_2CuO_4 close to half-filling [347], although other interpretations have also been put forward. Quantum fluctuations provide the system with a second option: the hole can hop to a site in the same sublattice by tunnelling, thereby avoiding the expense of paying the exchange energy, and allowing the hole to move within the antiferromagnetic state. In this case, the metallic state coexists naturally with antiferromagnetic correlations. The tunnelling matrix element between sites of the same sublattice determines effective mass. In order to obtain a better understanding of the role played

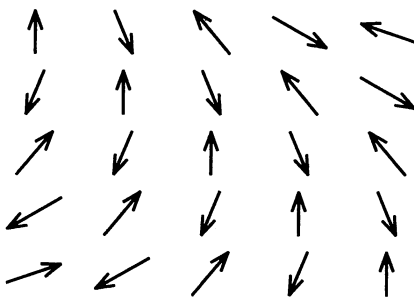


Fig. 11.10. Local spin orientations in a spiral phase. Spins have chirality in the (x, y) plane

by antiferromagnetic correlations in the metallic state, Anderson [341, 348] showed that spin degrees of freedom (spinons) can be distinguished from hole degrees of freedom (holons) by a decomposition of electron operators

$$a_{i\sigma} = f_{i\sigma} b_i^\dagger . \quad (11.67)$$

The fermion operator $f_{i\sigma}$ destroys a spinon and the boson operator b_i^\dagger creates a hole (holon). They must satisfy the condition

$$\sum_{i\sigma} \left(f_{i\sigma}^\dagger f_{i\sigma} + b_i^\dagger b_i \right) = 1 , \quad (11.68)$$

in order to avoid double occupation of any site. This condition couples degrees of freedom. An ingenious way of implementing the condition involves introducing a gauge field \mathbf{a} [349, 350] with the property that its circulation over one lattice unit is the chirality of those spins located at its peaks [351]. We can thereby justify a Ginzburg–Landau free energy [352] simultaneously describing both spinon pair formation and Bose condensation of holons. It is just the sum of spinon, holon and gauge field free energies, $F = F_s + F_h + F_g$. Coupling between degrees of freedom comes from the gauge field \mathbf{a} :

$$F_s = \int d^2r \left\{ \frac{\hbar^2}{2m_s} |[\nabla - 2i\mathbf{a}(\mathbf{r}) - 2ie\mathbf{A}(\mathbf{r})]\psi(\mathbf{r})|^2 + \alpha|\psi(\mathbf{r})|^2 + \frac{\beta}{2}|\psi(\mathbf{r})|^4 \right\} , \quad (11.69)$$

$$F_h = \int d^2r \left\{ \frac{\hbar^2}{2m_h} |[\nabla - i\mathbf{a}(\mathbf{r})]\phi(\mathbf{r})|^2 + a|\phi(\mathbf{r})|^2 + \frac{b}{2}|\phi(\mathbf{r})|^4 \right\} , \quad (11.70)$$

where \mathbf{A} is the vector potential of the magnetic induction and ψ, ϕ are order parameters for spinons and holons, respectively. Spin fluctuations induce gauge field fluctuations which scatter quasi-particles above their critical temperatures. They have short lifetimes in the normal state and this gives them unusual properties for a metal. The phase diagram for this model comprises several condensed phases and a metallic phase which is not a Fermi liquid. Some properties of the latter phase resemble those of the normal state of copper oxides. These descriptions do not provide any intuitive picture of electron correlations and a more physical view would seem necessary before such ideas could become widely accepted.

11.4.3 High Temperature Superconductivity

All studies of strongly correlated fermions are motivated by high temperature superconductivity in copper oxides such as La_2CuO_4 ($T_c \approx 40$ K) and $\text{YBa}_2\text{Cu}_3\text{O}_7$ ($T_c \approx 90$ K). Several mechanisms have been suggested to explain the exceptional properties of these materials. They are the only Mott insulators that can be easily doped to form metallic states. They have an antiferromagnetic state at half-filling, with a large exchange interaction of order

300 K. In addition, when doped with holes, their antiferromagnetism disappears in favour of a superconducting state with high critical temperature. Seven years after their discovery, the mechanism giving rise to this superconductivity has still not been firmly established. Among possible mechanisms, one proposes electron-electron coupling induced by interaction with magnons; as we have seen, this interaction can be quite significant when correlations are strong. There is as yet no quantitative microscopic theory for this coupling, but it can be understood intuitively in the weak coupling limit. When there are antiferromagnetic correlations, two holes can exchange short wavelength magnons. In perturbation theory [353], some series of diagrams can be summed to give the effective interaction between two electrons, induced by this exchange. The interaction is attractive if electron pairs have *d*-type spatial wave functions. When $t/U > 0.25$, the wave function of lowest energy is $d_{x^2-y^2}$, whilst at very strong couplings, the state d_{xy} would appear to have lowest energy. These wave functions have a node at the origin which also allows them to avoid Coulomb repulsion. The latter is only partly screened by other electrons, due to the low electron density. For other types of wave function, the effective pair interaction is repulsive. The superconductivity must therefore be of *d* type for the magnetic mechanism to be correct. We cannot at present estimate the magnitude of the electron-electron coupling in the strong coupling limit since elementary excitations are not sufficiently well known. Numerical simulations based on the Hubbard model would also seem to suggest a coupling of order J in the *d* channel. According to such calculations, only these wave functions can produce a superconducting state. Of course, the Hubbard model may just be an excessive simplification with regard to the structure of copper oxides, and several bands may actually be involved. Although some recent experiments have revealed a Josephson effect typical of a *d* state [354, 355], experimental aspects of the question have not been entirely settled [356, 357]. However, recent photoemission experiments on bismuth compounds have unambiguously identified a gap of form $\cos k_x - \cos k_y$, typical of a *d* symmetry [358].

A microscopic description of this state in the strong coupling regime has not yet been found. Today the task remains fascinating but difficult.

Part II

Superconductivity

12. Macroscopic Aspects of Superconductivity

12.1 Four Phenomena

Superconductivity was discovered in 1911, after Kamerlingh Onnes had opened the way to low temperature physics by liquifying helium. The discovery was made [359] for mercury whose resistance drops to zero (within the limits of experimental accuracy) below a critical temperature $T_c \approx 4.25$ K. Since then hundreds of zero resistance materials have been discovered. Up until 1987, critical temperatures of these materials all lay below 23.5 K, the critical temperature of the alloy Nb₃Sn. In most of these materials, the mechanism responsible for superconductivity is the electron–phonon interaction, which is well understood. In 1987, a new class of materials was discovered: the high temperature superconductors, with critical temperatures ranging between 40 K and 120 K. In these materials, the mechanism leading to superconductivity is not yet known. However, it is fairly clear that it is not the electron–phonon interaction. Moreover, all these materials contain atomic planes of copper and oxygen which play a key role in the mechanism inducing superconductivity [see Sect. 11.4.3(I)]. There are therefore many poorly understood features and for this reason, the present discussion will be limited to conventional superconductors.

Not only do thermal fluctuations destroy superconductivity, but a sufficiently intense magnetic field can push the superconductor into its normal (resistive) state. Kammerlingh Onnes determined the temperature variations of this critical field H_c from experimental data and found that

$$H_c(T) = H_c^0 \left[1 - \left(\frac{T}{T_c} \right)^2 \right], \quad (12.1)$$

plotted in Fig. 12.1 [360]. The critical field H_c^0 can be related to the critical temperature T_c . Since the critical field is zero at T_c , we are witnessing a second order transition. In zero field, the entropy is continuous at T_c , but the specific heat is discontinuous. When $H \neq 0$, transition takes place at $T < T_c$ and becomes (weakly) first order; latent heat is released at transition.

The zero resistance state can also be destroyed by large enough electrical currents. The critical current induces a magnetic field which can be related to the critical field by the Silsbee criterion: the critical current is approximately

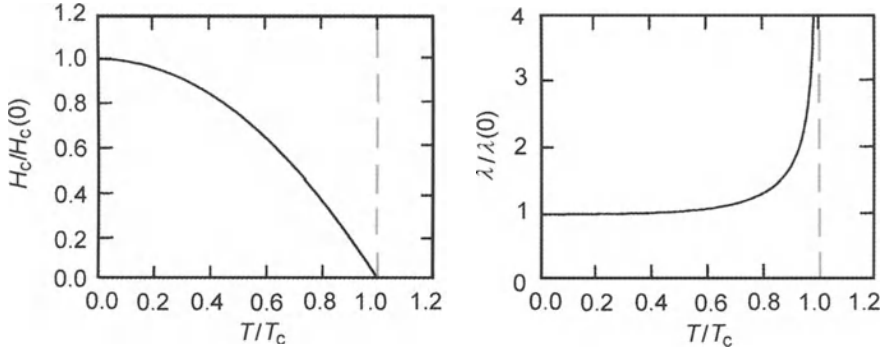


Fig. 12.1. *Left:* Temperature dependence of the critical field. At $T = T_c$, the critical field is zero and the transition is second order. At $T < T_c$ and $H = H_c(T)$, the transition becomes first order. *Right:* Temperature dependence of penetration depth λ

attained when the magnetic field at the surface of the sample equals the critical field.

But superconductivity is not just a zero resistance state. Meissner and Ochsenfeld [361] showed that a superconductor excludes all applied magnetic fields of intensity less than some critical value, which we shall specify. This is shown in Fig. 12.2. The superconductor is therefore a perfectly diamagnetic material, maintaining a $B \equiv 0$ state within it. This is the Meissner effect. More detailed studies have shown that, provided the magnetic field remains weak enough, it gradually diminishes at the superconductor surface over a depth λ_L of order 10^{-5} cm ≈ 0.1 μm . This is called the penetration depth. When a field H is applied, a permanent thermodynamic current appears at the superconductor surface in such a way as to screen the field. If J is the current per unit length of a superconducting cylinder, the field created by

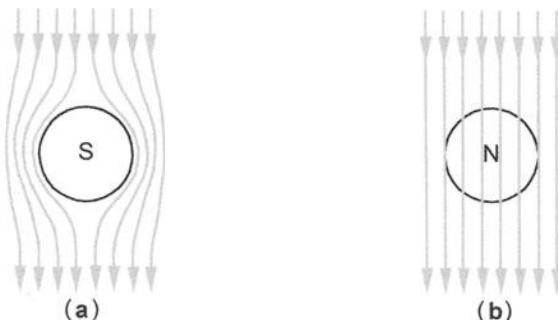


Fig. 12.2. Field lines around a superconductor. (a) When $H < H_c$, the system is perfectly diamagnetic. (b) When $H > H_c$, the system becomes normal

this solenoid is $J = H$, exactly cancelling the applied field. The penetration depth λ_L varies with temperature according to (see Fig. 12.1)

$$\lambda_L(T) = \frac{\lambda_L(0)}{[1 - (T/T_c)^4]^{1/2}}. \quad (12.2)$$

The divergence of λ_L at transition ($T \rightarrow T_c$) shows that we pass continuously from the normal metal, in which $\lambda = \infty$, to the superconducting state. In non-zero field, λ_L varies discontinuously from $\lambda = \infty$ to a finite value, and the transition is then first order.

If we compare magnetisation curves for various superconductors, we observe the two types of behaviour represented in Fig. 12.3. A type I superconductor is one in which diamagnetism remains perfect up to H_c ($H = -M, B = 0$) and becomes normal beyond that point. Reducing the field once again, the magnetisation reappears at some field value H_{c2} , called the nucleation field, which is less than H_c . This supercooling of the normal phase is due to the fact that type I superconductors have difficulty locally nucleating a superconducting region within a normal region. If there are defects, such as dislocations or macles, in the crystal lattice, these can modify such theoretical behaviour by smoothing out the transitions (see Fig. 12.3). Depending on the sample shape, there may also be an intermediate state (see

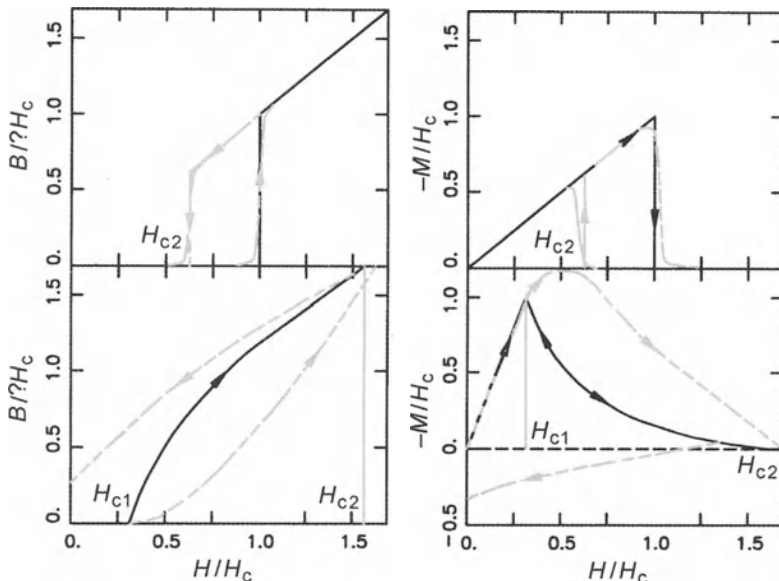


Fig. 12.3. Top: Type I superconductor. Induction and magnetisation as a function of applied field. When the magnetic field is reduced, superconductivity reappears at a field $H_{c2} < H_c$. Bottom: Type II superconductor. The Meissner effect is total up to H_{c1} . Between H_{c1} and H_{c2} , superconductivity persists in an inhomogeneous way then disappears beyond H_{c2} . Dotted lines are curves for impure samples

Sect. 12.7) in which normal and superconducting states coexist over a certain range of field values in the neighbourhood of H_c . For other superconductors, perfect diamagnetism persists only up to a magnetic field H_{c1} , less than H_c . Beyond this value, the magnetic field gradually penetrates in the form of flux lines (vortices); the magnetisation progressively decreases, until the nucleation field H_{c2} is reached, at which point superconductivity ceases. This kind of behaviour is referred to as type II superconductivity. In these materials, unlike the type I materials, superconductivity can easily be nucleated in an inhomogeneous way. In this case, H_{c2} may be well above the critical thermodynamic field H_c . Superconducting magnets can therefore be constructed. Between H_{c1} and H_{c2} , the material has no resistance, and contains a lattice of flux lines which can be treated simplistically as normal regions. This is the mixed state [362, 363, 364], also known as the Shubnikov phase. Such behaviour can be observed in clean materials, e.g., annealed NbTa. In dirty materials (with defects), vortices remain anchored onto impurities, leading to significant hysteresis and even paramagnetism in magnetisation curves, as shown in Fig. 12.3.

From a macroscopic point of view, the superconducting phase is a state which locally breaks the symmetry associated with gauge invariance,

$$\mathbf{A}'(r) \rightarrow \mathbf{A}(r) + \nabla \Lambda(r).$$

An order parameter ψ can be given which, as for any second order phase transition, grows from zero below the transition temperature.

As in any second order transition, the free energy and thermodynamic properties are very different in the superconducting state. The phonon specific heat grows as T^3 , $C_{\text{ph}} \approx BT^3$. By measuring their specific heat, we can determine the Debye temperature, characterising the maximal energy of optical phonons. If we subtract off phonon specific heat, we find that the specific heat of electrons in the superconducting state is [365]

$$C_{\text{el}} = a\gamma T_c \exp\left(-\frac{\Delta}{kT}\right). \quad (12.3)$$

This should be contrasted with the linear temperature dependence $C_{\text{el}} = \gamma T$ observed in Fermi liquids (γ is the Sommerfeld constant, equal to $k_B m p_F / 3\hbar^3$, assuming a spherical Fermi surface and one electron per ion in the crystal). Figure 12.4 illustrates this exponential behaviour [366]. It implies that there is an energy gap between ground state and excitations of the system, as in a semiconductor. Such a gap excludes any possibility of thermal conduction when $T \ll T_c$, since there is no state available to transport the corresponding entropy. This property is used to build low temperature thermal switches, activated by applying a field H greater than the critical field. Adiabatic demagnetisation systems, used to attain very low temperatures, are always equipped with such switches. Despite this gap, electrons from a normal metal can always be injected into a superconductor by a conversion process called Andreev reflection, which we shall study in Chap. 17. The existence of this

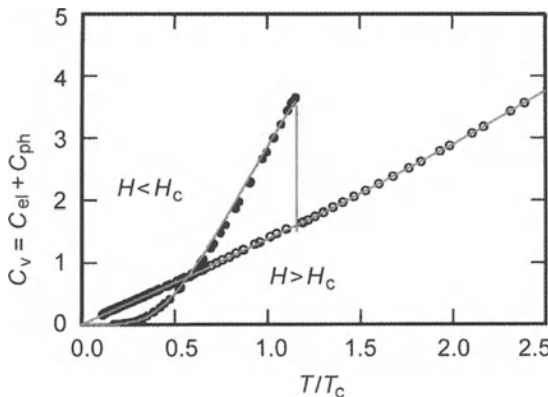


Fig. 12.4. Total specific heat (electron and phonon) of aluminium in zero field (black circles) and above the critical field (white circles) [366]

gap is related to the presence of 2-electron bound states, called Cooper pairs. Before tackling the electromagnetic properties of superconductors, we shall give an intuitive idea of the microscopic mechanism which gives rise to these bound states.

12.2 Electron–Phonon Interactions

At the beginning of the 1950s, a study of several samples corresponding to different isotopes of the same element (aluminium) showed that the critical temperature T_c and critical field varied as $1/\sqrt{M}$, where M is the atomic mass [367, 368]. This is an experimental demonstration that the crystal lattice plays an active role in superconductivity.

Imagine an electron at the centre of a unit cell in a cubic crystal. Coulomb interaction attracts lattice ions towards the centre of the cube formed by neighbouring ions. As the electron can move, it will not stay in this position for very long. In contrast, the ions have much greater inertia and take longer to come back to their equilibrium position. The result is an excess of ionic charge at the position occupied by the electron. This positive charge attracts another electron towards the position previously occupied by the first electron. There is therefore an attraction of two electrons towards each other via electron-induced lattice deformations. It is an interaction between electrons induced by the electron–phonon interaction.

An analogy is provided by two people lying on a rather soft mattress (the lattice). Each person creates a significant depression in the mattress, all the greater if they happen to be in the same place; whence an attractive force is induced by the flexibility of the lattice.

It is rather less obvious that such an interaction could give rise to electron bound states. We know that in three dimensions, a minimum attractive

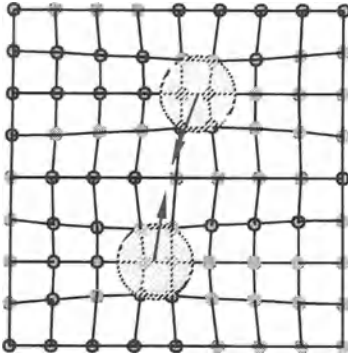


Fig. 12.5. Polarisation of the crystal lattice by conduction electrons. In a dynamic model, the attraction induced by excess ionic charge may exceed the Coulomb repulsion between electrons. In a static model, this would not be possible

interaction is needed in order to bind two electrons together. It is because there is a Fermi surface (acting via the Pauli principle) that an originally 3-dimensional problem is transformed into a 2-dimensional problem (on the Fermi surface). An infinitesimal electron-electron interaction is then sufficient to create a bound state. The binding energy is of the same order of magnitude as the critical temperature (of order 10 K). In general, this is about 10^{-3} times smaller than the electron kinetic energy (the Fermi energy). Consider a quadratic spectrum $\varepsilon(\mathbf{p}) = p^2/2m$. This can be linearised near ε_F ,

$$|\xi(\mathbf{p})| = \varepsilon(\mathbf{p}) - \varepsilon_F = v_F(p - p_F). \quad (12.4)$$

It is because the spectrum has a linear dependence (on $p - p_F$) near the Fermi level that a bound state is possible. We are interested in bound states of two electrons ($p > p_F$) or two holes ($p < p_F$). Let $\psi(\mathbf{r}_1, \mathbf{r}_2)$ be the wave function, a solution of the Schrödinger equation

$$[\mathcal{H}_0(\mathbf{r}_1) + \mathcal{H}_0(\mathbf{r}_2) + U(\mathbf{r}_1, \mathbf{r}_2)] \psi(\mathbf{r}_1, \mathbf{r}_2) = E\psi(\mathbf{r}_1, \mathbf{r}_2), \quad (12.5)$$

where the eigenstates of \mathcal{H}_0 are

$$\mathcal{H}_0(\mathbf{r}_1)\psi_{\mathbf{k}}(\mathbf{r}_1) = |\xi(\hbar\mathbf{k})|\psi_{\mathbf{k}}(\mathbf{r}_1), \quad (12.6)$$

and $\psi_{\mathbf{k}}(\mathbf{r}) = V^{-1/2} \exp(i\mathbf{k} \cdot \mathbf{r})$. The ground state does not involve any current. Indeed the centre of mass of the pair must have zero momentum; the two electrons have equal and opposite wave vectors. For an attractive and isotropic force, the ground state must be spatially symmetric and the spin wave function is therefore antisymmetric ($S = 0, l = 0$ state). We can expand $\psi(\mathbf{r}_1, \mathbf{r}_2)$ in terms of eigenstates of $\mathcal{H}_0(\mathbf{r}_1) + \mathcal{H}_0(\mathbf{r}_2)$ with these symmetries,

$$\psi(\mathbf{r}_1, \mathbf{r}_2) = V^{-1} \sum_{\mathbf{k}} b_{\mathbf{k}} \cos[\mathbf{k} \cdot (\mathbf{r}_1 - \mathbf{r}_2)] |S = 0\rangle, \quad (12.7)$$

where $S|0\rangle = (|\downarrow, \uparrow\rangle - |\uparrow, \downarrow\rangle)/\sqrt{2}$ is the singlet state of the two spins. Substituting into (12.5), we obtain the system of equations

$$2|\xi(\mathbf{k})|b_{\mathbf{k}} + \sum_{\mathbf{k}'} U_{\mathbf{kk}'} b_{\mathbf{k}'} = Eb_{\mathbf{k}}, \quad (12.8)$$

for amplitudes $b_{\mathbf{k}}$ forming the Cooper pair. As we shall see by studying the electron–phonon interaction in Chap. 14, the electron–phonon interaction potential can be approximated by a constant:

$$\begin{aligned} U_{\mathbf{kk}'} &= -U \text{ if } |\mathbf{k}| > k_{\min} = k_F - \omega_D/v_F, \\ &\quad \text{if } |\mathbf{k}'| < k_{\max} = k_F + \omega_D/v_F, \end{aligned} \quad (12.9)$$

and zero in all other cases (ω_D is the Debye frequency of the crystal). Defining the binding energy as $E = -2\Delta$, we obtain the amplitudes $b_{\mathbf{k}}$ from (12.8),

$$b_{\mathbf{k}} = \frac{1}{2} \frac{UA}{|\xi(\mathbf{k})| + \Delta}, \quad (12.10)$$

$$A = \sum_{k_{\min} < |\mathbf{k}| < k_{\max}} b_{\mathbf{k}}. \quad (12.11)$$

Δ can be determined from the eigenvalue equation. Summing the amplitudes $b_{\mathbf{k}}$, we eliminate A to obtain

$$1 = \frac{U}{2} \sum_{k_{\min} < |\mathbf{k}| < k_{\max}} \frac{1}{|\xi(\mathbf{k})| + \Delta} \approx \frac{n(\varepsilon_F)U}{2} \ln \left(\frac{\hbar\omega_D}{\Delta} \right), \quad (12.12)$$

where $n(\varepsilon_F)$ is the density of states at the Fermi level. The sum over wave vectors has been replaced by an integral over the range $\pm\hbar\omega_D$ in the vicinity of the Fermi level, and the linearised quasi-particle spectrum has been used. This linearisation replaces a 3-dimensional problem by a 2-dimensional problem, since wave vectors remain on the surface of the Fermi sphere. Bound states are thereby stabilised, depending logarithmically on potential U , as in two dimensions. The binding energy of the pair is then

$$E = 2\Delta = 2\hbar\omega_D \exp \left(\frac{-2}{n(\varepsilon_F)U} \right). \quad (12.13)$$

The exponent here differs by a factor of 2 relative to the BCS theory, but the physics is nevertheless correct on a qualitative level:

- this expression shows that Cooper pairs cannot be given by perturbation theory in U , because $U = 0$ is an essential divergence;
- the critical temperature $T_c \propto \Delta$ increases with $n(\varepsilon_F)U$;
- the maximal value that can be attained by Δ is limited by the Debye frequency ω_D . In practice, the critical temperature is between 10 and 100 times smaller than the Debye energy.

Raising the temperature enlarges the Fermi surface and thus decreases the Cooper pair binding energy. The latter goes to zero at T_c . In this sense, we can see that Cooper pairs could not exist above T_c , but appear collectively below T_c , and their number grows as the temperature decreases further. It is for this reason that we cannot consider the superconducting transition as

Bose condensation of pairs which already exist in some incoherent way above T_c . Unfortunately, some authors seem to entertain the idea that superconductivity is nothing but Bose condensation of Cooper pairs. Such a view is not valid.

Exercise

Determine the average size of a Cooper pair (see Sect. 12.5).

12.3 The Two-Fluid Model

The above study shows that some electrons in a superconductor form Cooper pairs. Let $n_s(T)$ be the pair density at temperature T . The density of remaining ‘electrons’ (which are in fact quasi-particles with properties similar to normal electrons) is then

$$n_n(T) = n_e - 2n_s(T). \quad (12.14)$$

This is the two-fluid model. Although the thermodynamics, and to a lesser degree also the transport, are affected by normal electrons in a superconductor, electromagnetic properties are dominated by Cooper pairs. This is because they involve electrons at the Fermi level. In particular, screening of magnetic fields is entirely due to Cooper pairs. The screening length λ_L is thus inversely proportional to the density of Cooper pairs. By dimensional analysis, λ_L can be related to n_s by $\lambda_L^2 r_c n_s \approx O(1)$, which brings in the classical electron radius $r_c = \mu_0 e^2 / m$. The latter measures the characteristic length of electromagnetic interaction. We deduce

$$\lambda(T) \propto \frac{1}{\sqrt{r_c n_s(T)}}. \quad (12.15)$$

Taking into account the temperature dependence of the penetration depth given in (12.2), we can conclude that

$$n_s(T) = \frac{n_e}{2} \left[1 - \left(\frac{T}{T_c} \right)^4 \right], \quad (12.16)$$

assuming that at zero temperature all electrons form Cooper pairs. At finite temperatures, we shall find in the BCS theory that the pair density is substantially smaller than $n_e/2$. Combining (12.14) and (12.16), we find that the density of ‘normal’ electrons varies with temperature according to

$$n_n = n_e \left(\frac{T}{T_c} \right)^4. \quad (12.17)$$

Although difficult to justify [373, 374], the two-fluid model describes charge transport in superconductors over distances which are large compared with

characteristic lengths λ_L and ξ . In this description, the total current is, below T_c , the sum of an ohmic current J_n carried by quasi-particles, and a superconducting current J_s carried by Cooper pairs. We know the electrodynamics of normal electrons, which combines Maxwell's equations with Ohm's law $J_n = \sigma E$, the constitutive equation relating normal currents to electric fields. However, we must also discover the constitutive equation governing the dynamics of a superconducting current. Note as a first step that Cooper pairs appear at T_c and must in some sense constitute the order parameter. This order parameter must therefore be related to the Cooper pair wave function, which suggests that Cooper pairs form a single macroscopic wave function. Macroscopic properties of a superconductor are then determined by this wave function, itself macroscopic, and it is this wave function which determines Cooper pair electrodynamics.

12.4 The London Equations

In 1935, the London brothers, Fritz and Heinz, put forward a constitutive equation relating the superconducting current to the electric field [374, 375, 376],

$$\frac{\partial(\Lambda J_s)}{\partial t} = \mathbf{E}, \quad (12.18)$$

$$\nabla \times (\Lambda \mathbf{J}_s) + \mathbf{B} = 0, \quad (12.19)$$

$$\Lambda = \mu_0 \lambda_L^2 = \frac{m_*}{n_s e_*^2}, \quad (12.20)$$

where the second London equation is obtained by combining the first with Maxwell's equation $\nabla \times \mathbf{E} + \partial \mathbf{B} / \partial t = 0$. More precisely, the time derivative of the second London equation is zero. It is therefore a constant and must equal 0 since $\mathbf{E} = \mathbf{B} = 0$ inside the superconductor. The effective mass and charge of a Cooper pair are denoted m_* and e_* , respectively ($m_* \approx 2m$ and $e_* \approx 2e$). These determine the phenomenological parameter Λ which we shall relate to the penetration depth λ_L .

The London equations are best motivated by quantum theoretical arguments. We saw in Chap. 2(I) that the momentum conjugate to position is \mathbf{p} and not the kinetic momentum $\boldsymbol{\pi} = m_* \mathbf{v}_s = \mathbf{p} - e_* \mathbf{A}$. In zero field, the Bloch theorem requires the ground state to have zero momentum $\mathbf{p} = 0$. If we postulate that the ground state wave function is rigid and cannot acquire momentum when a field is applied, we must conclude that $\langle \mathbf{p} \rangle = 0, \forall B$. Hence,

$$\langle \mathbf{v}_s \rangle = -\frac{e_* \mathbf{A}}{m_*}. \quad (12.21)$$

Since there are n_s Cooper pairs in the rigid ground state, the resulting current carried by this state is

$$\mathbf{J}_s = n_s e_* \langle \mathbf{v}_s \rangle = -\frac{n_s e_*^2}{m_*} \mathbf{A} = -\frac{\mathbf{A}}{\Lambda} . \quad (12.22)$$

Taking the derivative with respect to time, we obtain

$$\frac{\partial(\Lambda \mathbf{J})}{\partial t} = -\frac{\partial \mathbf{A}}{\partial t} = \mathbf{E} , \quad (12.23)$$

since the electric field $\mathbf{E} = -\nabla\Phi - \partial\mathbf{A}/\partial t$ and the potential Φ are both constant inside the metal. Finally, taking the curl of this equation, we obtain

$$\nabla \times \mathbf{E} = -\frac{\partial \mathbf{B}}{\partial t} = \frac{\partial \nabla \times (\Lambda \mathbf{J})}{\partial t} . \quad (12.24)$$

Since $\mathbf{B} + \nabla \times (\Lambda \mathbf{J})$ is constant and $\mathbf{B} = 0 = \mathbf{J}$ inside the superconductor, we arrive at the second London equation. If we now combine Ampère's theorem $\nabla \times \mathbf{H} = \mathbf{J}$ with the second London equation, we find that

$$\nabla \times (\nabla \times \mathbf{B}/\mu_0) = \nabla \times \mathbf{J} = -\mathbf{B}/\Lambda ,$$

and hence

$$\begin{aligned} \nabla \times (\nabla \times \mathbf{B}) &= \nabla(\nabla \cdot \mathbf{B}) - \nabla^2 \mathbf{B} \\ &= -\nabla^2 \mathbf{B} = -\frac{\mu_0}{\Lambda} \mathbf{B} = -\frac{1}{\lambda_L^2} \mathbf{B} . \end{aligned} \quad (12.25)$$

The magnetic field is therefore attenuated over a distance λ_L . The London equations account for the Meissner effect.

Equation (12.22) thus contains the two London equations, but since it is manifestly not invariant under gauge transformation, we must add a gauge condition $\nabla \cdot \mathbf{A} = 0$ to ensure that $\mathbf{A} \rightarrow 0$ inside the conductor. This condition is equivalent to charge conservation, thanks to the continuity equation $\nabla \cdot \mathbf{J} = 0 = -\partial\rho/\partial t$. This is the London gauge. Precise measurements have shown that the penetration depth $\lambda(T = 0)$ is always greater than λ_L . In the context of the London theory, this is only possible if the wave function ψ is not perfectly rigid in the ground state.

12.5 London and Pippard Superconductors

Combining the London equations, we were able to write down a local relation between superconducting current and vector potential,

$$\mathbf{J}_s(r) = K \mathbf{A}(r) , \quad \nabla \cdot \mathbf{A} = 0 , \quad (12.26)$$

where $K = 1/\Lambda = -n_s e_*^2/m_*$. In reality, Cooper pairs have non-local electrodynamics. Indeed, they have finite size. A Cooper pair is a wave packet whose constituent wave vectors lie in the interval $\delta k \approx \Delta/\hbar v_F$. Consequently, Cooper pairs have sizes of the order of

$$\xi = \frac{1}{\pi \delta k} = \frac{\hbar v_F}{\pi \Delta} \approx 1 \text{ }\mu\text{m} . \quad (12.27)$$

This coherence length ξ is several thousands of times greater than interatomic distances. It is important to understand how these extended objects can move around without interfering with other such objects. Indeed, these pairs interpenetrate and pass through one another without interaction. Such a process is only possible in quantum mechanics, reminiscent of the collisionless motion of free electrons through a crystal lattice. Since the correlation length is large, the superconducting current $\mathbf{J}_s(\mathbf{r})$ is not determined simply by the value of the potential \mathbf{A} at \mathbf{r} , but by its values over a volume of order ξ^3 about \mathbf{r} . The relation between \mathbf{J}_s and \mathbf{A} is therefore non-local:

$$J_s^i(\mathbf{r}) = \sum_j \int d^3r' K_{ij}(\mathbf{r} - \mathbf{r}') A_j(\mathbf{r}') . \quad (12.28)$$

In the limit of a field with slow spatial variations, we have

$$\int d^3r' K_{ij}(\mathbf{r} - \mathbf{r}') = \delta_{ij} \delta(\mathbf{r} - \mathbf{r}') K ,$$

and we return to the London equation. The characteristic length for field variations in a superconductor is the penetration depth λ_L . If this length is large compared with ξ , we come back to London electrodynamics.

In the opposite limit $\xi \gg \lambda_L$, we can draw an analogy with the penetration of an electromagnetic field in the anomalous skin effect regime. If a pair collides with the superconductor surface at a sufficiently large angle of incidence, it immediately emerges from the penetration depth, almost without interacting with the magnetic field. Only electrons at grazing incidence $\theta < \lambda/\xi$ interact with the field. Their number is then reduced to $n_s \lambda/\xi$, which we substitute into the penetration depth formula:

$$\lambda = \left(\frac{m_* \xi}{\mu_0 n_s \lambda \epsilon_*^2} \right)^{1/2} . \quad (12.29)$$

This defines the Pippard penetration depth [378]

$$\lambda_P = \left(\frac{m_*}{\mu_0 n_s \epsilon_*^2} \xi \right)^{1/3} = \lambda_L^{2/3} \xi^{1/3} . \quad (12.30)$$

In such superconductors, the kernel $K(\mathbf{r})$ can be calculated explicitly from the BCS theory to give the form of the non-local electrodynamics [see Sect. 14.9(II)]. As an example, the superconducting current is no longer given by the London equation but rather by

$$\mathbf{J}_s(\mathbf{r}) \approx \frac{3}{4\pi\xi_0\Lambda} \int d^3r' \frac{\mathbf{R}[\mathbf{R} \cdot \mathbf{A}(\mathbf{r}')] }{R^4} F(\mathbf{R}, T) , \quad (12.31)$$

where $\mathbf{R} = \mathbf{r} - \mathbf{r}'$ and $F(\mathbf{R})$ is a slowly varying function of temperature. The decrease in current is more complex here and will be analysed in Sect. 14.9(II).

Most pure elements are Pippard superconductors ($\xi \gg \lambda$). When impurities are present, electrons scatter above T_c with mean free path l . Such diffusive motion leads to spatial localisation of the electrons, and reduces the

average size of Cooper pairs (the coherence length) below T_c . This reduction is in the form of a geometric mean of coherence length in the proper limit (ξ_0) and mean free path, viz., $\xi \approx \sqrt{\xi_0 l}$. We thereby retrieve the London limit. Near T_c , the penetration depth diverges and all superconductors fall within the London limit.

12.6 Thermodynamics of the Transition

Consider a long cylinder placed in a magnetic field parallel to its axis. At the transition temperature, the Gibbs free energies per unit volume $g = f - BH$ are the same in both the normal and superconducting states:

$$g_n(H, T) = g_s(H, T). \quad (12.32)$$

This determines the *thermodynamic* critical field $H_c(T)$ at transition. The magnetic field only penetrates into the superconductor over the penetration depth and a surface current screens the field. The electromagnetic energy density $\mu_0 H_c^2/2$ is therefore concentrated within the thin layer of thickness λ_L , which has negligible volume $V \approx S\lambda_L$ (S being the surface area of the cylinder). Hence,

$$g_s(H, T) \approx g_s(H = 0, T) = f_s(T). \quad (12.33)$$

In the normal state, the magnetic field completely penetrates the superconductor and the electromagnetic energy per unit volume is $\mu_0 H^2/2$. The Gibbs free energy density at H_c is then

$$g_n(H_c, T) = f_n - \mu_0 H_c^2/2, \quad (12.34)$$

and we can deduce that

$$f_n(T) - f_s(T) = \frac{\mu_0 H_c^2(T)}{2}. \quad (12.35)$$

Differentiating with respect to temperature ($s = -\partial f / \partial T$), we can find the entropy difference between normal and superconducting states as a function of critical field,

$$s_n - s_s = -\mu_0 H_c \frac{dH_c(T)}{dT}, \quad (12.36)$$

plotted in Fig. 12.6. In the presence of a magnetic field, the latent heat at transition $L = T(s_n - s_s)$ is positive, because $dH_c/dT < 0$. In other words, the system absorbs heat in going from the superconducting to the normal state. Differentiating once more with respect to temperature, we obtain the specific heat $C = T(\partial S / \partial T)_V$ and hence

$$C_n - C_s = -\mu_0 T \left[H_c \frac{d^2 H_c}{dT^2} + \left(\frac{dH_c}{dT} \right)^2 \right]. \quad (12.37)$$

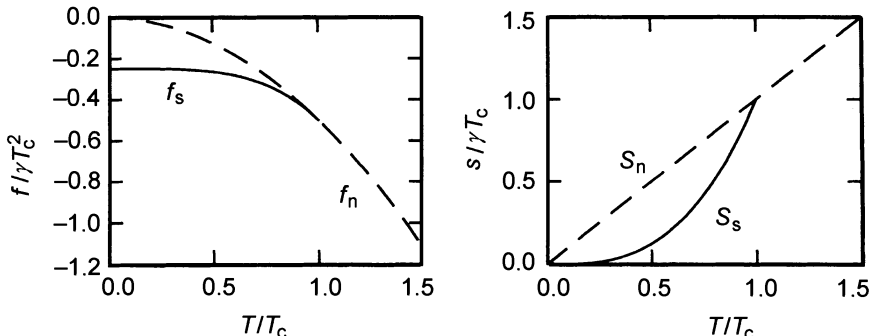


Fig. 12.6. *Left:* Free energy per unit volume in the superconducting state (*continuous curve*) and in the normal state (*dashed curve*). *Right:* Entropy per unit volume in the superconducting state (*continuous curve*) and in the normal state (*dashed curve*)

In particular, the jump in specific heat at transition is

$$\delta C = \mu_0 T_c \left(\frac{dH_c}{dT} \right)^2. \quad (12.38)$$

These exact thermodynamic relations are direct consequences of the Meissner effect. We will see that fluctuations at the superconducting transition occur over a range of reduced temperatures of order

$$\tau = (T - T_c)/T_c = (k_B T_c / \varepsilon_F)^4 \approx 10^{-12}.$$

The critical behaviour at transition is therefore of mean field type, i.e., the Landau theory is applicable. Whereas in magnetism there is only one energy scale, the coupling constant J , there is in the present case another scale, namely the Fermi energy, which introduces a cutoff frequency for fluctuations.

Exercise: Thermodynamics of Superconductors

The specific heat per unit volume of a metal can be represented by

$$C_s = aT^3 \quad (T < T_c), \quad C_n = bT^3 + \gamma T \quad (T > T_c), \quad (12.39)$$

where a and b are constants which can be related to the phonon spectrum of the metal and γ is the Sommerfeld constant. Using this result and the usual thermodynamic definitions, show the following.

1. The transition temperature in zero field is

$$T_c = \sqrt{\frac{3\gamma}{a - b}}. \quad (12.40)$$

2. The critical field $H_c = H(0)(1 - t^2)$, where $t = T/T_c$ and $H(0) = T_c \sqrt{2\gamma/\mu_0}$.

3. In zero field, the difference in internal energies between the two states reaches a maximum when $T = T_c/\sqrt{3}$.
4. If a magnetic field is increased very slowly up to a value above the critical field, the transition to the normal state is accompanied by cooling of the metal. Give a formula for the temperature drop.
5. If a magnetic field is applied suddenly, however, the metal is heated up rather than cooled when the field exceeds

$$H = H(0)\sqrt{(1 + 3t^2)(1 - t^2)} . \quad (12.41)$$

Exercise: Free Energy in the London Approximation

In the London approximation, the free energy of a superconductor is expressed as the sum of kinetic energies of pairs and magnetic energy, viz.,

$$F = \mathcal{E}_{\text{kin}} + \mathcal{E}_{\text{mag}} , \quad (12.42)$$

where

$$\mathcal{E}_{\text{kin}} = \int d^3r \frac{1}{2} m_* n_s v_s^2 . \quad (12.43)$$

Show that F can be expressed in the form

$$F = \frac{1}{2\mu_0} \int d^3r [B^2 + \lambda^2(\nabla \times \mathbf{B})^2] . \quad (12.44)$$

What contributions to the free energy are neglected in the London theory?

12.7 The Intermediate State

Previously we considered a very long sample in which field lines are not appreciably deformed. In most cases, the presence of a superconductor affects the value of the induction B at the sample surface and it may be very different to the applied induction B_a . We consider a superconducting sphere of radius R . Above the critical field, the magnetic induction \mathbf{B} is zero inside the superconductor, so that

$$\nabla \cdot \mathbf{B} = \nabla \times \mathbf{B} = \nabla^2 \mathbf{B} = 0 , \quad (12.45)$$

with boundary conditions

$$\mathbf{B} = \mathbf{B}_a \equiv \mu_0 \mathbf{H}_a \quad \text{when } \mathbf{r} \rightarrow \infty , \quad (12.46)$$

$$\mathbf{B} \cdot \hat{\mathbf{r}} = 0 \quad \text{when } r = R . \quad (12.47)$$

Solution of the magnetostatic problem shows that the field outside the sphere is a superposition of the applied field and a dipolar field which opposes \mathbf{B}_a ,

$$\mathbf{B} = \mathbf{B}_a + \frac{R^3}{2} \nabla \left(\frac{\mathbf{B}_a \cdot \mathbf{r}}{r^3} \right) . \quad (12.48)$$

It is easy to check that $\mathbf{B} = B_\theta \hat{\theta}$ is tangential to the surface of the sphere $\mathbf{B} \cdot \hat{r} = 0$ and that its amplitude is

$$B_\theta(r = R) = \frac{3}{2} B_a \sin \theta . \quad (12.49)$$

This is greater than the amplitude of the applied field in the sector between $\theta = 42^\circ$ and 138° containing the equatorial plane. Hence for $\theta = \pi/2$, $H = B/\mu_0$ reaches H_c when $B = 2\mu_0 H_c/3$. Let H_a be an applied field in the range

$$\frac{2H_c}{3} < H_a < H_c . \quad (12.50)$$

The field H then exceeds the critical field in a region of the sample surface. It should therefore become normal in these sectors. It is not possible for the whole sample to become normal since we would then have $H = H_a < H_c$ everywhere and this value is not sufficient for return to the normal state. We conclude that normal and superconducting regions must coexist and the sample is in the intermediate state. Had we chosen an ellipsoidal sample, we would have found such a state for fields in the range

$$1 - N_z < \frac{H}{H_c} < 1 , \quad (12.51)$$

where N_z is the ellipsoidal demagnetising factor as defined in Chap. 1(I). For a very long sample, $N_z = 0$; for a sphere, $N_z = 1/3$; for a cylinder with axis perpendicular to the field, $N_z = 1/2$; and for a plate perpendicular to the field, $N_z = 1$.

We shall now discuss domains formed in the intermediate state of a superconducting plate at $T = 0$. The problem was solved by Landau in a classic paper [369, 370, 371]. Many experiments indicate that the intermediate state in a plate comprises a lamellar structure of alternating normal and superconducting regions. This is shown in Fig. 12.7. Normal regions of thickness a are

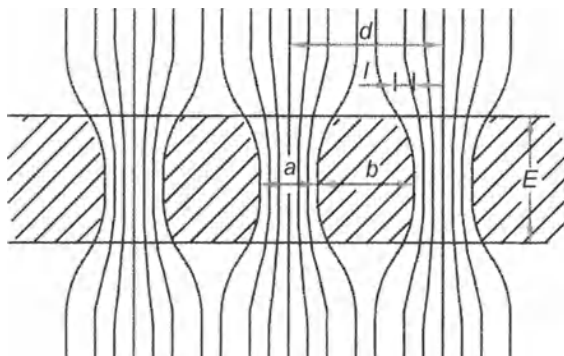


Fig. 12.7. (a) Sketch of field lines channelled into lamellas of thickness a across the plate of thickness E . The magnetic induction is B_a away from the plate and $\mu_0 H_c$ in normal regions of the plate

separated by superconducting regions of thickness b . Let $d = a + b$ and E the plate thickness.

Field lines spread out near the plate surface, over a relaxation length l . This length is approximately equal to the smaller of the two lengths a and b , which can be expressed by

$$\frac{1}{l} = \frac{1}{a} + \frac{1}{b}. \quad (12.52)$$

The stability of such a structure is essentially due to the fact that there is a free energy at the interface between normal and superconducting states. We have already seen that at the interface between two ferromagnetic domains the order parameter varies continuously between $+\sigma$ and $-\sigma$. The gradient of spin density gives rise to an excess free energy equal to

$$\frac{\Gamma}{2} \int (\nabla \sigma)^2 d^3 r.$$

By analogy, we associate a free energy per unit area to the variation of the superconducting order parameter at the interface between normal and superconducting regions; this is of order

$$\Gamma = \frac{\mu_0 H_c^2}{2} \delta, \quad (12.53)$$

where the length $\delta = \xi - \lambda$ is positive for type I superconductors and of order between 0.1 and 1 μm . Given this surface energy, the system seeks the configuration which minimises all contributions to the free energy of the lamellar structure. Some of these, such as the diamagnetic energy of screening currents, of order $\mu_0 H_c^2 \lambda_L / 2$, can be neglected in comparison with the interfacial free energy when $\xi \gg \lambda_L$. Others, such as the loss of condensation energy in normal regions, are not relevant to the selection of the lamellar structure (see Exercise C.1.4, Appendix C). We must still evaluate the electromagnetic free energy. Since the magnetic field in normal regions is equal to H_c , and since the density of lamellas in the normal state is $1/d$ per unit lamellar length, the magnetic energy per unit area of the plate is

$$f_{\text{em}} = \frac{\mu_0 H_c^2}{2d} (Ea + \gamma l^2). \quad (12.54)$$

The second term takes into account relaxation of field lines over a length l above the plate (the factor γ is a constant of order 1).

Analogously, given that there are two sides of length E to each normal lamella, the interfacial free energy per unit area of the plate associated with normal-superconducting interfaces is given by

$$f_{\text{ns}} = \Gamma \frac{2E}{d}, \quad (12.55)$$

where $1/d$ is once again the density of lamellas. If we introduce the volume fractions in normal and superconducting states,

$$\rho_n = \frac{a}{d}, \quad \rho_s = 1 - \rho_n = \frac{b}{d}, \quad (12.56)$$

the relaxation length is $l = d\rho_n\rho_s$, and the magnetic free energy of the lamellar structure is given by

$$f = f_{\text{em}} + f_{\text{ns}} = \frac{\mu_0 H_c^2}{2} \left(E\rho_n + \gamma d(\rho_n\rho_s)^2 + \frac{2E\delta}{d} \right). \quad (12.57)$$

For constant ρ_n , only the last two terms depend on d . The distance d between lamellas is found by minimising the free energy f ,

$$d = \frac{\sqrt{2E\delta}}{\rho_n\rho_s}. \quad (12.58)$$

Moreover, conservation of magnetic flux determines the values of ρ_n and ρ_s ,

$$\rho_n = \frac{H_a}{H_c}, \quad \rho_s = \frac{H_c - H_a}{H_c}, \quad (12.59)$$

since the magnetic field in normal regions is just H_c . The distance between lamellas is then the geometric mean of a microscopic distance 2δ of the same order as the coherence length, and a macroscopic distance E , the plate thickness. The intermediate state can be interpreted as a spontaneous phase separation into normal and superconducting regions. From this point of view, the existence of an interfacial free energy seems quite natural. More rigorous analysis of the Gibbs free energy G (see Exercise C.1.4, Appendix C) confirms the lamellar structure qualitatively, but makes a quantitative correction of these results.

Lamellar structures of this kind have been studied by scanning the superconducting surface with a submicron Hall probe, and also by magnetic decoration, i.e., powdering the superconducting surface with fine magnetic particles which follow field lines. Another approach is to study the Faraday rotation of light in a strongly rotating material deposited on the sample surface [379, 380]. Examples of structures observed are shown in Fig. 12.8. It can be seen that lamellas often fuse together and have defects. Moreover, cylindrical structures can be observed in the circular disks, showing that free energy differences between the various structures are often rather small, and hence difficult to determine theoretically.

It can also be shown that this structural free energy slightly lowers the critical field below H_c . The total free energy is a sum of the free energies in normal and superconducting regions, together with the excess energy associated with the structure, viz.,

$$F = \rho_s F_s + \rho_n F_n + \frac{B_a^2}{2\mu_0\rho_n} + \frac{f}{d}. \quad (12.60)$$

The minimum of F with respect to ρ_n occurs when

$$\rho_n = \frac{H_a}{H_c} \left[1 - 4 \frac{H_a}{H_c} \left(\frac{\delta}{d} \right)^{1/2} \right]^{-1/2}. \quad (12.61)$$

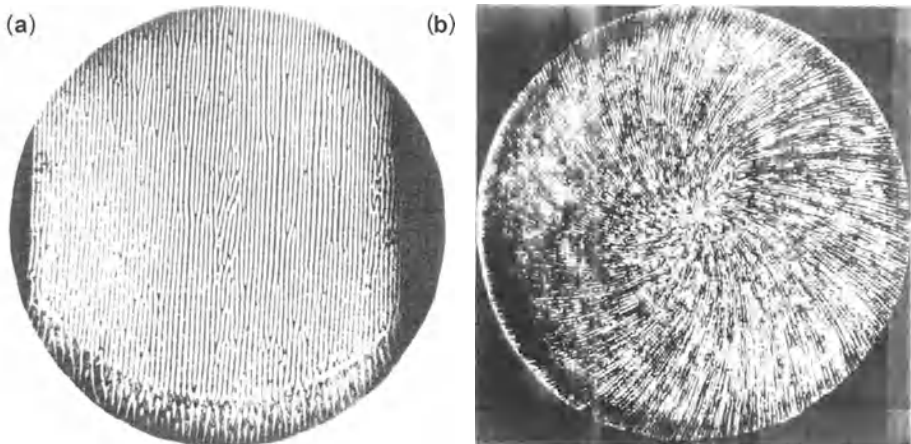


Fig. 12.8. (a) Lamellar structure observed on a tin disk in an oblique magnetic field at 15° to the normal. The temperature is $T = 2.165$ K, $T_c = 3.75$ K, and the field 0.95 Oe. Note that normal regions (dark) merge together in places. (b) When the magnetic field is suddenly decreased, magnetic flux escapes in a spiral motion of the lamellas about field lines

This implies, given the conservation of magnetic flux, that the critical field is reduced by a factor

$$H_{cI} = H_c \left[1 - 2 \left(\frac{\delta}{d} \right)^{1/2} \right]. \quad (12.62)$$

Many further refinements have been made to this study, involving interactions between lamellas, edge effects, and so on. Historically, explanation of the intermediate state was the great success of the London theory.

12.8 Critical Current in a Superconducting Wire

Consider a superconducting wire of radius a . According to Ampère's theorem, the current $\mathbf{J}(\mathbf{r})$ through a circle of radius \mathbf{r} is related to the magnetic field by

$$\int (\nabla \times \mathbf{H}) \cdot \hat{\mathbf{n}} \, dS = \oint \mathbf{H} \cdot d\mathbf{l} = 2\pi r H_\theta(\mathbf{r}) = J(r). \quad (12.63)$$

But the field H

$$H(r) = \frac{J(r)}{2\pi r} \quad (12.64)$$

is maximal when $r = a$. This defines the critical current

$$J_c = 2\pi a H_c. \quad (12.65)$$

This is Silsbee's rule [381]. It is not valid for thin films, of thickness smaller than λ_L . The critical currents of superconductors vary enormously from one material to another. In type II superconductors, they may exceed 10^9 A/cm^2 . This explains why high temperature superconductors are so interesting for industrial applications. If $J > J_c$, the surface field exceeds H_c and certain parts of the wire must be normal. But if a layer at the surface of the wire is normal whilst the centre is superconducting, all the current is carried in the centre, producing an even greater field at the surface. If we assume that the wire is normal, the current carried through a cross-section of radius r is $J(r) = (r/a)^2 J$ and

$$H(r) = \frac{rJ}{2\pi a^2}. \quad (12.66)$$

For the value $J = \alpha J_c$, we find $H(r) = \alpha H_c r/a$, which is less than H_c provided that $r < a/\alpha$.

These comments suggest that there is a core of radius $r_1 < a$ in the intermediate state, surrounded by a normal region. At the interface between normal and superconducting regions, we have $H(r) = H_c$. Since $H(r) = J(r)/2\pi r$, where $J(r)$ is the current within radius r , $J(r) = 2\pi r H_c$. This gives a current density for $r < r_1$

$$j(r) = \frac{1}{2\pi r} \frac{dJ(r)}{dr} = \frac{H_c}{r}. \quad (12.67)$$

In contrast, for $r_1 > r$, the system is normal and the current density is uniform with value

$$j(r) = \frac{J - J(r_1)}{\pi(a^2 - r_1^2)}. \quad (12.68)$$

These relations led London to propose the structure sketched in Fig. 12.9 for the intermediate state in the core of the wire [375]. This structure has since been observed experimentally [378]. The structure is justified by the following argument. If we consider two equipotential surfaces perpendicular to the cross-section, separated by distance z , we have $j(r) = \sigma E = \sigma \Phi/z$, where E is the electric field, Φ the potential difference and σ the conductivity in the normal state. Using (12.67), $\Phi = H_c z / \sigma r$. Since we have an equipotential, the condition $\Phi = \text{constant}$ requires z to be proportional to r . This is indeed the case in Fig. 12.9.

Since $J(r_1) = 2\pi r_1 H_c$, the continuity condition for the current at radius r_1 requires

$$\frac{J_c}{2\pi a r_1} = \frac{J - J_c r_1/a}{\pi(a^2 - r_1^2)}. \quad (12.69)$$

Putting $\rho = r_1/a$ and $\lambda = J/J_c$, we can determine ρ and therefore r_1 by solving (12.69), which we rewrite in the form

$$\rho^2 - 2\lambda\rho + 1 = 0. \quad (12.70)$$

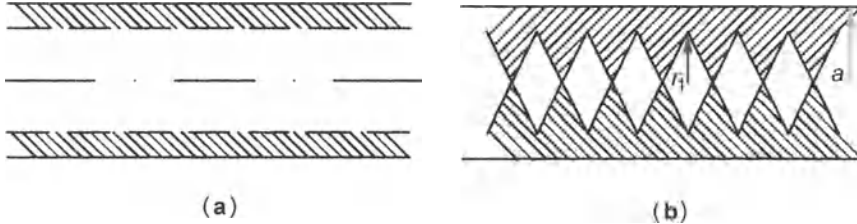


Fig. 12.9. (a) Unstable structure of a superconducting wire of radius a carrying a current J greater than the critical current. The central part would correspond to the superconducting state and the outer part to the normal state. (b) Mixed state proposed by London to describe the superconducting wire. The layer beyond radius r_1 is normal

The only physical solution, such that $\rho \rightarrow 0$ as $\lambda \rightarrow \infty$, is

$$\rho = \lambda - \sqrt{\lambda^2 - 1} . \quad (12.71)$$

Consider two equipotential surfaces a distance z apart. Ohm's law requires $\Phi = RJ$. But since R_n is the resistance in the normal state, the outer section has resistance $R_n a^2 / (a^2 - r_1^2)$ and carries current $J - J(r_1)$. Ohm's law then implies

$$\Phi = JR = [J - J(r_1)] R_n \frac{a^2}{a^2 - r_1^2} . \quad (12.72)$$

Replacing $J(r_1)$ by its value ρJ_c , we obtain the resistance of the wire as a function of the ratio $u = J/J_c$,

$$R = \frac{R_n}{2} \left[1 + (1 - u^{-2})^{1/2} \right] . \quad (12.73)$$

The London theory predicts a discontinuous jump in resistance by $R_n/2$ at J_c and a gradual saturation of the resistance up to R_n . Experiments show that the jump in resistance is slightly greater than this (of order $0.7R_n$) [382]. This can be explained by the reduction in H_c due to the free energy of the normal-superconducting interface, discussed in the last section. The microscopic theory proposed by Andreev [383] predicts a period of $(\xi^2 a)^{1/3}$ for the superconducting lozenges which constitute the mixed structure. If the superconductor has a large Hall resistance, the mixed structure looks more like a Christmas tree than stacked lozenges. There is also a dynamic model of the intermediate state in which interfaces are parallel to current flow and oscillate radially [384]. When there is a magnetic field, structures with interfaces parallel to the field are stabilised. This opens the way to structures quite different from those in the London model [387].

The London theory also explains the temperature dependence of a superconducting wire carrying a current J , in the neighbourhood of T_c . In this region, the critical current, proportional to H_c , is linear in $T - T_c$, so that

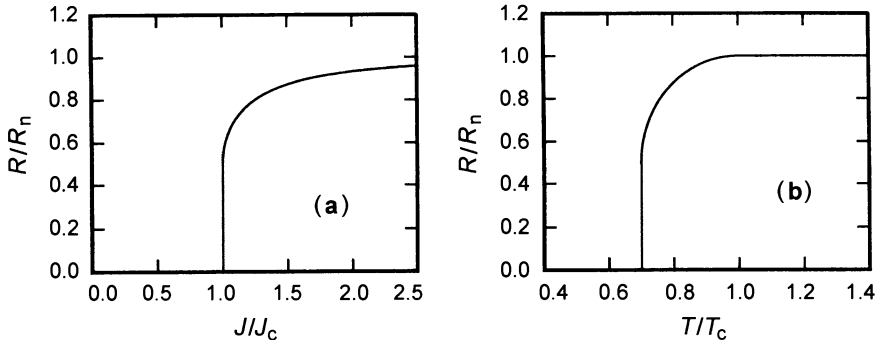


Fig. 12.10. (a) Evolution in resistance of a superconductor above the critical current J_c . The resistance makes a discontinuous jump by $R_n/2$ at J_c . (b) Temperature dependence of the resistance of a superconducting wire near T_c in the presence of a current J . The decrease in T_c is $\delta T_c = J/(dJ_c/dT)$

$$\begin{aligned} J_c &= \frac{dJ_c}{dT}(T_c - T) = \frac{dJ_c}{dH_c} \frac{dH_c}{dT}(T_c - T) \\ &= 2\pi a \frac{2H_c}{T_c}(T_c - T) = \frac{4\pi a H_c(T_c - T)}{T_c}. \end{aligned} \quad (12.74)$$

The critical temperature is reduced by a factor $\tau = J/(dJ_c/dT)$. Combining this with (12.73), we obtain the temperature dependence around T_c :

$$\frac{R}{R_n} = \frac{1}{2} \left(1 + \left[1 - \left(\frac{T_c - T}{\tau} \right)^2 \right]^{1/2} \right), \quad (12.75)$$

plotted in Fig. 12.10.

12.9 Two Types of Superconductor

We have seen that surface free energy between normal and superconducting states is at the origin of the intermediate state. Consider a plane interface between a normal and a superconducting region. Figure 12.11 shows the spatial variation of the mean binding energy $\Delta(T)$ of Cooper pairs, and also of the field H normally to the interface. The characteristic length over which Δ varies is, of course, the coherence length $\xi(T)$, of the same order as the size of the pairs. Moreover, equilibrium between a normal and a superconducting region requires $H = H_c$ in the normal phase. But the field is attenuated over distance λ_L which we have assumed much smaller than ξ in Fig. 12.11 (Pippard superconductor). To simplify the argument, we replace the gradual variations of Δ and H by abrupt interfaces located at average positions A and B such that the free energies are the same. There is then a normal phase with zero field in a region AB whose thickness is of order ξ . As $f_n - f_s = \mu_0 H_c^2/2$,

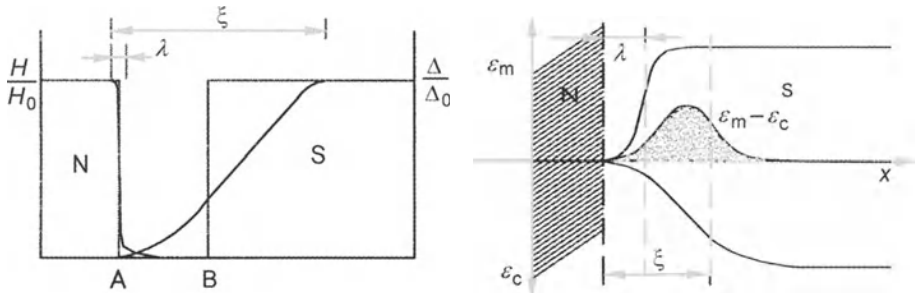


Fig. 12.11. *Left:* Spatial dependence of the gap $\Delta(T)$ and the local field at the interface of a Pippard superconductor. *Right:* Spatial dependence of the condensation energy ε_c and screening energy ε_m . The interfacial energy is the difference $\varepsilon_m - \varepsilon_c$ integrated over the volume

there is an excess free energy of $\mu_0 H_c^2 / 2$ throughout the volume of region AB. We deduce a free energy per unit area of

$$\Gamma = \xi \frac{\mu_0 H_c^2}{2}, \quad (12.76)$$

in agreement with the discussion of the intermediate state in Sect. 12.7.

In the opposite situation, where the penetration depth is such that $\lambda_L \gg \xi$ (London superconductor), the same argument shows that the surface free energy $\Gamma = -\lambda \mu_0 H_c^2 / 2$ is now negative. Although a negative surface free energy is difficult to justify in the context of the London theory, such superconductors do indeed exist in nature. Needless to say, the behaviour of these superconductors in a magnetic field is radically different to the behaviour studied previously. These are the type II superconductors. Abrikosov and Gorkov have shown that the change in behaviour between type I ($\Gamma > 0$) and type II ($\Gamma < 0$) occurs at the value $\kappa = 1/\sqrt{2}$ of the parameter $\kappa = \lambda/\xi$. To sum up,

$$\text{Type I} \iff \Gamma > 0 \iff \kappa < \frac{1}{\sqrt{2}}, \quad (12.77)$$

$$\text{Type II} \iff \Gamma < 0 \iff \kappa > \frac{1}{\sqrt{2}}. \quad (12.78)$$

The behaviour of type II superconductors is studied in Chap. 15(II).

13. Ginzburg–Landau Theory

Motivation

In 1950, Ginzburg and Landau devised a phenomenological theory of superconductivity [388] based on intuitive considerations which we shall develop in this chapter. At the time, the theory they proposed could not be justified in terms of a microscopic Hamiltonian. For this reason, their ideas were not taken very seriously in the West. In 1959, Gorkov showed [389] that the Ginzburg–Landau equations can be obtained from the microscopic theory of Bardeen, Cooper and Schrieffer [390] when the temperature is close enough to the critical temperature T_c . Since then the Ginzburg–Landau theory has been systematically used to describe macroscopic phenomena in superconductors. These are dominated by long wavelength variations of the free energy density. The simplicity of the theory means that it can often provide a manageable approach to situations in which the superconductivity is inhomogeneous, difficult to treat in the BCS theory. In addition, its intuitive aspect gives a concrete picture of the superconducting state. For experiments involving microscopic processes, such as the tunnel effect, photoemission spectra and nanostructures, details of the excitation spectrum come into the problem, and the Ginzburg–Landau theory is no longer adequate.

We consider wave functions of each Cooper pair j ,

$$\psi_c^j(\mathbf{r}) = V^{-1/2} a_j(\mathbf{r}) \exp i\phi_j(\mathbf{r}),$$

where $a_j(\mathbf{r})$ and $\phi_j(\mathbf{r})$ represent their amplitudes and phases, respectively. The coherence volume ξ^3 contains a large number of Cooper pairs which cannot be distinguished from one another. We therefore define an average wave function, or more exactly, a density of wave functions averaged over the volume ξ^3 . The average will only be non-zero if phases $\phi_j(\mathbf{r})$ are close together, in other words, if neighbouring Cooper pairs are coherent. In this case,

$$\psi(\mathbf{r}) = \frac{1}{\xi^3} \sum_{j \in \xi^3} \psi_j(\mathbf{r}_j) \propto \sqrt{n_s} \exp i\phi(\mathbf{r})$$

can be interpreted as the ground state wave function density. It is the order parameter introduced by Ginzburg and Landau. This discussion suggests identifying $|\psi(\mathbf{r})|^2$ with the density of Cooper pairs at the point \mathbf{r} , i.e.,

$$|\psi(\mathbf{r})|^2 = n_s . \quad (13.1)$$

In an N -particle system, we can define field operators creating and destroying particles at point \mathbf{r} , $\psi^\dagger(\mathbf{r})$ and $\psi(\mathbf{r})$, respectively [see Sect. 3.2(I) and Appendix B]. In a normally conducting metal, the expectation value of these operators is zero, whilst the expectation of the product $\psi^\dagger(\mathbf{r})\psi(\mathbf{r})$ is the particle density at \mathbf{r} . In a superconductor or superfluid, the operator $\psi(\mathbf{r})$ acquires a non-zero expectation $\langle\psi(\mathbf{r})\rangle$. Hence, at zero temperature we can write

$$\langle\psi^\dagger(\mathbf{r})\psi(\mathbf{r})\rangle = \langle\psi^\dagger(\mathbf{r})\rangle\langle\psi(\mathbf{r})\rangle . \quad (13.2)$$

We can then define the order parameter as the expectation value of operator $\psi(\mathbf{r})$. This relation can only be satisfied if the number of particles in the ground state remains indeterminate, which is clearly the case in the microscopic theory described in the next chapter. We should ask which symmetry is broken by the order parameter of a superconductor. We are generally free to choose the gauge $A(\mathbf{r})$ of the vector potential, which determines the phase of the wave function of each particle, i.e.,

$$\psi'(\mathbf{r}) = \psi(\mathbf{r}) \exp\left(\frac{2\pi i A(\mathbf{r})}{\Phi_0}\right) , \quad (13.3)$$

$$\mathbf{A}'(\mathbf{r}) = \mathbf{A}(\mathbf{r}) + \nabla A(\mathbf{r}) . \quad (13.4)$$

If the particles are independent, we can in principle choose a different gauge to describe the motion of each particle. But phase coherence between the various Cooper pairs means we must have the same gauge for all particles. The symmetry broken by the order parameter is therefore local gauge invariance. We must make the same choice of vector potential for all particles. The system thus selects a particular phase, just as a magnet selects a particular direction below the Curie temperature. In this case, we can change from one determination of the order parameter to another by making a rotation in spin space. In a superconductor, the operator $\exp(iN_{\text{op}}\chi/2)$ generates its phase (see Chap. 3). The operator N_{op} counts the number of particles in the system. More exactly, if ϕ is the phase of the order parameter, i.e., $\psi = |\psi| \exp(i\phi)$,

$$\exp(iN_{\text{op}}\chi/2)\psi = |\psi| \exp[i(\phi + \chi)] . \quad (13.5)$$

Choosing a particular phase for the order parameter amounts to choosing a particular gauge for the vector potential \mathbf{A} . This emphasises the physical significance of the electromagnetic gauge in this context. In superfluids, the symmetry broken by the order parameter is Galilean invariance.

We should establish the limits of application of the Ginzburg–Landau theory. Gorkov showed that the Ginzburg–Landau equations are equivalent to the BCS equations near T_c , provided that the two conditions

$$|\tau| = \frac{T_c - T}{T_c} \ll 1 , \quad \lambda \gg \xi_0 \quad (13.6)$$

are satisfied. In London superconductors, the first condition is the most important since the London penetration depth is always greater than the coherence length, at all temperatures. Since the penetration depth diverges near T_c , going as $\lambda \approx \lambda_0/2\sqrt{\tau}$, the second condition is equivalent to $|\tau| \ll \kappa^2/4$, where $\kappa = \lambda_0/\xi_0$. In Pippard superconductors, we have $\kappa \ll 1$ and this condition is the more restrictive. When these conditions are satisfied, Gorkov showed that the Ginzburg–Landau order parameter can be identified with the function

$$\psi(\mathbf{r}) = 0.326\sqrt{n_e} \frac{\Delta(\mathbf{r}, T)}{k_B T_c} \quad (13.7)$$

of the gap Δ in BCS theory. At equilibrium, the order parameter is uniform and functions Δ and ψ are real. Moreover, using the relation between $\Delta(T)$ and T_c given by the BCS theory,

$$\Delta = 3.06k_B T_c \sqrt{|\tau|} ,$$

the amplitude of the order parameter near T_c is roughly

$$|\psi(\mathbf{r})| = \sqrt{n_e |\tau|} = \sqrt{n_s} . \quad (13.8)$$

If the superconductor is not at equilibrium, as happens when there is an electric current, $\psi(\mathbf{r})$ and $\Delta(\mathbf{r})$ are complex.

13.1 Ginzburg–Landau Free Energy

As in the Landau theory of phase transitions, we assume that the order parameter is small near transition and that its spatial variations are slow enough to justify expanding the free energy density in powers of the order parameter in the vicinity of T_c :

$$\begin{aligned} f_s(\mathbf{r}, T) &= f_{n0}(T) + a|\psi(\mathbf{r})|^2 + \frac{b}{2}|\psi(\mathbf{r})|^4 \\ &\quad + \frac{1}{2m_*} \left| \left(\frac{\hbar}{i} \nabla - e_* \mathbf{A} \right) \psi(\mathbf{r}) \right|^2 + \mu_0 \frac{h^2(\mathbf{r})}{2} , \end{aligned} \quad (13.9)$$

where $f_{n0}(T) = f_{n0}(0) - \gamma T^2/2$ is the free energy of the normally conducting metal in zero field, and $\mathbf{h}(\mathbf{r})$ the local magnetic field. As in other second order phase transitions, $a = \alpha\tau$ ($\tau = T/T_c - 1$) changes sign at T_c . At thermodynamic equilibrium (no gradient) and in zero field ($h = 0$), the minimum of f_s with respect to $|\psi|^2$ is given by (see Fig. 13.1)

$$|\psi|^2 = -\frac{a}{b} = \frac{\alpha|\tau|}{b} \quad (T < T_c) , \quad (13.10)$$

and $\psi = 0$ when $T > T_c$. Using relation (13.8) between order parameter and pair density n_s near T_c , we deduce that n_s (and hence $1/\lambda^2$) is linear in τ

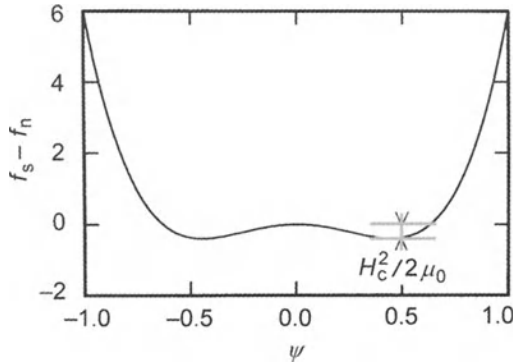


Fig. 13.1. The minimum of the free energy determines the ‘intensity’ $|\psi|^2$ of the order parameter, which is nothing other than the density n_s of Cooper pairs. The minimum value of the free energy determines the critical field

near T_c . This is consistent with the London theory. Below T_c , the critical field H_c is defined by the free energy difference $f_n(T) - f_s(T)$ [see (12.35)],

$$f_n(T) - f_s(T) = \mu_0 \frac{H_c^2(T)}{2} = \frac{(\alpha\tau)^2}{2b}. \quad (13.11)$$

This reproduces the temperature dependence of the critical field near T_c . Other terms included in the free energy density (13.9) are easily interpreted by separating the amplitude and phase of the order parameter, $\psi(\mathbf{r}) = |\psi(\mathbf{r})| \exp[i\phi(\mathbf{r})]$. They become

$$\frac{1}{2m_*} \left\{ \hbar^2 [\nabla |\psi(\mathbf{r})|]^2 + [\hbar \nabla \phi(\mathbf{r}) - e_* \mathbf{A}(\mathbf{r})]^2 |\psi(\mathbf{r})|^2 \right\} + \mu_0 \frac{\hbar^2(\mathbf{r})}{2}. \quad (13.12)$$

The first term is the additional energy induced by a gradient of the amplitude of the order parameter. This term is only relevant at T_c because, as soon as a becomes large enough, the first two terms of the free energy in (13.9) determine a deep minimum for $|\psi|$ which leaves little room for amplitude fluctuations. The second term gives the kinetic energy of a superconducting current in a gauge independent way. Indeed, the gauge transformation $A(\mathbf{r})$ induces translations of vector potential $\mathbf{A}' = \mathbf{A} + \nabla A$ and phase $\phi'(\mathbf{r}) = \phi(\mathbf{r}) + e_* A(\mathbf{r})/\hbar$ which leave $\hbar \nabla \phi - e_* \mathbf{A}$ invariant [see Chap. 2(I)]. In particular, the London gauge $\nabla \cdot \mathbf{A} = 0$ is chosen so as to maintain a stationary electron density and this implies that $\nabla \cdot \mathbf{J}_s = 0$. This condition is equivalent to $\nabla^2 \phi(\mathbf{r}) = 0$.

We now seek to relate parameters a and b to physical parameters H_c and λ_L introduced in the London theory. To this end, we shall neglect spatial variations of the order parameter. Kinetic energy of Cooper pairs then contributes

$$\varepsilon(\mathbf{r}) = \frac{e_*^2 A^2(\mathbf{r}) |\psi(\mathbf{r})|^2}{2m_*} \quad (13.13)$$

to the free energy density. This quantity can be compared with the electromagnetic contribution of the superconducting current to the free energy in the London theory,

$$\begin{aligned}\mathcal{E} &= \int d^3r dt \mathbf{J}_s(\mathbf{r}, t) \cdot \mathbf{E}(\mathbf{r}, t) = \int d^3r dt \frac{\mathbf{A}(\mathbf{r}, t)}{\mu_0 \lambda_L^2} \cdot \frac{\partial \mathbf{A}(\mathbf{r}, t)}{\partial t} \\ &= \frac{1}{2\mu_0 \lambda_L^2} \int d^3r A^2(\mathbf{r}) = \frac{\mu_0 \lambda_L^2}{2} \int d^3r J_s^2(\mathbf{r}).\end{aligned}\quad (13.14)$$

We can now relate the amplitude $|\psi|^2$ of the order parameter to the London penetration depth by identifying (13.13) with (13.14):

$$|\psi|^2 = \frac{m_*}{\mu_0 \lambda_L^2 e_*^2} = n_s^*. \quad (13.15)$$

Denoting the average velocity of Cooper pairs by \mathbf{v}_s , we see that the electromagnetic energy (13.14) of the supercurrent $\mathbf{J}_s = n_s^* e_* \mathbf{v}_s$ is just the kinetic energy $n_s^* m_* v_s^2 / 2$ of the Cooper pairs, and hence

$$m_* \mathbf{v}_s = \mathbf{p}_s - e_* \mathbf{A} = \hbar \nabla \phi - e_* \mathbf{A}. \quad (13.16)$$

This discussion shows quite clearly that the Ginzburg–Landau theory, like the London theory, is limited to local electrodynamics. This restricts it to the regime $\lambda(T) \gg \xi(0)$, which is naturally satisfied near T_c . Parameters $a = \alpha\tau$ and b in the free energy (13.9) can be related to physical parameters H_c and λ_L , which can be found by experiment. From (13.10), (13.11) and (13.15),

$$a(T) = -\frac{\mu_0 H_c^2}{n_s} = -\frac{(\lambda_L \mu_0 H_c e_*)^2}{m_*}, \quad (13.17)$$

$$b(T) = \frac{\mu_0 H_c^2}{n_s^2} = \mu_0 \left(\frac{e_*^2 \lambda_L^2 \mu_0 H_c}{m_*} \right)^2. \quad (13.18)$$

It is easy to check that $a(T) \rightarrow \alpha(T)|\tau|$ with $\alpha(T) = b(T)n_e$, and that $b(T) \rightarrow \text{const.}$ when $T \rightarrow T_c$, as in the Landau theory of phase transitions. In the next section, we will introduce the Ginzburg–Landau coherence length $\xi_{GL} = \hbar / \sqrt{2m_*|a|}$. Like the London penetration depth, this can be measured experimentally. It is therefore natural to express the critical field H_c in terms of λ_L and ξ_{GL} , using (13.17):

$$H_c = \frac{\Phi_0}{\mu_0} \frac{1}{2\pi\sqrt{2}\lambda_L(T)\xi_{GL}(T)}. \quad (13.19)$$

The above discussion implies that we can completely identify the London and Ginzburg–Landau theories when there are no spatial fluctuations in the order parameter. We can also compare with the microscopic BCS theory [see Chap. 14(II)] in the vicinity of T_c . This allows us to relate parameters α and b to microscopic parameters. To do so, we need to know the behaviour of the critical field near T_c according to the BCS theory:

$$H_c = 3.06k_B T_c \tau \sqrt{\frac{n(\varepsilon_F)}{2\mu_0}}.$$

Explicitly, we find

$$\alpha = 28.09 \frac{(k_B T_c)^2}{\mu_0 \varepsilon_F}, \quad (13.20)$$

$$b = \frac{\alpha}{n_e} = 3.35 \frac{\lambda_F^3 (k_B T_c)^2}{\mu_0 \varepsilon_F}, \quad (13.21)$$

where we have used the fact that, for an isotropic Fermi liquid, the density of states at the Fermi level is $n(\varepsilon_F) = 3n_e/2\varepsilon_F$ and the electron density is $n_e = 8\pi/3\lambda_F^3$.

The Ginzburg–Landau theory is not only applicable to clean superconductors. It can also be used when there are high concentrations of impurities, such as in alloys. In this case, parameters α and b are expressed in terms of the (elastic) mean free path between impurities, $l_e = v_F \tau_e$. This can be deduced by measuring conductivity σ_{xx} in the normal state and using Drude's formula $\sigma_{xx} = n_e e^2 l_e / p_F$. Here, n_e can be determined by measuring the Hall conductivity $\sigma_{xy} = n_e e / H$, and p_F can be found by measuring the Sommerfeld constant in the relation $C = \gamma T$ for the specific heat and using the fact that $\gamma = mp_F/3\hbar^3$ for a spherical Fermi surface. The correspondence between α, b and the microscopic parameters is then

$$\alpha = 0.303 \frac{\lambda_F}{l_e} k_B T_c, \quad (13.22)$$

$$\frac{\alpha}{b} = 1.331 \frac{l_e}{\xi_0} n_e = 1.331 \left(\frac{l_e^2}{3\xi^2} \right)^{1/2} n_e, \quad (13.23)$$

where $\xi_0 = \hbar v_F / 1.76\pi k_B T_c$. The effective coherence length of a dirty superconductor $\xi \approx (l_e \xi_0 / 3)^{1/2}$ is determined by the diffusive motion of electrons over a distance ξ . The amplitude of the order parameter ψ in the dirty limit $|\psi|^2 = \alpha \tau / b$ is reduced by disorder. It can be related to the gap parameter Δ . We use (13.23) and the relation $\Delta \approx 3.06k_B T_c \sqrt{\tau}$ near T_c given by BCS theory:

$$\psi_{\text{dirty}}(\mathbf{r}) = \left(\frac{\pi n_e \tau}{4\hbar k_B T_c} \right)^{1/2} \Delta(\mathbf{r}). \quad (13.24)$$

Comparing with (13.8), we find that $\psi_{\text{dirty}} \approx 3.2\psi_{\text{clean}} \sqrt{\tau_e k_B T_c / \hbar}$. Finally, if there are magnetic impurities, the order parameter decreases rapidly. Superconductivity persists in a small gapless region before disappearing [see Chap. 17(II)] [400, 401]. Such behaviour also occurs in highly disordered states $l_e \approx \lambda_F$. The Ginzburg–Landau theory must then be adapted since spatial fluctuations $\sqrt{\langle (n_s - \langle n_s \rangle)^2 \rangle}$ in n_s are much greater than $\langle n_s \rangle$ and dominate the free energy.

13.2 The Ginzburg–Landau Equations

To obtain the hydrodynamic behaviour of an inhomogeneous order parameter, we minimise the total free energy $F_s = \int d^3r f_s$ with respect to arbitrary variations $\delta\psi(\mathbf{r})$ of the order parameter. The simplest approach is to minimise F_s by treating $\psi(\mathbf{r})$ and $\psi^*(\mathbf{r})$ as independent variational parameters. The functional derivative of F_s with respect to $\psi^*(\mathbf{r})$ is then

$$\begin{aligned}\delta F_s &= \int d^3r \left[(a + b|\psi|^2)\psi + \frac{1}{2m_*}(-i\hbar\nabla - e_*\mathbf{A})\psi(i\hbar\nabla - e_*\mathbf{A}) \right] \delta\psi^* \\ &= 0.\end{aligned}\quad (13.25)$$

After integrating by parts, the last term becomes

$$\begin{aligned}\frac{i\hbar}{2m_*} \int d^2r \delta\psi^* \mathbf{n} \cdot (-i\hbar\nabla - e_*\mathbf{A})\psi \\ + \frac{1}{2m_*} \int d^3r \delta\psi^* (-i\hbar\nabla - e_*\mathbf{A})^2\psi.\end{aligned}\quad (13.26)$$

Choosing a variation $\delta\psi^*(\mathbf{r})$ which is zero on the superconductor surface, the surface term is clearly zero. In order to make the volume term zero for arbitrary variations in $\psi^*(\mathbf{r})$, we find that $\psi(\mathbf{r})$ must satisfy the first Ginzburg–Landau equation:

$$a\psi(\mathbf{r}) + b|\psi(\mathbf{r})|^2\psi(\mathbf{r}) + \frac{1}{2m_*}(-i\hbar\nabla - e_*\mathbf{A})^2\psi(\mathbf{r}) = 0.\quad (13.27)$$

This looks like the Schrödinger equation for a particle of mass m_* , charge e_* and energy $-a$ in a potential $b|\psi(\mathbf{r})|^2$. The analogy should not be taken literally. The dynamics of an order parameter in the presence of a time dependent field does not reduce to the dynamics of a particle. Finally, the free energy F must be minimised with respect to the vector potential. (We are merely generalising the deduction of Maxwell's equations from the Euler–Lagrange equations of the electromagnetic Lagrangian.) We obtain the two relations

$$\mathbf{J}(\mathbf{r}) = \frac{1}{\mu_0} \nabla \times [\nabla \times \mathbf{A}(\mathbf{r})] = \nabla \times \mathbf{H}(\mathbf{r}),\quad (13.28)$$

$$\begin{aligned}\mathbf{J} &= -i\frac{e_*\hbar}{2m_*}(\psi^*\nabla\psi - \psi\nabla\psi^*) - \frac{e_*^2}{m_*}|\psi|^2\mathbf{A} \\ &= \frac{e_*}{m_*}|\psi(\mathbf{r})|^2[\hbar\nabla\phi(\mathbf{r}) - e_*\mathbf{A}(\mathbf{r})] = e_*|\psi(\mathbf{r})|^2\mathbf{v}_s(\mathbf{r}).\end{aligned}\quad (13.29)$$

The first relation is one of Maxwell's equations and the second completes the Ginzburg–Landau equations by defining the current. If we neglect amplitude variations of the order parameter, we introduce the electromagnetic phase

$$\chi(\mathbf{r}) = \phi(\mathbf{r}) + \frac{2\pi}{\Phi_0} \int_0^{\mathbf{r}} \mathbf{A} \cdot d\mathbf{s}$$

to obtain the linearised Josephson relation [see Chap. 16(II)] from the second Ginzburg–Landau equation:

$$\mathbf{J}_s(\mathbf{r}) = \frac{\Phi_0}{2\pi\mu_0\lambda_L^2} \nabla\chi(\mathbf{r}) . \quad (13.30)$$

Finally, we must specify boundary conditions for the order parameter ψ . When Cooper pairs are reflected specularly from the interface with an insulating medium, de Gennes has shown on the basis of the BCS theory that ψ must satisfy the condition

$$(-i\hbar\nabla - e_*\mathbf{A})\psi(\mathbf{r}) \cdot \hat{\mathbf{n}} = 0 . \quad (13.31)$$

However, at the interface with a metal, the order parameter is only partially reflected [Andreev reflection, see Chap. 17(II)]. This is due to a change of wave vector between the two metals. In this case,

$$(-i\hbar\nabla - e_*\mathbf{A})\psi(\mathbf{r}) \cdot \hat{\mathbf{n}} = \frac{i\hbar}{\delta}\psi(\mathbf{r}) , \quad (13.32)$$

where the de Gennes length δ measures the distance over which the order parameter is attenuated in the normal metal [391]. If we neglect kinetic energy of Cooper pairs in the Ginzburg–Landau equation (13.27), the order parameter is uniform and given by its thermodynamic value $|\psi_0|^2 = n_s$. The second Ginzburg–Landau equation then becomes the London equation. Consequently, the London theory amounts to neglecting spatial variations in the order parameter.

Deviations of the order parameter from its equilibrium value $|\psi_0|^2 = |a|/b = n_s$ are generally small, and the reduced amplitude

$$f(\mathbf{r}) = \frac{\psi(\mathbf{r})}{\psi_0} = \frac{\psi(\mathbf{r})}{\sqrt{n_s}} \quad (13.33)$$

remains close to 1. The Ginzburg–Landau coherence length ξ_{GL} and electromagnetic wave vector \mathbf{k}_A are defined by

$$\xi_{GL}(T) = \frac{\hbar}{\sqrt{2m_*a(T)}} , \quad (13.34)$$

$$\mathbf{k}_A(\mathbf{r}) = \frac{2\pi\mathbf{A}(\mathbf{r})}{\Phi_0} , \quad (13.35)$$

where $\Phi_0 = h/|e_*| = h/2|e| = \phi_0/2$ is the flux quantum of a Cooper pair. The first equation can, of course, be inverted to give the parameter $a = \hbar^2/2m_*\xi_{GL}^2$ as a function of the coherence length (see Sect. 13.1). This parameter is related to the critical field and to the London penetration depth by (13.17). The thermodynamic critical field is attained when the magnetic flux through an area $\lambda_L(T)\xi_{GL}(T)$ is of the same order as the flux quantum (13.19). This is valid in either the dirty or the clean limit. According to definition (13.34), the Ginzburg–Landau coherence length diverges at the transition temperature. It is not therefore the same as the Pippard length ξ_0 , although it can be related to it in the clean and dirty limits by

$$\xi_{\text{GL}}(T) \approx 0.74 \frac{\xi_0}{\sqrt{|\tau|}} \quad (\text{clean}) , \quad (13.36)$$

$$\xi_{\text{GL}}(T) \approx 0.855 \sqrt{\frac{\xi_0 l_e}{|\tau|}} \quad (\text{dirty}) . \quad (13.37)$$

Using definitions (13.34) and (13.35), we can rewrite the Ginzburg–Landau equations (13.27) and (13.29) in reduced form:

$$\xi^2(T)[\nabla + i\mathbf{k}_A(\mathbf{r})]^2 f(\mathbf{r}) + f(\mathbf{r}) - |f(\mathbf{r})|^2 f(\mathbf{r}) = 0 , \quad (13.38)$$

$$\lambda_L^2 \nabla \times (\nabla \times \mathbf{k}_A) = \frac{i}{2} (f^* \nabla f - f \nabla f^*) - |f|^2 \mathbf{k}_A , \quad (13.39)$$

$$\hat{\mathbf{n}} \cdot [\nabla + i\mathbf{k}_A(\mathbf{r})] \psi(\mathbf{r}) = 0 . \quad (13.40)$$

As before, $\lambda_L(T)$ is the London penetration depth. In the dirty limit, we substitute the appropriate Ginzburg–Landau coherence length (13.37) and the effective penetration depth,

$$\lambda_{\text{eff}}(T) = \lambda_L(T) \left(\frac{\xi_0}{1.33l_e} \right)^{1/2} , \quad (13.41)$$

into the previous expressions. These were obtained by means of the correspondence between parameters a and b and the microscopic parameters ξ_0 and l given in (13.23).

We shall now show that $\xi(T)$ and $\lambda(T)$ determine the distances over which the order parameter and electromagnetic field vary, respectively. Neglecting the electromagnetic field, we linearise the first Ginzburg–Landau equation (13.38) by putting $f(x) = 1+g(x)$. Deviations g satisfy the linearised equation

$$\xi^2(T) \frac{d^2g}{dx^2} + [1 + g(x)] - [1 + 3g(x)] = 0 . \quad (13.42)$$

Solutions are exponentials $g = g_0 \exp[-\sqrt{2}x/\xi(T)]$, dying out over a distance $\xi(T)/\sqrt{2}$. If we neglect spatial variations of ψ , which is justified when transverse dimensions of the system are small compared with $\xi(T)$ (so that any gradient of the order parameter would make a prohibitive contribution to the free energy), the second Ginzburg–Landau equation (13.39) becomes

$$\nabla \times (\nabla \times \mathbf{A})(\mathbf{r}) = \nabla(\nabla \cdot \mathbf{A}) - \nabla^2 \mathbf{A} = -\mathbf{A}(\mathbf{r})/\lambda_L^2(T) . \quad (13.43)$$

We have the London equation once again. In the London gauge $\nabla \cdot \mathbf{A} = 0$, solutions of this equation are exponentials dying out over distance λ_L .

Exercise: Entropy of Superconductors

1. Show that in the Ginzburg–Landau theory, the Gibbs free energy in a fixed field H is given above and below T_c by

$$G_n(H, T) = V[f_n(T) - \mu_0 H^2/2], \quad (13.44)$$

$$G_s(H, T) = V \left[f_n(T) - \frac{|a|^2}{2b} + \frac{\mu_0}{2}(h^2 - 2hH) \right], \quad (13.45)$$

where $b = \mu_0 h$ is the average induction through the superconductor (non-zero for a type II superconductor) and $f_n(T)$ is the free energy per unit volume in zero field in the normal state.

2. Deduce the value of the thermodynamic critical field for a type I superconductor ($h = 0$), defined by the condition $G_s = G_n$.
3. Using the definition $S = -(\partial G / \partial T)_H$ of the entropy, show that entropies per unit volume in normal and superconducting states are given by

$$s_n = -\frac{\partial f_n}{\partial T}, \quad (13.46)$$

$$s_s = s_n + \frac{|a|}{b} \frac{\partial |a|}{\partial T}, \quad (13.47)$$

and show that s_s is less than s_n .

4. Show that s_s can also be expressed in the form

$$s_s = s_n + \mu_0 H_c \frac{\partial H_c}{\partial T}. \quad (13.48)$$

5. Using the temperature dependence of the critical field $H_c = H(0)(1-t^2)$, where $t = T/T_c$, plot $\Delta s = s_n - s_s$ as a function of temperature. Check that the system obeys Nernst's law by showing that $\Delta s \rightarrow 0$ when $T \rightarrow 0$.
6. A sample of tin is adiabatically heated from superconducting to normal state at temperature $T = 0.9T_c$. What is the decrease in temperature? Use the following information about tin: $T_c = 3.7$ K, $\mu_0 H(0) = 3 \times 10^{-2}$ T, and the specific heat at $t = 0.9$ is $c = 364 \text{ J m}^{-3} \text{ K}^{-1}$.

Exercise: Proximity Effect

Consider an interface between a normal metal, occupying half-space $x < 0$, and a superconductor, occupying half-space $x > 0$. Define a normalised order parameter $f = \psi(x)/\psi_{\text{eq}}$, where $\psi_{\text{eq}} = \sqrt{a/b}$. Boundary conditions for f are therefore

$$f \rightarrow 0, \quad \frac{df}{dx} \rightarrow 0 \quad \text{when } x \rightarrow -\infty, \quad (13.49)$$

$$f \rightarrow 1, \quad \frac{df}{dx} \rightarrow 0 \quad \text{when } x \rightarrow +\infty, \quad (13.50)$$

$$\left. \frac{df}{dx} \right|_0 = \frac{1}{\delta} f(0), \quad (13.51)$$

where δ is the de Gennes length.

1. Show that in zero field, the Ginzburg–Landau equations have a first integral compatible with the above boundary conditions, given by

$$\xi^2 \left(\frac{df}{dx} \right)^2 + f^2(x) - \frac{1}{2} f^4(x) = \frac{1}{2}, \quad (13.52)$$

where ξ is the Ginzburg–Landau coherence length.

2. Check that

$$f(x) = \tanh \left(\frac{x - x_0}{\sqrt{2}\xi} \right) \quad (13.53)$$

is a solution of this equation and express x_0 as a function of δ and ξ .

3. How does x_0 behave as $T \rightarrow T_c$? What can you conclude about the effects of proximity as T approaches T_c ?
4. What is the Ginzburg–Landau free energy per unit area $F(x)$ for the zone between 0 and x ? Define the interfacial free energy Γ from $F(x \rightarrow \infty)$ and the thermodynamic critical field H_c .
5. Define the penetration depth λ by

$$\Gamma = \mu_0 \frac{H_c^2}{2} \lambda. \quad (13.54)$$

What is its value as a function of ξ when the de Gennes length δ is negligible?

6. Repeat the same exercise for the interface between two superconductors with different critical temperatures. Describe behaviour when $T < \min(T_{c1}, T_{c2})$ and $T_{c2} < T < T_{c1}$. Compare the results with the Josephson effect.

13.3 Flux Quantisation

Consider a long tube of inner radius r_1 and outer radius r_2 (such that $\lambda \ll r_2 - r_1$), placed in a magnetic field $H_{\text{ext}} < H_c$. Let us suppose that the field varies in time. Integrating the first London equation around a circle lying completely within the cylinder, we obtain

$$\frac{\partial}{\partial t} \oint \Lambda \mathbf{J} dl = \oint \mathbf{E} dl = \int dS \nabla \times \mathbf{E} = -\frac{\partial}{\partial t} \int dS B. \quad (13.55)$$

Hence,

$$\oint \Lambda \mathbf{J} dl + \int dS B = \text{const.}$$

As the current only flows in a layer of thickness λ_L at the surface of the superconductor, we can conclude that

$$\Phi = \int B dS = \text{const.} \quad (13.56)$$

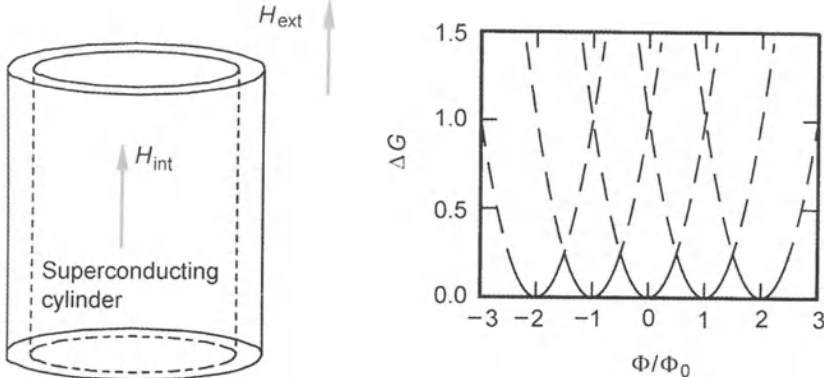


Fig. 13.2. *Left:* Superconducting cylinder of inner radius r_1 and outer radius r_2 in an external field of value H_{ext} far from the cylinder. We define $\Phi_{\text{ext}} = \pi r_1^2 \mu_0 H_{\text{ext}}$. *Right:* Various curves of the Gibbs free energy as a function of Φ_{ext} , for whole number values of trapped flux $\Phi_{\text{int}}/\Phi_0 = n$. The lower envelope of the curves corresponds to thermodynamic equilibrium. Transition from one curve to another can only occur if screening currents at the cylinder surface exceed the critical current

In other words, the superconducting cylinder screens fluctuations in the magnetic field. Ginzburg–Landau theory implies that this constant is a multiple of the flux quantum Φ_0 . The second Ginzburg–Landau equation (13.29),

$$\frac{m_*}{e_* \hbar} \frac{\mathbf{J}}{|\psi|^2} = \nabla \phi + \mathbf{k}_A , \quad (13.57)$$

can be integrated around the same path. Since the current is zero inside the superconductor, we find

$$0 = \oint \nabla \phi \cdot d\mathbf{l} + \oint \mathbf{k}_A \cdot d\mathbf{l} = 2n\pi + 2\pi \frac{\Phi}{\Phi_0} , \quad (13.58)$$

because periodic boundary conditions around the cylinder require the phase to be a multiple of 2π . This flux quantisation into integral multiples of the flux quantum Φ_0 ,

$$\Phi_0 = h/2e = 2.067857 \times 10^{-7} \text{ Oe cm}^2 , \quad (13.59)$$

was observed by Deaver and Fairbanks [392]. Through the Josephson effect [see Chap. 16(II)], flux can be measured to an accuracy of 10^{-6} to $10^{-8}\Phi_0$. Using a sensor of area 0.5 to 1 cm², we can detect fields smaller than 10^{-12} Oe $\equiv 10^{-16}$ T. These are typical values for the magnetic fields produced by synaptic currents in the human brain, and such techniques can be used in experimental study of human biomagnetism [393].

It is sometimes claimed that flux quantisation is just Bohr–Sommerfeld quantisation. However, the latter merely imposes a relation between the flux and the wave vector of the Cooper pairs, whereas in the present case, we also require the momentum expectation value $\langle \mathbf{p} \rangle$ to be zero in the ground

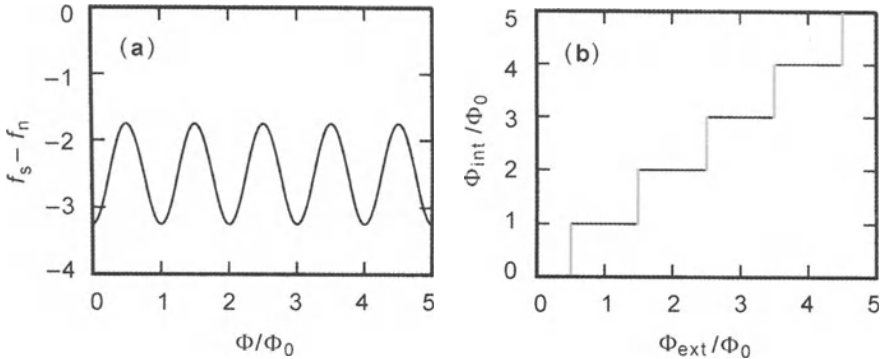


Fig. 13.3. *Left:* Variation of the free energy of pair condensation in a superconducting ring, associated with vector potential-induced torsion in the phase of the order parameter. If $f_s - f_n$ oscillates with an amplitude which is large compared with $k_B T$, the system will spontaneously select one of the minima. *Right:* For a sufficiently large applied external field, the energy of diamagnetic currents can cause the system to jump from one minimum to another. The result is a series of flux jumps of amplitude Φ_0 as the applied flux increases, observed by Deaver and Fairbank in 1961

state. Figure 13.3 shows the variation of the free energy, which has minima for integral values of Φ/Φ_0 . Flux is quantised as soon as the temperature is low enough to block the thermodynamic state in one of these minima. To understand how we may pass from one minimum to another by varying the applied flux, we must study the dependence of the free energy minimum on the external field.

We can use the Ginzburg–Landau equations to express the minimum value of the free energy. We start with expansion (13.9) of the free energy:

$$F_s = F_n + \frac{\mu_0 H^2}{2} + \int d^3r \mu_0 H_c^2 \left[-|f(\mathbf{r})|^2 + \frac{|f(\mathbf{r})|^4}{2} + \xi^2 |(\nabla + i\mathbf{k}_A)f(\mathbf{r})|^2 \right], \quad (13.60)$$

where we have replaced a and b by their expressions in terms of the critical field resulting from $-a|\psi_0|^2 = b|\psi_0|^4 = \mu_0 H_c^2$ [see (13.17) and (13.18)]. The first step is to integrate the kinetic term $|(\nabla + i\mathbf{k}_A)f(\mathbf{r})|^2$ by parts:

$$\begin{aligned} & \int [(\nabla + i\mathbf{k}_A)f(\mathbf{r})] \cdot [(\nabla - i\mathbf{k}_A)f^*(\mathbf{r})] d^3r \\ &= - \int d^3r f^*(\mathbf{r}) [(\nabla + i\mathbf{k}_A)^2 f(\mathbf{r})] + \text{surface terms}. \end{aligned} \quad (13.61)$$

With boundary conditions (13.31), surface terms do not contribute. We can then use the Ginzburg–Landau equation (13.27), whose solution corresponds to the minimum of the free energy, to express the kinetic term in terms of condensation energies

$$\xi^2 \int d^3r |(\nabla + ik_A)f(r)|^2 = \int d^3r (|f|^2 - |f|^4) .$$

Substituting into the free energy (13.60), we thus obtain its minimum value as defined by the Ginzburg–Landau equations:

$$F_s(H) = F_n + \frac{\mu_0}{2} \int d^3r [H^2(r) - |f(r)|^4 H_c^2] . \quad (13.62)$$

As mentioned in the previous chapter, we must consider the Gibbs free energy if we wish to study the transition from superconducting to normal state in non-zero field. For cylindrical geometry in external field H_{ext} , the magnetic induction is inhomogeneous in the superconducting state. In this case,

$$G_s(H) = F_s(H) - \mathbf{H}_{\text{ext}} \cdot \int \mathbf{B}(r) d^3r ,$$

$$G_n(H) = F_n - V\mu_0 H_{\text{ext}}^2/2 . \quad (13.63)$$

Hence, the difference between Gibbs free energies in superconducting and normal states is

$$G_s(H_{\text{ext}}) - G_n(H_{\text{ext}}) = \frac{\mu_0}{2} \int d^3r [(H(r) - H_{\text{ext}})^2 - H_c^2 |f(r)|^4] . \quad (13.64)$$

When $H_{\text{ext}} = H_c$, equality of the Gibbs free energies does not imply $f = 0$ ($\psi = 0$). The transition is first order, since the order parameter grows from a finite value below $T_c(H)$. The expression shows clearly that the critical field is determined by equilibrium between the positive diamagnetic energy (first term) and the negative energy of Cooper pair condensation (second term).

Expression (13.64) can be applied to the superconducting tube. Trapped flux $\Phi_{\text{int}} = n\Phi_0$ reduces the Gibbs free energy,

$$G_s(H_{\text{ext}}) - G_n(H_{\text{ext}}) = \frac{\mu_0}{2\pi r_1^2} (\Phi_{\text{int}} - \Phi_{\text{ext}})^2$$

$$+ \mu_0 \int_{r_1}^{r_2} \pi \rho d\rho [(H(r) - H_{\text{ext}})^2 - H_c^2 |f(r)|^4] , \quad (13.65)$$

where $\Phi_{\text{ext}} = \mu_0 H_0 / \pi r_1^2$. When $r_2 - r_1 \ll r_1$, the second term is small and thermodynamic equilibrium corresponds to the minimum of the first term with the added quantisation condition $\Phi_{\text{int}} = n\Phi_0$. The Gibbs free energy difference $G_s(H_{\text{ext}}) - G_n(H_{\text{ext}})$ is a set of parabolas (see Fig. 13.2) which intersect at $(n \pm 1/2)\Phi_0$. The difference $G_s(H_{\text{ext}}) - G_n(H_{\text{ext}})$ is minimal when n satisfies

$$(n - 1/2)\Phi_0 \leq \Phi_{\text{ext}} \leq (n + 1/2)\Phi_0 , \quad \Phi_{\text{int}} = n\Phi_0 . \quad (13.66)$$

If Φ_{ext} exceeds $(n + 1/2)\Phi_0$, thermodynamic equilibrium requires n to increase by one unit, as can be seen from Figs. 13.2 and 13.3. In practice, the system can only reach the minimum imposed by thermodynamics near the critical temperature. At lower temperatures, the flux inside remains quantised at $n\Phi_0$ as long as screening currents do not exceed the critical current

of the superconductor [see Sects. 12.8 and 16.6(II)]. The system remains in a metastable state (see Fig. 13.2). In conclusion, flux quantisation is due to:

- a thermodynamic state such that $\langle \mathbf{p} \rangle = 0$;
- the $2n\pi$ variation in the phase of the order parameter.

The behaviour of the phase was demonstrated in an ingenious experiment due to Little and Parks.

13.4 The Little–Parks Effect

When the cylinder thickness is small compared with the penetration depth, screening of the field is negligible and the order parameter has constant amplitude. There is no longer any real quantisation of flux, since screening currents are insufficient to impose a $\mathbf{j} = 0$ state within the superconductor. The system nevertheless remains sensitive to the enclosed magnetic flux which modulates its critical temperature. Since the cylinder thickness is small, the amplitude of the order parameter is constant and only its phase varies. Moreover, the vector potential $\mathbf{A} = \Phi_0 \mathbf{k}_A / 2\pi$ and the phase gradient $\nabla\phi$ are constant and can be expressed in terms of the magnetic flux Φ ,

$$\nabla\phi + \mathbf{k}_A = \frac{1}{2\pi r} \oint (\nabla\phi + \mathbf{k}_A) dl = \frac{1}{r} \left(n + \frac{\Phi}{\Phi_0} \right). \quad (13.67)$$

The Ginzburg–Landau free energy is then equal to

$$F_s - F_n = \alpha\tau|\psi|^2 + \frac{b}{2}|\psi|^4 + \frac{\hbar^2|\psi|^2}{2m_*r^2} \left(n + \frac{\Phi}{\Phi_0} \right)^2 + \mu_0 \frac{H^2}{2}. \quad (13.68)$$

The superconductor reaches its critical temperature when the coefficient of $|\psi|^2$ is zero [see Chap. 4(I)], that is,

$$\tau = \frac{\Delta T_c}{T_c} = -\frac{\hbar^2}{2m_*r^2\alpha} \left(n + \frac{\Phi}{\Phi_0} \right)^2. \quad (13.69)$$

Making use of correspondences between the parameter α and the BCS theory, we find that the decrease in T_c is given by

$$\frac{\Delta T_c}{T_c} = -0.55 \frac{\xi_0^2}{r^2} \left(n + \frac{\Phi}{\Phi_0} \right)^2 \quad (\text{clean}), \quad (13.70)$$

$$\frac{\Delta T_c}{T_c} = -0.72 \frac{\xi_0 l_e}{r^2} \left(n + \frac{\Phi}{\Phi_0} \right)^2 \quad (\text{dirty}). \quad (13.71)$$

As before, the value of n is chosen so as to minimise the decrease in T_c . The latter therefore follows the bottom of the parabolas centred on n , as shown in Fig. 13.4 [394, 395].

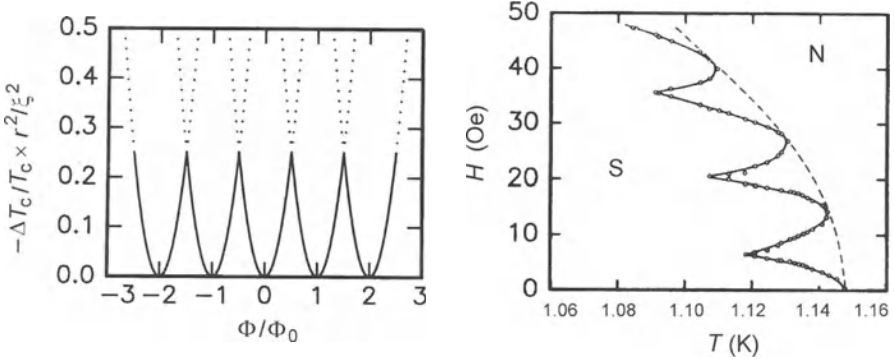


Fig. 13.4. *Left:* Decrease in T_c as a function of the magnetic flux imposed by an external field. *Right:* The experimental curve for an aluminium wire of diameter $1.32 \mu\text{m}$, obtained by Groff and Parks. Its envelope is the variation of H_c with T_c , neglected in our discussion

13.5 Critical Current in a Thin Film

A simple example in which the non-linear Ginzburg–Landau theory can be solved is provided by a thin film, whose thickness is small compared with the London penetration depth. In such conditions, the amplitude of the order parameter is constant, because the energy associated with variation of $|\psi|$ transverse to the film is extremely high. The current and free energy are given by

$$\mathbf{J}_s = e_* |\psi|^2 \mathbf{v}_s = \frac{e_* \hbar}{m_*} |\psi|^2 \left(\nabla \phi + \frac{2\pi \mathbf{A}}{\Phi_0} \right), \quad (13.72)$$

$$f_s - f_n = a |\psi|^2 + \frac{b}{2} |\psi|^4 + |\psi|^2 \frac{1}{2} m_* \mathbf{v}_s^2. \quad (13.73)$$

Because there is a non-zero kinetic energy, the minimum of $f_s - f_n$ is displaced relative to $|\psi|^2$:

$$|\psi|^2 = |\psi_0|^2 \left(1 - \frac{m_* \mathbf{v}_s^2}{2|a|} \right) = |\psi_0|^2 \left[1 - \left(\frac{\xi m_* \mathbf{v}_s}{\hbar} \right)^2 \right]. \quad (13.74)$$

The superconductor current is obtained by substituting this value of the order parameter into the expression for the current to give

$$\mathbf{J}_s = e_* |\psi_0|^2 \left[1 - \left(\frac{\xi m_* \mathbf{v}_s}{\hbar} \right)^2 \right] \mathbf{v}_s. \quad (13.75)$$

The maximum current is reached when $\partial J_s / \partial v_s = 0$, i.e., when $v_c = \hbar / \sqrt{3} \xi m_*$. We identify the maximal current value $J_s(v_c)$ with the critical current of the film,

$$J_c = \frac{2e_*\hbar n_s}{3\sqrt{3}m_*\xi} . \quad (13.76)$$

The condensate then has momentum

$$p_c = m_* v_c = \frac{\hbar}{\sqrt{3}\xi} , \quad (13.77)$$

which can be compared with the momentum in the BCS theory [396]. In the condensate frame (moving at speed v_s), the energy $E_p = \sqrt{\Delta^2 + \xi_p^2}$ of a quasi-particle of momentum $p - p_F = \xi_p/v_F$ is reduced by $\mathbf{p} \cdot \mathbf{v}_s$ [see Chap. 17(II)]. The critical current is reached when Cooper pairs can spontaneously dissociate into quasi-particles, i.e., when $E_p - \mathbf{p} \cdot \mathbf{v}_s < 0$. This implies

$$v_c \approx \frac{\Delta}{p_F} = \frac{2\hbar}{\pi m_* \xi_0} , \quad (13.78)$$

which is fairly close to the critical current obtained in the Ginzburg–Landau approximation. However, the general behaviour is quite different since, beyond v_c , the current falls off gradually in the Ginzburg–Landau theory, reaching zero at $\sqrt{3}v_c$, whereas it goes to zero suddenly at v_c in the BCS theory.

To sum up, in the London theory, which does not take the reduction in the order parameter into account, the critical current is reached when the condensate kinetic energy is of the same order as the magnetic energy of the critical field:

$$\frac{1}{2}n_s m_* v_s^2 = \frac{1}{2}\mu_0 \lambda_L^2 J_c^2 = \mu_0 \frac{H_c^2}{2} . \quad (13.79)$$

Hence, $J_c = H_c/\lambda_L = e_*\hbar/\sqrt{2}m_*\xi$, which is 1.84 times greater than the critical current in the Ginzburg–Landau theory.

13.6 Energy of an Interface Between Normal and Superconducting States

The variation of the order parameter at the interface between a normal and a superconducting region can be estimated using the Ginzburg–Landau theory. Let the interface lie in the (y, z) plane so that ψ (or $f = \psi/\psi_0$) and \mathbf{A} depend only on x . Currents and vector potential are all in the (y, z) plane and $\nabla\phi \cdot \hat{x} = 0$. We therefore choose a gauge such that $\phi = 0$, $\mathbf{A} = A\hat{y}$ and $\mathbf{H} = H\hat{z} = \hat{z}dA/dx$. The Ginzburg–Landau equations are then

$$0 = \xi^2 \frac{d^2 f}{dx^2} + [1 - [\xi k_A(x)]^2] f(x) - f^3(x) , \quad (13.80)$$

$$0 = \lambda_L^2 \frac{d^2 k_A}{dx^2} - f^2(x) k_A(x) . \quad (13.81)$$

These equations have a first integral obtained by multiplying the first equation by df/dx and the second by $\xi^2 dk_A/dx$ and adding them together:

$$\xi^2 \left(\frac{df}{dx} \right)^2 + \lambda_L \xi^2 \left(\frac{dk_A}{dx} \right)^2 + [1 - [\xi k_A(x)]^2] f^2(x) - \frac{f^4(x)}{2} = \frac{1}{2}. \quad (13.82)$$

Boundary conditions ($f \rightarrow 1$, $k_A \rightarrow 0$) on the superconductor side determine the constant of integration to be $1/2$. In general, the above equations can only be integrated numerically, except in the two physically relevant limiting cases. When $\xi \gg \lambda_L$, k_A is small in the region where df/dx varies. In this case, (13.82) simplifies to

$$\left(\xi \frac{df}{dx} \right)^2 = \frac{1}{2} [1 - f^2(x)]. \quad (13.83)$$

Its solution $f = \tanh(x/\xi\sqrt{2})$ behaves reasonably for positive values of x ($f \rightarrow 1$ for $x \rightarrow \infty$), but is meaningless when x is negative ($f < 0$). This poses no real problem since the region $x < 0$ does not contribute to surface energy. To estimate the interfacial free energy, we substitute $H_{\text{ext}} = H_c$ and $H = 0$ in the free energy (13.64) and make the change of variable $u = \tanh(x/\xi\sqrt{2})$ in the integral. The result is

$$\begin{aligned} \Gamma &= \mu_0 \frac{H_c^2}{2} \int_0^\infty [1 - f^4(x)] dx \\ &= \mu_0 \frac{H_c^2}{2} \sqrt{2}\xi \int_0^1 (1 + u^2) du = \mu_0 \frac{H_c^2}{2} \frac{4\sqrt{2}\xi}{3}. \end{aligned} \quad (13.84)$$

In the other limit $\lambda_L \gg \xi$, we can also use the above equations to evaluate the interfacial free energy, with the result:

$$\Gamma = -\frac{8(\sqrt{2}-1)}{3} \mu_0 \frac{H_c^2}{2} \lambda_L. \quad (13.85)$$

This energy is negative, favouring a structure divided into normal and superconducting regions in such a way as to maximise the area. The structure cannot divide itself up infinitely because there is a quantum limit to the size of normally conducting regions, which must contain exactly one quantum of flux Φ_0 . These structures are vortices, to be studied in Chap. 15(II). The change of behaviour from type I to type II happens when $\kappa = \lambda_L/\xi$ is equal to $1/\sqrt{2}$. For this particular value of κ , the interfacial energy is zero. When the external field equals the critical field, the free energy $G_s(H_c) - G_n(H_c) \equiv 0$ if the field is related to the order parameter by the particular solution

$$\mu_0 H(x) = \frac{dA}{dx} = \mu_0 H_c [1 - f^2(x)] = \frac{\Phi_0}{2\pi\xi^2} [1 - f^2(x)]. \quad (13.86)$$

Indeed, the integrand of (13.64) is then identically zero. In order to see that (13.86) is a solution of the Ginzburg–Landau equations for $\lambda = \xi/\sqrt{2}$, we first substitute it into (13.81) to obtain the second differential equation

$$\frac{df}{dx} = 2\pi \frac{f(x)A(x)}{\Phi_0}. \quad (13.87)$$

Then, inserting these two relations (13.86) and (13.87) into the first integral (13.82), we find that it does indeed constitute a particular solution of the Ginzburg–Landau equations.

13.7 Linearised Ginzburg–Landau Equations

The non-linear aspect of the Ginzburg–Landau equations, which expresses the screening mechanism of the order parameter, means that a numerical approach is required to obtain solutions in the most interesting cases. However, for certain highly inhomogeneous solutions, the non-linear term $b|\psi(\mathbf{r})|^4/2$ in the Ginzburg–Landau equations is much smaller than the kinetic term $\hbar^2|\nabla\psi(\mathbf{r})|^2/2m$. The minimum free energy is then found by balancing the kinetic term against the linear term $a|\psi(\mathbf{r})|^2$. The expectation value $\langle|\psi(\mathbf{r})|^2\rangle$ is then much smaller than the equilibrium value of the order parameter $|\psi_0|^2 = -a/b = n_s$. In these circumstances, we may neglect the non-linear term in the Ginzburg–Landau theory. Moreover, screening effects are negligible and the vector potential $A \approx A_{\text{ext}}$ is given by the applied field. This is exactly the situation encountered near the critical field H_{c2} , where superconductivity nucleates in an inhomogeneous way. The order parameter can then be determined from the linearised Ginzburg–Landau equation

$$\xi^2(T)(\nabla + ik_A)^2\psi(\mathbf{r}) = -\psi(\mathbf{r}). \quad (13.88)$$

The Ginzburg–Landau equations decouple and we can use the analogy with the Schrödinger operator to determine the order parameter of the linearised equation. Near H_{c2} , solutions of (13.88) with infinitesimal amplitude are also solutions of the full equations. If there is a sufficiently high concentration of magnetic impurities, superconductivity becomes gapless [see Chap. 17(II)]. In this case, spatial fluctuations of the order parameter dominate the thermodynamic average. Since the stiffness term $|\nabla\psi(\mathbf{r})|^2$ dominates, the linearised Ginzburg–Landau equations become suitable for describing transport over long wavelengths [402].

13.8 Nucleation of Superconductivity at H_{c2}

When $\mathbf{B} = B\hat{\mathbf{z}}$, we can choose the Landau gauge $A_y = Bx$. Then the linearised Ginzburg–Landau equation takes the form

$$\left[\nabla^2 + \frac{4i\pi}{\Phi_0} Bx \frac{\partial}{\partial y} - \left(\frac{2\pi B}{\Phi_0} \right)^2 x^2 \right] \psi(\mathbf{r}) = -\frac{\psi(\mathbf{r})}{\xi^2(T)}, \quad (13.89)$$

identical to the Schrödinger equation for an electron in a magnetic field. As for the Landau levels [see Chap. 2(I)], we seek solutions of the form

$$\psi(\mathbf{r}) = f(x) \exp -i(k_y y + k_z z). \quad (13.90)$$

We define reduced coordinates $X_0 = k_y l_B$ and $X = x/l_B$, where $l_B = [\Phi_0/2\pi B]^{1/2}$ is the magnetic length of a Cooper pair. In reduced form, (13.88) is just the equation for a harmonic oscillator:

$$\frac{d^2 f}{dX^2} - (X - X_0)^2 f(X) = -l_B^2 \left(\frac{1}{\xi^2} - k_z^2 \right) f(X). \quad (13.91)$$

Comparing this with the equation (2.36) for Landau levels, we identify $2\varepsilon_n$ with $l_B^2(1/\xi^2 - k_z^2)$, where ε_n is the energy of the Landau level in reduced units [see Sect. 2.3(I)],

$$\varepsilon_n = n + \frac{1}{2} = \frac{l_B^2}{2} \left(\frac{1}{\xi^2} - k_z^2 \right). \quad (13.92)$$

As in the case of the Landau levels, the flux enclosed in a state $\psi_n(\mathbf{r})$ (which we define as the average of $\pi\langle r^2 \rangle B = B \int d^2r |\psi(\mathbf{r})|^2 r^2$) is quantised in units of the flux quantum Φ_0 . This flux quantisation allows us to identify local solutions $\psi(\mathbf{r})$ for the order parameter with vortices, quantum entities to be studied in Chap. 15(II). In the Ginzburg–Landau equation (13.91), $\varepsilon_n = n + 1/2$ does not strictly speaking determine an energy (a free energy cannot be quantised!). However, the quantisation condition defines specific values of the magnetic field:

$$H_n = \frac{B}{\mu_0} = \frac{\Phi_0}{2\pi\mu_0(2n+1)} \left(\frac{1}{\xi^2} - k_z^2 \right). \quad (13.93)$$

The largest possible value for H_n is reached when $n = 0$ and $k_z = 0$. This is the strongest magnetic field permitting an inhomogeneous superconducting solution. It must therefore be the nucleation field H_{c2} , given by

$$H_{c2} = \frac{\Phi_0}{2\pi\mu_0\xi^2} = \sqrt{2}\kappa H_c. \quad (13.94)$$

The critical field H_{c2} coincides with the magnetic field for which the magnetic length $l_B = [\Phi_0/2\pi B]^{1/2}$ measuring the spatial extent of solutions of the Ginzburg–Landau equation is of the same order as the coherence length characterising the size of Cooper pairs. In other words, Cooper pairs cannot be compressed by a magnetic field without breaking them. In type I superconductors, $\kappa < 1/\sqrt{2}$, $H_{c2} < H_c$, whereas in type II superconductors, $H_{c2} > H_c$. Below H_{c2} , the order parameter is locally non-zero. Therefore, in a type I superconductor, an inhomogeneous solution $\psi(\mathbf{r})$ (corresponding to a local nucleation of the order parameter) is only possible below H_{c2} . There can be no nucleation of superconductivity between H_c and H_{c2} . In other words, if we gradually reduce the applied field around a type I superconductor, the system will remain in the normal state in $H_{c2} \leq H \leq H_c$. This is a supercooled state. Even though the superconducting state has lower free energy than the normal state, there can only be local nucleation of the superconducting phase below H_{c2} . At H_{c2} , the order parameter jumps discontinuously: the transition is first order. Magnetisation curves plotted in Fig. 12.3 reveal

precisely this hysteresis effect with regard to the order parameter. In type II superconductors, on the other hand, nucleation occurs well above H_c and the order parameter grows from zero when $H \leq H_{c2}$. Type II superconductors have a second order transition at $H = H_{c2}$. Likewise the order parameter and magnetisation are continuous at H_{c1} . This can be checked by examining the magnetisation curves plotted in Fig. 12.3.

For a disordered superconductor, the relation between nucleation critical field H_{c2} and thermodynamic critical field H_c is still given by (13.94). Disorder nevertheless reduces the coherence length $\xi \approx \sqrt{\xi_0 l_e}$ and thus increases κ . The thermodynamic field H_c typically has values around 10^3 Oe for ordinary superconductors (high temperature superconductors have much higher critical fields), and maximal values of κ are around 500. Hence the highest values which could be reached for the critical field H_{c2} in conventional superconductors are of order

$$H_{c2} < 10^3 \times 500 \text{ Oe} = 50 \text{ tesla.} \quad (13.95)$$

Because this value is so high, we may wonder whether the Zeeman energy of each electron in the Cooper pair ($S = 0$) would not be great enough to break the pair before the field H_{c2} was attained. This imposes a limit H_Z , called the Clogston limit [397], on the magnetic field,

$$H_Z < \frac{2\Delta}{\mu_B}, \quad (13.96)$$

to preserve the superconducting state. When $T_c = 20$ K, $H_c \approx 60$ T is of the same order of magnitude as H_{c2} . There is another much more restrictive condition on the anchoring of vortices [see Chap. 15(II)] so that the above fields effectively correspond to the maximum field accessible with superconducting magnets.

13.9 Surface Nucleation H_{c3}

Saint-James and de Gennes [398] have shown that near an interface with an insulating medium, the nucleation field is $H_{c3} = 1.695 H_{c2}$. This provides an opportunity to observe surface superconductivity above H_{c2} over a depth of order ξ . We choose \mathbf{H} along $\hat{\mathbf{z}}$ and \mathbf{A} along $\hat{\mathbf{y}}$. If the surface is perpendicular to \mathbf{H} , the boundary condition [see (13.31)],

$$\hat{\mathbf{n}} \cdot (\nabla + i\mathbf{k}_A) \psi = 0, \quad (13.97)$$

is equivalent to $\partial\psi/\partial z = 0$. This requires a solution with $k_z = 0$, as in the last section. The nucleation field is still equal to H_{c2} , since the boundary condition is the same as that for the nucleation critical field.

The situation is quite different when the surface is parallel to H . In this case, (13.97) implies $\partial\psi/\partial x = 0$. The harmonic oscillator wave function only satisfies these conditions if $x_0 = 0$ or $x_0 = \infty$. In fact our reasoning here is

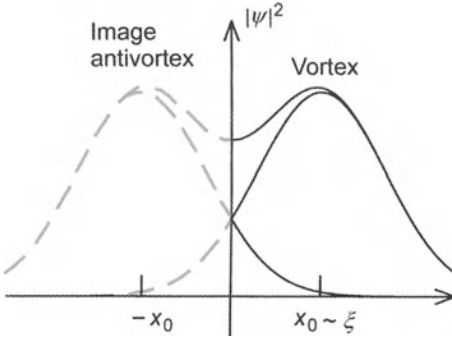


Fig. 13.5. Particular solution of the Ginzburg–Landau equations near a surface parallel to the magnetic field. These solutions can be constructed by superposing a vortex at distance x_0 (of order ξ) from the surface and a mirror image antivortex at $-x_0$ on the other side of the surface

not really valid, because the confinement potential due to the field is significantly modified at the surface (see Fig. 13.5). We could follow the example of Saint-James and de Gennes, solving the linearised Ginzburg–Landau equation (13.88) in terms of hypergeometric functions and determining the edge states. However, we can obtain a more physical idea of these states and their energies by using the usual variational methods of quantum mechanics [399]. To second order, the difference of Gibbs free energy is given by

$$G_s - G_n = \frac{\hbar^2}{2m_*} \int_0^\infty dx \left[-\frac{|\psi(x)|^2}{\xi^2} + |(\nabla + ik_A)\psi(x)|^2 \right]. \quad (13.98)$$

We choose order parameter $\psi = \exp(-ax^2 + ik_y y)$, with a and $k_y = x_0/l_B^2$ as variational parameters. Substituting this into the previous expression and evaluating the integrals, we obtain

$$\begin{aligned} I &= \frac{2m_*}{\hbar^2} (G_s - G_n) \\ &= \int_0^\infty dx \exp(-2ax^2) \left[-\frac{1}{\xi^2} + 4a^2 x^2 + \frac{(x - x_0)^2}{l_B^4} \right] \\ &= \frac{1}{2} \sqrt{\frac{\pi}{2a}} \left[-\frac{1}{\xi^2} + a + \frac{x_0^2 + (4a)^{-1}}{l_B^4} \right] - \frac{x_0}{2al_B^4}. \end{aligned} \quad (13.99)$$

Minimising this expression with respect to x_0 , we immediately find a relation between a and x_0 , viz.,

$$x_0 = \frac{1}{\sqrt{2\pi a}}. \quad (13.100)$$

Substituting this value into the previous expression, the integral is now only a function of a and ξ^2 :

$$I = \frac{1}{2} \sqrt{\frac{\pi}{2a}} \left[-\frac{1}{\xi^2} + a + \frac{1}{al_B^4} \frac{\pi - 2}{4\pi} \right]. \quad (13.101)$$

This is to be minimised with respect to a . In addition, at H_{c3} , the Gibbs free energies must be equal $G_n = G_s$. We therefore have two further relations,

$$a = \frac{1}{2\xi^2} = \frac{1}{2l_B^2} \sqrt{\frac{\pi - 2}{\pi}}, \quad (13.102)$$

which determine the approximate value of H_{c3} to be

$$H_{c3} = \sqrt{\frac{\pi}{\pi - 2}} \frac{\Phi_0}{2\pi\xi^2} = 1.66H_{c2}. \quad (13.103)$$

This is very close to the exact value found by Saint-James and de Gennes. The existence of surface superconductivity is important because it explains why many systems are able to carry a superconducting current in intense fields without any significant Meissner effect [403, 404]. In general, there is no surface superconductivity in an interface with a normal metal; all pairs formed at the interface can diffuse into the normal metal and break apart over a length $l_T = \sqrt{\hbar D/k_B T}$.

14. The BCS Theory of Superconductivity

14.1 The Electron–Phonon Interaction

From isotopic substitution experiments [405, 406], we know that the critical temperature and field of aluminium are proportional to $1/\sqrt{M}$, where M is the mass of the Al^{3+} ions in the lattice. Superconductivity is not therefore just an electronic phenomenon, but also involves lattice vibrations. Consider the two scattering processes between two electrons, shown in Fig. 14.1. In each case, a phonon is emitted by one electron and absorbed by the other. The two processes scatter two electrons initially in states $|\mathbf{p}\rangle$ and $|\mathbf{p}'\rangle$ into the *same* final states $|\mathbf{p}-\mathbf{k}\rangle$ and $|\mathbf{p}+\mathbf{k}\rangle$. We must therefore add together the amplitudes associated with each process. According to second order perturbation theory, the scattering amplitude can be expressed as the product of matrix elements at each vertex $V_{\mathbf{k}} \equiv V_{\mathbf{p}-\mathbf{k}, \mathbf{p}}$, divided by the energy difference between initial and intermediate states, viz.,

$$U_{\mathbf{k}}^a = \frac{|V_{\mathbf{k}}|^2}{\varepsilon_{\mathbf{p}} - \varepsilon_{\mathbf{p}-\mathbf{k}} - \hbar\omega_{\mathbf{k}}} , \quad (14.1)$$

since neither $\omega_{\mathbf{k}}$ nor $V_{\mathbf{k}}$ depend on the direction of \mathbf{k} . During the second process, it is the electron $|\mathbf{p}'\rangle$ which emits a phonon of wave vector $-\mathbf{k}$, and this phonon is then reabsorbed by the electron $|\mathbf{p}\rangle$. The scattering amplitude here is

$$U_{\mathbf{k}}^b = \frac{|V_{\mathbf{k}}|^2}{\varepsilon_{\mathbf{p}'} - \varepsilon_{\mathbf{p}'+\mathbf{k}} - \hbar\omega_{\mathbf{k}}} . \quad (14.2)$$

Energy is conserved during the scattering process, so that

$$\varepsilon_{\mathbf{p}} + \varepsilon_{\mathbf{p}'} = \varepsilon_{\mathbf{p}-\mathbf{k}} + \varepsilon_{\mathbf{p}'+\mathbf{k}} .$$

Hence we obtain the matrix element $U_{\mathbf{k}}$ for scattering

$$|\mathbf{p}\rangle \otimes |\mathbf{p}'\rangle \longrightarrow |\mathbf{p}-\mathbf{k}\rangle \otimes |\mathbf{p}'+\mathbf{k}\rangle$$

in the form

$$U_{\mathbf{k}} = U_{\mathbf{k}}^a + U_{\mathbf{k}}^b = -\frac{2|V_{\mathbf{k}}|^2\hbar\omega_{\mathbf{k}}}{(\hbar\omega_{\mathbf{k}})^2 - (\varepsilon_{\mathbf{p}} - \varepsilon_{\mathbf{p}-\mathbf{k}})^2} . \quad (14.3)$$

At long wavelengths, the matrix element $|V_{\mathbf{k}}|$ can be estimated by a crystal polarisability calculation [407],

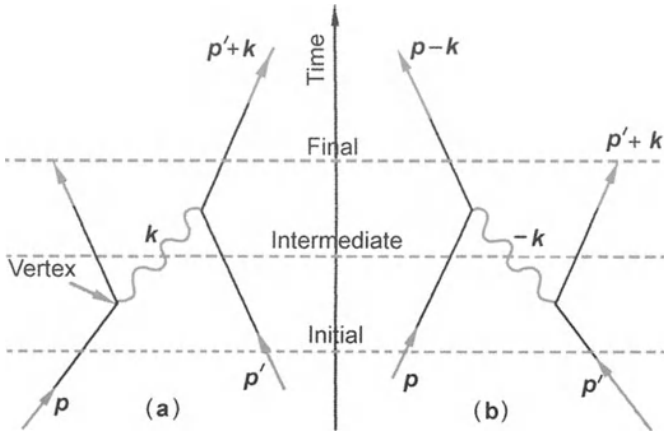


Fig. 14.1. (a) An electron of momentum \mathbf{p} emits a phonon of wave vector \mathbf{k} . This phonon is later reabsorbed by an electron of momentum \mathbf{p}' . (b) In this process, the electron of momentum \mathbf{p}' emits a phonon of wave vector $-\mathbf{k}$ which is reabsorbed by the first electron

$$|V_{\mathbf{k}}|^2 = \frac{p_F^2 \hbar \omega_{\mathbf{k}}}{2nmV} , \quad (14.4)$$

where n is the number of ions per unit volume, and m the electron mass. More precise estimates are difficult, because the matrix element depends on details of the electrostatic potential of ions in the crystal lattice. Note the reciprocal dependence on n , since the crystal becomes all the more polarisable as the ionic density decreases. In a simple solid, there is one conduction electron per ion and we replace n by $k_F^{-3} = \hbar^3/p_F^3$. This gives the matrix element of the electron-electron interaction induced by phonons:

$$U_{\mathbf{k}} = -\frac{2\varepsilon_F}{k_F^3 V} \frac{(\hbar \omega_{\mathbf{k}})^2}{(\hbar \omega_{\mathbf{k}})^2 - (\varepsilon_{\mathbf{p}} - \varepsilon_{\mathbf{p}-\mathbf{k}})^2} . \quad (14.5)$$

For electrons near the Fermi level, the interaction energy is a negative constant, independent of \mathbf{k} , since $\varepsilon_{\mathbf{p}} - \varepsilon_{\mathbf{p}-\mathbf{k}} \ll \hbar \omega_{\mathbf{k}}$. We could have obtained exactly the same result for a point interaction between electrons $U(\mathbf{r} - \mathbf{r}') = U_0 \delta(\mathbf{r} - \mathbf{r}')$, where $U_0 = -2\varepsilon_F/k_F^3$. The interaction induced by phonons is attractive and approximately equivalent to a local contact interaction between the electrons.

Since the interaction is independent of \mathbf{k} , which means that it is independent of the scattering angle between electrons, the electron orbital angular momentum remains unchanged. The interaction occurs at $l = 0$ and is therefore an s interaction. The electron spatial wave function remains symmetric when two particles are exchanged. The Pauli principle then requires an antisymmetric spin wave function. For the electrons to interact via a contact interaction, they must have antisymmetrised spin states. As the density of phonon states increases in proportion to $k^2 dk/d\omega$, phonons dominate at large

wave vectors, i.e., the edge of the zone $k \approx \pi/a$, at energies near the Debye energy $\hbar\omega_D$. For electrons with very different energy $\varepsilon_{\mathbf{p}} - \varepsilon_{\mathbf{p}'} \gg \hbar\omega_D$, the interaction becomes repulsive. Since electrons near the Fermi surface are the first to form Cooper pairs, we can say that the attraction due to phonons operates over an energy band of width $\hbar\omega_D$ and a momentum band of width $\delta p = \hbar\omega_D/v_F$.

In metals, the Coulomb repulsion will in part counterbalance this phonon-induced attraction [408]. As it is screened over a very short length r_s , of the same order as the interatomic distance, it can also be written as a contact term,

$$U_C(\mathbf{r} - \mathbf{r}') = \frac{e^2}{4\pi\varepsilon_0} r_s^2 \delta(\mathbf{r} - \mathbf{r}').$$

The ratio of Coulomb repulsion to phonon-induced attraction is thus of order

$$\frac{U_C}{U_{k=0}} = \frac{e^2 r_s^2 k_F^3}{8\pi\varepsilon_0\varepsilon_F} \approx \left(\frac{r_s}{\lambda_F} \right)^2 \frac{\pi e^2}{2\varepsilon_0\lambda_F\varepsilon_F} \approx 1 \quad (14.6)$$

in most metals, where $\lambda_F = h/p_F$ is the Fermi wavelength. This is why the total interaction $U_C + U_{ph}$ can be attractive in certain materials and repulsive in others. In fact, characteristic interaction times $\tau_C = h/\varepsilon_F$ for two electrons are much shorter than $1/\omega_D$. This reduces the Coulomb interaction by a logarithmic factor $\ln(\varepsilon_F/\hbar\omega_D) = \ln(M/m)$ [409, 410]. As the interaction constants are generally poorly known, we will assume an attractive interaction U which is constant over the interval $-\hbar\omega_D < \varepsilon_D < \hbar\omega_D$ for our study of superconductivity.

14.2 The BCS Hamiltonian

Consider a process in which an electron of momentum \mathbf{p} below the Fermi energy scatters into a state of momentum \mathbf{p}' above ε_F with amplitude t [423]. Such a process can be represented by the destruction via $a_{\mathbf{p}}$ of an electron of momentum \mathbf{p} followed by creation via $a_{\mathbf{p}'}^\dagger$ of an electron of momentum \mathbf{p}' . Matrix elements of the operator

$$t_{\mathbf{p}, \mathbf{p}'} = t a_{\mathbf{p}'}^\dagger a_{\mathbf{p}} \quad (14.7)$$

are equal to t if we have an initial state with one electron of momentum \mathbf{p} occupied and a final state with one electron of momentum \mathbf{p}' free; they are zero otherwise. This is a way of representing the process which includes constraints imposed by the Pauli principle through anticommutation relations

$$\{a_{\mathbf{p}}, a_{\mathbf{p}'}^\dagger\} = a_{\mathbf{p}} a_{\mathbf{p}'}^\dagger + a_{\mathbf{p}'}^\dagger a_{\mathbf{p}} = \delta_{\mathbf{p}, \mathbf{p}'} , \quad (14.8)$$

$$\{a_{\mathbf{p}}, a_{\mathbf{p}'}\} = \{a_{\mathbf{p}}^\dagger, a_{\mathbf{p}'}^\dagger\} = 0 . \quad (14.9)$$

We can specify the matrix elements of any process using this representation. Following the procedure described in Sect. 3.2(I) and Appendix B, the attractive contact interaction between two electrons is represented in second quantisation by

$$\begin{aligned} \mathcal{H} = & \sum_{\mathbf{p}\sigma} \varepsilon_{\mathbf{p}} a_{\mathbf{p}\sigma}^\dagger a_{\mathbf{p}\sigma} \\ & + \frac{U}{V} \sum_{-\hbar\omega_D < \varepsilon_{\mathbf{p}}, \varepsilon_{\mathbf{p}'} < \hbar\omega_D} a_{\mathbf{p}-\mathbf{q}, \uparrow}^\dagger a_{\mathbf{p}'+\mathbf{q}, \downarrow}^\dagger a_{\mathbf{p}, \uparrow} a_{\mathbf{p}', \downarrow}, \end{aligned} \quad (14.10)$$

where V is the volume of the system. The first term describes a system of non-interacting electrons. The electron interaction term respects energy and momentum conservation in the scattering process. Note, however, that when there is disorder, momentum is no longer a conserved quantum number. In that case, the Hamiltonian must be represented in real space with appropriate coupling constants [see Chap. 17(II)] [415]. Apart from the sign of U , which is negative here, this Hamiltonian is exactly the same as the Stoner Hamiltonian [see Chap. 11(I)].

Alternatively, destruction of an electron of momentum \mathbf{p} and spin σ is equivalent to creation of a hole of momentum $-\mathbf{p}$ and spin $-\sigma$. In this Landau description, quasi-particles are just electrons when $\varepsilon_{\mathbf{p}} > \varepsilon_F$ and holes when $\varepsilon_{\mathbf{p}} < \varepsilon_F$. Appearance and disappearance of quasi-particles is represented by operators

$$c_{\mathbf{p}, \sigma} = a_{\mathbf{p}, \sigma} \quad (\varepsilon_{\mathbf{p}} > \varepsilon_F), \quad (14.11)$$

$$c_{\mathbf{p}, \sigma} = a_{-\mathbf{p}, -\sigma}^\dagger \quad (\varepsilon_{\mathbf{p}} < \varepsilon_F). \quad (14.12)$$

In terms of quasi-particles, the present scattering process is written

$$t_{\mathbf{p}', \mathbf{p}} = t c_{\mathbf{p}, \sigma}^\dagger c_{-\mathbf{p}, -\sigma}^\dagger = t b_{\mathbf{p}, \sigma}^\dagger, \quad (14.13)$$

where $b_{\mathbf{p}, \sigma}^\dagger$ creates an electron-hole pair. The only difference between the two representations is that the number of particles is conserved in a finite system, whereas the number of quasi-particles is not.

If the interaction between electrons is attractive, bound states (Cooper pairs) between states $|\mathbf{p}, \sigma\rangle$ and $|-\mathbf{p}, -\sigma\rangle$ are energetically favoured at low temperatures [see Sect. 12.2(II)]. In terms of second quantisation operators, their wave function becomes

$$|\psi_C\rangle = \sum_{\mathbf{p}} b_{\mathbf{p}} a_{\mathbf{p}, \uparrow}^\dagger a_{-\mathbf{p}, \downarrow}^\dagger |0\rangle, \quad (14.14)$$

where Fourier components $b_{\mathbf{p}}$ are the Cooper pair condensation amplitudes defined in (12.10). The formation of a great number of pairs leads to instability of the Fermi surface describing macroscopic pair condensation, until condensation of one further pair involves a positive energy. If there is a macroscopic number of pairs below T_c , we expect the expectation value

$\langle a_{\mathbf{p}, \uparrow}^\dagger a_{-\mathbf{p}, \downarrow}^\dagger \rangle \approx b_{\mathbf{p}}^*$ to be non-zero. More precisely, consider the expectation of the interaction energy,

$$\frac{U}{V} \sum_{\mathbf{p}, \mathbf{p}', \mathbf{q}} \left\langle a_{\mathbf{p}-\mathbf{q}, \uparrow}^\dagger a_{\mathbf{p}'+\mathbf{q}, \downarrow}^\dagger a_{\mathbf{p}, \uparrow} a_{\mathbf{p}', \downarrow} \right\rangle . \quad (14.15)$$

This contains about N^3 terms, where N is the number of particles. Among these N^3 terms, each of the N^2 coherent terms

$$\frac{U}{V} \sum_{\mathbf{p}, \mathbf{q}} \left\langle a_{\mathbf{p}, \uparrow}^\dagger a_{-\mathbf{p}, \downarrow}^\dagger a_{\mathbf{q}, \uparrow} a_{-\mathbf{q}, \downarrow} \right\rangle \quad (14.16)$$

contributes an energy of order U/V , and of the same sign, to the interaction energy. This implies a total contribution of order $N^2 U/V$, which is indeed an extensive energy. The remaining $N^3 - N^2$ incoherent terms each make contributions of order U/NV to the energy, and the sign depends on the state under consideration. Given these random signs, they will make only a small contribution to the interaction energy for low energy states. It can in fact be shown [416] that their expectation value is zero in the BCS ground state,

$$\sum_{\mathbf{p}, \mathbf{p}' \neq -\mathbf{p}, \mathbf{q}} \left\langle \Psi_{\text{BCS}} \left| a_{\mathbf{p}-\mathbf{q}, \uparrow}^\dagger a_{\mathbf{p}'+\mathbf{q}, \downarrow}^\dagger a_{\mathbf{p}, \uparrow} a_{\mathbf{p}', \downarrow} \right| \Psi_{\text{BCS}} \right\rangle = 0 . \quad (14.17)$$

We are thus completely justified in neglecting the incoherent terms when determining the ground state. At finite temperatures, these terms become significant and gradually destroy the condensed state. In the superconducting state, the coherent contributions $\langle a_{\mathbf{p}, \uparrow}^\dagger a_{-\mathbf{p}, \downarrow}^\dagger \rangle$ and $\langle a_{\mathbf{q}, \uparrow} a_{-\mathbf{q}, \downarrow} \rangle$ acquire non-zero expectation values. This may seem surprising, since the Hamiltonian conserves particle number, whilst $a_{\mathbf{p}, \uparrow}^\dagger a_{-\mathbf{p}, \downarrow}^\dagger$ adds two particles. At constant particle number, the expectation value

$$\begin{aligned} \left\langle a_{\mathbf{p}, \uparrow}^\dagger a_{-\mathbf{p}, \downarrow}^\dagger \right\rangle &= \text{Tr} \left[\exp(-\beta \mathcal{H}) a_{\mathbf{p}, \uparrow}^\dagger c_{-\mathbf{p}, \downarrow}^\dagger \right] \\ &= \sum_{\alpha} \left\langle \alpha \left| \exp(-\beta \mathcal{H}) a_{\mathbf{p}, \uparrow}^\dagger c_{-\mathbf{p}, \downarrow}^\dagger \right| \alpha \right\rangle \end{aligned} \quad (14.18)$$

is identically zero, if we sum over a complete basis of common eigenstates of \mathcal{H} and $N_{\text{op}} = \sum_{\mathbf{p}\sigma} a_{\mathbf{p}\sigma}^\dagger a_{\mathbf{p}\sigma}$. In fact, a non-zero value of $\langle a_{\mathbf{p}, \uparrow}^\dagger a_{-\mathbf{p}, \downarrow}^\dagger \rangle$ amounts to restricting the sum to states of definite phase ϕ . Now, states with different phase ϕ differ macroscopically. The system would require an astronomical time to go from one state to the other. This is an example of a broken symmetry, in which the system selects a particular phase. The situation is exactly the same in a ferromagnet, whose magnetisation selects a particular direction below T_c . Thermodynamic fluctuations about a state of given phase ϕ are not great enough to explore states of different phase, so that the system is no longer ergodic. In the last chapter, we observed that the superconducting state globally breaks gauge invariance of the Hamiltonian under the unitary

transformation $S = \exp(iN_{\text{op}}\chi)$, where eigenvalues of N_{op} are particle numbers. The operator S transforms a ground state $|\Psi(\phi)\rangle$ of phase ϕ according to

$$\exp(iN_{\text{op}}\chi)|\Psi(\phi)\rangle = |\Psi(\phi + 2\chi)\rangle, \quad (14.19)$$

implying that the ground state is infinitely degenerate. Particle number and phase are therefore conjugate canonical variables, with $[N, \phi] = i$. This means we have an uncertainty relation

$$\delta N \delta \phi \approx 1. \quad (14.20)$$

For an isolated superconductor, N is fixed, the phase is indeterminate and we have $\langle a_{\mathbf{p},\sigma}^\dagger a_{-\mathbf{p},\sigma}^\dagger \rangle = 0$. We may well ask whether it is an observable quantity. For how could we observe a phase without adding or taking away a particle? Recent experiments on mesoscopic superconductors [417, 418] show that it is possible to measure the free energy difference between a superconductor with an even number of particles $N = 2n$ and one with an odd number $N = 2n+1$ [419]. Since we can distinguish states differing by only one electron, it would be useful to be able to specify their wave function and energy. Note that we can project states of known phase onto states of given particle number [see (14.52)]. These states do not necessarily correspond to a minimum free energy for fixed particle number [420], although experiments show that they are close.

In studying the BCS ground state, thermodynamic calculations will be limited to states of fixed phase, in which particle number is only specified on average by a chemical potential (in a grand canonical ensemble).

14.3 Mean Field Approximation and Diagonalisation of the BCS Hamiltonian

In the mean field approximation, we assume that $a_{\mathbf{p},\uparrow}^\dagger a_{\mathbf{q}-\mathbf{p},\downarrow}^\dagger$ differs only slightly from its expectation value. If the ground state is spatially uniform, we linearise the operator

$$a_{\mathbf{p},\uparrow}^\dagger a_{\mathbf{q}-\mathbf{p},\downarrow}^\dagger = b_{\mathbf{p}}^* + (a_{\mathbf{p},\uparrow}^\dagger a_{\mathbf{q}-\mathbf{p},\downarrow}^\dagger - b_{\mathbf{p}}^*) \quad (14.21)$$

around its expectation value

$$\langle a_{\mathbf{p},\uparrow}^\dagger a_{\mathbf{q}-\mathbf{p},\downarrow}^\dagger \rangle = b_{\mathbf{p}}^* \delta_{\mathbf{q},0}, \quad (14.22)$$

in the Hamiltonian (14.11). Keeping only terms of first order in the deviation from equilibrium, we obtain

$$\begin{aligned} \mathcal{H}_{\text{GC}} &= \mathcal{H} - \mu N_{\text{op}} \\ &= \sum_{\mathbf{p}} \xi_{\mathbf{p}} a_{\mathbf{p},\sigma}^\dagger a_{\mathbf{p},\sigma} + \sum_{\mathbf{p}} (a_{\mathbf{p},\uparrow}^\dagger a_{\mathbf{q}-\mathbf{p},\downarrow}^\dagger \Delta + a_{\mathbf{q}-\mathbf{p},\downarrow} a_{\mathbf{p},\uparrow} \Delta^*) - \sum_{\mathbf{p}} b_{\mathbf{p}}^* \Delta, \end{aligned} \quad (14.23)$$

where we have shifted the zero energy to the chemical potential, $\xi_{\mathbf{p}} = \varepsilon_{\mathbf{p}} - \mu$, and

$$\Delta = \frac{U}{V} \sum_{\mathbf{p}} b_{\mathbf{p}} \quad (14.24)$$

is the gap function. The latter is determined self-consistently from equations (14.22) and (14.24). The BCS Hamiltonian (14.23) has exactly the same form as the spin wave Hamiltonian encountered in Sect. 9.2(I), in the presence of an anisotropy transverse to the magnetic field. The only difference lies in the fact that we are dealing with fermions here. We proceed in the same way, defining a vector operator

$$X_{\mathbf{p}} = \begin{pmatrix} a_{\mathbf{p}, \uparrow} \\ a_{-\mathbf{p}, \downarrow}^\dagger \end{pmatrix}, \quad (14.25)$$

in order to put the BCS Hamiltonian into matrix form:

$$\mathcal{H} - \mu N_{\text{op}} = E_{\text{I}} + \sum_{\mathbf{p}} (\xi_{\mathbf{p}} + X_{\mathbf{p}}^\dagger H_{\mathbf{p}} X_{\mathbf{p}}), \quad (14.26)$$

where $E_{\text{I}} = - \sum_{\mathbf{p}} b_{\mathbf{p}}^* \Delta$ is the expectation value of the interaction, and matrix $H_{\mathbf{p}}$ is given by

$$H_{\mathbf{p}} = \begin{pmatrix} \xi_{\mathbf{p}} & \Delta \\ \Delta^* & -\xi_{\mathbf{p}} \end{pmatrix}. \quad (14.27)$$

The operators $a_{\mathbf{p}}^\dagger$ are fermions here. The Bogoliubov transformation [428]

$$X_{\mathbf{p}} = S_{\mathbf{p}} Y_{\mathbf{p}} = \begin{pmatrix} a_{\mathbf{p}, \uparrow} \\ a_{-\mathbf{p}, \downarrow}^\dagger \end{pmatrix} = \begin{pmatrix} u_{\mathbf{p}} & v_{\mathbf{p}}^* \\ -v_{\mathbf{p}} & u_{\mathbf{p}}^* \end{pmatrix} \begin{pmatrix} c_{\mathbf{p}, +} \\ c_{-\mathbf{p}, -}^\dagger \end{pmatrix} \quad (14.28)$$

must therefore be unitary, i.e., $S_{\mathbf{p}} S_{\mathbf{p}}^\dagger = 1$, in order to preserve anticommutation relations

$$\{X_{\mathbf{p}}, X_{\mathbf{p}}^\dagger\} = X_{\mathbf{p}} X_{\mathbf{p}}^{*T} + (X_{\mathbf{p}}^* X_{\mathbf{p}}^T)^T = 1 = \{Y_{\mathbf{p}}, Y_{\mathbf{p}}^\dagger\}. \quad (14.29)$$

This implies the relation

$$|u_{\mathbf{p}}|^2 + |v_{\mathbf{p}}|^2 = 1, \quad (14.30)$$

between matrix elements of S . By diagonalising the Hamiltonian, this unitary transformation S allows us to identify the quasi-particles of the superconductor $c_{\mathbf{k}}$, which have energies

$$E_{\mathbf{p}} = \pm \sqrt{\xi_{\mathbf{p}}^2 + |\Delta|^2}, \quad (14.31)$$

relative to the BCS ground state. The quasi-particle basis $c_{\mathbf{p}, \pm}$ is constructed so as to diagonalise the Hamiltonian $\mathcal{H} - \mu N_{\text{op}}$:

$$\begin{aligned}
\mathcal{H}_{\text{GC}} &= E_{\text{I}} + \sum_{\mathbf{p}} \left[\xi_{\mathbf{p}} + E_{\mathbf{p}} c_{\mathbf{p},+}^\dagger c_{\mathbf{p},+} - E_{-\mathbf{p}} c_{-\mathbf{p},-}^\dagger c_{-\mathbf{p},-} \right] \\
&= E_{\text{I}} + \sum_{\mathbf{p}} \left[\xi_{\mathbf{p}} - E_{-\mathbf{p}} + E_{\mathbf{p}} c_{\mathbf{p},+}^\dagger c_{\mathbf{p},+} + E_{-\mathbf{p}} c_{-\mathbf{p},-}^\dagger c_{-\mathbf{p},-} \right] \\
&= E_0 + \sum_{p < p_F} E_{\mathbf{p}} c_{\mathbf{p},+}^\dagger c_{\mathbf{p},+} + \sum_{p > p_F} E_{\mathbf{p}} c_{\mathbf{p},-}^\dagger c_{\mathbf{p},-} . \tag{14.32}
\end{aligned}$$

We have used anticommutation relations $\{c_{-\mathbf{p},-}, c_{-\mathbf{p},-}^\dagger\} = 1$ and the symmetry $E_{-\mathbf{p}} = E_{\mathbf{p}}$. This expression brings out the particle-hole duality between quasi-particles of types + and -. The energy E_0 is given by

$$E_0 = E_{\text{I}} + \sum_{\mathbf{p}} (\xi_{\mathbf{p}} - E_{\mathbf{p}}) . \tag{14.33}$$

Since

$$\begin{pmatrix} u_{\mathbf{p}} \\ -v_{\mathbf{p}} \end{pmatrix} \quad \text{and} \quad \begin{pmatrix} v_{\mathbf{p}}^* \\ u_{\mathbf{p}}^* \end{pmatrix} \tag{14.34}$$

are eigenvectors associated with eigenvalues $E_{\mathbf{p}}$ and $-E_{\mathbf{p}}$, the transformation S is defined by the corresponding systems of linear equations, whose solutions are

$$|u_{\mathbf{p}}|^2 = \frac{1}{2} \left(1 + \frac{\xi_{\mathbf{p}}}{|E_{\mathbf{p}}|} \right), \quad |v_{\mathbf{p}}|^2 = \frac{1}{2} \left(1 - \frac{\xi_{\mathbf{p}}}{|E_{\mathbf{p}}|} \right), \quad 2u_{\mathbf{p}}^* v_{\mathbf{p}} = -\frac{\Delta}{E_{\mathbf{p}}} . \tag{14.35}$$

The phases of Δ , $u_{\mathbf{p}}$ and $v_{\mathbf{p}}$ are not independent since the equation specifying the eigenvalue $(u_{\mathbf{p}}, -v_{\mathbf{p}})$ implies

$$\frac{\Delta v_{\mathbf{p}}}{u_{\mathbf{p}}} = \xi_{\mathbf{p}} - E_{\mathbf{p}} \tag{14.36}$$

must be real. If the order parameter has phase ϕ , then the phase of $v_{\mathbf{p}}$ relative to $u_{\mathbf{p}}$ is $-\phi$. We can choose $u_{\mathbf{p}}$ to be real, since the choice of phase here is arbitrary. The $c_{\pm\mathbf{p},\pm}$ are the elementary excitations above the superconductor ground state. They are linear combinations of electron and hole states. They can be obtained either by adding one particle to an N -electron state, or by removing one particle from an $(N+2)$ -electron state (equivalent to adding one hole). The quasi-particle dispersion relation is plotted in Fig. 14.2 as a function of $\xi_p = v_F(p - p_F)$, the quasi-particle energy in the normal state. From the Bogoliubov transformation, we obtain the expectation value of the condensation amplitude,

$$\begin{aligned}
b_{\mathbf{p}}^* &= \langle a_{\mathbf{p},\uparrow}^\dagger a_{-\mathbf{p},\downarrow}^\dagger \rangle = \left\langle \left(u_{\mathbf{p}}^* c_{\mathbf{p},+}^\dagger + v_{\mathbf{p}} c_{-\mathbf{p},-}^\dagger \right) \left(-v_{\mathbf{p}} c_{\mathbf{p},+} + u_{\mathbf{p}}^* c_{-\mathbf{p},-}^\dagger \right) \right\rangle \\
&= u_{\mathbf{p}}^* v_{\mathbf{p}} (1 - \langle n_{\mathbf{p},+} \rangle - \langle n_{\mathbf{p},-} \rangle) = -\frac{\Delta}{2E_{\mathbf{p}}} [1 - 2f(E_{\mathbf{p}})] , \tag{14.37}
\end{aligned}$$

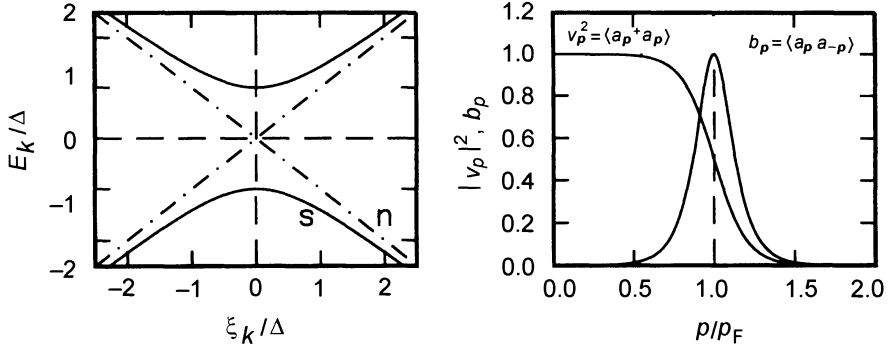


Fig. 14.2. *Left:* Elementary excitation spectrum (of quasi-particles) in the normal state (dashed lines) and in the superconducting state (continuous lines) as a function of linearised energy in the normal state ξ_p . The upper branch describes negatively charged quasi-particles (electron type), whilst quasi-particles on the lower branch are positively charged (hole type). *Right:* Electron distribution $|v_p|^2$ in the BCS ground state. In the normal state, this distribution is discontinuous at p_F , but decreases continuously over the interval $\delta p \approx \Delta/v_F$, where the condensation amplitude b_p is large

where the amplitude $u_p^* v_p$ is determined by (14.35), and f is the Fermi function. The number of thermally excited quasi-particles $n_{\mathbf{p},\pm} = c_{\mathbf{p},\pm}^\dagger c_{\mathbf{p},\pm}$ is zero at $T = 0$. Figure 14.2 illustrates the \mathbf{p} dependence of $|v_p|^2 = 1 - |u_p|^2$ and the condensation amplitude b_p . We observe that $|v_p|$ tends to 1 inside the Fermi sea, whereas b_p only becomes significant within Δ of p_F . This shows that, in BCS theory, electrons within the Fermi surface contribute to the ground state wave function, and in this sense form pairs. It is in fact the order parameter Δ which plays the role of a potential coupling together states $|\mathbf{p}, \uparrow\rangle$ and $|- \mathbf{p}, \downarrow\rangle$. But we must beware! The mean field approximation neglects many terms initially present in the BCS Hamiltonian, which may in principle affect internal states. As these states are inert with respect to all transport properties, their exact nature is of little importance.

From the gap function (14.24) and the values of u_p, v_p given by (14.35), we find the equation for the gap:

$$\Delta = \frac{U}{V} \sum_{\mathbf{p}} b_{\mathbf{p}} = \frac{|U|}{V} \sum_{\mathbf{p}} \frac{\Delta}{2E_{\mathbf{p}}} , \quad (14.38)$$

where the sum is over all states in the range $-\hbar\omega_D < \xi_{\mathbf{p}} < \hbar\omega_D$. Taking the continuous limit, this self-consistency condition becomes

$$1 = \frac{n(\varepsilon_F)|U|}{2} \int_{-\hbar\omega_D}^{\hbar\omega_D} \frac{d\xi}{\sqrt{\Delta^2 + \xi^2}} = n(\varepsilon_F)|U| \sinh^{-1} \frac{\hbar\omega_D}{\Delta} , \quad (14.39)$$

where $n(\varepsilon_F)$ is the density of states at the Fermi level (per spin). In the weak coupling limit $n(\varepsilon_F)|U| \ll 1$, the gap is given by

$$\Delta = \frac{\hbar\omega_D}{\sinh[1/n(\varepsilon_F)|U|]} \approx 2\hbar\omega_D \exp \frac{-1}{n(\varepsilon_F)|U|} . \quad (14.40)$$

The representation (14.32) and (14.33) gives the energy of the BCS state as

$$E_{\text{BCS}} = \sum_{\mathbf{p}} 2\xi_{\mathbf{p}} v_{\mathbf{p}}^2 + E_I = \sum_{\mathbf{p}} \xi_{\mathbf{p}} \left(1 - \frac{\xi_{\mathbf{p}}}{E_{\mathbf{p}}} \right) - \frac{\Delta^2 V}{|U|} . \quad (14.41)$$

Since the energy of the normal state is

$$E_n = \sum_{p < p_F} 2\xi_p , \quad (14.42)$$

the energy difference between BCS and normal states is

$$\begin{aligned} E_{\text{BCS}} - E_n &= \sum_{p > p_F} \left(\xi_p - \frac{\xi_p^2}{E_p} \right) + \sum_{p < p_F} \left(-\xi_p - \frac{\xi_p^2}{E_p} \right) + \Delta \sum_{\mathbf{p}} b_{\mathbf{p}} \\ &= 2 \sum_{p > p_F} \xi_p \left(1 - \frac{\xi_p}{E_p} \right) - \sum_{\mathbf{p}} \frac{\Delta^2}{E_p} \\ &\approx 2n(\varepsilon_F)U \int_0^\infty d\xi \left(\xi - \frac{\xi^2}{E} - \frac{\Delta^2}{2E} \right) \\ &= -\frac{n(\varepsilon_F)V\Delta^2}{2} . \end{aligned} \quad (14.43)$$

We identify the condensation energy of Cooper pairs with $\mu_0 H_c^2 V / 2$, where H_c is the thermodynamic critical field,

$$H_c = \left[\frac{n(\varepsilon_F)}{2\mu_0} \right]^{1/2} \Delta . \quad (14.44)$$

Since Δ is proportional to the Debye energy $\hbar\omega_D$, which varies as $1/\sqrt{M}$ with atomic mass, the isotopic effect $H_c \propto M^{-1/2}$ is predicted by the above formula provided that $n(\varepsilon_F)$ and U do not change from one isotope to another. Although $n(\varepsilon_F)$ is not affected by isotopic substitution, U is determined by the electrons as well as the phonons. We therefore expect significant deviations from the isotopic effect. Such deviations have been observed and analysed using more careful descriptions of the electron–phonon interaction [412, 413, 414].

We can now calculate the density of states of a superconductor. Since there is a bijective correspondence between electrons $a_{\mathbf{p}}$ and quasi-particles $c_{\mathbf{p}}$, we have

$$n_s(E) dE = n_n(\xi) d\xi . \quad (14.45)$$

This implies

$$\begin{aligned} n_s(E) = n_n(\varepsilon_F) \frac{d\xi}{dE} &= \frac{E}{(E^2 - \Delta^2)^{1/2}} \quad \text{if} \quad E \equiv |\varepsilon - \varepsilon_F| > \Delta , \\ n_s(E) &= 0 \quad \text{if} \quad E \equiv |\varepsilon - \varepsilon_F| < \Delta . \end{aligned} \quad (14.46)$$

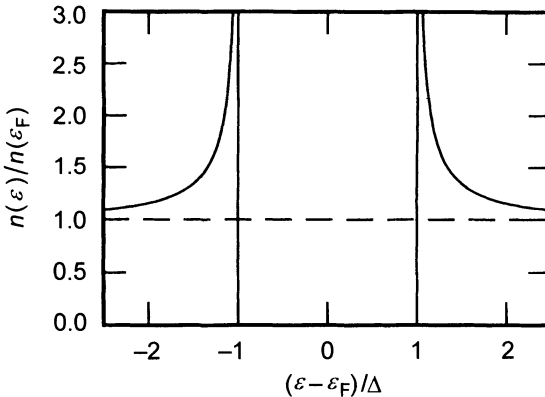


Fig. 14.3. Density of states for a superconducting metal near ε_F . The dashed line corresponds to the normally conducting state ($T \gg T_c$) and the continuous curve to the superconducting state at zero temperature. The density of states is zero in the gap. Since particle number is conserved, this implies that the density of states must be greater than in the normal state both above and below the gap. At finite temperatures, the gap closes

The density of states has a singularity just below ($-\Delta$) and just above (Δ) the gap. As the total number of states is conserved, those located in the gap are pushed above and below $\pm\Delta$, as can be seen from the excitation spectrum in Fig. 14.3. At finite temperatures, singularities in the density of states at $E = \pm\Delta$ are rounded off. It can be shown that even above T_c , electron-electron interactions induce a reduction in the density of states which gradually develops as we approach T_c .

14.4 BCS Wave Function and Coherent States

When we apply the operator $\mathcal{H}_{\text{GC}} - E_{\text{I}}$ of (14.23) to the state

$$|\Psi_{\text{BCS}}\rangle = \prod_{\mathbf{p} < p_F} \left(u_{\mathbf{p}} + v_{\mathbf{p}} a_{\mathbf{p},\uparrow}^\dagger a_{-\mathbf{p},\downarrow}^\dagger \right) |0\rangle, \quad (14.47)$$

we obtain

$$(H_{\text{BCS}} - E_{\text{I}}) |\Psi_{\text{BCS}}\rangle = \prod_{\mathbf{p} < p_F} \left[\Delta^* v_{\mathbf{p}} + \Delta u_{\mathbf{p}} a_{\mathbf{p},\uparrow}^\dagger a_{-\mathbf{p},\downarrow}^\dagger \right] |0\rangle. \quad (14.48)$$

As amplitudes $u_{\mathbf{p}}$ and $v_{\mathbf{p}}$ satisfy

$$\Delta u_{\mathbf{p}} - \xi_{\mathbf{p}} v_{\mathbf{p}} = -E_{\mathbf{p}} v_{\mathbf{p}}, \quad (14.49)$$

$$\xi_{\mathbf{p}} u_{\mathbf{p}} - \Delta^* v_{\mathbf{p}} = E_{\mathbf{p}} u_{\mathbf{p}}, \quad (14.50)$$

we deduce that $|\Psi_{\text{BCS}}\rangle$ is an eigenvector of $H_{\text{BCS}} - E_{\text{I}}$ with eigenvalue $\sum_{\mathbf{p} < p_F} (\xi_{\mathbf{p}} - E_{\mathbf{p}})$, the ground state energy. It is therefore the wave function of

the BCS ground state. This wave function is not an eigenstate of the number operator N_{op} , but rather of the variable ϕ canonically conjugate to it. Indeed, N_{op} generates the phase of the wave function, since

$$\exp(iN_{\text{op}}\phi/2)|\Psi_{\text{BCS}}\rangle = \prod_{\mathbf{p}} \left[|u_{\mathbf{p}}| + |v_{\mathbf{p}}| \exp(i\phi) a_{\mathbf{p},\uparrow}^\dagger a_{-\mathbf{p},\downarrow}^\dagger \right] |0\rangle . \quad (14.51)$$

We can therefore project the BCS states onto states of definite particle number [422], by taking the Fourier transform with respect to the phase:

$$\begin{aligned} |\Psi\rangle_N &= \int_0^{2\pi} \exp(-iN\phi/2) |\Psi_{\text{BCS}}(\phi)\rangle d\phi \\ &= \left(\prod_{\mathbf{p}} u_{\mathbf{p}} \right) \left(\sum_{\mathbf{p}} \frac{v_{\mathbf{p}}}{u_{\mathbf{p}}} a_{\mathbf{p},\uparrow}^\dagger a_{-\mathbf{p},\downarrow}^\dagger \right)^{N/2} |0\rangle \end{aligned} \quad (14.52)$$

is an N -particle eigenstate of the number operator. Notice that the BCS state is a superposition of states each containing an even number of electrons. We can check that states $c_{\pm\mathbf{p},\pm}^\dagger$ are excitations above the BCS state and are obtained by adding an electron or a hole to the system, i.e.,

$$c_{\mathbf{p},+}|\Psi_{\text{BCS}}\rangle = c_{-\mathbf{p},-}|\Psi_{\text{BCS}}\rangle = 0 , \quad (14.53)$$

$$c_{\mathbf{p},+}^\dagger|\Psi_{\text{BCS}}\rangle = a_{\mathbf{p},\uparrow}^\dagger \prod_{q \neq p} \left(u_q + v_q a_{q,\uparrow}^\dagger a_{-q,\downarrow}^\dagger \right) |0\rangle . \quad (14.54)$$

We also find that $c_{\mathbf{p},\pm}^\dagger|\Psi_{\text{BCS}}\rangle$ is orthogonal to $|\Psi_{\text{BCS}}\rangle$, i.e.,

$$\langle \Psi_{\text{BCS}} | c_{\mathbf{p},+}^\dagger | \Psi_{\text{BCS}} \rangle = 0 .$$

More generally, any state with an odd number of electrons is orthogonal to the BCS state. However, a pair of quasi-particles $c_{\mathbf{p},+}^\dagger c_{\mathbf{q},+}^\dagger$ can be added or removed from the ground state without changing the particle number expectation. In other words, any transition from the BCS ground state must conserve electron number parity. This property can be used to measure the density of states of a superconductor by the tunnel effect.

We still have to specify the charge, current and speed of a quasi-particle. In order to do so, it is convenient to form a spatially localised wave packet within some length $\delta\mathbf{r} \approx 1/\delta\mathbf{k}$, and identify the charge within this volume. Consider the state

$$|\mathbf{k}\rangle_{\text{QP}} = \sum_{\mathbf{p}} \alpha_{\mathbf{p}-\mathbf{k}} c_{\mathbf{p},+}^\dagger |\Psi_{\text{BCS}}\rangle , \quad (14.55)$$

where coefficients $\alpha_{\mathbf{q}}$ are normalised $\sum_{\mathbf{q}} |\alpha_{\mathbf{q}}|^2 = 1$. Charge is measured by the density operator $\rho(\mathbf{r}) = \psi^\dagger(\mathbf{r})\psi(\mathbf{r})$ [see Sect. 3.2(I) and Appendix B]:

$$\rho(\mathbf{r}) = \frac{1}{V} \sum_{\mathbf{p}, \mathbf{q}} \exp[i(\mathbf{p} - \mathbf{q}) \cdot \mathbf{r}] a_{\mathbf{p}}^\dagger a_{\mathbf{q}}^\dagger$$

$$\begin{aligned}
&= \frac{1}{V} \sum_{\mathbf{p}, \mathbf{q}} \exp[i(\mathbf{p} - \mathbf{q}) \cdot \mathbf{r}] \left[(u_{\mathbf{q}} v_{\mathbf{p}} + v_{\mathbf{q}} u_{\mathbf{p}}) (c_{\mathbf{q},-}^\dagger c_{\mathbf{p},+}^\dagger + c_{\mathbf{q},+} c_{\mathbf{p},-}) \right. \\
&\quad \left. + (u_{\mathbf{p}} u_{\mathbf{q}} - v_{\mathbf{p}} v_{\mathbf{q}}) (c_{\mathbf{q},-}^\dagger c_{\mathbf{p},-} + c_{\mathbf{p},+}^\dagger c_{\mathbf{q},+}) + 2v_{\mathbf{p}}^2 \delta_{\mathbf{p},\mathbf{q}} \right]. \quad (14.56)
\end{aligned}$$

Its expectation value in the wave packet state $|\mathbf{k}\rangle_{QP}$ is

$${}_{QP}\langle \mathbf{k} | \rho(\mathbf{r}) | \mathbf{k} \rangle_{QP} = \quad (14.57)$$

$$\frac{N}{V} + \frac{1}{V} \sum_{\mathbf{p}, \mathbf{q}} \alpha_{\mathbf{p}-\mathbf{k}} \alpha_{\mathbf{q}-\mathbf{k}} (u_{\mathbf{p}} u_{\mathbf{q}} - v_{\mathbf{p}} v_{\mathbf{q}}) \exp[i(\mathbf{p} - \mathbf{q}) \cdot \mathbf{r}].$$

The first term comes from the uniform density of the BCS ground state. The second term measures the charge of the quasi-particle. Integrated over the wave packet, its charge Q is approximately

$$Q \approx e(u_{\mathbf{k}}^2 - v_{\mathbf{k}}^2) = e \frac{\xi_{\mathbf{k}}}{E_{\mathbf{k}}} = e \frac{\xi_{\mathbf{k}}}{\sqrt{\xi_{\mathbf{k}}^2 + \Delta^2}}, \quad (14.58)$$

assuming $\delta\mathbf{k}$ sufficiently narrow compared with $\Delta/\hbar v_F$ to be able to neglect the variation of $u_{\mathbf{k}}$ and $v_{\mathbf{k}}$ over the wave packet. This charge depends on the quasi-particle energy and changes sign at the Fermi surface. Such a sign change is to be expected since quasi-particles correspond to electrons and holes above T_c . It is rather more surprising to find that, although quasi-particles are electron-hole linear combinations, Q is not exactly equal to $\pm|e|$. The whole charge cannot be localised in the wave packet, part of the charge being distributed over the ground state. In this sense, quasi-particles are not completely independent of the rest of the electron gas.

The current carried by the quasi-particle can be evaluated as the expected value of the current operator

$$\mathbf{j} = \frac{e\hbar}{2mi} (\psi^\dagger \nabla \psi - \psi \nabla \psi^\dagger),$$

over the wave packet. This gives

$$\langle |\mathbf{j}(\mathbf{r})| \rangle = e \frac{\hbar \mathbf{k}}{m}, \quad (14.59)$$

which agrees with the usual definition of current.

By definition, the group velocity of a wave packet is

$$\mathbf{v}_G = \frac{\nabla_{\mathbf{k}} E_{\mathbf{k}}}{\hbar} = \frac{\xi_{\mathbf{k}}}{E_{\mathbf{k}}} \frac{\hbar \mathbf{k}}{m}, \quad (14.60)$$

implying that the quasi-particle speed is reduced below T_c by a factor $\xi_{\mathbf{k}}/E_{\mathbf{k}}$. In conclusion, the current carried by a quasi-particle is not given by the charge multiplied by the group velocity. This amounts to saying that charge is not conserved, if we consider only quasi-particles. It is impossible to describe the system only in terms of quasi-particles, since the rest of the charge is carried by the ground state.

It can be shown that correlation functions $C(\mathbf{r} - \mathbf{r}')$ in the BCS state die out over a distance $\xi_0 = \hbar v_F / \pi \Delta$, the coherence length of the superconductor, just as we might expect.

14.5 Finite Temperatures

As quasi-particles $c_{\mathbf{p},+}$ are fermions, their thermal occupation probability is $\langle n_{\mathbf{p}} \rangle = f(E_{\mathbf{p}}) = 1/[\exp(\beta E_{\mathbf{p}}) + 1]$. We deduce that the condensation amplitude at finite temperatures is:

$$\begin{aligned} b_{\mathbf{p}} &= \langle a_{\mathbf{p},\uparrow} a_{-\mathbf{p},\downarrow} \rangle = u_{\mathbf{p}}^* v_{\mathbf{p}} [1 - f(E_{\mathbf{p}}) - f(E_{-\mathbf{p}})] \\ &= u_{\mathbf{p}}^* v_{\mathbf{p}} [1 - 2f(E_{\mathbf{p}})] . \end{aligned} \quad (14.61)$$

The equation for the gap (14.38) then becomes

$$\begin{aligned} 1 &= n(\varepsilon_F) |U| \int d^3 p \frac{1 - 2f(E_p)}{E_p} \\ &= n(\varepsilon_F) \int_0^{\hbar\omega_D} d\xi \frac{\tanh(\beta \sqrt{\xi^2 + \Delta^2})/2}{\sqrt{\xi^2 + \Delta^2}} . \end{aligned} \quad (14.62)$$

The critical temperature T_c is reached when the gap Δ is zero. Putting $x_c = \hbar\omega_D/k_B T_c$,

$$1 = n(\varepsilon_F) |U| \left[\ln x_c \tanh x_c/2 - \int_0^{x_c} dx \ln x \frac{d}{dx} (\tanh x/2) \right] . \quad (14.63)$$

Table 14.1. Critical temperature, critical field, Debye temperature and gap for some pure superconducting elements

El.	T_c [K]	H_c	θ_D [K]	$\frac{2\Delta}{k_B T_c}$	El.	T_c [K]	H_c	θ_D [K]	$\frac{2\Delta}{k_B T_c}$
Al	1.176	105	420	3.53	Re	1.7	200	430	3.0
Be	0.026	—	1160	—	Rh	0.0003	—	269	—
Cd	0.56	29.6	200	3.44	Ru	0.5	69	600	—
Ga	1.083	59.3	325	3.50	Sn	3.75	305	195	3.59
Hf	0.13	12.1	2200	—	Ta	4.4	831	230	3.63
Hg	4.16	411	71	3.95	Tc	7.8	1410	351	—
In	3.4	281.5	109	3.65	Th	1.37	—	170	—
Ir	0.14	19	425	—	Ti	0.4	60	430	—
La(α)	4.88	808	142	3.72	Tl	2.4	181	80	3.63
Mo	0.92	90	460	—	U	1.1	—	200	—
Nb	9.25	1970	277	3.65	V	5.35	1400	338	3.50
Np	0.075	—	188	—	W	0.0154	1.15	550	3.54
Os	0.65	70	500	—	Zn	0.9	55	319	3.44
Pa	1.3	—	—	—	Zr	0.5	54	290	—
Pb	7.23	803	96	3.95					

In the weak coupling limit $x_c \gg 1$, the second term is equal to $\ln \pi/2\gamma$, where $\gamma = \exp 0.577 = 1.781$ is the Euler constant. We can then deduce the relation between the critical temperature and the gap,

$$2\Delta(0) = \frac{2\pi}{\gamma} k_B T_c = 3.52 k_B T_c . \quad (14.64)$$

The functional dependence of the gap on reduced temperature, defined by $\tau = (T_c - T)/T_c$, can be determined by mathematical study of the gap equation near T_c [40]:

$$\Delta = 3.06 k_B T_c \sqrt{\tau} . \quad (14.65)$$

This behaviour is typical in the mean field approximation. Likewise, the narrowing of the gap at very low temperatures is exponentially small,

$$\Delta(T) = \Delta(0) - [2\pi\Delta(0)k_B T_c]^{1/2} \exp(-\Delta/k_B T) . \quad (14.66)$$

In contrast to the case for magnets, this exponential behaviour is not affected by Goldstone modes. The particles are charged, which raises the energy of collective modes to the plasma frequency ω_p (of the order of 1 eV for metals). They then play no further role in low energy processes [see Sect. 17.7(II)] [427, 428, 429]. The temperature dependence of the gap in lead is plotted in Fig. 14.4 and compared with the BCS prediction.

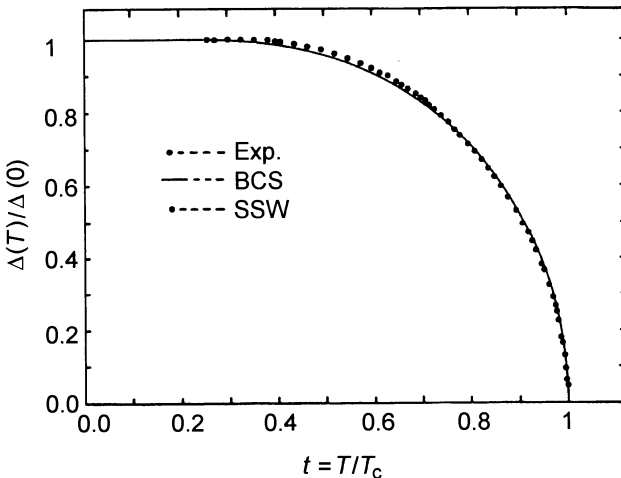


Fig. 14.4. Temperature dependence of the gap in lead, observed using a Pb/Pb tunnel junction [426], and comparison with BCS theory

14.6 Thermodynamic Properties

All thermodynamic functions can be determined from the gap equation (14.62). We use the Hamiltonian $\mathcal{H}(\lambda) = H_0 + \lambda U_{\text{int}}$ to interpolate between the free particle Hamiltonian ($\lambda = 0$) and the BCS Hamiltonian ($\lambda = 1$). Differentiating the free energy

$$F = -\frac{1}{\beta} \ln \text{Tr} \exp[-\beta \mathcal{H}(\lambda)] \quad (14.67)$$

with respect to λ , we find the expected value of the interaction energy,

$$\frac{\partial F}{\partial \lambda} = \frac{1}{Z} \text{Tr} \{ \exp[-\beta \mathcal{H}(\lambda)] U_{\text{int}} \} = \langle U_{\text{int}} \rangle. \quad (14.68)$$

Moreover, the expected value $\langle U_{\text{int}} \rangle = E_I = -\Delta \sum_p b_p$ of the interaction energy is related to the gap function by [see (14.24)]

$$\lambda E_I = \lambda \langle U_{\text{int}} \rangle = -\frac{\Delta^2(T, \lambda)V}{\lambda|U|}, \quad (14.69)$$

where the gap function $\Delta(T, \lambda)$ is the solution of equation (14.62) with an interaction λU . The free energy difference between superconducting and normal states can be obtained by substituting $\langle U_{\text{int}} \rangle$ (14.69) into (14.68), then integrating λ from 0 to 1,

$$F_s(T) - F_n(T) = V \int_0^1 d\lambda \frac{\Delta^2(T, \lambda)}{\lambda^2|U|}. \quad (14.70)$$

Combining this expression and the gap equation, we can derive the energy, entropy and specific heat near the critical temperature:

$$F_s(T) - F_n(T) = -0.474k_F^3V \frac{k_B^2(T - T_c)^2}{\varepsilon_F}, \quad (14.71)$$

$$S_s(T) - S_n(T) = 0.948k_F^3V k_B \frac{k_B(T - T_c)}{\varepsilon_F}, \quad (14.72)$$

$$C_s(T) - C_n(T) = 0.948k_F^3V k_B \frac{k_B T_c}{\varepsilon_F}. \quad (14.73)$$

We can also express these thermodynamic functions in terms of the Sommerfeld constant $\gamma = k_F^3/3\varepsilon_F$, as we did in Chap. 12(II). These functions are plotted below T_c in Figs. 12.4 and 12.6.

14.7 The Tunnel Effect

When two metals are separated by a thin layer of oxide (several Fermi wavelengths across), electrons can cross this barrier by the tunnel effect. If one of the metals is a superconductor, the tunnelling current is directly proportional to its density of states, which can thereby be measured experimentally [430].

The tunnel effect coupling is a small perturbation and can be represented by an additional interaction,

$$\mathcal{H}_T = \sqrt{\frac{S}{V_R V_L}} \sum_{\mathbf{p}, \mathbf{q}, \sigma} (T_{\mathbf{pq}} a_{\mathbf{p}, \sigma}^\dagger \alpha_{\mathbf{q}, \sigma} + T_{\mathbf{pq}}^* a_{\mathbf{p}, \sigma} \alpha_{\mathbf{q}, \sigma}^\dagger) . \quad (14.74)$$

Operators $a_{\mathbf{p}}^\dagger$ and $\alpha_{\mathbf{p}}^\dagger$ are operators creating electrons on the right and left of the barrier, respectively. The normalisation factor depends on the volumes of metal V_R and V_L on the right and left of the barrier, as well as the area S of the junction. The first term transfers an electron from right to left with amplitude $T_{\mathbf{pq}}$, while the second term describes the opposite process. Momentum in the plane of the barrier is conserved in this process. In general, $T_{\mathbf{pq}}$ is only significant when p_z and q_z are large, i.e., of the order of p_F and q_F , respectively, z being the direction perpendicular to the barrier. (In a semi-classical model, the tunnelling amplitude $T_{\mathbf{pq}}$ is proportional to $\exp[-k_F d / \cos \theta]$, where θ is the angle of incidence with respect to the normal. When $k_F d$ is of the order of 10, the transition amplitude falls by a factor of 2 between $\theta = 0$ and $\theta = 25^\circ$.) This is why $T_{\mathbf{pq}}$ depends strongly on \mathbf{p}_\perp and \mathbf{q}_\perp , the momenta in the barrier plane. The tunnelling current is the speed at which electrons on the right are transferred to the left. Consider the current operator

$$\begin{aligned} J_{op} &= e \frac{\partial N_L}{\partial t} = \frac{ie}{\hbar} \left[\mathcal{H} + \mathcal{H}_T, \sum_{\mathbf{p}, \sigma} a_{\mathbf{p}, \sigma}^\dagger a_{\mathbf{p}, \sigma} \right] \\ &= \frac{ie}{\hbar} \left[\mathcal{H}_T, \sum_{\mathbf{p}, \sigma} a_{\mathbf{p}, \sigma}^\dagger a_{\mathbf{p}, \sigma} \right] \\ &= -\frac{ie}{\hbar} \sum_{\mathbf{p}, \mathbf{q}, \sigma} (T_{\mathbf{pq}} a_{\mathbf{p}, \sigma}^\dagger \alpha_{\mathbf{q}, \sigma} - T_{\mathbf{pq}}^* \alpha_{\mathbf{q}, \sigma}^\dagger a_{\mathbf{p}, \sigma}) . \end{aligned} \quad (14.75)$$

This can be interpreted as the difference between right-to-left and left-to-right currents. Since J_{op} does not commute with Hamiltonian \mathcal{H} , we calculate the transition rate using the Fermi golden rule.

Assume to begin with that the two metals are normal. The potential difference U between the two metals maintains a difference of chemical potential $\mu_L - \mu_R = eU$. For an initially occupied right-hand state $|p, \sigma\rangle$, the transition probability per unit time is

$$w_{R \rightarrow L} = \frac{1}{\hbar} \int |\langle R | \mathcal{H}_T | L \rangle|^2 n_R(\varepsilon_R) [1 - f(\varepsilon_R)] V_R \frac{d\Omega_q}{2\pi} \delta(\varepsilon_R - \varepsilon_L - eU) , \quad (14.76)$$

where we have integrated over the directions of final state wave vectors q . In this formula, $n_R(\varepsilon_R)V_R$ is the density of states per unit energy on the right, and $1 - f(\varepsilon_R)$ restricts the sum to unoccupied states. The right-to-left current is obtained by summing over all possible initial states, viz.,

$$J_{R \rightarrow L} = \frac{e}{h} V_R V_L \int_{-\infty}^{\infty} \frac{d\Omega_q}{2\pi} \frac{d\Omega_p}{2\pi} d\varepsilon_L |\langle R | \mathcal{H}_T | L \rangle|^2 n_L(\varepsilon_L) f(\varepsilon_L) n_R(\varepsilon_L + eU) [1 - f(\varepsilon_L + eU)] . \quad (14.77)$$

It is useful to average the transmission coefficient over the angles of \mathbf{p} and \mathbf{q} , putting

$$|T|^2 = \int \frac{d\Omega_q}{2\pi} \frac{d\Omega_p}{2\pi} |T_{pq}|^2 . \quad (14.78)$$

If we then subtract the contributions of right-to-left and left-to-right currents, we obtain the current per unit area $j = J/S$ in the form:

$$\begin{aligned} j &= \frac{e^2}{h} |T|^2 \int_{-\infty}^{\infty} n_L(\varepsilon) n_R(\varepsilon + eU) \\ &\quad [f(\varepsilon)[1 - f(\varepsilon + eU)] - f(\varepsilon + eU)[1 - f(\varepsilon)]] \\ &= \frac{e^2}{h} |T|^2 \int_{-\infty}^{\infty} n_L(\varepsilon) n_R(\varepsilon + eU) [f(\varepsilon) - f(\varepsilon + eU)] . \end{aligned} \quad (14.79)$$

In normal metals, the density of states at the Fermi level is constant. When $\beta eU \gg 1$, the ohmic current is

$$j = GU = \frac{e^2}{h} |T|^2 n_R(\varepsilon_F) n_L(\varepsilon_F) U . \quad (14.80)$$

We now assume that the left-hand metal is a superconductor. We begin by separating (\mathbf{p}, \uparrow) and $(-\mathbf{q}, \downarrow)$ terms in the right-to-left tunnel coupling:

$$\mathcal{H}_T^{R \rightarrow L} \propto \sum_{\mathbf{p}, \mathbf{q}} \left(T_{\mathbf{p}, \mathbf{q}} a_{\mathbf{p}, \uparrow}^\dagger \alpha_{\mathbf{q}, \uparrow} + T_{-\mathbf{p}, -\mathbf{q}} a_{-\mathbf{p}, \downarrow}^\dagger \alpha_{-\mathbf{q}, \downarrow} \right) . \quad (14.81)$$

Electron operators a^\dagger can be rewritten in terms of superconductor quasi-particle operators c^\dagger using the Bogoliubov transformation,

$$a_{\mathbf{p}, \uparrow}^\dagger = u_{\mathbf{p}}^* c_{\mathbf{p}, +}^\dagger + v_{\mathbf{p}} c_{-\mathbf{p}, -} , \quad (14.82)$$

$$a_{-\mathbf{p}, \downarrow}^\dagger = -v_{\mathbf{p}} c_{\mathbf{p}, +}^\dagger + u_{\mathbf{p}}^* c_{-\mathbf{p}, -} . \quad (14.83)$$

The annihilation operator $c_{-\mathbf{p}, -}$ does not contribute since its projection on the BCS state is zero. Finally, since states $|\mathbf{q}, \uparrow\rangle$ and $|-\mathbf{q}, \downarrow\rangle$ are distinguishable, tunnelling probabilities are additive:

$$|\langle R | \mathcal{H}_T | L \rangle|^2 \propto |u_{\mathbf{p}}^*|^2 |T_{\mathbf{p}, \mathbf{q}}|^2 + |v_{\mathbf{p}}^*|^2 |T_{-\mathbf{p}, -\mathbf{q}}|^2 . \quad (14.84)$$

When there is no magnetic field, this expression reduces to $|T_{\mathbf{p}, \mathbf{q}}|^2$ (time reversal invariance requires $T_{\mathbf{p}, \mathbf{q}} = T_{-\mathbf{p}, -\mathbf{q}}^*$). Condensation amplitudes of the superconductor no longer appear, which allows us to apply the above analysis. The differential conductance per unit area of the junction is

$$\begin{aligned} G_{ns} &= \frac{dj}{dU} = \frac{e^2}{h} |T|^2 n_R(\varepsilon_F) \int_{-\infty}^{\infty} d\varepsilon n_R(\varepsilon) \left[-\frac{\partial f(\varepsilon + eU)}{\partial U} \right] \\ &= G_{nn} \frac{n_R^s(\varepsilon_F + eU)}{n_R^n(\varepsilon_F)} , \end{aligned} \quad (14.85)$$

where we have replaced the derivative of the Fermi function by a δ -function ($T \ll T_c$). In this limit, the differential conductance is a direct measure of the density of states of the superconductor. At finite temperatures, there is a gradual thermal broadening. When the two metals are superconductors, the above model gives the tunnelling current as an integral over their respective densities of states. In the BCS theory, the tunnelling current

$$j_{ss} = \frac{G_{nn}}{e} \int_{-\infty}^{\infty} \frac{|\varepsilon| d\varepsilon}{(\varepsilon^2 - \Delta_R^2)^{1/2}} \frac{|\varepsilon + eU|}{[(\varepsilon + eU)^2 - \Delta_R^2]^{1/2}} [f(\varepsilon) - f(\varepsilon + eU)] \quad (14.86)$$

can be evaluated exactly when the two superconductors are identical, so that $\Delta_L = \Delta_R \equiv \Delta$,

$$\frac{j_{ss}}{G_{nn}U} = E \left[\sqrt{1 - \left(\frac{2\Delta}{eU} \right)^2} \right] - 2 \left(\frac{\Delta}{eU} \right)^2 K \left[\sqrt{1 - \left(\frac{2\Delta}{eU} \right)^2} \right], \quad (14.87)$$

where E and K are the elliptic integrals [see also Sect. 16.1(II)]. At zero temperature, it can be seen from Fig. 16.3 in Chap. 16(II) that there is no current across the junction when $e|U| \leq \Delta_L + \Delta_R$. At this point the potential is sufficient to create a hole on one side and a particle on the other. When gaps Δ_R and Δ_L are significantly different, the tunnelling current can have a structure in the interval $[0, (\Delta_R + \Delta_L)/e]$ around $eU = \Delta_L - \Delta_R$ at finite temperature, as can be seen in Fig. 16.3. This is due to a finite quasi-particle density in one of the superconductors. These structures provide a simple way of finding the gap of the two superconductors forming the junction.

We have not taken into account any pair tunnel effect between the two superconductors. This is an important process, giving rise to the Josephson effect studied in Chap. 16(II).

14.8 Nuclear Relaxation and Ultrasound Absorption

These are incoherent scattering processes in a normal metal, represented by an interaction term

$$\mathcal{H}_s = \sum_{\mathbf{p}, \mathbf{p}', \sigma, \sigma'} B_{\mathbf{p}, \sigma}^{\mathbf{p}', \sigma'} a_{\mathbf{p}', \sigma'}^\dagger a_{\mathbf{p}, \sigma}. \quad (14.88)$$

In a superconductor, initially incoherent processes can acquire a certain degree of coherence via the superconductor wave function. Rewriting electron operators in terms of associated quasi-particles,

$$a_{\mathbf{p}, \uparrow}^\dagger = u_{\mathbf{p}}^* c_{\mathbf{p}, +}^\dagger + v_{\mathbf{p}} c_{-\mathbf{p}, -}, \quad (14.89)$$

$$a_{\mathbf{p}, \downarrow}^\dagger = -v_{\mathbf{p}} c_{-\mathbf{p}, -} + u_{\mathbf{p}}^* c_{\mathbf{p}, -}^\dagger, \quad (14.90)$$

the Hamiltonian \mathcal{H}_s scatters quasi-particles by four processes:

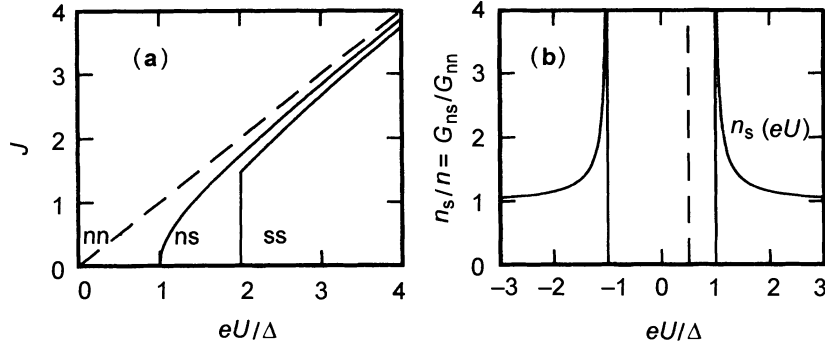


Fig. 14.5. (a) Tunnelling current in a normal n-i-n junction (dashed line), an n-i-s junction (continuous curve) and an s-i-s junction (continuous curve). In the n-i-n junction, the behaviour is ohmic $J = GU$. In an n-i-s junction, the current increases as $U^{1/2}$ above the threshold $eU = \Delta$. In an s-i-s junction, the threshold is 2Δ . (b) Differential conductance $G = dj/dU$ of an n-i-s junction can be used to obtain a direct measurement of the density of states of a superconductor

$$\mathcal{H}_s = \sum_{\mathbf{p}, \mathbf{p}', \sigma, \sigma', \tau, \tau'} B_{\mathbf{p}, \sigma}^{\mathbf{p}', \sigma'} \left[u_{\mathbf{p}} u_{\mathbf{p}'}^* c_{\mathbf{p}', \sigma'}^\dagger c_{\mathbf{p}, \sigma} + v_{\mathbf{p}}^* v_{\mathbf{p}'} \rho_\sigma^\tau \rho_{\sigma'}^{\tau'} c_{-\mathbf{p}', \tau'}^\dagger c_{-\mathbf{p}, \tau} \right. \\ \left. + u_{\mathbf{p}} v_{\mathbf{p}'} \rho_\sigma^\tau c_{-\mathbf{p}', \tau'} c_{\mathbf{p}, \tau} + u_{\mathbf{p}'} v_{\mathbf{p}} \rho_{\sigma'}^{\tau'} c_{\mathbf{p}', \tau'}^\dagger c_{-\mathbf{p}, \tau} \right]. \quad (14.91)$$

Spin factors ρ_σ^τ are defined by

$$\rho_+^- = -1, \quad \rho_-^+ = 1, \quad \rho_+^+ = \rho_-^- = 0. \quad (14.92)$$

As before, $c^\dagger c$ processes describe scattering of a quasi-particle, whilst $c^\dagger c^\dagger$ and cc processes describe creation or destruction of two quasi-particles, respectively. In order to calculate transition probabilities, we must combine processes involving the same initial and final states. There are then two terms from the scattering processes:

$$\langle \mathbf{p}', \sigma' | \mathcal{H}_s | \mathbf{p}, \sigma \rangle = u_{\mathbf{p}} u_{\mathbf{p}'} B_{\mathbf{p}, \sigma}^{\mathbf{p}', \sigma'} - v_{\mathbf{p}} v_{\mathbf{p}'} \sum_{\tau, \tau'} \rho_{\sigma'}^{\tau'} \rho_\sigma^\tau B_{-\mathbf{p}, \tau}^{-\mathbf{p}', \tau'}. \quad (14.93)$$

The second term involves the matrix element between two states of opposite spin and momentum. We must therefore consider two cases, depending on the symmetry of the Hamiltonian under time reversal, i.e., depending on the sign of η in

$$\sum_{\tau, \tau'} \rho_{\sigma'}^{\tau'} \rho_\sigma^\tau B_{-\mathbf{p}, \tau}^{-\mathbf{p}', \tau'} = \eta B_{\mathbf{p}, \sigma}^{\mathbf{p}', \sigma'}. \quad (14.94)$$

The interaction $V\delta(\mathbf{p} - \mathbf{p}')$ is scalar for ultrasound and is invariant under $t \rightarrow -t$. This is case I, $\eta = 1$. Nuclear relaxation is induced by interaction with an electromagnetic field $e\mathbf{p} \cdot \mathbf{A}/m$, which is odd under time reversal $\mathbf{p} \rightarrow -\mathbf{p}$. This is case II, where $\eta = -1$. Before evaluating matrix elements, note that \mathcal{H}_s

can in principle spatially modulate the gap and induce a collective excitation of the condensed state [429]. These collective modes can be excited by an electromagnetic interaction, whereas ultrasound does not have this effect. We evaluate coherence factors $u_{\mathbf{p}}u_{\mathbf{p}'} - \eta v_{\mathbf{p}}v_{\mathbf{p}'}$ from definition (14.35),

$$C_{\mathbf{p}}^{\mathbf{p}'} \equiv (u_{\mathbf{p}}u_{\mathbf{p}'} - \eta v_{\mathbf{p}}v_{\mathbf{p}'})^2 = \frac{1}{2} \left(1 + \frac{\xi_{\mathbf{p}}\xi_{\mathbf{p}'}}{E_{\mathbf{p}}E_{\mathbf{p}'}} - \eta \frac{\Delta^2}{E_{\mathbf{p}}E_{\mathbf{p}'}} \right) . \quad (14.95)$$

As for the tunnel effect, we average the matrix element B over all possible directions of \mathbf{p} and \mathbf{p}' , and also over spin components:

$$|B|^2 = \sum_{\sigma, \sigma'} \int \frac{d\Omega_{\mathbf{p}}}{4\pi} \frac{d\Omega_{\mathbf{p}'}}{4\pi} |B_{\mathbf{p}, \sigma}^{\mathbf{p}', \sigma'}|^2 . \quad (14.96)$$

The absorbed power is given by

$$W = \sum_{\mathbf{p}, \mathbf{p}'} w \hbar\omega , \quad (14.97)$$

where w is the transition rate per unit time, calculated using the Fermi golden rule,

$$w = 2\pi\omega |B|^2 C_{\mathbf{p}}^{\mathbf{p}'} n_s(E_{\mathbf{p}}) n_s(E_{\mathbf{p}'}) \delta(E_{\mathbf{p}'} - E_{\mathbf{p}} - \hbar\omega) \times \{f(E_{\mathbf{p}})[1 - f(E_{\mathbf{p}'})] - f(E_{\mathbf{p}'})[1 - f(E_{\mathbf{p}})]\} , \quad (14.98)$$

where n_s is the density of states of the superconductor and f the Fermi function. When we sum over all energies $\xi_{\mathbf{p}}$, the second (odd) term in the coherence factor (14.95) disappears. Putting together these results, and substituting in the BCS density of states (14.46), we obtain the relation between absorption in the superconducting and normal states,

$$W_s = \frac{W_n}{\hbar\omega} \int dE dE' \frac{EE' - \eta\Delta^2}{(E^2 - \Delta^2)^{1/2}(E'^2 - \Delta^2)^{1/2}} \times [f(E) - F(E')] \delta(E' - E - \hbar\omega) . \quad (14.99)$$

The exact nature of the absorption in a superconductor depends above all on the sign η , that is, on time reversal properties. As an example, we shall first describe ultrasound absorption, in which $\eta = 1$.

Ultrasound Absorption

We assume that the sound wave frequency $\hbar\omega$ is much smaller than the gap and the temperature. The energies E and E' of the scattered quasi-particles are each very close to Δ or to $-\Delta$. Ultrasound absorption is then given explicitly by

$$\frac{W_s}{W_n} = - \int_{|E| > \Delta} dE \frac{\partial f}{\partial E} = \frac{2}{1 + \exp(\beta\Delta)} . \quad (14.100)$$

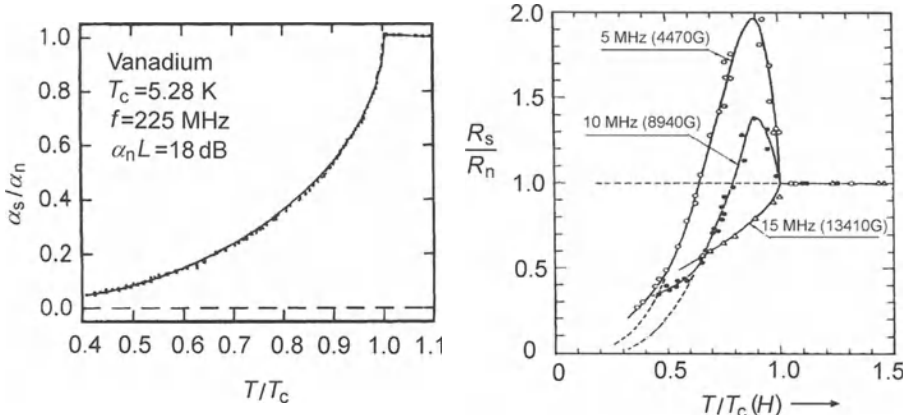


Fig. 14.6. Ultrasound attenuation (left) in vanadium and nuclear relaxation rate $R = 1/T_1$ (right) in the compound A15, V_3Sn , below T_c . Although the two systems behave very differently near T_c , they both become exponential for $T \ll T_c$, a characteristic feature of the gap

This decreases exponentially at low temperatures. Ultrasound absorption decreases monotonically from the critical temperature T_c . This behaviour is plotted in Fig. 14.6 for vanadium [433] and has been observed in many superconductors. Such behaviour is very different from nuclear relaxation, in which $\eta = 1$.

Nuclear Relaxation

In this context, the relevant frequency is the nuclear precession frequency, always very small compared with Δ/\hbar . Nuclear relaxation processes are rather complex so we shall restrict the discussion to differences between superconducting and normal states. Taking the limit $E' - E \rightarrow 0$, the longitudinal relaxation time T_1 is

$$\frac{T_{ln}}{T_{ls}} = - \int_{|E| > \Delta} dE \frac{E^2 + \Delta^2}{E^2 - \Delta^2} \frac{\partial f}{\partial E}. \quad (14.101)$$

This diverges logarithmically near Δ . In reality, the divergence in the density of states at Δ is smoothed out and the integral converges. However, nuclear relaxation reaches a maximum just below T_c and there is a singularity (the Hebel–Schlieter singularity [432]). This is shown in Fig. 14.6 for the compound A15, V_3Sn [434]. The difference in behaviour between ultrasound and nuclear relaxation processes is explained by the different coherence factors of \mathbf{p} and $-\mathbf{p}$ states. These experiments provide spectacular confirmation of the BCS wave function. In particular, a 2-fluid model would not describe this effect. Without going into the details, it is worth mentioning the thermal conductivity of the superconductor. Heat diffusion has two distinct origins:

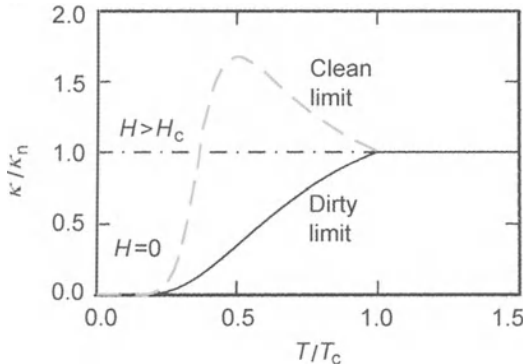


Fig. 14.7. Thermal conductivity of a superconductor below T_c . At low temperatures, there are no quasi-particles available to transport entropy. Thermal conductivity then decreases exponentially. This property is used to build heat switches; the superconductor transition is brought about by applying a magnetic field above the critical field. In clean systems, the increase in mean free path at first causes a rise in thermal conductivity

- scattering of quasi-particles on residual phonons at finite temperatures;
- scattering of quasi-particles on non-magnetic impurities.

The second of these processes is also represented by the generic Hamiltonian (14.88). In terms of quasi-particles, scattering from impurities reduces to

$$\mathcal{H}_s = \sum_{\mathbf{p}, \mathbf{p}', \sigma} c_{\mathbf{p}', \sigma}^\dagger c_{\mathbf{p}, \sigma} (u_{\mathbf{p}} u_{\mathbf{p}'} - v_{\mathbf{p}} v_{\mathbf{p}'}), \quad (14.102)$$

which conserves quasi-particle energy and spin. Thermal conductivity associated with scattering from impurities corresponds to case I, undergoing the same exponential decrease at low temperatures, since there are no more quasi-particles to transport entropy. This is shown in Fig. 14.7. When there are magnetic impurities, time reversal invariance is broken and all properties of the superconductor are significantly altered [see Sect. 17.8(II)].

In clean systems, effects are dominated by scattering from phonons. Temperature behaviour is then different. Reducing the temperature, the electron mean free path increases and thermal conductivity at first increases below T_c , before following the exponential decrease in the number of thermally excited quasi-particles. This is shown in Fig. 14.7.

14.9 Electromagnetic Screening

The BCS theory provides a very accurate description of the non-local electrodynamics in a superconductor. The Meissner effect in weak fields is a good illustration of the microscopic aspects of electromagnetic screening. There are

two contributions to the diamagnetic energy of an electron in an electromagnetic field [see Chap. 2(I)]. These are represented by their matrix elements

$$\langle \mathbf{q} | \mathcal{H}_1^d | \mathbf{k} \rangle = \mu_B [\mathbf{k} \cdot \mathbf{A}(\mathbf{q} - \mathbf{k}) + \mathbf{q} \cdot \mathbf{A}(\mathbf{q} - \mathbf{k})] , \quad (14.103)$$

$$\langle \mathbf{q} | \mathcal{H}_2^d | \mathbf{k} \rangle = \frac{e^2}{2m} \sum_{\mathbf{p}} \mathbf{A}(\mathbf{p}) \cdot \mathbf{A}(\mathbf{q} - \mathbf{p} - \mathbf{k}) , \quad (14.104)$$

where the vector potential is represented by its Fourier transform, so that we may calculate $\langle \mathbf{q} | (\mathbf{A} \cdot \nabla + \nabla \cdot \mathbf{A}) | \mathbf{k} \rangle$ and $\langle \mathbf{q} | A^2(\mathbf{r}) | \mathbf{k} \rangle$. Since each term scatters a \mathbf{k} electron into a state \mathbf{q} , their representation in second quantisation is

$$\begin{aligned} \mathcal{H}_1^d &= \mu_B \sum_{\mathbf{q}, \mathbf{p}, \sigma} (2\mathbf{q} - \mathbf{p}) \cdot \mathbf{A}(\mathbf{p}) a_{\mathbf{q}, \sigma}^\dagger a_{\mathbf{q}-\mathbf{p}, \sigma} , \\ \mathcal{H}_2^d &= \frac{e^2}{2m} \sum_{\mathbf{q}, \mathbf{p}, \mathbf{p}', \sigma} \mathbf{A}(\mathbf{p}) \cdot \mathbf{A}(\mathbf{p}') a_{\mathbf{q}, \sigma}^\dagger a_{\mathbf{q}-\mathbf{p}-\mathbf{p}', \sigma} . \end{aligned} \quad (14.105)$$

Since we are considering weak fields, energy shifts can be found from perturbation theory. \mathcal{H}_1 does not contribute to first order because there is no current in the ground state. In a normally conducting metal, the second order contribution from \mathcal{H}_1 exactly balances (at zero frequency) the first order contribution from \mathcal{H}_2 . We cannot describe diamagnetism without taking the Landau levels into account. In a superconductor, we must reexpress electron operators a and a^\dagger in terms of superconductor eigenstates (the quasi-particles c and c^\dagger). We find the same four processes as in the previous section, viz.,

$$\begin{aligned} \sum_{\sigma} a_{\mathbf{q}, \sigma}^\dagger a_{\mathbf{k}, \sigma} &= u_{\mathbf{q}} u_{\mathbf{k}} \left(c_{\mathbf{q}, +}^\dagger c_{\mathbf{k}, +} + c_{\mathbf{q}, -}^\dagger c_{\mathbf{k}, -} \right) \\ &\quad + v_{\mathbf{q}} v_{\mathbf{k}} \left(c_{-\mathbf{q}, -}^\dagger c_{-\mathbf{k}, -} + c_{-\mathbf{q}, +}^\dagger c_{-\mathbf{k}, +} \right) \\ &\quad + u_{\mathbf{q}} v_{\mathbf{k}} \left(c_{\mathbf{q}, +}^\dagger c_{-\mathbf{k}, -}^\dagger - c_{\mathbf{q}, -}^\dagger c_{-\mathbf{k}, +}^\dagger \right) \\ &\quad + v_{\mathbf{q}} u_{\mathbf{k}} \left(c_{-\mathbf{q}, -} c_{\mathbf{k}, +} - c_{-\mathbf{q}, +} c_{\mathbf{k}, -} \right) . \end{aligned} \quad (14.106)$$

At zero temperature, matrix elements of the first, second and last terms in the ground state do not contribute to second order. However, the third term adds two quasi-particles \mathbf{q} and $\mathbf{p} - \mathbf{q}$ to the ground level and then removes them. (At finite temperatures, we must take the other terms into account because there are quasi-particles in the initial state.) These ground state matrix elements are

$$\langle \mathbf{q}, \mathbf{p} - \mathbf{q} | \mathcal{H}_1^d | 0 \rangle = \mu_B (u_{\mathbf{q}} v_{\mathbf{q}-\mathbf{p}} - v_{\mathbf{q}} u_{\mathbf{q}-\mathbf{p}}) (2\mathbf{q} - \mathbf{p}) \cdot \mathbf{A}(\mathbf{p}) . \quad (14.107)$$

Now, in the London gauge, \mathbf{A} is transverse to \mathbf{p} , that is, $\mathbf{p} \cdot \mathbf{A}(\mathbf{p}) = 0$. The energy of the intermediate state is $E_{\mathbf{q}} + E_{\mathbf{p}-\mathbf{q}}$ above the ground state energy, so the contribution to the diamagnetic energy from \mathcal{H}_1^d is, to second order,

$$E_1^d = -4\mu_B^2 \sum_{\mathbf{q}} \frac{|\mathbf{q} \cdot \mathbf{A}(\mathbf{p})|^2}{E_{\mathbf{q}} + E_{\mathbf{p}-\mathbf{q}}} C_{\mathbf{q}}^{\mathbf{q}-\mathbf{p}} , \quad (14.108)$$

where

$$C_{\mathbf{q}}^{\mathbf{k}} \equiv [u_{\mathbf{q}} v_{\mathbf{k}} - v_{\mathbf{q}} u_{\mathbf{k}}]^2 \quad (14.109)$$

depends explicitly on the coherence factors. The second diamagnetic contribution comes from the expected value of \mathcal{H}_2^d in the BCS state. Only the second term in (14.106) can contribute when $\mathbf{k} = \mathbf{q}$. Its energy is

$$E_2^d = \frac{e^2}{m} \sum_{\mathbf{q}} v_{\mathbf{q}}^2 \sum_{\mathbf{p}} |\mathbf{A}(\mathbf{p})|^2 . \quad (14.110)$$

Since $\xi_{\mathbf{q}}$ is odd around ε_F (14.35), the sum over $|v_{\mathbf{q}}|^2$ gives $n_e/2$, where n_e is the electron density. There is a screening current associated with this energy change:

$$J_2(\mathbf{p}) = \frac{\delta E_2^d}{\delta \mathbf{A}(\mathbf{p})} = -\frac{e^2 n_e}{m} \mathbf{A}(\mathbf{p}) \equiv -K_2 \mathbf{A}(\mathbf{p}) . \quad (14.111)$$

This coincides precisely with London local electrodynamics (12.22). All non-local diamagnetic contributions are contained in E_1^d . Expanding the coherence factor $C_{\mathbf{q}}^{\mathbf{k}}$ and replacing amplitudes $u_{\mathbf{q}}, v_{\mathbf{q}}$ by their definition (14.35), we obtain

$$C_{\mathbf{q}}^{\mathbf{k}} = \frac{1}{2} \frac{E_{\mathbf{q}} E_{\mathbf{k}} - \xi_{\mathbf{q}} \xi_{\mathbf{k}} - \Delta^2}{E_{\mathbf{q}} E_{\mathbf{k}}} . \quad (14.112)$$

In order to evaluate the energy E_1^d explicitly, we choose a coordinate system with z -axis along \mathbf{p} and y -axis along \mathbf{A} (since they are orthogonal). Expressing vector \mathbf{q} in spherical coordinates $\mathbf{q} \equiv (q, \theta, \phi)$, we have

$$\mathbf{q} \cdot \mathbf{A} = q A \sin \phi \sin \theta . \quad (14.113)$$

It is also convenient to shift the sum over \mathbf{q} by $\mathbf{p}/2$, in order to symmetrise expressions. Finally, since the penetration depth ($\simeq \hbar/p$) is always large compared with the Fermi wavelength, the quasi-particle energy is

$$\xi_{\mathbf{q} \pm \mathbf{p}/2} = \frac{\hbar^2}{2m} \left[\left(\mathbf{q} \pm \frac{\mathbf{p}}{2} \right)^2 - q_F^2 \right] = \xi_{\mathbf{q}} \pm \hbar^2 v_F \frac{p}{2} \cos \theta . \quad (14.114)$$

We now convert the sum over \mathbf{q} into an integral over ξ ,

$$\sum_{\mathbf{q}} q^2 \dots \rightarrow \int \frac{q^2 dq d\Omega}{(2\pi)^3} q^2 \dots \rightarrow \frac{q_F^4}{(2\pi)^3 \hbar v_F} \int d\xi d\Omega \dots , \quad (14.115)$$

to obtain the diamagnetic energy E_1^d in the desired form,

$$E_1^d \equiv -K_1(\mathbf{p}) \frac{\mathbf{A}^2(\mathbf{p})}{2} = -\frac{4\mu_B^2 q_F^4}{3\pi^2 \hbar v_F} I(\mathbf{p}) \frac{\mathbf{A}^2(\mathbf{p})}{2} , \quad (14.116)$$

where

$$I(\mathbf{p}) = \frac{3}{8\pi} \int_{-\infty}^{\infty} d\xi d\Omega \sin^2 \phi \sin^2 \theta \frac{C_{\mathbf{q}-\mathbf{p}/2}^{\mathbf{q}+\mathbf{p}/2}}{E_{\mathbf{q}+\mathbf{p}/2} + E_{\mathbf{q}-\mathbf{p}/2}} . \quad (14.117)$$

For a metal with approximately spherical Fermi surface $q_F^3 = 3\pi^2 n_e$, we can simplify the factor to the left of $I(\mathbf{p})$:

$$K_1(\mathbf{p}) = \frac{n_e e^2}{m} I(\mathbf{p}) . \quad (14.118)$$

The integral I can only be calculated explicitly in two limiting cases. When the penetration depth $\lambda \approx 1/p \gg \xi$, the second term in (14.114) is a small correction and the integral $I(\mathbf{p})$ is of order ξ^2/δ^2 . The energy E_1^d is much smaller than E_2^d , and the electrodynamics is just as described in the London theory. In the opposite limit, we obtain

$$I(\mathbf{p}) \approx \frac{3\pi}{4p\xi} - 1 . \quad (14.119)$$

In this case, the electrodynamics is non-local, since

$$K(\mathbf{p}) = K_1(\mathbf{p}) + K_2(\mathbf{p}) = \frac{3\pi}{4} \frac{n_e e^2}{m} \frac{1}{p\xi} \quad (14.120)$$

diverges when $p \rightarrow 0$. $1/p$ is of the same order as the penetration depth λ , so this expression amounts to reducing the electron density in the superconductor by a factor λ/ξ . This confirms the physical argument used in Sect. 12.5(II). In this limit, the magnetic field does not have exponential spatial dependence. Indeed, screening is small over short distances compared with λ , because $K(p \gg 1/\lambda)$ is very small. However, over large distances, divergence of K leads to a rapid decrease in the current. Despite the modification in the states imposed by boundary conditions near the surface (located at $x = 0$), the image method can be used when reflection of Cooper pairs is specular, to reduce the problem to one in an infinite medium, adapting boundary conditions on the magnetic field. In an infinite medium, both vector potential and current must be continuous at $x = 0$. We must therefore require a discontinuity in the magnetic field, from $-\mathbf{H}_0$ at $x = 0^-$ to $+\mathbf{H}_0$ at $x = 0^+$. An inhomogeneous term is thereby introduced into the Helmholtz equation for the vector potential [see Sect. 12.4(II)],

$$\nabla \times \mathbf{H} = 2H_0 \hat{\mathbf{y}} \delta(x) - \frac{1}{\mu_0} \nabla^2 \mathbf{A} = J \Leftrightarrow \frac{1}{\mu_0} \frac{d^2 A_y}{dx^2} = 2H_0 \delta(x) - J_y . \quad (14.121)$$

This is easily solved in Fourier transform space:

$$A_y(x) = -\frac{2\mu_0 H_0}{\pi} \int_0^\infty \frac{\cos px}{p^2 + K(p)} dp , \quad (14.122)$$

$$H(x) = \frac{2H_0}{\pi} \int_0^\infty \frac{p \sin px}{p^2 + K(p)} dp . \quad (14.123)$$

Since the field does not decrease exponentially, we define the penetration depth by

$$\lambda = \frac{1}{H_0} \int_0^\infty H(x) dx = \frac{2}{\pi} \int_0^\infty \frac{dp}{p^2 + K(p)} . \quad (14.124)$$

In the Pippard limit, this becomes

$$\lambda_P = \frac{2}{\pi} \int_0^\infty \frac{qdq}{q^3 + q_0^3} \quad \text{where} \quad \frac{1}{q_0} = \left(\frac{4m\xi}{3\pi\mu_0 n_{ee} e^2} \right)^{1/3} . \quad (14.125)$$

This integral can be calculated exactly, yielding $\lambda_P = 4\pi/3q_0$. Up to a numerical factor, we have found the dependence $\lambda_P \sim \lambda_L^{2/3} \xi^{1/3}$ obtained in Sect. 12.5(II). When we go into real space, we must respect the London gauge condition, which gives a tensorial character to the kernel $K(\mathbf{R} \equiv \mathbf{r} - \mathbf{r}')$ of (12.28). Finally, the Fourier transform of $1/q$ is $1/R^2$, so we obtain the spatial decrease of the current once more.

Electromagnetic Response

The above study can be extended to finite frequencies [431, 437]. We can then relate diamagnetism to complex conductivity. From the definition of the electric field $\mathbf{E} = -\partial\mathbf{A}/\partial t = -i\omega\mathbf{A}$, it is straightforward to relate complex conductivity to the response function $K(\mathbf{p}, \omega)$,

$$\mathbf{J}(\mathbf{p}, \omega) = \sigma(\mathbf{p}, \omega) \mathbf{E}(\mathbf{p}, \omega) = i\omega\sigma(\mathbf{p}, \omega)\mathbf{A} = -K(\mathbf{p}, \omega)\mathbf{A} . \quad (14.126)$$

When the frequency tends to zero, we have seen that $K(\mathbf{p}, \omega)$ tends to a constant. The complex conductivity of a superconductor is therefore imaginary and diverges as $1/\omega$. This amounts to saying that its dielectric constant diverges as $1/\omega^2$, instead of $1/\omega$ for a normal metal. Another consequence is that, for small frequencies compared with the gap, the conductivity is identically zero! This paradoxical result is easy to explain [438]. The appearance of an energy gap pushes any spectral weight which was located below the gap into the zero frequency response. The conductivity is infinite at zero frequency but zero at all frequencies below the gap. This is shown on the experimental curve in Fig. 14.8 obtained by Morse and Bohm [439]. This dependence of the real and imaginary parts of the conductivity is totally consistent, as is easily checked using the Kramers–Kronig relations [see Sect. 8.4.2(I)]. At finite temperatures, the imaginary conductivity σ_i follows the gap,

$$\sigma_i = \sigma_n \frac{\pi\Delta}{\hbar\omega} \tanh \frac{\Delta}{2k_B T} . \quad (14.127)$$

Comparing with London electrodynamics, we can at low temperatures identify the density of Cooper pairs with the gap $n_s \simeq \Delta$, whereas close to T_c , $n_s \simeq \Delta^2$. This identification is a key feature of Ginzburg–Landau theory.

Finally, the reflectivity of a metal depends on both real and imaginary parts [441]. The reflectivity of a superconductor remains close to unity below the gap, but at very high frequencies, we come back to the conductivity of a metal in its normal state (see Fig. 14.8). This is to be expected because the superconducting state only affects low energy properties of a metal.

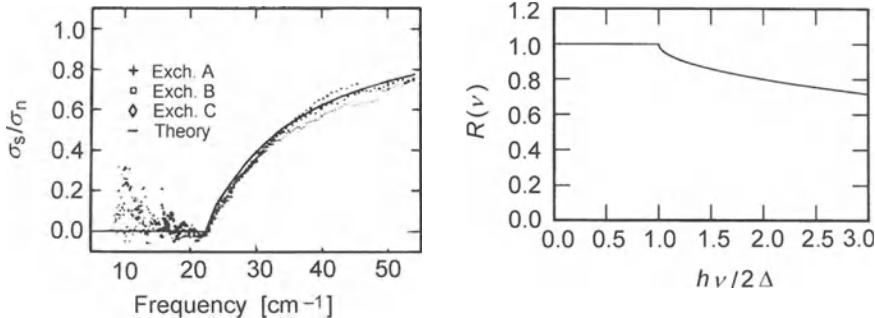


Fig. 14.8. *Left:* Frequency dependence of the real part σ_1 of the complex conductivity of a superconductor. Note that the conductivity is infinite at $\omega = 0$ but zero in the gap. Above the gap, the dynamic conductivity is finite and tends towards the conductivity of the normal state. *Right:* Reflectivity of a superconductor as a function of frequency ω

14.10 Conclusion

The BCS theory of superconductivity is the only non-perturbative theory of an N -body system which we are at present able to solve. It therefore plays a rather special role and has been applied in some very varied contexts, from atomic nuclei to neutron stars. The two main ingredients are a weak attraction between electrons due to phonons, and a mean field approximation allowing us to neglect incoherent contributions of the interaction potential. The BCS theory has been confirmed by many experiments. The density of states can be measured by the tunnel effect. Absorption phenomena depend on coherence factors which lead to quite different behaviour when different quantities are measured. Study of electromagnetic properties provides a rather precise reconstruction of Pippard non-local electrodynamics. Microwave absorption can be used to exhibit the gap in the energy spectrum.

Despite its many successes, the BCS theory cannot explain high temperature superconductivity [see Sects. 11.4.3(I) and 17.9(II)]. In addition, materials referred to as heavy fermions are not explained by the BCS theory, at least not in its original form. The BCS mechanism does not therefore seem to be the only one giving rise to an instability in the Fermi surface and pair condensation. Finally, experiments in mesoscopic physics impose spatial constraints, as well as constraints on particle number. This will necessitate a more precise formulation of superconductivity in heterogeneous media, since the order parameter varies over very small distances. In conclusion, charge constraints induce quantum fluctuation effects in the phase which mean that the BCS theory must be extended.

15. Vortices in Type II Superconductors

15.1 Isolated Vortices

In previous chapters, we observed that the free energy of an interface between normal and superconducting regions was negative $\Gamma_{\text{ns}} < 0$ when the London penetration depth exceeded the coherence length (divided by $\sqrt{2}$). When there is a magnetic field, a highly divided structure is therefore energetically favoured, in which normal and superconducting phases coexist [442], in such a way as to limit the positive diamagnetic energy of screening currents. We shall now study this mixed state. It is easy to see that it will be governed by quantum effects. Consider a normal region enclosed within the superconductor and traversed by a magnetic field. Around this region, a screening current must circulate in the superconductor. Consider a circular path of radius r around the normal region. The Bohr–Sommerfeld quantisation rule (or equivalently, the second Ginzburg–Landau equation) applied to a Cooper pair in orbital (vortex) motion around this path, leads to

$$\oint \mathbf{p}_s \, d\mathbf{l} = m_* \oint \mathbf{v}_s \, d\mathbf{l} = m_* v_s 2\pi r = nh . \quad (15.1)$$

The circulation is therefore quantised and the speed of pairs decreases as $1/r$,

$$v_s = \frac{n\hbar}{m_* r} . \quad (15.2)$$

Of course, this conclusion is no longer valid if r becomes comparable with ξ , the size of the pairs. In addition to this, pairs are charged and generate a screening current which dies out over a distance of order λ_L . The above expressions are thus limited to the region in which screening can be neglected, that is, $r \ll \lambda_L$. As regards possible values of n , the lowest energy structures correspond to $n = 1$. The energy of two vortices with coincident centres (the case $n = 2$) is always greater than the energy obtained when they are separated. (If this were not the case, all vortices would condense on top of one another, thereby causing a separation into two homogeneous phases. Such is only possible when the interfacial energy is positive $\Gamma_{\text{ns}} > 0$.)

The energy per unit length of a vortex is dominated by the kinetic energy of Cooper pairs over the volume in which diamagnetic currents are circulating. This volume is that contained between two cylinders of radii ξ and λ_L , viz.,

$$\begin{aligned}\varepsilon_{\text{vort}} &= \frac{n_s}{2} \int_{\xi}^{\lambda_L} \frac{m_* v_s^2}{2} 2\pi r dr = \frac{\pi n_s \hbar^2}{2m_*} \int_{\xi}^{\lambda_L} \frac{dr}{r} \\ &= \frac{\pi n_s \hbar^2}{2m_*} \ln \kappa = \frac{\Phi_0^2}{8\pi\mu_0\lambda_L^2} \ln \kappa.\end{aligned}\quad (15.3)$$

Here $n_s/2$ is the density of Cooper pairs. The orbital momentum $|\mathbf{L}|$ of one Cooper pair in orbital motion at radius r is rm_*v_s where v_s is given by (15.2). The magnetic moment per pair $|\boldsymbol{\mu}| = e_*|\mathbf{L}|/m_*$ contributes

$$\mu = n_s e_* \int_{\xi}^{\lambda_L} r v_s 2\pi r dr \approx n_s \frac{e_* \hbar}{2m_*} \lambda_L^2 = 2\pi n_s \mu_B \lambda_L^2 = \frac{\Phi_0}{2\mu_0} \quad (15.4)$$

to the magnetic moment per unit length. A magnetic field therefore lowers the energy of a vortex by $-\mu B$. A vortex can appear if it would reduce the total energy, i.e., if the sum of kinetic and magnetic energies $\varepsilon_{\text{vort}} - \mu B$ is negative. This definition defines the critical field H_{c1} ,

$$H > H_{c1} = \frac{\varepsilon_{\text{vort}}}{\mu_0 \mu} = \frac{\Phi_0}{4\pi\mu_0\lambda_L^2} \ln \kappa. \quad (15.5)$$

This is the field above which vortices can appear in the superconductor. Below H_{c1} , the Meissner effect is total; above H_{c1} , the Meissner effect is only partial. Comparing with the Ginzburg–Landau theory [see (13.19)], we can relate H_{c1} to the thermodynamic field H_c ,

$$H_{c1} = \frac{H_c}{\sqrt{2}\kappa} \ln \kappa, \quad (15.6)$$

where $\kappa = \lambda_L/\xi$. As for the nucleation field H_{c2} , this relation remains valid for dirty superconductors, where $\xi \approx \sqrt{\xi_0 l_e}$ and $\kappa \gg 1$. As H_{c2} increases, H_{c1} decreases. This is summarised in the equations:

$$H_{c1} \approx \frac{H_c}{\kappa} \ll H_c \ll H_{c2} \approx \kappa H_c, \quad (15.7)$$

$$H_{c1} H_{c2} \approx H_c^2. \quad (15.8)$$

In the following, we shall consider an extreme type II superconductor, that is, one for which $\kappa \gg 1$. Let the magnetic field be slightly greater than H_{c1} , so that the vortex density is small enough to justify neglecting interactions between vortices. We seek solutions to the Ginzburg–Landau equations for one vortex. The vortex wave function must have the axially symmetric form

$$\psi(\mathbf{r}) = \psi_0 f(r) \exp(-i\phi). \quad (15.9)$$

Its phase varies by 2π over one turn, in order to carry one quantum of circulation. Implicitly, this phase requires the symmetric gauge

$$\mathbf{A} = A(r)\hat{\phi}, \quad A(r) = \frac{\mu_0}{r} \int_0^r r' h(r') dr'. \quad (15.10)$$

Near the vortex centre where the magnetic field is maximal,

$$A(r) \approx \frac{\mu_0 h(0)r}{2}, \quad (15.11)$$

and far from the centre, $A(r)$ is determined by the flux $\Phi_0 = \oint \mathbf{A} \cdot d\mathbf{l}$,

$$k_A = \frac{2\pi A(r)}{\Phi_0} \approx \frac{1}{r}. \quad (15.12)$$

With these conventions, the Ginzburg–Landau equations only depend on r :

$$f - f^3 + \xi^2 \left[\frac{1}{r} \frac{d}{dr} \left(r \frac{df}{dr} \right) - \left(\frac{1}{r} - k_A(r) \right)^2 f \right] = 0, \quad (15.13)$$

$$\mu_0 \lambda_L^2 \frac{2\pi J_\phi}{\Phi_0} = -\lambda_L^2 \frac{d}{dr} \left(\frac{1}{r} \frac{d(rk_A)}{dr} \right) = f^2 \left(\frac{1}{r} - k_A \right), \quad (15.14)$$

since we have

$$\frac{1}{r} \frac{\partial \psi(\mathbf{r})}{\partial \phi} = -\frac{i}{r} \psi(\mathbf{r})$$

for the solution (15.9) chosen above to describe the vortex. At the vortex centre, $k_A = 2\pi A/\Phi_0 \approx \pi \mu_0 h(0)r/\Phi_0 = r/S$ where S is an area of order l_B^2 and l_B is the magnetic length. We seek a solution of form $f(r) = Cr^n$, satisfying the first Ginzburg–Landau equation,

$$Cr^n - C^3 r^{3n} - \xi^2 \left[\left(\frac{1}{r} - \frac{r}{S} \right)^2 Cr^n - n^2 Cr^{n-2} \right] = 0. \quad (15.15)$$

We must have $n = 1$, so that the dominant term $r^{n-2}(1 - n^2)$ for small r is zero. The next order in the expansion in powers of r is easily obtained, and the coefficient C determined, giving

$$f(r) = \frac{r}{2\xi} \left[1 - \frac{r^2}{8\xi^2} \left(1 + \frac{h(0)}{H_{c2}} \right) \right]. \quad (15.16)$$

As we would expect, $f(r)$ relaxes over a distance of order ξ , the coherence length, reaching a value close to 1 when $r > \xi$. If $\lambda \gg \xi$, variations in the order parameter can be neglected. The curl of the second Ginzburg–Landau equation is then just the London equation, since $e_* |\psi|^2 / m_* = 1 / \mu_0 \lambda_L^2$:

$$\lambda_L^2 \nabla \times \mathbf{J}_s + \mathbf{h} = \hat{\mathbf{z}} \frac{\Phi_0}{\mu_0} \delta(\mathbf{r}), \quad (15.17)$$

$$\nabla \times \mathbf{h} = \mathbf{J}_s. \quad (15.18)$$

The inhomogeneous term $(\Phi_0/\mu_0)\delta(\mathbf{r})$ has been introduced in order to take into account the rapid variation of $f(r)$ at the core of the vortex, approximately represented by a δ -function. It is determined by calculating the magnetic flux through a disk of radius $r \gg \lambda_L$, which must equal Φ_0/μ_0 , since each vortex carries one flux quantum. Using $\mathbf{J} = \nabla \times \mathbf{H}$ and replacing the double curl by the Laplacian, the magnetic field is found to obey the Helmholtz equation,

$$\lambda_L^2 \nabla^2 h - h = -\frac{\Phi_0}{\mu_0} \delta(\mathbf{r}) . \quad (15.19)$$

This has solution

$$h(r) = \frac{\Phi_0}{2\pi\mu_0\lambda_L^2} K_0\left(\frac{r}{\lambda_L}\right) , \quad (15.20)$$

where K_0 is the modified Bessel function of order 0. At large distances, this function dies out exponentially, being proportional to $\exp(-r/\lambda_L)$. At short distances, h behaves logarithmically. This is a direct consequence of circulation quantisation, which implies that the current density must decrease as $1/r$ [see (15.2)]. Of course, the logarithmic divergence has a cutoff at some distance of the same order as the coherence length ξ , when the order parameter drops to zero. There are therefore three different regimes:

$$h(r) \approx h(0) [1 - C(r/\xi)^2] , \quad r \ll \xi , \quad (15.21)$$

$$h(r) \approx \frac{\Phi_0}{2\pi\mu_0\lambda_L^2} \left(\ln \frac{\lambda_L}{r} + 0.12 \right) , \quad \xi \ll r \ll \lambda_L , \quad (15.22)$$

$$h(r) \approx \frac{\Phi_0}{2\pi\mu_0\lambda_L^2} \sqrt{\frac{\pi\lambda_L}{2r}} \exp(-r/\lambda_L) , \quad \lambda_L \ll r . \quad (15.23)$$

Once we know the distribution of the magnetic field and order parameter, we can find the free energy per unit vortex length. If we neglect the loss of pair condensation energy in the vortex core (of order $\mu_0 H_c^2 \xi^2 / 2 \ll \mu_0 H_c^2 \lambda_L^2 / 2$), the free energy of the vortex can be calculated in the London approximation as the sum of the magnetic energy and the kinetic energy of pairs, which is nothing but the diamagnetic energy of the screening current. Hence,

$$\begin{aligned} \varepsilon_{\text{vort}} &= \frac{\mu_0}{2} \int 2\pi r dr [h^2 + H_c^2(1 - f^4)] \\ &\approx \frac{\mu_0}{2} \int 2\pi r dr [h^2 + \lambda_L^2 (\nabla \times \mathbf{h})^2] . \end{aligned} \quad (15.24)$$

This is a free energy per unit length and is therefore a tension, which can also be written

$$\varepsilon_{\text{vort}} = \frac{\Phi_0 h(0)}{2} = \frac{\Phi_0^2}{4\pi\mu_0\lambda_L^2} \ln \kappa = \frac{\mu_0 H_c^2}{2} 4\pi\xi^2 \ln \kappa . \quad (15.25)$$

This agrees with the estimate (15.3) based on kinetic energy of diamagnetic currents. This energy is $4 \ln \kappa$ times greater than the free energy of pair condensation lost in the vortex core. It is of order $(\ln \kappa)/4$ times the magnetic energy $\mu_0 h^2/2$ integrated over area $\pi\lambda_L^2$, since $h \approx \Phi_0/\pi\mu_0\lambda_L^2 = 2H_{c1}/\ln \kappa$.

15.2 Interactions Between Vortices

Diamagnetic currents in a vortex induce a magnetic moment per unit length μ . This has been estimated in (15.4). As we bring a vortex located at \mathbf{r}_2

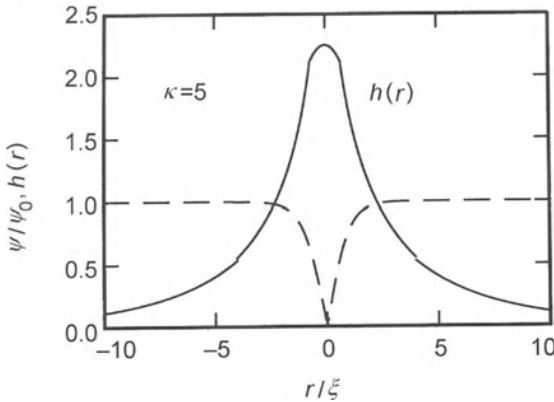


Fig. 15.1. Structure of an Abrikosov vortex in a superconductor for which $\kappa = \lambda_L/\xi$ takes the value 5. The field maximum at the vortex centre is of order $h(0) \approx 2H_{c1}$. In the vortex core, there are localised quasi-particle states which contribute to the specific heat [see Chap. 17(II)]

towards another at \mathbf{r}_1 , the field $h(|\mathbf{r}_1 - \mathbf{r}_2|)$ it produces at \mathbf{r}_1 increases the energy of vortex 1, because \mathbf{h} and $\boldsymbol{\mu}$ are opposite (diamagnetic currents create a field which opposes \mathbf{h}). Since the interaction between the two vortices is symmetric, the vortex at \mathbf{r}_1 will also increase the energy of the vortex at \mathbf{r}_2 . The total interaction energy is therefore

$$\varepsilon_{\text{int}} \approx 2 \frac{\Phi_0}{2} h(|\mathbf{r}_1 - \mathbf{r}_2|) = \frac{\Phi_0^2}{2\pi\mu_0\lambda_L^2} K_0(|\mathbf{r}_1 - \mathbf{r}_2|/\lambda_L), \quad (15.26)$$

and the interaction is repulsive. It behaves logarithmically at short distances and becomes exponentially small at large distances (15.23). (Such exponential behaviour is a natural consequence of electromagnetic screening, which does not exist in superfluids. In that case, the vortex interaction remains logarithmic even at large distances.) Choosing $\mathbf{r}_1 - \mathbf{r}_2$ along the x -axis, the force exerted in that direction by vortex 1 on vortex 2 is

$$f_x = \frac{\partial \varepsilon_{\text{int}}}{\partial x_2} = -\Phi_0 \frac{\partial h}{\partial x_2} = \Phi_0 J_y(r_1 - r_2), \quad (15.27)$$

where the Maxwell equation $\nabla \times \mathbf{h} = \mathbf{J}$ has been used. For an arbitrary number of vortices, supercurrents are additive and the total force on any one vortex is

$$\mathbf{f} = \mathbf{J}_s \times \boldsymbol{\Phi}_0, \quad (15.28)$$

where $\boldsymbol{\Phi}_0$ is along the vortex axis and \mathbf{J}_s is the total current at the vortex centre. Static equilibrium is only possible when the resultant current due to all other vortices is zero at the location of the vortex in question. The only way to achieve this is to place all vortices over a regular lattice, such as a

triangular or square lattice. However, it can be shown that the square lattice constitutes an unstable equilibrium because the force, which is repulsive, increases monotonically when a vortex is displaced from its equilibrium position. In contrast, the triangular lattice is stable and generally has the lower energy. In practice, triangular vortex lattices are the ones most commonly observed. The Abrikosov lattice was observed for the first time by neutron scattering [443], then by magnetic decoration [444], then by scanning tunnelling microscopy [445], and finally by Hall probe scanning [446]. However, square and even rectangular lattices have been observed in certain materials. It is thought that these structures are stabilised by the crystal lattice, which introduces an anisotropy into the order parameter [445] and thereby lowers the free energy of lattices with the same symmetry as the crystal lattice. When κ is close to $1/\sqrt{2}$, we can also observe coexisting Meissner and Shubnikov phases [447]. This state resembles the intermediate state in type I superconductors.

15.3 The Abrikosov Vortex Lattice

The Abrikosov lattice is a periodic arrangement of vortices [448]. It can be studied in great detail near H_{c2} , that is, close to the threshold at which superconductivity nucleates. The present discussion will be purely qualitative, referring the interested reader to the book by Abrikosov [449] for more exhaustive analysis. At the nucleation threshold, we may begin by considering the linearised Ginzburg–Landau equations, whose solutions correspond to the harmonic oscillator ground state ($n = 1$ Landau level):

$$\psi_k(\mathbf{r}) = \exp(i k_y y) \exp\left[-\frac{(x - x_k)^2}{2\xi^2}\right], \quad (15.29)$$

where the $x_k = k_y l_B^2$ are in the first instance arbitrary. Any linear combination will also satisfy the linearised equations. We must consider the non-linear term in order to determine the structure. Regularly spaced wave vectors k_y , $k_n = nq$ describe spatial periodicity in the y direction with spacing $a_y = 2\pi/q$. This implies a distance $a_x = ql_B^2$ between centres x_k . We deduce that x and y periodicities must be related by

$$a_x a_y = \frac{\Phi_0}{B}. \quad (15.30)$$

In other words, the basic lattice unit must contain one quantum of flux. To describe a regular lattice, we choose an order parameter which is a linear combination of the $\psi_k(\mathbf{r})$, viz.,

$$\psi_A(\mathbf{r}) = \sum_n C_n \psi_{k_n}(\mathbf{r}). \quad (15.31)$$

In a rectangular lattice, all the C_n are equal. This order parameter can also describe a triangular lattice if we choose $C_{2n+1} = iC_{2n}$. We may consider

$\psi_A(\mathbf{r})$ as an order parameter depending on variational parameters C_n and q , to be determined by minimising the total Ginzburg–Landau free energy. This means including both the linear terms $\propto |\psi_A(\mathbf{r})|^2$ and the non-linear terms $\propto |\psi_A(\mathbf{r})|^4$. We can now show that the structure with minimal energy is controlled by the parameter

$$\beta_A = \langle \psi_A^4(\mathbf{r}) \rangle / \langle \psi_A^2(\mathbf{r}) \rangle^2 ,$$

in the sense that this structure is the one determined by the smallest value of β_A . We put $\psi_A(\mathbf{r}) = C\psi_A^0(\mathbf{r})$, where the function $\psi_A^0(\mathbf{r})$ is normalised, $\langle |\psi_A^0(\mathbf{r})|^2 \rangle = 1$. Minimising $f_s - f_n$ with respect to C requires

$$C^2 = -a/b \frac{\langle |\psi_0(\mathbf{r})|^2 \rangle}{\langle |\psi_0(\mathbf{r})|^4 \rangle} .$$

The condensation energy is then

$$\langle f_s - f_n \rangle = -\frac{a^2}{2b} \frac{\langle |\psi_0(\mathbf{r})|^2 \rangle^2}{\langle |\psi_0(\mathbf{r})|^4 \rangle} = -\frac{a^2}{2b\beta_A} . \quad (15.32)$$

This is indeed minimal for the smallest value of β_A . In the square lattice, we find $\beta_A = 1.18$, whilst in the triangular lattice, $\beta_A = 1.16$. The triangular structure is therefore slightly favoured. As the flux per lattice unit is fixed at Φ_0 , the distance between vortices is slightly greater in the triangular lattice than in the square lattice. If a_Δ is the side of an equilateral triangle, its area is $A = a_\Delta^2 \sqrt{3}/4$. The magnetic flux through an elementary Wigner–Seitz cell (which has area $2A$, as shown in Fig. 15.2) must be Φ_0 . We deduce that

$$a_\Delta = \sqrt{\frac{2}{\sqrt{3}}} \left(\frac{\Phi_0}{B} \right)^{1/2} = 1.075 a_\square , \quad (15.33)$$

where $a_\square = \sqrt{\Phi_0/B}$ is the distance between vortices in the square structure. Consequently, it is the triangular structure which has the lowest energy, since interaction energy between vortices decreases with distance. Finally, as in any

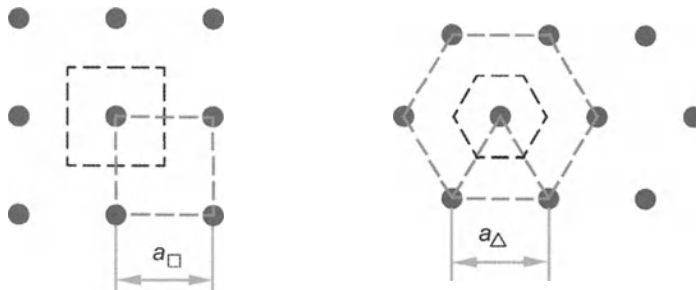


Fig. 15.2. Structure of square and triangular vortex lattices. Dashed lines show the boundary of the Wigner–Seitz cell

crystal, the Abrikosov lattice will melt when thermal fluctuations are sufficiently great [453, 454, 455, 457, 458, 459, 460]. This is observed in high temperature superconductors, in which vortices can form a liquid before superconductivity disappears at T_c . And if the crystal is highly disordered, the Abrikosov lattice may give way to a glassy structure, the vortex glass [461, 462]. It now seems widely accepted that there is a vortex glass in granular high temperature superconductors.

15.4 Magnetisation Curves

Below H_{c1} , the Meissner effect is total and magnetisation opposes field, so that $\mathbf{H} = \mathbf{B}/\mu_0 - \mathbf{M} = -\mathbf{M}$. Above H_{c2} , superconductivity disappears, $\mathbf{H} = \mathbf{B}/\mu_0$ and $\mathbf{M} = 0$. Between H_{c1} and H_{c2} , the magnetisation decreases monotonically because vortex density and density of normal regions gradually increase. This variation of magnetisation is shown in Fig. 12.3. Just above H_{c1} , vortex separation is controlled by the exponential part of their interaction. We therefore expect an optimal distance of order $a = (\Phi_0/B)^{1/2}$. The free energy variation above H_{c1} is then of order

$$F = H_{c1}B + \alpha \exp\left(-\frac{1}{\lambda_L}\sqrt{\frac{\Phi_0}{B}}\right),$$

where the second term is the contribution to the free energy from interaction between vortices. As $H = \partial F/\partial B$, we expect B to decrease logarithmically with $H - H_{c1}$. More quantitative analysis confirms this argument and B is given by

$$B = \frac{2\Phi_0}{\sqrt{3}\lambda_L^2 \ln[3H_{c1}/(H - H_{c1})]}, \quad (15.34)$$

near H_{c1} . The susceptibility is singular at H_{c1} and the transition is thus of second order.

15.5 Potential of a Vortex Near a Surface

By studying vortex behaviour near surfaces, we can show that there is a surface potential which tends to prevent vortices from entering the superconductor. If there are no vortices, the field at the superconductor surface dies out exponentially over the London penetration depth. When a vortex approaches the surface, we must add an image vortex in order to preserve boundary conditions $\mathbf{J}_s \cdot \hat{\mathbf{n}} = 0$. Let $\mathbf{r}_1 = (x, 0)$ be the position of the vortex and $\mathbf{r}_2 = (-x, 0)$ the position of its image in the superconductor surface $x = 0$. The magnetic field produced by the two vortices satisfies the London equation with two dipolar sources at \mathbf{r}_1 and \mathbf{r}_2 ,

$$\lambda^2 \nabla^2 \mathbf{H} - \mathbf{H} = -\frac{\Phi_0}{\mu_0} \hat{z} [\delta(\mathbf{r} - \mathbf{r}_1) + \delta(\mathbf{r} - \mathbf{r}_2)] . \quad (15.35)$$

When the vortex is there, the total magnetic field $\mathbf{H} = h(\mathbf{r})\hat{z}$ is thus given by

$$h(\mathbf{r}) = H_0 \exp(-x/\lambda_L) + \frac{\Phi_0}{2\pi\mu_0\lambda_L^2} \left[K_0 \left(\frac{|\mathbf{r} - \mathbf{r}_1|}{\lambda_L} \right) + K_0 \left(\frac{|\mathbf{r} - \mathbf{r}_2|}{\lambda_L} \right) \right] . \quad (15.36)$$

This magnetic field distribution determines the Gibbs free energy in an applied field H_0 ,

$$G_s(H_0) - G_s(0) = \frac{\mu_0}{2} \int dV [h^2(\mathbf{r}) + \lambda_L^2 (\nabla \times \mathbf{J})^2] - \mu_0 H_0 \int dV h(\mathbf{r}) , \quad (15.37)$$

where $\mathbf{J} = \nabla \times \mathbf{H}$. It is not easy to evaluate the energy of a vortex from this expression and we shall merely discuss the final result when $x \geq \xi$. Expressed as a potential $U(x) = G_s(H_0) - G_s(0)$, we have

$$U(x) = \Phi_0 \left[H_0 \exp \left(-\frac{x}{\lambda_L} \right) - \frac{\Phi_0}{4\pi\mu_0\lambda_L^2} K_0 \left(\frac{2x}{\lambda_L} \right) - H_0 + H_{c1} \right] . \quad (15.38)$$

We must introduce a cutoff for the logarithmic divergence of K_0 at short distances in order to take into account the vortex core. Using the definition

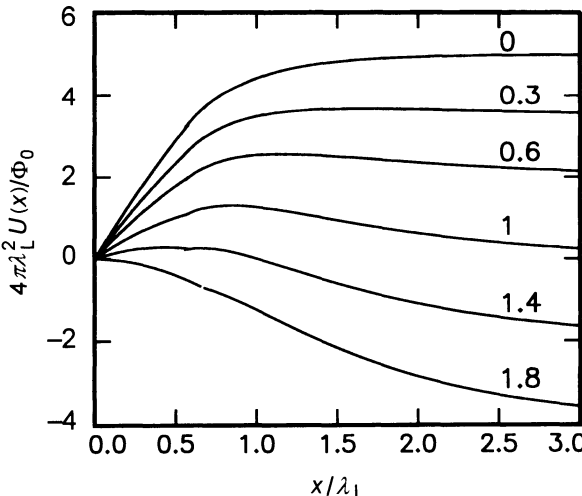


Fig. 15.3. Vortex potential near a surface. Up to fields quite close to the thermodynamic critical field H_c , there is a potential barrier which tends to keep vortices out of the superconductor

of H_{c1} , we find that the potential is zero for $x < \xi$. At large distances, $U(x)$ tends to a positive constant when $H_0 < H_{c1}$ but becomes negative when $H_0 > H_{c1}$. The general behaviour is plotted in Fig. 15.3. For a rather wide range of fields, we observe a potential barrier which prevents vortices from penetrating the superconductor. This potential barrier exists right up to fields near the thermodynamic critical field H_c . However, in real systems, the field, which is maximum in corners, may exceed H_c locally. Inhomogeneities may also allow vortices to enter.

15.6 Dissipation by Vortex Flow

Today type II superconductors can be used to produce intense magnetic fields, up to 20 T. This is the result of long term technological development, required to overcome the inherent problem of type II superconductors, which is vortex motion. It is easy to see that motion of a vortex will induce a dissipation of energy, equivalent to a finite resistance. Moreover, any vortex flow will reduce the magnetic field of a magnet, which no longer functions in persistent mode. An electric current J_{ext} exerts a force per unit length on the vortex equal to

$$\mathbf{f} = \mathbf{J}_{\text{ext}} \times \Phi_0 . \quad (15.39)$$

Multiplying by the number of vortices per unit area $n_v = B/\Phi_0$, we deduce the force per unit volume on the vortex lattice:

$$\mathbf{F} = \mathbf{J}_{\text{ext}} \times \mathbf{B} . \quad (15.40)$$

There are then two alternatives. One possibility is that inhomogeneities are sufficient to hold the lattice in place (pinning). A small displacement of the lattice causes an equal and opposite restoring force, so that it in fact remains stationary. No energy is then dissipated. Alternatively, the lattice moves and there must be a dissipative process. Such a process must be all the more efficient as the velocity \mathbf{v}_L is large, in order to limit acceleration of the lattice. We therefore have a viscous force,

$$\mathbf{f}_v = -\eta \mathbf{v}_L . \quad (15.41)$$

In the stationary regime, the velocity

$$\mathbf{v}_L = \frac{\mathbf{J}_{\text{ext}} \times \Phi_0}{\eta} \quad (15.42)$$

is perpendicular to the applied current \mathbf{J}_{ext} , as happens for the Hall current. Displacement of the vortices induces an electric field. If there is induction \mathbf{B} in the lattice frame, then there will be an electric field \mathbf{E} in the laboratory frame, given by

$$\mathbf{E} = -\mathbf{v}_L \times \mathbf{B} . \quad (15.43)$$

Combining the previous two equations, we deduce that the electric field is parallel to the applied current,

$$\mathbf{E} = \frac{\Phi_0 B}{\eta} \mathbf{J}_{\text{ext}} . \quad (15.44)$$

This induces energy dissipation characterised by a resistivity

$$\rho = \frac{|\mathbf{E}|}{|\mathbf{J}_{\text{ext}}|} = \frac{\Phi_0 B}{\eta} . \quad (15.45)$$

At the critical field H_{c2} , the system is in the normal state, with resistivity ρ_n . We can therefore determine the viscosity

$$\eta = \frac{\mu_0 H_{c2} \Phi_0}{\rho_n} . \quad (15.46)$$

When the field exceeds the depinning limit, the superconductor resistivity is

$$\rho = \rho_n \frac{B}{\mu_0 H_{c2}} . \quad (15.47)$$

Microscopically, the simplest approach to explaining this dissipation is to determine the electric field distribution near a vortex moving with velocity v_L . Bardeen and Stevens have shown by this type of analysis that the electric field is that of a dipole [463]. Referring to Fig. 15.4, the electric field is uniform and maximal at the centre of the vortex core. If we assume that the vortex core is normal, there is then an ohmic resistance in the core and dissipation occurs, as can be observed experimentally [450].

There is some reason to doubt the existence of a normal region at the vortex centre, since the order parameter is only zero at one point. Caroli, de Gennes and Matricon have studied the quasi-particle spectrum in the vortex core [451, 452]. They have shown that there is a finite density of low energy excitation at the vortex centre [see Chap. 17(II)]. When the vortex moves, thermally excited core states contribute to energy dissipation.

A further consequence of these core states is the existence of a finite quasi-particle density of states in the gap:

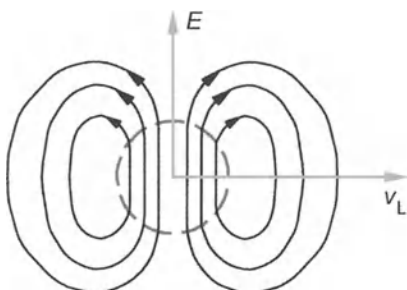


Fig. 15.4. Electric field near a moving vortex. The *dashed curve* shows the boundary of the normal core of the vortex

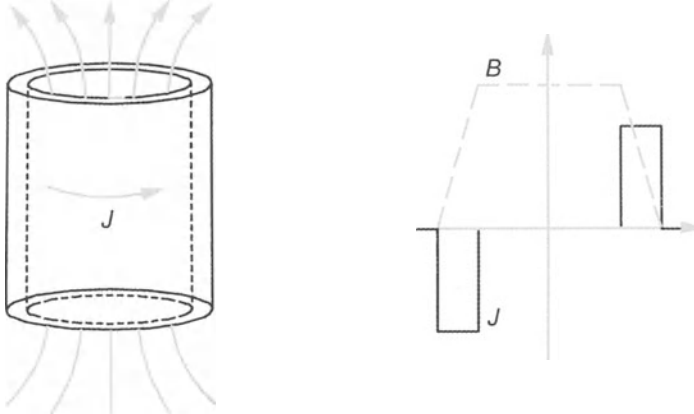


Fig. 15.5. *Left:* Flux trapped in a type II superconducting cylinder. *Right:* Profile of current density J and magnetic induction B across the cylinder

$$n_s(\varepsilon_F) \approx n_n(\varepsilon_F) \frac{B}{\mu H_{c2}} . \quad (15.48)$$

These quasi-particles can transport entropy. They then contribute to the specific heat, which becomes linear at low temperatures:

$$C(B, T) = C_n(T) \frac{B}{\mu H_{c2}} . \quad (15.49)$$

In order to visualise the consequences of such dissipation, we model a superconducting solenoid, operating in persistent mode, by a cylinder containing flux trapped by a superconducting current (see Fig. 15.5). If the thickness d is small compared with the diameter D , the current density J_{ext} is approximately uniform. It can be determined by Ampère's theorem, applied to two circles of diameters $D + 2r$ and $D + 2(r + \delta r)$. By Stokes's theorem, we relate the difference between the two circulations to the enclosed current:

$$\oint H(r) dl - \oint H(r + \delta r) dl = \pi(D + 2r)[H(r) - H(r + \delta r)] \\ = -\pi(D + 2r)J\delta r , \quad (15.50)$$

implying

$$\left| \frac{d\mathbf{H}}{dr} \right| = -|\mathbf{J}(r)| . \quad (15.51)$$

There is therefore a radial force on each vortex given by

$$f(r) = \Phi_0 |\mathbf{J}(r)| = \Phi_0 \left| \frac{dH}{dr} \right| . \quad (15.52)$$

Unless this force is balanced by another force (by pinning, for example), vortices flow radially, each carrying with them a quantum of flux. This in

turn reduces the trapped flux and also the current. The flux decrease induces an electromotive force and hence an electric field $E = \mathcal{E}/\pi D$,

$$\mathcal{E} = \pi DE = -\frac{d\Phi}{dt} = \Phi_0 \frac{dn_{\text{vort}}}{dt} = n_{\text{vort}} \Phi_0 \pi D v_L = B \pi D v_L , \quad (15.53)$$

since the vortex flow dn_{vort} across a circle of perimeter πD is $n_{\text{vort}} \times \pi D \times v_L dt$. In practice, this provides a reasonable description of what happens when a region of a superconducting magnet makes the transition to the normal phase. It is worth remembering the magnitude of the electromagnetic energy in a large 20 T coil, of magnetic volume 10 m³: $E = 10 \times (20)^2 / 2\mu_0 = 159$ MJ. In transition, the magnetic flux decreases rapidly and the voltage \mathcal{E} may reach several MV. This could be catastrophic if the magnet were not designed accordingly. In order to stabilise these magnets, superconducting wires are held in a copper matrix of relatively low resistance. This serves to limit the voltage developed in the superconductor. In addition, the system is so designed that most of the current, and hence the energy, is dissipated outside the magnet. The time required to discharge the current from the magnet is the ratio $\tau = L/R$ of the inductance of the magnet (several MH) to the resistance of the power supply (several ohms). This discharge time determines the value of $\mathcal{E} = B \times (\pi D^2/4)/\tau$.

Equation (15.53) can be interpreted in a different way. dn_{vort}/dt is the rate of decrease of the number of flux quanta enclosed within the cylinder, and has dimensions of frequency ν . We can relate n_{vort} to the total phase accumulated by the order parameter

$$\Delta\phi = \oint \nabla\phi \cdot d\mathbf{l} = 2\pi n$$

around the cylinder, so that ν may be interpreted as the Josephson frequency

$$e_*\mathcal{E} = 2e\mathcal{E} = \hbar \frac{\Delta\phi}{\Delta t} = h\nu \quad (15.54)$$

corresponding to voltage \mathcal{E} , generated around the cylinder. When a voltage appears across the terminals of a SQUID [a superconducting ring with an s-i-s Josephson junction, see Chap. 16(II)], there is a screening current which oscillates in the junction with frequency ν , associated with vortices passing round the circuit. There is therefore a precise analogy between the dissipative process considered here and the current (generally reactive) through a Josephson junction.

15.7 Observing Vortex Motion

We consider two superconducting films of length L and width w , separated by an insulating layer as shown in Fig. 15.6 [464, 465]. When a current passes lengthwise through the upper film, it induces a force on the vortex lattice. As

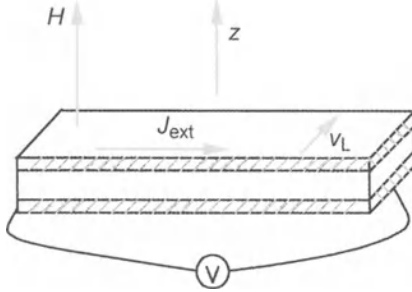


Fig. 15.6. Two superconducting films separated by an insulating layer. A current J_{ext} above the depinning threshold passes through the top film. Voltage $V = \mathcal{E}$ is detected across the terminals of the bottom film, in the same direction as J_{ext}

soon as the depinning threshold is exceeded, this force induces a uniform motion of the vortices, of velocity v_L perpendicular to the current. The motion of the vortex lattice can be detected by the lower film. The flow of vortices through the film reduces the magnetic flux enclosed in the electric circuit and hence induces an electromotive force \mathcal{E} perpendicular to the vortex flow. The associated electric field is in the same direction as the applied current in the upper film. A voltage therefore develops across the lower film, without the application of any current. As in the previous example, vortex velocity v_L can be determined by measuring this voltage:

$$\mathcal{E} = LB|v_L|. \quad (15.55)$$

This is a vortex detector, sometimes called a flux transformer, since it converts a vortex flow into a voltage. Finally, a flow of entropy S can be associated with the vortex flow. Indeed, vortex cores contain low-energy quasi-particles which can transport entropy. One consequence is that a temperature difference should develop in the direction of vortex flow so as to generate an entropy flow in the opposite direction and thereby balance the entropy flow carried by vortices. This is the Ettinghausen effect, which can be used to measure the entropy of a vortex as a function of temperature [466, 468].

15.8 Vortex Pinning

When inhomogeneities are introduced into a superconducting material on a scale of the same order or greater than ξ , these irregularities generate potential barriers which hinder vortex motion and collectively pin the vortex lattice. As an example, consider a small hole of diameter d in a superconducting film. The condensation energy lost in a vortex core is of the same order of magnitude as the total energy $\epsilon_{\text{vort}} = \mu_0 H_c^2 \xi^2$. If the vortex is at distance ξ from the hole, or actually in the hole, it is an energy which need no longer

be paid. Vortices are therefore attracted towards the hole by a force which can be estimated as

$$f_{\text{pinning}} = \mu_0 H_c^2 \xi . \quad (15.56)$$

However, the force on a vortex is of order (15.39),

$$f_L = \Phi_0 J_{\text{ext}} = 2\pi\sqrt{2}\mu_0 H_c \lambda_L \xi J_{\text{ext}} , \quad (15.57)$$

where we have used the definition of the thermodynamic critical field in terms of λ_L and ξ , namely $\mu_0 H_c = \Phi_0 / 2\pi\sqrt{2}\lambda_L \xi$. Equating these two forces, we obtain the critical current required to depin the vortex:

$$J_{\text{ext}} \approx \frac{H_c}{\lambda_L} . \quad (15.58)$$

In practice, there are collective effects due to the vortex lattice and inhomogeneities in alloys which are difficult to describe exactly [469]. We are therefore limited to rather primitive models, although they provide a reasonable description of the behaviour of materials in use at the present time.

15.9 Strong Pinning Limit. The Bean Model

At high vortex density, the lattice becomes extremely rigid and we may expect vortices either to be pinned or to move en bloc. In this situation, a macroscopic model may be adequate [470]. We have seen that the magnetic force per unit volume on the vortex lattice is

$$\mathbf{F} = \mathbf{J}_{\text{ext}} \times \mathbf{B} . \quad (15.59)$$

In practice, in superconducting magnets, it is only the total current which is fixed, whereas the current distribution and therefore also its density are determined by the field. For example, in the solenoid model, we found that $J = dH/dr$ (15.51). As long as the force $|\mathbf{F}|$ does not exceed the pinning threshold F_c (which may depend on B),

$$|\mathbf{F}| = JB = B \frac{dH}{dr} = \frac{d}{dr} \left(\frac{B^2}{2\mu_0} \right) > F_c(B) , \quad (15.60)$$

and the vortex lattice remains stationary. The stability condition is just that the gradient of the electromagnetic energy should not exceed F_c . If we neglect the field outside the solenoid $B \approx 0$, the maximal magnetic field within the solenoid is

$$\frac{B^2}{2\mu_0} = \int_{r_{\min}}^{r_{\max}} F_c(B) dr . \quad (15.61)$$

Assuming F_c independent of B , the maximal field increases as the square root of the thickness of the superconducting material. Since this thickness is

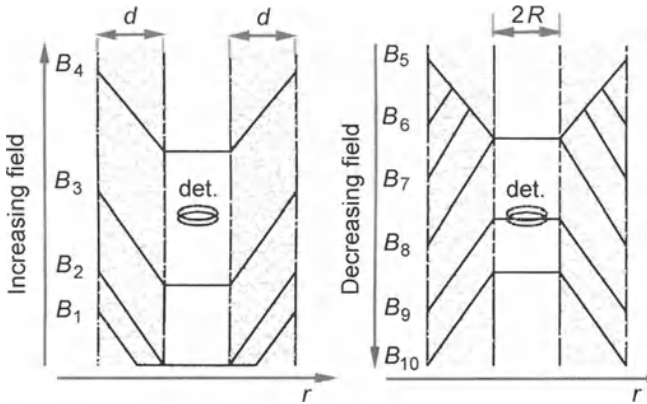


Fig. 15.7. Flux density across a superconducting cylinder of thickness d for increasing field (left) and decreasing field (right). These curves show the magnetic hysteresis associated with currents trapped by vortex pinning

generally of the same order as the radius, we deduce that the required quantity of superconducting wire increases as B^4 . This explains the impressive size of 20 T Nb₃Sn-NiTi superconducting magnets.

Clearly, F_c cannot remain constant down to $B = 0$, because the critical depinning current $J_c \approx F_c/B$ would then be infinite. For this reason, it seems more physical to treat J_c as constant. This is the Bean model. In this case, $F_c \propto B$ and flux density profiles are then straight lines of slope J_c . An example is shown in Fig. 15.7, where we have plotted the profiles of B across a solenoid of thickness d as the external field H is increased. The field within the solenoid is measured with a detector and gives an idea of the current. Evidently, the solenoid can screen a maximal field of

$$H_s = J_c d \quad (15.62)$$

If having gone above this value, the field is reduced and then reversed, as shown in Fig. 15.7, a certain part of the magnetic flux remains trapped in the solenoid, by pinning of flux lines. Magnetisation curves are also hysteretic, a limiting factor in the use of superconducting magnets with alternating currents.

15.10 Thermal Transport of Flux Lines

At finite temperatures, thermal agitation can lift vortices above local barriers. Such thermal processes may cause a reduction of the field within type II superconducting magnets operating in persistent mode. This could not happen in a type I superconductor. Anderson and Kim [471] have shown that the field falls logarithmically according to

$$B = B_0[1 - \alpha \ln(t/t_0)] . \quad (15.63)$$

This behaviour is also observed in disordered magnets and glasses. The form of this relation results from activating the relaxation rate of a flux line above an energy barrier D ,

$$\gamma = \gamma_0 \exp\left(-\frac{D}{kT}\right) , \quad (15.64)$$

where γ_0 is a microscopic frequency, i.e., an oscillation frequency of the vortex in its potential well. Relaxation of the magnetisation is given by an average over the barrier distribution $f(D)$,

$$\begin{aligned} M &= \int dD f(D) \exp(-\gamma t) \\ &= \int dD f(D) \exp\left[-\exp\left(-\frac{D}{k_B T} + \ln(t/t_0)\right)\right] . \end{aligned} \quad (15.65)$$

The exponential of an exponential can be replaced by 0 if the argument is positive and by 1 if it is negative. This produces a step function Θ with argument $\Theta(D - k_B T \ln t)$. Approximating $f(D)$ by a constant, we obtain Anderson and Kim's formula. In practice, the magnetic viscosity $\alpha \equiv (1/M)dM/dt$ of magnets made from NiTi and Nb₃Sn is very small, so that the field reduction caused by vortex activation is extremely low. However, the effect is of key importance in developing magnets from high temperature superconducting materials, since these must operate at 77 K. Experimental studies show that thermal transport is difficult to control in a satisfactory way in these materials. A great deal of technological innovation will be needed before we can build the 1000 T magnets everyone is dreaming about!

16. The Josephson Effect and Quantum Interferometers

16.1 Quasi-Particle Tunnelling Current

The semi-classical approximation, discussed in Chap. 2(I), can be used to determine the amplitude $\psi(\mathbf{r}_1)$ of a stationary wave function at any point \mathbf{r}_1 from knowledge of its amplitude $\psi(\mathbf{r}_0)$ at some other point \mathbf{r}_0 :

$$\psi(\mathbf{r}_1) = a \exp \left[i \frac{S(\mathbf{r}_1, \mathbf{r}_0)}{\hbar} \right] \psi(\mathbf{r}_0), \quad (16.1)$$

where the semi-classical action is given by $S = \int_{\mathbf{r}_0}^{\mathbf{r}_1} \mathbf{p}(\mathbf{r}) \cdot d\mathbf{r}$. When there is a potential barrier between \mathbf{r}_0 and \mathbf{r}_1 , the momentum $m\mathbf{v}$ becomes imaginary. As long as $|S|$ remains comparable with the quantum of action (Planck's constant \hbar), the probability of transition from \mathbf{r}_0 to \mathbf{r}_1 is finite. The potential barrier is not large enough to localise the particle on one side or the other. This is the tunnel effect. An insulator between two metals is just such a barrier. However, the condition on the action $S \approx \hbar$ requires the thickness of the barrier to be less than a few atomic layers, if the tunnelling probability is to remain appreciable. This can be achieved very simply for many metals, because they naturally form an oxide layer consisting of a few atomic planes [473]. We then place another metal on the other side to form a junction. Depending on the metals used, we obtain an n-i-n, s-i-n or s-i-s junction, where n and s mean normal metal or superconducting metal, respectively, and i indicates a thin layer of insulating material. The only difficulty here is that the insulating layer rarely has uniform thickness. The tunnelling amplitude decreases exponentially with thickness so that particles will tend to pass through in places where resistance is least.

We first consider the n-i-n junction. A voltage U across the junction shifts the chemical potentials μ_1 and μ_2 apart by an energy eU , as shown in Fig. 16.1. We can estimate the tunnelling current using Fermi's golden rule: the current is the product of the number of initial states N_1 contributing to the current, the density of available final states ρ_2 , and the average matrix element of the current operator between initial and final states. The number of initial states is the product of the density of states $n_1(\epsilon_F)$ with the volume V_1 and the potential difference $\mu_2 - \mu_1 = eU$ across the junction. Likewise, the density of final states is $\rho_2 = n_2(\epsilon_F)V_2$. Finally, we parametrise the matrix element of the current

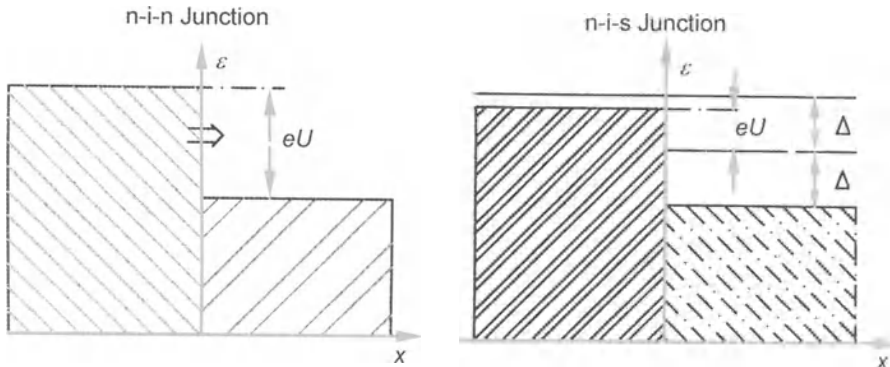


Fig. 16.1. *Left:* n-i-n junction, polarised by a potential U . *Right:* Density of states of an n-i-s junction, polarised by a potential U

$$\langle i|J_{\text{op}}|f\rangle \approx ev_F|T|^2/\hbar$$

by the transmission coefficient $|T|^2$ of the barrier (v_F is the speed of electrons at the Fermi level). We then merely divide by the area of the junction to obtain the tunnelling current:

$$J = 2\pi^2 \frac{e^2}{h} N_1 N_2 |T|^2 \frac{V_1 V_2}{S} U = GU = \frac{e^2}{h} gU, \quad (16.2)$$

where G is the conductance of the junction and g is the dimensionless conductance, measured in units of the quantum of conductance e^2/h . This formula shows that the junction behaves like an ohmic resistance, i.e., $J \propto U$.

We shall now consider an n-i-s junction between a normally conducting and a superconducting metal. On the superconducting side, electrons form Cooper pairs of binding energy 2Δ . The chemical potential of the superconductor is thus exactly in the middle of the gap. Suppose that an electron from the normal metal is transferred into the superconductor. The electron does not enter in the form of a Cooper pair and its energy is less than the quasi-particle energy by an amount Δ . In order to transport the electron, we must supply this energy, either through a voltage polarising the junction or by a photon of energy $h\nu \geq \Delta$. As the density of states $n_2(\epsilon_F)$ is zero between $\mu_2 - \Delta$ and $\mu_2 + \Delta$ (at $T = 0$), there is no available state for an electron whose energy lies within this range. The tunnelling current is therefore zero from 0 to $U = \Delta/e$. Above this value, we can use (16.2) provided that we integrate the density of states between Δ and eU ,

$$J = \frac{G}{e} \int_{\Delta}^{eU} \epsilon(\epsilon^2 - \Delta^2)^{-1/2} d\epsilon = \frac{G}{e} \sqrt{(eU)^2 - \Delta^2}. \quad (16.3)$$

This is plotted in Fig. 14.5. Equivalently, we can use the differential conductance $G_{\text{ns}} = dJ/dU = G_{nn} N_s/N_n$ as a measure of the density of states of the superconductor (see Fig. 14.3).

When we consider a junction between two identical superconductors, the same reasoning shows that there is no tunnelling current unless $eU > 2\Delta$, the energy required to break a pair. When this condition is fulfilled, we calculate the tunnelling current by integrating over both initial and final densities, $n_1(\varepsilon_F)$ and $n_2(\varepsilon_F)$, to give

$$\begin{aligned} J &= -\frac{G}{e} \int_{\Delta-eU/2}^{eU/2-\Delta} \frac{(eU/2)^2 - \varepsilon^2}{[(eU/2 + \Delta)^2 - \varepsilon^2]^{1/2} [(eU/2 - \Delta)^2 - \varepsilon^2]^{1/2}} \quad (16.4) \\ &= GU \left[E \left(\sqrt{1 - (2\Delta/eU)^2} \right) - 2(\Delta/eU)^2 K \left(\sqrt{1 - (2\Delta/eU)^2} \right) \right], \end{aligned}$$

where K and E are the elliptic integrals of first and second kind, viz.,

$$\begin{aligned} K(u) &= \int_0^{\pi/2} \frac{d\phi}{\sqrt{1 - u^2 \sin^2 \phi}}, \\ E(u) &= \int_0^{\pi/2} d\phi \sqrt{1 - u^2 \sin^2 \phi}. \quad (16.5) \end{aligned}$$

The tunnelling current is plotted in Fig. 16.2. It jumps discontinuously from 0 to $\pi J_n/4$ when the voltage reaches $2\Delta/e$.

We can also assess the current-voltage characteristic of a tunnel junction between two different superconductors with gaps Δ_1 and Δ_2 . At zero temperature, the conductance threshold is $U = (\Delta_1 + \Delta_2)/e$ and the characteristic is similar to that shown in Fig. 14.5. At non-zero temperatures, when $\Delta_1 \ll \Delta_2$ and $T \leq T_{c1}$, there are a certain number of thermally excited quasi-particles in superconductor 1 which contribute to the tunnelling conductance when $U \approx (\Delta_2 - \Delta_1)/2$ (see Fig. 16.2) [473, 474]. This gives a current peak for the following reason: further increasing the voltage above this value, the tunnelling current begins to fall because the density of states in superconductor 2

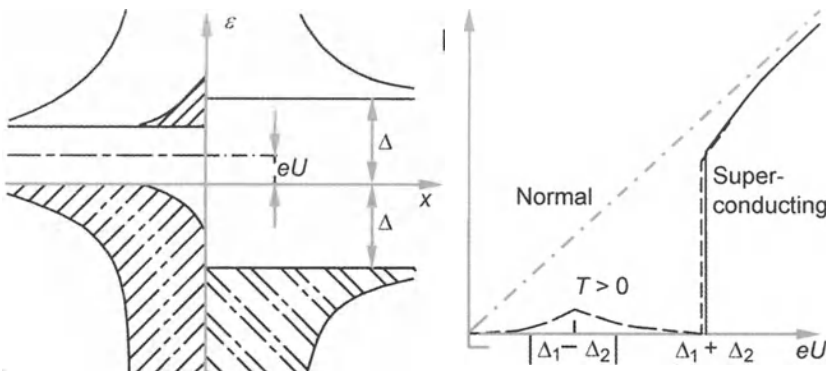


Fig. 16.2. *Left:* Density of states of an s-i-s junction at non-zero temperatures, between two superconductors of different gap. *Right:* Current-voltage characteristic for an s-i-s junction at non-zero temperatures when gaps Δ_1 and Δ_2 are very different

decreases monotonically above the gap. Finally, when $U > (\Delta_1 + \Delta_2)/e_*$, the whole density of states contributes to the tunnelling current, which therefore rises rapidly, as shown in Fig. 16.2.

16.2 The Josephson Effect

In the above discussion, we only included contributions of quasi-particles to the tunnelling current. Since these are thermally excited above the ground state, this process is no longer possible at low temperatures, unless the junction is polarised above the threshold. However, there is another process in which the two electrons making up a Cooper pair tunnel simultaneously and coherently between the two superconductors. A pair tunnel effect must necessarily couple the ground states of the two superconductors. A collective state forms between the two superconductors, which can be visualised as a superposition of their order parameters. In fact, the tunnel effect is associated with the penetration of a wave function through a barrier. The penetration of the ground state (the condensate) of one superconductor into the other is thus just as probable as the same process with regard to their quasi-particles. Saying that the two superconductors can have a common collective state amounts to saying that Cooper pairs may form with one electron in each superconductor.

The pair tunnelling probability is similar to that for individual electrons. If this coherent phenomenon corresponds to formation of a general condensate over the two superconductors, there will be a non-zero supercurrent even when the voltage (although not the phase difference) between them is zero. We can estimate the order of magnitude of this current by calculating the additional energy associated with the tunnel junction. This must be proportional to the product $\psi_1(\mathbf{r}) \times \psi_2(\mathbf{r})$, or equivalently, to $\Delta_1(\mathbf{r}) \times \Delta_2(\mathbf{r})$. The simplest expression, symmetric in $\psi_1(\mathbf{r})$ and $\psi_2(\mathbf{r})$, is

$$\begin{aligned} \mathcal{E} &= C \int dy dz \left[|\psi_1(\mathbf{r})\psi_2(\mathbf{r})| - \frac{1}{2} [\psi_1(\mathbf{r})\psi_2^*(\mathbf{r}) + \psi_1^*(\mathbf{r})\psi_2(\mathbf{r})] \right] \\ &= C \int dy dz |\psi_1(\mathbf{r})\psi_2(\mathbf{r})| [1 - \cos(\theta_1 - \theta_2)] , \end{aligned} \quad (16.6)$$

where C is a constant and the junction lies in the (y, z) -plane. The zero energy has been chosen for a phase difference $\theta_1 - \theta_2 = 0$ between the two superconductors. The energy of the junction therefore depends on the phase difference between the two superconductors. We can understand this dependence by considering the effect of applying a magnetic field, described by a vector potential $\mathbf{A} = -By\hat{\mathbf{x}}$ oriented along the normal to the junction (the x -axis). Given gauge invariance, the energy of the junction depends on the electromagnetic phase difference [see (2.25)],

$$\mathcal{E} = C \int dy dz |\psi_1(\mathbf{r})\psi_2(\mathbf{r})| \left[1 - \cos \left(\theta_1 - \theta_2 + \frac{2\pi\Phi(y)}{\Phi_0} \right) \right] , \quad (16.7)$$

where $\Phi(y) = \int_2^1 A_x dx = Byd$ is the magnetic flux between $y = 0$ and y inside a junction of thickness d . (In the following section, we shall see that we must add the London penetration depths of the two superconductors to the geometrical thickness of the junction.) We found in Sect. 2.2(I) that a sensitive dependence of energy on magnetic flux induces a current density across the junction equal to

$$j = -\frac{\delta\mathcal{E}}{\delta\Phi} = \frac{2\pi}{\Phi_0} C |\psi_1 \psi_2| \sin\left(\theta_1 - \theta_2 + \frac{2\pi\Phi(y)}{\Phi_0}\right). \quad (16.8)$$

In zero field, this takes the form of the Josephson relation

$$j = j_c \sin(\theta_1 - \theta_2). \quad (16.9)$$

In other words, a phase difference induces a current across the junction which is periodic in $\theta = \theta_1 - \theta_2$. There are many examples where the Josephson relation is not exactly sinusoidal [475], as can be seen in Fig. 16.3. To account for these deviations, we often use a parametrisation of the Josephson current inspired by the behaviour of SQUIDS:

$$j = j_c \sin \chi, \quad \chi = \theta + \alpha \sin \theta, \quad (16.10)$$

where α takes values between 0 and $+\infty$. The Josephson limit (16.9) corresponds to small values of α , whereas for $\alpha \geq 1$, the current is a non-linear and hysteretic function of θ . Each increment in the Josephson current describes a phase shift which corresponds to nucleation of a vortex in the junction and which is accompanied by energy dissipation [see Chap. 17(II)]. α parametrises dissipative effects in the tunnel junction, whatever their origins. Using the microscopic theory of the Josephson effect [477], the critical current j_c of the junction can be related to the conductance $G = 1/R$ of the normal state junction:

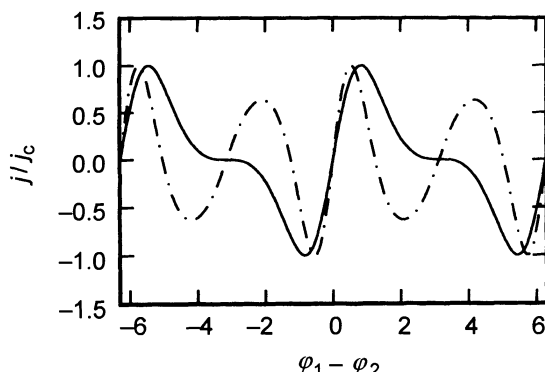


Fig. 16.3. Behaviour of a dissipative Josephson junction for $\alpha = 1$ (continuous curve) and $\alpha = 2$ (dashed curve). The parameter α measures non-linear effects in the junction which induce dissipative jumps when vortices nucleate

$$j_c = \frac{\pi}{2} G \Delta(T) \tanh \frac{\Delta(T)}{k_B T}, \quad (16.11)$$

so that in the neighbourhood of T_c ,

$$j_c = \pi \frac{\Delta^2(T)}{4 R k_B T_c}. \quad (16.12)$$

In practice, the Josephson effect can only be observed when the resistivity of the tunnel junction is sufficiently low (between 0.1Ω and $10^{-4} \Omega$). When the resistivity is higher, electromagnetic fluctuations (Nyquist noise is proportional to the resistance R) tend to destroy the Josephson current. For low resistivities, critical currents are of order $1\text{--}10^3 \text{ A/cm}^2$, much smaller than the critical currents of type II superconductors ($\approx 10^9 \text{ A/cm}^2$). For this reason, the Josephson effect is sometimes referred to as weak superconductivity.

The Josephson effect is not only observed in s-i-s junctions, but also in superconductors containing a weak link, such as the microbridge shown in Fig. 16.4. If the current through the microbridge exceeds the critical current, it then becomes normal and behaves like a Josephson junction between two superconductors [478]. This behaviour can be described using the Ginzburg–Landau theory. The equation satisfied by the normalised order parameter $f(\mathbf{r}) = \psi(\mathbf{r})/\psi_0$ in zero magnetic field is [see Sect. 13.2(II), equation (13.38)]

$$\xi_{\text{GL}}^2(T) \nabla^2 f(\mathbf{r}) + f(\mathbf{r}) - |f^2(\mathbf{r})|f(\mathbf{r}) = 0. \quad (16.13)$$

If the length of the microbridge is small compared with the coherence length ξ , the first term is $(\xi/L)^2$ times greater than the other two. Hence f satisfies the Laplace equation

$$\nabla^2 f(\mathbf{r}) = 0 \quad (16.14)$$

in the microbridge, with boundary conditions appropriate to its geometry, and asymptotic behaviour $f(\mathbf{r}) \rightarrow \exp i\theta_1$ and $f(\mathbf{r}) \rightarrow \exp i\theta_2$ far away on either side of the microbridge. We therefore seek a solution of form

$$f(\mathbf{r}) = u(\mathbf{r}) \exp i\theta_1 + [1 - u(\mathbf{r})] \exp i\theta_2, \quad (16.15)$$

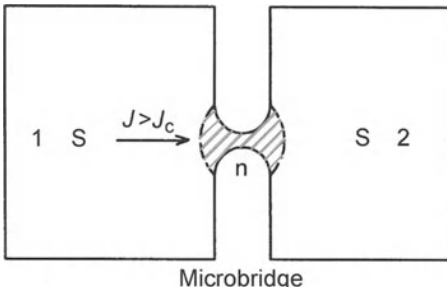


Fig. 16.4. Microbridge operating above the critical current and behaving like a Josephson junction

where the function $u(\mathbf{r})$ tends to 1 inside superconductor 1, and 0 inside superconductor 2. It is easy to check that $u(\mathbf{r})$ also satisfies Laplace's equation. Without knowing the exact form of the function $u(\mathbf{r})$, we can still calculate the current through the junction (when $\mathbf{A} = 0$),

$$\begin{aligned} j &= -i \frac{e_* \hbar}{2m_*} |\psi_0|^2 [f^*(\mathbf{r}) \nabla f(\mathbf{r}) - f(\mathbf{r}) \nabla f^*(\mathbf{r})] \\ &= \frac{e_* \hbar}{m_*} |\psi_0|^2 \nabla u(\mathbf{r}) \sin(\theta_1 - \theta_2). \end{aligned} \quad (16.16)$$

This has the same form as (16.9). The critical current is indeed proportional to $|\psi_0|^2 \propto \Delta^2$, as in (16.12) for a tunnel junction near T_c .

16.3 Microscopic Origins of the Josephson Effect

The current operator associated with tunnelling Hamiltonian H_T was given in Chap. 14(II) [see (14.75)],

$$J = -\frac{ie}{\hbar} \sum_{\mathbf{p}, \mathbf{q}, \sigma} (T_{\mathbf{pq}} a_{\mathbf{p}, \sigma}^\dagger b_{\mathbf{q}, \sigma} - T_{\mathbf{pq}}^* b_{\mathbf{q}, \sigma}^\dagger a_{\mathbf{p}, \sigma}), \quad (16.17)$$

where $a_{\mathbf{p}, \sigma}^\dagger$ and $b_{\mathbf{q}, \sigma}^\dagger$ are operators creating electrons on the left and right of the junction, respectively. The expectation value of the current operator in the BCS state $\langle \psi_{\text{BCS}} | J | \psi_{\text{BCS}} \rangle$ [see Chap. 14(II)] is zero because the momentum of the BCS state is itself zero. We must therefore pursue this calculation to second order to obtain the thermodynamic current,

$$\langle J \rangle = \langle \psi_1 | J | \psi_{\text{BCS}} \rangle + \langle \psi_{\text{BCS}} | J | \psi_1 \rangle, \quad (16.18)$$

where $|\psi_1\rangle$ is the wave function perturbed by H_T , viz.,

$$|\psi_1\rangle = \sum_m \frac{\langle m | H_T | \psi_G \rangle}{E_G - E_m + i\eta} |\psi_m\rangle. \quad (16.19)$$

The sum is taken over all excited quasi-particle states above the ground state $|G\rangle \equiv |\text{BCS}\rangle$. Using the expressions for H_T and J , we obtain the Josephson current explicitly [479],

$$\begin{aligned} J &= -\frac{ie}{\hbar} \sum_{\mathbf{p}, \mathbf{q}, \mathbf{p}', \mathbf{q}', \sigma, m} \left[\frac{T_{\mathbf{pq}} T_{\mathbf{p}'\mathbf{q}'}^*}{D_m} \langle G | a_{\mathbf{p}, \sigma}^\dagger b_{\mathbf{q}, \sigma} | m \rangle \langle m | a_{\mathbf{p}', \sigma'}^\dagger b_{\mathbf{q}', \sigma'} | G \rangle \right. \\ &\quad \left. - \frac{T_{\mathbf{pq}}^* T_{\mathbf{p}'\mathbf{q}'}^*}{D_m} \langle G | b_{\mathbf{p}, \sigma}^\dagger a_{\mathbf{q}, \sigma} | m \rangle \langle m | b_{\mathbf{p}', \sigma'}^\dagger a_{\mathbf{q}', \sigma'} | G \rangle \right], \end{aligned} \quad (16.20)$$

where the energy denominator D_m is given by

$$D_m^{-1} = (E_G - E_m + i\eta)^{-1} + (E_G - E_m - i\eta)^{-1}. \quad (16.21)$$

Each term involves the destruction of two particles on one side of the junction ($b_{\mathbf{q}} b_{\mathbf{q}'}$) and the appearance of two particles on the other side ($a_{\mathbf{p}}^\dagger a_{\mathbf{p}'}^\dagger$). This is indeed a description of Cooper pair tunnelling. In the tunnelling current, we neglected terms which only involve quasi-particles ($a^\dagger b)(b^\dagger a)$; these give rise to the usual tunnelling current, discussed in Sect. 16.1. We continue calculation of the Josephson current by rewriting operators a and b in terms of superconductor quasi-particles c and d . This is done using the Bogoliubov transformation (14.28) [see Chap. 14(II)]. We assume that amplitudes u and v are complex and related by the phase of the order parameters of the two superconductors,

$$|u_{\mathbf{p}}| = |v_{\mathbf{p}}| \exp i\phi_1, \quad |u_{\mathbf{q}}| = |v_{\mathbf{q}}| \exp i\phi_2. \quad (16.22)$$

Moreover, time reversal symmetry of the tunnelling Hamiltonian leads to symmetry relations $T_{\mathbf{p}, \mathbf{q}} = T_{-\mathbf{p}, -\mathbf{q}}^*$. We then group terms to obtain the Josephson current

$$\begin{aligned} J = 4 \frac{e}{\hbar} \sum_{\mathbf{p}, \mathbf{q}} |T_{\mathbf{pq}}|^2 & (u_{\mathbf{p}}^* v_{\mathbf{p}} u_{\mathbf{q}} v_{\mathbf{q}}^* - u_{\mathbf{p}} v_{\mathbf{p}}^* u_{\mathbf{q}}^* v_{\mathbf{q}}) \\ & \left[\frac{n_{\mathbf{p}} n_{\mathbf{q}}^\dagger}{E_{\mathbf{p}} - E_{\mathbf{q}}} - \frac{n_{\mathbf{p}} n_{\mathbf{q}}}{E_{\mathbf{p}} + E_{\mathbf{q}}} + \frac{n_{\mathbf{p}}^\dagger n_{\mathbf{q}}^\dagger}{E_{\mathbf{p}} + E_{\mathbf{q}}} - \frac{n_{\mathbf{q}}^\dagger n_{\mathbf{p}}}{E_{\mathbf{p}} - E_{\mathbf{q}}} \right], \end{aligned} \quad (16.23)$$

where $n_{\mathbf{p}} = c_{\mathbf{p}}^\dagger c_{\mathbf{p}}$ and $n_{\mathbf{q}} = d_{\mathbf{q}}^\dagger d_{\mathbf{q}}$ are quasi-particle occupation number operators. The conjugate operators $n_{\mathbf{p}}^\dagger$ can be reexpressed as $n_{\mathbf{p}}^\dagger = 1 - n_{\mathbf{p}}$ using operator commutation relations. Likewise, definitions (14.35) of coherence factors $u_{\mathbf{p}}$ and $v_{\mathbf{p}}$ give an expression for $|u_{\mathbf{p}}||v_{\mathbf{p}}| = |\Delta|/2E_{\mathbf{p}}$ in terms of the quasi-particle energy $E_{\mathbf{p}} = \sqrt{\xi_{\mathbf{p}}^2 + \Delta^2}$ in the BCS theory. We then define the angular average of the tunnelling matrix element

$$|T|^2 = \frac{V_1 V_2}{S} \int \frac{d\Omega_{\mathbf{p}}}{2\pi} \frac{d\Omega_{\mathbf{q}}}{2\pi} |T_{\mathbf{pq}}|^2, \quad (16.24)$$

where $d\Omega_{\mathbf{p}}$ and $d\Omega_{\mathbf{q}}$ are solid angles in the directions of vectors \mathbf{p} and \mathbf{q} . Normalisation factors have been taken into account in replacing the discrete sum by the integral over all possible directions of vectors \mathbf{p} and \mathbf{q} on the Fermi surface. Finally, expressing the superconductor density of states in the form $n_s(\xi) = n(\varepsilon_F)|\xi|/E(\xi)$ and Fermi factors in terms of hyperbolic tangents, we obtain the Josephson current in the form

$$\begin{aligned} J_s = -\frac{2e}{\hbar} |T|^2 \frac{V_1 V_2}{S} \sin(\phi_1 - \phi_2) n_1(\varepsilon_F) n_2(\varepsilon_F) \Delta_1 \Delta_2 \\ \int_{\Delta_1}^{\infty} \int_{\Delta_2}^{\infty} dE_1 dE_2 \frac{E_1 \tanh(\beta E_1/2) - E_2 \tanh(\beta E_2/2)}{(E_1^2 - E_2^2)(E_1^2 - \Delta_1^2)^{1/2}(E_2^2 - \Delta_2^2)^{1/2}}. \end{aligned} \quad (16.25)$$

The integral over E_1 and E_2 can be calculated explicitly by the residue method. The conductance G_n of the normal state junction is

$$G_n = 2\pi^2 n_1(\varepsilon_F) n_2(\varepsilon_F) |T|^2 \frac{V_1 V_2}{S} \frac{e^2}{h} = g \frac{e^2}{h}. \quad (16.26)$$

We do therefore retrieve the form $J = J_c \sin(\phi_1 - \phi_2)$ for the Josephson current, where the critical current J_c can now be expressed in terms of the conductance of the junction, and the superconductor gaps Δ_1 and Δ_2 ,

$$J_c = \frac{2G}{e} \frac{\Delta_1 \Delta_2}{\Delta_1 + \Delta_2} K \left(\frac{|\Delta_1 - \Delta_2|}{\Delta_1 + \Delta_2} \right). \quad (16.27)$$

This is the Ambegaokar-Baratoff formula [477]. We can not only obtain the Josephson effect from the microscopic theory, but also its exact dependence on temperature and the parameters of the superconductors.

16.4 The Josephson Effect in a Magnetic Field

Apply a magnetic field of induction $B(x)\hat{z}$ along the z -axis in the plane of the junction, as shown in Fig. 16.5. The vector potential in the Landau gauge is

$$\mathbf{A} = -B(x)y\hat{x}. \quad (16.28)$$

In the insulating layer, $B(x)$ varies only slightly, and on either side, it decreases as $\exp(-x/\lambda)$. The phase difference induced by the magnetic field is of order

$$\int_2^1 A_x dx = B(0)yl, \quad (16.29)$$

where $l = 2\lambda(T) + d$ is dominated by the London penetration length $\lambda(T)$. The current density in the junction when there is an applied field is therefore

$$j = j_c \sin \left(\theta_1 - \theta_2 + \frac{2\pi B y l}{\Phi_0} \right). \quad (16.30)$$

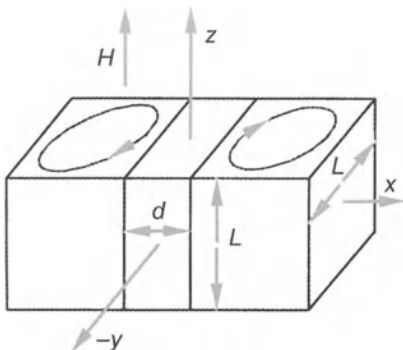


Fig. 16.5. Geometry of a Josephson junction in a magnetic field. Screening currents in the superconductors have been represented on their surfaces

The current density varies over the whole width L_y of the junction, even changing sign. Indeed, the Josephson current tries to screen the magnetic field in the junction. In practice, it is the total current

$$\begin{aligned} I &= L_z \int_0^{L_y} j(y) dy \\ &= j_c \frac{\Phi_0 L_z}{Bl} \left[\cos(\theta_1 - \theta_2) - \cos \left(\theta_1 - \theta_2 + \frac{2\pi BL_y l}{\Phi_0} \right) \right] \\ &= I_c \frac{\Phi_0}{\pi\Phi} \sin \frac{\pi\Phi}{\Phi_0} \sin \left(\theta_1 - \theta_2 + \frac{\pi\Phi}{\Phi_0} \right), \end{aligned} \quad (16.31)$$

which we actually measure. In this expression, $I_c = j_c L_y L_z$ is the critical current of the junction. Whatever the phase difference $\theta_1 - \theta_2$, the current vanishes each time the flux in the junction is a whole number of flux quanta [481]. If we adjust the phase difference $\theta_1 - \theta_2$, the maximal current I_{\max} that the junction can carry is given by

$$I_{\max} = I_c \left| \frac{\sin(\pi\Phi/\Phi_0)}{\pi\Phi/\Phi_0} \right|. \quad (16.32)$$

In practice, the curve plotted in Fig. 16.6 is used to determine the magnetic thickness of the junction, $l = d + 2\lambda(T) \approx 2\lambda(T)$, and hence the penetration depth.

In wide Josephson junctions, the magnetic field induced by the Josephson current can no longer be neglected. Let

$$\theta = \theta_1 - \theta_2 + 2\pi \int_2^1 A_x dx / \Phi_0$$

be the electromagnetic phase determining the Josephson current. Between y and $y + \delta y$, the phase difference across the junction increases by an amount

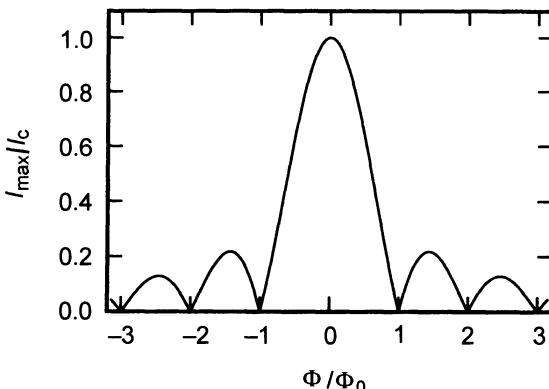


Fig. 16.6. Variation of the maximal Josephson current with magnetic flux in the junction. The curve is the same as for the light intensity diffracted by a slit in optics

$$\theta(y + \delta y) - \theta(y) = \frac{2\pi B(y)}{\Phi_0} l \delta y . \quad (16.33)$$

The magnetic induction is therefore proportional to the gradient of the Josephson phase,

$$B(y) = \frac{\Phi_0}{2\pi l} \frac{\partial \theta}{\partial y} . \quad (16.34)$$

In addition, Ampère's theorem relates the magnetic field to the current:

$$j_x = \frac{\partial H}{\partial y} , \quad (16.35)$$

which can be equated with the Josephson current $j = j_c \sin \theta$ in the junction. Substituting in the two previous equations, we find that the Josephson phase satisfies the pendulum equation

$$\frac{\partial^2 \theta}{\partial y^2} = \frac{\sin \theta}{\lambda_J^2} , \quad (16.36)$$

where the Josephson length λ_J is

$$\lambda_J = \sqrt{\frac{\Phi_0}{2\pi l j_c \mu_0}} . \quad (16.37)$$

To begin with, let us assume that the flux in the junction remains small compared with the flux quantum, and that the phase difference $\theta = \theta_1 - \theta_2 \approx 0$ is negligible. In this case the Josephson angle is small and we can linearise (16.36). The solution is an exponential:

$$\theta = \theta_0 \exp(-y/\lambda_J) , \quad H = -j_c \lambda_J \exp(-y/\lambda_J) . \quad (16.38)$$

In this limit, the Josephson current can screen the applied field over a length λ_J . For a critical Josephson current of 10^2 A/cm², the screening length $\lambda_J \approx 10^{-2}$ cm = 100 μm is much longer than the penetration depth λ_L . The junction may be considered as narrow when screening is negligible, i.e., if $L_y \ll \lambda_J$. In the opposite limit, there exists a weak Meissner effect. In the large magnetic field limit, we can use the first integral of the pendulum equation,

$$\left(\frac{\partial \theta}{\partial y} \right)^2 = k_0^2 - \frac{2}{\lambda_J^2} \cos \theta , \quad (16.39)$$

$$y - y_0 = \int_{\pi}^{\theta} d\phi \left(k_0^2 - \frac{2}{\lambda_J^2} \cos \phi \right)^{-1/2} , \quad (16.40)$$

to understand the physical behaviour of the phase in the junction. The integration constant k_0 is the maximal angular frequency in the junction. When it is very large, the Josephson phase increases linearly across the junction. This is the limit in which we neglect screening by the Josephson current and

kinetic energy dominates potential energy in the pendulum analogy. There is a soliton-type solution, obtained by choosing $k_0^2 = 2/\lambda_J^2$,

$$\theta(y) = 4 \arctan \left[\exp \left(\frac{y - y_0}{\lambda_J} \right) \right], \quad (16.41)$$

which describes a vortex centred at y_0 . The flux enclosed by this vortex,

$$\Phi = l \int_{-\infty}^{\infty} B(y) dy = l \frac{\Phi_0}{2\pi l} [\theta(\infty) - \theta(-\infty)] = \Phi_0, \quad (16.42)$$

is indeed equal to one flux quantum. A Josephson junction in a magnetic field therefore resembles a 2-dimensional type II superconductor, since vortices start to appear at the field value

$$H_{c1} = \frac{2\Phi_0}{\pi^2 \mu_0 \lambda_J l}. \quad (16.43)$$

When there are several vortices in the junction, interactions between them can significantly alter their structure.

16.5 The AC Josephson Effect

When the current is greater than the critical value J_c , superconductivity is destroyed near the junction and a voltage appears. The time dependence of the order parameter on either side of the junction is $\psi_1(t) \propto \exp(-i\mu_1 t/\hbar)$ and $\psi_2(t) \propto \exp(-i\mu_2 t/\hbar)$, where the difference in chemical potential between the two superconductors is imposed by the potential difference: $\mu_2 - \mu_1 = 2eU = -2|e|U$ [482, 483]. (A thermal gradient can also induce a difference in chemical potential. The difference in chemical potential is that of pairs, which can differ from that of quasi-particles in a non-equilibrium situation [see Chap. 17(II)].) If we neglect the vector potential arising from the current, the phase difference between the two superconductors is

$$\theta_2 - \theta_1 = -\frac{(\mu_2 - \mu_1)t}{\hbar} = \frac{2|e|Ut}{\hbar}, \quad (16.44)$$

$$\frac{d\theta}{dt} = -\frac{\mu_2 - \mu_1}{\hbar} = \frac{2|e|U}{\hbar}. \quad (16.45)$$

This relation can be viewed as a consequence of gauge invariance. Adding a phase θ to the wave function, the vector potential and electrostatic potential U must be simultaneously modified by

$$\mathbf{A} \rightarrow \mathbf{A} + \frac{2\pi}{\Phi_0} \nabla \theta, \quad U \rightarrow U - \frac{2\pi}{\Phi_0} \frac{\partial \theta}{\partial t}, \quad (16.46)$$

in order to leave equations of motion and physical fields

$$\mathbf{E} = -\frac{\partial \mathbf{A}}{\partial t} - \nabla U, \quad \mathbf{B} = \nabla \times \mathbf{A}, \quad (16.47)$$

invariant. Equation (16.45) then follows from (16.46).

If the voltage is constant, the phase θ grows linearly in time and the Josephson current across the junctions oscillates in time according to

$$j = j_c \sin \left(\theta_0 + \frac{2\pi U}{\Phi_0} t \right), \quad (16.48)$$

at the Josephson frequency

$$f_J = \frac{\omega_J}{2\pi} = \frac{2eU}{h} = \frac{U}{\Phi_0}. \quad (16.49)$$

This takes the value 483.6 GHz for a voltage of 1 mV. Above the critical current, the Josephson junction acts as a voltage-frequency converter. It can therefore be used as a voltage standard. Indeed, the conversion factor is just the flux quantum, known to very great accuracy. At the present time, the definition of the volt is based on the AC Josephson effect. Its accuracy has been tested by comparing the Josephson frequencies of two junctions made from different superconductors. The measured difference $|\Delta f_J|/f_J \leq 10^{-16}$ [484] gives some idea of the precision of the Josephson effect! Finally, the switching time between superconducting ($j < j_c$) and resistive ($j > j_c$) states of the junction is of order $1/f_J \leq 10$ ps. Semiconductor circuits are still no rival for the speed of these Josephson circuits, which are mainly used for military purposes, due to their high cost. In practice, the voltage U is measured at fixed current. The latter comprises the Josephson current and a normal (ohmic) component which is of order U/R when $U \gg 2\Delta$. The total current is then

$$j = j_c \sin \theta + \frac{\hbar}{2eR} \frac{\partial \theta}{\partial t}. \quad (16.50)$$

This equation can be inverted and integrated to give the Josephson phase as a function of current:

$$\theta = 2 \arctan \left[\sqrt{1 - \left(\frac{j_c}{j} \right)^2} \tan \left(\frac{\sqrt{j^2 - j_c^2} e R t}{\hbar} \right) + \frac{j_c}{j} \right]. \quad (16.51)$$

This in turn specifies the voltage $U(t) = (\Phi_0/2\pi)\partial\theta/\partial t$ across the junction for fixed current j [478],

$$U(t) = R \frac{j^2 - j_c^2}{j + j_c \cos(\omega t - \theta_1)}, \quad (16.52)$$

where

$$\omega = \frac{2\pi R}{\Phi_0} \sqrt{j^2 - j_c^2}, \quad \theta = \arccos \left(\frac{j_c}{j} \right). \quad (16.53)$$

When the current is much greater than the critical value, the junction is ohmic. However, near j_c , the amplitude of the alternating voltage is close to Rj_c , as can be seen from Fig. 16.7. The average voltage across the junction is then [485, 486]

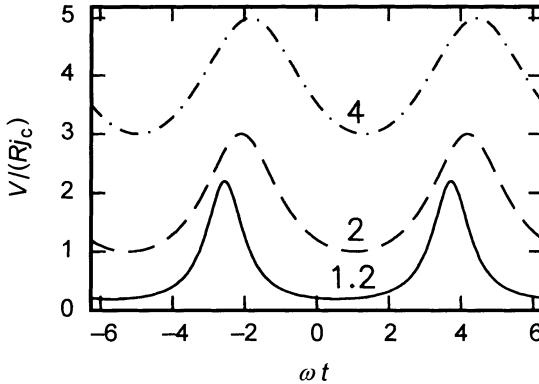


Fig. 16.7. Voltage across a Josephson junction at constant current above the critical current j_c . The three curves correspond to $j = 1.2j_c$, $j = 2j_c$ and $j = 4j_c$, respectively

$$\overline{U} = \frac{1}{2\pi} \int_0^{2\pi} U(\phi) d\phi = R\sqrt{j^2 - j_c^2} = \frac{\hbar\omega}{2e}. \quad (16.54)$$

We shall consider the opposite problem, in which an alternating voltage is applied to the junction:

$$U(t) = U_0 + v \cos \Omega t. \quad (16.55)$$

We wish to find the current in the junction. The second Josephson equation (16.45) gives the phase as the integral of the voltage,

$$\theta(t) = \frac{2\pi}{\Phi_0} (U_0 t + \frac{v}{\Omega} \sin \Omega t + \theta_0). \quad (16.56)$$

The Josephson current is then given by

$$\begin{aligned} \frac{j}{j_c} &= \sin \theta(t) \\ &= \sin \left[\frac{2\pi}{\Phi_0} (U_0 t + \theta_0) \right] \cos \left(\frac{v}{\Phi_0 f} \sin \Omega t \right) \\ &\quad + \cos \left[\frac{2\pi}{\Phi_0} (U_0 t + \theta_0) \right] \sin \left(\frac{v}{\Phi_0 f} \sin \Omega t \right). \end{aligned} \quad (16.57)$$

Anharmonic terms can be expanded in Fourier series,

$$\cos(a \sin \Omega t) = A_0 + 2 \sum_{n=1}^{\infty} A_{2n} \cos 2n\Omega t, \quad (16.58)$$

$$\sin(a \sin \Omega t) = 2 \sum_{n=1}^{\infty} B_{2n-1} \sin(2n-1)\Omega t, \quad (16.59)$$

where coefficients $A_{2n} = J_{2n}(a)$ and $B_{2n-1} = J_{2n-1}(a)$ are Bessel functions with argument $a = v/\Phi_0 f$. In the expression for the current, we find terms of type

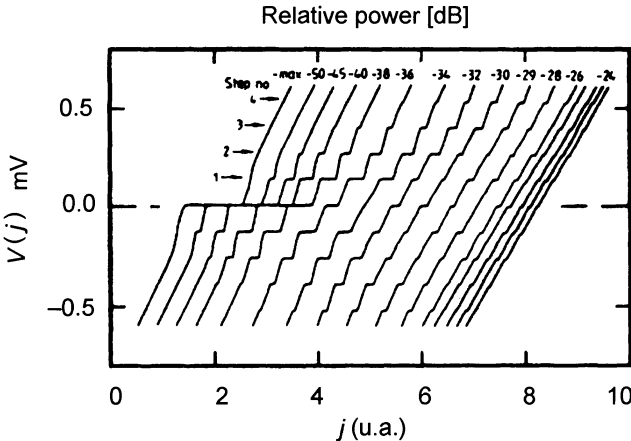


Fig. 16.8. $U(j)$ characteristic for an s-i-s junction. Each curve corresponds to one amplitude v of the alternating voltage, and they are shifted horizontally relative to one another. The two current directions $+j$ and $-j$ are plotted on each curve

$$j_c J_n(a) \sin \left[\left(\frac{2\pi U_0}{\Phi_0} \pm n\Omega \right) t + \theta_0 \right]. \quad (16.60)$$

Each time the voltage reaches the value $U_0 = n\Phi_0 f$, there is a time independent term of amplitude

$$|\bar{j}_n| = j_c J_n(a) \sin \theta_0. \quad (16.61)$$

There are resonances in the curve $j(U)$, in addition to the quasi-particle current studied at the beginning of this chapter [487]. Experimenters often prefer to measure $U(j)$. This exhibits hysteresis effects because resonances in the curve $j(U)$ lead to several possible values of U for the same j . As experiments show, these resonances appear as steps in the $U(j)$ curve, known as Shapiro steps after their discoverer. These steps can be understood as regions in which the AC Josephson current is synchronised with harmonics of the applied frequency Ω . The current-voltage characteristic of an Ni-Ni junction, observed experimentally by Grimes and Shapiro [489], is shown in Fig. 16.8. The Shapiro steps are clearly visible.

16.6 Quantum Interferometers. The AC SQUID

Josephson circuits are now commonly used to measure magnetic fields by interferometry. Applications are not limited to research and development. Earthquakes are usually preceded by large fluctuations in the terrestrial magnetic field in the region of the epicentre. In principle, this provides roughly 36 hours' notice before the quake. Observation stations have been set up in

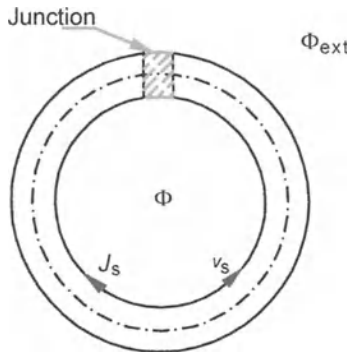


Fig. 16.9. An AC SQUID is made of a Josephson junction inserted into a superconducting ring. The supercurrent circulates in the opposite direction to the phase gradient $\theta = \theta_1 - \theta_2$

California to monitor the Earth's magnetic field, and the Japanese are beginning a similar programme. Another interesting application is measurement of the magnetic fields produced by the human heart and brain [490, 491]. This is useful in study of cerebral activity and in detection of certain pathologies, such as heart failure and epilepsy. The advantage of this type of instrumentation is its high sensitivity and non-invasiveness (other techniques used for brain studies require electrodes to be placed on the cortex).

The interferometers used in such applications are AC and DC SQUIDs, Superconducting QUantum Interference Devices. The AC SQUID comprises a superconducting ring in which a Josephson junction has been introduced, as shown in Fig. 16.9 [492, 493, 494]. These interferometers are based on the relation between phase difference across the junction and enclosed flux. Since the current is zero inside the superconductor, the line integral of the second Ginzburg–Landau equation along a path joining each side of the junction is zero. Hence,

$$0 = \int_1^2 \nabla\theta \cdot dl + \frac{2\pi}{\Phi_0} \int_1^2 \mathbf{A} \cdot dl \approx \theta_2 - \theta_1 \pm 2n\pi + 2\pi \frac{\Phi}{\Phi_0}, \quad (16.62)$$

where we have approximated the line integral $\int_1^2 \mathbf{A} \cdot dl \approx \oint \mathbf{A} \cdot dl = 2\pi\Phi/\Phi_0$. This amounts to neglecting the magnetic flux inside the junction. For small phase differences $\theta = \theta_2 - \theta_1$, we can also integrate the second Ginzburg–Landau equation across the junction, giving

$$\begin{aligned} \theta_2 - \theta_1 &\approx \int_1^2 \nabla\theta \cdot dl + \frac{2\pi}{\Phi_0} \int_1^2 \mathbf{A} \cdot dl \\ &\approx e_* \Lambda_L \oint j_s \cdot dl \approx e_* \Lambda_L j_s l. \end{aligned} \quad (16.63)$$

The charge $e_* = -2|e|$ of a Cooper pair is negative, so the Josephson current j_s across the junction circulates in the opposite direction to the phase gradient. Combining the relation

$$2\pi \left(n - \frac{\Phi}{\Phi_0} \right) = 0 \quad (16.64)$$

between phase difference and flux with the Josephson relation, we obtain the current in the SQUID as

$$j_s = -j_c \sin \theta = -j_c \sin \frac{2\pi\Phi}{\Phi_0} . \quad (16.65)$$

We cannot determine the flux Φ_{ext} applied to the SQUID from this relation alone, because the Josephson current screens the flux to a certain extent. The simplest way to assess screening is to introduce the inductance L of the circuit, similar to the inductance of a single turn of a coil,

$$L = \mu_0 r \ln(r/a) . \quad (16.66)$$

For a diameter of 3 mm, L is of order 3×10^{-9} H. The flux enclosed inside the ring can then be related to the applied flux by

$$\Phi = \Phi_{\text{ext}} + L j_s . \quad (16.67)$$

Provided the current remains below the critical value, we can use (16.65) to obtain

$$\frac{2\pi\Phi}{\Phi_0} + \frac{2\pi L j_c}{\Phi_0} \sin \frac{2\pi\Phi}{\Phi_0} = \frac{2\pi\Phi_{\text{ext}}}{\Phi_0} . \quad (16.68)$$

If this were not so, a flux quantum would enter the ring and j_s would decrease abruptly by Φ_0/L . We observe that $\Phi = \Phi_{\text{ext}}$ whenever Φ is a half-integral multiple of the flux quantum. The behaviour of Φ/Φ_0 as a function of Φ_{ext}/Φ_0 depends crucially on the value of $L j_c/\Phi_0$, as can be seen by calculating the derivative

$$\frac{d\Phi}{d\Phi_{\text{ext}}} = \left(1 + \frac{2\pi L j_c}{\Phi_0} \cos \frac{2\pi\Phi}{\Phi_0} \right)^{-1} . \quad (16.69)$$

If $2\pi L j_c < \Phi_0$, the slope of Φ as a function of Φ_{ext} is always positive. Otherwise, the slope changes sign by going through $\pm\infty$, and the enclosed flux can assume several possible values for each value of Φ_{ext} , as shown in Fig. 16.10. When $2\pi L j_c \gg \Phi_0$, screening currents are large and the enclosed flux is initially reduced to $\Phi \approx \Phi_{\text{ext}}/(1+2\pi L/\Phi_0)$. In practice, the inductance is chosen so that $2\pi L j_c \geq \Phi_0$. Two coils are adjoined to the AC SQUID. The first coil couples the magnetic flux Φ_{ext} which we wish to measure. The second coil modulates the magnetic flux at a high frequency around $\Phi_{\text{ext}}^{\text{dc}}$, with large enough amplitude $\Phi_{\text{ext}}^{\text{rf}}$ to make the enclosed flux Φ follow a hysteresis curve when expressed in terms of

$$\Phi_{\text{ext}} = \Phi_{\text{ext}}^{\text{dc}} + \Phi_{\text{ext}}^{\text{rf}} \cos \omega t .$$

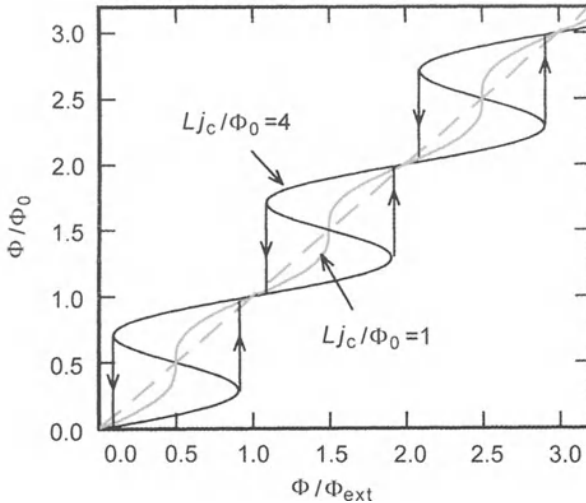


Fig. 16.10. Behaviour of Φ/Φ_0 as a function of Φ_{ext}/Φ_0 for three different values of Lj_c/Φ_0 . Vertical lines correspond to flux increments when a flux quantum enters the ring

This coil is part of a resonant circuit with high quality factor. Associated with the area enclosed within the hysteresis curve $\Phi(\Phi_{\text{ext}})$, there is dissipation which affects the quality factor. The latter can then be measured. More precisely, the work done on the SQUID to change Φ_{ext} is $dW = -HdB = -J_s d\Phi_{\text{ext}}$, that is

$$dW = -J_s d\Phi_{\text{ext}} = \frac{1}{L} (-LJ_s) d\Phi_{\text{ext}} = \frac{1}{L} (\Phi_{\text{ext}} - \Phi) d\Phi_{\text{ext}}. \quad (16.70)$$

The energy dissipated is thus

$$W = \frac{1}{2L} \left[\langle \Phi_{\text{ext}}^2 \rangle - \left\langle \oint \Phi d\Phi_{\text{ext}} \right\rangle \right]. \quad (16.71)$$

The first term is

$$\frac{1}{2L} \left(\Phi_{\text{ext}}^{\text{dc}2} + \frac{1}{2} \Phi_{\text{ext}}^{\text{rf}2} \right)$$

and therefore varies with $\Phi_{\text{ext}}^{\text{dc}}$, whilst the second term measures the area enclosed in one of the loops of Fig. 16.10 and does not change over a certain range of values of $\Phi_{\text{ext}}^{\text{dc}}$. In practice, a counteraction is introduced which injects a flux in such a way as to balance the applied flux $\Phi_{\text{ext}}^{\text{dc}}$. The static flux can then be kept zero (flux locking). By this method, magnetic fluxes can be measured to an accuracy greater than $10^{-5}\Phi_0$, i.e., 2×10^{-20} Wb. For a coil of diameter 1 cm, this flux corresponds to a magnetic induction of 2×10^{-12} G. With such extreme sensitivity, very small variations in magnetic field can be detected. Currents can also be measured, by injecting them into

the SQUID coupling coil. In a resistance measurement using a bridge, we try to reduce a current to zero by varying a reference resistance. We can once again use a SQUID to detect the current zero. However, we should remember that Nyquist noise $\bar{v}^2 = \sqrt{4k_B RT} \Delta f$ in the resistance to be measured increases with the value of the resistance (and the temperature). For this reason, the SQUID is particularly useful when measuring low resistances at low temperatures.

16.7 Flux Transformers

In magnetisation measurements, it is rarely possible, or even desirable, to put the sample or the patient into a SQUID. Flux quantisation is used to transfer the relevant magnetisation into the SQUID. We use two superconducting coils of inductances L_{input} and L_{signal} , connected by an entirely superconducting circuit. The total flux through both coils must be kept constant; that is, if the flux in the signal coil increases because of the magnetisation being measured, then the flux in the other coil must go down in such a way that the total flux in the circuit remains the same. It suffices to place the input coil around the SQUID to detect the signal. Quantitatively speaking, if we apply flux Φ_{ext} in a signal coil with N turns, the current induced in the circuit is

$$N\Phi_{\text{ext}} = (L_{\text{signal}} + L_{\text{input}})J = 0. \quad (16.72)$$

If M is the coefficient of mutual inductance between the SQUID and the input coil, the flux coupled inside the SQUID is

$$\Phi_{\text{SQUID}} = \frac{MN\Phi_{\text{ext}}}{L_{\text{signal}} + L_{\text{input}}}. \quad (16.73)$$

In practice, three coils are used. Two of them are identical but wound in opposite directions. They are placed in the uniform magnetic field which magnetises the sample under investigation. When the sample is not present, no flux is induced since the windings are balanced. The sample is then placed in one of the coils so that the total flux produced by the uniform field is only proportional to the magnetisation of the sample. Figure 16.11 shows a typical experimental arrangement, but there exist many variations (e.g., plane structures, multiple-coil structures) depending on the type of measurement required.

16.8 Mechanical Analogy for the AC SQUID

Static and dynamic properties of the AC SQUID can be described through a mechanical model suggested by Anderson [495]. The Hamiltonian of the AC SQUID contains three contributions,

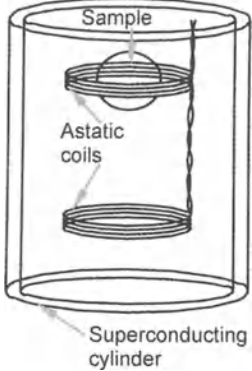


Fig. 16.11. Astatic configuration: two coils wound in opposite directions, each with inductance $L_{\text{signal}}/2$. The magnetic field can be trapped in a superconducting tube, as shown here, or be applied by an outer coil

$$\mathcal{H} = \mathcal{H}_M + \mathcal{H}_E + \mathcal{H}_J . \quad (16.74)$$

$\mathcal{H}_M = LJ_s^2/2$ is the magnetic energy of screening currents, \mathcal{H}_E the electrical energy in the capacitance formed by the tunnel junction (neglected up to now), and \mathcal{H}_J the Josephson coupling energy (16.6). Using (16.64), the magnetic energy is

$$\begin{aligned} \mathcal{H}_M &= \frac{(LJ_s)^2}{2L} = \frac{(\Phi_{\text{ext}} - \Phi)^2}{2L} = \frac{\Phi_0^2}{8\pi^2 L} \left(\frac{2\pi\Phi_{\text{ext}}}{\Phi_0} - \frac{2\pi\Phi}{\Phi_0} \right)^2 \\ &= \frac{\Phi_0^2}{8\pi^2 L} \left(\frac{2\pi\Phi_{\text{ext}}}{\Phi_0} - \theta + 2n\pi \right)^2 . \end{aligned} \quad (16.75)$$

The capacitance energy is found from the Josephson relation to be

$$\mathcal{H}_E = \frac{CU^2}{2} = \frac{C}{2} \left(\frac{d\Phi}{dt} \right)^2 = \frac{C\Phi_0^2}{8\pi^2} \left(\frac{d\theta}{dt} \right)^2 . \quad (16.76)$$

Concerning the Josephson coupling, the extra energy in the condensate induced by a phase difference θ across the junction is

$$\mathcal{H}_J = \frac{j_c\Phi_0}{2\pi} (1 - \cos \theta) = \frac{j_c\Phi_0}{2\pi} \left(1 - \cos \frac{2\pi\Phi}{\Phi_0} \right) . \quad (16.77)$$

The only dynamical variable in the total AC SQUID Hamiltonian is $\phi = 2\pi\Phi/\Phi_0$, which can be interpreted here as the collective coordinate of the condensate:

$$\mathcal{H} = \frac{\Phi_0^2}{8\pi^2 L} (\phi_{\text{ext}} - \phi)^2 + \frac{C\Phi_0^2}{8\pi^2} \left(\frac{d\phi}{dt} \right)^2 + \frac{j_c\Phi_0}{2\pi} (1 - \cos \phi) . \quad (16.78)$$

Dissipation is essential to the correct operation of the SQUID, whether it be associated with quasi-particle tunnelling current or Josephson radiation. It is given simply in terms of a resistance R across the terminals of the junction:

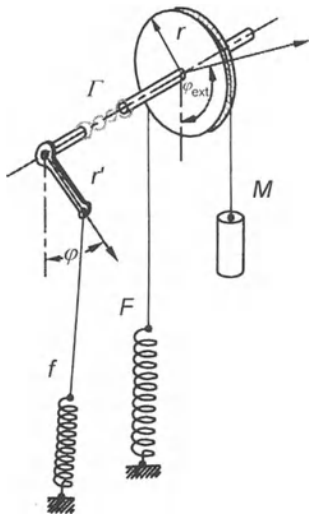


Fig. 16.12. Mechanical analogy for the SQUID (from Varoquaux, E.)

$$\frac{dW}{dt} = \frac{U^2}{R} = \frac{1}{R} \left(\frac{d\Phi}{dt} \right)^2 = \frac{\Phi_0^2}{4\pi^2 R} \left(\frac{d\phi}{dt} \right)^2. \quad (16.79)$$

The mechanical analogy is illustrated in Fig. 16.12. The system consists of a pendulum with moment of inertia I , for which the restoring force f is supplied by a spring. The angle ϕ which plays the role of the reduced flux $\phi = 2\pi\Phi/\Phi_0$ in the SQUID, marks the position of the pendulum. The pendulum is driven by a flywheel via a spring of stiffness Γ . The angular position of the flywheel plays the role of the external flux. The flywheel can itself be driven by a motor at constant angular speed $\phi_{\text{ext}} = \omega t$, or by the combination of the mass M and the spring F shown in the figure, which gives it a large amplitude ($> 2\pi$) sinusoidal motion. The Hamiltonian for this system includes the elastic energy of the spring Γ , and the kinetic and potential energies of the pendulum,

$$\mathcal{H} = \frac{\Gamma}{2}(\phi_{\text{ext}} - \phi)^2 + \frac{I}{2} \left(\frac{d\phi}{dt} \right)^2 + f(1 - \cos \phi). \quad (16.80)$$

The equation of motion is then

$$\Gamma(\phi_{\text{ext}} - \phi) = f \sin \phi + I \frac{d^2\phi}{dt^2} + \eta \frac{d\phi}{dt}, \quad (16.81)$$

where we have put in a phenomenological term η to describe friction. The dynamical equation for the AC SQUID is identical if we make the correspondence between magnetic and kinetic energies, capacitance energy and energy of the coupling spring Γ , and Josephson energy and potential energy of the pendulum:

$$\begin{aligned}
 \frac{\Phi_{\text{ext}} - \Phi}{L} &= j_c \sin \frac{2\pi\Phi}{\Phi_0} + C \frac{d^2\Phi}{dt^2} + \frac{1}{R} \frac{d\Phi}{dt} \\
 &= j_c \sin \theta + C \frac{dU}{dt} + \frac{U}{R} \\
 &= -j_s - j_D - j_n .
 \end{aligned} \tag{16.82}$$

Here j_s is the Josephson current, j_D the displacement current, only important at high frequencies (near the Josephson frequency, of order 10 GHz), and in fact negligible up to several hundred MHz, and j_n is the ohmic quasi-particle current which allows the fast relaxation of the flux Φ to its equilibrium value. In the mechanical model, a discontinuous jump in the flux occurs when ϕ is close to π (ϕ_{ext} is greater than π because the spring is soft). At some point, the pendulum swings round and reaches a new equilibrium position after several rapid oscillations, and this corresponds to the flux jump.

16.9 The DC SQUID

Figure. 16.13 shows the set up of a DC SQUID, composed of a ring with two Josephson junctions. To operate the device, a current larger than the critical current is applied and the average voltage measured. The latter depends on the flux enclosed in the ring (there is also a component oscillating at the Josephson frequency, which is averaged out by the detection system). Screening currents are also present in the DC SQUID. However, unlike in the AC SQUID, they do not play a key role with regard to operation of the circuit. We shall first identify the critical current of the circuit. Let θ_1 and θ_2 be the phase differences between the two superconductors at the terminals of junctions 1 and 2, respectively. The condition requiring uniform phase of the order parameter along a circle lying in the ring relates these phase differences to the flux according to

$$2\pi \left(\frac{\Phi}{\Phi_0} + n \right) = \theta_1 + \theta_2 . \tag{16.83}$$

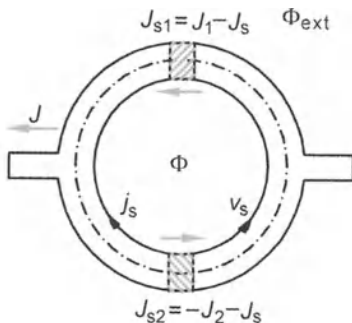


Fig. 16.13. DC SQUID. The total current through the interferometer is $J = J_1 + J_2$

Let j_s be the screening supercurrent circulating in the ring. The total current j through the circuit is composed of the current in each junction j_1 and j_2 . When j reaches its critical value, the supercurrents in each junction are $j_1 - j_s$ and $j_2 + j_s$, so that the total current is $j_1 + j_2$. The Josephson relations at each junction are

$$j_{s1} = j_1 - j_s = -j_{c1} \sin \theta_1 , \quad (16.84)$$

$$j_{s2} = -j_2 - j_s = -j_{c2} \sin \theta_2 = j_{c2} \sin \left(\theta_1 - \frac{2\pi\Phi}{\Phi_0} \right) . \quad (16.85)$$

We have used (16.83) relating phase differences and flux. The total current through the DC SQUID is then

$$J_S = j_{s1} - j_{s2} = j_1 + j_2 = -j_{c1} \sin \theta_1 - j_{c2} \sin \left(\theta_1 - \frac{2\pi\Phi}{\Phi_0} \right) . \quad (16.86)$$

The critical current is the maximum value of J_S obtainable by adjusting the phase difference θ_1 . To keep the analysis as simple as possible, we assume to begin with that the screening flux Lj_s is negligible. The flux inside the SQUID is then just the applied flux. The angle θ_1 is chosen so as to minimise the kinetic energy of the current, i.e.,

$$\frac{dJ_S}{d\theta_1} = 0 = -j_{c1} \cos \theta_1 - j_{c2} \cos \left(\theta_1 - \frac{2\pi\Phi}{\Phi_0} \right) . \quad (16.87)$$

This condition determines the critical current,

$$J_c = [(j_{c1} - j_{c2})^2 + 4j_{c1}j_{c2} \cos^2(\pi\Phi_{\text{ext}}/\Phi_0)]^{1/2} . \quad (16.88)$$

In the present case, where $j_{c1} = j_{c2} = j_c$, this simplifies to

$$J_c = 2j_c |\cos(\pi\Phi_{\text{ext}}/\Phi_0)| .$$

This function is plotted in Fig. 16.14. Maxima are reached for integral multiples of the flux quantum, while minima correspond to half-integral multiples. When screening currents are no longer negligible, we must determine the screening current j_s self-consistently in terms of θ_1 and Φ_{ext} using

$$2j_s = j_c \left[\sin \theta_1 - \sin \left(\theta_1 - \frac{2\pi}{\Phi_0} (\Phi_{\text{ext}} + Lj_s) \right) \right] . \quad (16.89)$$

We can then determine the flux inside the SQUID, $\Phi = \Phi_{\text{ext}} + Lj_s$, and substitute it into (16.83). The critical current is obtained by maximising J_S with respect to θ_1 . Apart from a reduction in the oscillation amplitude, the variation of the critical current with applied flux is qualitatively the same [496]. The DC SQUID is operated around half-integer flux values. As for the AC SQUID, two coils are coupled to it. One of these couples the flux being measured to the SQUID and the other modulates the flux and applies a counteractive flux. A current just above J_c is applied, and the flux modulated with amplitude about $\pm\Phi_0/2$. The Josephson phases then oscillate

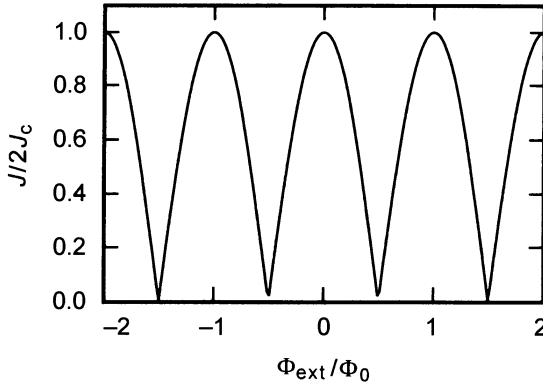


Fig. 16.14. Critical current of a DC SQUID as a function of applied flux when screening currents can be neglected. The curve shows that the double junction acts as an interferometer for Cooper pairs propagating in each branch of the circuit

very rapidly. There is nonetheless a mean voltage (modulated by the flux). The amplitude of this mean voltage is

$$\Delta U \approx \frac{R\Phi_0}{2L}, \quad (16.90)$$

where R is the tunnelling resistance of the junction. The sensitivity of voltage to flux is $dU/d\Phi_{\text{ext}} = R/L$ around $\Phi = \Phi_0/2$ (see Fig. 16.14). As for the AC SQUID, a flux-locked mode is used, applying a flux which exactly balances the measured flux, so that the output signal remains zero at all times [492, 497].

16.10 Electromagnetic Waves

In non-zero field, progressive electromagnetic waves can be generated in a Josephson junction, and they can be detected experimentally [498, 499]. The energy transported by the wave is generally too low to be able to use the Josephson junction as a source of electromagnetic radiation. When there is a vector potential $\mathbf{A} = -By\hat{x}$ and a voltage U , the Josephson current is given by

$$j = j_c \sin \left(\theta_0 + \frac{2\pi Ut}{\Phi_0} + \frac{2\pi Bl y}{\Phi_0} \right), \quad (16.91)$$

which describes a progressive wave of speed

$$c = \frac{\omega}{k} = \frac{U}{Bl}. \quad (16.92)$$

The Josephson current slips transversely at the junction with constant speed c [500]. These waves can be excited by applying a constant external voltage U . In the mechanical analogy for the AC SQUID, the Josephson phase has

spontaneous oscillation modes with which we may associate a current j given by

$$j = j_c \sin \theta + \frac{\Phi_0}{2\pi R} \frac{\partial \theta}{\partial t} + \frac{C\Phi_0}{2\pi} \frac{\partial^2 \theta}{\partial t^2}. \quad (16.93)$$

This current is coupled to the electromagnetic field by Ampère's theorem,

$$j = \frac{\partial H}{\partial y}. \quad (16.94)$$

In addition the magnetic induction affects the phase difference between the two superconductors, which varies across the junction according to

$$B = \frac{\Phi_0}{2\pi l} \frac{\partial \theta}{\partial y}. \quad (16.95)$$

Combining these relations, we obtain a dynamical equation

$$\frac{\partial^2 \theta}{\partial y^2} - \frac{1}{c_0^2} \left(\frac{\partial^2 \theta}{\partial t^2} + \gamma \frac{\partial \theta}{\partial t} \right) = \frac{\sin \theta}{\lambda_J^2}, \quad (16.96)$$

where

$$\gamma^{-1} = RC, \quad c_0^2 = \frac{\mu_0}{4\pi l C \Phi_0^2}. \quad (16.97)$$

When there is no dissipation ($R = \infty$), we retrieve the sine-Gordon equation. We described the solutions of this equation in 1 + 1 dimensions (y and t) in Chap. 10(I). They are either progressive waves, referred to as Swihart waves in the present context, or solitons, which are vortices here. In practice, boundary conditions on the order parameter constrain possible wavelengths to integer fractions of the width of the junction. Consequently, there exist discrete frequencies associated with stationary waves in the junction. Applying a static voltage U , these waves can be excited. They can be observed either in the curves $j(U)$, or by direct detection of emitted UHF radiation [501, 502].

17. Inhomogeneous Superconductivity

In certain structures, the order parameter $\Delta(\mathbf{r})$ has such large spatial variations that its average over the coherence length ξ no longer represents the average properties of the system. In these circumstances, the Ginzburg–Landau theory is no longer relevant. For example, a vortex now has an internal structure (the core states) which is not considered in the Ginzburg–Landau theory. For other mesoscopic structures, in which superconductors and normal metals come together within distances much smaller than ξ and λ_L , coherent electron transport and an unusual electronic spectrum can be observed. And in highly disordered superconductors ($l_e \approx l_F$), spatial fluctuations of the order parameter are so large that the energy gap disappears, although superconductivity is not suppressed. These phenomena all require a short-distance description of superconductivity. Today we have at our disposal a whole range of tools with which to describe both inhomogeneous superconductivity and also non-equilibrium phenomena, such as superconductivity in non-uniform electromagnetic fields. We shall use concrete examples here to bring out the physics of these mathematical methods, which are complex enough to obscure their physical import at times.

17.1 The Bogoliubov–de Gennes Equations

The self-consistent method due to Bogoliubov and de Gennes [503, 504] treats the interaction between two electrons as a contact interaction,

$$U_{\text{int}}(\mathbf{r}, t; \mathbf{r}', t') = U(\mathbf{r})\delta(\mathbf{r} - \mathbf{r}')\delta(t - t') ,$$

by analogy with the BCS theory. The method is therefore only applicable to processes of low energy compared with the Debye energy $\omega \ll \omega_D$ and for which the mean free path is large compared with the Fermi wavelength. More quantitatively, retardation effects induced by the electron-phonon interaction are relevant over distance scales smaller than

$$\lambda_c = \frac{v_F}{\omega_D} \approx \frac{\epsilon_F}{\hbar\omega_D} \frac{\lambda_F}{4\pi} ,$$

that is, roughly $10\lambda_F \approx 10 \text{ \AA}$ for typical superconductors. The potential $U(\mathbf{r})$ between electrons can be considered as an average effective potential

over distances of order λ_c . Between this lower limit and the coherence length ξ , we can make a microscopic description of superconductivity in a mean field approximation. We just linearise the interaction between electrons,

$$U_{\text{int}} = \sum_{\sigma, \tau} \int d^3r \frac{U(\mathbf{r})}{2} \psi_\sigma^\dagger(\mathbf{r}) \psi_\sigma(\mathbf{r}) \psi_\tau^\dagger(\mathbf{r}) \psi_\tau(\mathbf{r}), \quad (17.1)$$

about its expected value at temperature T . Using Wick's theorem [505], $\langle U_{\text{int}} \rangle$ contains three terms,

$$\begin{aligned} s\langle U_{\text{int}} \rangle &= \sum_{\sigma, \tau} \int d^3r \frac{U(\mathbf{r})}{2} [\langle \psi_\sigma^\dagger(\mathbf{r}) \psi_\sigma(\mathbf{r}) \rangle \langle \psi_\tau^\dagger(\mathbf{r}) \psi_\tau(\mathbf{r}) \rangle \\ &\quad - \langle \psi_\sigma^\dagger(\mathbf{r}) \psi_\tau(\mathbf{r}) \rangle \langle \psi_\tau^\dagger(\mathbf{r}) \psi_\sigma(\mathbf{r}) \rangle + \langle \psi_\sigma^\dagger(\mathbf{r}) \psi_\tau^\dagger(\mathbf{r}) \rangle \langle \psi_\sigma(\mathbf{r}) \psi_\tau(\mathbf{r}) \rangle], \end{aligned} \quad (17.2)$$

which describe the Hartree energy, the exchange energy and the Cooper pair condensation energy, respectively. The superconducting state $|S\rangle$ is a singlet state so the exchange term (the second term here) is only non-zero when $\sigma = \tau$, in which case it equals half the Hartree term. We can thereby reduce the interaction between electrons to an effective interaction,

$$U_I = U_m(\mathbf{r}) \sum_{\sigma} [\psi_\sigma^\dagger(\mathbf{r}) \psi_\sigma(\mathbf{r}) + \Delta(\mathbf{r}) \psi_\uparrow^\dagger(\mathbf{r}) \psi_\downarrow^\dagger(\mathbf{r}) + \Delta^*(\mathbf{r}) \psi_\uparrow(\mathbf{r}) \psi_\downarrow(\mathbf{r})]. \quad (17.3)$$

Molecular potentials

$$U_m(\mathbf{r}) = U(\mathbf{r}) \langle \psi_\uparrow^\dagger(\mathbf{r}) \psi_\uparrow(\mathbf{r}) \rangle = U(\mathbf{r}) \langle \psi_\downarrow^\dagger(\mathbf{r}) \psi_\downarrow(\mathbf{r}) \rangle, \quad (17.4)$$

$$\Delta(\mathbf{r}) = U(\mathbf{r}) \langle \psi_\uparrow(\mathbf{r}) \psi_\downarrow(\mathbf{r}) \rangle = -U(\mathbf{r}) \langle \psi_\downarrow(\mathbf{r}) \psi_\uparrow(\mathbf{r}) \rangle, \quad (17.5)$$

are self-consistently determined from expectation values of the two operators $\psi_\sigma^\dagger(\mathbf{r}) \psi_\sigma(\mathbf{r})$ and $\psi_\uparrow^\dagger(\mathbf{r}) \psi_\downarrow^\dagger(\mathbf{r})$, measuring electron density and Cooper pair density, respectively, at temperature T . The effective Hamiltonian $\mathcal{H}_{\text{eff}} = \mathcal{H}_0 + U_I$ is quadratic, as in the BCS theory:

$$\mathcal{H}_{\text{GC}} = \mathcal{H}_{\text{eff}} - \mu N_{\text{op}} = E_I \quad (17.6)$$

$$+ \int d^3r \left[\sum_{\sigma} \psi_\sigma^\dagger(\mathbf{r}) \mathcal{H}_e(\mathbf{r}) \psi_\sigma(\mathbf{r}) + \Delta(\mathbf{r}) \psi_\uparrow^\dagger(\mathbf{r}) \psi_\downarrow^\dagger(\mathbf{r}) + \Delta^*(\mathbf{r}) \psi_\downarrow(\mathbf{r}) \psi_\uparrow(\mathbf{r}) \right].$$

This can be diagonalised by the generalised Bogoliubov transformation. \mathcal{H}_e is the Hamiltonian for one electron,

$$\mathcal{H}_e = \frac{1}{2m} \left[\frac{\hbar}{i} \nabla - e \mathbf{A}(\mathbf{r}) \right]^2 + U(\mathbf{r}) - \mu, \quad (17.7)$$

in the potential $U(\mathbf{r}) = U_0(\mathbf{r}) + U_m(\mathbf{r})$ resulting partly from the disorder (first term) and partly from the molecular potential (second term). Let ξ_n be the eigenvalues of \mathcal{H}_e corresponding to eigenvectors $\phi_n(\mathbf{r})$. By analogy with the BCS theory, \mathcal{H}_{GC} is rewritten in matrix form as follows:

$$\mathcal{H}_{\text{GC}} = E_{\text{I}} + \sum_n \xi_n + \int d^3r X^\dagger(\mathbf{r}) H(\mathbf{r}) X(\mathbf{r}) , \quad (17.8)$$

where $H(\mathbf{r})$ and $X(\mathbf{r})$ are given by

$$H(\mathbf{r}) = \begin{pmatrix} \mathcal{H}_e & \Delta(\mathbf{r}) \\ \Delta^*(\mathbf{r}) & -\mathcal{H}_e^* \end{pmatrix} , \quad X(\mathbf{r}) = \begin{pmatrix} \psi_\uparrow(\mathbf{r}) \\ \psi_\downarrow^\dagger(\mathbf{r}) \end{pmatrix} . \quad (17.9)$$

Note that, when there is a magnetic field, $\mathcal{H}_e^* \neq \mathcal{H}_e$. We then define eigenstates,

$$\chi_n^+(\mathbf{r}) = \begin{pmatrix} u_n(\mathbf{r}) \\ -v_n(\mathbf{r}) \end{pmatrix} , \quad \chi_n^-(\mathbf{r}) = \begin{pmatrix} v_n^*(\mathbf{r}) \\ u_n^*(\mathbf{r}) \end{pmatrix} , \quad (17.10)$$

solutions of the generalised Schrödinger equation

$$H(\mathbf{r})\chi_n^\pm(\mathbf{r}) = \pm E_n \chi_n^\pm(\mathbf{r}) . \quad (17.11)$$

These are normalised by

$$\int d^3r [|u_n(\mathbf{r})|^2 + |v_n(\mathbf{r})|^2] = 1 , \quad (17.12)$$

in such a way as to preserve the fermion commutation relations in the χ_n basis. Relations (17.10–17.12) are the Bogoliubov–de Gennes equations, generalising the BCS theory to inhomogeneous systems. Amplitudes $u_n(\mathbf{r})$ and $-v_n(\mathbf{r})$ are electron and hole components of a quasi-particle wave function. When the gap tends to zero, or when the energy E_n is much larger than the gap, eigenstates χ_n become pure electron or hole states again. Field operators can be expressed in this new quasi-particle basis:

$$\psi_\uparrow(\mathbf{r}) = \sum_n [u_n(\mathbf{r}) c_{n,+} + v_n^*(\mathbf{r}) c_{n,-}^\dagger] , \quad (17.13)$$

$$\psi_\downarrow^\dagger(\mathbf{r}) = \sum_n [-v_n(\mathbf{r}) c_{n,+} + u_n^*(\mathbf{r}) c_{n,-}^\dagger] , \quad (17.14)$$

where $c_{n,+}$ and $c_{n,-}$ are operators destroying quasi-particle states $\chi_n^+(\mathbf{r})$ and quasi-hole states $\chi_n^-(\mathbf{r})$ of energy $\pm E_n$. The Hamiltonian is diagonal in this basis,

$$\begin{aligned} \mathcal{H}_{\text{GC}} = E_{\text{I}} + \sum_n (\xi_n - E_n) \\ + \sum_{n, E_n > \mu} E_n c_{n,+}^\dagger c_{n,+} + \sum_{n, E_n < \mu} E_n c_{n,-}^\dagger c_{n,-} . \end{aligned} \quad (17.15)$$

We can therefore determine the self-consistency relations satisfied by the molecular potentials,

$$U_m(\mathbf{r}) = -U(\mathbf{r}) \sum_n \{|u_n(\mathbf{r})|^2 f(E_n) + |v_n(\mathbf{r})|^2 [1 - f(E_n)]\} , \quad (17.16)$$

$$\Delta(\mathbf{r}) = U(\mathbf{r}) \sum_n u_n^*(\mathbf{r}) v_n(\mathbf{r}) [1 - 2f(E_n)] , \quad (17.17)$$

in terms of solutions u_n and v_n of the Bogoliubov–de Gennes equations. In practice, $U_m(\mathbf{r})$ differs only slightly from the Hartree–Fock energy in the normal state and does not require a self-consistency calculation. The same is clearly not true of the gap $\Delta(\mathbf{r})$. In practice, the main application of the Bogoliubov–de Gennes equations is to clean inhomogeneous systems $l_e \gg \xi$. In these systems, we can determine solutions $u(\mathbf{r})$ and $v(\mathbf{r})$ explicitly. The simplest example is provided by a current with slow spatial variation flowing through a superconductor.

17.2 Semi-Classical Approximation

Even when the current is varying slowly in space, the Ginzburg–Landau equations imply that the phase of the order parameter must vary rapidly. For this reason, we seek a solution of the Bogoliubov–de Gennes equations in the form

$$\Delta(\mathbf{r}) = \Delta \exp[i\phi(\mathbf{r})], \quad (17.18)$$

$$u_{\mathbf{k}}(\mathbf{r}) = u_{\mathbf{k}} \exp i[\mathbf{k} \cdot \mathbf{r} + \phi(\mathbf{r})/2], \quad (17.19)$$

$$v_{\mathbf{k}}(\mathbf{r}) = v_{\mathbf{k}} \exp i[\mathbf{k} \cdot \mathbf{r} - \phi(\mathbf{r})/2], \quad (17.20)$$

where the wave vector \mathbf{k} is of order k_F , much larger than the phase gradient $|\nabla\phi|$. After substituting into the Bogoliubov–de Gennes equations (17.10–17.12), $u_{\mathbf{k}}$ and $v_{\mathbf{k}}$ are eigenstates of the linear system

$$\left\{ \frac{\hbar^2}{2m} \left[\mathbf{k} + \frac{1}{2}(\nabla\phi + \mathbf{k}_A) \right]^2 + U - \mu \right\} u_{\mathbf{k}} - \Delta v_{\mathbf{k}} = \tilde{E}_{\mathbf{k}} u_{\mathbf{k}}, \quad (17.21)$$

$$\Delta u_{\mathbf{k}} + \left\{ \frac{\hbar^2}{2m} \left[\mathbf{k} - \frac{1}{2}(\nabla\phi + \mathbf{k}_A) \right]^2 + U - \mu \right\} v_{\mathbf{k}} = -\tilde{E}_{\mathbf{k}} v_{\mathbf{k}}. \quad (17.22)$$

As in previous chapters, we have introduced an electromagnetic wave vector $\mathbf{k}_A = 2\pi\mathbf{A}/\phi_0$, and U is the electrostatic potential. When the phase ϕ is time dependent, the electrostatic potential U must be replaced by the covariant potential $U \rightarrow U + (\hbar/2)\partial\phi/\partial t$. For a current with slow spatial variation, the same is true of the condensate momentum,

$$\mathbf{P}_s = \frac{\hbar}{2}(\nabla\phi + \mathbf{k}_A). \quad (17.23)$$

The above linear system determines the local quasi-particle spectrum $\tilde{E}(\mathbf{k})$ as a function of $\xi_{\mathbf{k}}$ [503, 508],

$$\tilde{\xi}_{\mathbf{k}} = \xi_{\mathbf{k}} + U + \frac{P_s^2}{2m}, \quad \xi_{\mathbf{k}} = \frac{\hbar^2 k^2}{2m} - \mu, \quad (17.24)$$

$$\tilde{E}_{\mathbf{k}} = E_{\mathbf{k}} + \mathbf{P}_s \cdot \frac{\hbar \mathbf{k}}{m}, \quad E_{\mathbf{k}} = \pm \sqrt{\tilde{\xi}_{\mathbf{k}}^2 + \Delta^2}. \quad (17.25)$$

The excitation spectrum is no longer isotropic and the gap closes when $P_s \approx P_c = \Delta/v_F$. This condition specifies the critical current of a superconductor

at zero temperature. Likewise, amplitudes $u_{\mathbf{k}}$ and $v_{\mathbf{k}}$ are given by the energies $E_{\mathbf{k}}$,

$$u_{\mathbf{k}}^2 = \frac{1}{2} \left(1 + \frac{\tilde{\xi}_{\mathbf{k}}}{E_{\mathbf{k}}} \right), \quad v_{\mathbf{k}}^2 = \frac{1}{2} \left(1 - \frac{\tilde{\xi}_{\mathbf{k}}}{E_{\mathbf{k}}} \right), \quad 2u_{\mathbf{k}}^*v_{\mathbf{k}} = -\frac{\Delta}{E_{\mathbf{k}}}, \quad (17.26)$$

and not by quasi-particle energies $\tilde{E}_{\mathbf{k}}$, so that we retrieve electron states $u_{\mathbf{k}} = 1$ or hole states $v_{\mathbf{k}} = 1$ in the normal phase. The pair kinetic energy $P_s^2/2m$ is negligible compared with the Debye energy, so the self-consistency condition (17.22) is almost unaffected by the current. Since Δ is still given by its value at $P_s = 0$, the current j_s is always proportional to P_s ,

$$j_s = n_s e_* v_s = n_s e_* \frac{P_s}{m_*}, \quad (17.27)$$

up to the critical current, when it falls sharply to zero. This behaviour should be contrasted with the current obtained near T_c in the Ginzburg–Landau theory in Sect. 13.5(II). In that case, the maximum was reached well below the critical current for a momentum equal to $2/3\sqrt{3}$ the momentum of the critical current.

In conclusion, for a given energy \tilde{E} and direction $\hat{\mathbf{k}}$, there are two wave vectors \mathbf{k}_+ and \mathbf{k}_- , collinear with $\hat{\mathbf{k}}$,

$$\hbar k_{\pm} = (2m)^{1/2} \left[\mu \pm \sqrt{\left(\tilde{E} - P_s v_F \right)^2 - \Delta^2} \right]^{1/2}, \quad (17.28)$$

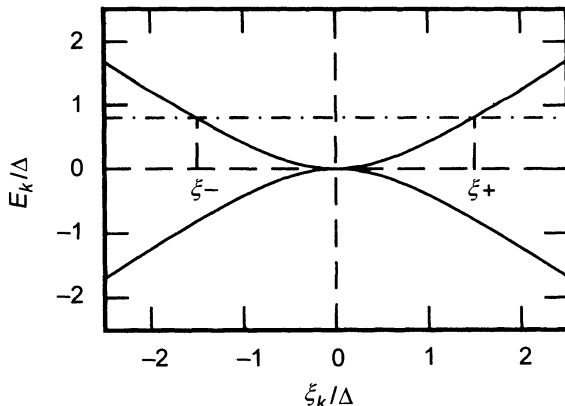


Fig. 17.1. Excitation spectrum of a superconductor carrying a current close to the critical current, in the direction of the applied current. At a given energy \tilde{E} , there are two collinear wave vectors k_{\pm} for which corresponding quasi-particles have the same energy

such that the corresponding quasi-particles have the same energy $\tilde{E}_{\mathbf{k}_+} = \tilde{E}_{\mathbf{k}_-}$ (see Fig. 17.1). Hence, in a wave packet describing a quasi-particle of energy \tilde{E} , there is always interference between components \mathbf{k}_+ and \mathbf{k}_- , with period

$$\frac{1}{|\mathbf{k}_+ - \mathbf{k}_-|} \approx v_F/\xi_{\mathbf{k}}$$

of the same order as the coherence length. The semi-classical approximation is therefore only applicable when (applied or molecular) potentials vary slowly over this length scale, which severely limits its use.

17.3 Vortex Core States

The Bogoliubov–de Gennes equations can be used to describe the microscopic structure of a vortex [503, 509, 510, 511]. At low temperatures, this structure is qualitatively different from the one obtained in Chap. 14(II) in the context of the Ginzburg–Landau theory. When the temperature is such that $k_B T_c \gg k_B T \geq \Delta^2/E_F$, the order parameter attains its asymptotic value over a distance $\xi_1 = \xi_0 T/T_c$ much shorter than the coherence length ξ_0 . The maximal current density j_s is five times greater than the critical current and the magnetic field has an angular point in the core. Because the diameter of the core is diminished, there is a logarithmic reduction in the density of states per unit length of the vortex:

$$n_v = \frac{2\pi^3}{3} n(\varepsilon_F) \frac{\xi_0^2}{\ln(T_c/T)} . \quad (17.29)$$

The flux carried by the vortex is quantised and this requires a 2π variation in the phase of the order parameter around the vortex, of form $\Delta = \Delta(r) \exp(-i\phi)$ in cylindrical coordinates. The structure of amplitudes u and v is determined by this cylindrical symmetry,

$$u(\mathbf{r}) = a \exp(ik_{\parallel}z) \exp[i(\mu - 1/2)\phi] f_+(k_{\perp}r) , \quad (17.30)$$

$$v(\mathbf{r}) = a \exp(ik_{\parallel}z) \exp[i(\mu + 1/2)\phi] f_-(k_{\perp}r) , \quad (17.31)$$

where k_{\parallel} and k_{\perp} are the wave vector components parallel and perpendicular to the vortex, and functions f_+ and f_- remain to be found. We also introduce the angle Θ between the wave vector and the z -axis of the vortex, so that $k_{\parallel} = k_F \cos \Theta$, $k_{\perp} = k_F \sin \Theta$. Finally, flux quantisation and the fermionic nature of elementary excitations mean that the quasi-particle wave function must be multiplied by -1 after a complete rotation around the vortex. Hence 2μ must be odd, i.e., $\mu = \pm 1/2, \pm 3/2$, and so on. In a type II superconductor $\kappa = \lambda/\xi \gg 1$, we can neglect the vector potential $A_\phi \approx \mu_0 h(0)r/2$ relative to the kinetic energy of Cooper pairs $p \approx \hbar/r$, because

$$\frac{e\mu_0 h(0)r^2}{2\hbar} \approx \left(\frac{r}{\lambda}\right)^2 \ll 1 .$$

Radial wave functions f_+ and f_- are determined by the Bogoliubov–de Gennes equations,

$$\frac{d^2 f_+}{du^2} + \frac{1}{u} \frac{df_+}{du} + \left(\mu - \frac{1}{2} \right)^2 \frac{f_+}{u^2} - \delta(\mathbf{r}) f_- = (1 + \alpha) f_+, \quad (17.32)$$

$$\frac{d^2 f_-}{du^2} + \frac{1}{u} \frac{df_-}{du} + \left(\mu + \frac{1}{2} \right)^2 \frac{f_-}{u^2} + \delta(\mathbf{r}) f_+ = (1 - \alpha) f_-, \quad (17.33)$$

where

$$u = k_{\perp} r, \quad \delta(\mathbf{r}) = \frac{2m\Delta(\mathbf{r})}{\hbar^2 k_{\perp}^2}, \quad \alpha = \frac{2m\varepsilon}{\hbar^2 k_{\perp}^2}, \quad (17.34)$$

and ε is the energy of the core state relative to the Fermi level. At very short distances $r \ll \xi_1$, δ is negligible, the Bogoliubov–de Gennes equations decouple and their solutions,

$$\begin{aligned} f_+(u) &= J_{\mu-1/2}[(1+\alpha)u], \\ f_-(u) &= J_{\mu+1/2}[(1-\alpha)u], \end{aligned} \quad (17.35)$$

are Bessel functions vanishing at $r = 0$, unless $\mu = \pm 1/2$. This suggests parametrising the solutions by

$$\begin{aligned} f_+(u) &= g_+(u) H_{\nu}(u), \\ f_-(u) &= g_-(u) H_{\nu}(u), \end{aligned} \quad (17.36)$$

absorbing rapid variations of f_{\pm} into the Hankel functions $H_{\nu} = J_{\nu} + iN_{\nu}$ of order $\nu = \sqrt{\mu^2 + 1/4}$. This leaves only slowly varying g_{\pm} over length scale ξ_1 . The second derivatives

$$\frac{d^2 g_{\pm}}{du^2} \approx \frac{1}{k_{\perp} \xi_1} \frac{dg_{\pm}}{du}$$

can be neglected, and the derivative $dH_{\nu}/du \approx iH_{\nu}$ for large values of the argument. g_{\pm} are therefore solutions of the system of differential equations

$$2i \frac{dg_+}{du} - \delta(u) g_- = \left(\alpha + \frac{\mu}{u^2} \right) g_+, \quad (17.37)$$

$$2i \frac{dg_-}{du} + \delta(u) g_+ = - \left(\alpha + \frac{\mu}{u^2} \right) g_-. \quad (17.38)$$

Right-hand terms are small for low energy levels $\alpha \ll \delta(\infty)$, $\mu \ll k_F \xi_1$, and can be treated by perturbation theory. To zeroth order,

$$g_+ = ig_- \propto \exp[-K(u)] \quad \text{with} \quad K(u) = -\frac{1}{2} \int_0^u \delta(u') du'.$$

We must take the calculation to first order:

$$\begin{aligned} g_+(u) &= \exp[i\psi(u)/2] g_0(u), \\ g_-(u) &= -i \exp[-i\psi(u)/2] g_0(u), \end{aligned} \quad (17.39)$$

where the phase $\psi(u) \ll 1$ is obtained by quadrature,

$$\psi(u) = \int_u^\infty du \left(\alpha + \frac{\mu}{u^2} \right) \exp \{2[K(u) - K(u')]\} . \quad (17.40)$$

Eigenvalues α_μ are found by matching together solutions (17.35) and (17.36), using asymptotic expansions of the Bessel functions. We obtain

$$\alpha_\mu = \mu \frac{\int_0^\infty \frac{\delta(u)}{u} \exp[-2K(u)] du}{\int_0^\infty \exp[-2K(u)] du} . \quad (17.41)$$

Let ξ_1 be the scale over which the order parameter relaxes towards its equilibrium value. Making the following approximation,

$$\begin{aligned} \Delta(r) &= \Delta_0 \frac{r}{\xi_1}, \quad r < \xi_1, \\ \Delta(r) &= \Delta_0, \quad r > \xi_1, \end{aligned} \quad (17.42)$$

we obtain

$$2K(r) = \frac{2r - \xi_1}{\xi_0 \sin \Theta} \quad \text{for } r > \xi_1 .$$

This determines the core state energy by quadrature as

$$\varepsilon_\mu(\Theta) \approx \frac{\mu \Delta_0^2}{\varepsilon_F \sin^2 \Theta} \ln \left(\frac{\pi \xi_0 \sin \Theta}{2 \xi_1} \right) . \quad (17.43)$$

Because the energy levels are very closely spaced, we define the density of states integrated over all angles Θ by

$$n_v = n(\varepsilon_F) \frac{\pi^3 \xi_0^2}{\ln(\xi_0/\xi_1)} \int_0^\pi \sin^3 \Theta d\Theta , \quad (17.44)$$

in agreement with (17.29).

The order of magnitude of ξ_1 remains to be determined, using the self-consistency condition

$$\Delta(\mathbf{r}) = U(\mathbf{r}) \sum_{\mu, \Theta} u_\mu^*(\mathbf{r}) v_\mu(\mathbf{r}) \tanh[\beta \varepsilon_\mu(\Theta)/2] . \quad (17.45)$$

States $\mu = \pm 1/2$, for which u^*v behaves linearly for small r , strongly renormalise the spatial dependence of the gap near the core. Expanding the two terms of (17.45) for small values of r , we obtain

$$\Delta_0 \frac{r}{\xi_1} = \sum_\Theta \Delta_0 \frac{k_F \sin \Theta r}{2} \tanh \frac{\varepsilon_{1/2}}{2k_B T} \quad (17.46)$$

$$\begin{aligned} \Leftrightarrow \frac{1}{\xi_1} &= \frac{\pi k_F}{2} \int_0^\pi d\Theta \sin^2 \Theta \tanh \frac{\varepsilon_{1/2}}{2k_B T} \\ &\approx \frac{\pi^2}{8\xi_0} \frac{\Delta_0}{k_B T} \ln(\xi_0/\xi_1) , \end{aligned} \quad (17.47)$$

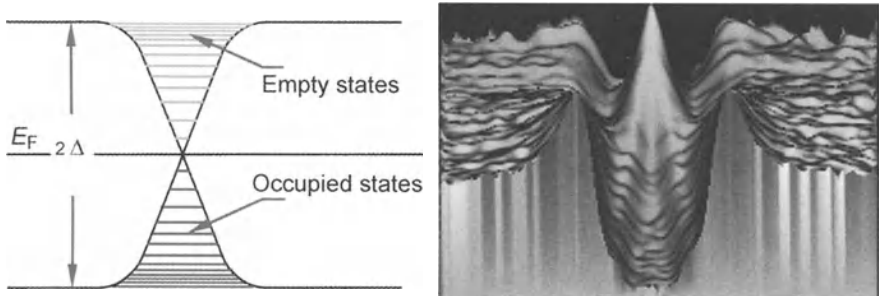


Fig. 17.2. *Left:* Density and spatial extent of core states as a function of position. *Right:* Spatial variation in the density of states near a vortex in NbSe₂, measured using a scanning tunnelling microscope [512]. Far from the core, the gap in the tunnelling conductance is visible, whilst the density of states has a marked peak at the centre of the core

since $\varepsilon_{1/2}$ is small compared with the temperature. It can also be checked that the current density j_s increases linearly between $r = 0$ and $r = \xi_1$, where it reaches a plateau of order

$$j_s = \frac{e_*}{m_*} n_s \frac{3\pi\hbar}{2\xi_0} = \frac{\pi}{2} e n(\varepsilon_F) v_F \Delta_0 = \frac{3\pi}{2} j_c . \quad (17.48)$$

This is about 5 times the critical current in a homogeneous superconductor. Core states were detected experimentally by scanning tunnelling spectroscopy several years ago [512]. Figure 17.2 shows the variation in density of states near a vortex.

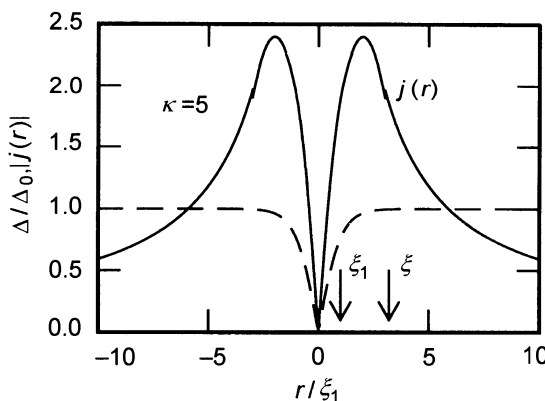


Fig. 17.3. Spatial variation of the order parameter and screening current in a vortex at $T/T_c = 0.3$

17.4 Interface Between a Superconductor and a Normal Metal. Andreev Reflection

When an electron with energy below the gap is incident on an interface between normally conducting and superconducting metals, it cannot penetrate the superconductor in the form of a quasi-particle. We may therefore expect it to be reflected with unit probability. However, this does not take into account the possibility of converting the electron into a Cooper pair, balancing energy and charge by reflection of a hole. Such a process would convert an ohmic current in the normal metal into a supercurrent in the superconductor. We can obtain an intuitive feel for Andreev reflection by considering the interface between two normal and superconducting regions in the intermediate state of a type I superconductor [see Sect. 12.7(I)]. In this case, the order parameter varies very slowly over distances of order λ_F and we may use the semi-classical approximation. We can thus represent the excitation spectrum as a function of the distance from the interface (see Fig. 17.4). The velocity $v = \partial\varepsilon(k)/\partial(\hbar k)$ of the incident electron gradually decreases to zero at point A, then changes sign when the quasi-particle changes branch. The reflected quasi-particle has a wave vector slightly less than k_F and velocity opposite to that of the incident electron. It is therefore a hole. The wave vector is only slightly affected by Andreev reflection (in both length and direction), since we move from a state just above ε_F to one just below. The process is the same everywhere on the Fermi surface. Hence, Andreev reflection is not particularly sensitive to the quality of the interface, which only has an effect over distances much smaller than ξ . Conversion of an electron into a hole is strictly forbidden in the normal metal because of energy and momentum conserva-

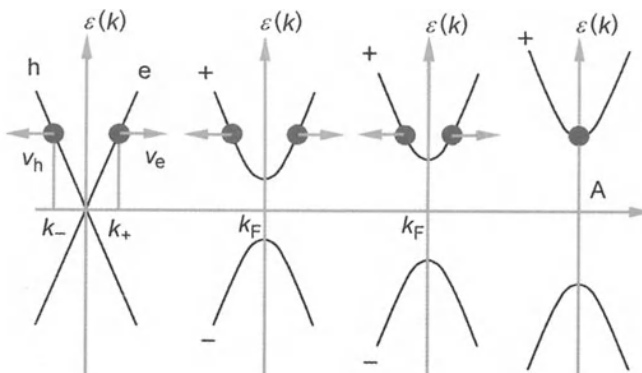


Fig. 17.4. An incident electron gradually becomes a quasi-particle. Its velocity changes sign at point A as it moves from one branch of the spectrum to the other. The wave vector of the reflected particle is close to the incident wave vector but its velocity is opposite. It is therefore a hole

tion. In contrast, near a superconductor, eigenstates are electron-hole linear combinations and conversion is then possible.

In order to analyse Andreev reflection in the clean limit $l_e \geq \xi$, we assume to begin with that the order parameter $\Delta = 0$ for $x \leq 0$ and $\Delta = \Delta_0$ for $x > 0$. Its value will then be recalculated in a self-consistent way. Solutions of the Bogoliubov-de Gennes equations on either side of the interface are

$$\begin{aligned}\psi_{<}(x) &= [A \exp(i k_+ x) + B \exp(-i k_+ x)] \begin{pmatrix} 1 \\ 0 \end{pmatrix} \\ &\quad + [C \exp(i k_+ x) + D \exp(-i k_+ x)] \begin{pmatrix} 0 \\ 1 \end{pmatrix},\end{aligned}\quad (17.49)$$

$$\psi_{>}(x) = E \exp(i \lambda_+ x) \begin{pmatrix} 1 \\ \gamma \end{pmatrix} + F \exp(-i \lambda_- x) \begin{pmatrix} 1 \\ \gamma^* \end{pmatrix}. \quad (17.50)$$

Waves A and B describe incident and reflected electrons, whilst C and D describe a hole with velocity directed along either $-\hat{x}$ or \hat{x} , respectively. Wave vectors k_+ and k_- of electron and hole states depend on their energy E and also components $\mathbf{q} = (0, q_y, q_z)$ parallel to the interface:

$$\begin{aligned}\frac{\hbar^2 k_+^2}{2m} &= \mu - \frac{\hbar^2 \mathbf{q}^2}{2m} + E = \xi_q + E = \xi_q(1 + \varepsilon_q), \\ \frac{\hbar^2 k_-^2}{2m} &= \mu - \frac{\hbar^2 \mathbf{q}^2}{2m} - E = \xi_q - E = \xi_q(1 - \varepsilon_q),\end{aligned}\quad (17.51)$$

where $\mu \approx \varepsilon_F$ is the chemical potential of the metal and $\varepsilon_q = E/\xi_q$ is a small correction ($\ll 1$). As there is no state in the superconductor with energy $|E| < \Delta$, solutions of the Bogoliubov-de Gennes equations for $x > 0$ are evanescent:

$$\frac{\hbar^2 \lambda_{\pm}^2}{2m} = \xi_q \pm i\sqrt{\Delta^2 - E^2} = \xi_q(1 \pm i\eta_q), \quad (17.52)$$

$$\gamma = \frac{\Delta}{E + i\sqrt{\Delta^2 - E^2}}. \quad (17.53)$$

Note that $|\gamma| = 1$. In these states, electron and hole components have the same relative weight. Since $\eta_q \ll 1$, like ε_q , all of k_+ , k_- , λ_+ and λ_- are close to k_x . More precisely, these wave vectors are given approximately by

$$k_{\pm} = k_x \pm \frac{E}{\hbar v_x}, \quad \lambda_{\pm} = k_x \pm i \frac{\sqrt{\Delta^2 - E^2}}{\hbar v_x}, \quad (17.54)$$

where $v_x = \hbar k_x/m$. Quantum mechanics requires continuity of the wave function at the interface and also conservation of flux:

$$A + B = E + F, \quad C + D = E\gamma + F\gamma^*, \quad (17.55)$$

$$\begin{aligned}k_+(A - B) &= \lambda_+ E - \lambda_- F, \\ k_-(C - D) &= \lambda_+ \gamma E - \lambda_- \gamma^* F.\end{aligned}\quad (17.56)$$

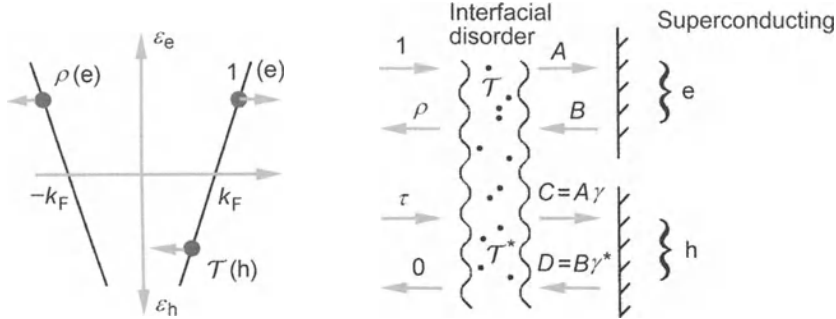


Fig. 17.5. An incident electron is reflected partly in the form of an electron and partly in the form of a hole. The reflection amplitude ρ , due to interfacial disorder, is parametrised by the transmission matrix \mathcal{T} . The effect of interfacial disorder on holes is represented by the matrix \mathcal{T}^* , because they are conjugate to electron states

This linear system is easy to solve, because $k_+ - \lambda_+ \ll k_+$ and $k_- - \lambda_- \ll k_-$, so that

$$\begin{aligned} B &\approx F, & A &\approx E, \\ D &\approx \gamma^* F, & C &\approx E\gamma. \end{aligned} \quad (17.57)$$

In the case where only one electron is incident ($A = 1, D = 0$), there is a complete conversion to holes ($C = \gamma, B = 0$). Conversely, when just one hole is incident ($D = 1, A = 0$), a whole electron is reflected by the interface ($B = 1/\gamma^*, C = 0$). In practice, the interface is not perfect and an electron is always partially reflected by disorder just in front of the interface. We can then parametrise its effect by means of a transmission matrix \mathcal{T} . When there is no magnetic field, \mathcal{T} must have form

$$\mathcal{T} = \begin{pmatrix} \frac{e^{-i\beta}}{t} & \frac{r}{t} e^{-i(\alpha-\beta)} \\ \frac{r}{t} e^{i(\alpha-\beta)} & \frac{e^{i\beta}}{t} \end{pmatrix} \quad (17.58)$$

for electrons, and \mathcal{T}^* for holes (see Fig. 17.5). In this formula, $R = r^2$ and $T = t^2$ are reflection and transmission coefficients in the normal state. The transmission matrix between incident and reflected electron amplitudes (1 and ρ) and transmitted hole amplitude (τ) is obtained by simply multiplying the transmission matrices associated with electrons and holes by the Andreev reflection matrix:

$$\begin{pmatrix} 1 \\ \rho \end{pmatrix} = \mathcal{T}^{-1} \begin{pmatrix} \gamma^{*-1} & 0 \\ 0 & \gamma^{-1} \end{pmatrix} \mathcal{T}^* \begin{pmatrix} \tau \\ 0 \end{pmatrix}. \quad (17.59)$$

We can then find the electron reflection coefficient and hole transmission coefficient,

$$R = |\rho|^2 = \frac{4r^2 \sin(\delta - \alpha)}{1 + 4r^4 - 2r^2 \cos 2(\delta - \alpha)},$$

$$T = 1 - R = \frac{t^4}{1 + 4r^4 - 2r^2 \cos 2(\delta - \alpha)} . \quad (17.60)$$

The angle δ parametrises the electron energy relative to the gap,

$$\cos \delta = \frac{E}{\Delta} . \quad (17.61)$$

These relations generalise the BTK impedance factors [524], in a model where impurities are described by a $\delta(\mathbf{r})$ potential at the interface. Figure 17.6 illustrates the significance of phase factor α in our general model of interfacial disorder. It modifies the phases of conjugate electron and hole states in a way analogous to the superconductor. To fully appreciate the effect of each term, it is instructive to determine the current-voltage characteristic of the interface. In a simplified approach, we determine the transmitted current using a semiconductor model:

$$I = 2n(\varepsilon_F)ev_F S \int_{-\infty}^{\infty} [f_{\rightarrow}(\varepsilon) - f_{\leftarrow}(\varepsilon)] d\varepsilon , \quad (17.62)$$

where $f_{\rightarrow}(\varepsilon)$ and $f_{\leftarrow}(\varepsilon)$ are the non-equilibrium distributions of incident electrons (\rightarrow) and charges reflected by the interface (\leftarrow). S is the area of the n-s junction. Without solving the Boltzmann equation, we assume that $f_{\rightarrow}(\varepsilon)$

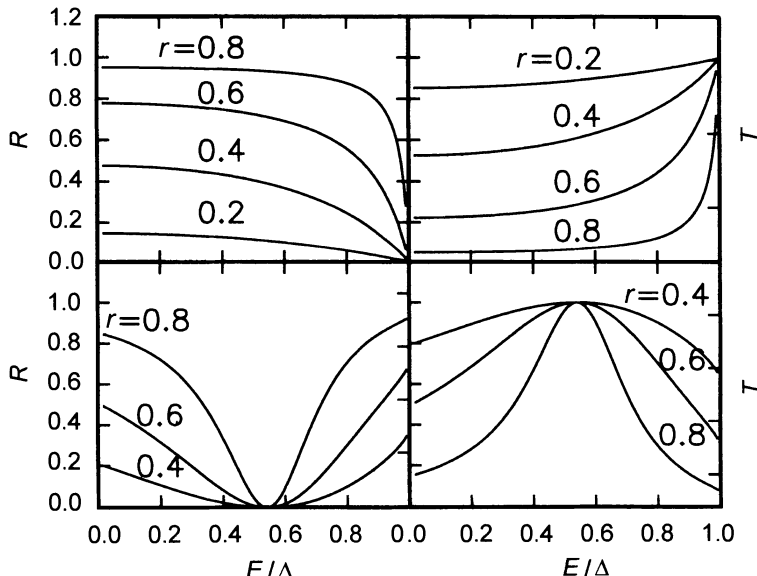


Fig. 17.6. Top: Interfacial reflection and transmission coefficients parametrised by a real reflection amplitude r . The transmission amplitude equals 1 at the gap level, whatever the value of r . Bottom: The same quantity but taking into account the complex phase $\alpha = 1$ rad of the reflection coefficient. In this case, the transmission coefficient equals 1 in the middle of the gap

is determined by the equilibrium distribution of a reservoir maintained at potential V relative to the superconductor, i.e.,

$$f_{\rightarrow}(\varepsilon) = f_0(\varepsilon - eV). \quad (17.63)$$

Likewise, the distribution of reflected charges is determined by coefficients R and T , together with the equilibrium distributions of the reservoir, so that

$$f_{\leftarrow}(\varepsilon) = T(\varepsilon)f_0(\varepsilon + eV) + R(\varepsilon)f_0(E - eV). \quad (17.64)$$

Making use of symmetries relative to the Fermi level, the total current (17.62) becomes

$$I = 2n(\varepsilon_F)e v_F S \int_{-\infty}^{\infty} [f_0(\varepsilon - eV) - f_0(\varepsilon)] [1 + T(\varepsilon) - R(\varepsilon)] d\varepsilon. \quad (17.65)$$

At zero temperature, the current is simply proportional to $1 + T(eV) - R(eV)$. Temperature averages reflection and transmission coefficients over an energy range $\delta\varepsilon = k_B T$. Finally, for voltages below the gap, $T(eV) = 1 - R(eV)$, so that current-voltage curves reduce to the electron-hole conversion coefficient represented in Fig. 17.6. We thus observe the effect of the phase difference α , which is to shift the resonance usually located at the gap energy down towards lower energies.

We may now determine the density of states near the interface and solve for the pair potential $\Delta(\mathbf{r})$. As each of these quantities is related to normal and anomalous Green functions (G and F) on either side of the interface, we define them from the Bogoliubov-de Gennes solutions

$$\begin{aligned} G_{\omega}(x, x') &= \sum_{\mathbf{k}} \left[\frac{u_{\mathbf{k}}(x)u_{\mathbf{k}}^*(x')}{\omega + i\eta - \varepsilon(\mathbf{k})} + \frac{v_{\mathbf{k}}^*(x)v_{\mathbf{k}}(x')}{\omega + i\eta + \varepsilon(\mathbf{k})} \right], \\ F_{\omega}^{\dagger}(x, x') &= \sum_{\mathbf{k}} \left[\frac{v_{\mathbf{k}}(x)u_{\mathbf{k}}^*(x')}{\omega + i\eta - \varepsilon(\mathbf{k})} - \frac{u_{\mathbf{k}}^*(x)v_{\mathbf{k}}(x')}{\omega + i\eta + \varepsilon(\mathbf{k})} \right]. \end{aligned} \quad (17.66)$$

It is important to include all states in the sum, including propagating quasi-particles of energy greater than Δ . The local density of states and the pair potential is simple to deduce [534],

$$\begin{aligned} n(x, \omega) &= -\frac{1}{\pi} \text{Im}[G_{\omega}(x, x)], \\ \Delta^*(x) &= U(x) \int_0^{\infty} \frac{d\omega}{\pi} \text{Im}[F_{\omega}^{\dagger}(x, x)]. \end{aligned} \quad (17.67)$$

Substituting the explicit solutions

$$\begin{aligned} \psi_{<}(x) &= \begin{pmatrix} \exp(i\mathbf{k}_+ \cdot \mathbf{x}) + \rho \exp(-i\mathbf{k}_+ \cdot \mathbf{x}) \\ \tau \exp(i\mathbf{k}_- \cdot \mathbf{x}) \end{pmatrix}, \\ \psi_{>}(x) &= E \exp(i\lambda_+ x) \begin{pmatrix} 1 \\ \gamma \end{pmatrix} + F \exp(-i\lambda_- x) \begin{pmatrix} 1 \\ \gamma^* \end{pmatrix}, \end{aligned} \quad (17.68)$$

into the definitions (17.66), we obtain

$$n(x, E) = n(\varepsilon_F) \int_0^{\pi/2} \sin \theta \, d\theta \{1 + \operatorname{Re}[\rho \exp(2iEx/\hbar v_x)]\} , \quad (17.69)$$

with $v_x = v_F \cos \theta$ and the reflection amplitude ρ given by

$$\rho = \exp i(\alpha - 2\beta) \frac{r \sin(\delta - \alpha)}{\exp i(\alpha - \delta) - r^2 \exp i(\delta - \alpha)} . \quad (17.70)$$

After integrating over all angles of incidence, the density of states is

$$n(x, E) = n(\varepsilon_F) \{1 + \operatorname{Re}[\rho f(2Ex/\hbar v_F)]\} , \quad (17.71)$$

where $f(y) = \int_1^\infty \exp(iyx) dx/x^2$ describes oscillations as a function of position, illustrated in Fig. 17.7. These oscillations, known as Rowell oscillations [535], have a period which depends on the energy relative to the Fermi level. When $E = \Delta$, the period is ξ . The density of states in the normal metal depends not only on position but also on energy. These oscillations have recently been observed by scanning tunnelling microscopy [537, 538]. All this structure in the energy spectrum, acquired by proximity with the normal metal, leads to a great number of effects in mesoscopic structures near superconductors. When quasi-particles are injected from the superconductor into the normal metal, there are very similar oscillations in the density of states. These manifest themselves by an oscillation in the current transmitted through a superconducting film as a function of its thickness d_s (Tomasch oscillations [536]). In the analysis we have presented here, any transverse scattering of the electron at the interface has been ignored. This is not a very realistic viewpoint. When multiple scattering between transverse modes is taken into account, we find that the transmission coefficient is strengthened [526]. When there is

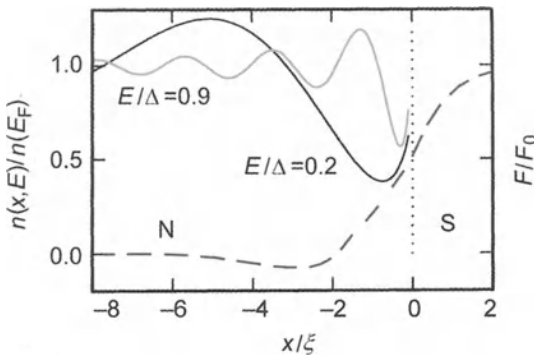


Fig. 17.7. Oscillations in the density of states near an interface with a superconductor. The oscillation period depends on the energy and is of order ξ when $E = \Delta$. The phase of the oscillations depends on the exact nature of the disorder. The dashed curve represents the spatial dependence of the pair amplitude F across the interface

significant disorder in the normal metal, both electron and hole have diffusive motions. We can describe the behaviour of the density of states averaged over the disorder, together with the average characteristics of the junction, using a generalisation of the Boltzmann equation to inhomogeneous superconductors. The corresponding transport equations are rather formal and do not provide a transparent physical description of proximate structures [527, 528]. Despite certain difficulties associated with averaged boundary conditions on the interface, specific problems can in principle be solved [529, 530].

At non-zero temperatures, another source of interfacial resistance appears. A certain proportion of the electron states in the normal metal have energy above the gap. These states of charge e will be injected into quasi-particle states of charge $e(u_k^2 - v_k^2)$. The charge difference is usually absorbed into the superconductor ground state. But this conversion of part of the charge of a quasi-particle state towards the ground state must involve an inelastic process. Such processes (scattering by phonons) are rare at low temperatures. Consequently, the conversion of an electron state in the normal metal into a quasi-particle takes place over a non-equilibrium charge length λ_Q which may be very large [533, 531, 532]. In order to balance the charge accumulating at the interface, the condensate must move so as to remain electrically neutral. An additional potential difference results, equivalent to an extra resistance in the junction.

A very similar calculation determines the pair amplitude,

$$F(\mathbf{r}) = \langle \psi_\downarrow(\mathbf{r})\psi_\uparrow(\mathbf{r}) \rangle = \int_0^{E_D} \frac{d\omega}{\pi} F_\omega(\mathbf{r}, \mathbf{r}), \quad (17.72)$$

shown as a dashed curve in Fig. 17.7. This reveals that the amplitude of the order parameter is reduced in the superconductor, similar to the prediction of the Ginzburg–Landau theory. However, in the normal metal, the pair amplitude oscillates with period of order ξ because of the singularity in the reflection coefficient (see Fig. 17.6). At finite temperatures, the drop in pair amplitude in the normal metal becomes exponential, over a thermal length $l_T = h v_F / k_B T$ [515, 516, 517]. If there is an interaction $U(\mathbf{r})$ between electrons in the normal metal, this pair amplitude induces a potential $\Delta(\mathbf{r}) = U(\mathbf{r})F(\mathbf{r})$ which is attractive or repulsive, depending on the sign of U . We have assumed the density of states to be identical on either side of the interface. When this is not the case, it is the ratio $F(r)/n(r)$ which is continuous. A discontinuity, which is easy to account for, is therefore introduced into the pair amplitude. Since the pair amplitude extends into the normal metal, it is quite natural to find a Josephson current between two superconductors separated by a normal metal.

17.5 S-N-S Junctions and Andreev States

In the previous study, interfacial disorder has two effects: firstly, it modifies the transparency of the interface, and secondly, it alters phase relations of electron-hole pairs reflected from the interface. In order to simplify the study of s-n-s junctions, these effects will only be discussed in the physical analysis of results. The geometry of this sandwich is shown in Fig. 17.8. The relative phase of the two superconductors is maintained by an external circuit at a value $\chi = \chi_2 - \chi_1$. Solutions in each region can be classified according to the sign of wave vectors k_+ and k_- as follows:

$$\begin{aligned}\psi^+(x) &= A \exp(i k_+ x) \begin{pmatrix} 1 \\ 0 \end{pmatrix} + C \exp(i k_- x) \begin{pmatrix} 0 \\ 1 \end{pmatrix}, \quad |x| < d, \\ \psi^-(x) &= B \exp(-i k_+ x) \begin{pmatrix} 1 \\ 0 \end{pmatrix} + D \exp(-i k_- x) \begin{pmatrix} 0 \\ 1 \end{pmatrix}, \quad |x| < d, \\ \psi^>(x) &= E \exp[i\lambda_+(x-d)] \begin{pmatrix} e^{i\chi_2} \\ \gamma \end{pmatrix}, \quad x > d, \\ \psi^->(x) &= F \exp[-i\lambda_-(x-d)] \begin{pmatrix} e^{i\chi_2} \\ \gamma^* \end{pmatrix}, \quad x > d, \\ \psi^<(x) &= G \exp[i\lambda_-(x+d)] \begin{pmatrix} \gamma \\ e^{-i\chi_1} \end{pmatrix}, \quad x < -d, \\ \psi^-<(x) &= H \exp[-i\lambda_+(x+d)] \begin{pmatrix} \gamma^* \\ e^{-i\chi_1} \end{pmatrix}, \quad x < -d.\end{aligned}\tag{17.73}$$

We now match the solutions and their derivatives at $x = \pm d$ to obtain the relations,

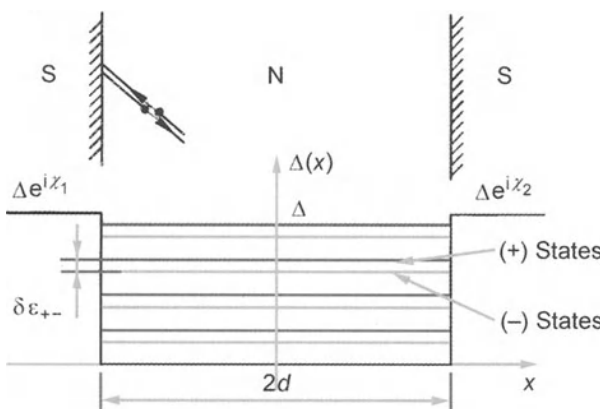


Fig. 17.8. S-n-s junction of length $2d$ between two superconductors of phase χ_1 and χ_2 . The families of states + and - form two ladders of Andreev levels separated by $\delta\varepsilon$

$$\begin{aligned}
 E &= A\gamma \exp i[k_+d - \chi_2] = C \exp(ik_-d), \\
 F &= A \exp(-ik_+d) = C\gamma \exp i[-k_-d + \chi_1], \\
 G &= B \exp -i[k_+d + \chi_2] = D\gamma \exp(-ik_-d), \\
 H &= B\gamma \exp(ik_+d) = D \exp i[k_-d + \chi_1].
 \end{aligned} \tag{17.74}$$

These imply the condition quantising energy levels,

$$\gamma^2 \exp 2i(k_+ - k_-)d = \exp(\mp i\chi). \tag{17.75}$$

In an s-n-s junction, it is not the electron wave vector which is quantised, but rather the difference between electron and reflected hole wave vectors. Depending on the sign of the phase χ , there are two ladders of Andreev levels, + and -. Their energies are found using approximation (17.54) of wave vectors k_{\pm} ,

$$E_n^{\pm} = \frac{\hbar v_x}{4d} [2(n\pi + \delta) \mp \chi]. \tag{17.76}$$

As in the previous section, interfacial disorder shifts the phase δ by an arbitrary amount α , regardless of the relative phase of the superconductors. Since each energy level carries a current $j_n^{\pm} = -\partial E_n^{\pm}(\chi)/\partial\chi$, there is a Josephson current through the junction, unless the \pm ladders coincide ($\chi = 0, \pm n\pi$). The current is therefore a periodic function of phase difference. The form of the total current depends sensitively on the value of the temperature relative to the correlation energy $E_c = \hbar v_F/2d$. E_c is a measure of the rigidity of Andreev states under changes in their boundary conditions ($\chi = 0$ and $\chi = \pm\pi$) on either side of the junction. At $T = 0$, the current shown in Fig. 17.9 exhibits a sawtooth form, but when $k_B T \geq E_c/2$, we have once again the sinusoidal Josephson current,

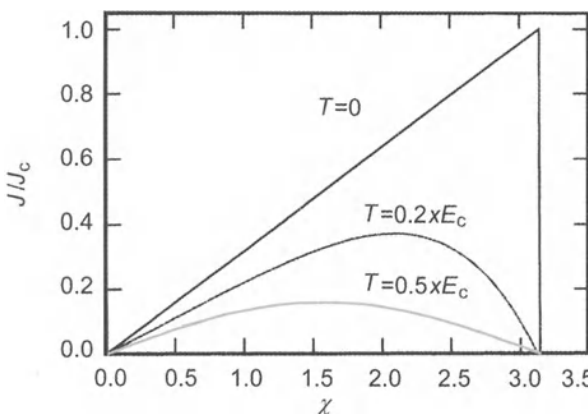


Fig. 17.9. Phase dependence of the Josephson current in an s-n-s junction for various temperatures

$$J = J(T) \sin \chi, \quad J(T) = J_0 \frac{12}{\pi} \exp(-2\pi k_B T/E_c). \quad (17.77)$$

Although the maximal current $J_0 = n_e e \pi E_c / p_F$ is large, $J(T)$ decreases exponentially with junction thickness and temperature, as would be expected. If there is disorder, we define $E_c = \hbar/\tau_D$, where $\tau_D = D/(2d)^2$ is the time taken by the electron to diffuse from one side of the junction to the other. Any disorder in the junction reduces the correlation energy E_c , but multiple scattering on an interface increases transmission coefficients and partly counters this reduction.

17.6 Electromagnetic Properties of Proximity Structures

Because of their rigidity, Andreev states can screen an electromagnetic field. When there is an interaction between electrons in the normal metal (attractive or repulsive), there is a further contribution to the diamagnetic energy coming from the pair amplitude in the normal metal. The expected value of the interaction contributes to the free energy and its magnetic field dependence follows that of the pair amplitude. To begin with, we shall neglect this contribution in the normal region.

Consider a metallic film of thickness d near a superconductor of thickness $d_s \gg \xi$. Assuming that electrons and holes are reflected specularly at the free surface of the normal metal, we may use the image method [see Sect. 14.9(II)] to relate this geometry to the s-n-s junction of thickness $2d$ studied previously. For each wave vector, there is a family of $N = 2d\Delta/\hbar v_x$ Andreev states which can screen an electromagnetic field. From their wave functions, electron states can be expressed in terms of Andreev states,

$$a_{\mathbf{k}\uparrow}^\dagger = \frac{1}{\sqrt{2}} (c_{\mathbf{k}_+}^\dagger + c_{\mathbf{k}_-}) , \quad a_{\mathbf{k}\downarrow}^\dagger = \frac{1}{\sqrt{2}} (-c_{\mathbf{k}_+}^\dagger + c_{\mathbf{k}_-}) , \quad (17.78)$$

as for a superconductor. (Note that boundary conditions (17.74) imply $A = \pm C$.) The interaction with the external magnetic field, described by \mathcal{H}_1 and \mathcal{H}_2 [see (14.105)] has the same form as for a superconductor [see (14.106)], except that there is no gap. It is the Andreev states of energy less than Δ which contribute to screening. This is a crucial difference because Andreev states extend over the whole normal region; their coherence length is of order $2d$. At low temperatures, this length is much greater than the penetration depth. In this Pippard regime, the dominant contribution comes from grazing incidence states (small v_x). In other words, screening is due to the lowest energy Andreev states. At zero temperature, the penetration depth can be calculated explicitly [539],

$$\lambda(T=0) = \frac{3\pi}{4} \left(\frac{2d\lambda_L^2}{6\pi} \right)^{1/3} , \quad (17.79)$$

where $\lambda_L = \sqrt{m/\mu_0 n_e e^2}$ is the London penetration depth. It is just as though the pair coherence length had been replaced by the thickness $2d$ of the junction. More detailed study of the screening current distribution shows that the junction overscreens the field; the sign of the current changes in the junction. At finite temperatures, screening is only effective over a length $l_T = \sqrt{\hbar v_F/k_B T}$. The thermal energy exceeds the correlation energy beyond this length. Such behaviour is just the opposite to what happens in superconductors (see Fig. 12.1). The penetration depth in that case only varies near T_c .

When there is a significant electron-electron interaction in the normal metal, we must add orbital magnetism induced by the pair potential to Andreev screening [515, 541]. It has paramagnetic sign if the interaction is repulsive and diamagnetic sign if it is attractive. There may then be competition between Andreev screening and paramagnetism induced by interactions. Such competition could explain why paramagnetism has been found to completely dominate proximate diamagnetism in recent experiments [542].

17.7 Gapless Superconductivity

In BCS theory, Cooper pairs can form because states $|\mathbf{k}\rangle$ and $|-\mathbf{k}\rangle$ are degenerate. Any attractive interaction can then induce an instability in the Fermi surface [see Sects. 12.2 and 14.3(II)]. When there are non-magnetic impurities, the Bogoliubov-de Gennes theory shows that this same degeneracy exists. Indeed, Anderson's theorem [543] asserts that any perturbation not removing time reversal degeneracy has no significant effect on superconductivity. Maki and de Gennes have shown that perturbations breaking time reversal invariance (e.g., magnetic field, current, magnetic impurities) will only suppress superconductivity if electron scattering is chaotic [545, 547]. This is because all memory of the accumulated phase must be lost.

A magnetic field induces a linear increase $\phi \approx 2ev \cdot At/\hbar$ in the relative phase of two electrons forming a Cooper pair, and this is not a priori consistent with the ergodicity condition. Nevertheless, when there is scattering (by impurities, walls and so on), electrons have Brownian motion. The phase then diffuses randomly $\overline{\theta^2} \simeq \overline{\dot{\theta}^2} t \tau_{\text{el}}$. This guarantees a loss of coherence over a time scale of $\tau_H^{-1} \simeq DH/\Phi_0^2$, where D is the diffusion coefficient.

This is typical for scattering by magnetic impurities. The exchange interaction between localised spins and the conduction electron,

$$U_{\text{int}} = \sum_i J(\mathbf{R}_i - \mathbf{r}) \mathbf{S}_i \cdot \boldsymbol{\sigma}(\mathbf{r}), \quad (17.80)$$

fluctuates rapidly in time. A conduction electron will only stay in a given spin state for a time of order

$$\alpha \equiv \frac{\hbar}{\tau_s} \simeq x \frac{\overline{J^2} S(S+1)}{\varepsilon_F}, \quad (17.81)$$

where x is the concentration of magnetic impurities and $\overline{J^2}$ is the spatial average of $J^2(\mathbf{r})$. Of course, such changes in spin direction are not compatible with the singlet state of a Cooper pair. Abrikosov and Gorkov [544] have shown that the fall in critical temperature depends on the decoherence energy α according to

$$\ln \frac{T_c}{T_{c0}} = \psi\left(\frac{1}{2}\right) - \psi\left(\frac{1}{2} + \frac{\alpha}{2\pi k_B T_c}\right), \quad (17.82)$$

where $\psi(x) = d \ln \Gamma(x)/dx$ is the digamma function. For low decoherence, the decrease in T_c is linear,

$$\delta T_c = \frac{\pi \alpha}{4k_B}.$$

Superconductivity disappears completely when the decoherence energy equals half the gap Δ_0 . These predictions have been confirmed in many experimental studies on superconducting transition metals and rare earths [549]. The effective exchange coefficient J between a magnetic impurity and the conduction electrons is temperature dependent (the Kondo effect), and hence superconducting reentrant phenomena are possible. As an example, the compound $\text{La}_{0.37}\text{Ce}_{0.63}\text{Al}_2$ is superconducting between 0.18 and 1.2 K but becomes normal again below 0.18 K [552]. In parallel with lowering of the critical temperature, the superconductor density of states is significantly modified by addition of magnetic impurities, as can be seen from Fig. 17.10 [550]. Scanning tunnelling spectroscopy has shown that the measured gap is not the same as the thermodynamic gap predicted by BCS theory. Abrikosov and Gorkov noticed that, before it disappears, superconductivity persists with no

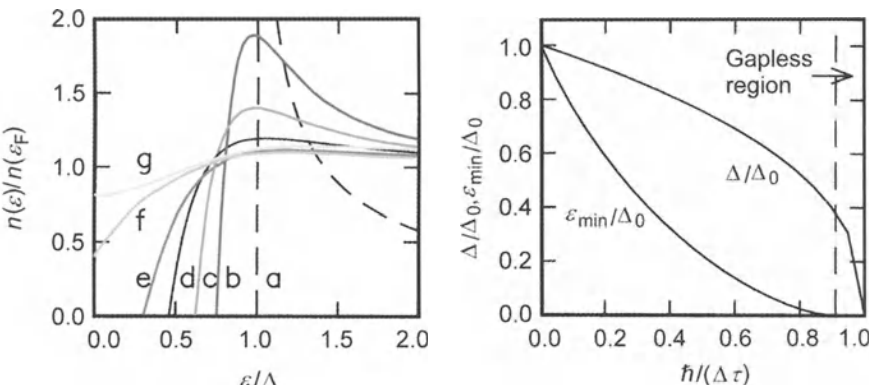


Fig. 17.10. *Left:* Energy dependence of the density of states for various values of the decoherence parameter α [550]. Curve (a) $\alpha = 0$, (b) $\alpha = 0.07$, (c) $\alpha = 0.15$, (d) $\alpha = 0.25$, (e) $\alpha = 0.4$, (f) $\alpha = 1.1$, (g) $\alpha = 1.8$. *Right:* Dependence of the thermodynamic gap Δ and minimal energy ε_{\min} required to excite a quasi-particle on the decoherence α [551]. When $0.91 < 2\alpha/\Delta_0 < 1$, gapless superconductivity is possible

gap. In this region, a quasi-particle can be excited by an infinitesimal energy whilst maintaining a state without resistance. The London equations are a direct consequence of rigidity of the condensate wave function, which implies the existence of a persistent current $j = -\partial E/\partial\phi$. Likewise an argument due to Kohn, W., shows that a rigid state is accelerated by an electric field and is therefore a state without resistance [553]. On the other hand, there is nothing to say there must be a gap in the energy spectrum. Normal mesoscopic structures can carry a persistent current. However, many quasi-particles are excited in a gapless superconductor and are not part of the condensate. Only a fraction of the electrons are in the condensed state, even at zero temperature.

Microscopic description of gapless superconductivity is a formidable exercise. Fortunately it can be avoided by using the Ginzburg–Landau theory, as de Gennes has shown. In discussing the nucleation of superconductivity near H_{c2} , we noted that when the gap disappears, it is justifiable to use the linearised Ginzburg–Landau equations. Here the gap is zero at all temperatures. At long wavelengths, we can then describe the order parameter as the lowest energy diffusive mode, a solution of

$$\hbar D(\nabla + i\mathbf{k}_A)^2\Delta = -2\alpha\Delta, \quad (17.83)$$

even at $T = 0$ [503]. This constitutes a considerable simplification. It also allows us to identify the coherence length with the Ginzburg–Landau length at $T = 0$,

$$\xi = \sqrt{\frac{\hbar D}{2\alpha}}. \quad (17.84)$$

Of course, we can no longer justify identifying this length with a mean size for the Cooper pairs, given the very large fluctuations in the order parameter.

Interest in inhomogeneous superconductors was revived by studies of indium oxide. In certain regions of its phase diagram, it passes directly from the superconducting state to an insulating state by application of a magnetic field [554, 556]. For the moment, there is no microscopic description of this phenomenon.

17.8 Collective Modes

Goldstone's theorem predicts a collective mode associated with fluctuations in the phase of the order parameter. But this Anderson–Bogoliubov mode [557] involves a local charge oscillation in which normal and superfluid components of the electron density are in simultaneous motion. The long range Coulomb interaction increases the frequency of this mode to the plasma frequency (of the order of 1 eV), thereby rendering it unobservable. The collective modes of a superconductor must alone maintain a constant local electron density. This is possible if normal and superfluid components move in opposite directions

in such a way as to produce a constant total electron density. Since quasi-particles and condensate are not in equilibrium, the quasi-particle relaxation time is related to the non-equilibrium charge time τ_Q mentioned earlier. This mode involves an oscillation of the normal component, and is therefore dissipative. The larger the motion of the normal component required to balance oscillation of the superfluid component, the greater the dissipation will be. This explains why the mode has only been observed near the critical temperature [558], where the superfluid density is low and its motion can be balanced by a low amplitude oscillation of the normal component. For a disordered superconductor, the frequency and dissipation factor of this mode are of order

$$\omega \approx c_{\text{CG}} q - i\gamma/2 \quad \text{where} \quad c_{\text{CG}} = \sqrt{\frac{2D\Delta}{\hbar}}, \quad \gamma = \frac{\hbar\pi\Delta^2}{2k_B T \tau_{\text{el}}}, \quad (17.85)$$

D is the electron diffusion coefficient, τ_{el} the elastic collision time, and Δ the order parameter at time T . This mode is not hydrodynamic, in the sense that its frequency is high compared with the inelastic relaxation rate of order $1/\tau_Q$, but small compared with $1/\tau_{\text{el}}$. Such non-hydrodynamic behaviour greatly complicates analysis, requiring a kinetic theory which couples normal and superfluid components. (Most transport phenomena can be treated using a generalised Boltzmann equation for the quasi-particles. Indeed, the condensate quickly adjusts to maintain local equilibrium with quasi-particles [508].) The relevant hydrodynamic equations are [559, 561]:

1. Local charge conservation $\nabla \cdot (\mathbf{j}_n + \mathbf{j}_s) = 0$.
2. The constitutive equation for the normal component of the current \mathbf{j}_n , that is, Ohm's law $\mathbf{j}_n = \sigma \mathbf{E}$.
3. The superfluid continuity equation, giving the dynamics of its chemical potential,

$$2en(\varepsilon_F) \frac{\pi\Delta}{4k_B T} \frac{\partial \mu_s}{\partial t} + \nabla \cdot \mathbf{j}_s = 0. \quad (17.86)$$

4. The constitutive equation of the superfluid current (the London equation),

$$\frac{\partial \mathbf{j}_s}{\partial t} = -\frac{en_s}{m} \nabla \mu_s + \frac{e^2 n_s}{m} \mathbf{E}. \quad (17.87)$$

Although this mode involves balanced motion of normal and superfluid components, there is no connection with the second sound of a superfluid. There is no oscillation of temperature and entropy here.

Some methods for describing the average properties of non-equilibrium superconductors have been developed to a high degree. However, the general theory is so complex that a considerable number of approximations have to be made before arriving at a physically transparent description. These approximations are specific to each particular problem and it would not be appropriate to describe them here.

The particularity of inhomogeneous superconductors is that they have spatially and energetically dependent spectral properties (density of states). Distribution functions are therefore inadequate to describe them. Deviations from equilibrium couple both distribution functions and spectral quantities. Given the mathematical complexity of the problem, it is not easy to know whether certain physical phenomena may not have been forgotten.

17.9 Conclusions and Perspectives

The present view of superconductivity is to a large extent dominated by the BCS theory. The successes of this theory with regard to conventional superconductors are indeed undeniable. It has since been extended to inhomogeneous superconductors, as well as strongly coupled superconductors. Among recent successes, the BCS theory has explained superconductivity in fullerenes [562]. Despite the rather high critical temperatures of these materials (≥ 30 K), this superconductivity is due to electron-phonon coupling on C_{60} spheres. Hence, Cooper pairs form on the fullerenes. The high critical temperatures compared with those for intercalated graphite compounds would appear to result from curvature of carbon planes, providing optimal electron-phonon coupling [563, 564]. The simplicity of the BCS theory gives a rather idyllic view of superconductivity which has been seriously put into question by several families of new materials over the past ten years or so. These are the organic superconductors [565]. Their quasi-one-and two-dimensional structures are difficult to reconcile with the BCS theory. However, it is the superconductors with strong electron correlations, such as heavy fermions and high temperature superconductors, which pose the greatest difficulties for the BCS theory, and more generally, for condensed matter physics.

To appreciate the extent of these difficulties, let us recall that in the BCS theory, Cooper pairs appear at the same temperature as macroscopic phase coherence. We know that such a scenario is not essential for superconductivity. Pairs may form at energies much higher than the critical temperature T_c , superconductivity manifesting itself as the Bose condensation of pre-existing pairs [566]. This happens in granular superconductors, and also in arrays of Josephson junctions: pairs appear at the critical temperature of the massive material before macroscopic phase coherence is established by Josephson coupling. Excitons in semiconductors also have binding energies much higher than the energy at which the system is likely to condense into a superfluid state. In principle, it is not difficult to obtain a large binding energy for pairs. But it is difficult to have a high condensation temperature at the same time. Indeed an interaction strong enough to bind two electrons must inevitably give rise to a large mass renormalisation. This will in turn reduce the critical temperature accordingly. Moreover, when the attractive interaction is located at precise sites over the lattice, structural instabilities will tend to localise pairs and create an insulating system. Finally, whatever the origin of

the attractive interaction between electrons, it will always be in competition with Coulomb repulsion. In high temperature superconductors, the coherence length $\xi \propto 1/\Delta \simeq 1/k_B T_c$, which is a measure of the size of the Cooper pairs, is so short (several times the atomic spacing) and the electron density so low that the Coulomb interaction is not screened on the scale of the Cooper pair. Coulomb repulsion is therefore an essential factor. Unlike the electron-phonon interaction, it is not easy to understand this competition in such a way that the attractive interaction wins out, just by playing with the time scales over which it is effective, given the length scales involved.

We may therefore say that superconductivity is a phenomenon occurring at low temperatures. Either the attractive force is weak and pair binding energy is low, or the attractive force is strong and the temperature at which coherence develops is greatly reduced, unless the system becomes unstable. Superconducting compounds with high critical temperature are cuprates made up of CuO_2 planes. These are undoped Mott insulators. We must then add to all the above problems the fact that the Coulomb interaction is extremely effective in Mott insulators. In these materials, superconductivity would appear to be an extraordinary phenomenon, difficult to reconcile within the context of our present knowledge.

During the last few years, study of antiferromagnetic ladder structures [see Chap. 10(I)] has developed in parallel with investigation of high temperature superconductors. These systems are similar in many respects. The only difference arises from the quasi-one-dimensional nature of ladders compared with the two-dimensional structure of CuO_2 planes. In fact, certain ladder compounds, such as the $\text{SrCu}_n\text{O}_{2n-1}$ family, derive from the same materials. At the same time, it was also realised that spin ladders on the one hand, and cuprates in certain doping regimes on the other, both manifest a spin gap. Such a gap is typical of spin liquid states described in Chap. 10(I). It would thus seem useful to understand how charge carriers (holes) can induce a spin gap in cuprates, which are normally antiferromagnetic. Moreover, studies of hole motion in antiferromagnetic ladders should reveal the nature of the attractive coupling between holes. Partial answers to these questions already exist. On a ladder it is preferable to place two holes at the ends of a rung because electrons on neighbouring sites then gain more quantum delocalisation energy (hopping energy in a Hubbard model) [567]. This energy exceeds the Coulomb repulsion for holes placed at adjacent sites. We may then say that the two holes are confined by the antiferromagnetic medium. In such a ladder structure, there is also a natural separation of charge and spin degrees of freedom which facilitates the appearance of phase coherence between pairs. Superconductivity has recently been observed in the doped Mott insulator $\text{Sr}_{0.4}\text{Ca}_{13.6}\text{Cu}_{24}\text{O}_{41.8}$, whose structure contains ladders [569]. This gives credence to these ideas. In two dimensions, hole confinement amounts to locally excluding holes from the antiferromagnetic medium [570]. For neutral holes, this would normally lead to a phase separation. But here, the electrostatic

cost of such a phase separation is prohibitive. The system prefers a dynamic generation of charge inhomogeneities in which holes are confined in charge stripes, and these look very much like ladders. There is experimental evidence for such structures [568]. Among other things they explain the spin gap, which is a property of confined regions without holes. Paradoxically, the most difficult point is to explain macroscopic phase coherence over the whole system. If we can base the high coherence energy on the spin-charge separation in striped structures, a Josephson coupling is also required to block the phases of all inhomogeneous structures. A magnetic Josephson effect between spin ladders has indeed been proposed [571], but the idea must be generalised to violently fluctuating two-dimensional structures. To sum up, we lack any real understanding of coherence processes in strongly correlated electron systems.

This discussion reveals the extent to which very fundamental aspects of condensed matter physics escape proper understanding. High temperature superconductivity has literally exploded the carefully constructed edifice built up during the previous thirty years. The problems raised go beyond the study of superconductivity and magnetism. Their solution may lead to the production of new materials whose technological impact would be considerable. Indeed, physics has shown on many occasions that technological and social revolutions could be generated by intelligent exploitation of some new discovery. We must therefore conclude that the scientific future of condensed matter physics is likely to be a brilliant one, offering remarkable scientific and industrial opportunities over at least the next ten years.

A. Representations of Continuous and Point Groups

A.1 General Notions

This appendix gives only the minimal requirements for using representations of symmetry groups in solid state physics. Many text books deal with this subject in greater detail and some are given in the Bibliography. Physical systems are often invariant under certain symmetry operations forming a group G . For example, electrons in an atom are subject to a central potential which is invariant under the group of rotations. Likewise, electrons in a solid are in a periodic potential which has translational invariance, but is also invariant under the point group of the lattice. There are 32 point symmetry groups in three dimensions, compatible with translational invariance of a crystal lattice. Wave functions corresponding to stationary solutions of the Schrödinger equation form a vector space, or state space. When we apply an operation g in the symmetry group G , we associate with the transformation $\mathbf{r} \Leftrightarrow \mathbf{r}' = g^{-1}\mathbf{r}$ of real space, a transformation of the function space,

$$\psi_\alpha(\mathbf{r}) \Leftrightarrow \psi'_\alpha(\mathbf{r}) = \psi_\alpha(\mathbf{r}') = \Gamma(g)[\psi_\alpha(\mathbf{r})] = \sum_{\beta} \Gamma(g)_{\alpha\beta} \psi_\beta(\mathbf{r}) . \quad (\text{A.1})$$

These relations define the transformation law $\Gamma(g)$ for wave functions under elements of the group G . The wavefunctions $\psi'_\alpha(\mathbf{r})$ are also stationary solutions of the Schrödinger equation, since $V(\mathbf{r}') = V(g^{-1}\mathbf{r}) = V(\mathbf{r})$. The set of transformations $\Gamma(g)$ of the wave function vector space forms a group isomorphic to G , since the definition (A.1) implies $\Gamma(gs) = \Gamma(g)\Gamma(s)$, and this generates a group structure. It is in fact a representation of the group G on the wave function space. Choosing a basis of this space, we obtain a matrix representation of the transformations $\Gamma(g)$. Elements of the matrix $\Gamma(g)_{\alpha\beta}$ are defined by (A.1). The size of the matrix defines the dimension of the representation. For any given representation Γ of the group, we can associate a complex number with every element g of the group by the relation

$$\chi_\Gamma(g) = \text{Tr} [\Gamma(g)] = \sum_{\alpha} \Gamma(g)_{\alpha\alpha} . \quad (\text{A.2})$$

This is called the character of g in the representation Γ . Changing the basis for the wave function space by a unitary transformation, characters are in-

variant, because the trace of a matrix product is itself invariant under cyclic permutation,

$$\mathrm{Tr}[U^\dagger \Gamma(g) U] = \mathrm{Tr}[\Gamma(g) U U^\dagger] = \mathrm{Tr}[\Gamma(g)] .$$

In quantum mechanics, representations must preserve the norm and are therefore unitary. This implies for the characters

$$\chi_\Gamma(g^{-1}) = \chi_\Gamma^*(g) . \quad (\text{A.3})$$

We can often relate several elements g and g' of a group by the existence of some s such that $g' = s^{-1}gs$. This is an equivalence relation and the set of group elements related to any given g is therefore an equivalence class, called a conjugacy class. As an example, the symmetry group of the cube contains four axes of symmetry of order 3 along the diagonals of the cube. As we can change from one axis to another by cyclic permutation of the axes, these symmetry elements belong to the same conjugacy class. Such classes are useful because the character is constant over each class:

$$\chi(g') = \mathrm{Tr}[\Gamma(s^{-1}gs)] = \mathrm{Tr}[\Gamma(s^{-1})\Gamma(g)\Gamma(s)] = \chi(g) . \quad (\text{A.4})$$

For finite groups, the number of elements h in the group is called the order of the group. If there are p conjugacy classes, each one containing $n(i)$ elements, we have $h = \sum_{i=1}^p n(i)$. Each representation will have only p characters. There are two trivial representations of any such group. Firstly, there is the identity representation I , of dimension 1, which leaves every state ψ invariant. Its characters are all equal to 1. Secondly, consider a vector space of dimension h equal to the order of the group and index a basis ψ_s by the elements s of the group G . We can then define the regular representation $\Gamma_{\text{reg}}(g)$ which maps ψ_s to ψ_{gs} . This representation has dimension h . The character of the identity in G is always equal to the dimension of the representation.

Given two state spaces 1 and 2 (e.g., associated with spatial and spin wave functions), we can construct a product vector space made up of tensor products of states. Consider two representations Γ_1 and Γ_2 of the same group acting in spaces 1 and 2, respectively. Then there is a representation $\Gamma_1 \otimes \Gamma_2$ of G on the product space. For each element $g \in G$, it relates the state $\psi \otimes \chi$ to the state $[\Gamma_1(g)\psi] \otimes [\Gamma_2(g)\chi]$. Characters of the product representation are products of characters. Its dimension is the product of dimensions of the constituent spaces.

When certain subspaces of the state space remain invariant under the action of all elements $\Gamma(g)$, the representation is said to be reducible. Matrices associated with the elements $\Gamma(g)$ can then be decomposed into block diagonal form by the choice of some particular basis for the vector space. If there is no invariant subspace, the representation is irreducible. The regular representation of a group is generally reducible and so too are the product representations. A finite group containing p conjugacy classes has only p distinct irreducible representations. It can be shown that

$$\sum_{i=1}^p (\dim \Gamma_i)^2 = h . \quad (\text{A.5})$$

This relation can be extremely useful for determining the dimensions of representations of a finite group. For example, one of the symmetry groups of a cubic crystal is the tetrahedral group T , which is of order 12 and contains 4 conjugacy classes: $I(1)$ identity, $C_2(3)$ rotation by π (order 2), $C_3(4)$ rotation by $2\pi/3$ (order 3), $C_3^2(4)$ rotation by $4\pi/3$. Since one of these representations is the identity, of dimension 1, we must have

$$1^2 + (\dim \Gamma_2)^2 + (\dim \Gamma_3)^2 + (\dim \Gamma_4)^2 = 12 . \quad (\text{A.6})$$

This equation can only be satisfied if $\dim \Gamma_2 = 1$, $\dim \Gamma_3 = 1$ (representations E and E^*) and $\dim \Gamma_4 = 3$ (representation F). Knowing the irreducible representations, we can identify subspaces which are invariant under group transformations. These subspaces correspond to degenerate energy levels of the Hamiltonian \mathcal{H} which has symmetry group G :

$$\begin{aligned} \mathcal{H}(\mathbf{r})\psi_\alpha(\mathbf{r}) &= \varepsilon_\alpha \psi_\alpha(\mathbf{r}) \Rightarrow \\ \mathcal{H}(\mathbf{r}')\psi_\alpha(\mathbf{r}') &= \mathcal{H}(\mathbf{r}) \sum_\beta \Gamma(g)_{\alpha\beta} \psi_\beta(\mathbf{r}) \\ &= \sum_\beta \Gamma(g)_{\alpha\beta} \varepsilon_\beta \psi_\beta(\mathbf{r}) \\ &= \varepsilon_\alpha \sum_\gamma \Gamma(g)_{\alpha\gamma} \psi_\gamma(\mathbf{r}) \Rightarrow \\ \varepsilon_\alpha \Gamma(g)_{\alpha\gamma} &= \Gamma(g)_{\alpha\gamma} \varepsilon_\gamma , \end{aligned} \quad (\text{A.7})$$

where orthogonality of wave functions has been used. When a representation is irreducible, there are always non-diagonal matrix elements $\Gamma(g)_{\alpha\gamma} \neq 0$. We therefore find $\varepsilon_\alpha = \varepsilon_\gamma$. Irreducible representations thus correspond to distinct multiplets of the Hamiltonian and help us determine their degeneracy, without explicitly solving the Schrödinger equation. When a perturbation V is applied, the symmetry group G' of $\mathcal{H} + V$ is smaller and forms a subgroup of G . Some previously irreducible representations Γ of G may become reducible representations of G' . In general, they decompose into r irreducible representations Γ_i ,

$$\Gamma_G(g \in G') = \bigoplus_{i=1}^r \Gamma_i(g \in G') , \quad (\text{A.8})$$

for some r . Some irreducible representations may appear a_i times in this decomposition, where the number a_i is called the multiplicity. From the previous relation, we see that the dimension of a reducible representation is the sum of dimensions of irreducible representations occurring in the decomposition (including any multiplicities). Wave function bases of subspaces associated with each irreducible representation Γ_i give the new multiplet structure when

the perturbation V has removed degeneracy in multiplets of \mathcal{H} . If there are r irreducible representations in the above decomposition, then there will be r multiplets, each containing $\dim \Gamma_i$ states. We need a method for finding the irreducible representations of G' occurring in the decomposition of Γ_G . This is achieved by means of orthogonality relations between characters. Consider two irreducible representations i and j with characters $\chi_i(g)$ and $\chi_j(g)$. The orthogonality relation between these two characters is

$$\sum_{g \in G} \chi_i(g) \chi_j^*(g) = h \delta_{ij} . \quad (\text{A.9})$$

Since all elements within the same conjugacy class have the same character, the sum can be taken over conjugacy classes:

$$\sum_C \chi_i(C) \chi_j^*(C) n(C) = h \delta_{ij} , \quad (\text{A.10})$$

where C is an index running over the set of conjugacy classes and $n(C)$ is the number of elements in conjugacy class C . This orthogonality relation gives the decomposition of a reducible representation Γ_0 into irreducible representations Γ_i :

$$\begin{aligned} \Gamma_0 &= \bigoplus_{i=1}^p a_i \Gamma_i , \\ a_i &= \frac{1}{h} \sum_C \chi_0(C) \chi_i^*(C) n(C) . \end{aligned} \quad (\text{A.11})$$

A.2 Representations of the Rotation Group

A familiar example is provided by representations of the rotation group in three dimensions. We choose $|j, m\rangle$ as a basis for the vector space, simultaneous eigenstates of J^2 and J_z , where \mathbf{J} is the angular momentum. Rotation through angle θ about an axis along unit vector $\hat{\mathbf{n}}$ transforms eigenstate $|j, m\rangle$ by

$$\begin{aligned} \Gamma|j, m\rangle &= \exp\left(-i\theta \frac{\hat{\mathbf{n}} \cdot \mathbf{J}}{\hbar}\right) |j, m\rangle \\ &= \sum_{m'} \langle j, m' | \exp\left(-i\theta \frac{\hat{\mathbf{n}} \cdot \mathbf{J}}{\hbar}\right) |j, m\rangle |j, m'\rangle \\ &= \sum_{m'} \Gamma_{mm'}^j(\hat{\mathbf{n}}, \theta) |j, m'\rangle . \end{aligned} \quad (\text{A.12})$$

Γ_j is the restriction of the representation Γ to the subspace defined by eigenvalue $\hbar^2 j(j+1)$ of J^2 . It is an irreducible representation. Matrix elements $\Gamma_{mm'}^j(\hat{\mathbf{n}}, \theta)$ define the matrix representation of Γ_j of dimension $2j+1$ in the basis $|j, m\rangle$. The characters of Γ_j only depend on the rotation angle θ ,

because changing the quantisation axis from $\hat{\mathbf{n}}$ to $\hat{\mathbf{z}}$ corresponds to conjugating Γ by some unitary matrix U , $\Gamma \rightarrow U^\dagger \Gamma U$, and this leaves characters unchanged. Hence,

$$\begin{aligned}\chi_j(\theta) &= \sum_{m=-j}^j \exp(-im\theta) \\ &= 1 + 2 \cos \theta + \dots + 2 \cos j\theta = \frac{\sin(j+1/2)\theta}{\sin \theta/2}.\end{aligned}\quad (\text{A.13})$$

The characters can also be found from the recurrence relation

$$\chi_j(\theta) - \chi_{j-1}(\theta) = 2 \cos j\theta, \quad (\text{A.14})$$

and the first two values (spin 0 and spin 1/2)

$$\chi_0 = 1, \quad \chi_{1/2}(\theta) = 2 \cos \theta/2. \quad (\text{A.15})$$

For this continuous group, the orthogonality relation between characters $\chi_j(\theta)$ and $\chi_{j'}(\theta)$ takes the form

$$\frac{1}{\pi} \int_0^\pi d\theta (1 - \cos \theta) \chi_j(\theta) \chi_{j'}^*(\theta) = \delta_{ij'}. \quad (\text{A.16})$$

These relations can be used to find the decomposition of a product representation, such as transformations of wave functions which are products of an orbital and a spin state $|l, m_l\rangle \otimes |s, m_s\rangle$ under rotation by θ about axis $\hat{\mathbf{n}}$. For this representation, characters are products of constituent characters,

$$\chi_{l \otimes s}(\theta) = \frac{1}{2 \sin^2(\theta/2)} [\cos(l-s)\theta - \cos(l+s+1)\theta]. \quad (\text{A.17})$$

We then use orthogonality relations between characters to obtain the decomposition of $\Gamma_l \otimes \Gamma_s$ into irreducible representations Γ_j of the rotation group,

$$\Gamma_l \otimes \Gamma_s = \bigoplus_j a_j \Gamma_j, \quad (\text{A.18})$$

where the multiplicity $a_j = 1$ if $|l-s| \leq j \leq l+s$ and $a_j = 0$ otherwise. These relations are easily checked using (A.13), (A.16) and (A.17). We thus obtain the basic rules for addition of angular momenta.

Let us consider the addition of $2N$ spin 1/2 systems, frequently arising in studies of magnetism. We seek the multiplicity a_l of representations Γ_l ($0 \leq l \leq N$) occurring in the decomposition of the product representation $\Gamma_{1/2}^{2N}$,

$$(\Gamma_{1/2})^{2N} = \bigoplus_{l=0}^N a_l \Gamma_l, \quad (\text{A.19})$$

which has character

$$\chi_{2N} = \chi_{1/2}^{2N}(\theta) = (2 \cos \theta/2)^{2N}. \quad (\text{A.20})$$

Substituting χ_{II} and the character (A.13) of Γ_l into the orthogonality relation (A.16), we obtain

$$\begin{aligned} a_l &= \frac{1}{\pi} \int_0^\pi d\theta (1 - \cos \theta) (2 \cos \theta / 2)^{2N} \frac{\sin(l + 1/2)\theta}{\sin \theta / 2} \\ &= \frac{2}{\pi} \int_0^\pi d\theta \sin \theta / 2 \sin(l + 1/2)\theta (2 \cos \theta / 2)^{2N}. \end{aligned} \quad (\text{A.21})$$

Rewriting the product $2 \sin \theta / 2 \sin(l + 1/2)\theta = \cos l\theta - \cos(l + 1)\theta$, the multiplicity a_l appears as the difference of two integrals,

$$a_l = I_{2N}^l - I_{2N}^{l+1}, \quad (\text{A.22})$$

where the integrals are given by

$$\begin{aligned} I_{2N}^l &= \frac{1}{\pi} \int_0^\pi \cos l\theta (2 \cos \theta / 2)^{2N} d\theta \\ &= \frac{2}{\pi} 2^{2N} \int_0^{\pi/2} \cos 2l\theta (\cos \theta)^{2N} d\theta. \end{aligned} \quad (\text{A.23})$$

These can be calculated using

$$\int_0^{\pi/2} \cos 2lx \cos^{2N} x dx = \frac{\pi}{2^{2N+1}} C_{2N}^{N-l}. \quad (\text{A.24})$$

Hence $I_{2N}^l = C_{2N}^{N-l}$ and coefficients a_l are now expressed as the difference of two binomial coefficients, viz.,

$$\begin{aligned} a_l &= C_{2N}^{N-l} - C_{2N}^{N-l-1} \\ &= \frac{(2N)!}{(N-l)!(N+l)!} - \frac{(2N)!}{(N-l-1)!(N+l+1)!} \\ &= \frac{(2N)!}{(N-l)!(N+l+1)!} [(N+l+1) - (N-l)] \\ &= (2l+1) \frac{(2N)!}{(N-l)!(N+l+1)!}. \end{aligned} \quad (\text{A.25})$$

Whereas the ferromagnetic state $l = N$ appears only once in this decomposition, the antiferromagnetic state $l = 0$ occurs roughly 2^{2N-1} times. This large degeneracy in the ground state is only removed by considering interactions which break rotation invariance.

A.3 Point Groups

These groups arise for solids in which rotation invariance is broken by the crystal lattice. The relevant finite groups and their representations must be compatible with translation invariance of the crystal. The operations of the 32 groups are shown in Fig. A.1. Among these groups, some have inversion

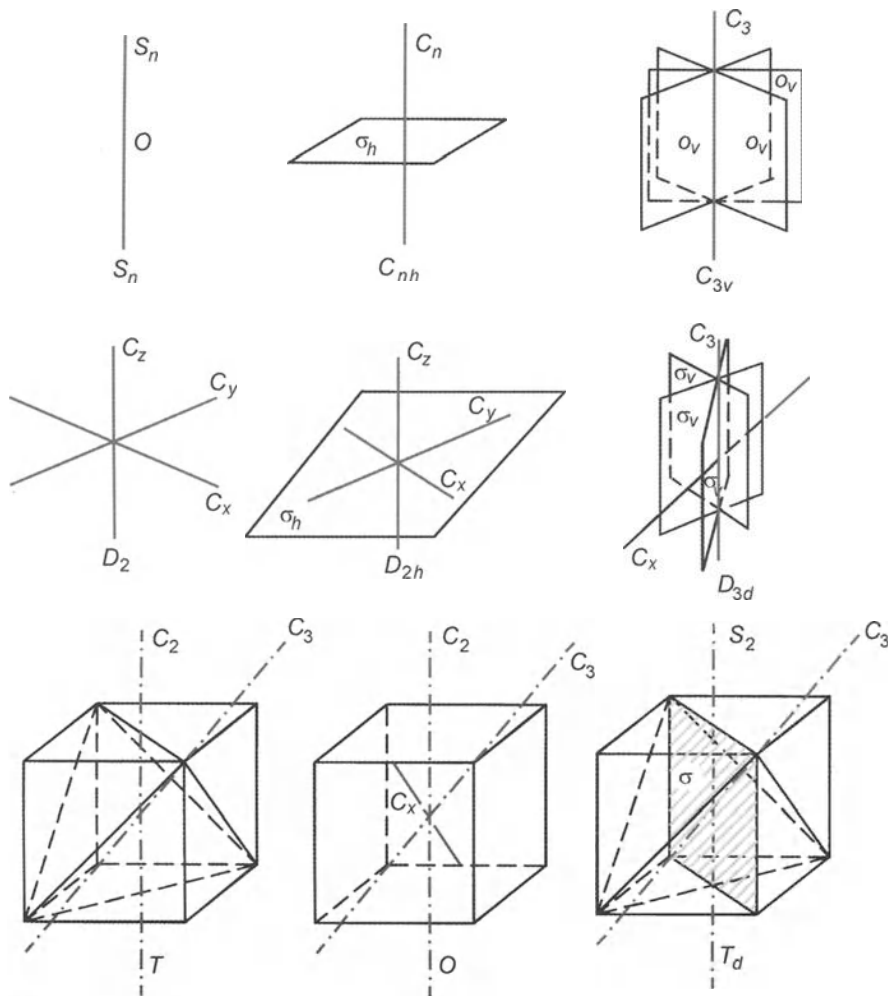


Fig. A.1. Point group symmetry operations

symmetry, that is, they are invariant under $i : \mathbf{r} \rightarrow -\mathbf{r}$. They can then be factorised in the form $G_h = G \times C_i$, where the group $C_i = (E, i)$ is of order 2, E being the identity. The number of conjugacy classes and representations is doubled and the associated characters are products of characters of constituent representations. The 16 remaining groups G can be divided into 7 classes depending on the type of lattice: triclinic, monoclinic, orthorhombic, tetragonal, rhombohedral, hexagonal and cubic.

- The axes of a triclinic structure form a non-orthonormal frame. The only symmetry of such a structure is the identity.

- In a monoclinic structure, the \hat{z} axis is perpendicular to \hat{a}_1 and \hat{a}_2 , a non-orthonormal basis of the (x, y) -plane. The possible groups are: C_2 , order 2, generated by rotation through $\theta = \pi$ about \hat{z} ; and C_{1h} , generated by mirror symmetry in the plane containing \hat{a}_1 and \hat{a}_2 .
- The orthorhombic structure has three mutually orthogonal basis axes. The unit cell has sides of different lengths. There are two basic groups: the order 2 dihedral group D_2 , which is the first in a family D_n of dihedral groups, generated by a symmetry C_n of order n about an axis \hat{z} and n symmetries of order 2 about axes perpendicular to \hat{z} ; and the group C_{2v} containing a symmetry of order 2 about \hat{z} and two mirror symmetries in planes which intersect along \hat{z} .
- In the tetragonal structure, two sides of the unit cell are equal. The basic groups are C_4 , S_4 , D_4 , C_{4v} and D_{2d} . The group $S_{n=4}$ is generated by an improper rotation, product of a rotation of order $n = 4$ and a mirror symmetry. As for C_{2v} , the group C_{4v} has an order 4 symmetry about \hat{z} and $n = 4$ mirror symmetries in planes intersecting along \hat{z} .
- The group $D_{n=2,d}$ has $4n = 8$ elements and is obtained by adding to the $2n$ elements of $D_{n=2}$, $2n$ further elements generated by n diagonal reflection planes containing the \hat{z} axis and equidistant from the $n C_2$ axes of order 2 perpendicular to \hat{z} . In the rhombohedral structure, the three axes \hat{a}_1 , \hat{a}_2 and \hat{a}_3 of the unit cell are at angles $2\pi/3$ to one another. The elementary groups C_3 , S_6 , D_3 , C_{3v} and D_{3d} all possess an order 3 symmetry (at least), and their construction has been described above.
- The hexagonal structure has \hat{z} axis perpendicular to axes \hat{a}_1 and \hat{a}_2 , which are at angle $2\pi/3$ to one another. The possible groups on this structure are C_6 , C_{3h} , C_{6h} , D_6 , C_{6v} , D_{3h} and D_{6h} , all described previously.
- A cubic structure has two new basic symmetry groups. The group T is the group of rotations leaving a regular tetrahedron invariant. There are three order 2 axes through the midpoints of opposite sides of the tetrahedron, and four order 3 axes through the vertices of the tetrahedron and the centres of opposite faces. The order 2 axes are equivalent (we can change from one to another by using one of the order 3 rotations), and so too are the order 3 axes (conjugating this time with the order 2 rotations to change from one axis to another). The other new group is O , containing those rotations which leave the cube invariant. It contains three order 4 axes through the centres of opposite faces, and four order 3 axes through opposite vertices of the cube. There are also six order 2 axes joining the midpoints of opposite sides. It can be generated by adding an order 3 axis to the group D_4 . The group T_d is the full symmetry group of the tetrahedron, which also contains the mirror symmetries in planes containing one side and the midpoint of the opposite side. The group T_d is isomorphic to O via the mapping $S_4 \leftrightarrow C_4$, $C_3 \leftrightarrow C_3$ and $\sigma \leftrightarrow C_2$.

Table A.1. The 32 point groups and their representations. For each group, conjugacy classes are specified by the type of symmetry, and the number of elements in them is given in brackets. Representations are given with their dimension in brackets using conventions explained in the text

Group	Conjugacy class (number of elements)	Representations (dimension)
Triclinic		
$C_1(1)$	$E(1)$	$A(1)$
$S_2(2)$	$E(1) i(1)$	$A_g(1) A_u(1)$
Monoclinic		
$C_2(2)$	$E(1) C_2(1)$	$A(1) B(1)$
$C_{1h}(2)$	$E(1) \sigma_h(1)$	$A'(1) A''(1)$
$C_{2h}(4)$	$E(1) C_2(1) i(1) \sigma_h(1)$	$A_g(1) A_u(1) B_u(1)$
Orthorhombic		
$D_2(4)$	$E(1) C_z(1) C_y(1) C_x(1)$	$A_1(1) B_3(1) B_1(1) B_2(1)$
$C_{2v}(4)$	$E(1) C_2(1) \sigma_v(1) \sigma_{v'}(1)$	$A_1(1) B_2(1) A_2(1) B_1(1)$
$D_{2h}(8)$	$E(1) C_z(1) C_x(1) C_y(1) i(1) \sigma_h(1) \sigma_v(1) \sigma_i(1)$	$A_{1g}(1) B_{3g}(1) B_{1g}(1) B_{2g}(1) A_{1u}(1) B_{3u}(1) B_{1u}(1) B_{2u}(1)$
Tetragonal		
$C_4(4)$	$E(1) C_4(1) C_2(1) C_4^3(1)$	$A(1) B(1) E(1) E^*(1)$
$S_4(4)$	$E(1) S_4(1) C_2(1) S_4^3(1)$	$A(1) B(1) E(1) E^*(1)$
$C_{4h}(8)$	$E(1) C_4(1) C_2(1) C_4^3(1) i(1) S_4(1) S_2(1) S_4^3(1)$	$A_g(1) B_g(1) E_g(1) E_g^*(1) A_u(1) B_u(1) E_u(1) E_u^*(1)$
$D_4(8)$	$E(1) C_4^2(1) C_4(2) C_2(2) C_{2'}(2)$	$A_1(1) A_2(1) B_1(1) B_2(1) E(2)$
$C_{4v}(8)$	$E(1) C_4^2(1) C_4(2) \sigma_v(2) \sigma_{v'}(2)$	$A_1(1) A_2(1) B_1(1) B_2(1) E(2)$
$D_{2d}(8)$	$E(1) C_2(1) S_4(2) C_2(2) \sigma_d(2)$	$A_1(1) A_2(1) B_1(1) B_2(1) E(2)$
$D_{4h}(16)$	$E(1) C_4^2(1) C_4(2) C_2(2) C_{2'}(2) i(1) \sigma_h(1) S_4(2) \sigma_v(2) \sigma_{v'}(2)$	$A_g^1(1) A_g^2(1) B_g^1(1) B_g^2(1) E_g(2) A_u^1(1) A_u^2(1) B_u^1(1) B_u^2(1) E_u(2)$
Rhombohedral		
$C_3(3)$	$E(1) C_3(1) C_3^2(1)$	$A(1) E(1) E^*(1)$
$S_6(6)$	$E(1) C_3(1) C_3^2(1) i(1) S_3(1) S_3^2(1)$	$A_g(1) E_g(1) E_g^*(1) A_u(1) E_u(1) E_u^*(1)$
$D_3(6)$	$E(1) C_3(2) C_x(3)$	$A_1(1) A_2(1) E(2)$
$C_{3v}(6)$	$E(1) C_3(2) \sigma_v(3)$	$A_1(1) A_2(1) E(2)$
$D_{3d}(6)$	$E(1) C_3(2) C_x(3) i(1) S_3(2) S_x(3)$	$A_g^1(1) A_g^2(1) E_g(2) A_u^1(1) A_u^2(1) E_u(2)$
Hexagonal		
$C_6(6)$	$E(1) C_6(1) C_3(1) C_2(1) C_6^4(1) C_6^5(1)$	$A(1) B(1) E^1(1) E^{1*}(1) E^2(1) E^{2*}(1)$
$C_{3h}(6)$	$E(1) C_3(1) C_3^2(1) i(1) S_3(1) S_3^2(1)$	$A_g(1) E_g(1) E_g^*(1) A_u(1) E_u(1) E_u^*(1)$
$C_{6h}(12)$	$E(1) C_6(1) C_3(1) C_2(1) C_6^4(1) C_6^5(1) i(1) S_6(1) S_3(1) \sigma_h(1) S_6^4(1) S_6^5(1)$	$A_g(1) B_g(1) E_g^1(1) E_g^{1*}(1) E_g^2(1) E_g^{2*}(1) A_u(1) B_u(1) E_u^1(1) E_u^{1*}(1) E_u^2(1) E_u^{2*}(1)$
$D_6(12)$	$E(1) C_6^3(1) C_6^2(2) C_6(2) C_2(3) C_{2'}(3)$	$A_1(1) A_2(1) B_1(1) B_2(1) E_2(2) E_1(2)$
$C_{6v}(12)$	$E(1) C_6^3(1) C_6^2(2) C_6(2) \sigma_v(3) \sigma_{v'}(3)$	$A_1(1) A_2(1) B_1(1) B_2(1) E_1(2) E_2(2)$
$D_{3h}(12)$	$E(1) \sigma_h(1) S_6^2(2) S_6(2) C_2(3) \sigma_v(3)$	$A'_1(1) A'_2(1) A''_1(1) A''_2(1) E'(2) E''(2)$
$D_{6h}(24)$	$E(1) C_6^3(1) C_6^2(2) C_6(2) C_2(3) C_{2'}(3) i(1) \sigma_h(1) S_3(2) S_6(2) \sigma_v(3) \sigma_d(3)$	$A_g^1(1) A_g^2(1) B_g^1(1) B_g^2(1) E_g^2(2) E_g^1(2) A_u(1) A_u^1(1) B_u^1(1) B_u^2(1) E_u^2(2) E_u^1(2)$
Cubic		
$T(12)$	$E(1) C_2(3) C_3(4) C_3^2(4)$	$A(1) E(1) E^*(1) F(3)$
$T_h(24)$	$E(1) C_2(3) C_3(4) C_3^2(4) i(1) S_2(3) S_3(4) S_3^2(4)$	$A_g(1) E_g(1) E_g^*(1) F_g(3) A_u(1) E_u(1) E_u^*(1) F_u(3)$
$O(24)$	$E(1) C_3(8) C_4^2(3) C_2(6) C_4(6)$	$A_1(1) A_2(1) E(2) F_2(3) F_1(3)$
$T_d(24)$	$E(1) C_3(8) S_2^2(3) \sigma_d(6) S_4(6)$	$A_1(1) A_2(1) E(2) F_1(3) F_2(3)$
$O_h(48)$	$E(1) C_3(8) C_4^2(3) C_2(6) C_4(6) i(1) S_3(8) \sigma_h(3) \sigma_d(6) S_4(6)$	$A_g^1(1) A_g^2(1) E_g(2) F_g^2(3) F_g^1(3) A_u(1) A_u^1(1) E_u(2) F_u^2(3) F_u^1(3)$

A.4 Representations of Point Groups

The number of irreducible representations of each group is given by the number of conjugacy classes and their dimensions by (A.5). Letters A , B , E or F denote the type of representation. One-dimensional representations are denoted by letters A or B , depending on whether basis states (wave functions) are even or odd under the main rotation symmetry generating the group. For example, the basis state in the B representation of group C_2 is such that

$$\psi_B(\mathbf{r}') = \psi_B(-x, -y, z) = -\psi_B(x, y, z).$$

Hence the character $\chi_B(c_2)$ of this rotation is not equal to 1 (whereas $\chi_A(c_2) = 1$). Letter E denotes two-dimensional representations. However, in Table A.1, some representations which are complex conjugates of one another like $E(1)$ and $E^*(1)$ are actually one-dimensional. The letter E is used because time reversal symmetry, which leaves the Hamiltonian invariant, permutes the basis states of representations E and E^* . These two one-dimensional representations therefore form a doublet of degenerate states, unless some magnetic perturbation removes the degeneracy by breaking invariance under $t \rightarrow -t$. Letter F denotes three-dimensional representations. Finally, for groups $G_h = G \times C_i$, the index g (gerade) indicates a representation in which basis states are even with respect to parity (inversion), whilst an index u (ungerade) means that they are odd.

Explicit determination of characters for these representations involves orthogonality relations, cyclic properties of certain subgroups and use of (A.3). Details are given in the references cited in the bibliography. Many groups are product groups:

$$\begin{aligned} C_{3h} &= C_3 \times C_i, & C_{4h} &= C_4 \times C_i, & C_{6h} &= C_6 \times C_i, \\ D_{2h} &= D_2 \times C_i, & D_{4h} &= D_4 \times C_i, & S_6 &= C_3 \times C_i, \\ D_{3d} &= D_4 \times C_i, & D_{6h} &= D_6 \times C_i, & T_h &= T \times C_i, \\ O_h &= O \times C_i. \end{aligned} \tag{A.26}$$

The irreducible representations are products of representations and the characters are products of characters. The tables below only specify characters of factor groups. Many groups are isomorphic and have the same character table, which greatly reduces the number of tables.

A.5 Application to the Crystalline Field

Representations of point groups are used to determine electronic multiplets in crystals. In Sect. 2.13(I), we discussed the limit of the strong crystalline field affecting the $4d$ and $5d$ shells, and sometimes also the $3d$ shell. The basic

multiplets are then determined by the crystalline field with the Hund term as perturbation. In a cubic crystal with symmetry group O , the representation of the ground state of an ion with a single electron in the outer d shell is F_2 , of dimension 3 [see Sect. 2.13(I)]. The configuration of this electron in a crystalline orbit belonging to the F representation is denoted $4f_2^1$ or $5f_2^1$, in complete analogy with the corresponding atomic notation $4d^1$ or $5d^1$. To obtain the multiplet structure of an ion with two d electrons in a cubic crystal (configuration $4f_2^2$ or $5f_2^2$, e.g., Nb^{3+} or Ta^{2+}), we decompose the representation $F_2 \otimes F_2$ into irreducible representations of group O . The character table of $F_2 \otimes F_2$ is found by taking the squares of entries in the character table A.7 for F_2 , i.e.,

	E	$C_3(8)$	$C_4^2(3)$	$C_2(6)$	$C_4(6)$
$F_2 \otimes F_2$	9	0	1	1	1

Since the group O is order 24, we apply the orthogonality relation (A.11) and use Table A.7 to obtain the decomposition of $F_2 \otimes F_2$ for this symmetry group:

$$F_2 \otimes F_2 = A_1 \oplus E \oplus F_2 \oplus F_1 . \quad (\text{A.27})$$

There are therefore four different multiplets. The Hund term then determines the ground state. Coulomb repulsion is always smallest in a spatially antisymmetric $S = 1$ state. Both F_1 and F_2 have this antisymmetry. For $n f_2^2$ configurations in octahedral symmetry, the ground state is 3F_1 ($S = 1$) and the first excited state is 3F_2 [576].

Table A.2. Character tables for groups C_1 , C_i , C_2 , C_s , C_{2h} , C_{2v} and D_2

C_i			E	i	C_{2h}			E	C_2	σ_h	i	
C_2			E	C_2	C_{2v}			E	C_2	σ_v	$\sigma_{v'}$	
C_s			E	σ	D_2			E	C_z	C_x	C_y	
C_1	$ $	E	A_g	A_1	A_g	A_1	A_1	1	1	1	1	
A	$ $	1	A_g	A	A'	1	1	B_g	B_2	B_3	1	-1
A_u	$ $		A_u	B	A''	1	-1	A_u	A_2	B_1	1	1
								B_u	B_1	B_2	1	-1

Let us now consider the case of iron Fe^{++} which has 6 d electrons. In a strong crystalline field, the energy difference between crystalline orbits f and e is greater than the Hund term. The six electrons then occupy the three f orbitals (configuration $3f_2^6$) and the total spin is zero. This state is not magnetic and belongs to the identity representation A_1 of the group O [576]. When the Hund term is large enough to align spins, the electrons go into the crystalline configuration $3f_2^4e^2$. As one of the f_2 orbitals is full, this

Table A.3. Character tables for groups C_3 , C_{3v} and D_3 , with $\varepsilon = \exp(-2\pi i/3)$

C_3	E	C_3	C_3^2	C_{3v}	D_3	E	$C_3(2)$	$\sigma_v(3)$
						E	$C_3(2)$	$C_x(3)$
A	1	1	1	A_1	A_1	1	1	1
E	1	ε	ε^2	A_2	A_2	1	1	-1
E^*	1	ε^2	ε	E	E	2	-1	0

Table A.4. Character table for groups C_4 , S_4 and S_6 , with $\varepsilon = \exp(2\pi i/6)$

C_4	E	C_4	C_2	C_4^3	C_6	E	C_6	C_6^2	C_6^3	C_6^4	C_6^5
	E	S_4	S_4^2	S_4^3	A	1	1	1	1	1	1
A	A	1	1	1	B	1	-1	1	-1	1	-1
B	B	1	-1	1	E_1	1	ε^2	- ε	1	ε^2	- ε
E	E	1	i	-1	E_1^*	1	- ε	ε^2	1	- ε	ε^2
E^*	E^*	1	-i	-1	E_2	1	ε	ε^2	-1	- ε	- ε^2
					E_2^*	1	- ε^2	- ε	-1	ε^2	ε

Table A.5. Character table for groups C_{4v} , D_4 and D_{2d}

C_{4v}	E	C_4^2	$C_4(2)$	$\sigma_v(2)$	$\sigma_{v'}(2)$
D_4	E	C_4^2	$C_4(2)$	$C_2(2)$	$C_{2'}(2)$
	E	C_2	$S_4(2)$	$C_2(2)$	$\sigma_d(2)$
A_1	A_1	A_1	1	1	1
A_2	A_2	A_2	1	1	-1
B_1	B_1	B_1	1	1	-1
B_2	B_2	B_2	1	1	-1
E	E	E	2	-2	0
				0	0

Table A.6. Character table for groups C_{6v} , D_6 and D_{3h}

D_6	E	C_6^3	$C_6^2(2)$	$C_6(2)$	$C_2(3)$	$C_{2'}(3)$
C_{6v}	E	C_6^3	$C_6^2(2)$	$C_6(2)$	$\sigma_v(3)$	$\sigma_{v'}(3)$
	E	σ_h	$S_6^2(2)$	$S_6(2)$	$C_2(3)$	$\sigma_v(3)$
A_1	A_1	A'_1	1	1	1	1
A_2	A_2	A'_2	1	1	1	-1
B_1	B_2	A''_1	1	-1	1	-1
B_2	B_1	A''_2	1	-1	1	-1
E_2	E_1	E'	2	2	-1	-1
E_1	E_2	E''	2	-2	-1	1
				1	0	0
				0	0	0

Table A.7. Character table for groups T , O and T_d , with $\varepsilon = \exp(-2\pi i/3)$

T	E	$C_2(3)$	$C_3(4)$	$C_3^2(4)$	O		E	$C_3(8)$	$C_4^2(3)$	$C_2(6)$	$C_4(6)$
					T_d	E	$C_3(8)$	S_4^2	$\sigma_d(6)$	$S_4(6)$	
A	1	1	1	1	A_1	A_1	1	1	1	1	1
E	1	1	ε	ε^2	A_2	A_2	1	1	1	-1	-1
E^*	1	1	ε^2	ε	E	E	2	-1	2	0	0
F	3	-1	0	0	F_2	F_2	3	0	-1	1	-1
					F_1	F_1	3	0	-1	-1	1

configuration is equivalent to $3f_2^2e^2$. The character table of this representation $F_2 \otimes F_2 \otimes E \otimes E$ is obtained by straightforward multiplication of characters:

	E	$C_3(8)$	$C_4^2(3)$	$C_2(6)$	$C_4(6)$
$F_2 \otimes F_2$	9	0	1	1	1
$E \otimes E$	4	1	4	0	0
$F_2 \otimes F_2 \otimes E \otimes E$	36	0	4	0	0

The decomposition is

$$F_2 \otimes F_2 \otimes E \otimes E = 2A_1 \oplus 2A_2 \oplus 4E \oplus 4F_2 \oplus 4F_1. \quad (\text{A.28})$$

The state with lowest energy is 5F_2 . This is a magnetic state ($S = 2$).

When the Hund term dominates the crystalline field (3d shell), the configuration of an isolated ion may also be used to obtain the elementary multiplet. In this case, multiplets of the isolated ion are determined by the Hund rules [see Sect. 3.3(I)]: 2D for a $3d^1$ configuration such as V^{4+} and Ti^{3+} , and 3F for a $3d^2$ configuration such as V^{3+} . The corresponding representations of the rotation group are Γ_2 and Γ_3 , respectively. To decompose these into irreducible representations of the crystal, we construct the character tables of Γ_l , $l = 2, 3$ in the point group. As an example, consider a cubic symmetry. For any rotation of order n , its character in Γ_l is

$$\chi_l(2\pi/n) = \frac{\sin(l + 1/2)(2\pi/n)}{\sin(\pi/n)}. \quad (\text{A.29})$$

As the group O contains only rotation symmetries of orders 4, 3 and 2, this equation gives the character tables of Γ_2 and Γ_3 for conjugacy classes of O .

Using orthogonality relations (A.11) and Table A.7 once again, we can obtain the decomposition of these representations in terms of irreducible representations of the octahedral group:

$$\begin{aligned} \Gamma_2 &= E \oplus F_2, \\ \Gamma_3 &= A_2 \oplus F_1 \oplus F_2. \end{aligned} \quad (\text{A.30})$$

	E	$C_3(8)$	$C_4^2(3)$	$C_2(6)$	$C_4(6)$
Γ_2	5	-1	1	1	-1
Γ_3	7	1	-1	-1	-1

Note that representations F_1 and F_2 appear in this decomposition of Γ_3 , representation of the multiplet of the isolated ion, and also in the decomposition of the product representation $F_2 \otimes F_2$ of crystalline orbits. This is to be expected since symmetry considerations disregard the relative magnitude of the Hund term and crystalline field. Note also that multiplets E and F_2 occur in the decomposition of Γ_2 ($3d^1$ configuration). This agrees with the result obtained in Sect. 2.13(I) by selecting linear combinations of $l = 2$ orbitals respecting the crystal symmetries.

Representations of symmetry groups $G_h = G \times G_i$ are obtained from those of G . Representations Γ_l do not contain inversion and split into Γ_l^g and Γ_l^u depending on the sign of $\chi(i)$. It follows that the decomposition of Γ_l^g only involves g representations of G_h . Likewise, representations Γ_l^u only contain u representations.

Angular momentum j is approximately a good quantum number in the rare earths. Study of crystalline fields requires character tables for half-integral representations of the point groups. The simplest approach is to adjoin an element R to the group, corresponding to rotation by 2π in a 4π periodic space. This doubles the sizes of the point groups. When $\chi(R) = 1$, we find the same tables as before. When $\chi(R) = -1$, we construct the table by multiplying characters. Decomposition into irreducible representations is then carried out as in the above examples.

Representations of crystal symmetry groups can also be used to obtain optical or Raman selection rules, exactly as representations of the rotation group determine atomic selection rules.

B. Second Quantisation

B.1 State Space for N Free Fermions

For N independent particles, the Hamiltonian is the sum of the Hamiltonians for each particle,

$$\mathcal{H} = \sum_i \mathcal{H}_0^i. \quad (\text{B.1})$$

As the Hamiltonian is separable, the N -fermion wave function is a linear combination of products of N wave functions of the 1-particle Hamiltonian \mathcal{H}_0 . The Pauli principle considerably reduces the number of possible linear combinations, since the wave function must be completely antisymmetric under exchange of any two fermions. A basis for the N -fermion wave functions is given by Slater determinants of N distinct wave functions of the Hamiltonian \mathcal{H}_0 ,

$$\langle \dots \mathbf{r}_j \sigma_j \dots | \psi_N \rangle = \frac{1}{\sqrt{N!}} \begin{vmatrix} \phi_1(\mathbf{r}_1, \sigma_1) & \phi_2(\mathbf{r}_1, \sigma_1) & \cdots & \phi_n(\mathbf{r}_1, \sigma_1) \\ \phi_1(\mathbf{r}_2, \sigma_2) & \phi_2(\mathbf{r}_2, \sigma_2) & \cdots & \phi_n(\mathbf{r}_2, \sigma_2) \\ \vdots & \vdots & \ddots & \vdots \\ \phi_1(\mathbf{r}_n, \sigma_n) & \phi_2(\mathbf{r}_n, \sigma_n) & \cdots & \phi_n(\mathbf{r}_n, \sigma_n) \end{vmatrix}, \quad (\text{B.2})$$

where σ_j are spin variables (\uparrow and \downarrow). It is hardly worth specifying the exact form of this wave function, imposed by the Pauli principle. It is more useful to specify which states are occupied amongst the possible states of \mathcal{H}_0 . The latter are generally far more numerous than the number of particles N . Then the above state can be specified by

$$|\psi_N\rangle = |\alpha, \beta, \dots, \mu\rangle \equiv |\{N_\mu\}\rangle, \quad (\text{B.3})$$

where $\{N_\mu\} \equiv \alpha, \dots, \mu$ are N states chosen amongst the eigenstates of \mathcal{H}_0 . We may always add a further particle, provided we antisymmetrise over all coordinates. We must specify the state in which the particle is added. This is done using a creation operator a_ν^\dagger . We must also specify its phase relative to the N -particle wave function. The state

$$|\psi_{N+1}\rangle = (-1)^N a_\nu^\dagger |\psi_N\rangle = (-1)^N a_\nu^\dagger |\{N_\mu\}\rangle = (-1)^N |\alpha \dots \mu \nu\rangle \quad (\text{B.4})$$

describes $N + 1$ particles in states $\alpha, \dots, \mu, \nu \equiv \{N_\mu\} + \nu$. We also define a destruction operator for the fermion in state ν by

$$|\psi_N\rangle = |\{N_\mu\}\rangle = (-1)^N a_\nu |\psi_N, \nu\rangle = (-1)^N a_\nu |\{N_\mu\}, \nu\rangle . \quad (\text{B.5})$$

In Dirac notation, these operators become

$$a_\nu = |\{N_\mu\}\rangle \langle \{N_\mu\}, \nu| , \quad a_\nu^\dagger = |\{N_\mu\}, \nu\rangle \langle \{N_\mu\}| . \quad (\text{B.6})$$

By successive application of creation operators, we can construct a completely antisymmetrised N -fermion state from the vacuum, denoted $|0\rangle$. The latter is considered here to be the state containing no particles. We have

$$|\psi_N\rangle = (-1)^P \prod_{\nu \in \{N_\mu\}} a_\nu^\dagger |0\rangle , \quad (\text{B.7})$$

where $(-1)^P$ is a phase factor. As an example, wave functions for one and two particles are

$$\langle \mathbf{r}_1 | a_\alpha^\dagger | 0 \rangle = \langle \mathbf{r}_1 | \alpha \rangle = \phi_\alpha(\mathbf{r}_1) , \quad (\text{B.8})$$

$$\begin{aligned} \langle \mathbf{r}_1, \mathbf{r}_2 | a_\beta^\dagger a_\alpha^\dagger | 0 \rangle &= \langle \mathbf{r}_1, \mathbf{r}_2 | \beta, \alpha \rangle \\ &= \phi_\alpha(\mathbf{r}_2) \phi_\beta(\mathbf{r}_1) - \phi_\beta(\mathbf{r}_2) \phi_\alpha(\mathbf{r}_1) . \end{aligned} \quad (\text{B.9})$$

The N -fermion ground state, often called the Fermi sea, is obtained by choosing the set $\{N_\mu\}$ of the N lowest energies determined by \mathcal{H}_0 (including spin degeneracy). An arbitrary N -fermion state is a linear combination of states of the form (B.7) with different sets $\{N_\mu\}$. From definitions (B.4) and (B.5), the following anticommutation relations are satisfied:

$$\begin{aligned} \{a_\mu, a_\nu\} &= \{a_\mu^\dagger, a_\nu^\dagger\} = 0 , \\ \{a_\mu, a_\nu^\dagger\} &= a_\mu a_\nu^\dagger - a_\nu^\dagger a_\mu = \delta_{\mu\nu} . \end{aligned} \quad (\text{B.10})$$

These guarantee antisymmetry of N -fermion states. The number operator, or occupation operator, is defined by

$$n_\nu = a_\nu^\dagger a_\nu . \quad (\text{B.11})$$

This measures the level of occupation of state ν , since

$$\begin{aligned} n_\nu |\{N_\mu\}\rangle &= 0 \quad \text{if } \nu \notin \{N_\mu\} , \\ n_\nu |\{N_\mu\}\rangle &= 1 \quad \text{if } \nu \in \{N_\mu\} . \end{aligned} \quad (\text{B.12})$$

B.2 Other Representations

From the operator a_ν^\dagger creating an electron in state ν , we can define new operators creating the electron in other states. Amongst these, we define field operators

$$\begin{aligned} \psi_\sigma(\mathbf{r}) &= \sum_\nu \phi_\nu(\mathbf{r}) a_{\nu, \sigma} , \\ \psi_\sigma^\dagger(\mathbf{r}) &= \sum_\nu \phi_\nu^*(\mathbf{r}) a_{\nu, \sigma}^\dagger , \end{aligned} \quad (\text{B.13})$$

where σ is a spin index and the sum extends over a complete set of eigenstates $\phi_\nu(\mathbf{r})$ of \mathcal{H}_0 . These operators create or destroy a particle at \mathbf{r} , as can be seen from the anticommutation relations,

$$\begin{aligned} \left\{ \psi_\sigma(\mathbf{r}), \psi_{\sigma'}^\dagger(\mathbf{r}') \right\} &= \sum_{\mu, \nu} \phi_\nu^*(\mathbf{r}') \phi_\mu(\mathbf{r}) \left\{ a_{\nu, \sigma}, a_{\mu, \sigma'}^\dagger \right\} \\ &= \delta_{\sigma \sigma'} \sum_\mu \phi_\mu^*(\mathbf{r}') \phi_\mu(\mathbf{r}) = \delta(\mathbf{r} - \mathbf{r}') \delta_{\sigma \sigma'} . \end{aligned} \quad (\text{B.14})$$

The interpretation of $\psi^\dagger(\mathbf{r})$ and $\psi(\mathbf{r})$ as creation and destruction operators for particles at \mathbf{r} follows from

$$\begin{aligned} \langle 0 | \psi_{\sigma'}^\dagger(\mathbf{r}') \psi_\sigma(\mathbf{r}) | 0 \rangle &= 0 , \\ \langle 0 | \psi_\sigma(\mathbf{r}) \psi_{\sigma'}^\dagger(\mathbf{r}') | 0 \rangle &= \delta(\mathbf{r} - \mathbf{r}') \delta_{\sigma \sigma'} . \end{aligned} \quad (\text{B.15})$$

A basis of states for the Hamiltonian \mathcal{H}_0 containing a periodic lattice potential is given by the Bloch states $\phi(\mathbf{k}, \mathbf{r})$, with wave vector \mathbf{k} [see Sect. 3.4(I)]. Their Fourier transforms are the Wannier states $\phi(\mathbf{r} - \mathbf{R}_i)$, which correspond to atomic orbitals localised around the ion at \mathbf{R}_i [see Sect. 3.6(I), (3.61) and (3.63)]. These states can be used to express the field operator:

$$\psi(\mathbf{r}) = \sum_i \phi(\mathbf{r} - \mathbf{R}_i) a_i = \frac{1}{\sqrt{V}} \sum_i \sum_{\mathbf{k}} \exp(-i\mathbf{k} \cdot \mathbf{R}_i) \phi(\mathbf{k}, \mathbf{R}) a_i . \quad (\text{B.16})$$

The operator

$$a_{\mathbf{k}} = \frac{1}{\sqrt{V}} \sum_i \exp(-i\mathbf{k} \cdot \mathbf{R}_i) a_i \quad (\text{B.17})$$

then destroys a Bloch state of wave vector \mathbf{k} . Field operators can be expressed just as well in the Wannier basis as in the Bloch basis:

$$\psi(\mathbf{r}) = \sum_{\mathbf{k}} \phi(\mathbf{k}, \mathbf{r}) a_{\mathbf{k}} . \quad (\text{B.18})$$

This is a particularly useful representation because the Hamiltonian is often diagonalised in such a basis. We define the operator $\rho_\sigma(\mathbf{r})$,

$$\rho_\sigma(\mathbf{r}) = \psi_\sigma^\dagger(\mathbf{r}) \psi_\sigma(\mathbf{r}) , \quad (\text{B.19})$$

which measures the density of spin σ particles at \mathbf{r} . This operator also has a Fourier decomposition,

$$\begin{aligned} \rho_\sigma(\mathbf{q}) &= \int \frac{d^3 r}{V} \exp(-i\mathbf{q} \cdot \mathbf{r}) \rho(\mathbf{r}) \\ &= \int \frac{d^3 r}{V} \exp(-i\mathbf{q} \cdot \mathbf{r}) \sum_{\mathbf{k}, \mathbf{k}'} \phi^*(\mathbf{k}, \mathbf{r}) \phi(\mathbf{k}', \mathbf{r}) a_{\mathbf{k}}^\dagger a_{\mathbf{k}'} \\ &= \frac{1}{V} \sum_{\mathbf{k}, \mathbf{k}'} S(\mathbf{k}, \mathbf{k}', \mathbf{q}) a_{\mathbf{k}}^\dagger a_{\mathbf{k}'} , \end{aligned} \quad (\text{B.20})$$

where the structure factor

$$S(\mathbf{k}, \mathbf{k}', \mathbf{q}) = \int d^3r \exp(-i\mathbf{q} \cdot \mathbf{r}) \phi^*(\mathbf{k}, \mathbf{r}) \phi(\mathbf{k}', \mathbf{r})$$

is a delta function $\delta(\mathbf{k} - \mathbf{k}' - \mathbf{q})$ when the Bloch states reduce to plane waves. Since the density operator is Hermitian $\rho^\dagger(\mathbf{r}) = \rho(\mathbf{r})$, its Fourier components satisfy $\rho_\mathbf{q}^\dagger = \rho_{-\mathbf{q}}$.

When there are no interactions, an operator $a_\beta^\dagger a_\alpha$ describes excitation of a particle from state α to state β . If the 1-particle Hamiltonian \mathcal{H}_0 is diagonal in basis ϕ_μ , the N -particle Hamiltonian \mathcal{H} is a sum of diagonal terms $\varepsilon_\mu^0 a_\mu^\dagger a_\mu$, each of which describes the energy of state μ multiplying its occupation number.

We define the *normal ordering* of an operator acting on the N -particle state space by moving all creation operators to the left and all destruction operators to the right, e.g.,

$$a_\alpha^\dagger a_\beta, \quad a_\alpha^\dagger a_\beta^\dagger a_\delta a_\gamma.$$

Its expectation value in an N -particle state is zero unless it changes none of the occupation numbers of 1-particle states. This is the case if each creation operator index coincides with a destruction operator index, and vice versa. Then the expectation value is found by contracting indices. The contraction of the following operators is:

$$\langle U_{\alpha\beta} a_\alpha^\dagger a_\beta \rangle = U_{\alpha\alpha} n_\alpha, \quad (\text{B.21})$$

$$\langle v_{\alpha\beta;\gamma\delta} a_\alpha^\dagger a_\beta^\dagger a_\delta a_\gamma \rangle = (v_{\alpha\beta;\alpha\beta} - v_{\alpha\beta;\beta\alpha}) n_\alpha n_\beta. \quad (\text{B.22})$$

When v is a constant, independent of the state, the last term is zero.

B.3 Representation of Operators in Second Quantisation

We make a distinction between quadratic operators coupled to the density (such as a static potential due to an electromagnetic field or impurities) and operators coupling the density at two different points (such as an interparticle potential). Let $\phi_\mu(\mathbf{r})$ be a basis of eigenstates of \mathcal{H}_0 , defined by

$$\mathcal{H}_0(\mathbf{r}) \phi_\mu(\mathbf{r}) = \left[-\frac{\hbar^2}{2m} \nabla^2 + V(\mathbf{r}) \right] \phi_\mu(\mathbf{r}) = \varepsilon_\mu^0 \phi_\mu(\mathbf{r}). \quad (\text{B.23})$$

The representation of the Hamiltonian in second quantisation is

$$\int d^3r \psi^\dagger(\mathbf{r}) \mathcal{H}_0 \psi(\mathbf{r}) = \sum_\mu \varepsilon_\mu^0 a_\mu^\dagger a_\mu, \quad (\text{B.24})$$

which is diagonal, as anticipated. It is in this sense that second quantisation is useful: the expectation value of this Hamiltonian,

$$\langle \phi_N | \mathcal{H}_0 | \phi_N \rangle = \sum_{\mu} \varepsilon_{\mu} \langle n_{\mu} \rangle , \quad (\text{B.25})$$

is given by the occupation of each 1-particle state. We thereby avoid all the complexities of the N -particle antisymmetric wave function. Of course, we may adopt any representation \mathbf{k} in which the Hamiltonian is diagonal. Any perturbation $U(\mathbf{r})$ coupled to the density (i.e., a potential) has representation

$$\int d^3r \psi^{\dagger}(\mathbf{r}) U(\mathbf{r}) \psi(\mathbf{r}) = \sum_{\mu, \nu} U_{\mu\nu} a_{\mu}^{\dagger} a_{\nu} , \quad (\text{B.26})$$

where

$$U_{\mu\nu} = \int d^3r \phi_{\mu}^{*}(\mathbf{r}) U(\mathbf{r}) \phi_{\nu}(\mathbf{r}) . \quad (\text{B.27})$$

Once again, in some other representation \mathbf{k} , we express the potential by Fourier transform:

$$U(\mathbf{q}) = \frac{1}{V} \int d^3r \exp(-i\mathbf{q} \cdot \mathbf{r}) U(\mathbf{r}) . \quad (\text{B.28})$$

In second quantisation, the potential becomes

$$\frac{1}{V} \sum_{\mathbf{k}, \mathbf{k}', \mathbf{q}} U(\mathbf{q}) S(\mathbf{k}, \mathbf{k}', \mathbf{q}) a_{\mathbf{k}}^{\dagger} a_{\mathbf{k}'} = \sum_{\mathbf{k}, \mathbf{k}'} U_{\mathbf{k}, \mathbf{k}'} a_{\mathbf{k}}^{\dagger} a_{\mathbf{k}'} , \quad (\text{B.29})$$

where the structure factor S defined previously is a delta-function $\delta(\mathbf{k}-\mathbf{k}'-\mathbf{q})$ when the Bloch states reduce to plane waves.

Representation of an interaction potential $V(\mathbf{r}, \mathbf{r}')$ between particles is more complex because it couples the densities at \mathbf{r} and \mathbf{r}' , whence its representation

$$\mathcal{N} \left[\frac{1}{2} \int d^3r \rho(\mathbf{r}) V(\mathbf{r}, \mathbf{r}') \rho(\mathbf{r}') \right] = \frac{1}{2} \sum_{\alpha\beta;\gamma\delta} v_{\alpha\beta;\gamma\delta} a_{\alpha}^{\dagger} a_{\beta}^{\dagger} a_{\delta} a_{\gamma} , \quad (\text{B.30})$$

where \mathcal{N} normal orders. The matrix element of the potential is

$$v_{\alpha\beta;\gamma\delta} = \int d^3r d^3r' \phi_{\alpha}^{*}(\mathbf{r}) \phi_{\beta}^{*}(\mathbf{r}') V(\mathbf{r}, \mathbf{r}') \phi_{\gamma}(\mathbf{r}) \phi_{\delta}(\mathbf{r}') . \quad (\text{B.31})$$

It should be emphasised that indices do not occur in the same order in the matrix element of V and in its representation in terms of second quantisation operators. This is crucial since antisymmetry of wave functions is absorbed by second quantisation operators. For the interaction to have the right sign, we must always change its sign when two fermion operators are permuted. In this case, there were two permutations: firstly, the operators were normal ordered, and then γ and δ were swapped to remove a minus sign. In general, V does not depend on spin. The matrix elements are then zero, unless the total index $\alpha \equiv (i\sigma)$ is the same as $\gamma = (j\sigma)$ and likewise, β is the same as δ [see Chap. 3(I)].

We may, of course, represent the interaction potential in the Bloch wave basis,

$$\frac{1}{2} \sum_{\mathbf{k}, \mathbf{k}', \mathbf{q}} V(\mathbf{k}, \mathbf{k}', \mathbf{q}) a_{\mathbf{k}-\mathbf{q}}^\dagger a_{\mathbf{k}'+\mathbf{q}}^\dagger a_{\mathbf{k}'} a_{\mathbf{k}} . \quad (\text{B.32})$$

Each term describes a scattering process between two particles with initial momentum states \mathbf{k} and \mathbf{k}' and final states $\mathbf{k} - \mathbf{q}$, $\mathbf{k}' + \mathbf{q}$. Vector \mathbf{q} is therefore the momentum transferred in the collision. When the Bloch states are plane waves, $V(\mathbf{k}, \mathbf{k}', \mathbf{q})$ only depends on \mathbf{q} , the momentum transfer. If the system is not translation invariant, we may still find a representation of the interaction in the form (B.32) [see Sect. 11.4.1(I)], but we must now add a further sum over wave vectors of the reciprocal lattice.

B.4 Perturbation Theory

To first order, the shift in energy of a state is calculated by taking the expectation of the perturbation in that state,

$$\langle \psi_N | \mathcal{H}_{\text{pert}} | \psi_N \rangle . \quad (\text{B.33})$$

Since interaction potentials are represented in normal ordered form, the only non-zero contributions to this expectation come from contractions of second quantisation operators occurring in $\mathcal{H}_{\text{pert}}$ (see Sect. B.2). For quadratic operators, the matrix element reduces to

$$\left\langle \psi_N \left| \sum_{\mu\nu} U_{\mu\nu} a_\mu^\dagger a_\nu \right| \psi_N \right\rangle = \sum_\mu U_{\mu\mu} \langle n_\mu \rangle , \quad (\text{B.34})$$

where $\langle n_\mu \rangle$ is the occupation number of the state μ in the state $|\psi_N\rangle$. For quartic operators (such as an interparticle potential), the procedure is the same, giving

$$\frac{1}{2} \sum_{\alpha\beta;\gamma\delta} v_{\alpha\beta;\gamma\delta} \langle \psi_N | a_\alpha^\dagger a_\beta^\dagger a_\delta a_\gamma | \psi_N \rangle = \frac{1}{2} \sum_{\alpha\beta} (v_{\alpha\beta;\alpha\beta} - v_{\alpha\beta;\beta\alpha}) \langle n_\alpha n_\beta \rangle . \quad (\text{B.35})$$

This expression involves spin indices in both α and β . To obtain spin states of the N particles, we must consider not only the diagonal matrix elements of V but also its off-diagonal matrix elements in spin space. As V does not depend explicitly on spin, $v_{i\sigma, j\sigma'; k\sigma, l\sigma'}$ is independent of σ and σ' , but off-diagonal terms also involve operators $a_{i\sigma}^\dagger a_{j\sigma'}^\dagger a_{i\sigma'} a_{j\sigma}$ which are no longer just the product of two densities. They can nevertheless be decomposed in terms of density and polarisation using identities (3.25) and (3.27). We then diagonalise the 2×2 matrix in spin space to obtain the new energy levels and eigenstates. Diagonal and off-diagonal terms in spin space are often represented by the two Feynman diagrams shown in Fig. B.1.

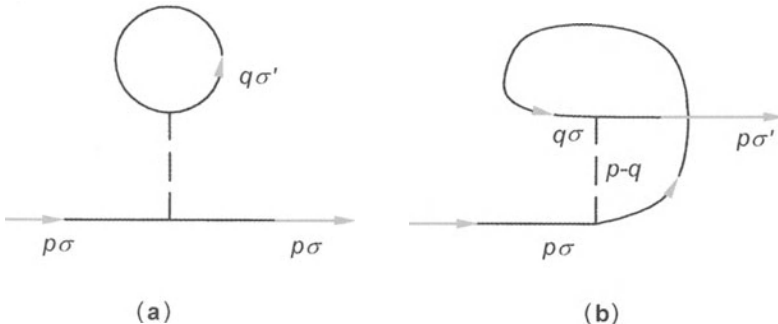


Fig. B.1. Feynman diagrams contributing to the Hartree–Fock approximation for a spin-independent potential. (a) The Hartree term only involves the density and is spin-independent. (b) The Fock term is not diagonal in spin space. It depends on both density and magnetisation

These eigenstates can also be found from a first order perturbative expansion of N -particle states,

$$|\psi_N\rangle = |\phi_N\rangle + \frac{1}{E^0 - \mathcal{H}} \mathcal{H}_{\text{pert}} |\psi_N\rangle , \quad (\text{B.36})$$

where \mathcal{H} is the unperturbed N -particle Hamiltonian. We can rewrite this equation explicitly in the 1-particle case. These states generally depend explicitly on spin even if $\mathcal{H}_{\text{pert}}$ does not, because of the matrix structure of operators $1/(E_0 - \mathcal{H})$ and $\mathcal{H}_{\text{pert}}$. We define operators b_α^\dagger and b_α creating and destroying one particle in these perturbed states and so obtain an effective Hamiltonian,

$$\mathcal{H}_{\text{eff}} = \sum_\mu \varepsilon_{\text{HF}}^\mu b_\mu^\dagger b_\mu , \quad (\text{B.37})$$

which is diagonal in this basis. We see that to first order we may just redefine the 1-particle states, which then become the new elementary excitations of the system. For this reason, they are called quasi-particles.

C. Exercises

C.1 Magnetism

C.1.1 Magnetic Textures

Consider n spins of magnitude S placed around a 1-dimensional ring, where S is large enough to justify a classical model. The position of spin $i \in [1, n]$ on the ring is given by an angle θ . A radial magnetic field $B(\theta) = B\hat{e}_r$ of uniform intensity is applied. Spins interact via an exchange interaction which is assumed to be ferromagnetic to begin with. To simplify, we shall assume that the direction of the classical spin vector lies in the plane spanned by \hat{e}_r and \hat{e}_z , and is located by an angle χ , as shown in Fig. C.1. χ may depend on i , i.e., on θ . Such a spin configuration is called a magnetic texture. The Hamiltonian is

$$H = -J \sum_{i=1}^n \left[\tilde{\mathbf{S}}_i \cdot \tilde{\mathbf{S}}_{i+1} + |\gamma| \mathbf{B}(\theta) \cdot \tilde{\mathbf{S}}_i \right], \quad (\text{C.1})$$

identifying $i = n + 1$ with $i = 1$.

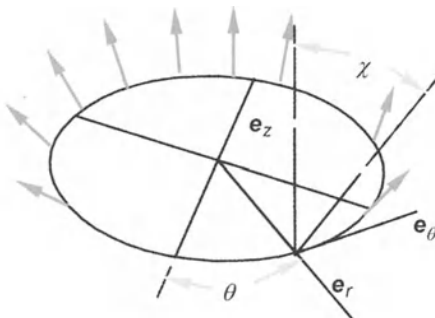


Fig. C.1. Spin ring in an inhomogeneous magnetic field with angle χ . Local cylindrical coordinates are used at position θ

- When χ is independent of θ , calculate the energy of the ring as a function of χ , B and J . What is the equilibrium value of χ ?

2. When $B = 0$ and χ is independent of θ , calculate the exchange field \tilde{h}_{ex} on a spin in the ring, together with its gradient $\nabla \tilde{h}_{\text{ex}}$ and $\nabla^2 \tilde{h}_{\text{ex}}$. What is the couple on each spin? For what value of χ is the couple zero? Deduce the stationary textures? Do they correspond to energy minima or maxima?
3. Still in zero field, consider a texture such that $\chi(\theta) \ll 1$. Expanding χ in Fourier series,

$$\chi(\theta) = \sum_j \chi_j \cos(k_j \theta - \omega_j t), \quad (\text{C.2})$$

what are the possible values of k_j ? Write down the linearised Bloch equations for the deviation of the spins from equilibrium $\sigma_i = S - Se_z$ and deduce the dispersion relation $\omega_j(k_j)$.

4. Assume that the radial magnetic field is no longer uniform, but given by

$$\tilde{B} = B \cos \theta \hat{e}_r. \quad (\text{C.3})$$

Write down the Bloch equations linearised around $S\hat{e}_z$ for this inhomogeneous magnetic field. What are the spin wave precession frequencies? Is there an analogy with the Josephson effect?

5. Assuming antiferromagnetic exchange J , and $B = 0$, what are the energies of rings with even and odd numbers of spins?

C.1.2 Long Range Exchange Interaction Between Spin 1/2 Particles and the Mean Field Approximation

The aim is to show that the mean field approximation becomes exact for long range exchange interactions, even for quantum spin 1/2 systems. Consider a magnet containing $2N$ spin 1/2 particles. Exchange is long range when, in the thermodynamic limit,

$$\sum_j |J_{ij}| \rightarrow \infty, \quad (\text{C.4})$$

and short range when this quantity remains finite. We shall make a simple model of long range interactions in which all exchange couplings J_{ij} are equal to $J_0/2N$, for all i, j . The factor $1/2N$ in the definition of the exchange constant guarantees that the energy is an extensive quantity when the exchange interaction has infinite range. The following results will be useful:

- Adding $2N$ spin 1/2 particles, the total spin l may take on any of the $N + 1$ integer values between 0 and N . Each of these values occurs

$$a_l = \frac{2l+1}{2N+1} C_{2N+1}^{N-l} = (2l+1) \frac{(2N)!}{(N-l)!(N+l+1)!} \quad (\text{C.5})$$

times in the sum. In other words, the decomposition of the representation $(D_{1/2})^{2N}$ of $2N$ spins into irreducible representations of the rotation group is given by (see Appendix A)

$$(D_{1/2})^{2N} = \bigoplus_{l=0}^N a_l D_l . \quad (\text{C.6})$$

- For large n , an approximate value of the factorial is given by Stirling's formula

$$\ln(n!) = n(\ln n - 1) . \quad (\text{C.7})$$

1. To begin with, we consider a ferromagnetic Hamiltonian in an external field H along the z -axis,

$$\mathcal{H} = - \sum_{i>j}^{2N} J_{ij} \mathbf{S}_i \cdot \mathbf{S}_j + |\gamma| \sum_i S_i^z H . \quad (\text{C.8})$$

What are the good quantum numbers of the Hamiltonian \mathcal{H} ? Deduce the exact energy levels.

2. What is the degeneracy of each level in a field $H \neq 0$ and in zero field?
3. We now assume that the applied field H is identically zero. What is the probability P_l that the total spin equals l at temperature T ? By a qualitative argument, explain why P_l has a maximum for some value \bar{l} (to be determined in the next question), and show that fluctuations around \bar{l} are small (i.e., $P_l \ll P_{\bar{l}}$ for $l \neq \bar{l}$).
4. Neglecting fluctuations around \bar{l} , find the partition function $Z_{\bar{l}}$ and free energy $F_{\bar{l}}$ in zero magnetic field. For what value of \bar{l} is the free energy minimal? Deduce that the system has a phase transition at a critical temperature T_c , to be found shortly (assume that \bar{l} is small compared with N near T_c).
5. Deduce the entropy and specific heat near T_c . Compare results with the mean field.
6. Assume now that the applied field H is no longer zero. Find the dependence of \bar{l} on H . Assume that $1 \ll \bar{l} \ll N$. Compare results with the mean field equations.
7. At low temperatures $T/T_c \ll 1$, determine the partition function and free energy.
8. What is the specific heat? Why do we not retrieve Bloch's $T^{3/2}$ law? Physical arguments should be given.
9. Assume now that coupling $J_0 < 0$ is antiferromagnetic. Does the system have a phase transition? Give physical arguments to justify the result.

C.1.3 Spin-Flop Transition for an Antiferromagnet

The aim here is to study the phase diagram for an antiferromagnetic system of spins $S = 1$ placed on a simple cubic lattice of $2N$ sites. Antiferromagnetic exchange $J > 0$ is between nearest neighbours and at each site, spins are subject to a uniaxial ionic anisotropy $D(\mathbf{S} \cdot \hat{\mathbf{n}})^2$.

1. Consider first a set of $2N$ free spins $S = 1$ subject to a magnetic field \mathbf{H} and ionic anisotropy D . Each spin is described by the Hamiltonian

$$\mathcal{H} = |\gamma| \mathbf{S} \cdot \mathbf{H} + D(\mathbf{S} \cdot \hat{\mathbf{n}})^2. \quad (\text{C.9})$$

Let θ be the angle between \mathbf{H} and $\hat{\mathbf{n}}$. The anisotropy energy $d = D\hbar^2$ is small compared with the magnetic energy $B = \mu H$. Show that the energy levels of \mathcal{H} are given to first order by

$$\begin{aligned}\varepsilon_+ &= B + \frac{d}{2} (\cos^2 \theta + 1) , \\ \varepsilon_0 &= d \sin^2 \theta = d (1 - \cos^2 \theta) , \\ \varepsilon_- &= -B + \frac{d}{2} (\cos^2 \theta + 1) .\end{aligned}\quad (\text{C.10})$$

Plot the Zeeman diagram for $\theta = 0$ and $\theta = \pi/2$. Recall that

$$S_z = \hbar \begin{pmatrix} 1 & 0 & 0 \\ 0 & 0 & 0 \\ 0 & 0 & -1 \end{pmatrix}, \quad S_x = \frac{\hbar}{\sqrt{2}} \begin{pmatrix} 0 & 1 & 0 \\ 1 & 0 & 1 \\ 0 & 1 & 0 \end{pmatrix}. \quad (\text{C.11})$$

2. What is the free energy and the magnetisation M of the N spins? At low temperatures, describe the general appearance of $M(\theta)$ for fixed magnetic field and temperature. Describe also the magnetisation curves $M(H)$ for $\theta = 0$ and $\theta = \pi/2$.
3. Consider now the full Hamiltonian for $2N$ interacting spins,

$$\mathcal{H} = \sum_{\alpha, i=1}^{i=2N} \mathbf{S}_i \cdot \mathbf{S}_{i+\alpha} + \sum_{i=1}^{i=2N} [|\gamma| \mathbf{h} \cdot \mathbf{S}_i + D(\mathbf{S}_i \cdot \hat{\mathbf{z}})^2], \quad (\text{C.12})$$

where the sum over α is taken over nearest neighbours. The applied external field \mathbf{h} and anisotropy axis $\hat{\mathbf{n}}$ are assumed to lie along the z -axis. Show that in the molecular field approximation, the above Hamiltonian reduces to an effective Hamiltonian

$$\begin{aligned}\mathcal{H} \approx \sum_{i=1}^N &[|\gamma| (\mathbf{h}_b + h\hat{\mathbf{z}}) \cdot \mathbf{S}_i^a + D(\mathbf{S}_i^a \cdot \hat{\mathbf{z}})^2 \\ &+ |\gamma| (\mathbf{h}_a + h\hat{\mathbf{z}}) \cdot \mathbf{S}_i^b + D(\mathbf{S}_i^b \cdot \hat{\mathbf{z}})^2].\end{aligned}\quad (\text{C.13})$$

Express molecular fields \mathbf{h}_a and \mathbf{h}_b for the two sublattices a and b in terms of J , expected values $\langle \mathbf{S}_i \rangle^a$ and $\langle \mathbf{S}_i \rangle^b$, and the number of neighbours z at each site.

4. Let us now study this Hamiltonian. Let $\boldsymbol{\sigma}_a = \langle \mathbf{S}_i \rangle^a / \hbar$ and $\boldsymbol{\sigma}_b = \langle \mathbf{S}_i \rangle^b / \hbar$ be order parameters for each sublattice. Let θ_a and θ_b be angles from the z -axis to $\boldsymbol{\sigma}_a$ and $\boldsymbol{\sigma}_b$. Write down the free energy of the system in zero field as a function of θ_a , θ_b and $h_m = 2Jz\hbar^2/\mu$. (Use the results of the first question and assume that $\beta\mu h_m \gg 1$.) Find the angles θ_a and θ_b which minimise the free energy, depending on the sign of the anisotropy D . Determine the Néel temperature in zero field, assuming $B_m = \mu h_m \gg d$.

5. The external field $h\hat{z}$ is now non-zero. We consider the low temperature limit $\beta d \gg 1$. In this limit the molecular field is much larger than the applied field, so that $|h_a| \approx |h_b| \approx |h_m|$. Consider first an Ising type anisotropy $D < 0$. Determine equilibrium angles ϕ_a and ϕ_b as a function of the magnetic field. Show that, at a critical value h_{sf} of the field, the spin configuration swings round from a configuration which is collinear with the field to one which is non-collinear (to be specified shortly). Is this spin-flop transition first or second order?
6. In the low temperature limit $\beta d \ll 1$, find the magnetisation in each phase, and describe its general dependence on the magnetic field.
7. Estimate the critical temperature of the non-collinear phase when $H > H_{sf}$. Plot the general appearance of the magnetisation curve around $T_c(H)$.
8. What happens in a planar-type anisotropy $D > 0$?
9. Plot the phase diagram in the (H, T) -plane for both $D < 0$ and $D > 0$, specifying the structure of each phase. Is there a tricritical point?

C.1.4 Spin Waves and Quantum Fluctuations in Antiferromagnets

In this exercise, we consider quantum fluctuations around an antiferromagnetic Néel state and their effects in spaces of different dimensions. We assume that the crystal lattice, of lattice constant a and composed of $2N$ spins, is bipartite, i.e., it can be divided into two sublattices A and B , each containing N spins. Let z denote the lattice coordination (number of neighbours). The Heisenberg spin S Hamiltonian is

$$\mathcal{H} = |J| \sum_{\langle ij \rangle} \mathbf{S}_i \cdot \mathbf{S}_j , \quad (\text{C.14})$$

where the $\langle ij \rangle$ sum is over nearest neighbours in sublattices A and B , i.e., $i \in A$ and $j \in B$.

1. Show that the classical Néel state $\mathbf{S}_i = S \hat{\Omega}$, $\mathbf{S}_j = -S \hat{\Omega}$, where $\hat{\Omega}$ is a unit vector, minimises the classical energy E_{cl} , but that its quantum equivalent

$$|N\rangle = \prod_{i \in A, j \in B} |S, S\rangle_i \otimes |S, -S\rangle_j \quad (\text{C.15})$$

is not an eigenstate of the Hamiltonian. Find the expectation value $\langle N | \mathcal{H} | N \rangle$.

2. Show that the transformation

$$S_j^z \rightarrow \tilde{S}_j^z = -S_j^z , \quad S_j^x \rightarrow \tilde{S}_j^x = S_j^x , \quad S_j^y \rightarrow \tilde{S}_j^y = -S_j^y , \quad (\text{C.16})$$

leaves commutation relations invariant. Applying this transformation to all spins in sublattice B , without altering spins in sublattice A , show that the Heisenberg Hamiltonian can be represented by

$$\mathcal{H} = -|J| \sum_{\langle ij \rangle} S_i^z \tilde{S}_j^z + \frac{|J|}{2} \sum_{\langle ij \rangle} \left(S_i^+ \tilde{S}_j^+ + S_i^- \tilde{S}_j^- \right). \quad (\text{C.17})$$

Using the expansion of operators \mathbf{S} and $\tilde{\mathbf{S}}$ in powers of $1/S$ (the Holstein–Primakoff transformation),

$$S_i^+ = \sqrt{2S} a_i^\dagger, \quad S_i^- = \sqrt{2S} a_i, \quad S_i^z = -S + a_i^\dagger a_i, \quad (\text{C.18})$$

write the Hamiltonian \mathcal{H} in the form

$$\begin{aligned} \mathcal{H} &= E_{\text{cl}} + 2|J|Sz \sum_{\mathbf{k}} \left[a_{\mathbf{k}}^\dagger a_{\mathbf{k}} + \frac{\gamma_{\mathbf{k}}}{2} \left(a_{\mathbf{k}}^\dagger a_{-\mathbf{k}}^\dagger + a_{\mathbf{k}} a_{-\mathbf{k}} \right) \right], \\ \gamma_{\mathbf{k}} &= \frac{1}{z} \sum_j \exp i \mathbf{k} \cdot \boldsymbol{\delta}_{ji}, \end{aligned} \quad (\text{C.19})$$

where $\boldsymbol{\delta}_{ij} = \mathbf{R}_j - \mathbf{R}_i$ and the sum is over all sites j neighbouring a given site i .

3. Let us now diagonalise this Hamiltonian using a Bogoliubov transformation,

$$a_{\mathbf{k}} = u_{\mathbf{k}} c_{\mathbf{k}} + v_{\mathbf{k}} c_{-\mathbf{k}}^\dagger, \quad (\text{C.20})$$

for bosons, $|u_{\mathbf{k}}|^2 - |v_{\mathbf{k}}|^2 = 1$. This can be parametrised by a hyperbolic angle,

$$u_{\mathbf{k}} = \cosh \theta_{\mathbf{k}}, \quad v_{\mathbf{k}} = \sinh \theta_{\mathbf{k}}, \quad (\text{C.21})$$

which is real and even under $\mathbf{k} \rightarrow -\mathbf{k}$.

Show that anomalous contributions $c_{\mathbf{k}}^\dagger c_{-\mathbf{k}}^\dagger$ and $c_{\mathbf{k}} c_{-\mathbf{k}}$ cancel out if

$$\tanh 2\theta_{\mathbf{k}} = -\gamma_{\mathbf{k}}. \quad (\text{C.22})$$

Deduce the canonical form of the Hamiltonian in terms of spin waves,

$$\mathcal{H} = E_0 + \sum_{\mathbf{k}} \omega_{\mathbf{k}} c_{\mathbf{k}}^\dagger c_{\mathbf{k}}, \quad (\text{C.23})$$

and find the dispersion relation $\omega_{\mathbf{k}}$. Deduce that quantum fluctuations lower the ground state energy, i.e., $E_0 < E_{\text{cl}}$.

Show that near $\mathbf{k} = 0$ and $\mathbf{k} = \pi \equiv (\pi, \pi, \pi)$, the spin wave dispersion relation is linear:

$$\omega_{\mathbf{k}} = 2|J|S\sqrt{2z}|\mathbf{k}|a, \quad \omega_{\mathbf{k}} = 2|J|S\sqrt{2z}|\mathbf{k} - \pi|a. \quad (\text{C.24})$$

4. Let us now determine the ground state $|\psi_0\rangle$ of the antiferromagnet when there are quantum fluctuations. Since there are no excited magnons in the ground state, we should have

$$c_{\mathbf{k}} |\psi_0\rangle = 0, \quad (\text{C.25})$$

i.e., $|\psi_0\rangle$ is the vacuum state for magnons. Deduce that

$$|\psi_0\rangle = \mathcal{N} \exp\left(\frac{1}{2} \sum_{\mathbf{k}} u_{\mathbf{k}} a_{\mathbf{k}}^\dagger a_{-\mathbf{k}}^\dagger\right) |0\rangle , \\ u_{\mathbf{k}} = \tanh \theta_{\mathbf{k}} , \quad (C.26)$$

and determine the normalisation factor \mathcal{N} .

5. Let us now evaluate the suppression of alternating magnetisation M^\dagger by fluctuations,

$$\Delta M^\dagger = \frac{1}{2N} \left\langle \sum_i \exp(i\pi R_i) S_i^z \right\rangle - S . \quad (C.27)$$

Show that it is determined by the magnon thermal occupation number $n_{\mathbf{k}} = [\exp(\beta\omega_{\mathbf{k}}) - 1]^{-1}$,

$$\Delta M^\dagger = \frac{1}{2} + \frac{1}{2N} \sum_{\mathbf{k}} \left(n_{\mathbf{k}} + \frac{1}{2} \right) \frac{1}{(1 - \gamma_{\mathbf{k}}^2)^{1/2}} . \quad (C.28)$$

In three dimensions, we can conclude that the alternating magnetisation decreases quadratically with temperature,

$$\Delta M^\dagger = a_3 + b_3 \left(\frac{k_B T}{2|J|Sa} \right)^2 , \quad (C.29)$$

where

$$a_3 = \frac{1}{2N} \sum_{\mathbf{k}} \frac{1}{(1 - \gamma_{\mathbf{k}}^2)^{1/2}} - 1 , \quad b_3 = \frac{1}{6^{5/2}} . \quad (C.30)$$

Comparing with a ferromagnet, what conclusion can be drawn?

C.1.5 Order by Disorder: Ground State Selection Processes in Antiferromagnets Frustrated by Thermal Fluctuations

There exist in nature a certain number of crystal lattices with triangular units in their unit cells. For example, in the face-centred cubic crystal, atoms in the centre of each face form an equilateral triangle. When the spins located at these sites interact antiferromagnetically, frustration occurs because not all antiferromagnetic bonds can be satisfied at once. This effect manifests itself through a large-scale degeneracy in the ground state. Such degeneracy can only be removed by other processes, which we shall now investigate. The simplest model in which these phenomena play any role is a 2-dimensional XY model with classical spins placed on a square lattice, as shown in Fig. C.2. The unit length is chosen to be the lattice constant. The model is frustrated because there are antiferromagnetic interactions between nearest neighbours (along the sides of squares, with exchange constant J_1), and also between second nearest neighbours (along diagonals of squares, with exchange constant J_2). The Hamiltonian describing this magnet is therefore

$$\mathcal{H} = \sum_{ij} J_{ij} \mathbf{S}_i \cdot \mathbf{S}_j = \sum_{ij} J_{ij} \cos(\theta_i - \theta_j) , \quad (\text{C.31})$$

where J_{ij} equals J_1 between nearest neighbours (along sides of squares) and J_2 between second nearest neighbours. Angle θ_i measures the angular position of spin i in the (x, y) -plane relative to the x -axis.

1. If $J_2 = 0$, what is the ground state of the magnet at zero temperature? What is its energy? Let N be the total number of sites in the lattice. If $J_2 \neq 0$ but $J_2 \ll J_1$, the ground state remains the same. What is its energy? What molecular fields act on spins in the two sublattices (\uparrow and \downarrow)? Why are magnetisations m_\uparrow and m_\downarrow of the two sublattices equal and opposite? What is the mean field equation for these magnetisations? Deduce the value of the critical temperature as a function of J_1 and J_2 .
2. In the limit $J_1 \rightarrow 0$, show that the magnet decouples into two independent antiferromagnetic sublattices A and B (each one having its own \uparrow and \downarrow sublattices, as shown in Fig. C.2). At zero temperature, what is the ground state energy? When J_1 is small but non-zero, what are the molecular fields exerted by sublattice A on sublattice B , and vice versa? Deduce that the A and B lattices remain independent, so that the ground state remains infinitely degenerate. Do so by showing that the energy of the system is independent of the angle $\phi = \theta_A - \theta_B$ between sublattices A and B , and give its value as a function of J_2 and N . What are the mean field equations for the magnet? Deduce its critical temperature.
3. At zero temperature, compare ground state energies for the two phases studied above. For which value of J_2/J_1 does the system transit from phase 1 (question 1 above) to phase 2 (question 2)? When the system is made to go from phase 1 to phase 2 by varying J_2/J_1 , is the transition first or second order?
4. In the rest of this exercise, we shall be concerned only with phase 2. Its ground state is illustrated in Fig. C.2. Recall that this state is infinitely degenerate and can be specified by the angle $\phi = \theta_A - \theta_B$ between sub-

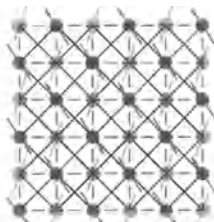


Fig. C.2. On the square lattice shown here, there are antiferromagnetic interactions between nearest neighbours (along sides of squares, with exchange constant J_1) and also between second nearest neighbours (along diagonals, with exchange constant J_2)

lattices A and B . We shall investigate fluctuations around the state ϕ . Show that these can be represented by the Hamiltonian

$$\delta\mathcal{H} = \sum_{ij} [4|J_2|\delta_{ij} - J_{ij}\cos(\theta_i - \theta_j)]\delta\theta_i\delta\theta_j. \quad (\text{C.32})$$

Define Fourier transforms of quantities A and $\delta\theta$ by

$$A(\mathbf{q}) = \sum_{mn, rs} \exp\{-i[q_x(m-r) + q_y(n-s)]\} A_{mn, rs},$$

$$\delta\theta_{\mathbf{q}} = \frac{1}{\sqrt{N}} \sum_{mn} \exp[-i(q_x m + q_y n)] \delta\theta_{mn}, \quad (\text{C.33})$$

where $[m, n]$ and $[r, s]$ are Cartesian coordinates of sites i and j , respectively. Show that in Fourier space the fluctuations [see (C.32)] can be represented by

$$\delta\mathcal{H} = \sum_{\mathbf{q}} A(\mathbf{q}) |\delta\theta_{\mathbf{q}}|^2, \quad (\text{C.34})$$

where

$$A_{\mathbf{q}} = 4|J_2|(1 - \cos q_x \cos q_y) - 2J_1(\cos q_x - \cos q_y) \cos \phi. \quad (\text{C.35})$$

5. Equation (C.34) describes a sum of independent harmonic fluctuations about the ground state ϕ . Using the treatment of Gaussian fluctuations near a phase transition described in Sect. 4.2(I) (Ornstein-Zernike theory), show that the contribution to the free energy made by fluctuations is

$$F(\phi, T) = E_0 - \frac{k_B T}{2} \sum_{\mathbf{q}} \ln \left(\pi \frac{k_B T}{A(\mathbf{q})} \right). \quad (\text{C.36})$$

Give a physical interpretation of

$$\Delta S(\phi) = -\frac{1}{2} \sum_{\mathbf{q}} \ln A(\mathbf{q}). \quad (\text{C.37})$$

Bear in mind that the Ornstein-Zernike theory describes fluctuations in three dimensions, whereas we are working in two dimensions here.

6. A rather lengthy calculation leads to the result

$$\Delta S(\phi) \approx a + b \left(\frac{J_1 \cos \phi}{J_2} \right)^2, \quad (\text{C.38})$$

where a and b are positive constants. Deduce that the free energy is minimal when $\cos \phi = \pm 1$. In other words, thermal fluctuations select a ground state in which the two sublattices A and B are collinear.

Disorder, manifested through the lack of some fraction of the spins over the lattice, is another factor leading to selection of the ground state. However, in this case, the values selected are $\phi = \pm\pi/2$. Disorder therefore favours non-collinear structures in which sublattices A and B are orthogonal, in competition with thermal fluctuations [577].

C.2 Superconductivity

C.2.1 Superconductors Under Pressure

1. Referring to the Meissner effect, show that the magnetisation of a type I superconducting sample of volume v is

$$\begin{aligned} m_s &= -v_s H \quad (T < T_c) , \\ m_n &= 0 \quad (T > T_c) . \end{aligned} \quad (\text{C.39})$$

2. Define the magnetic Gibbs free energy of the sample and its differential by

$$\begin{aligned} G_S &= U_S - Ts - Pv - \mu_0 Hm , \\ dG_S &= -sdT + vdP - \mu_0 mdH . \end{aligned} \quad (\text{C.40})$$

Recalling that the Gibbs free energy is constant over the coexistence surface $H_c(T, P)$, whose trace in the $P = 0$ plane is shown in Fig. 12.1(II), show that the Clausius–Clapeyron equations of a superconductor are:

$$\mu_0 \left(\frac{\partial H_c}{\partial T} \right)_P = -\frac{s_n - s_s}{m_n - m_s} = -\frac{1}{v_s H_c} (s_n - s_s) , \quad (\text{C.41})$$

$$\mu_0 \left(\frac{\partial H_c}{\partial P} \right)_T = \frac{1}{v_s H_c} (v_n - v_s) , \quad (\text{C.42})$$

$$\left(\frac{\partial P}{\partial T} \right)_{H_c} = \frac{s_n - s_s}{v_n - v_s} . \quad (\text{C.43})$$

3. Applying the third law of thermodynamics, deduce that

$$\left(\frac{\partial H_c}{\partial T} \right)_P = 0 \quad \text{at} \quad T = 0 , \quad (\text{C.44})$$

as can be seen from Fig. 12.1(II).

4. From the definition of the specific heat at constant pressure $C_p = T(\partial S/\partial T)_P$, use (C.41) to show that

$$C_p^n - C_p^s = -\mu_0 \frac{v_s T}{2} \left(\frac{\partial^2 H_c^2}{\partial T^2} \right)_P , \quad (\text{C.45})$$

and that $C_p^s > C_p^n$ at transition.

5. Define the isothermal compressibility and isobaric expansion coefficient by

$$\kappa = -\frac{1}{v} \left(\frac{\partial v}{\partial P} \right)_T , \quad \beta = \frac{1}{v} \left(\frac{\partial v}{\partial T} \right)_P . \quad (\text{C.46})$$

Show from (C.42) and (C.43) that

$$\frac{\mu_0}{2} \left(\frac{\partial^2 H_c^2}{\partial P^2} \right)_T = \kappa_s - \kappa_n , \quad (\text{C.47})$$

$$\frac{\mu_0}{2} \left(\frac{\partial^2 H_c^2}{\partial P \partial T} \right) = \beta_n - \beta_s . \quad (\text{C.48})$$

6. In zero field, show that these relations are equivalent to

$$C_p^n - C_p^s = -\mu_0 v T \left(\frac{\partial H_c}{\partial T} \right)_P^2, \quad (\text{C.49})$$

$$\kappa_n - \kappa_s = -\mu_0 \left(\frac{\partial H_c}{\partial P} \right)_T^2, \quad (\text{C.50})$$

$$\beta_n - \beta_s = \mu_0 \left(\frac{\partial H_c}{\partial P} \right)_T \left(\frac{\partial H_c}{\partial T} \right)_P. \quad (\text{C.51})$$

7. Using the identity

$$\left(\frac{\partial H_c}{\partial P} \right)_T = - \left(\frac{\partial T_c}{\partial P} \right)_{H_c} \left(\frac{\partial H_c}{\partial T} \right)_P, \quad (\text{C.52})$$

show that T_c depends on the pressure according to

$$\left(\frac{\partial T_c}{\partial P} \right)_{H_c=0} = v T_c \frac{\beta_n - \beta_s}{C_p^n - C_p^s} = \frac{\kappa_n - \kappa_s}{\beta_n - \beta_s}. \quad (\text{C.53})$$

C.2.2 Superconductor Arrays

We consider a square superconductor array of period l . We aim to determine the dependence of the critical field H_c and temperature T_c on the flux enclosed in each cell. Since T_c is determined by the temperature at which the coefficient of $|\psi|^2$ vanishes, the linearised Ginzburg–Landau equations are applicable. We define the flux ϕ through a cell as $\phi = Bl^2$ and the angle $\gamma = 2\pi\phi/\phi_0$. Likewise, it is useful to introduce the angle $\theta = l/\xi_{\text{GL}}$, where ξ_{GL} is the Ginzburg–Landau coherence length.

1. Why can the order parameter ψ be treated as constant over the cross section of a wire (assumed small relative to l)? Give physical arguments.

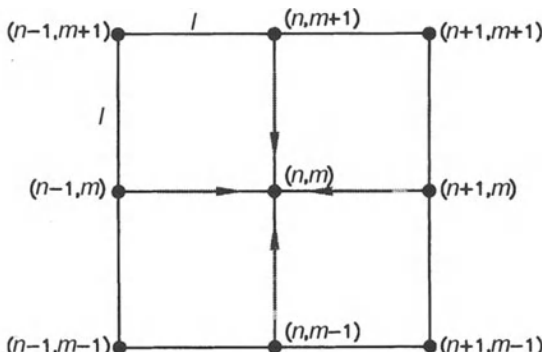


Fig. C.3. Square array of superconducting wires, with lattice constant l . Values of the order parameter are denoted $\psi(-1, 0)$, $\psi(0, 0)$, $\psi(1, 0)$, and so on

2. Kirchoff's law requires current conservation at each node. Express this conservation law in terms of order parameters $\psi_\alpha(s)$ on each wire α ending at the node under consideration, where s is the coordinate along each wire.
3. Choosing a particular $x = 0, y = 0$ as the centre of the array, express the vector potential \mathbf{A} as a function of the flux enclosed in each cell, adopting the Landau gauge.
4. Integrate the linearised Ginzburg–Landau equations along horizontal wires $(0, 0) \rightarrow (1, 0)$ and $(-1, 0) \rightarrow (0, 0)$. Express integration constants in terms of the (complex) values of ψ at points $(0, 0), (1, 0)$ and $(-1, 0)$.
5. Integrate the linearised Ginzburg–Landau equations along vertical wires $(0, 0) \rightarrow (0, 1)$ and $(0, -1) \rightarrow (0, 0)$. Express results in terms of the nodal values of ψ .
6. From these results, determine the condition imposed by current conservation on nodal values of the order parameter.
7. Since the array is periodic, Bloch's theorem specifies an order parameter at node (n, m) in the form

$$\psi(n, m) = f_q(n) \exp(iqm) . \quad (\text{C.54})$$

From the previous question, find the equation satisfied by the function $f_q(n)$.

8. What symmetries exist when $\gamma \rightarrow -\gamma$ and $\gamma \rightarrow \gamma + 2\pi$?
9. We now seek the behaviour of uniform solutions ($q = 0$) for small values of γ . Show that in the continuous limit, the finite difference equation obtained is that of a harmonic oscillator. Deduce that for small values of γ , we must have

$$\gamma = 4(1 - \cos \theta) . \quad (\text{C.55})$$

Deduce the critical field H_{c2} of the array as a function of l and ξ_{GL} .

10. When γ is close to π , so that $\gamma = \pi + \delta$, find the critical field H_{c2} of the array by analogous reasoning.

C.2.3 Superconductivity in an Inhomogeneous Magnetic Field

The aim here is to investigate nucleation of superconductivity in a superconducting film lying in the (x, y) -plane. The film is assumed thin enough to be able to neglect screening of a field applied along the z -axis. The magnetic field is spatially modulated in the \hat{x} direction,

$$\mathbf{B} = b \sin(qx) \hat{z} . \quad (\text{C.56})$$

(A field of this kind can be produced by placing ferromagnetic wires parallel to the y -axis on the superconductor surface. The $\uparrow\downarrow$ alternation of the order parameter between adjacent wires is ensured by their dipolar interaction.) Near the nucleation threshold, the amplitude $|\psi(x, y)|^2$ of the order parameter is small. This justifies using the linearised Ginzburg–Landau equations.

We seek the reduction in critical temperature as a function of b and a possible current \mathbf{J} .

1. Find the vector potential from which \mathbf{B} derives in the Landau gauge.
2. We seek solutions of the linearised Ginzburg–Landau equations in the form

$$\psi(x, y) = \exp(\mathrm{i}k_y y) \phi(x). \quad (\text{C.57})$$

Find the equation satisfied by $\phi(x)$.

3. We begin by looking for solutions with $k_y = 0$. In this case, what is the mean current in the $\hat{\mathbf{y}}$ direction?
4. When the spatial period $\lambda = 2\pi/q$ is much smaller than the coherence length ξ_{GL} , determine the variation of the Ginzburg–Landau coherence length with b and q . Using the definition of ξ_{GL} in terms of parameter a in the Ginzburg–Landau free energy, and its temperature dependence near T_c , deduce the reduction in T_c as a function of the various parameters.
5. For any q , use the analogy with the Schrödinger equation in a periodic potential to justify a solution of type

$$\phi(x) = \exp(\mathrm{i}k_x x) u_{k_x}(x), \quad (\text{C.58})$$

and discuss its properties. What is the relation between k_x and the applied current in the $\hat{\mathbf{x}}$ direction?

6. Sketch the energy bands of the corresponding Schrödinger equation as a function of k_x across the Brillouin zone $[-q, q]$. Consider both the weak and strong field limits. Sketch also the x dependence of the order parameter in both cases.
7. Proceeding by analogy with the Schrödinger equation, what is the correspondence between the ground state energy and the value of ξ_{GL}^{-1} in the linearised Ginzburg–Landau equation? Show that the reduction in critical temperature is periodic in the current J_x . When b is small, estimate ΔT_c as a function of b and q and show that ΔT_c is minimal when

$$b\lambda^2 = \frac{\Phi_0}{2}. \quad (\text{C.59})$$

C.2.4 Intermediate State of a Type I Superconductor

Consider an extreme type I superconductor $\xi \gg \lambda_L$. We shall investigate the lamellar structure for a superconducting plate of thickness E embedded in a uniform magnetic field H (see Fig. 12.7).

1. Plot on the same graph the x variation of the Ginzburg–Landau order parameter ψ and the magnetic field H at the centre of the plate $z = 0$. Specify at which points and over what distances these quantities relax from one value to another, and give the order of magnitude of ψ and H in each region, using physical arguments.

2. We shall now examine a lamella of width b . Consider a variational solution of the order parameter in the interval $[-d/2, d/2]$, with value at $z = 0$ given by

$$\psi(x) = \frac{\psi_0}{\exp[(|x| - b/2)/\delta] + 1} . \quad (\text{C.60})$$

ψ_0 and δ are parameters whose physical significance will be established shortly. We need first to estimate the contribution of diamagnetic screening currents to the Gibbs free energy, over the interval $[-d/2, d/2]$. Which is the most significant contribution in the London gauge: the contribution from variations in the order parameter, or that due to the vector potential?

3. Estimate other contributions to the Gibbs free energy, taking into account relaxation of lines near the surface of the plate.
4. What constraint arises from flux conservation?
5. Find the period d of the structure by minimising the Gibbs free energy under the constraint imposed by flux conservation.
6. Discuss the physical significance of these results and explain why the London theory gives a qualitatively correct description of the intermediate state if we introduce a surface free energy at the normal-superconducting interface. What is the physical origin of this interfacial energy?
7. Give a numerical estimate for d when the plate is made of aluminium ($H_c = 105$ Oe, $T_c = 1.2$ K and $v_F = 2.03 \times 10^6$ m/s) and has thickness 1 mm, and the applied field is 50 Oe.
8. Sketch magnetic field lines at the plate surface. Compare values of H at the centre of normal regions and at the plate surface with H_c . What can be concluded? Is it possible to have superconducting regions within normal regions at the plate surface? If so, suggest a plausible structure.

When $\delta < b$, a useful integral approximation is

$$\int_{-d/2}^{d/2} \frac{dx}{\{\exp[(|x| - b/2)/\delta] + 1\}^n} = b - 2\delta \ln n . \quad (\text{C.61})$$

Bibliography

Chapter 1

1. Goldfarb, R.B., Fickett, F.R. (1985) NIST publication **696**
2. Morrish, A.H. (1965) The Physical Principles of Magnetism, pp. 3–15. Wiley, New York
3. Callen, H.B. (1960) Thermodynamics. Wiley, New York
4. Einstein, A., de Haas, W.J. (1915) Verh. Deut. Phys. Ges. **17**, 152. Ibid. (1916) **18**, 173, 423
5. Barnett, S.J. (1925) Phys. Rev. **6**, 171

Chapter 2

6. Sakurai, J.J. (1976) Advanced Quantum Mechanics. Addison-Wesley, 86-87
7. Feynman, R.P., Leighton, R.B., Sands, M. (1966) Lectures on Physics, Vol. II, Chap. 15. Addison-Wesley
8. Gutzwiller, M.C. (1991) Chaos in Classical and Quantum Mechanics. Springer
9. Merzbacher, E. (1960) Quantum Mechanics. Wiley, New York
10. Aharonov, Y., Bohm, D. (1959) Phys. Rev. **115**, 485
11. Washburn, S., Webb, R.A. (1986) Adv. in Phys. **35**, 375
12. Aronov, A.G., Sharvin, Y.V. (1987) Rev. Mod. Phys. **59**, 755
13. Aharonov, Y., Casher, A. (1984) Phys. Rev. Lett. **53**, 319
14. Elion, W.J., Wachters, J.J., Sohn, L.L., Mooij, J.E. (1993) Phys. Rev. Lett. **71**, 2311
15. Büttiker, M., Imry, Y., Landauer, R. (1983) Phys. Lett. A **96**, 365
16. Lévy, L.P., Dolan, G., Dunsmuir, J., Bouchiat, H. (1990) Phys. Rev. Lett. **64**, 2074
17. Chandrasekar, V., Webb, R.A., Brady, M.J., Ketchen, M.B., Gallagher, W.J., Kleinsasser, A. (1992) Phys. Rev. Lett. **67**, 3578
18. Mailly, D., Chapelier, C., Benoît, A. (1993) Phys. Rev. Lett. **70**, 2020
19. Willett, R., Eisenstein, J.P., Stormer, H.L., Tsui, D.C., Gossard, A.C., English, J.H. (1987) Phys. Rev. Lett. **59**, 1776
20. von Klitzing, K., Dorda, G., Pepper, M. (1981) Phys. Rev. Lett. **45**, 494
21. Prange, R. (1986) The Quantum Hall Effect. Springer
22. Pruisken, A.M.M. (1988) Phys. Rev. Lett. **61**, 1297
23. Polyakov, D.G., Shklovskii, B.I. (1993) Phys. Rev. Lett. **70**, 3796
24. Halperin, B.I. (1982) Phys. Rev. B **25**, 2185
25. Büttiker, M., (1988) Phys. Rev. B **38**, 9375

26. MacDonald, A. (1994) Mesoscopic Quantum Physics, les Houches Summer School, France. North Holland
27. Laughlin, R.B. (1981) Phys. Rev. B **23**, 5632
28. van Leeuwen, M. (1921) J. Phys. **2**, 361
29. Lévy, L.P., Reich, D.H., Pfeiffer, L., West, K. (1993) Physica B **189**, 204
30. Richter, K., Ullmo, D., Jalabert, R.A. (1996) Phys. Rep. **276**, 1
31. Landau, L.D. (1930) Z. Phys. **64**, 629
32. Peierls, R. (1933) Z. Phys. **80**, 763
33. Peierls, R. (1976) Surprises in Theoretical Physics. Princeton University Press, Princeton
34. de Haas, W.J., van Alphen, P.M. (1936) Proc. Amsterdam Acad. **33**, 1106
35. Shoenberg, D. (1984) Magnetic Oscillations in Metals. Cambridge University Press, Cambridge
36. Shoenberg, D. (1984) J. Low Temp. Phys. **56**, 417
37. Wiegers, S.A.J., Specht, M., Lévy, L.P., Simmons, M.Y., Ritchie, D.A., Cava, A., Etienne, B., Martinez, G., Wyder, P. (1997) Phys. Rev. Lett.
38. Dingle, R.B. (1952) Proc. Roy. Soc. **A211**, 500
39. Dingle, R.B. (1952) Proc. Roy. Soc. **A211**, 517
40. Abrikosov, A.A. (1988) Fundamental Theory of Metals, p.177. North Holland
41. Ballentine, L.E. (1990) Quantum Mechanics, p.326. Prentice Hall
42. Bethe, H., Salpeter, E. (1957) Quantum Mechanics of One and Two Electron Atoms, pp.19-20 and p.228. Springer
43. Geier, S., Bergmann, G. (1992) Phys. Rev. Lett. **68**, 2520
44. Dzyaloshinskii, I.E. (1957) Zh. Eksp. Fiz. [Sov. Phys. JETP] **6**, 821; Sov. Phys. JETP **6**, 1259]
45. Moriya, T. (1960) Phys. Rev. **120**, 91
46. Hutchings, M.T. (1964) Solid State Physics **16**, Seitz, E.F., Turnbull, D. (Eds.). Academic Press
47. Jahn, H.A., Teller, E. (1937) Proc. Roy. Soc. (London) **A161**, 220
48. Jahn, H.A. (1938) Proc. Roy. Soc. (London) **A164**, 356
49. Bates, C.A. (1978) Phys. Rep. **35**, 187
50. Kugel, K.I., Khomskii, D.I. (1982) Usp. Fiz. Nauk. **136**, 621 [Sov. Phys. Usp. **25**, 231]
51. Kanamori, J. (1960) J. Appl. Phys. (Supp.) **31**, 14S
52. Kramers, H.A. (1930) Proc. Amsterdam Acad. **33**, 959

Chapter 3

53. Heisenberg, W. (1926) Z. Phys. **38**, 441
54. Dirac, P.A.M. (1926) Proc. Roy. Soc. **112A**, 661
55. van Vleck, J.H. (1932) The Theory of Electric and Magnetic Susceptibilities. Oxford University Press, Oxford
56. Hund, F. (1927) Linienspektren und periodisches System der Elemente. Springer
57. Heitler, W. (1927) Z. Phys. **46**, 47; (1928) Z. Phys. **47**, 835; (1928) Z. Phys. **51**, 805
58. London, F. (1928) Z. Phys. **46**, 455; (1928) Z. Phys. **50**, 24
59. Herring, C. (1962) In Rado and Suhl (Eds.) Magnetism Vol. IIB, 1-181. Wiley, New York
60. Sugiura, Y. (1927) Z. Phys. **45**, 484
61. Bowers, K.D., Owen, W. (1955) Rep. Prog. in Phys. **18**, 304

62. Stevens, K.W.H. (1976) Phys. Rep. **24**, 1
63. Anderson, P.W. (1962) In Rado and Suhl (Eds.) Magnetism Vol. IIB, 25–83. Wiley, New York
64. Bullett, D.W. (1980) In Seitz and Turnbull (Eds.) Solid State Physics **35**, 129. Academic Press
65. Nozières, P. (1970) Theory of Interacting Fermi Systems. Benjamin, New York; (1970) Symposium Kastler, p.370. Presses Universitaires de France
66. Kramers, H.A. (1934) Physica **1**, 182

Chapter 4

67. Landau, L.D. (1969) In: Men of Physics: L.D. Landau. Pergamon Press
68. Landau, L.D. (1978) Statistical Physics. Pergamon Press
69. Anderson, P.W. (1984) Basic Notions in Condensed Matter Physics. Benjamin Cummings
70. Mermin, N.D., Wagner, H. (1966) Phys. Rev. Lett. **17**, 1133, 1307
71. Kosterlitz, J.M., Thouless, D.J. (1972) J. Phys. C **5**, L124; (1973) J. Phys. C **6**, 1181
72. Bean, C.P., Rodbell, D.S. (1962) Phys. Rev. **126**, 104
73. Ornstein, L.S., Zernike, K. (1914) Proc. K. Ned. Acad. Wet. **17**, 793
74. Birgeneau, R., Shirane, G., Blume, M., Koehler, W.C. (1974) Phys. Rev. Lett. **33**, 110
75. Levanyuk, A.P. (1959) Zh. Eksp. Teor. Fiz. **36**, 810 [JETP (1959)]
76. Fisher, M.E. (1974) Rev. Mod. Phys. **46**, 597
77. Ma, S.K. (1976) Modern Theory of Critical Phenomena. Benjamin
78. Ma, S.K. (1976) In: Domb, C., Green, M.S. (Eds.) Phase Transitions and Critical Phenomena Vol. 6, 250. Academic Press
79. Wilson, K. (1983) Rev. Mod. Phys. **55**, 583
80. Amit, D. (1984) Field Theory, the Renormalisation Group and Critical Phenomena. World Scientific
81. Kadanoff, L.P. (1966) Physics **2**, 263
82. Wilson, K., Fisher, M. (1972) Phys. Rev. Lett. **28**, 240
83. de Gennes, P.G. (1972) Phys. Lett. A **38**, 339
84. Wilson, K.G. (1975) Rev. Mod. Phys. **47**, 773
85. Abrahams, E., Anderson, P.W., Licciardello, D.C., Ramakrishnan (1979) Phys. Rev. Lett. **42**, 673
86. Widom, B. (1965) J. Chem. Phys. **43**, 3892; (1965) J. Chem. Phys. **43**, 3898
87. Stanley, E. (1971) Critical Phenomena. Oxford University Press, Oxford
88. Lévy, L.P. (1988) Phys. Rev. B **38**, 4963
89. Griffiths, R.B. (1965) Phys. Rev. Lett. **14**, 623
90. Ho, J.T., Lister, J.D. (1969) Phys. Rev. Lett. **22**, 603
91. Ho, J.T., Lister, J.D. (1970) Phys. Rev. B **2**, 4523
92. Ahlers, G. (1980) Rev. Mod. Phys. **52**, 580
93. Hohenberg, P.C., Halperin, B.I. (1977) Rev. Mod. Phys. **49**, 435

Chapter 5

94. Langevin, M.P. (1905) *J. Physique* **4**, 678
95. Weiss, P. (1907) *J. Physique* **6**, 661
96. Brillouin, L. (1927) *J. Phys. Radium* **8**, 74
97. Onsager, L. (1936) *J. Amer. Chem. Soc.* **58**, 1486
98. Thouless, D., Anderson, P.W., Palmer, R.G. (1977) *Philos. Mag.* **35**, 593
99. Mézard, M., Parisi, G., Virasoro, M.A. (1987) *Spin Glass Theory and Beyond*. World Scientific
100. Edwards, S.F., Anderson, P.W. (1975) *J. Phys. F* **5**, 965
101. Sherrington, D., Kirkpatrick, S. (1978) *Phys. Rev. B* **17**, 4384
102. Néel, L. (1932) *Ann. Physique* **17**, 64
103. Harris, A.B., Rastelli, E., Tassi, A. (1990) *J. Appl. Phys.* **67**, 5445
104. Anderson, P.W. (1950) *Phys. Rev.* **79**, 705
105. ter Haar, D., Lines, M.E. (1962) *Proc. Roy. Soc. (London)* **A254**, 521
106. Smart, J.S. (1966) *Effective Field Theories of Magnetism*. Saunders, Philadelphia
107. Tyabliakov, S.V. (1967) *Methods in the Quantum Theory of Magnetism*. Plenum, New York
108. Elser, V. (1989) *Phys. Rev. Lett.* **62**, 2405
109. Chandra, P., Coleman, P., Ritchey, I. (1993) *J. Phys. I (France)* **3**, 591
110. Harris, A.B., Kallin, C., Berlinsky, A.J. (1992) *Phys. Rev. B* **45**, 7084
111. Chalker, J.T., Holdsworth, P.C., Shender, E.F. (1993) *Phys. Rev. Lett.* **68**, 855
112. von Delft, J., Henley, C. (1993) *Phys. Rev. B* **48**, 965
113. Sindsingre, P., Lecheminant, P., Lhuillier, C. (1994) *Phys. Rev. B* **50**, 3108
114. Kawamura, H. (1984) *J. Phys. Soc. Jpn.* **53**, 2452
115. Kawamura, H., Miyashita, S. (1984) *J. Phys. Soc. Jpn.* **53**, 4113
116. Bernu, B., Lhuillier, C., Pierre, L. (1992) *Phys. Rev. Lett.* **69**, 2590
117. Bernu, B., Lecheminant, P., Lhuillier, C., Pierre, L. (1992) *Phys. Rev. B* **50**, 10048
118. Henley, C.L. (1987) *Phys. Rev. Lett.* **62**, 2056
119. Fisher, M.E., Nelson, D.R. (1974) *Phys. Rev. Lett.* **32**, 1350
120. Harris, A.B., Berlinsky, A.J., Bruder, C. (1990) *J. Appl. Phys.* **68**
121. Villain, J., Bidaux, R., Carton, J.P., Conte, R. (1980) *J. Physique* **41**, 1263
122. Larson, B.E., Henley, C.L. (1991) Unpublished
123. Lallemand, P., Diep, H.T., Ghazali, A., Toulouse, G. (1985) *J. Physique Lett.* **46**, 1087
124. Binder, K., Young, A.P. (1986) *Rev. Mod. Phys.* **58**, 801
125. Mydosh, J. (1990) *Spin Glasses*. North Holland
126. Nattermann, T., Villain, J. (1988) In: *Phase Transitions* **11**, 5
127. Aharony, A., Imry, Y., Ma, S.K. (1976) *Phys. Rev. Lett.* **37**, 1364

Chapter 6

128. Ising, E. (1925) *Z. Phys.* **31**, 253
129. Onsager, L. (1944) *Phys. Rev.* **65**, 117
130. Onsager, L. (1949) *Nuov. Cimento Suppl.* **6**, 261
131. Yang, C.N. (1952) *Phys. Rev.* **85**, 808
132. Yang, C.N., Lee, T.D. (1952) *Phys. Rev.* **87**, 404, 410

133. de Gennes, P.G. (1979) *Scaling Concepts in Polymer Physics*. Cornell University Press, 265
134. Lieb, E.H., Mattis, D.C. (1966) *Mathematical Physics in One Dimension*. Academic Press, New York
135. Thomson, C.J. (1972) In: *Phase Transitions and Critical Phenomena*, Domb, C., Green, M.S. (Eds.). Academic Press, New York
136. McCoy, B.M., Wu, T.T. (1973) *The 2D Ising Model*. Harvard University Press, Cambridge
137. Baxter, M. (1982) *Exactly Solvable Models in Statistical Mechanics*. Rodney, New York
138. Hornreich, R.M., Liebermann, R., Schuster, H.G., Selke, W. (1979) *Z. Physik B* **35**, 91
139. Selke, W. (1988) *Phys. Rep.* **170**, 213
140. Temperley, H.N.V. (1972) In: *Phase Transitions and Critical Phenomena* **1**, 227, Domb, C., Green, M.S. (Eds.). Academic Press, New York
141. Kac, M. (1966) In: *Brandeis Lectures*, Chrétien, M., Gross, E.P., Dreser, S. (Eds.). Gordon and Breach, New York
142. Lines, M.E. (1979) *Phys. Rep.* **55**, 133
143. Glauber, R.J. (1963) *J. Math. Phys.* **4**, 294
144. Kawasaki, K. (1966) *Phys. Rev.* **145**, 224
145. Suzuki, M., Kubo, R. (1968) *J. Phys. Soc. Jpn.* **24**, 51
146. Lévy, L.P., Ogielski, A.T. (1989) *J. Math. Phys.* **30**, 683
147. Hohenberg, P.C., Halperin, B.I. (1977) *Rev. Mod. Phys.* **49**, 435

Chapter 7

148. Mermin, N.D., Wagner, H. (1966) *Phys. Rev. Lett.* **17**, 1133, 1307
149. Bogoliubov, N.N. (1962) *Phys. Abh. Sowjet.* **6**, 113, 229
150. Hohenberg, P.C. (1967) *Phys. Rev.* **158**, 383
151. Lieb, E., Schultz, T., Mattis, D. (1961) *Ann. Phys. N.Y.* **16**, 407
152. Steiner, M., Villain, J., Windsor, C. (1976) *Adv. Phys.* **25**, 87
153. Jordan, P., Wigner, E.P. (1928) *Z. Phys.* **47**, 631
154. Tenant, D.A., Perring, T.G., Cowley, R.A., Nagler, S.E. (1993) *Phys. Rev. Lett.* **70**, 4003
155. Bethe, H. (1931) *Z. Physik* **71**, 205
156. Hulthén, L. (1938) *Arkiv. Math. Astron. Fysik* **26A**, 11
157. des Cloizeaux, J., Pearson, J.J. (1962) *Phys. Rev.* **128**, 2131
158. Griffiths, R.B. (1964) *Phys. Rev.* **133**, A768
159. Yang, C.N., Yang, C.P. (1966) *Phys. Rev.* **147**, 303; (1966) *Phys. Rev.* **150**, 321; (1956) *Phys. Rev.* **151**, 258
160. Faddeev, L.D., Thakhtajan, L.A. (1981) *Phys. Lett. A* **83**, 375
161. Takahashi, M., Suzuki, M. (1972) *Prog. Theor. Phys.* **48**, 2187
162. Luther, A., Peschel, I. (1974) *Phys. Rev. B* **9**, 2911
163. Shastry, B.S. (1988) *Phys. Rev. Lett.* **60**, 639
164. Haldane, F.D.M. (1988) *Phys. Rev. Lett.* **60**, 635
165. Gaudin, J. (1970) *La fonction d'onde de Bethe*. CEA ed.
166. Nozières, P. (1992) *Liquide de Fermi à une dimension. Méthodes de perturbation et Ansatz de Bethe*. Lecture course at the Collège de France
167. Kosterlitz, J.M., Thouless, D.J. (1972) *J. Phys. C* **5**, L124; (1973) *J. Phys. C* **6**, 1181
168. Berezinskii, V.L. (1972) *Sov. Phys. JETP* **34**, 610

169. Kosterlitz, J.M., Thouless, D.J. (1978) *Prog. Low Temp. Phys.* **VIIIB**, 371
170. Nelson, D.R. (1983) *Phase Transitions* **7**, 1, Domb and Green (Eds.). Academic Press
171. Bishop, D.J., Reppy, J.D. (1978) *Phys. Rev. Lett.* **40**, 1727
172. Rudnick, I. (1978) *Phys. Rev. Lett.* **40**, 1454
173. Agnolet, G., McQueeney, D.F., Reppy, J.D. (1989) *Phys. Rev. B* **39**, 8934
174. Fisher, M.P.A., Lee, D.H. (1989) *Phys. Rev. B* **39**, 2756
175. Schön, G., Zaikin, A.D. (1990) *Phys. Rep.* **198**, 237
176. de Nijs, M., Rommelse, K. (1989) *Phys. Rev. B* **40**, 4709
177. Nozières, P. (1991) Lectures at the Beg Rohu Summer School. In: Solids far from equilibrium, Godrèche, C. (Ed.). Cambridge University Press, Cambridge

Chapter 8

178. Langevin, P. (1908) *Compt. Rend. Acad. Sci. (Paris)* **146**, 530
179. Einstein, A. (1905) *Ann. Physik* **19**, 371
180. Marshall, W., Lovesey, S.W. (1971) *Theory of Thermal Neutron Scattering*. Clarendon Press, Oxford
181. Squires, G.L. (1978) *Introduction to the Theory of Thermal Neutron Scattering*. Cambridge University Press, Cambridge
182. Lovesey, S.W., Springer, T. (Eds.) (1977) *Dynamics of Solids and Liquids by Neutron Scattering, Topics in Current Physics Vol. 3*. Springer
183. Onsager, L. (1931) *Phys. Rev.* **38**, 2265
184. Onsager, L., Machtap, S. (1953) *Phys. Rev.* **91**, 1505
185. Johnson, J.B. (1928) *Phys. Rev.* **32**, 97
186. Nyquist, H. (1928) *Phys. Rev.* **32**, 110
187. Brillouin, L. (1934) *Helv. Phys. Acta* **1** Suppl., 47
188. Réfrigier, P., Ocio, M., Bouchiat, H. (1987) *Europhys. Lett.* **3**, 503
189. Bernard, W., Callen, H.B. (1959) *Rev. Mod. Phys.* **31**, 1017
190. Callen, H.B., Welton, T.A. (1951) *Phys. Rev.* **83**, 34
191. Callen, H.B., Greene, R.F. (1951) *Phys. Rev.* **86**, 702
192. Villain, J. (1993) *Cours de physique statistique*, p. 65
193. Kubo, R. (1957) *J. Phys. Soc. Japan* **12**, 570
194. Chester, G.V. (1963) *Rep. Prog. Phys.* **26**, 411
195. Kubo, R. (1966) *Rep. Prog. Phys.* **29**, 255
196. Landau, L., Lifshitz, E. (1967) *Mécanique Quantique*, pp. 172-3 and 221-4. Éditions Mir
197. Ocio, M., Bouchiat, H., Monod, P. (1985) *J. Phys. Lett. (Paris)* **46**, 647
198. Sleator, T., Hahn, E.L., Hilbert, C., Clarke, J. (1987) *Phys. Rev. B* **36**, 1969
199. Sommerfeld, A. (1953) *Thermodynamics*. Academic Press
200. Kwok, P.C., Schultz, T.D. (1969) *J. Phys. C* **2**, 1196
201. Casimir, H.B.G. (1945) *Rev. Mod. Phys.* **17**, 343
202. Büttiker, M. (1986) *Phys. Rev. Lett.* **57**, 1761
203. Büttiker, M. (1988) *I.B.M. J. Res. Dev.* **32**, 317
204. Peterson, R. (1967) *Rev. Mod. Phys.* **39**, 69
205. Efremov, G.F. (1968) *Zh. Eksp. Teor. Fiz.* **55**, 2322 [(1969) Sov. Phys. JETP **28**, 1232]
206. Lévy, L.P., Ogielski, A.T. (1989) *J. Math. Phys.* **30**, 683
207. Abragam, A. (1960) *The Principles of Nuclear Magnetism*. Oxford University Press, Oxford
208. Bloembergen, N. (1961) *Nuclear Magnetic Relaxation*. W.A. Benjamin

209. Goldman, M. (1970) Spin Temperature and Nuclear Magnetic Resonance in Solids. Oxford University Press, Oxford
210. Slichter, C.P. (1985) Principle of Magnetic Resonance. Springer
211. Low, W. (1960) Paramagnetic Resonance in Solids. In: Solid State Physics, Suppl. 2, Seitz and Turnbull (Eds.). Academic Press
212. White, R.W. (1983) Quantum Theory of Magnetism. Springer
213. Ruckenstein, A.E. (1988) J. Low Temp. **70**, 327
214. Bloembergen, N., Purcell, E.M., Pound, R.V. (1948) Phys. Rev. **73**, 679
215. Sparks, M. (1964) Ferromagnetic Relaxation. McGraw Hill
216. Kittel, C. (1960) Lecture Notes on Magnetism. Université Paris-Sud, Orsay
217. Keffer, F. (1966) Spin-waves, Handbuch der Physik. Springer
218. Bloembergen, N. (1950) Phys. Rev. **78**, 572
219. Landau, L., Lifshitz, L. (1935) Physik Z. Sowjet. **8**, 153
220. Gilbert, T. (1955) Phys. Rev. **100**, 1234

Chapter 9

221. Kadanoff, L.P., Martin, P.C. (1963) Ann. Phys. **24**, 419
222. Forster, D. (1975) Hydrodynamic Fluctuations, Broken Symmetry and Correlation Functions. Benjamin Cummings
223. Ruckenstein, A.E. (1984) Ph.D. Thesis, Cornell University
224. Goldstone, J. (1961) Nuov. Cim. **19**, 154
225. Goldstein, H. (1950) Classical Mechanics, 255–263. Addison-Wesley, New York
226. Lévy, L.P., Ruckenstein, A.E. (1984) Phys. Rev. Lett. **55**, 1427
227. Holstein, T., Primakoff, H. (1940) Phys. Rev. **58**, 1048
228. White, R.M. (1983) Quantum Theory of Magnetism. Springer
229. Bogoliubov, N.N. (1958) Zh. Eksp. Teor. Fiz. **34**, 58 [(1958) Sov. Phys. JETP **34**, 41]
230. Keffer, F. (1966) Handbuch der Physik, Vol. 18. Springer
231. Balian, R., Brézin, E. (1969) Nuovo Cim. B **LXIV**, 37
232. Walker, L.R. (1958) J. Appl. Phys. **29**, 318
233. Damon, R.W., Eshbach, J.R. (1981) J. Phys. Chem. Solids **19**, 308
234. Osheroff, D.D., Cross, M.C. (1987) Phys. Rev. Lett. **59**, 97
235. Bloch, F. (1930) Z. Phys. **61**, 206
236. Dyson, F. (1956) Phys. Rev. **102**, 1217
237. Reich, D.H., Lévy, L.P., Hawthorne, D. (1991) J. Appl. Phys. **69**, 5950
238. Villain, J. (1974) J. Physique **35**, 27
239. Schwinger, J. (1952) On Angular Momentum. US Atomic Energy Commission Rpt. NYO-3071
240. Azzouz, M., Douçot, B. (1992) Phys. Rev. B **47**, 8660
241. Andreev, A.F., Marchenko, V.I. (1976) Zh. Eksp. Teor. Fiz. **70**, 1522 [(1976) Sov. Phys. JETP **43**, 794]
242. Halperin, B.I., Hohenberg, P.C. (1969) Phys. Rev. **88**, 188
243. Henley, C.L., Sompolinsky, H., Halperin, B.I. (1982) Phys. Rev. B **25**, 5849

Chapter 10

244. Kaganov, M.I., Chubukov, A.V. (1987) Usp. Fiz. Nauk. **153**, 537 [Sov. Phys. Usp. **30**, 1015]
245. Haldane, F.D.M. (1983) Phys. Lett. A **93**, 454
246. Haldane, F.D.M. (1983) Phys. Rev. Lett. **50**, 1153
247. Schulz, H.J., Ziman, T. (1986) Phys. Rev. B **33**, 6545
248. Schulz, H.J. (1986) Phys. Rev. B **34**, 6372
249. Kugel, K.I., Khomskii, D.I. (1982) Sov. Phys. Usp. **85**, 231
250. De Nijs, M., Rommelse, K. (1989) Phys. Rev. B **40**, 4709
251. Ablowitz, M.J., Segur, H. (1981) Solitons and the Inverse Scattering Transform. SIAM ed., Philadelphia
252. Lamb, G.L. (1981) Elements of Soliton Theory. Wiley, New York
253. Villain, J. (1974) J. de Physique (Paris) **35**, 27
254. Rubinstein, J. (1970) J. Math. Phys. **11**, 258
255. Forest, G., McLaughlin, D.W. (1982) J. Math. Phys. **23**, 1248
256. Haldane, F.D.M. (1992) Phys. Rev. Lett. **57**, 1488
257. Auerbach, A. (1994) Interacting Electrons and Quantum Magnetism. Springer
258. Mikeska, H.J. (1982) Phys. Rev. B **26**, 5213
259. Dashen, R.F., Hasslacher, B., Neveu, A. (1974) Phys. Rev. D **10**, 4114; ibid. Phys. Rev. D **10**, 4130; ibid. Phys. Rev. D **10**, 4139
260. Dashen, R.F., Hasslacher, B., Neveu, A. (1975) Phys. Rev. D **12**, 3424
261. Maki, K. (1981) Phys. Rev. B **24**, 3991
262. Mikeska, H.J., Vaz da Costa, B., Fogedby, H.C. (1989) Z. Phys. B **77**, 119
263. Lévy, L.P. (1985) Phys. Rev. B **31**, 7077
264. Rajaraman, R. (1982) Solitons and Instantons. Elsevier
265. Faddeev, L.D., Takhtajan, L.A. (1987) Hamiltonian Methods in the Theory of Solitons. Springer
266. Takhtajan, L.A. (1977) Phys. Lett. A **64**, 235
267. Fogedby, H.C. (1980) J. Phys. A **13**, 1467
268. Haldane, F.D.M. (1982) J. Phys. C **15**, L1309
269. Takhtajan, L.A. (1982) Phys. Lett. A **87**, 479
270. Lieb, E., Schultz, T.D., Mattis, D.C. (1962) Ann. Phys. **16**, 407
271. Affleck, I., Lieb, E. (1986) Lett. Math. Phys. **12**, 57
272. Marshall, W. (1955) Proc. Roy. Soc. London **A232**, 48
273. Lieb, E., Mattis, D.C. (1962) J. Math. Phys. **3**, 749
274. Majumdar, C.K., Ghosh, D.K. (1969) J. Math. Phys. **10**, 1388; ibid. **10**, 1399
275. Liang, S., Douçot, B., Anderson, P.W. (1988) Phys. Rev. Lett. **61**, 365
276. Kekule von Stradonitz, A. (1866) Lehrbuch der organischen chemie. Erlangen
277. Sutherland, W. (1988) Phys. Rev. B **37**, 3788
278. Majumdar, C.K., Ghosh, D.K. (1969) J. Math. Phys. **10**, 1388; ibid. **10**, 1399. Majumdar, C.K., Krishan, K., Mubayi, V. (1972) J. Phys. C **5**, 2869
279. Shastry, B.S., Sutherland, W. (1981) Phys. Rev. Lett. **47**, 964
280. Chitra, R., Pati, S.K., Krishnamurthy, H.R., Sen, D., Ramasesha, S. (1995) Phys. Rev. B **52**, 6591
281. Haldane, F.D.M. (1982) Phys. Rev. B **25**, 4925
282. Kennedy, T. (1990) J. Cond. Matter **3**, 5757
283. Affleck, I., Kennedy, T., Lieb, E.H., Tasaki, H. (1987) Phys. Rev. Lett. **59**, 799; ibid. (1988) Comm. Math. Phys. **115**, 477
284. Hagiwara, M., Katsumata, K., Affleck, I., Halperin, B.I., Renard, J.P. (1990) Phys. Rev. Lett. **65**, 3181
285. Arovas, D.P., Auerbach, A., Haldane, F.D.M. (1988) Phys. Rev. Lett. **60**, 531
286. Botet, R., Jullien, R. (1983) Phys. Rev. B **37**, 613

287. Takahashi, M. (1989) Phys. Rev. Lett. **62**, 2313
 288. White, S.R., Huse, D.A. (1993) Phys. Rev. B **48**, 3844
 289. Golinelli, O., Jolicoeur, T., Lacaze, R. (1992) Phys. Rev. B **45**, 9798; ibid.
 (1992) **B46**, 10854; ibid. (1994) **B50**, 3037
 290. Laughlin, R.B. (1983) Phys. Rev. Lett. **50**, 1395
 291. Affleck, I. (1985) Nucl. Phys. B **B57**, 397
 292. Affleck, I. (1989) In Brézin, E., Zinn-Justin, J. (Eds.) Champs, Cordes et
 Phénomènes Critiques. Elsevier
 293. Gell-Mann, M., Lévy, M. (1960) Nuov. Cimm. **16**, 1729
 294. Shankar, R. (1990) Nucl. Phys. B **330**, 433
 295. Shankar, R., Read, N. (1990) Nucl. Phys. B **336**, 457
 296. Ge, M.L., Niu, Y. (1989) J. Phys. A **22**, L457
 297. Berry, M.V. (1984), Proc. Roy. Soc. London **A392**, 45

Chapter 11

298. Pines, D. (1955) Solid State Phys. **1**, 368; Pines, D. (1954) Phys. Rev. **92**, 626
 299. Nozières, P., Pines, D. (1958) Phys. Rev. **111**, 442
 300. Wigner, E. P. (1934) Phys. Rev. **46**, 1002
 301. Rosenbaum, T., et al. (1985) Phys. Rev. Lett. **52**
 302. Herring, C. (1968) In Rado and Suhl (Eds.) Magnetism Vol. 4. Academic Press
 303. Wohlfarth, E.P. (1980) Ferromagnetic Materials **I**, 1. North Holland
 304. Vonsovky, S.V., Turov, E.A. (1953) Sov. Phys. JETP **24**, 419
 305. Zener, C., Heikes, R.R. (1953) Rev. Mod. Phys. **25**, 191
 306. Weiss, R.J., de Marco, J.J. (1958) Rev. Mod. Phys. **30**, 59
 307. Batterman, B.N. (1959) Phys. Rev. Lett. **2**, 47
 308. Pobell, F., et al. (1986) Phys. Rev. Lett. **57**
 309. Stoner, E.C. (1938) Proc. Roy. Soc. (London) **A165**, 372
 310. Gorkov, L.P. (1984) Usp. Fiz. Nauk. **144**, 381 [(1984) Sov. Phys. Usp. **27**,
 809] See also (1986) Proc. Yamada Conf. XV, Physica **143B**
 311. Lomer, W.M. (1962) Proc. Phys. Soc. (London) **80**, 489
 312. Overhauser, A.W. (1962) Phys. Rev. **128**, 1437
 313. Kohn, W. (1959) Phys. Rev. Lett. **2**, 393
 314. Johnson, M.A., Silsbee, R. (1984) Phys. Rev. Lett. **57**
 315. Izuyama, T., Kim, E.J., Kubo, R. (1963) J. Phys. Soc. Jpn. **18**, 1025
 316. Nozières, P. (1970) Symposium Kastler, p.381. Presses Universitaires de
 France
 317. Doniach, S., Engelsberg, S. (1966) Phys. Rev. Lett. **17**, 750
 318. Berk, N.F., Schrieffer, J.R. (1966) Phys. Rev. Lett. **17**, 433
 319. Béal-Monod, M.T. (1982) Physica **110B**, 1987; (1983) Proc. 3rd Magnetic
 Magnetism, 279–303
 320. Schultz, S., Dunifer, G. (1967) Phys. Rev. Lett. **18**, 283
 321. Johnson, B.R., et al. (1984) Phys. Rev. Lett. **52**, 1508
 322. Masuhara, N., et al. (1984) Phys. Rev. Lett. **53**, 1168
 323. Ruckenstein, A., Lévy, L.P. (1988) Phys. Rev. B **39**, 183
 324. Moriya, T. (1985) Spin Fluctuations in Itinerant Electron Magnetism.
 Springer
 325. Hirsh, J.E. (1990) Phys. Rev. B **41**, 6820
 326. des Cloizeaux, J. (1959) J. de Phys. et Rad. **20**, 606; ibid. **20**, 751
 327. Keldysh, L.V., Kopaev, Y.V. (1964) Fiz. Tver. Tel. **6**, 2791 [(1965) Sov. Phys.
 Solid State **6**, 2219]

328. Rice, T.M. (1970) Phys. Rev. B **2**, 3619
 329. Kulikov, N.I., Tugushev, V.V. (1984) Usp. Fiz. Nauk. **144**, 643 [(1985) Sov. Phys. Usp. **27**, 954]
 330. Moriya, T., Usami, K. (1977) Solid State Comm. **23**, 935
 331. Fawcett, E. (1988) Rev. Mod. Phys. **60**, 209
 332. Hubbard, J. (1963) Proc. Roy. Soc. (London) **A276**, 238
 333. Lieb, E.H., Wu, F.Y. (1968) Phys. Rev. Lett. **20**, 1445
 334. Mott, N.F. (1990) Metal Insulator Transitions. Taylor and Francis
 335. Anderson, P.W. (1988) In: Broglie, R.A., Schrieffer, J.R. (Eds.) E. Fermi Summer School Varenna, Frontiers in Many-Particle Physics p.1. North Holland
 336. Rice, T.M. (1994) Strongly Interacting Fermions and High T_c Superconductivity, Doucot, B., Zinn-Justin, J. (Eds.). Elsevier Science
 337. Metzner, W., Vollhardt, D. (1987) Phys. Rev. Lett. **59**, 121; (1988) Phys. Rev. B **37**, 7382; (1989) Phys. Rev. Lett. **62**, 324
 338. Georges, A., Kotliar, G., Krauth, W., Rozenberg, M.J. (1996) Rev. Mod. Phys. **68**, 13
 339. Gutzwiller, M.C. (1963) Phys. Rev. Lett. **10**, 159; (1964) Phys. Rev. A **134**, 923; (1965) Phys. Rev. A **137**, 1726
 340. Brinkman, W.F., Rice, T.M. (1970) Phys. Rev. B **2**, 4302; (1970) Phys. Rev. B **2**, 1324
 341. Anderson, P.W. (1987) Science **235**, 1196; (1990) Phys. Rev. Lett. **65**, 2306
 342. Kanamori, J. (1963) Prog. Theor. Phys. **30**, 275
 343. Ballentine, L.E. (1990) Quantum Mechanics, 328. Prentice Hall
 344. Kadanoff, L.P., Baym, G. (1962) Quantum Statistical Mechanics. Benjamin, New York
 345. Varma, C.M., et al. (1989) Phys. Rev. Lett. **63**, 1996
 346. Shraiman, B., Siggia, E. (1989) Phys. Rev. Lett. **62**, 1564
 347. Cheong, S.W., et al. (1991) Phys. Rev. Lett. **67**, 1791
 348. Baskaran, G., Zou, Z., Anderson, P.W. (1987) Solid State Comm. **63**, 973
 349. Ioffe, L., Larkin, A. (1989) Phys. Rev. B **39**, 8988
 350. Lee, P.A., Nagaosa, N. (1992) Phys. Rev. B **46**, 5621
 351. Wen, X., Wilczek, F., Zee, A. (1989) Phys. Rev. B **39**, 11413
 352. Nagaosa, N., Lee, P.A. (1992) Phys. Rev. B **45**, 966
 353. Scalapino, D.J., Loh, E., Hirsch, J.E. (1987) Phys. Rev. B **35**, 6694
 354. Wollman, D.A., Van Harlingen, D.J., Lee, W.C., Ginsberg, D.M., Leggett, A.J. (1993) Phys. Rev. Lett. **71**, 2134
 355. Mathai, M., Gim, Y., Black, R.C., Amar, A., Wellstood, J. (1995) Phys. Rev. Lett. **74**, 4523
 356. Chaudhari, P., Lin, S.Y. (1994) Phys. Rev. Lett. **72**, 1084
 357. Sun, A.G., Gajewski, D.A., Maple, M.B., Dynes, R.C. (1994) Phys. Rev. Lett. **72**, 2267
 358. Ding, H., Campuzano, J.C., Bellman, A., Yokoya, T., Randeira, M., Norman, M., Takahashi, T., Katayama-Yoshida, H., Jennings, G. (1995) Phys. Rev. Lett. **74**, 2784; ibid. (1995) **74**, 4951

Chapter 12

359. Omnès, H.K. (1911) Comm. Phys. Lab. Univ. Leiden 119b, 120b, 122b, 124c
 360. Omnès, H.K. (1914) Comm. Phys. Lab. Univ. Leiden 139f
 361. Meissner, W., Ochsenfeld, R. (1933) Naturwiss. **21**, 787

362. Shubnikov, L.V., de Haas, W.J. (1930) Comm. Phys. Lab. Univ. Leiden 207, 210; (1930) Proc. Acad. Amsterdam **33**, 418
363. de Haas, W.J., Voogd, J. (1931) Comm. Phys. Lab. Univ. Leiden 208b, 214b
364. Kinsel, T., Lynton, E.A., Serin, B. (1964) Rev. Mod. Phys. **36**, 105
365. Corak, W.S., Satterthwaite, C.B., Wexler, A. (1954) Phys. Rev. **96**, 1442; (1954) Phys. Rev. **99**, 1442; (1956) Phys. Rev. **102**, 656
366. Phillips, N.E. (1959) Phys. Rev. **114**, 676
367. Maxwell, E. (1950) Phys. Rev. **78**, 477
368. Reynolds, C.A., Serin, B., Wright, W.H., Nesbitt, L.B. (1950) Phys. Rev. **78**, 487
369. Landau, L. (1937) Phys. Z. Sowjet. **11**, 129
370. Landau, L. (1943) J. Phys. USSR **7**, 99
371. Andreev, A. (1966) Z. Eksp. Teor. Phys. **51**, 1510 [(1966) Sov. Phys. JETP **24**, 1019]
372. Pethick, C.J., Smith, H. (1979) Ann. Phys. **119**, 133
373. Smith, H., Jensen, H.H. (1989) Transport Phenomena. Oxford University Press, Oxford
374. London, F., London, H. (1935) Z. für Phys. **96**, 359
375. London, F. (1937) Une conception nouvelle de la supraconductivité. Hermann
376. London, F. (1950) Superfluids. Wiley, New York
377. Haenssler, F., Rinderer, L. (1967) Helv. Phys. Acta **40**, 659
378. Pippard, A.B. (1953) Proc. Roy. Soc. London **A216**, 547; (1955) Proc. Roy. Soc. London **A248**, 97
379. Sharvin, Y.V. (1957) Z. Eksp. Teor. Fiz. **33**, 1341 [(1958) Sov. Phys. JETP **6**, 1031]
380. Haenssler, F., Rinderer, L. (1965) Phys. Lett. **16**, 29
381. Silsbee, F.B. (1916) J. Wash. Acad. Sci. **6**, 597
382. Mukherjee, B.K., Baird, D.C. (1968) Phys. Rev. Lett. **21**, 996
383. Andreev, A.F. (1968) Zh. Eksp. Teor. Fiz. **54**, 1510 [(1968) Sov. Phys. JETP **27**, 809]
384. Gorter, C.J. (1957) Physica **23**, 45
385. Gorter, C.J., Potters, M.J. (1958) Physica **24**, 169
386. Chandrasekar, B.S., Dinewitz, I.J., Ferrell, D.E. (1966) Phys. Rev. Lett. **20**, 321
387. van Gurp, G.J. (1967) Phys. Lett. A **24**, 528

Chapter 13

388. Ginzburg, V.L., Landau, L.D. (1950) Zh. Eksp. Teor. Fiz. **20**, 1064
389. Gorkov, L.P. (1959) Zh. Eksp. Teor. Fiz. **36**, 1918; (1959) Zh. Eksp. Teor. Fiz. **37**, 833; (1959) Zh. Eksp. Teor. Fiz. **37**, 1407
390. Bardeen, J., Cooper, L.N., Schrieffer, J.R. (1957) Phys. Rev. **108**, 1175
391. de Gennes, P.G. (1964) Rev. Mod. Phys. **36**, 225
392. Deaver, D.S., Fairbank, W.M. (1961) Phys. Rev. Lett. **7**, 43
393. Lounasmaa, O.V., Hari, R. (1990) La Recherche **21**, 874
394. Little, W.A., Parks, R.D. (1962) Phys. Rev. Lett. **9**, 9; (1964) Phys. Rev. A **133**, 97
395. Groff, R.P., Parks, R.D. (1967) In Malkov, M.P. (Ed.) Proc. of LT10, Vol. IIA. Viniti, Moscow
396. Bardeen, J. (1962) Rev. Mod. Phys. **34**, 667
397. Clogston, A.M. (1962) Phys. Rev. Lett. **9**, 266

398. Saint James, D., de Gennes, P.G. (1963) Phys. Rev. Lett. **7**, 306
 399. Tinkham, M. (1975) Introduction to Superconductivity, 133. Krieger
 400. Levine, J.L. (1967) Phys. Rev. **155**, 373
 401. Abrikosov, A.A., Gorkov, L.P. (1960) Z. Eksp. Teor. Fiz. **39**, 1781 [(1961) Sov. Phys. JETP **12**, 1243]
 402. de Gennes, P.G. (1989) Superconductivity of Metals and Alloys. Addison-Wesley
 403. Chevrel, R., Sergent, M., Prigent, J. (1971) J. Sol. State Chem. **3**, 515
 404. Fisher, O., Jones, H., Bongi, G., Sergent, M., Chevrel, R. (1974) J. Phys. C **7**, L450

Chapter 14

405. Maxwell, E. (1950) Phys. Rev. **78**, 477
 406. Reynolds, C.A., Serin, B., Wright, W.H., Nesbitt, L.B. (1950) Phys. Rev. **78**, 487
 407. Abrikosov, A.A. (1988) Fundamental Theory of Metals, 53–56. North Holland
 408. de Gennes, P.G. (1989) Superconductivity of Metals and Alloys. Addison-Wesley
 409. Eliashberg, G. (1960) Zh. Eksp. Teor. Fiz. [(1960) Sov. Phys. JETP **38**, 966; ibid. **39**, 1437]
 410. Mahan, G.D. (1990) Many-Particle Physics, 773. Plenum Press
 411. Engelhardt, J.J., Webb, G.W., Matthias, B.T. (1967) Science **155**, 191
 412. Garland, J.W. (1963) Phys. Rev. Lett. **11**, 114; (1967) Phys. Rev. **153**, 460
 413. Morel, P., Anderson, P.W. (1962) Phys. Rev. **125**, 1263
 414. McMillan, W.L., Rowell, J.M. (1969) In: Parks, R.D. (Ed.) Superconductivity Chap. 11. Marcel Dekker, New York
 415. Gorkov, L.P. (1963) Zh. Eksp. Teor. Fiz. **44**, 767
 416. Rickayzen, G. (1967) Theory of Superconductivity, 167. Wiley, New York
 417. Lafarge, P., Joyez, P., Estève, D., Urbina, C., Dévoret, M.H. (1993) Phys. Rev. Lett. **70**, 994
 418. Tuominen, M.T., et al. (1992) Phys. Rev. Lett. **69**, 1997
 419. Eiles, T.M., Martinis, J., Dévoret, M. (1993) Phys. Rev. Lett. **70**, 1863
 420. Jankó, B., Smith, A., Ambegaokar, V. (1994) Phys. Rev. B **50**, 1152
 421. Bogoliubov, N.N. (1958) Zh. Eksp. Teor. Fiz. **34**, 58 [(1958) Sov. Phys. JETP **34**, 41]
 422. Anderson, P.W. (1967) The Josephson Effect and Quantum Coherence in Superconductors and Superfluids. In: Gorter, G.J. (Ed.) Prog. in Low Temp. Phys. V. North Holland
 423. Bardeen, J., Cooper, L.N., Schrieffer, J.R. (1957) Phys. Rev. **108**, 1175
 424. Schrieffer, J.R. (1964) Theory of Superconductivity. Benjamin
 425. Rickayzen, G. (1969) In: Parks, R.D. (Ed.) Superconductivity. Marcel Dekker, New York
 426. Gasparovic, R.F., Taylor, B.N., Eck, R.E. (1966) Solid State Comm. **4**, 59
 427. Anderson, P.W. (1958) Phys. Rev. **110**, 827
 428. Bogoliubov, N.N. (1958) Nuov. Cim. **7**, 794
 429. Martin, P. (1969) In: Parks, R.D. (Ed.) Superconductivity. Marcel Dekker, New York
 430. Giaver, I. (1960) Phys. Rev. Lett. **5**, 147; (1960) **5**, 464; (1961) Fisher, J.C., Giaver, I. J. Appl. Phys. **32**, 171

431. Abrikosov, A.A., Khalatnikov, I.M. (1958) *Usp. Fiz. Nauk.* **95**, 551 [(1958) Sov. Phys. Uspekhi]
432. Hebel, L.C., Schlichter, C.P. (1959) *Phys. Rev.* **113**, 1504
433. Levy, M., Kagiwada, R., Rudnick, I. (1963) *Phys. Rev.* **132**, 2039
434. Madsuda, Y., Okubo, N. (1969) *J. Phys. Soc. Japan* **26**, 309
435. MacLaughlin, D.K. (1976) In: Ehrenreich, Seitz, Turnbull (Eds.) *Solid State Physics* Vol. 31. Academic Press
436. Guénault, A.M. (1961) *Proc. Roy. Soc. A* **294**, 420
437. Mattis, D.C., Bardeen, J. (1958) *Phys. Rev.* **111**, 412
438. Tinkham, M., Ferrell, R.A. (1959) *Phys. Rev. Lett.* **2**, 331
439. Morse, R.W., Bohm, H.V. (1957) *Phys. Rev.* **108**, 1094
440. Palmer, L.H., Tinkham, M. (1968) *Phys. Rev.*
441. Ashcroft, N.W., Mermin, N.D. (1976) In: Holt, Rinehart, Winston (Eds.) *Solid State Physics*, 778

Chapter 15

442. Abrikosov, A.A. (1957) *Zh. Eksp. Teor. Fiz.* **32**, 1442
443. Cribier, D., Jacrot, B., Rao, L.M., Farnoux, B. (1964) *Phys. Lett.* **9**, 106
444. Essmann, U. (1967) *Phys. Lett. A* **24**, 526; *Phys. Status Solidi* **20**, 95
445. Hess, H.F., Robinson, R.B., Dynes, R.C., Valles, J.M., Waszczak, J.V. (1989) *Phys. Rev. Lett.* **62**, 214
446. Chang, A.M., Hallen, H.D., Harriott, L., Hess, H.F., Kao, H.L., Kwo, J., Miller, R.E., Wolfe, R., van der Ziel, J. (1992) *Appl. Phys. Lett.* **61**, 1974
447. Essmann, U. (1972) *Phys. Lett. A* **41**, 477
448. Abrikosov, A.A. (1961) *Zh. Eksp. Teor. Fiz.* **39**; *ibid.* **41**
449. Abrikosov, A.A. (1988) *Fundamental Theory of Metals*, 410–419. North Holland
450. Strand, A.R., Hemstead, C.F., Kim, Y.B. (1964) *Phys. Rev. Lett.* **13**, 794
451. Caroli, C., de Gennes, P.G., Matricon, J. (1965) *J. Physique Lettres* **9**, 307
452. de Gennes, P.G. (1989) *Superconductivity of Metals and Alloys*, 153. Addison-Wesley
453. Safar, H., Gammel, P., Bishop, D.J., Mitzi, D.B., Kapitulnick, A. (1992) *Phys. Rev. Lett.* **68**, 2672
454. Bishop, D.J., Gammel, P.L., Murray, C.A. (1992) *Science* **255**, 165
455. Charalambous, M., et al. (1992) *Phys. Rev. B* **45**, 5091
456. Charalambous, M., et al. (1995) *Phys. Rev. Lett.* **75**, 2578
457. Fisher, D.S., Fisher, M.P.A., Huse, D. (1991) *Phys. Rev. B* **43**, 130
458. Huse, D., Fisher, M.P.A., Fisher, D.S. (1992) *Nature* **358**, 553
459. Farrell, D.E. (1994) In: Ginsberg, D. (Ed.) *Physical Properties of High Temperature Superconductors*. World Scientific
460. Blatter, G., Feigelman, M.V., Geshkenbein, V.B., Larkin, A.I., Vinokur, V.M. (1994) *Rev. Mod. Phys.* **66**, 1125
461. Yeshurun, Y., Malozemoff, A.P. (1988) *Phys. Rev. Lett.* **60**, 2202
462. Nelson, D.R., Vinokur, V.M. (1993) *Phys. Rev. B* **48**, 13060
463. Bardeen, J., Stevens, M.J. (1965) *Phys. Rev.* **140**, A1197
464. Giaver, I. (1965) *Phys. Rev. Lett.* **15**, 825
465. Kim, Y.B., Stevens, M.J. (1969) In: Parks, R.D. (Ed.) *Superconductivity*, Chap. 19. M. Dekker, New York
466. Salomon, P.R., Otter Jr., F.A. (1967) *Phys. Rev.* **164**, 608
467. Salomon, P.R. (1969) *Phys. Rev.* **179**, 475

468. Vidal, F. (1973) Phys. Rev. B **8**, 1982
 469. Thuneberg, E.V., Kurkijärvi, J., Rainer, D. (1984) Phys. Rev. B **29**, 3914
 470. Bean, C.P. (1962) Phys. Rev. Lett. **8**, 250; (1964) Rev. Mod. Phys. **36**, 31
 471. Anderson, P.W. (1962) Phys. Rev. Lett. **9**, 309
 472. Anderson, P.W., Kim, Y.B. (1964) Rev. Mod. Phys. **36**, 39

Chapter 16

473. Giaver, I. (1960) Phys. Rev. Lett. **5**, 147
 474. Nicol, J., Shapiro, S., Smith, P.H. (1960) Phys. Rev. Lett. **5**, 461
 475. Avenel, O., Varoquaux, E. (1985) Phys. Rev. Lett. **55**, 2704
 476. Varoquaux, E., Meisel, M.W., Avenel, O. (1986) Phys. Rev. Lett. **57**, 2291
 477. Ambegaokar, V., Baratoff, A. (1963) Phys. Rev. Lett. **10**, 486; ibid. (1963) **11**, 104
 478. Aslamasov, A., Larkin, A.I. (1969) Pis'ma Eksp. Teor. Fiz. **9**, 150 [(1969) Sov. Phys. JETP Lett.]
 479. Josephson, B.D. (1962) Phys. Rev. Lett. **1**, 251; (1964) Rev. Mod. Phys. **36**, 216; (1965) Adv. Phys. **14**, 419
 480. Ferrell, R., Prange, R. (1963) Phys. Rev. Lett. **10**, 479
 481. Rowell, J.M. (1963) Phys. Rev. Lett. **11**, 200
 482. Rieger, T.J., Scalapino, D.J., Mercereau, J.E. (1972) Phys. Rev. Lett. **28**, 1112
 483. Clarke, J. (1968) Phys. Rev. Lett. **28**, 1363
 484. (1985) Search and Discovery, Phys. Today, April
 485. McCumber, D.E. (1968) J. Appl. Phys. **39**, 2503; (1968) **39**, 3113
 486. Stewart, W.C. (1968) Appl. Phys. Lett. **12**, 277
 487. Shapiro, S. (1963) Phys. Rev. Lett. **11**, 80
 488. Shapiro, S., Janus, A.R., Holly, S. (1964) Rev. Mod. Phys. **36**, 223
 489. Grimes, C.C., Shapiro, S. (1968) Phys. Rev. **169**, 397
 490. Lounasmaa, O.V., Hari, R. (1990) La Recherche **21**, 223; (1989) Science **224**, 439
 491. Williamson, S., et al. (Eds.) (1990) Advances in Magnetism. Plenum Press
 492. Webb, R.A., Giffard, R.P., Weatley, J.C. (1973) J. Low Temp. Phys. **13**, 383
 493. Lounasmaa, O.V. (1974) Experimental Principles and Methods Below 1 K. Academic Press
 494. Clarke, J. (1990) In: Superconducting Devices, 51. Academic Press
 495. Anderson, P.W. (1964) In: Caianello, E.R. (Ed.) Lectures on the Many-Body Problem **2**, 113. Academic Press
 496. De Bruyn Ouboter, R., De Waele, A.T. (1970) Prog. Low Temp. Phys. **6**, 243
 497. Clarke, J. (1973) Proc. IEEE **61**, 8
 498. Swihart, J.C. (1961) J. Appl. Phys. **32**, 461
 499. Eck, R.E., Scalapino, D.J., Taylor, B.N. (1965) Phys. Rev. Lett. **13**, 15
 500. Kulik, I.O. (1965) Pis'ma Zh. Eksp. Teor. Fiz. **64**, 946
 501. Langenberg, D., Scalapino, D., Taylor, B., Eck, R. (1965) Phys. Rev. Lett. **15**, 294
 502. Dmitrenko, I.M., Yanson, I.K. (1965) Zh. Eksp. Teor. Fiz. **48** [(1965) Sov. Phys. JETP **22**, 1190]

Chapter 17

503. de Gennes, P.G. (1989) Superconductivity of Metals and Alloys. Addison-Wesley
504. Bogoliubov, N.N., Tolmachev, V.V., Shirkov, D.V. (1959) A New Method in the Theory of Superconductivity. Consultant Bureau, New York
505. Fetter, A.L., Walecka, J.D. (1971) Quantum Theory of Many-Particle Systems. McGraw-Hill, New York
506. Gorkov, L.P. (1958) *Zh. Eksp. Teor. Fiz.* **34**, 735 [(1958) Sov. Phys. JETP **7**, 505]
507. Abrikosov, A.A., Gorkov, L.P. (1958) *Zh. Eksp. Teor. Fiz.* **35**, 1558 [(1959) Sov. Phys. JETP **8**, 1090]
508. Aronov, A.G., Galperin, Y.M., Gurevich, V.L., Kozub, V.I. (1986) In: Langenberg, D.V., Larkin, A.I. (Eds.) Nonequilibrium Superconductivity. Elsevier
509. Caroli, C., de Gennes, P.G., Matricon, J. (1964) *Phys. Lett.* **9**, 307; (1965) *Phys. Kondens. Materie* **3**, 380
510. Kramer, L., Pesch, W. (1974) *Z. Physik* **269**, 59
511. Gygi, F., Schlüter, M. (1990) *Phys. Rev. B* **41**, 822
512. Hess, H.F., et al. (1989) *Phys. Rev. Lett.* **62**, 214
513. Pippard, A.B., Shepherd, J.G., Tindali, D.A. (1971) *Proc. Roy. Soc. A* **324**, 17
514. Pippard, A.B. (1981) In: Gray, K. (Ed.) Nonequilibrium Superconductivity and Kapitza Boundaries, Chap. 12. Plenum, New York
515. de Gennes, P.G. (1964) *Rev. Mod. Phys.* **36**, 225
516. Werthamer, N.R. (1963) *Phys. Rev.* **132**, 2440
517. de Gennes, P.G., Guyon, E. (1963) *Phys. Lett.* **3**, 168
518. de Gennes, P.G. (1963) *Phys. Lett.* **5**, 22
519. Deutscher, G., de Gennes, P.G. (1969) In: Parks, R. (Ed.) Superconductivity 1005–1033. Marcel Dekker, New York
520. Andreev, A.F. (1964) *Zh. Eksp. Teor. Fiz.* **46**, 185, 1823 [(1964) Sov. Phys. JETP **19**, 1228]
521. McMillan, W.L. (1968) *Phys. Rev.* **175**, 559
522. Kulik, I.O. (1969) *Zh. Eksp. Teor. Fiz.* **57**, 1745 [(1970) Sov. Phys. JETP **30**, 944]
523. Bardeen, J., Johnson, J.L. (1972) *Phys. Rev. B* **5**, 72
524. Blonder, G.E., Tinkham, M., Klapwijk, T.M. (1982) *Phys. Rev. B* **25**, 4515
525. van Wees, B.J., de Vries, P., Magnéé, P., Klapwijk, T.M. (1992) *Phys. Rev. Lett.* **69**, 510
526. Beenakker, C.W.J. (1992) *Phys. Rev. B* **46**, 12841
527. Eilenberger, G. (1968) *Z. Phys.* **214**, 195
528. Usadel, K.D. (1970) *Phys. Rev. Lett.* **25**, 507
529. Nazarov, Y.V. (1994) *Phys. Rev. Lett.* **73**, 420
530. Zhou, F., Spivak, B., Zyuzin, Z. (1995) *Phys. Rev. B* **52**, 4467
531. Tinkham, M., Clarke, J. (1972) *Phys. Rev. Lett.* **28**, 1366
532. Clarke, M. (1981) In: Gray, K. (Ed.) Nonequilibrium Superconductivity and Kapitza Boundaries, Chap. 11. Plenum, New York
533. Pethick, C.J., Smith, H. (1981) In: Gray, K. (Ed.) Nonequilibrium Superconductivity and Kapitza Boundaries, Chap. 12. Plenum, New York
534. Rickayzen, G. (1980) Green's Functions and Condensed Matter. Academic Press
535. Rowell, J.M., McMillan, W.L. (1966) *Phys. Rev. Lett.* **16**, 453
536. Tomasch, W.J. (1966) *Phys. Rev. Lett.* **15**, 16

537. Tessmer, S.H., van Harlingen, D.J., Lyding, J.W. (1993) Phys. Rev. Lett. **70**, 3135
538. Guéron, S., Pothier, H., Birge, N.O., Estève, D., Dévoret, M.H. (1996) Phys. Rev. Lett. **77**, 3025
539. Zaikin, A.D. (1982) Solid State Comm. **41**, 533
540. Lévy, L.P. (1996) Submitted to Phys. Rev. B
541. Altshuler, B.L., Khmelnitskii, D.E., Spivak, B.Z. (1983) Solid State Comm. **48**, 841
542. Mota, A.C., Visani, P., Pollini, A. (1989) J. Low Temp. Phys. **76**, 465
543. Anderson, P.W. (1959) J. Phys. Chem. Solids **11**, 26
544. Abrikosov, A.A., Gorkov, L.P. (1961) Zh. Eksp. Teor. Fiz. [(1961) Sov. Phys. JETP **12**, 1243]
545. de Gennes, P.G. (1964) Phys. Kond. Materie **3**, 79
546. de Gennes, P.G., Sarma, G. (1963) J. Appl. Phys. **34**, 1380
547. Maki, K. (1963) Prog. Theor. Phys. Japan **29**, 333; ibid. (1964) **31**, 731; ibid. (1964) **32**, 29
548. Maki, K. (1969) In: Parks, R. (Ed.) Superconductivity, Chap. 18. Marcel Dekker, New York
549. Woolf, M.A., Rief, F. (1965) Phys. Rev. **137**, A557
550. Ambegaokar, V., Griffin, A. (1964) Phys. Rev. **137**, A1151
551. Skalski, S., Betheber-Matibet, O., Weiss, P.R. (1964) Phys. Rev. **136**, A1500
552. Winzer, K. (1973) Z. Physik. **265**, 139
553. Kohn, W. (1964) Phys. Rev. **133**, A171
554. Hebard, A., Paalanen, M. (1990) Phys. Rev. Lett. **65**, 927
555. Hebard, A., Paalanen, M., Ruel, R. (1991) Phys. Rev. Lett. **69**, 1604
556. Fisher, M.P.A. (1990) Phys. Rev. Lett. **65**, 923
557. Anderson, P.W. (1958) Phys. Rev. **110**, 827; ibid. (1958) **112**, 1900
558. Carlson, R.V., Goldman, A.M. (1973) Phys. Rev. Lett. **31**, 880; ibid. (1975) **34**, 11; (1976) J. Low Temp. Phys. **27**, 67
559. Schmid, A., Schön, G. (1975) J. Low Temp. Phys. **20**, 207
560. Schmid, A. (1981) In: Gray, K.E. (Ed.) Nonequilibrium Superconductivity, Phonons and Kapitza Boundaries. Plenum, New York
561. Schön, G. (1986) In: Langenberg, D.V., Larkin, A.I. (Eds.) Nonequilibrium Superconductivity, 589. Elsevier
562. Hebard, A.F. (1992) Physics Today **26**, November issue
563. Schluter, M., Lannoo, M., Needels, M., Baraff, G.A. (1968) Phys. Rev. Lett. **68**, 526
564. Pietronero, L. (1992) Europhys. Lett. **17**, 365
565. Jérôme, D. (1995) In: Douçot, B., Zinn-Justin, J. (Eds.) Strongly Interacting Fermions and High T_c Superconductivity. Elsevier Science; (1994) In: Farges, J.P. (Ed.) Organic Superconductors. Marcel Dekker, New York
566. Nozières, P., Saint-James, D. (1982) J. Physique **43**, 1133
567. Dagotto, E., Rice, T.M. (1996) Science **271**, 618
568. Trankada, J.M., Sternleib, B.J., Axe, J.D., Nakamura, Y., Ushida, S. (1995) Nature **375**, 561; ibid. (1996) Submitted to Phys. Rev. Lett.
569. Uehara, M., Nagata, T., Ahilistu, J., Takahashi, H., Moti, N., Kinoshita, K. (1996) Phys. Soc. Japan, to be published
570. Schrieffer, J.R., Zang, S.C., Wen, X.G. (1988) Phys. Rev. Lett. **60**, 944
571. Emery, V.J., Kivelson, S.A., Zachar, O. (1996) Submitted to Phys. Rev. B

Appendix A

- 572. Hammermesh, M. (1964) Group Theory and its Application to Physical Problems. Addison-Wesley
- 573. Serre, J.P. (1967) Représéntation linéaire des groupes finis. Hermann, Paris
- 574. Wigner, E.P. (1959) Group Theory and its Application to the Quantum Mechanics of Atomic Spectra. Academic Press
- 575. Pikus, G.E., Bir, G.L. (1974) Symmetry and Strain Effects in Semiconductors. Wiley, New York
- 576. Schläfer, H.L. (1967) Einfürung in die Ligandenfeldtheorie. Akademische Verlaganstalt, Frankfurt

Appendix C

- 577. Henley, C. (1989) Phys. Rev. Lett. **62**, 2056

Index

- Abrikosov
 - criterion 284
 - lattice 342–344
- Absorption 150, 163
 - ultrasound 327–330
- Adiabatic
 - demagnetisation 19, 50, 108
 - phase 212
 - response 149, 152–159
 - susceptibility 153, 159
- Aharonov–Casher effect 28
- AKLT state 223
- Ampère’s theorem 4, 272, 280, 348, 365, 379
- Andreev
 - reflection 390–396
 - state 397–399
- Angular momentum
 - orbital 67
 - spin 67
 - topological 232
 - total 45
- Anisotropy
 - ionic 52, 189
 - uniaxial 112, 117, 174, 185, 189
- Anomalous
 - skin effect 273
 - Zeeman effect 46
- Antiferrromagnetism 71, 77, 110–113
 - destruction by holes 258
- Antisymmetrisation operator 72
- Antisymmetry 310, 417, 421
 - of wave functions 61, 235, 256
- Approximation
 - Hartree–Fock 74, 101
 - Heitler–London 71
 - mean field 77, 81, 101, 128, 314–319, 430
 - random phase 244
 - semi-classical 24, 26, 355, 384–386
- Band width 74, 237, 253
- BCS state 319
- BCS theory 249, 309–336
 - density of states 318
 - gap 315, 317
 - Hamiltonian 311–314
- Bloch
 - equation 166–169, 192
 - law 196
 - state 24, 47, 74, 423
 - theorem 28
 - wave 28
- Bogoliubov transformation 249, 315
 - for bosons 191
- Bogoliubov–de Gennes equations 381–384
- Bohm–Aharonov effect 26
- Bohr magneton 45
- Bohr–Sommerfeld rules 33, 337
- Bose condensation 259, 270
- Bose–Einstein statistics 195
- Boson 186
- Breather 210
 - dispersion relation 211
- Brillouin function 48, 105
- Canonical variable 33, 208, 209, 229
- Cauchy theorem 163
- Causality 149, 162
- Charge
 - fractional 37
 - magnetic 7, 193
 - quasi-particle 320
 - topological 141, 210
- Chemical potential 37, 40, 314
- Chromium 238, 248, 251
 - spin density wave 252
- Classical spin 49, 186
- Coherence length 273, 339, 386
 - Ginzburg–Landau 289, 292
- Collective coordinates 57, 226
- Commutation relation 33, 45, 135, 315, 422

- Condensation
 - amplitude 250, 312, 316
 - Bose 259, 270
 - of eigenvalues 122
- Conductivity
 - Drude 290, 335
 - electrical 164
 - Hall 35, 290
 - of superconductor 335
 - thermal 179, 330
- Configuration 68, 78, 220
- Conservation law 179, 184, 202
- Constitutive equation 4, 179, 271
- Contraction of operators 76, 424
- Cooper pair 30, 267, 285, 312, 337, 356
 - effective mass 271
- Correlation
 - energy 398
 - length 81, 90
- Correlation function 147, 155, 199
 - in BCS state 322
 - in Ising model 121–126
 - in XY model 144, 214–216
- Coupling constant 206
- Creation and annihilation operators 64, 187, 286, 421
- Critical
 - current 263, 280–283, 300, 359, 366, 377, 384
 - exponent 93
 - field
 - H_{c1} 266, 338, 344
 - H_{c2} 265, 304, 338
 - H_{c3} 305
 - thermodynamic 263, 274, 288, 318, 338
 - phenomena 93
 - slowing down 129–130
 - temperature 103, 143, 322
- Crystalline field 53, 57, 416
- Curie's
 - constant 49, 104, 107, 236
 - law 49, 161
- Curie–Weiss law 103
- Cyclotron
 - frequency 30
 - radius 30
- d* band 44, 74, 236
- de Gennes length 292
- Debye energy 269, 311, 318
- Demagnetising factor 7, 277
- Density of states
- at Fermi level 41, 44, 235
 - at Landau level 37
 - at n-s interface 394
 - BCS 318
 - in two dimensions 32
 - of superconductor 401
 - phonon 310
- Detailed balance, principle of 127
- Diamagnetism 26, 399
 - Landau 40
 - of superconductor 265
- Dielectric constant 145, 164
- Diffusion
 - of heat 180
 - of spins 180
- Dingle's criterion 42
- Dipolar relaxation 171
- Dipole–dipole interaction 61, 147, 171
- Dispersion relation
 - breather 211
 - spin-wave 183, 246
- Displacement current 4
- Dissipation 157, 345–349
- Domain
 - magnetic 107
 - superconducting 277, 341
- Drude conductivity 290, 335
- Dynamic susceptibility 199
- Dzyaloshinskii–Moriya interaction 52
- Effective mass 24, 26, 30, 44
- Einstein
 - coefficient 159
 - equations 159
- Einstein–de Haas effect 20
- Elastic collision time 35
- Electrical conductivity 164
- Electromagnetic
 - response 335
 - screening 331–335, 399
- Electron
 - correlations 71, 81, 255–258
 - density 64, 77
 - polarisation 77
- Electron–electron interaction 310
- Electron–phonon interaction 267–270, 309, 381
- Elementary excitation 185, 188
- Entropy 19
 - in Ising model 119
 - of superconductor 275, 324, 350
 - spin 1/2 49
- Ergodicity
 - at phase transition 89, 185

- Evolution operator 147, 167
- Exchange 61, 236
 - anisotropy 73
 - biquadratic 74, 223
 - frequency 177
 - Hamiltonian 72, 188
 - narrowing 172
- Excitonic
 - gap 250
 - insulator 239, 248–252
- Expansion coefficient 123, 439
- Extended state 37
- Extensive variable 4, 13

- Fermi
 - energy 32
 - fluid 30, 77
 - golden rule 162, 325, 329, 355
 - level 35, 310
 - liquid 266, 290
 - surface 43, 268, 334
 - nesting 237, 248
- Fermion gas 135
- Ferrimagnetism 113
- Ferromagnetism 71
 - weak 247
- Field
 - crystalline 53, 57
 - magnetic 3
 - molecular 77, 101–105
 - reaction 104, 108–110
- Field operator 64, 422
- Filling factor 32, 157
- Fine structure constant 47
- Fixed point 97
- Fluctuation 133, 147
 - of order parameter 90, 102, 196
 - quantum 206, 212
- Fluctuation-dissipation theorem 106, 152–159
- Flux quantisation 295–299
- Flux quantum 30, 292, 296, 304, 339, 364, 366
- Flux transformer 373
- Fock term 80, 81
- Fractional charge 37
- Free energy 14, 104
 - classical 39
 - Ginzburg–Landau 287–290, 343
 - in Ising model 119
 - Landau 86
 - of superconductor 324
- Frustration 114, 435–438

- Gap
 - BCS theory 315, 317
 - excitonic 250
 - Haldane 225
 - Hall effect 37
 - of superconductor 266
 - spin-wave 204
- Gapless superconductivity 400–402
- Gauge invariance 24, 28, 266, 286, 288
- Gibbs free energy 15, 274
- Ginzburg–Landau
 - coherence length 289, 292
 - equations 291–295, 303, 339
 - free energy 287–290, 343
 - theory 285–307, 335, 402
 - validity 286
- Glauber dynamics 127
- Goldstone
 - mode 181
 - theorem 181
- Grand canonical potential 16, 40
- Griffiths relation 99
- Group representation 407–420
- Gutzwiller wave function 139, 254
- Gyromagnetic factor 21, 180

- Haas–van Alphen effect 40, 41
- Haldane gap 225
- Half-filling 258
- Hall conductivity 35, 290
- Hamiltonian
 - BCS 311–314
 - exchange 72, 188
 - in XY model 134
 - Ising 117
 - magnetic 23
 - tunnelling 325, 361
 - Zeeman 45, 148, 187
- Harmonic oscillator 30, 185
- Hartree term 80, 81
- Hartree–Fock
 - approximation 74, 101
 - equation 76
- Heat 12, 14
- Hebel–Schlichter singularity 330
- Heisenberg exchange Hamiltonian 61, 70, 75
- Heitler–London approximation 71
- Helimagnetism 113, 204
- Helmholtz equation 194, 339
- Hermite polynomial 31
- Hole 67, 258, 390

- Holstein–Primakoff Transformation 185–192
- Hopping integral 74, 78
- Hubbard model 252–260
- Hund rules 63, 67, 417
- Hydrodynamic mode 168, 179–204
- Hydrogen molecule 68
- Hyperscaling relation 99
- Hysteresis, magnetic 4, 106, 352

- Incompressible state 37
- Inductance 157
- Induction, magnetic 3, 102
- Inhomogeneous superconductivity 381–406
- Instability, thermodynamic 106
- Instanton 214
- Intensive variable 13
- Interfacial energy 278, 284, 301, 337
- Intermediate state 265, 276–281, 390
 - resistance 282
- Internal energy 12, 104
- Ising
 - Hamiltonian 117
 - model 117–131
 - spin 108
- Isothermal
 - compressibility 131, 439
 - response 149–152
 - susceptibility 18, 159
- Isotopic effect 267, 309, 318
- Itinerant magnetism 44, 235–260

- Jahn–Teller distortion 56–58, 68
- Jordan–Wigner transformation 135
- Josephson
 - current 359, 398
 - effect 349, 358–379
 - frequency 367
 - length 365
- Junction
 - microbridge 360
 - n-i-n 325, 355
 - n-i-s 326, 356
 - s-i-s 327, 357
 - s-n-s 397

- Kagomé lattice 114
- Kekulé state 219
- Kinetic energy 79
- Kinetic momentum 24, 211
- Knight shift 169

- Kosterlitz–Thouless transition 141–146, 215
- Kramers
 - degeneracy 58
 - doublet 60
- Kramers–Kronig Relations 162–164
- Kubo formulas 161

- Ladder operator 33, 45
- Lagrange multiplier 201, 229
- Landau gauge 25, 30
- Landau levels 30, 40
- Landau theory 85, 103
 - validity 92, 275
- Landé factor 20, 30
- Langevin
 - equation 103
 - force 147
- Laplace equation 360
- Larmor frequency 167
- Latent heat 84, 263, 275
- Lattice gas 117, 130–131
- Lee and Yang
 - distribution 125
 - zeros 124
- Legendre transformation 15
- Level repulsion 178
- Lieb–Schultz–Mattis theorem 216
- Ligand 74, 78
- Lindhard susceptibility 241
- Linear response 128, 147–178
- Local equilibrium 166, 179
- Local polarisation 104
- Localised state 37
- London
 - equations 271, 339
 - gauge 272, 288, 332, 335
 - penetration depth 270, 289
- Long range interaction 102, 430
- Lorentz
 - force 24
 - transformation 209

- Magnetic
 - charge 7, 193
 - coordination 102
 - domain 107
 - field 3
 - hysteresis 4, 106, 352
 - induction 3, 102
 - length 30
 - monopole 4, 231
 - polarisation 245

- resistance 157
- scalar potential 5
- vector potential 7
- work 11
- Magnetic moment
 - giant 245
 - of vortex 338, 340
 - orbital 39
- Magnetisation 3
 - alternating 111, 183
 - of superconductor 265
- Magneto-elastic coupling 57, 87, 123
- Magneto-mechanical factor 20
- Magneto-optics 115
- Magnetocaloric effect 19
- Magnetostatic mode 168, 193
- Magnetostriction 123
- Magnon 184–192
 - anharmonic effects 189
 - lifetime 189
 - non-linear 197–198
 - thermodynamics 195–197
- Majumdar–Ghosh state 221
- Marshall theorem 217
- Maxwell's equations 4, 193, 271
- Mean field approximation 77, 81, 101, 128, 314–319, 430
- Meissner effect 264, 272, 275, 331, 338, 344
- Mermin–Wagner theorem 85, 133
- Micro bridge junction 360
- Mixed state 337
- Molecular field 77, 101–105, 382
- Mott transition 254
- Néel state 81, 220
- Néel temperature 111
- Nesting, of Fermi surface 237, 248
- Noise, electromagnetic 155, 360
- Non-equilibrium charge length 396
- Non-linear commutation relations 45
- Non-linear response 165
- Non-linear σ model 226–233
- Non-local electrodynamics 27, 272, 334
- Normal order 65, 189, 424
- Nuclear Magnetic Resonance (NMR) 164
 - pulsed 166
- Nuclear relaxation 330
- Nucleation 106, 265, 303, 305
- Number operator 65, 186, 313, 422
- Ohm's law 271
- Onsager
 - equations 109
 - reciprocity relations 149, 165
- Orbital magnetism 39
- Order by disorder 435
- Order parameter 83, 102, 285
 - Edwards–Anderson 109
 - non-local 225
 - symmetry 202, 286, 313
- Orthogonality
 - catastrophe 70
 - of wave functions 79
- Oscillation
 - Haas–van Alphen 40
 - Rowell 395
 - Tomasch 395
- Overlap integral 66, 69, 75
- Paramagnetism
 - Curie 49
 - Pauli 43
- Paramagnon 247
- Partition function 48, 51, 110
 - in Ising model 118
 - lattice gas 131
- Pauli matrices 44
- Pauli principle 61, 64, 78
- Pendulum equation 365
- Penetration depth 264, 400
 - London 270, 289
 - Pippard 273, 335
- Periodicity of spin states 185, 212, 231
- Permanent current 27
- Permeability 5
- Permutation operator 63, 69, 72
- Phase transition
 - first order 84, 263, 265
 - second order 83, 344
 - singularity 84, 93
 - symmetry 83
- Phonon
 - density of states 310
 - specific heat 266
- Pinning
 - of domain walls 107
 - of vortices 346
- Planck's law 159
- Point group 412
 - representation 416
- Poisson
 - bracket 182, 208
 - equation 7
 - formula 40

- Principal parts 163
- Projection operator 64, 80, 222, 224, 320
- Proximity effect 394
- Quantum
 - of action 355
 - of conductance 35, 356
- Quantum effects 82
- Quantum Hall effect 34–38
 - fractional 37
- Quasi-particle 76, 312, 315, 356, 395
 - charge 320
- Random phase approximation 244
- Rare earths 44, 53, 69, 236
- Reaction field 104, 108–110
- Reciprocity theorem 9, 155
- Reflectivity, of superconductor 335
- Relaxation time
 - longitudinal 169, 330
 - transverse 169
- Renormalisation 198
 - of fluctuations 93–97
- Representation
 - of point groups 416
 - of rotation group 410
- Resistance, in intermediate state 282
- Resonance
 - ferrimagnetic 176
 - ferromagnetic 173
 - nuclear magnetic (NMR) 164
 - pulsed 166
- Response function 149
- Restoring force 133, 181, 375
- Rigidity of wave function 28, 38, 271, 399
- Rotating frame 166, 180
- Rotation
 - group 410–412
 - invariance 72
- Rowell oscillation 395
- Scaling
 - function 99
 - law 98–100
 - dynamical 129
- Scattering amplitude 256
- Schrödinger equation 24, 74
- Schwinger boson 201
- Screening
 - electromagnetic 331–335, 399
 - Thomas–Fermi 242
- Second quantisation 64, 421–427
- Semi-classical limit, of spin 212
- Semiconductor model, of junction 326
- Shapiro steps 369
- Shubnikov phase 266
- Silsbee criterion 263, 281
- Sine–Gordon equation 208–214, 379
- Singlet 63, 218
- Slater determinant 79, 421
- Soliton 207, 366, 379
- Sommerfeld constant 244, 266, 290, 324
- Specific heat
 - constant field 14
 - constant magnetisation 13, 131
 - constant volume 131
 - discontinuity at T_c 275
 - in Ising model 119
 - of phonons 266
 - of superconductor 266, 324
 - singularity at T_c 87
 - spin 1/2 49, 104
- Speed of sound 124, 180
- Spherical harmonics 45
- Spin
 - chain 135–139, 205–233
 - degeneracy 32
 - density wave 44, 113, 238, 248–252
 - glass 109, 114
 - hydrodynamics 201–204
 - liquid 114, 205
 - operator 66
 - soft 201
 - temperature 166
 - torsion 182
 - wave 104, 179–204, 246, 433
 - dispersion relation 183, 246
 - gap 204
 - spectroscopy 198
- Spin 1/2 44, 102
- Spin-flop transition 112, 178, 431
- Spin-orbit interaction 47, 67
- Spin-Peierls transition 206
- Spinon 136
- Spiral phase 258
- SQUID
 - AC 369–373
 - DC 376–378
 - mechanical analogy 373
- Stark effect 56
- Stereographic projection 186, 231
- Stokes's theorem 348
- Stoner
 - criterion 237

- excitation 246
- model 242–248, 312
- – susceptibility 246
- Structure factor 148
- Sublattice 110, 176
- Sum rule 163
- Superconducting array 439
- Superconductivity
 - gapless 400–402
 - high temperature 259, 263, 336, 404
 - inhomogeneous 381–406
 - thermodynamics 274
 - type I 265, 284
 - type II 284, 366
- Superconductor under pressure 438
- Supercooling 106, 265, 304
- Superexchange 77
- Superheating 106
- Susceptance, isothermal 17
- Susceptibility 4
 - adiabatic 153, 159
 - antiferromagnetic 111
 - dynamic 199
 - in Ising model 121
 - in Stoner model 246
 - in XY model 141
 - isothermal 18, 159
 - Landau 40
 - Lindhard 241
 - longitudinal 111
 - Pauli 44
 - transverse 111, 157
 - van Vleck 51
- Swihart wave 379
- Symmetric gauge 25, 32
- Thermal
 - conductivity 179, 330
 - length 396
 - transport 352
- Thermodynamics
 - of magnons 195–197
 - of spins 48
 - of superconductor 274
- Thomas–Fermi screening 242
- Time reversal invariance 58, 164, 328, 362
- $t - J$ model 255
- Tomasch oscillation 395
- Topological
 - charge 210
 - angular momentum 232
 - charge 141
 - order 85, 134
- Transfer matrix 119–121, 139
- Transition
 - ion 53, 67
 - metal 44, 236
- Triangular lattice 114
- Tricritical point 88
- Triplet 63, 218
- Tunnelling 215, 324–327, 355–358, 390–396
 - current 327, 355–358
 - Hamiltonian 325, 361
- 2-level system 157
- Two-fluid model 270
- Ultrasound absorption 327–330
- Uncertainty principle 314
- Units, CGS and MKSA 4
- Valence 70
- Valence bond state 218–226
- Van der Waals isothermal 106
- Van Leeuwen theorem 39
- Van Vleck formula 25
- Variational method 81, 306
- Vector model of spins 45
- Vector potential
 - electric 29
 - magnetic 7
- Villain representation 201, 208
- Viscosity 180, 347
- Vortex 134, 266, 337–353, 366, 379
 - core states 347, 386–389
 - flow 345–350
 - interaction potential 341, 344
 - lattice 342–344
 - magnetic moment 338, 340
 - pinning 350
 - wave function 338
- Vortex-antivortex pair 145
- Walker mode 193
- Wannier state 47, 74, 79, 423
- Wick theorem 382
- Widom relation 99
- Wigner crystal 236
- Wigner–Eckart theorem 45, 73
- XY model 133–146
- Zeeman
 - effect 44
 - energy 43
 - Hamiltonian 45, 148, 187



Location: <http://www.springer.de/phys/>

**You are one click away
from a world of physics information!
Come and visit Springer's
Physics Online Library**

Books

- Search the Springer website catalogue
- Subscribe to our free alerting service for new books
- Look through the book series profiles

You want to order?

Email to: orders@springer.de

Journals

- Get abstracts, ToC's free of charge to everyone
- Use our powerful search engine LINK Search
- Subscribe to our free alerting service LINK Alert
- Read full-text articles (available only to subscribers of the paper version of a journal)

You want to subscribe?

Email to: subscriptions@springer.de

Electronic Media

- Get more information on our software and CD-ROMs
- Email to: helpdesk-em@springer.de

You have a question on
an electronic product?

.....● Bookmark now:

**http://
www.springer.de/phys/**

Springer · Customer Service
Haberstr. 7 · D-69126 Heidelberg, Germany
Tel: +49 6221 345200 · Fax: +49 6221 300186
d&p · 6437a/MNT/SF · Gha.



Springer